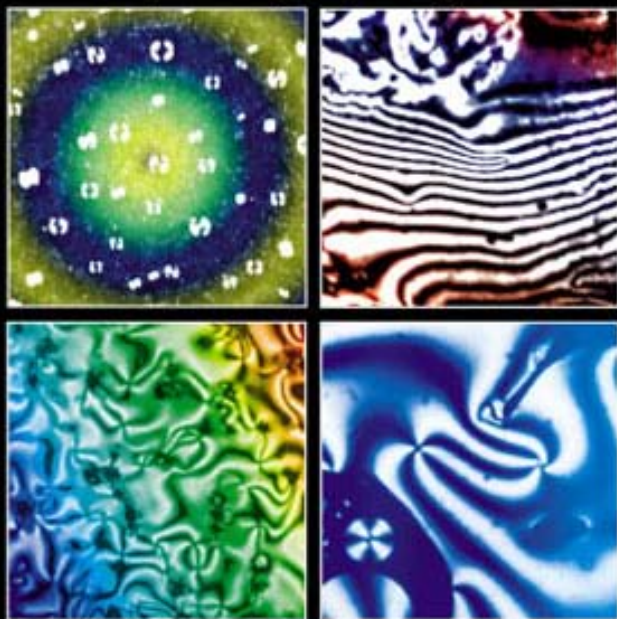Xin-Jiu Wang · Qi-Feng Zhou
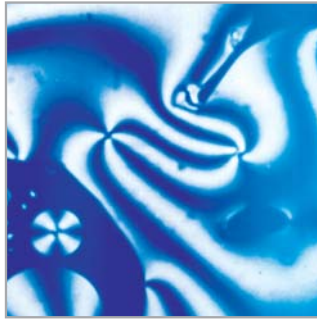
LIQUID CRYSTALLINE
POLYMERS

LIQUID CRYSTALLINE POLYMERS

This page intentionally left blank

LIQUID CRYSTALLINE POLYMERS

Xin-Jiu Wang

Avery Research Center, USA

Qi-Feng Zhou

Peking University, China

World Scientific

British Library Cataloguing-in-Publication Data
A catalogue record for this book is available from the British Library.

LIQUID CRYSTALLINE POLYMERS

Contents

This page intentionally left blank

Preface

The liquid crystal and the polymer are two different disciplines of science and technology. They meet together producing the liquid crystalline polymer or, if you prefer, the polymeric liquid crystal. The liquid crystalline polymer combines mesogenic units and high molecular weight, and thus exhibits excellent anisotropic physical properties while possessing the advantage of easy processing and convenient molecular tailoring. The liquid crystalline polymer not only possesses the individual properties of each of its parents, but also exhibits intrinsic features that its parents do not have. In such a sense, the liquid crystalline polymer is a new state of matter.

Both the liquid crystal and the polymer are of about the same age, but the polymer has successfully penetrated every walk of human life. On the other hand, the liquid crystal had kept itself quiet for a half century until the early 70's. Since then, it has caught the vast interest of both science and industry. It has been applied especially in the display industry, such as in portable TVs and notebook and desktop computers. Two important events symbolized the liquid crystal's coming of age: Professor P. G. de Gennes, a French physicist, won the Noble Prize in 1991 and Professor G. W. Gray, a British chemist, was awarded the Kyoto Prize in 1995.

In tracing back the history of the liquid crystalline polymer itself, the German scientist D. Vorlander should be mentioned. It was he who first pointed out that the long shape of the polymer does not prevent the polymer from exhibiting liquid crystallinity. The polymeric liquid crystallinity was first found in the tobacco mosaic virus in solution around 1940, and later found in the poly-peptide solution. The initial theoretical basis for the rigid liquid crystalline polymer is attributed to the

efforts of Onsager and Flory, both Noble Prize laureates. The liquid crystalline polymer has been a constant challenge to theoretical scientists to fully explain and exactly predict the behaviors of it and its substantial members, *i.e.*, network and gel. In addition, the understanding of liquid crystalline polymers may provide an insight into biological systems.

S. L. Kwolek, a woman scientist of DuPont, invented the liquid crystal aromatic polyamides which eventually paved the way to the first commercial liquid crystalline polymer product—poly-p-phenyleneterephthalamide under the trade name Kevlar. She recently recalled, "When I dissolved the PBA (poly-p-aminobenzamide) polymer at 10% concentration in tetramethylurea with 6.5% LiCl, the solution was unusually fluid, turbid, stiropalescent, and butter-milk-like in appearance." The fiber that was spun turned out to be extremely strong with a modulus of 430 gpd! This discovery in 1964 remains a milestone of this field. In recognition of her contribution, the American Society of Chemistry Industry awarded Kwolek the 1997 Perkin Medal.

The liquid crystalline polymer has since developed far beyond imagination that a decade ago. The liquid crystalline polymer family has so far included the main chain-, side chain-, and crosslinked- (*i.e.* network or elastomer) types, and their solutions and gels. The liquid crystal phases cover nematic, cholesteric and smectics. Although the science of the liquid crystalline polymer is not fully mature, it has attracted significant research interests and has already made tremendous progress. As investments and human resources continue, the liquid crystalline polymer is expected to have an even brighter future.

The liquid crystalline polymer industry now covers diverse products, from high modulus rope to high strength composite, from the tennis racket to the radial tire cord, from the cover layer of the optical fiber to the microwave oven, from the bullet-proof vest to thermal insulated clothing, and from the electro-optic display to non-linear optical material, *etc.*

The authors, X. J. Wang (XJW), a condensed matter physicist, and Q. F. Zhou (QFZ), a polymer chemist, have found joint research interest in this fascinating material since the middle of the 80's. They have collaborated on several projects. In 1994, they successfully organized an IUPAC conference on liquid crystalline polymers in Beijing. XJW is now working as a senior research scientist in Avery Research Center, Avery Dennison Company, USA. While QFZ is working as a professor in the Department of Polymer Science and Engineering, Peking University, China.

This book consists of six chapters. The first chapter highlights the concept of liquid crystals, including chemical structure, phase classification, defect and texture, and continuum theory. This chapter is carefully prepared in order to meet the needs of readers who are not specialized in liquid crystals. The second chapter is associated with the theoretical descriptions of liquid crystalline polymers, networks, and gels which deal with subjects such as the formation of liquid crystallinity in polymer system, phase transition and phase diagram, the molecular weight effect, chain conformation, physics properties, *etc.* In Chapter 3, the molecular engineering of liquid crystalline polymers is introduced. The molecular composition and the molecular weight play essential roles in the molecular design, which are reviewed in detail. In addition, some unusual liquid crystalline polymers are discussed in the chapter. Chapter 4 is devoted to the phase identification of liquid crystalline polymers. The techniques involved cover polarizing microscopy, thermal analysis, X-ray diffraction and others. Chapters 5 and 6 summarize the properties and applications of liquid crystalline polymers. Chapter 5 deals mainly with mechanical performance in fiber and composites. Chapter 6 introduces the elasticity and viscosity and rheology of liquid crystalline polymers, as well as other important properties.

<div align="right">

Xin-Jiu Wang and Qi-Feng Zhou
Pasadena, CA, USA, 2002

</div>

This page intentionally left blank

Chapter 1

Liquid Crystal States of Matter

1.1.   LIQUID CRYSTAL STATES

As we know, there are three basic states of matter, solid, liquid, and gaseous states. These states of matter can be transformed into each other at appropriate conditions. In the solid state (generally meaning the crystalline state), the building blocks, such as atoms, or molecules, or clusters of molecules are packed closely and regularly, forming a crystal lattice. The X-ray diffraction of the state shows many regular diffraction spots. Over 95% of matter on the earth exist in the form of the crystalline state. The types of crystal structure are enormous. The physical properties of crystals are basically anisotropic. The crystals have a constant melting temperature (except for amorphous solids). Two different crystal planes make a constant angle. As the temperature of matter increases the thermal movement of atoms or molecules become so severe that the crystal lattice is dissolved and fluidity appears. At this temperature, matter does not have a regular shape and anisotropic properties any more. It becomes a liquid. In the liquid state, the atoms or molecules are no longer arranged in a regular order, but they are still bonded to each other tightly, though not in the tightest packing. Compared with the crystal state, the volume change of a liquid is not great but the liquid does not have a regular shape and can flow. Because of gravity the surface of liquids is usually flat. Increasing the temperature further up beyond the melting point, matter is transformed to the gaseous state. In the gaseous state, no short-range order exists. The interaction between the constituent molecules is extremely weak. Due to thermal excitation the molecules fill the container uniformly and hence the

gas no longer has a flat surface. Generally, as the temperature increases progressively, matter at first appears in the form of a crystal solid, and then a liquid and finally the gaseous state. Exceptionally, a few materials may be heated directly from the solid into the gas state, that is, by sublimation, such as for iodine. Conversely, some substances may be transformed directly from gas to solid, which is called sublimation as well. Water vapor condensing to ice is an example of sublimation.

As the understanding about the states of matter became deeper, people had found that in addition to the above mentioned well-known three states, there exist other states of matter in nature, such as the plasma state, amorphous solid, liquid crystal state, superconductor, neutron state, etc. Among them the liquid crystal state is the subject of this book.

The liquid crystal state is a kind of state whose order is between the crystal solid and isotropic liquid states. In the crystal state, there is a long range order in position and orientation, while in the liquid state there are no long range ordering in either of them. Figure 1.1 is a comparison of the crystal (a), the liquid crystal (b) and the liquid (c) states.

The liquid crystal was once considered a rare state in the nature, but so far over eighty thousand liquid crystalline compounds have actually been found, making them a great family of matter.

The discovery of the liquid crystal state should be traced back to a story taking place one hundred years ago. Austria botanist F. Reinitzer observed a peculiar phenomenon in 1888 — under a microscope (Reinitzer, 1888), cholesteryl nonanoate melted into a cloudy liquid at 145.5 °C; as the temperature rose to 178.5 °C, it suddenly became clear. When cooling down, the substance briefly appeared violet-blue just before becoming an

(a)	(b)	(c)
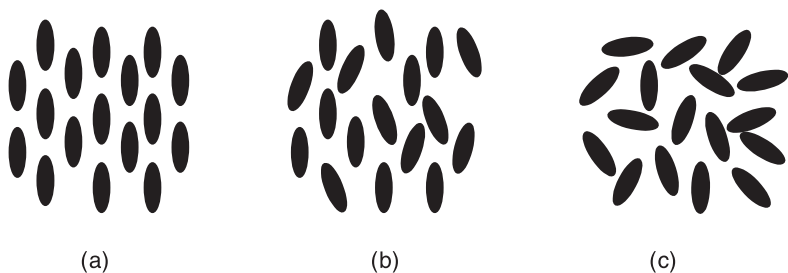
Figure 1.1.   The schematics of (a) crystal, (b) liquid crystal and (c) liquid.

opaque liquid, and then finally a white solid crystal. Reinitzer was puzzled about what he observed: why were there two melting points between the crystal (solid) and clear (liquid) states. He sent the sample together with his observation to German physicist Otto Lehmann who later made detailed observations by means of the polarizing microscope equipped with a heat stage. He at last concluded that cholesteryl nanonoate in the temperature range of 145.5 °C and 178.5 °C must be in a new state of matter. After a few years of hesitation, he finally named this state of matter, the **liquid crystal** (Lehmann, 1900). Later somebody proposed that the term "mesogenic state" might be an appropriate nomenclature for the new state, because it may avoid possible confusion. In spite of this problem, people have seemed to prefer the term liquid crystal due to its vivid description and the term liquid crystal has since been widely adopted, while the term mesogen or mesogenic is now used for a compound that is able to show the liquid crystal state. Contemporary knowledge tells us that cholesteryl nanonoate actually exhibits two liquid crystal phases in the temperature range of 178.5 °C and 145.5 °C. As the temperature decreases, the first blue color is that of the blue phase of the liquid crystal, and the second violet-blue color results from the cholesteric phase of the liquid crystal. More than twenty liquid crystal phases have since been discovered. The blue phase and cholesteric phase are two of them.

One enlightenment that can be drawn from the discovery of the liquid crystal is that despite the fact that Reinitzer and Lehmann pursued different fields and were in different countries, the cooperation between them inaugurated a new field of science — the liquid crystal. Actually the whole development of the field of the liquid crystal has demonstrated this type of cooperation.

As early as 1850, a German scientist discovered, in fact, the possibility of the liquid crystal when he found that natural fats exhibited two melting points. With increasing temperature, the substance starts to become cloudy at around 52 °C and is completely opaque at 58 °C, and then becomes clear at 62.5 °C. This observation should be the earliest record of the "discovery" of the liquid crystal. At around the same time, the cholesterol derivative exhibited a striking color when it cooled from the isotropic liquid state. Unfortunately, these phenomena were not given enough attention or correctly explained. The researchers themselves did not realize that they were approaching the entrance of a new field of science. Therefore, the discovery of the liquid crystal should be attributed to Reinitzer and Lehmann.

1.2.   APPEARANCE AND LIGHT SCATTERING OF LIQUID CRYSTALS

The liquid crystal state is a state of matter which is different from the liquid and solid states. Liquid crystals can flow as a liquid does. Typically, the viscosity of the liquid crystals such as the nematic liquid crystal is in the order of magnitude of 1×10^{-2} Pa.s., a value greater than that of water whose viscosity is about 1×10^{-3} Pa.s. Some liquid crystals, such as high order modifications — smectic liquid crystals, are very viscous. A liquid is transparent, but a liquid crystal is normally milky. This is because the fluctuation of the orientation of the molecular long axes of the liquid crystals causes strong light scattering. The scattering of liquid crystals is as high as one million times that of conventional isotropic liquids. The milky appearance becomes one of the identifications of the liquid crystals.

As we know, the scattering of matter is caused by the fluctuation of their refractive index (or optical dielectric constant). The local compression or dilution of mass density in bulk isotropic liquids modifies in turn the local refractive index. The change can be expressed in the form of the dielectric constant as

$$\varepsilon(\boldsymbol{r}) = \varepsilon + \varepsilon' \phi(\boldsymbol{r}), \tag{1.1}$$

where ε is the average dielectric constant, $\phi(\boldsymbol{r})$ is the bulk compressibility and $\boldsymbol{r}$ is the distance vector of a point in the material, ε' is the fluctuation of the dielectric constant. According to light scattering rules, the cross-section of light scattering of isotropic liquids, σ_I, is given by

$$\sigma_I \propto \varepsilon'^2 \langle |\phi(\boldsymbol{k})|^2 \rangle, \tag{1.2}$$

where $\phi(\boldsymbol{k})$ is the Fourier transformation of $\phi(\boldsymbol{r})$, and $\langle \ldots \rangle$ indicates the statistical average. The average in the bracket can be written as

$$\langle |\phi(\boldsymbol{k})^2| \rangle = \frac{V k_B T}{B}, \tag{1.3}$$

where V is the volume of the sample, $1/B$ is the isothermal compressibility coefficient, and k_B is the Boltzmann constant.

Liquid crystals are optically anisotropic media with the exception of the cubic phases, such as the D-phase and blue phase. The refractive index or dielectric constant of liquid crystals varies according to the orientation of the molecular axes (or the optical axes). For example, the nematic liquid crystals are optically uniaxial and exhibit remarkable birefringence, that

is, their refractive indices of ordinary and extraordinary light, n_o and n_e, are different. The difference of these two refractive indices, the birefringence denoted as $\Delta n = n_e - n_o$, is generally great, say, about 0.1. Due to the thermal fluctuation, the optical axes of nematic molecules always vary from point to point and from time to time. The effect of this phenomenon is much more significant than the density fluctuation. Little energy is required for causing the fluctuation of the optical axes of nematic molecules, so that the thermal fluctuation of the refractive index is significant even at the ambient temperature. This effect results in strong light scattering. The cross-section of light scattering in the nematics is expressed by

$$\sigma_N \propto \varepsilon_a^2 \langle |\delta \boldsymbol{n}(\boldsymbol{k})|^2 \rangle, \tag{1.4}$$

where ε_a is the optical dielectric anisotropy ($\varepsilon_\parallel - \varepsilon_\perp$), *i.e.*, the difference of dielectric constants parallel and perpendicular to the optical axis. $\delta \boldsymbol{n}(\boldsymbol{k})$ is the Fourier transformation of the optical axis fluctuation $\delta \boldsymbol{n}(\boldsymbol{r})$. The detailed calculation gives the statistical average of $\langle |\delta \boldsymbol{n}(\boldsymbol{k})|^2 \rangle$ as follows

$$\langle |\delta \boldsymbol{n}(\boldsymbol{k})|^2 \rangle \propto \frac{V k_B T}{K q^2}, \tag{1.5}$$

where K is an elastic constant associated with the change of optical axis. According to the estimate made by de Gennes (1973) $K \sim U/a$ and $B \sim U/a^3$ (a is the molecular dimension, about $1\,\mathrm{nm}$, U is the binding energy), q is the difference between the incident and scattering wave-vectors of light. $2\pi/q$ is about the order of visible light's wavelength. Suppose $\varepsilon' \sim \varepsilon_a \sim 1$, thus the ratio of scattering cross-sections of nematic liquid crystal and isotropic liquid is

$$\frac{\sigma_N}{\sigma_I} \propto \left(\frac{\varepsilon_a}{\varepsilon'} \right)^2 \cdot \frac{B}{K q^2} \approx \frac{1}{(aq)^2} \approx 10^5 \text{--} 10^6. \tag{1.6}$$

The ratio reaches up to one million times. This explains why the liquid crystal is in fact very turbid while ordinary liquid is transparent. The light scattering varies for different phases of the liquid crystals. For example, owing to the suppression of molecules into layers the light scattering of the smectic A phase is less than the nematic liquid crystal. For the smectic C phase, the fluctuation of the projection of tilted molecules onto smectic layers (the c-vector) causes stronger scattering than that in the smectic A phase.

The above analysis is one example of the anisotropic properties of liquid crystals. It is these anisotropic properties that make liquid crystals and provide for its wide applications.

1.3.   CHEMICAL STRUCTURE OF LIQUID CRYSTALS

1.3.1.   Basic molecular structure of rodic liquid crystals

Most liquid crystalline molecules are highly anisotropic, and to a good approximation they can be regarded as rigid rods or ellipsoids of revolution with lengths l greater than their widths d. The molecular weight ranges from a few hundreds Daltons for low molecular mass liquid crystals to hundreds of thousands Daltons for polymeric liquid crystals.

The basic structure of low molecular mass liquid crystals or monomers of liquid crystalline polymers is schematically shown below

$$R \text{---}\langle A \rangle\text{---H---}\langle B \rangle\text{---X}$$
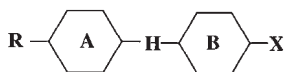
where X is a side group, R is a terminal group, A and B are aromatic rings, and H is a linking group.

1. Side group:

The following side chains are extensively studied: alkyl group (C_nH_{2n+1}); alkoxy group $(C_nH_{2n+1}O)$ and alkenyl (C_nH_{2n-1}) or alkenyloxy $(C_nH_{2n-1}O)$ group. The length and flexibility of the side chain affect the type of liquid crystal phases and the phase transition. In general, for homologues, the compounds with small n show no mesogenic phase. As n increases, the monotropic liquid crystal phase appears. As n further increases the nematic phase occurs and thereafter smectic phases may appear. As n varies the even-odd alternation occurs: the compounds in odd carbon numbers in the side chains have the higher transition temperature whereas compounds in even numbers have lower transition temperatures.

2. Terminal group:

The terminal group primarily contributes to the dielectric anisotropy and the refractive indices, which in turn affects the threshold voltage and optical properties in display applications, respectively. Common terminal groups are alkyl, alkoxy, cyano, nitro, isocyanate (NCS), sulfide and halides such as F, Cl, CF_3 and OCF_3.

3. Aromatic rings:

Most liquid crystal compounds consist of two or more aromatic rings. Those aromatic rings can be a totally saturated cyclohexane, a cyclocyclohexane, an unsaturated biphenyl, terphenyl, or combinations of them. Usually, the longer the ring, the higher the melting temperature.

4. Linking group:

The linking group makes an important contribution to the phase transition and physical properties such as the birefringence. The following linking groups have been well studied

(1) Saturated groups, such as ethylene (C_2H_4)
(2) Esters
(3) Unsaturated groups containing a double bond or a triple bond such as stilbene, azoy, schiff base, tolane or acetylene, and diacetylene.

5. Lateral group:

By substituting the hydrogen in the 2-, 3-, or 4-position of a phenyl ring by cyano, fluoro, or chloro polar group, one can modify the physical properties of liquid crystals. In most cases, the lateral substitution will broaden the molecule, thus reducing lateral attractions and lowering the nematic and smectic phase stability. Not only do the nature and size of the substitution affect the liquid crystal properties, but also the position of the group can have a significant effect.

6. Chiral center:

Replace the terminal group by a chiral center and the chiral nematic and smectic phases can be obtained.

The liquid crystal molecules or monomers are generally 2–4 nm in length and 0.4–0.6 nm in width. Experiments and theories demonstrate that for compounds showing the liquid crystal phase, their axial ratio or ratio of length to width (or to diameter) must be greater than a certain value, approximately 4.

1.3.2.   Discotic liquid crystals

Disc-like molecules may also exhibit the liquid crystal phase. de Gennes predicted this possibility in his famous book "The Physics of Liquid Crystals"

(1973). A few years later Chandrasekhar (1977) successfully synthesized this kind of discotic liquid crystal. There is a rigid flat aromatic core connected with 3, 4, 6, 8, 9 flexible side chains. Some examples of the discotic liquid crystal molecules are shown in Figure 1.2. Generally, the
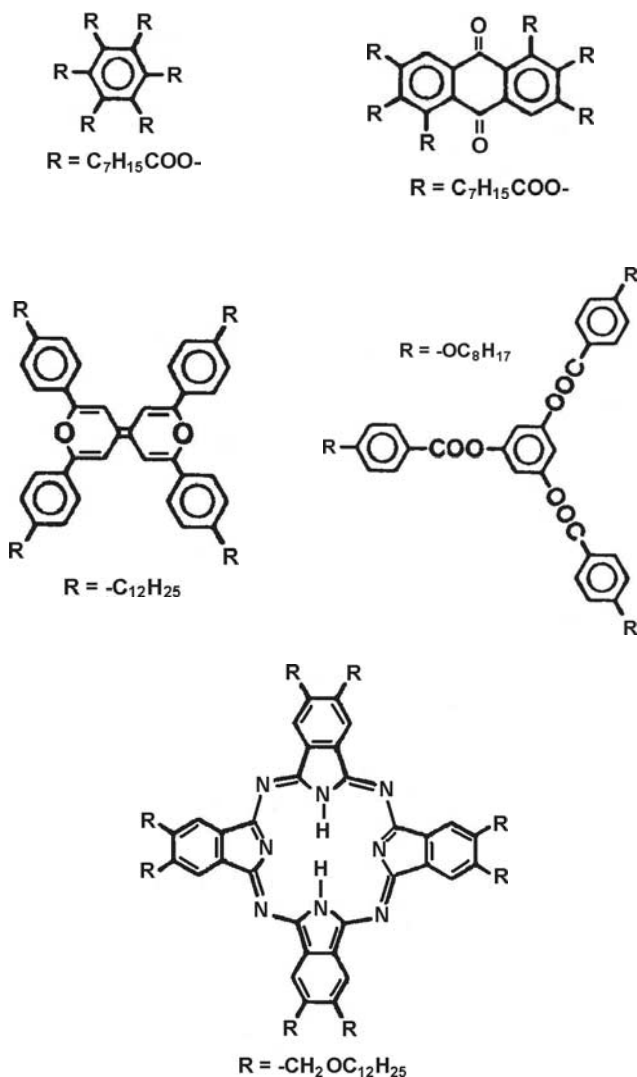
Figure 1.2.   Examples of discotic liquid crystal molecules.

discotic liquid crystal molecules are about 1 nm in thickness and a few nm in diameter.

1.3.3. Amphiphilic liquid crystals

Another important member of the liquid crystal family is the solution of amphiphilic molecules. The amphiphilic molecules are tadpole-like. A polar, hydrophilic group is at one end of the amphiphilic molecule while a non-polar, hydrophobic group is at the other end. Two examples are shown in Figure 1.3. Soap in solution, for example, is a liquid crystal. One end of this molecule, $-COO-Na^+$ is a polar group and is soluble in water, while the other end is a hydrocarbon paraffin group $CH_3(CH_2)_{14}^-$, dissolved in water.

The liquid crystalline materials exhibit the liquid crystal phase in different ways. Some of them exhibit the liquid crystal phase at a certain range of temperatures, while some exhibit the liquid crystal phase according to their concentration in solution. The former are called thermotropic liquid crystals, and the latter lyotropic liquid crystals. The
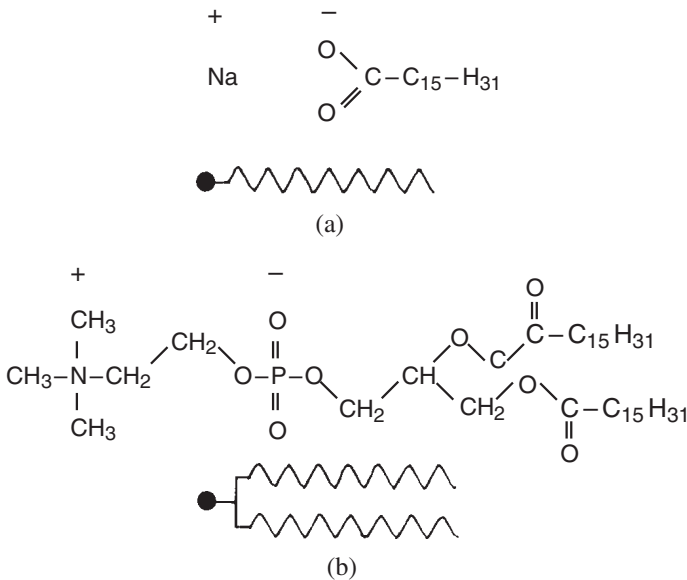
Figure 1.3. Two amphiphilic liquid crystal molecules: (a) sodium laurate; (b) dipalmitoylphosphatidylcholine. (From Collings, 1990.)

above-mentioned rod-like molecules are mainly thermotropic liquid crystals, and the amphiphilic molecules are lyotropic liquid crystals. But, very long, very rigid polymer solutions can exhibit the lyotropic liquid crystal phase.

Liquid crystalline polymers are a kind of polymer that show liquid crystal phases. They are composed of low molecular mass liquid crystals, which can be either rod-like or disc-like, or rod- and disc-like together in one. The constituent blocks may be of very complicated two-dimensional or three dimensional shape. They may be composed of amphiphilic molecules as well. According to the way the mesogenic units are incorporated into the polymers, the liquid crystalline polymers can be classified as main chain liquid crystalline polymers in which the mesogenic units are connected in the backbone, or side chain liquid crystalline polymers in which the mesogenic units are attached to the backbone as side pendants. The mesogenic units may be incorporated in both ways, that is, a part as the backbone and the other part as side groups attached to the backbone. This kind of liquid crystalline polymer is called the combined liquid crystalline polymer. The side groups may be attached to the backbone through their centers (side-on mode or laterally attached), or through their ends (end-on or terminally attached), or off-center attached (shoulderly attached). Figure 1.4 depicts some examples of liquid crystalline polymers.

Liquid crystalline polymers may be crosslinked to each other to form a network that retains the liquid crystal feature. The liquid crystal networks deform when a stress is applied as rubber does. They exhibit rubber elasticity.

A typical example of a thermotropic liquid crystalline polymers is the polyesters and the mesogen substituted polysiloxane. The aromatic amide, the super strength fiber known commercially as Kevlar belongs to the lyotropic liquid crystalline polymers. The other important lyotropic liquid crystalline polymers are poly(γ-benzyl-L-glutamate), abbreviated as PBLG, cellulose derivatives, the tobacco mosaic virus, *etc.*
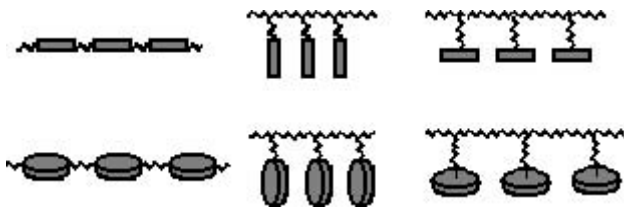
Figure 1.4.   The liquid crystalline polymers.

1.4.   POLYMORPHISM OF LIQUID CRYSTALS

MBBA, 4-methoxybenzylidene-4'-butylaniline was the first compound which showed the liquid crystal phase at room temperature. The chemical formulae of MBBA is as follows
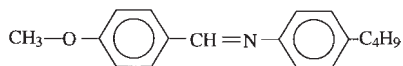
MBBA shows only the nematic liquid crystal phase (denoted as N phase), its phase sequence being

$$I \xleftrightarrow{47} N \xleftrightarrow{20} K$$

where I denotes the isotropic liquid phase, and K the crystal phase. The figures are the transition temperatures in degrees Celsius between adjacent phases. We will apply this expression when dealing with the phase sequences hereafter.

A few liquid crystals have a more complicated phase behavior, showing more than one liquid crystal phase. The series of terephthalylidene-bis-alkylanilines (TBnA) is particularly interesting in presenting an unusually broad polymorphism. For example, TPBA

has a phase sequence as follows

$$I \xleftrightarrow{233} N \xleftrightarrow{212} S_A \xleftrightarrow{179} S_C \xleftrightarrow{149} S_F \xleftrightarrow{140} S_G \xleftrightarrow{61} S_H \longleftrightarrow K,$$
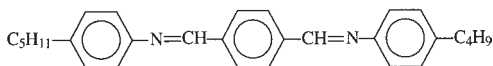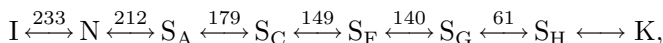
where S_A, S_C, S_F, S_G and S_H denote the smectic A, smectic C, smectic F, smectic G and smectic H phases.

Molecules with non-symmetric carbon atoms may exhibit a chiral structure, *e.g.*, the compound (8SI) of chemical formulae
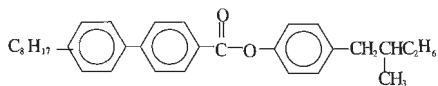
shows a phase sequence as follows

$$I \longleftrightarrow Ch \longleftrightarrow S_A \longleftrightarrow S_C{}^* \longleftrightarrow S_I{}^* \longleftrightarrow S_J{}^* \longleftrightarrow S_G{}^* \longleftrightarrow K,$$
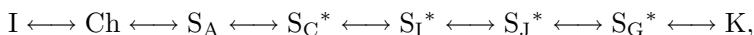
where Ch or N* denotes the cholesteric phase, and S_I, S_J are the smectic I and J phase. The asterisk denotes the counterpart chiral phases. The names smectic A, B, C, *etc.* were named purely in the chronological sequence in which the phases were discovered. The letter designation does not imply any information about the arrangement of the molecules, the symmetry, or other features.

We now introduce the classification of the liquid crystal phases and their structural features.

There are two fundamental orderings in the materials: positional order and orientational order. At low temperatures, matter exhibits a crystal state. The atoms or molecules are arranged regularly and periodically. Both position and orientation exhibit a long range order. When heated, matter may become an isotropic liquid through two ways, by losing the orientational order first while retaining the translational order, and hence becoming a plastic crystal, or alternatively, by losing the translational order while keeping the orientational order. These latter materials are liquid crystals.

In fact, with increasing temperature, these materials may not completely lose their translational order while retaining their orientational order. All liquid crystals are characterized by their orientational order, but liquid crystal phases show varying amounts of translational order with the only exception of nematics. Apart from the above basic symmetries, there is another important symmetry — bond orientation symmetry. This symmetry is important when dealing with hexatic phases. Liquid crystals are classified in terms of following criterion:

(1) translational order
(2) bond orientational order
(3) correlation between smectic layers
(4) with chirality?
(5) cubic structure?

1.4.1.   No translational order — Nematics

The nematic liquid crystal, N phase, is the only liquid crystal phase without any long range translational order. Nematics are the most important member in the family of the liquid crystals and are widely used in the display industry.

In nematics, the molecules tend to be parallel to each other. The preferred direction of parallel orientation is characterized by the director,
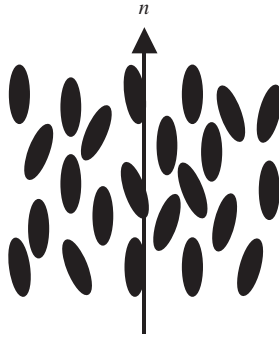
Figure 1.5.   The nematic liquid crystals.

denoted by a unit vector $\boldsymbol{n}$. The director $\boldsymbol{n}$ actually has the up and down symmetry. The nematic liquid crystal is shown in Figure 1.5.

This phase has a symmetrical axis C_∞ along the director. In addition, there is a reflection-symmetry plane perpendicular to the axis C_∞ and a mirror-symmetry plane through the C_∞ axis. Therefore, the local symmetry of nematics can be expressed by the $D_{\infty h}$ group. Of course, nematics have three dimensional translational symmetry.

The structural factor of the nematic phase reflects the breaking of the rotational symmetry. The large X-ray scattering angle sphere (short distance) shrinks toward the circle perpendicular to the director while the small scattering angle intensity is compressed along the $\boldsymbol{n}$ axis. There are two X-ray diffuse spots at $\boldsymbol{q} = q_0\boldsymbol{n}$ with $q_0 = 2\pi/l$ (l the molecular length) and two diffuse rings around $\boldsymbol{q} = q_1\boldsymbol{n} \times \boldsymbol{k}$ with approximately $q_1 = 2\pi/a$ (a the distance between neighboring molecules).

1.4.2.   One-dimensional translational order — Smectic A and C phases

As the temperature is further cooled, the molecules begin to segregate into planes giving rise to a smectic A or smectic C phase. In addition to the orientational order that the nematic phase shows, the smectic A and C phases exhibit a one-dimensional translational order, and can therefore form layered structures. There is a liquid-like motion of the rods in each layer and no correlation of the molecular positions from one layer to the next. In each layer, the mass centers of the molecules are randomly distributed as
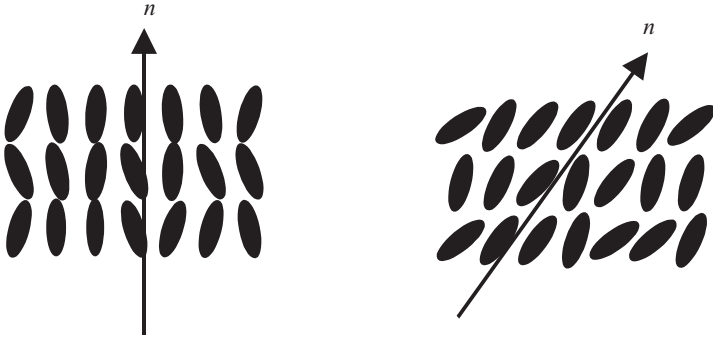
Figure 1.6.   The smectic A and C phases.

in isotropic liquids. The layers can easily slide. The molecular arrangement in the smectic A and C phases are schematically shown in Figure 1.6.

In the smectic A phase, molecules tend to be perpendicular to the smectic layers. The layer thickness d is roughly the same as the molecular length l. The thickness of the layers in the case of liquid crystalline polymers is about the order of the monomer's length. But in the smectic C phase, the molecules in the layers are parallel and tilted in arrangement with respect to the normal of the layers by a tilt angle θ. The layer thickness of the smectic C phase is $d = l \cos \theta$. The ordering of the smectic A and C phases are both higher than the nematic phase so that they appear at a lower temperature than the nematics do. The smectic A phase appears first as the temperature decreases if a compound shows both the smectic A and C phases.

The positional correlation in the smectic A phase can be described as a sinusoidal modulation of the average mass density

$$\langle n(\boldsymbol{r}) \rangle = n_0 + 2 n_{q_0} \cos(q_0 z), \tag{1.7}$$

where $q_0 = 2\pi/l$ and the z axis is along the layer normal. The Fourier transformation of this function leads to two Bragg peaks away from $q = 0$ in the structural factor:

$$S(q) \propto |\langle n_{q_0} \rangle|^2 [\delta(q_z - q_0 e_z) + \delta(q_z + q_0 e_z)]. \tag{1.8}$$

The thermal fluctuations destroy the ideal long-range periodic order of the smectic phase and there are power-law singularities rather than the

delta function in $S(\boldsymbol{q})$ at $\boldsymbol{q} = \pm q_0 \boldsymbol{e}_z$. Thus, the peaks in the smectic structural factor are called quasi-Bragg peaks, and the smectics are thus said to be characterized by quasi-long-range order (QLRO) in one dimensional position rather than a true long-range order (LRO). As the smectic phase is approached on cooling from the nematic phase, the diffuse spots in the nematic structural factor are sharpened and eventually become the quasi-Bragg peaks of the smectic phase. The experimental structural factor of the smectic phase has basically confirmed the expectation in Equation (1.8) which has only two quasi-Bragg peaks (at $\pm q_0$).

The local symmetry of smectic A phase is the same as that of the nematics, *i.e.*, its point group is $D_{\infty h}$, while the symmetry of the smectic C phase is C_{2h} (a C_2 symmetry axis plus a reflection plane perpendicular to the axis). In addition, both smectic phases exhibit a one-dimension translational order. Owing to the difference in symmetry, the smectic phases show different optical properties. The smectic A phase is optically uniaxial, but the smectic C phase is optically biaxial.

1.4.3.   Two-dimensional translational order within layers with weak correlation along the third dimension — Hexatic phases

There are the smectic B, F and I phases belonging to this kind of liquid crystal, the so-called hexatic phase. The newly discovered smectic M phase is also catalogued to the hexatic liquid crystal phase. These hexatic phases have a six-fold symmetry which can be observed from the X-ray scattering intensity at $q = 2\pi/a$.

In addition to the one-dimensional order which forms the layer structure, there is a two-dimensional translational order within the layers. The molecules of this class of liquid crystals are arranged into a hexatic lattice with a correlation length of tens of nm that is one order of magnitude higher than that in the S_A and S_C phases within layers. In addition, there is two dimensional, long range bond symmetry. In the literature, the S_B, S_F, S_I phases are sometimes called stack hexatic phases.

Assuming θ is the angle that the vector connecting neighboring molecules makes with respect to the x-axis, the hexatic order is defined by

$$\Psi_6 = \exp(6i\theta). \tag{1.9}$$
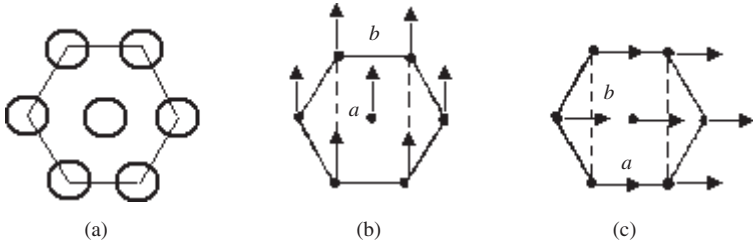
Figure 1.7.   The smectic liquid crystal (a) B, (b) F and (c) I phases.

The Fourier transformation of the smectic B phase is characterized by its six-fold bond-orientational order, expressed as a Fourier series in χ

$$S(q) = \sum_p S_{6p}(q_\parallel, q_\perp) \cos(6p\chi). \qquad (1.10)$$

There is a long-range orientational order in the plane but no long-range positional order. In the smectic B phase, only the first harmonic $S_6(q_\parallel, q_\perp)$ is significant. As the temperature is further reduced to that of the smectic crystalline L phase, which is going to be mentioned in a later section, more and more harmonics in χ become important. Figure 1.7 schematizes the three phases.

In the hexatics, there is no chemical bond between neighboring molecules. The hexatic bond order can be viewed as resulting from the loss of the long-range positional but not orientational order of a hexagonal crystal.

The molecular tilt order of the smectic C phase can coexist with the hexatic order, leading to smectic F and I phases depicted in Figure 1.7.

In the smectic B phase, the molecules within the layers are aligned perpendicularly to the layers, but the molecules of the S_F and S_I phases within layers are tilted with respect to the layer normal by a tilt angle. The azimuthal of the tilt direction or the projections onto the smectic layers of the S_F and S_I phases are different. In the former, the projections of molecules onto the layer point to the edge of the hexatic, while in the latter, to the apex. The difference seems not so significant, but S_F and S_I liquid crystals are not miscible, and there is a phase transition between them when the temperature varies.

The S_B phase can be regarded as a hexatic structure. S_F and S_I phases have the base-centered monoclinic structure in the nomenclature

of crystallography even though the correlation between layers in these two smectic phases is weak.

The smectic M phase, discovered in 1990, may be classified as a hexatic phase. The molecules are tilted within layers but are not miscible with the S_F and S_I phases. The structural details are under investigation.

1.4.4.   Three-dimensional translational order but correlation is weaker than that in crystals

This class of liquid crystals includes the smectic liquid crystal L, G, and J phases, and the higher ordered ones: the smectic liquid crystal E, H, and K phases.

Compared with the previously mentioned class of liquid crystals, S_B, S_F, S_I, and S_M, this class of liquid crystals exhibits a stronger correlation between smectic layers, the correlation length ranging from tens to hundreds of layers. The way of stacking of successive layers may be either $AAA\ldots$, $ABABAB\ldots$ or $ABCABC\ldots$. These six smectic liquid crystals are actually very similar to real crystals, but they do exhibit a significant disorder in both translation and orientation. Dynamic experiments demonstrated that they exhibit rather different characteristics from real crystals, such as the dielectric relaxation and the Mossbauer spectrum. The X-ray diffraction of these liquid crystals shows reflections of only less than five orders. In addition, as the transition to a real crystal happens, a relatively large amount of transition enthalpy and volume change occurs. These variations are in general one order of magnitude greater than those transitions occurring between liquid crystals.

In the S_L phase, the molecules are perpendicular to layers and are arranged in a hexatic lattice within layers. This symmetry is the same as that of the S_B phase. Both of the S_L and S_B phases are optically uniaxial, their molecules within smectic layers rotate more freely around their long axes or rotate in groups simultaneously. In some of the literature, the S_B phase is called the hexatic B phase while the S_L phase is named the S_B phase or crystal B phase. The molecules within the S_G and S_I phases are tilted with respect to the layers while the molecules of the S_L phase are aligned more or less perpendicularly to the layers. The stacking of molecules within the layer of the S_L, S_G and S_J phases is similar to those shown in Figure 1.7 as well. The crystallography classifications of these three liquid crystal phases are the same as those of the S_B, S_F and S_I phases.

(a) H   (b) K

(c) E
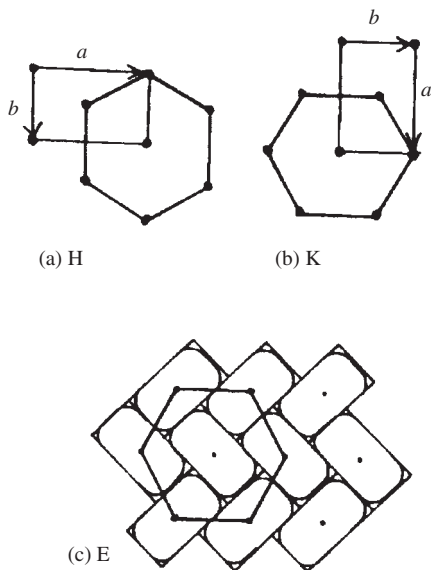
Figure 1.8.   The smectic (a) H, (b) K and (c) E phases.

The structural relation of the S_G and S_J phases with the S_L phase is similar to that in the hexatic series, *i.e.* of the S_F and S_I phases with the S_B phase.

The molecules of the S_E phase within the smectic layers tend to be perpendicular to the smectic layers, but they are unable to rotate freely with respect to the long molecular axis. This phenomenon has been verified by X-ray diffraction experiments that demonstrated that the packing of molecules within layers in the S_E phase is too close for them to rotate freely. Incoherent quasi-elastic neutron scattering has illustrated that the molecules of the S_E phase can vibrate at a frequency of 10^{11}Hz within a 180 degree range. Only those molecules with enough energy can go over the energy barrier from one hemi-circle to the other hemi-circle. The molecular packing within the S_E layer is schematically shown in Figure 1.8. In order to demonstrate that the molecules cannot rotate freely they are depicted as ellipses in the figure where the cross-section of the molecules are arranged herringbone-like. The S_E phase is of a monoclinic structure.

The S_H and S_K phases differ from the S_E phase only in their tilted molecules within the layers. The molecules of the S_H phase are tilted to the

edge of the hexatic while in S_K phase to the apex. Both of the S_H and S_K phases are of a monoclinic structure.

1.4.5.   Chiral liquid crystals

1.4.5.1.   Cholesterics

In this liquid crystal phase, the molecules have non-symmetrical carbon atoms and thus lose mirror symmetry. Otherwise optically active molecules are doped into host nematogenic molecules to induce the chiral liquid crystals. The liquid crystals consisting of such molecules show a helical structure. The most important chiral liquid crystal is the cholesteric liquid crystals. As discussed in Section 1.2, the cholesteric liquid crystal was the first discovered liquid crystal and is an important member of the liquid crystal family. In some of the literature, it is denoted as the N* phase, the chiral nematic liquid crystal. As a convention, the asterisk is used in the nomenclature of liquid crystals to mean the chiral phase. Cholesteric liquid crystals have beautiful and interesting optical properties, *e.g.*, the selective reflection of circularly polarized light, significant optical rotation, circular dichroism, *etc.*

The molecules in cholesteric liquid crystals are arranged as thin layers. The molecules lie in the layers and are parallel to each other, but the director rotates along the helical axis continuously and uniformly. The helical pitch is much greater than the spacing of successive molecular layers. In general the helical pitch of cholesteric liquid crystals is of the order of visible light's wavelength — about a few hundreds nm. The pitch of those cholesteric liquid crystals induced by doping with optically active molecules is larger, *e.g.*, up to a few microns. A schematic of cholesteric liquid crystals is illustrated in Figure 1.9.

1.4.5.2.   Chiral smectic liquid crystals

Almost all the smectic phases, in which the molecules are arranged in layers and are tilted with respect to the layers, have counterpart chiral phases. The most important one of this class is the chiral smectic C phase — S_{C*} phase. In these chiral liquid crystal phases, the molecules are tilted at a constant angle with respect to the layer normal but the tilt azimuthal rotates uniformly along the chiral axis and forms a helical structure.
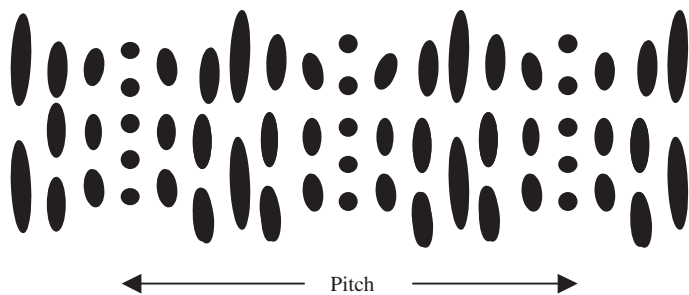
Figure 1.9.   The cholesteric liquid crystal.

The local symmetry group of the S_C^* phase is a C_2 group and thus the S_C^* phase has helical electricity. The spontaneous polarization, P_s, is perpendicular to the layer normal and molecular axis. Due to its helical structure P_s changes its direction uniformly, evolving along the helical axis so that the S_C^* phase does not show a measurable ferroelectricity except in the unwinding of its helical structure. The S_C^* phase is one of the very important liquid crystal phases that has a prospective application in fast response display. The detailed structure of the S_C^* phase will be shown in Chapter 6.

Once the helical structure of the S_C^* phase is unwound, ferroelectricity is displayed (see Chapter 6 for the details). In recent years, many experimental studies have revealed that some liquid crystal compounds show new types of smectic phases with complex tilt and dipole order, such as the anti-ferroelectric smectic C phase, S_{CA}^* phase, and the ferrielectric smectic C phase, $S_{C\gamma}^*$ phase. For instance, in the S_{CA}^* phase, the spontaneous polarization P_s is opposite for successive layers. It was found experimentally that the chiral S_O phase is in fact similar to the anti-ferroelectric S_{CA}^* phase.

The twisted-grain-boundary phase, TGB (Renn and Lubensky, 1988) was discovered recently in which topological defects create a new symmetry rather than simply destroy the old one. It occurs in some chiral liquid crystals (Goodby *et al.,* 1988) and is characterized by an array of equally spaced twist-grain boundaries in the smectic A or C liquid crystal as shown in Figure 1.10. In this phase, the average director twists like a cholesteric while regularly spaced molecular planes are configured like a smectic. One
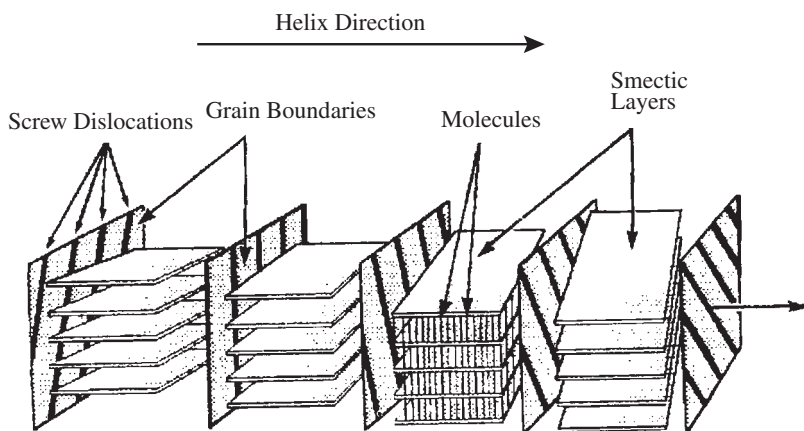
Figure 1.10. The TGB phase of liquid crystals. (From Goodby *et al.*, 1993. Reproduced by permission of Taylor & Francis, <http://www.tandf.co.uk/journals/tf/02678292.html>)

would reasonably expect it to appear between the cholesteric and smectic A, or smectic C phases.

1.4.6. Cubic phases

1.4.6.1. D phase

The D phase is the one cubic liquid crystal phase which was discovered independently in 1957 by G. Gray (Gray *et al.*, 1957) and D. Demus (1957) when they were studying the following compounds

$$CnH_{2n+1}O - \underset{R}{\bigcirc\bigcirc} - COOH$$
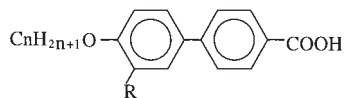
where R is either $-NO_2$ or $-CN$, and n = 16 or 18. These compounds display a phase between the S_A (or N) and S_C phase and were called the Smectic D, S_D phase. Actually the D phase does not have a layered structure that is characteristic of all smectic phases. The structure has been studied in detail by Etherington *et al.* (Etherington *et al.*, 1985, 1986) through X-ray diffraction, a second-harmonic-generation experiment and modeling. The space group and molecular packing of the phase was proposed. It was thus suggested that it was better to call the S_D phase the D phase.

The D phase had been found in only four compounds until recently (Paschke *et al.*, 1994). The four compounds are the 16 and 18 members of the $4'$-n-alkoxy-$3'$-nitrobiphenyl-4-carboxylic acids (AnBC) synthesized by Gray *et al.* in 1957 and the n = 16 and 18 members of the analogous $3'$-cyano compounds (ACBC) prepared by Goodby and Gray (1980). Detail experiments (Etherington *et al.*, 1985, 1986) verified that the compound (CN:18) is of space group P23 or Pm3, and is optically isotropic with no apparent optical rotation. Recently, Paschke *et al.* (1994) found that the D phase appears in more members of the above series of cyano compounds with n = 15 to 22. The temperature range of the D phase becomes wider as n increases.

1.4.6.2.   Another D-like cubic phase

Later Demus *et al.* (1984) found that the following compounds exhibits the cubic phase as well

$$C_nH_{2n+1}O-\langle\bigcirc\rangle-(CONH)_2-\langle\bigcirc\rangle-OC_nH_{2n+1}$$

where $n \geq 8$. The cubic phase appears at a temperature below the S_C phase and is not miscible with the above D phase. Recently some CN-substituted analogous compounds were found to show this phase.

It is clear that the cubic unit cell is very large and accommodates more than 100 molecules. It can be assumed that the molecules are aligned in parallel in micelles or in bundles, and the preferred direction is randomly oriented in dynamic equilibrium. The lattice elements form a three-dimensional cubic lattice with a long-range order.

The molecular packing and the mechanism of phase transition of the cubic phases have been attracting much research interest worldwide.

1.4.6.3.   Blue phase

Some cholesteric materials show the blue phase as the temperature increases from that of the cholesteric phase and before it reaches that of the isotropic phase. The blue phase is a cubic phase. There have been three blue phases found so far: BP I, BP II and BP III phases. It is now understood that the BP I phase is a body-centered cubic, the BP II phase is a primitive cubic and the BP III phase is a fog phase with no structural symmetry. Generally the temperature range of the blue phase is quite narrow, less than 1 degree

centigrade. The blue phase possesses a helical structure and its pitch is less than that of the corresponding cholesteric phase. It is optically isotropic, but with remarkable optical activity. The molecules in the blue phase are packed into a double helical structure. The networks of defects is believed to play an important role in constructing the structure.

The blue phase has a similar structure to that of the D phase, in spite of the remarkable difference in the lattice parameter. The lattice parameter of the former is hundreds of nm while that of the latter is less than 10 nm.

In general, if all the liquid crystal phases would exist together for a particular material, the phase sequence would be as follows

$$I \longleftrightarrow N \longleftrightarrow BP \longleftrightarrow Ch \longleftrightarrow S_A \longleftrightarrow D \longleftrightarrow S_C \longleftrightarrow S_B \longleftrightarrow S_I \longleftrightarrow S_L \longleftrightarrow$$
$$\longrightarrow S_F \longleftrightarrow S_J \longleftrightarrow S_G \longleftrightarrow S_E \longleftrightarrow S_K \longleftrightarrow S_H \longleftrightarrow K.$$

The chiral counterparts should appear in the sequence immediately following their non-chiral phases *i.e.*, at a lower temperature. The re-entrant phase is an exception. They may appear in reverse order, *e.g.*, as temperature decreases the re-entrant nematic phase appears at a temperature lower than that for the S_A phase

$$N \longleftrightarrow S_A \longleftrightarrow N_{re} \longleftrightarrow S_{Are},$$

where N_{re} and S_{Are} are the re-entrant N and S_A phase, respectively. Only those liquid crystal materials with strong polar group are able to show the re-entrant phases.

1.4.7.   Discotic liquid crystals

The liquid crystals discussed so far are composed of rod-like molecules. As discussed in the last section, disc-like molecules may show liquid crystal phases and are called discotic liquid crystals. The first discotic liquid crystal was synthesized by Chandrasekhar (1977) and many more discotic liquid crystals have since been discovered.

The simplest discotic liquid crystal phase is the nematic discotic phase, N_D, in which the normals of the molecular discs tend to align with respect to a preferred direction, *i.e.*, the director, but the mass centers of molecules do not have any positional order. The discs in Figure 1.11 represent the disc-like molecules, the molecules are packed in the way a pile of coins is packed randomly. The discotic nematic phase has its chiral counterpart, *i.e.*, the
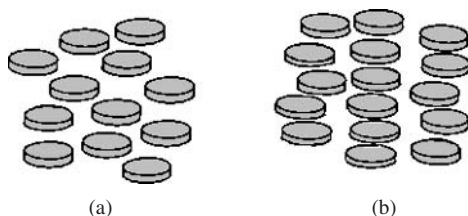
Figure 1.11.   The discotic nematic (a) and column phases (b).
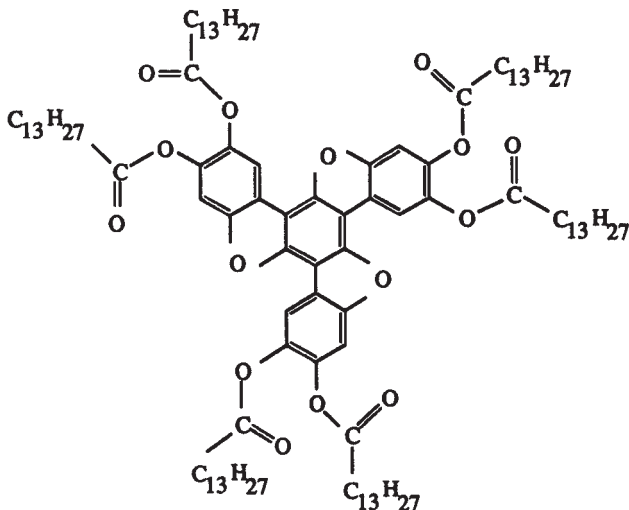
Figure 1.12.   An example of a typical disc-like molecule.

$N_D{}^*$ phase. A phase similar to the rod-like smectic liquid crystal phase is the column phase in which molecules are packed as columns parallel to each other. The columns are arranged in a hexatic or rectangular array. Inside the columns, the spacings of the molecules are either constant or random. The axes of the columns may be tilted with respect to the normal of discotic molecules. Figure 1.12 sketches the chemical formulae of one example of a discotic liquid crystal molecule.

There is another class of liquid crystals, the bowlic liquid crystal phase, whose molecules are bowl-like or pyramid-like, as is shown in Figure 1.13. Because of the breaking down of the up-down symmetry, the bowlic phase shows an even higher order and may be able to show ferroelectricity (Lam, 1986; Wang *et al.*, 1989).
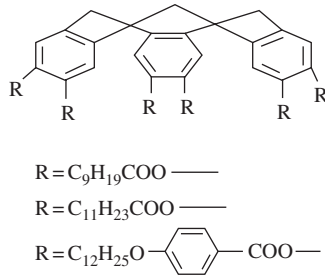
Figure 1.13. A bowlic liquid crystal molecule.

1.4.8. Lyotropic liquid crystals

1.4.8.1. Amphiphilic liquid crystals

Liquid crystal phases also appear in response to changes in the concentration of water, oil, surfactants, or other species in a wide variety of molecular mixtures. These are called lyotropic liquid crystals.

When amphiphilic molecules dissolve in water, their polar heads tend to be close to each other while the non-polar hydrophobic tails are as far away from water as possible. Depending on the concentration, the amphiphilic molecules aggregate to form spheres, or columns, or a laminar structure, see Figure 1.14.

In Figure 1.14 the tadpoles represent amphiphilic molecules, and the solid circles are the polar heads of amphiphilic molecules, *i.e.*, the hydrophilic parts, while the zig-zag lines are the hydrophobic groups. The typical phase diagram is depicted in Figure 1.15.

As the concentration increases, the amphiphilic molecules form micelles and then form columns. The columns are arranged into a hexatic array. As the concentration further increases, the system forms a laminar structure, *i.e.*, a smectic liquid crystal phase. Sometimes, a cubic phase may appear between the micelle and hexatic phases. In fact, the micelles are packed to form a cubic phase. The three phases are all liquid crystal phases: hexatic phase, laminar phase and cubic phase. As seen in the figure, the phase diagram of amphiphilic molecules actually depends on the temperature as well. T_{K} in Figure 1.15 is the Kraft temperature, below which the system is phase separated into crystal and water.
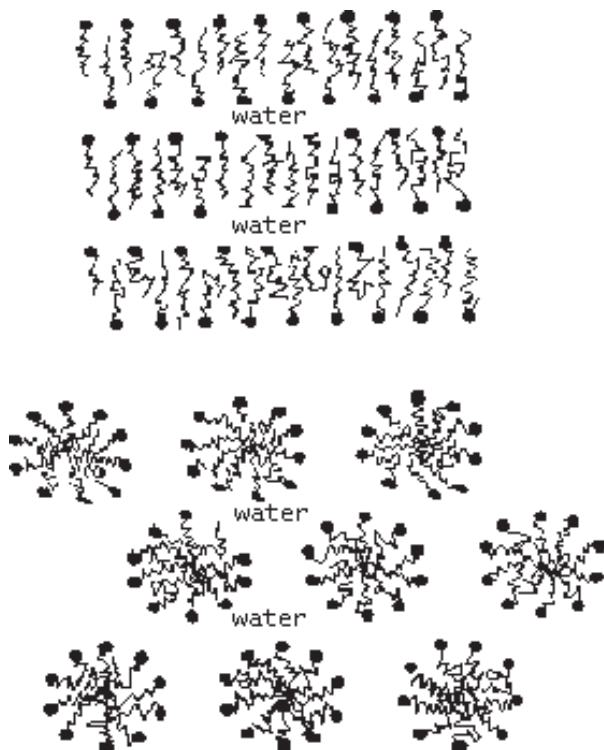
Figure 1.14.   The amphiphilic liquid crystals. (From Collings, 1990.)

1.4.8.2.   *Lyotropic liquid crystals consisting of long rigid molecules*

A few non-amphiphilic molecules are able to show liquid crystallinity in solution at a certain range of concentration, such as PBLG, DNA, the tobacco mosaic virus, *etc.* They are of great molecular mass, very rigid, rod-like and have a very long anisotropic shape. They are typical macromolecules and are lyotropic liquid crystals. This class of liquid crystals does not aggregate to form sphere, column or laminar structures. These lyotropic systems depend on the properties of the solvent. They are one of major interest of this book and will be discussed in detail later.

1.4.9.   Induced liquid crystals

Some materials are themselves not liquid crystals, or do not display the liquid crystal phase at a certain temperature or solvent concentration. But,
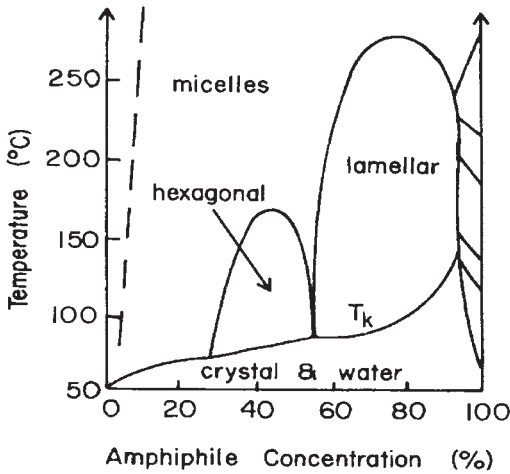
Figure 1.15.   The typical phase diagram of amphiphilic molecules. (From Collings, 1990.)

they may become liquid crystals when subjected to certain external conditions, such as pressure, electric field, magnetic field, irradiation, *etc.* The liquid crystal phase may also be induced when two non-liquid crystalline materials are mixed together.

1.5.   CONTINUUM THEORY OF LIQUID CRYSTALS

1.5.1.   Order parameter

The atoms in crystals are not always fixed in a perfectly ordered position except at the absolute temperature! Due to the thermal movement, atoms more or less deviate from their equilibrium position. For the same reason, the orientational order in liquid crystals is not perfect either. Because of the thermal fluctuation, the orientation and position of liquid crystals vary constantly. If the positions and orientations of liquid crystal molecules are frozen at a moment in time, the picture should look like that shown in Figure 1.5. The molecules tend to align along a preferred direction, but imperfectly. This preferred direction is defined as the director $\boldsymbol{n}$. Because the molecules are moving all the time, they are not fixed at a constant

position and do not point in a constant direction, although they have a greater chance of orienting along the director. In other words, at a certain moment more molecules are oriented along the director than otherwise. How close are the molecules aligned along the director? A parameter is needed to quantitatively describe the extent of the molecules' being oriented along the director. This statistical quantity is the order parameter, denoted conventionally as S.

Because the liquid crystals are up and down symmetrical, obviously $\langle \cos \theta \rangle$ (θ is the angle the molecular long axis makes with respect to the director) is not an appropriate candidate for the order parameter. What if $\langle \cos^2 \theta \rangle$ is adopted? If so, for perfect alignment, the order parameter $S = 1$; but for the disordered distribution $S = 1/3$. For the sake of convenience, it is hoped that for the random distribution, *i.e.*, the isotropic phase, $S = 0$, and for the perfect orientation, $S = 1$. Therefore, the statistical average of the second Legendre polynomial P_2 is chosen as the order parameter

$$S = \langle P_2(\cos \vartheta) \rangle = \left\langle \tfrac{3}{2} \cos^2 \theta - \tfrac{1}{2} \right\rangle. \qquad (1.11)$$

If the liquid crystalline molecules are not cylindrically symmetrical, S must be expressed by a tensor (traceless tensor). The nematic liquid crystal state (a uniaxial symmetrical system) is the main concern of the book. For such a phase, the order parameter can be denoted by the scalar in Equation 1.11.

The order parameter S is a very important quantity in a partially ordered system. It is the measure of the extent of the anisotropy of the liquid crystal physical properties, *e.g.*, elastic constants, viscosity coefficients, dielectric anisotropy, birefringence, and so on. S is temperature dependent and decreases as the temperature increases. The typical temperature dependence of S is shown in Figure 1.16.

As the temperature reaches the clear point T_c or isotropization temperature T_i, S jumps abruptly down to zero. The phenomenon implies that the nematic-isotropic transition is of first order.

The combination of S and $\boldsymbol{n}$ appropriately describes the ordering of liquid crystals. S is the microscopic feature of molecular orientation while $\boldsymbol{n}$ is the macroscopic characteristic of liquid crystal orientation. In general, the molecular dimension of liquid crystals is about a few nm in length and a few tenth of a nm in width. The range of variation of $\boldsymbol{n}(\boldsymbol{r})$ is in the order of the magnitude of microns. $\boldsymbol{n}(\boldsymbol{r})$ is in fact the average orientation of a
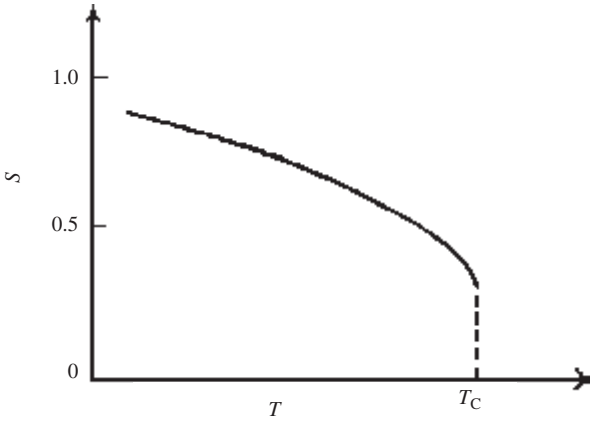
Figure 1.16.   The order parameter versus temperature.

small bulk sample of a hundred of thousand molecules, whose scale is much greater than the molecular dimension. When dealing with the orientational distortions and defects in liquid crystals, the analysis of $n(r)$ is appropriate.

1.5.2.   Distortions of liquid crystals

The liquid crystals can be deformed by applying external fields. Even a small electric or magnetic field, shear force, surface anchoring, *etc.*, is able to make significant distortion or deformation to liquid crystals. Thus, n is actually a function of position r. According to the symmetry of liquid crystals there exist three kinds of deformations in liquid crystals: splay, twist and bend deformations, shown in Figure 1.17. The short bars in the figure represent the projections of the local directors.

The three kinds of deformations are associated with the variation of n, *i.e.* ∇n. For the splay deformation, the divergence of the n vectors, $\nabla \cdot n$, is not zero; for the twist deformation, $n \cdot \nabla \times n \neq 0$, and for the bend deformation, $n \times \nabla \times n \neq 0$. In order to describe the meaning of the three formulae, it is supposed that in the undeformed sample, n points along the z direction. These three deformations can hence be written in the form of components as follows

$$\frac{\partial n_x}{\partial x} + \frac{\partial n_y}{\partial y}, \quad \frac{\partial n_y}{\partial x} - \frac{\partial n_x}{\partial y}, \quad \frac{\partial n_y}{\partial z}\mathbf{i} + \frac{\partial n_x}{\partial z}\mathbf{j}. \tag{1.12}$$
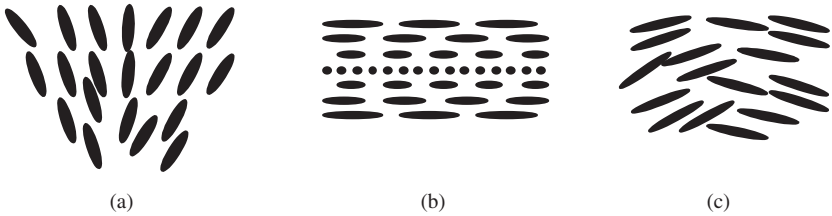
Figure 1.17.   Three basic deformations in liquid crystals: (a) splay; (b) twist and (c) bend.

The strain increases the energy of the solid as a stress is applied. The distortion of the director in liquid crystals causes an additional energy in a similar way. The energy is proportional to the square of the deformations and the correspondent coefficients are defined as the splay elastic constant, K_{11}, twisted elastic constant K_{22} and bend elastic constant K_{33}, i.e., the respective energies are the half of

$$K_{11}(\nabla \cdot \boldsymbol{n})^2; \quad K_{22}(\boldsymbol{n} \cdot \nabla \times \boldsymbol{n})^2; \quad K_{33}(\boldsymbol{n} \times \nabla \times \boldsymbol{n})^2. \qquad (1.13)$$

These three elastic modulii are different in liquid crystals. Generally, K_{11} and K_{33} are greater than K_{22}, which implies that the twist deformation is the easiest one to occur. K_{33} is the largest constant for rod-like polymers while for semi-flexible polymers in a concentrated solution and for thermotropic polymers K_{11} is usually the largest. K_{22} for liquid crystalline polymers is about the same in values as those for small molecular mass liquid crystals. But the above conclusion is not always valid. $K_{ii}(i = 1, 2, 3)$ are functions of the temperature. The ratios between them varies with temperature. For example, at temperatures near the transition to the S_A phase, K_{22} may become the greatest term of the three elastic constants. The three elastic constants are all small, that is the reason why liquid crystals deform easily. For the liquid crystal compound MBBA, the three elastic constants at $20\,^{\circ}$C are: $K_{11} = 5.8 \times 10^{-12}$ N, $K_{22} = 3.3 \times 10^{-12}$ N and $K_{33} = 7.0 \times 10^{-12}$ N. The reorientation of the liquid crystal as a bulk does not give off energy and the spatial orientation of liquid crystals may be determined by an electric or a magnetic field, or by surface alignment agents (SiO, lecithin, B-L films, *etc.*), or by a surface rubbing polyimide and so on.

The elasticity theory of liquid crystals was proposed by Oseen (1933) and Zocher (1933), and then modified by Frank into the form that has since

been accepted (1958). According to the Frank theory, the elastic energy of a deformed nematic liquid crystal can be expressed as

$$F = F_0 + \left(\frac{1}{2}\right) \int_V d^3\boldsymbol{r} [K_{11}(\nabla \cdot \boldsymbol{n})^2 + K_{22}(\boldsymbol{n} \cdot \nabla \times \boldsymbol{n})^2$$
$$+ K_{33}(\boldsymbol{n} \times \nabla \times \boldsymbol{n})^2], \tag{1.14}$$

where F_0 is the constant term for an undeformed sample.

Because of the spontaneously helical structure in the cholesteric liquid crystals, the second term in the integral must be revised to

$$\frac{1}{2}K_{22}\left(\boldsymbol{n} \cdot \nabla \times \boldsymbol{n} + \frac{2\pi}{P_0}\right)^2, \tag{1.15}$$

where P_0 is the intrinsic helical pitch. The supplement favors the molecular twist. The form illustrates that without an external field, the director of liquid crystals is naturally twisted with the period of the helix being the pitch P_0.

The form of free energy for smectic liquid crystals is different. If there are no defects in the smectic liquid crystals, the curl of $\boldsymbol{n}$, $\nabla \times \boldsymbol{n}$, must be zero. Thus, no twist and bend deformations exist in the smectic liquid crystals. In addition, there is an energy penalty associated with the translational deformation. For example, the displacement of smectic layer $\boldsymbol{u}$ will cause an additional term of elastic energy

$$\frac{1}{2}B\left(\frac{d\boldsymbol{u}}{dz}\right)^2, \tag{1.16}$$

where B is the elastic modulus, assuming that the z axis is perpendicular to the layers for the undeformed sample.

The elasticity theory has been used in dealing for example with the response of liquid crystals to external fields (electric, magnetic, mechanical force), defects, *etc.*

The above argument is suitable for polymer liquid crystals as well. In fact, the static properties of polymer liquid crystals are basically the same as those for the low molecular mass liquid crystals. But their dynamics are quite different because of their polymeric structure.

1.5.3. Frederiks transitions

We now apply the elasticity theory of liquid crystals to analyze the deformation of liquid crystals under an external magnetic field.
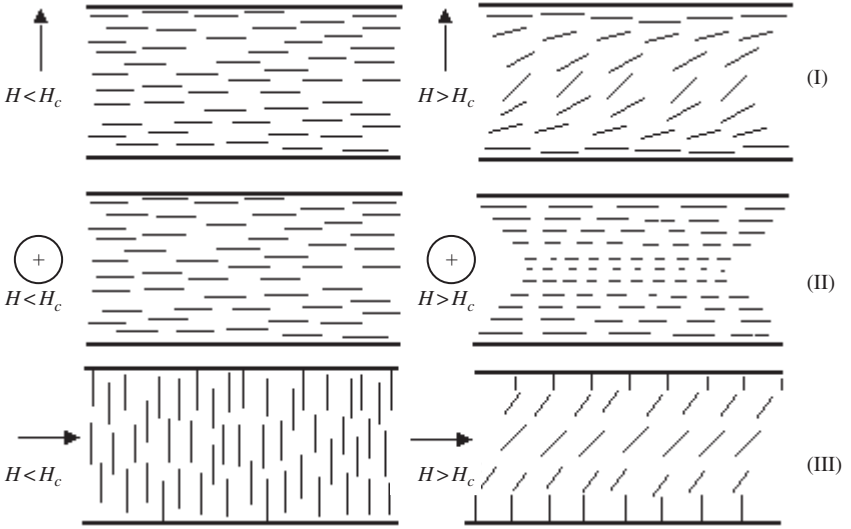
Figure 1.18.   The Frederiks transitions I, II and III. The arrows represents the direction of the applied magnetic field $\boldsymbol{H}$.

A sheet of nematic liquid crystals sandwiched between two parallel glass plates that have been surface treated to align the liquid crystal molecules on the glass plates in the homogeneous configuration is shown in Figure 1.18(I). The applied magnetic field $\boldsymbol{H}$ is perpendicular to the director. Because the nematic liquid crystals are paramagnetic, without surface anchoring the liquid crystal molecules would all be reoriented along the magnetic field. In the presence of surface anchoring, the competition between surface anchoring and the external magnetic field will cause the director of the liquid crystal to undergo a deformation.

The magnetic contribution to the free energy density of the liquid crystal has the form

$$-\left(\frac{1}{2}\right)\chi_a(\boldsymbol{n}\cdot\boldsymbol{H})^2, \tag{1.17}$$

where χ_a is the anisotropy of magnetic susceptibility. Then the free energy of the liquid crystal is

$$F = \left(\frac{1}{2}\right)\int_V d^3\boldsymbol{r}[K_{11}(\nabla\cdot n)^2$$
$$+ K_{22}(\boldsymbol{n}\cdot\nabla\times\boldsymbol{n})^2 + K_{33}(\boldsymbol{n}\times\nabla\times\boldsymbol{n})^2 - \chi_a(\boldsymbol{n}\cdot\boldsymbol{H})^2]. \tag{1.18}$$

Using a coordinate system with the z axis along the $\boldsymbol{H}$ direction and the x axis along the $\boldsymbol{n}$ direction of the undeformed sample, the director is written as

$$\boldsymbol{n} = (\cos\theta, 0, \sin\theta),$$

and the magnetic field as

$$\boldsymbol{H} = (0, 0, H).$$

Substituting $\boldsymbol{n}$ and $\boldsymbol{H}$ into Equation 1.18, the free energy of a unit area of a liquid crystal sheet of thickness d, F_s is

$$F_s = \frac{1}{2}\int_{-d/2}^{d/2}[(K_{11}\cos^2\theta + K_{33}\sin^2\theta)\left(\frac{d\theta}{dz}\right)^2 - \chi_a H^2 \sin^2\theta]dz. \quad (1.19)$$

It is noted that there is no twisted deformation in liquid crystals, thus the K_{22} term does not appear in F_s. If the deformation is not so great, the splay deformation is dominant. When the deformation becomes greater, the bend deformation becomes more important.

The free energy is at its minimum when the liquid crystal is at equilibrium. One can obtain the minimum by means of the Euler-Lagrange functional method.

From the symmetry of the liquid crystal layer the following boundary condition exists

$$z = \pm d/2, \quad \theta = 0;$$

and

$$z = 0, \quad \theta = \theta_m \quad \text{and} \quad \frac{d\theta}{dz} = 0,$$

where θ_m is the deformation angle of the liquid crystal director at the midplane of the sample, and, in fact, is the maximum deformation angle of the sample. By substituting them into the Euler-Lagrange differential equation, the dependence of θ_m on the external magnetic field can be implicitly expressed as

$$\int_0^{\theta_m}\sqrt{\frac{K_{11}\cos^2\theta + K_{33}\sin^2\theta}{\sin^2\theta_m - \sin^2\theta}}d\theta = \sqrt{\chi_a}\cdot\frac{Hd}{2}. \quad (1.20)$$

As θ_m approaches zero, the magnetic threshold field $\boldsymbol{H}_c$ is then given by

$$H_c = \frac{\pi}{d}\sqrt{\frac{K_{11}}{\chi_a}}. \quad (1.21)$$

Since the applied magnetic field $\boldsymbol{H}$ is less than $\boldsymbol{H}_c$ no deformation occurs. If $\boldsymbol{H}$ is greater than $\boldsymbol{H}_c$, θ_m depends on the value of $\boldsymbol{H}$. The elastic constant K_{11} may be determined through measuring H_c. The ratio of K_{11} to K_{33} can be evaluated from the curve of θ_m versus H, or accordingly from the transmittance versus H or the electric capacitance versus H.

The reorientation of liquid crystals in this geometrical arrangement is named Frederiks transition I (Frederiks & Zolina, 1933). By appropriately designing the alignment of undeformed liquid crystals and the direction of the magnetic field, as shown in Figure 1.18 II and III, the Frederiks transition II and III occur. From them, K_{22} and K_{33} can be determined through the magnetic threshold field. In fact, K_{22} is more difficult to measure than K_{11} and K_{33}. The Frederiks transition may also occur when an electric field is applied instead. Because of the large dielectric anisotropy of liquid crystals, the electric threshold field is very small, about 0.1 volt/micron. In the above argument, the formulae are valid as long as the liquid crystal sample is pure enough, otherwise the conduction effect will cause other effects.

1.5.4.   The twisted — and supertwisted — nematic liquid crystals

The twisted nematic (TN) and supertwisted nematic (STN) liquid crystals are widely used in liquid crystal displays. The former is used in wrist watches and calculators while the latter is used in notebook computers.

The TN cell is schematically shown in Figure 1.19. The liquid crystal sandwiched between two indium-tin-oxide (ITO) coated glass plates is about a few microns in thickness. The liquid crystal molecules on the top and bottom plates are homogeneously aligned and twisted by an angle of $\pi/2$. The liquid crystal molecules have a positive dielectric anisotropy $\varepsilon_a > 0$ so that an electric field will rotate the liquid crystal director up. The threshold voltage is given by

$$V_c = \pi \sqrt{\frac{\frac{K_{11}+(K_{33}-2K_{22})}{4}}{\varepsilon_a}}. \tag{1.22}$$

V_c is typically of order of one volt. Now, polarizers are mounted on the top and bottom glass plates such that their polarization directions are along or normal to the neighboring liquid crystal molecules on both plates. When
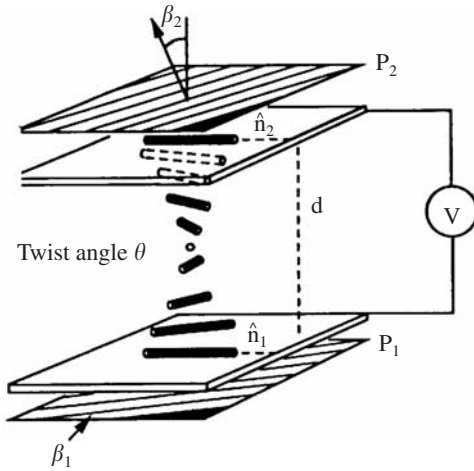
Figure 1.19.   The twisted nematic cell. The twist angle $\theta = \pi/2$ and the two polars make an angle $\Psi = 0$ or $\pi/2$.

the voltage is off, the cell is transparent. When the voltage is on, the cell becomes dark.

STN has a twist angle greater than 180 degrees and its electric-optical response is much steeper so that they can be driven in the multiplexing displays such as those found in the SVGA format color notebook computers.

1.6.   DEFECTS IN LIQUID CRYSTALS

The local translational and orientational order of atoms or molecules in a sample may be destroyed by singular points, lines or walls. The discontinuities associated with the translational order are the dislocations while the defects associated with the orientational order are the disclinations. Another kind of defect, dispirations, are related to the singularities of the chiral symmetry of a medium. The dislocations were observed long after the research on them began. The dislocations in crystals have been extensively studied because of the requirement in industry for high strength materials. On the contrary, the first disclination in liquid crystals was observed as early as when the liquid crystal was discovered in 1888, but the theoretical treatment on disclinations was quite a recent endeavor.

There is only the orientational order in nematics so that only disclinations may appear with no dislocations. In the other kinds of liquid crystals,

the dislocation may appear because of the discontinuity of the translational order.

1.6.1.   The Volterra process

Both dislocation and disclination can be produced by the well-known Volterra process. Take a cylinder of a medium and do the following operations in sequence on it:

(1) cut off a thin cylinder of diameter r_c along the axis of the cylinder;
(2) cut a plane via the axis of cylinder and then move two opposite slips of the cut plane by a displacement of either translation $\boldsymbol{b}$ or rotation $\boldsymbol{\omega}$, or both together. Hence the relative displacement of two slips is

$$\boldsymbol{d}(\boldsymbol{r}) = \boldsymbol{b} + \boldsymbol{\omega} \times \boldsymbol{r}; \tag{1.23}$$

(3) If $\boldsymbol{b}$ or $\boldsymbol{\omega}$ is consistent with the translational or orientational symmetrical element of the matter, the gap resulting from the displacement $\boldsymbol{d}$ can be filled by a piece of bulk medium and two slips will fit perfectly with the filled piece. If the operation (2) makes the medium overlap, we need to take away an additional piece of medium instead and thus still keep the perfect fit of the two slips.
(4) The medium will then relax to a new state owing to the internal interactions. Consequently, a singular line L is left.

The six basic Volterra processes are depicted in Figure 1.20, among them the three intrinsic processes on $\boldsymbol{b}$ produce dislocations while the three intrinsic operations associated with $\boldsymbol{\omega}$ produce disclinations. In Figure 1.20, assuming $\boldsymbol{\sigma}$ is the normal of the cut plane,

(a) $\boldsymbol{b} \perp \boldsymbol{L}$, but $\boldsymbol{b} \parallel \boldsymbol{\sigma}$, the line L is an edge dislocation;
(b) $\boldsymbol{b} \perp \boldsymbol{L}$, and $\boldsymbol{b} \perp \boldsymbol{\sigma}$, L is an edge dislocation;
(c) $\boldsymbol{b} \parallel \boldsymbol{L}$, L is a screw dislocation;
(d) $\boldsymbol{\omega} \parallel \boldsymbol{L}$, L is a wedge disclination;
(e) $\boldsymbol{\omega} \perp \boldsymbol{L}$, but $\boldsymbol{\omega} \parallel \boldsymbol{\sigma}$, L is a twist disclination;
(f) $\boldsymbol{\omega} \perp \boldsymbol{L}$, and $\boldsymbol{\omega} \perp \boldsymbol{\sigma}$, L is a twist disclination.

The dislocations have been extensively studied so we limit ourselves mainly to the disclination. Figure 1.21 sketches a sample of nematic liquid crystals, the short bars denoting the directors which all lie on the sheet of paper. Now cut the sample along the normal and via the line L, see
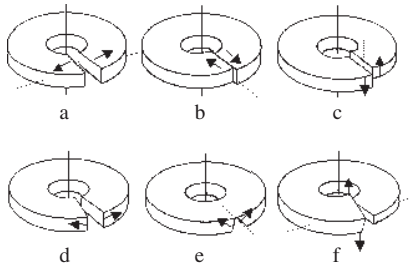
Figure 1.20.   The Volterra process.
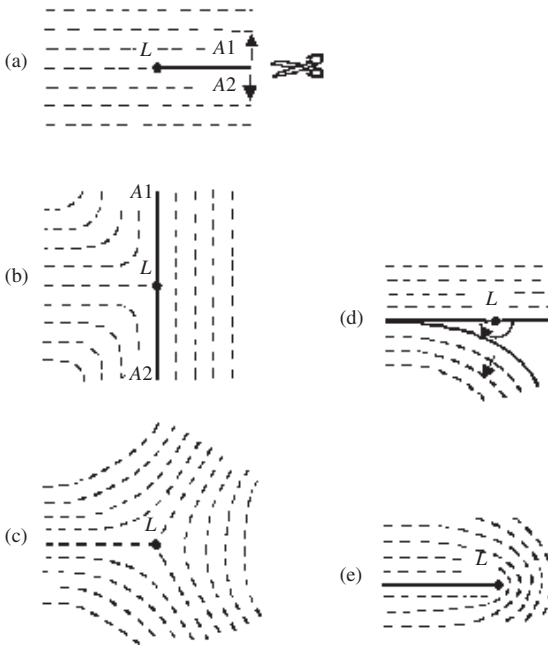
Figure 1.21.   The Volterra process generating $\pm 1/2$ disclinations (c and e).

Figure 1.21(a), and rotate the two opposite slips of the cut A1 and A2 by π. π is a symmetry element. Insert a new sample piece of liquid crystals and arrange their director to fit the directors on the A1 and A2 slips, as shown Figure 1.21(b). The liquid crystals then relax themselves to the configuration shown in Figure 1.21(c). A disclination with the strength of $-1/2$

appears. It is a wedge disclination. If the same amount of liquid crystals is needed to be moved, as shown in Figure 1.21(d), the final picture of the director field will look like that shown in Figure 1.21(e). The disclination line L is then $+1/2$ in strength.

There is a simple process to produce a disclination: rotate the directors on two slips respectively by ω_1 and ω_2 and make $\omega_1 - \omega_2 = \omega$. Thus the same disclination line is produced. The process is named the de Gennes-Friedel process. One can prove that the de Gennes-Friedel process is equivalent to the Volterra process for nematic liquid crystals. The operation P_v of the Volterra process can in fact be divided into the translation and rotation steps, *i.e.*, first, translate the directors (T) and then rotate them around themselves (P_g). The latter is actually the de Gennes-Friedel process. In other words

$$P_v = P_g + T. \tag{1.24}$$

Because there is no dislocation in nematics which have only translational symmetry, consequently

$$P_v = P_g. \tag{1.25}$$

1.6.2.   Strength of disclination in nematics

The relative rotation of two opposite slips is $\omega = 2m\pi$ where m is the strength of the disclination, which can be either an integer or semi-integer, *i.e.*, $\pm 1/2$, ± 1, $\pm 3/2$, *etc.*. The general definition of the strength of the disclination is the sum of the deformation angles, in radian measure, made with respect to a laboratory axis when going along a closed contour around the disclination

$$m = \frac{1}{2\pi} \oint_L d\psi, \tag{1.26}$$

where ψ is the angle of the director with respect to a certain direction, *e.g.*, the x axis and L is the closed contour. For convenience, we calculate instead the sum of the angles θ of the directors with respect to the tangents of the closed contour, *i.e.*

$$m = 1 + \frac{1}{2\pi} \oint_L d\theta. \tag{1.27}$$

The sign of m depends on whether $\boldsymbol{n}$ and the closed contour (*i.e.*, the Burger's circle) have the same direction.

The algebraic sum of the disclinations are not arbitrary, and the sum of all the strengths in a medium is a topological constant, *i.e.*, the Euler
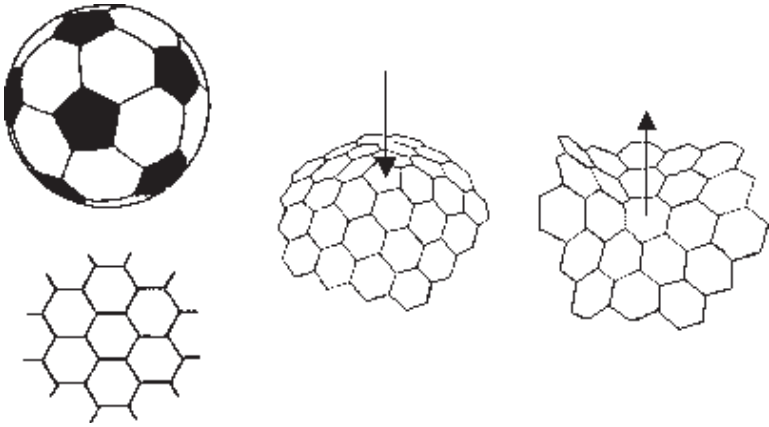
Figure 1.22.   The Poincare theorem on a soccer ball.

characteristic. This is the so-called Poincare theorem. For example, for a spherical surface or any smooth surface that is topologically equivalent to a spherical surface, the sum of strengths of all disclinations must be equal to 2, the Euler characteristic of a spherical surface. We give some examples to demonstrate the theorem.

For a terrestrial globe, either the longitude or latitude lines' distribution, construct at the south and north poles, a $m = 1$ disclination each. A soccer ball, shown in Figure 1.22, consists of twelve black mosaic pentagons and a number of hexagons. Each pentagon actually corresponds to a $+1/6$ disclination, the total strength of the twelve pentagons counts to $+2$. A $-1/6$ disclination shown in the same figure only produces a locally saddle surface. A buckminster fullerene molecule is a similar example. For a volleyball and a basketball, one observes the same rule. For a bulk sample, the sum of all the disclinations should be about zero. In liquid crystals, $m = \pm 1/2$ and ± 1 disclinations appear frequently but the disclinations with high strength are seldom observed because they cause large energy. The director configuration in the vicinity of various strength disclinations are depicted in Figure 1.23.

Assume the nematic liquid crystals to be a homogeneous planar structure, *i.e.*, the directors lie in the x–y plane, making an angle ϕ with respect to the x axis. For simplicity, we further suppose that all the three elastic constants are equal, *i.e.*, $K_{11} = K_{22} = K_{33} = K$. Thus the energy density
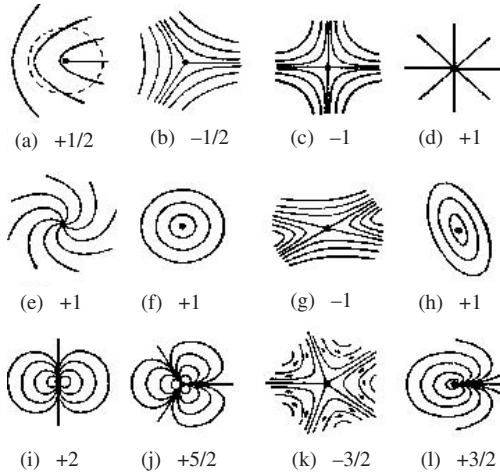
Figure 1.23.   The director configurations of disclinations with various strengths.

of the director field is

$$F = \left(\frac{1}{2}\right) K(\nabla \boldsymbol{n})^2. \tag{1.28}$$

Hence the equilibrium condition is defined by the equation

$$\Delta \phi = 0. \tag{1.29}$$

The solutions may be as follows

$$\phi = 0, \qquad \text{the uniform nematic; or} \tag{1.30a}$$

$$\phi = qz + \phi_0, \quad \text{the uniform cholesteric; or} \tag{1.30b}$$

$$\phi = m\theta + \phi_0, \quad \text{the singular solution.} \tag{1.30c}$$

If the disclination line is a wedged one and is along the z axis, then the solution of Equation (1.30c) is

$$\phi = m \cdot tg^{-1}\left(\frac{y}{x}\right) + C \tag{1.31}$$

and if the disclination is along the y axis, then the solution is

$$\phi = m \cdot tg^{-1}\left(\frac{z}{x}\right) + C. \tag{1.32}$$

The configuration of Equation (1.32) is associated with a twist disclination. Both twist and wedge disclinations are shown in Figure 1.24, where the disclination line is normal to this sheet of paper.

(a)   (b)
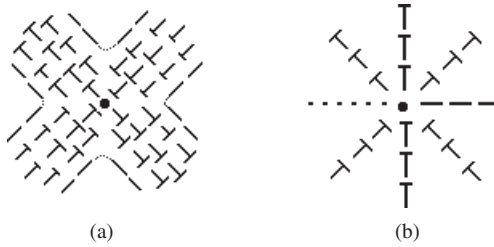
Figure 1.24.   A wedge (a) and a twist (b) disclination.

Substitute the solution back into Equation (1.28). The energy per unit length of an isolated disclination in a cylindrical sample of a diameter R is given by

$$F = E_c + \pi K m^2 \ln\left(\frac{R}{r_c}\right), \qquad (1.33)$$

where E_c is the core energy of the disclination, whose contribution is not so significant, presumably equal to $\pi K m^2$. This equation indicates that F tends to infinity as R approaches infinity. It is not the case because the disclinations likely appear in pairs with opposite signs. The energy of such a pair is hence

$$F = 2\pi K m^2 \ln\left(\frac{d}{2r_c}\right), \qquad (1.34)$$

where d is the separation of the two disclinations. Thus, the deformation area is confined to a limited dimension. The disclinations with the opposite signs tend to approach each other in order to reduce the energy, and may eventually annihilate together. Figure 1.25 shows an example that a $+1$ and a $-1/2$ disclination annihilating to become a $+1/2$ disclination.

An important conclusion obtained from Equation (1.33) is that the deformation energy is proportional to the square of the disclination strength m. The equation is derived for a special case but the above conclusion is universal, with only the coefficient being different. It is expected that a $m = 2$ disclination is likely to divide into two $m = 1$ disclinations or so, in order to achieve a more stable configuration.
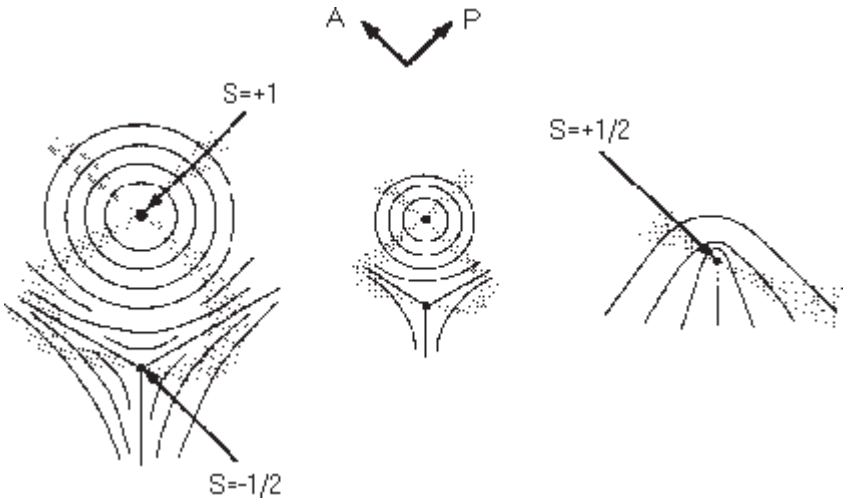
Figure 1.25.   A $+1$ and a $-1/2$ disclinations annihilate to become a $+1/2$ disclination. (From Shiwaku *et al.*, 1995)

1.6.3.   Point disclinations

Assume a point disclination located in a nematic droplet of radius R. The point disclination can be classified according to their Poincare characteristic angle α as a knot point ($\alpha = 0$), focus point ($0 < \alpha < \pi/2$), center ($\alpha = \pi/2$), saddle-focus point ($\pi/2 < \alpha < \pi$) or saddle point ($\alpha = \pi/2$). For a knot point, one has a spherically symmetrical radial configuration and then

$$F = 8\pi KR.$$

For a center point, one has a tangential bipolar configuration and

$$F = 5\pi KR.$$

While for a saddle defect, *i.e.*, a hyperbolic configuration

$$F = \left(\frac{8}{5}\right)\pi KR.$$

More complex configurations with a tilted director orientation at the surface have also been reported by Hobdell & Windel (1995) and Madhusudana & Sumathy (1983). It is illustrated that the knot defect has the highest energy while the saddle defect gives the lowest.
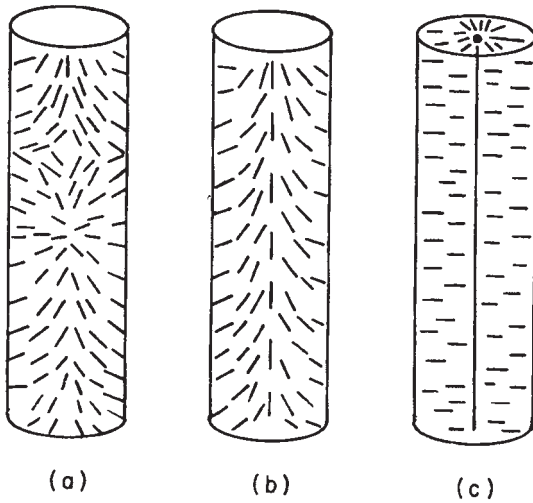
Figure 1.26. A point singularity escape in the third dimension. (From Collings, 1990. Reproduced by permission of Taylor & Francis, <http://www.tandf.co.uk/journals/tf/02678292.html>)

The bulk energy of the point defects is proportional to the dimension of the sample. On the other hand, the planar structure of a disclination line contributes to the bulk energy in proportion to the logarithm of the ratio R to r_c. The latter term is much greater than unity if R is large enough for optical observation. In a capillary of radius R, the directors are homeotropically aligned with the wall. The planar solution would lead to a line disclination of $m = +1$, as shown in Figure 1.26(c). But the directors are likely to escape from the center of the disclination $m = 1$ towards a series of point defects of $m = 1$ and $m = -1$, see Figure 1.26(a), the knot and saddle points and may eventually become a non-singular configuration, shown in Figure 1.26(b). It is the so-called escape in the third dimension.

The disclination line of $m = \pm 1/2$ and disclination point of $m = \pm 1$ are frequently observed in liquid crystals. In some cases high strength disclinations may be observed, such as in a thin layer of small molecular mass liquid crystals, polymer liquid crystals, lyotropic liquid crystals, binary thermotropic liquid crystals, *etc.*

If the inequality of the three elastic constants is taken into account, the disclination configurations are slightly different. Even though the energy for same $|m|$ is different. The integration of defects produces the textures of liquid crystals. Owing to the thermal fluctuation of the molecules and

the temperature dependence of the elastic constants and birefringence, the optical textures of liquid crystals are significantly associated with temperature.

The disclinations may split or annihilate due to interactions. The disclinations of the same sign tend to repel each other while those of opposite signs attract each other and may eventually annihilate.

Because of the additional translational order, the dislocations can exist in the cholesteric and smectic liquid crystals, which makes the texture of these liquid crystals even more complicated. Each liquid crystal phase shows characteristic textures and thus the optical texture becomes an important means to differentiate the phase of the liquid crystals. Liquid crystalline polymers have the same topologically stable defects as small molecular mass liquid crystals do, but the textures may be different due to the difference in the energetic stability of the same topological defects in both low molecular mass and polymeric liquid crystals (Kleman, 1991). In Chapter 3 we will discuss the textures in detail.

1.6.4.   Defects in smectic A phase

The homotopy group of the smectic A phase is

$$
\begin{aligned}
\Pi_0(S_A) &= 1, \\
\Pi_1(S_A) &= Z \otimes Z_2, \\
\Pi_2(S_A) &= Z, \\
\Pi_3(S_A) &= Z,
\end{aligned}
\tag{1.35}
$$

where Z is the translational dislocation normal to the smectic layers with the Burger vector being the multiple layer thickness; Z_2, is a cyclic group of two elements. There is no topological stable singular wall, but there are topological stable singular lines, composed not only of the disclination lines associated with Z_2 but also of the dislocation lines associated with Z. $\Pi_3(S_A) = Z$ implies that there are topological solitons.

The deformations in the smectic A phase liquid crystals are the bending of the smectic layer (accordingly to the splay of the directors) and the dilation or compression of the layers. The energy is thus

$$
F = \frac{1}{2}B\left(\frac{\partial u}{\partial z}\right)^2 + \frac{1}{2}K_{11}(\nabla \cdot \boldsymbol{n})^2,
\tag{1.36}
$$
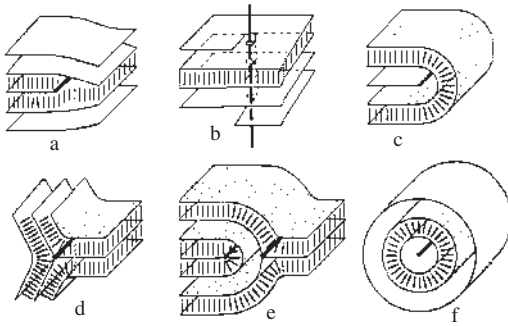
Figure 1.27. Typical dislocations (a, b) and disclinations (c–f) in smectic A liquid crystals. (From Kurik & Lavrentovich, 1988.)

where u is the displacement of the layer and B is the elastic modulus. The equilibrium state is governed by (assuming $\lambda^2 = K_{11}/B$)

$$\frac{\partial^2 u}{\partial z^2} - \lambda^2 \frac{\partial^4 u}{\partial x^4} = 0. \tag{1.37}$$

The typical dislocations (a, b) and disclinations (c-f) are shown in Figure 1.27.

The edge dislocation

Suppose the edge dislocation is along the y axis and the Burger vector has a thickness of one layer. The smectic layer is in the x–y plane. At equilibrium, the displacement $\boldsymbol{u}$ is expressed by

$$u(x, z) = \frac{d}{4} + \frac{d}{4\pi} \int \frac{dq}{iq} \exp(iqx - \lambda|z|q^2) \tag{1.38}$$

and the deformation angle θ between the layer normal and the z axis is given by

$$\theta = \frac{1}{4\sqrt{\pi}} \frac{d}{(\lambda |z|)^{1/2}} \exp\left(-\frac{x^2}{4\lambda |z|}\right). \tag{1.39}$$

It is illustrated that the deformation disappears rapidly in the x-direction and decays slowly in the z-direction. The deformation energy is independent of sample dimension. It is concluded that the dissolution of the dislocation doesn't reduce the energy.

The screw dislocation

There is a helical structure surrounding the screw dislocation line. The screw dislocation is perpendicular to the smectic layer and the deformation is

$$u = \frac{b}{2\pi} tg^{-1}\left(\frac{y}{x}\right). \tag{1.40}$$

The screw dislocation affects neither the lattice dilation nor the bending of the layer. Thus it isn't associated with an energy penalty.

The focal-conic texture

The smectic layers are flexible, *i.e.*, it is relatively easy for bending deformation, but the layers are difficult to compress. The bending of the smectic layers can be expressed by two principal curvatures R_1 and R_2, *i.e.*,

$$F = \frac{1}{2}K_{11}\int\left(\frac{1}{R_1} + \frac{1}{R_2}\right)^2 d\tau. \tag{1.41}$$

For a point on an ellipse, $R_1 \cdot R_2 > 0$; for a point on a hyperbolic, $R_1 \cdot R_2 < 0$.

For a defect point forming a spherical surface, see Figure 1.28(a), where $R = R_1 = R_2 = \infty$, the energy is

$$F = 8\pi K_{11}R.$$

For a Dupin cyclide comprised a circle base and a straight line core, shown in Figure 1.28(b),

$$F = 2\pi^2 K_{11}R\left[\ln\left(\frac{2R}{r_c}\right) - 2\right].$$

If the base is an ellipse and the core is a hyperbolic curve, shown in Figure 1.28(c), the Dupin cyclide has the energy

$$F = \pi K_{11}(1 - e^2)p\ln(a/r_c),$$
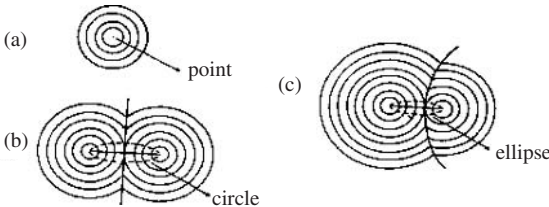
Figure 1.28.   The Dupin cyclides (a) a point and sphere; (b) a circle and a straight line; (c) an ellipse and a hyperbolic curve.

where e, p and a are the eccentricity, perimeter and semi-principal diameter. The last case is favorable from the energy point of view. The three possibilities are shown in Figure 1.28. A series of the Dupin cyclides are knitted to each other to construct the focal-conic texture.

1.6.5. Defects in the smectic C phase

The projections of the director on the smectic C layer construct a c-vector (or c-director) field. The distortion of the c-director and the displacement of the layer are two parts of the defects in the smectic C phase. Because the c-director is apolar, there are only the integer disclinations. In addition, there is no escape in the third dimension because the c-director is confined in layers. Neither topological stable singular walls nor points exist in the smectic C sample according to the homotopy argument.

1.6.6. Dispiration in the smectic C* phase

The helical structure of the c-director in the smectic C* phase makes the defects different from those in the smectic C phase. As the Volterra process produces a screw dislocation, for example, along the z axis and the Burger vector $b = d$, it must be accompanied by a parallel wedge disclination in the c-director, in the form

$$\phi = -\frac{b}{p} tg^{-1}\left(\frac{y}{x}\right) + qz. \tag{1.42}$$

It is named the wedge dispiration, designated as $(b, -b/p)$. Similarly, an edge dislocation of the Burger vector b must be accompanied by a partial twist disclination, designated as the twist dispiration $(b, b/p)$.

1.6.7. Defects in the cholesteric phase

The χ-, λ- and τ-disclinations

The order tensor of the cholesteric liquid crystal is a symmetrical matrix, or a set of three orthogonal vectors: $\boldsymbol{n}$, $\boldsymbol{q}$ and $\boldsymbol{n} \times \boldsymbol{q}$.

It is known that there is no topological stable singular wall and point but there are topological stable singular lines which are characterized by the Q group, $Q(C0, \overline{C0}, C1, C2, C3)$. The classification of the cholesteric
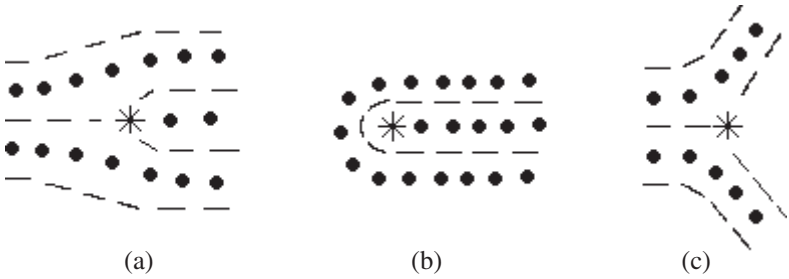
Figure 1.29. The schematics of (a) χ-disclination, (b) λ-disclination and (c) τ-disclination. (Modified from Collings, 1990.)

liquid crystal was made by Kleman & Friedel (1969) as the χ-, λ- and τ-disclinations shown in Figure 1.29:

(1) χ-disclination: semi-integer turn (*i.e.*, the multiple π rotation) around the helical axis;
(2) λ-disclination: multiple π rotation around the director;
(3) τ-disclination: multiple π rotation around $\boldsymbol{n} \times \boldsymbol{q}$.

Compared with the homotopy classification, each element in the homotopy Q group corresponds to the above defects in the following way

$C0$: $\lambda(2n)$, $\tau(2n)$ and $\chi(2n)$
$\overline{C0}$: $\lambda(2n+1)$, $\tau(2n+1)$ and $\chi(2n+1)$
$C1$: $\lambda(n+1/2)$
$C2$: $\tau(n+1/2)$
$C3$: $\chi(n+1/2)$

It is apparent that the two classifications are consistent, but the homotopy approach is more powerful in further analysis because there is a relation between the group elements, which is associated with the interactions between the defects.

The cholesteric liquid crystal can be regarded as a layered structure so that it also shows the focal-conic texture, especially for large pitch cholesteric liquid crystals.

The texture of cholesteric liquid crystals is rather complicated. Both disclination and dislocation exist together. The typical texture is shown in Figure 1.30.
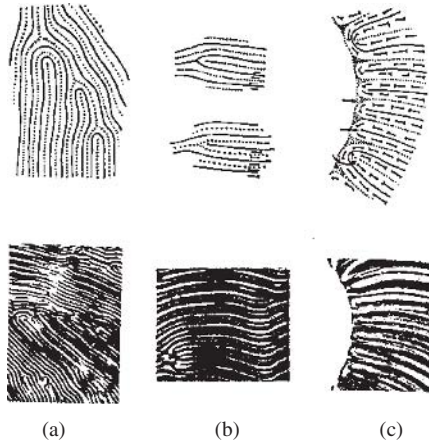
Figure 1.30.   Typical finger-print textures in cholesteric liquid crystals: schematics (upper) and images (lower). (From Bouligand & Kleman, 1970.)

The Cano wedge

The Cano wedge can be used to measure the cholesteric pitch. Two substrates are wedged by a small angle 2γ. The cholesteric liquid crystal between the substrates is homogeneously aligned. Under polarized microscopy, the equally spaced disclinations appear at the middle of the wedge. The separation of the lines $2d$ is associated with the pitch P

$$P = 8d \tan \gamma. \tag{1.43}$$

This technique has been applied to measure the pitch of cholesteric liquid crystals.

1.6.8.   Textures

Under the polarized optical microscope, the liquid crystal films show colorful patterns, *i.e.*, the optical textures. Each liquid crystal phase shows its typical texture which provides the means to identify the phase of the liquid crystals. The typical textures are the Schlieren, threadlike, homeotropic, homogeneous, marble, finger-print, focal-conic, Dupin cyclide, fan-shape, sanded, mosaic, and so on. They are the integrations of many typical defects mentioned above. Demus & Richter (1978) were the first to review

the textures of liquid crystals in detail. Later, Gray and Goodby (1984) summarized the textures of the smectic liquid crystal phases.

1.6.9.   Homotopy classification of defects in liquid crystals

Now we briefly discuss the topological homotopy theory that classifies defects in liquid crystals and judges the stability of the defects according to the symmetry of liquid crystals.

The singularities in the liquid crystals cause the deformation of the director field of liquid crystals and thus affect the symmetry of liquid crystals. This idea provides an approach to analyze the characteristics of the defects. The order vectors (or scalars, or tensors) of various liquid crystals are not the same. The director n is the order vector of the nematic liquid crystals, but the order for the cholesteric liquid crystals is a symmetric matrix, *i.e.*, a tensor. Because the order vector space is thus a topological one, any configuration of the director field of liquid crystals is thus represented by a point in the order vector space. The order vector space (designated by M) is associated with the symmetry of liquid crystals. The topologically equivalent defects in liquid crystals constitutes the homotopy class. The complete set of homotopy classes constitutes a homotopy group, denoted $\Pi_r(M)$. r is the dimension of the sub-space surrounding a defect, which is related to the dimension of the defect (point, line or wall) d', and the dimension of the liquid crystal sample d by

$$d' = d - r - 1. \qquad (1.44)$$

For a three-dimensional nematic liquid crystal for example, the $r = 0$ case corresponds for example to a defect with $d' = 2$, which means a disclination wall; for $r = 1$, $d' = 1$ corresponds to a disclination line; for $r = 2$, $d = 0$ corresponds to a disclination point. It is known that the order vector space of three dimensional nematic liquid crystals is the projection plane P_2. Its homotopy group of the zero rank ($r = 0$) is

$$\Pi_0(P_2) = 1.$$

In the other words, there is no topologically stable disclination wall.

The homotopy group of the first rank ($r = 1$) is

$$\Pi_1(P_2) = Z_2.$$

This is a cycle group of two elements, one of two elements is in fact the disclination line of $|m| = 1/2$, the other element corresponds to the $|m| = 1$ disclination line, which is not topologically stable.

The homotopy group of the second rank is

$$\Pi_2(P_2) = Z,$$

where Z is the integer group and corresponds to the topologically stable disclination points of integer strength.

The conclusions are consistent with our knowledge of the defects in nematic liquid crystals.

Similarly, homotopy theory can be applied to other liquid crystal phases, such as the cholesteric and smectic liquid crystals (Mermin, 1979; Wang, 1986).

This page intentionally left blank

Chapter 2

Theories of Liquid Crystalline Polymers

The purpose of this chapter is to explain theoretically the formation of liquid crystal phases in polymer systems and to provide the basic concepts for designing and synthesizing liquid crystalline polymers. Liquid crystalline polymers combine features of both polymers and liquid crystals, thus we discuss the materials from two sides: liquid crystallinity and polymer properties. Theoretical descriptions have encountered many difficulties in the past. One is that the present theoretical understanding of neither polymers or liquid crystals is complete.

The initial understanding of liquid crystalline compounds is attributed to German chemist Daniel Vorlander who proposed in 1908 an empirical rule (Vorlander, 1908): liquid crystal phases can be formed by molecules of the utmost linear shape. This revealed his insight into the relationship between the formation of liquid crystal phases and the shape of molecules. At that time, the empirical rule aided in the design and synthesis of liquid crystalline compounds, especially in the Halle Group. In the period from the discovery of liquid crystals in 1888 to 1908 when Vorland proposed his rule, less than 200 liquid crystalline compounds were found. In the next fifteen years, the number of synthetic liquid crystalline compounds reached as many as 2000. Vorland assumed the existence of liquid crystalline polymers in his paper in 1923 (Vorland, 1923). Under the subheading "The Nature of 'Infinite' Long Molecules" in this paper, he asked "What happens to the molecules when they become longer and longer?", and then answered "According to my experiences, a border for this (liquid crystal) state does not exist as the length of molecule increases." A few years later, the liquid crystal phase was first discovered in the solution of the tobacco mosaic

virus (Bawden & Pirie, 1937). This virus is a rigid polymer a few hundreds nanometers long. Another typical example of a long rigid polymer is poly(γ-benzyl-L-glutamate) (PBLG) which exhibits the liquid crystal phase in solution (1950). A few efforts have been made to establish the theoretical basis of this class of liquid crystalline polymers. Among those, the most important theories were the virial expansion by physicist L. Onsager in 1949 (Onsager, 1949) and the lattice model by chemist P. J. Flory in 1956 (Flory, 1956). These two scientists were both made Noble Laureates in chemistry for their contributions in thermodynamics and polymer science, respectively. Their theories propose that liquid crystal phases arise for purely steric reasons; relatively dense systems of long rigid rods easily form a liquid crystal phase. These two theories will be introduced in the first two sections of this chapter.

Rigid polymers are not the only class of polymers which can show liquid crystal phases. These phases are also found in the melts of polymers in which mesogenic units are incorporated in the backbone (main chain polymers) or attached as pendants to the backbone (side chain polymers). These liquid crystalline polymers will be discussed in later sections.

Three main kinds of liquid crystal states: nematic, cholesteric and smectic can occur in polymer systems. However, we will restrict the discussion to nematic polymers below, since it may be too early to adequately elaborate on the other two phases.

2.1.   ONSAGER THEORY FOR RIGID — ROD LIQUID CRYSTALLINE POLYMERS

Onsager (1949) was the first to study theoretically the rigid-rod system in solution which is composed of identical long cylindrical rods with length L and diameter D, and where L much greater than D. Only the steric interaction is considered in this theory and the following requirements must be met:

(1) No penetration between rods, so that the steric interaction can be expressed as

$$V_{ij} = \begin{cases} \infty, & \text{if molecule } i \text{ and } j \text{ overlap} \\ 0, & \text{otherwise} \end{cases} \qquad (2.1)$$

(2) The rods are long enough. The molecules can be cylindrical, semi-sphero-cylindrical or even lathe. The basic conclusions for these molecular shapes are quite similar. In the text below, only the solutions of cylindrical molecules are described. The calculation can be easily extended to deal with disc-like molecules by varying the length-to-breadth ratio.

(3) The solution is dilute. In a dilute solution, the density of the system, $\rho = N/V$, with N being the total number of rods in a solution of volume V, is small. Thus the volume fraction of rods in the solution is

$$\Phi = \frac{\pi D^2}{4} L \rho. \tag{2.2}$$

2.1.1. The partition function

The orientational distribution function of rods with long axis $\boldsymbol{a}$ is designated by $f(\boldsymbol{a})$. $\rho f(\boldsymbol{a}) \mathrm{d}\Omega_{\mathbf{a}}$ is the number of rods which point to the solid angle $\mathrm{d}\Omega$ centered at $\boldsymbol{a}$.

First of all, we examine the partition function Z — an important function in thermodynamics and statistics, and calculate the free energy of the system according to the formula

$$F = -k_B T \ln Z, \tag{2.3}$$

where T is the Kelvin temperature and k_B is the Boltzmann constant. The thermodynamical quantities associated with the equilibrium state can then be obtained. The calculation is similar to that for a simple fluid with N identical spherical particles, however it is more complicated because of the anisotropic shape. The partition function is the volume in the phase space or the summation over all the possible configurations that the system adopts. For the system of cylindrical molecules, the partition function is given by

$$Z = \frac{1}{N! h^{6N}} \int \cdots \int \exp(-\beta U) d\tau_1 d\tau_2 \cdots d\tau_N, \tag{2.4}$$

where $\beta = 1/(k_B T)$. The Planck constant h is introduced in the denominator to make Z dimensionless. The factor of $1/N!$ arises from the indistinguishability of N molecules. A rigid rod has 6 degrees of freedom, three from translational motion and the rest from rotational motion. The infinitesimal volume element τ_i of the phase space is

$$d\tau_i = d\mathbf{r_i} \cdot d\mathbf{p_i} \cdot d\theta_i \cdot d\phi_i \cdot d\psi_i \cdot dp_{\theta i} \cdot dp_{\phi i} \cdot dp_{\psi i},$$
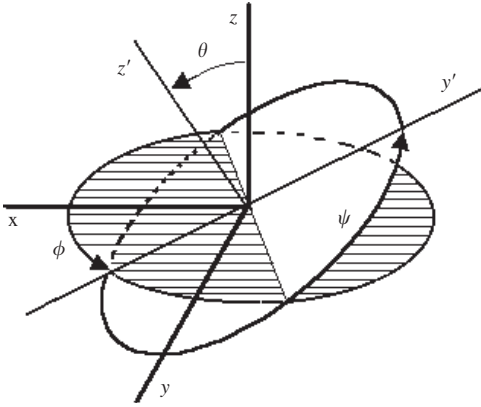
Figure 2.1.   The Euler angle definition for a rigid rod.

where $\boldsymbol{r}$ is the positional coordinates and θ, ϕ and ψ are the Euler's angles (see Figure 2.1), $\boldsymbol{p}$, p_θ, p_ϕ, and p_ψ are the conjugate momenta.

The total energy of the system, U, is the sum of the kinetic energy of each rigid rod T_i (translation and rotation) and potential energy V_i.

The translational kinetic energy of a rigid rod T_{ti} is simply

$$T_{ti} = \frac{1}{2m}(p_x^2 + p_y^2 + p_z^2), \tag{2.5}$$

where m and $\boldsymbol{p}(p_x,\ p_y$ and $p_z)$ are the mass and kinetic momenta (components).

The rotational kinetic energy of a rigid rod is more complicated and we adopt the form from the literature as follows

$$T_{ri} = \frac{p_\theta^2}{2I_1} + \frac{(p_\phi - p_\psi \cos\theta)^2}{2I_1 \sin^2\theta} + \frac{p_\psi^2}{2I_2}, \tag{2.6}$$

where I_1 and I_2 are principal inertial moments around the long and the short axes, respectively. The total energy of the system is the sum of the two contributions

$$T = \sum_{i=1}^{N}(T_{ti} + T_{ri}) = \sum_{i}^{N} T_i. \tag{2.7}$$

The potential energy of rigid rods is not only a function of the relative distance ($\boldsymbol{r}_{ij}$) of the mass centers of two rigid rods but is also associated with the orientations of two molecules ($\boldsymbol{a}_i$ and $\boldsymbol{a}_j$). It is expressed as

$$V_{ij} = V_{ij}(\boldsymbol{r}_{ij}; \boldsymbol{a}_i, \boldsymbol{a}_j). \tag{2.8}$$

The total potential energy is the sum of the interaction of all pairs of rods not repeatedly counted. There are $N(N-1)$ terms of such interaction potentials, and is written as

$$V = \sum_i \sum_{j>i}^{N} V_{ij}(\boldsymbol{r}_{ij}; \boldsymbol{a}_i, \boldsymbol{a}_j), \tag{2.9}$$

where the summation is made for all i and j (j must be greater than i).

The partition function is then given by

$$\begin{aligned}
Z(N,V,T) = {} & \frac{1}{N!h^{6N}} \int \cdots \int d^{3N}x\, d^{3N}p \\
& \times \int \cdots \int d^N\theta\, d^N\phi\, d^N\psi\, d^N p_\theta\, d^N p_\phi\, d^N p_\psi \\
& \times \exp\left\{ -\beta \left[\sum_i^N T_i(p) + \sum_{i<j}^N V_{ij}(r; a_i, a_j) \right] \right\},
\end{aligned} \tag{2.10}$$

where $dxdydz$ is written as d^3x and $dp_x dp_y dp_z$ is written as d^3p. The integral for translational moments is

$$(2\pi m k_B T)^{3N/2}$$

while the integration for the angular moments gives

$$(2\pi I_1 \sqrt{2\pi I_2})^N \prod_i^N \sin\theta_i.$$

The integrad in Equation 2.10 is independent of the Euler angle ψ and thus the integral with respect to ψ is $(2\pi)^N$. Substituting these integrals back into Equation 2.10, the partition function is reduced to the form

$$Z(N,V,T) = \frac{1}{N!A^N} \int \cdots \int d^N\Omega\, d^{3N}x \exp\left(-\beta \sum_{i<j}^N V_{ij} \right), \tag{2.11}$$

where

$$A = \frac{h^6}{\{(2\pi m k_B T)^{3/2}(2\pi I_1 k_B T)(2\pi I_2 k_B T)^{1/2}(2\pi)\}}$$

and is dependent on the molecular mass m, the inertial moments I_1 and I_2 and is a function of the temperature. Ω is the solid angle

$$d\Omega = \sin\theta d\theta d\phi.$$

The remaining integrad is associated with the potential only. Two tricks are adopted here:

(1) Substitute the integration over angles into the summation. Divide the unit spherical surface into K solid angles of $\Delta\omega$, the number of molecules whose axes point to each solid angle $\Delta\omega$ being N_α (N_α is an integer). The integral over $d\Omega$ is then equivalent to summing all the possible combinations $\{N_1, N_2, \ldots, N_\alpha, \ldots, N_k\}$, and $\sum_{\alpha=1}^{k} N_\alpha = N$. The partition function in Equation 2.11 becomes

$$Z(N,V,T) = \frac{1}{N!A^N} \sum_{\{N_\alpha\}} \frac{N!(\Delta\omega)^N}{N_1!N_2!\ldots N_\alpha!\ldots N_k!}$$

$$\times \int \cdots \int d^{3N}x \exp\left(-\beta\sum_{i<j}^{N} V_{ij}\right) \equiv \sum_{\{N_\alpha\}} Z(\{N_\alpha\}),$$

(2.12)

where

$$Z(\{N\}) = \frac{(\Delta\omega)^N}{A^N \prod_{\alpha=1}^{k} N_\alpha!} \int \cdots \int d^{3N}x \exp\left(-\beta\sum_{i<j}^{N} V_{ij}\right). \qquad (2.13)$$

Denote the maximal term in Equation 2.12 by $Z(\{N_a\})_{\max}$. Apparently the following inequality exists

$$Z(\{N_a\})_{\max} < Z(N,V,T) < N^k Z(\{N_a\})_{\max}.$$

Take the logarithm of each term in the inequality and divide by N. The following inequality is obtained

$$\frac{1}{N}\ln Z(\{N_\alpha\})_{\max} < \frac{1}{N}\ln Z < \frac{1}{N}[\ln Z(\{N_\alpha\})_{\max} + k\ln N].$$

As N approaches infinity, $\ln N/N$ approaches zero. Therefore, $\ln Z/N$ can be replaced by $(1/N)\ln(Z\{N_\alpha\})_{\max}$. As a result, one needs only to calculate

$Z(\{N_\alpha\})$ and minimize with respect to $\{N_\alpha\}$. $Z(\{N_\alpha\})$ hence has the form

$$Z(\{N_\alpha\}) = \frac{(\Delta\omega)^N}{A^N \prod_{\alpha=1}^{k} N_\alpha!} \int \cdots \int d^{3N}x \prod_{i<j}^{N} \exp(-\beta V_{ij}). \qquad (2.14)$$

(2) Introduce the Mayer function Q_{ij}, replace $\exp(-V_{ij}/k_BT)$ by $1 + Q_{ij}$. When i and j molecules are not overlapped the term Q_{ij} vanishes; otherwise $Q_{ij} = -1$. Substituting into Equation 2.14, the multi-products in the equation are reduced to the power expansion of Q_{ij}. Here the cluster expansion is used.

When the density of molecules is not very high the quadratic term of ϕ is very small and the higher terms of ϕ must be further reduced. So that we retain only the linear term and then

$$Z(\{N_\alpha\}) = \frac{(\Delta\omega)^N}{A^N \prod_{\alpha=1}^{k} N_\alpha!} \left[V^N + V^{N-2} \sum_{i<j}^{N} \int\int Q_{ij} d^3 r_i d^3 r_j \right]$$

$$= \left(\frac{\Delta\omega \cdot V}{A} \right)^N \frac{1}{\prod_{\alpha=1}^{k} N_\alpha!} \left(1 + \frac{1}{2V} \sum_{i\neq j}^{N} \int Q_{ij} d^3 r_{ij} \right). \qquad (2.15)$$

The factor $\frac{1}{2}$ in the second term is present because the summation in Equation 2.15a is carried out only for i less than j. It is shown that ϕ_{ij} is a function of the distance of i and j molecules, r_{ij}, and the relative orientation angles (α and β respectively) of the two molecules. It may be more accurate if we write ϕ_{ij} as $\phi_{\alpha\beta}(r_{ij})$. The orientations of N_α rigid rods within the α-th tiny solid angle are the same. The summation with respect to i and j in the second term in Equation 2.15b can be further reduced to the summation with respect to α, *i.e.*,

$$\sum_{i\neq j}^{N} \int Q_{ij}(r_{ij}) d^3 r_{ij} = \sum_{\alpha,\beta=1}^{k} N_\alpha(N_\beta - \delta_{\alpha\beta}) \int Q_{\alpha\beta}(r) d^3 r, \qquad (2.16)$$

where $\delta_{\alpha\beta}$ is the Knoneck Delta: $\delta = 1$ as $\alpha = \beta$; $\delta = 0$ as α is not equal to β. If N is very large, N_β is large as well, so that the term of $\delta_{\alpha\beta}$ is negligible. The integral in Equation 2.16 is the second virial coefficient β_1. $Q_{\alpha\beta} = -1$ when the rods collide, otherwise $Q_{\alpha\beta} = 0$. Therefore, β_1 is,

in fact, the negative of the exclusion volume V^{ex} of the two rigid rods. Substituting into Equation 2.15 then

$$Z(\{N_\alpha\}) = \left(\frac{\Delta\omega \cdot V}{A}\right)^N \frac{1}{\prod_{\alpha=1}^k N_\alpha!} \left(1 - \frac{1}{2V}\sum_{i\neq j}^N N_\alpha N_\beta V^{ex}\right). \quad (2.17)$$

Take the logarithm for the partition function Z and apply the Sterling formula

$$\ln N_\alpha! \approx N_\alpha \ln N_\alpha$$

hence

$$\frac{\ln Z(\{N_\alpha\})}{N} = \ln\frac{\Delta\omega \cdot V}{A} - \sum_{\alpha=1}^k \left(\frac{N_\alpha}{N}\ln\frac{N_\alpha}{N} + \frac{N_\alpha}{N}\ln N\right)$$

$$+ \frac{1}{N}\ln\left(1 - \frac{N^2}{2V}\sum_{\alpha,\beta}^k \frac{N_\alpha}{N}\frac{N_\beta}{N}V^{ex}\right). \quad (2.18)$$

Introducing the orientation function $f(\Omega)$ of rods

$$\frac{N_\alpha}{N} = f(\Omega_\alpha)(\Delta\omega).$$

We transfer the summation back to an integration. Note that $\rho = N/V$. Finally Equation 2.18 is reduced to

$$\frac{1}{N}\ln Z(\{N_\alpha\}) = -\ln(A\rho) - \int f(\Omega)\ln f(\Omega)d\Omega$$

$$- \frac{\rho}{2}\iint d\Omega d\Omega' f(\Omega)f(\Omega')V^{ex}(\Omega - \Omega'), \quad (2.19)$$

where the orientation function is normalized to unity

$$\int f(\Omega)d\Omega = 1. \quad (2.20)$$

The fourth term in Equation 2.14, $\sum_{i<j,l<m}^N Q_{ij}Q_{lm}$ contributes the term

$$-\frac{\rho^2}{3}\iiint \beta_2(\Omega, \Omega', \Omega'')f(\Omega)f(\Omega')f(\Omega'')d\Omega d\Omega' d\Omega'',$$

where β_2 is the third virial coefficient. The third virial term can be neglected if

$$|\beta_1|\rho \gg |\beta_2|\rho^2.$$

This holds in the second virial approximation.
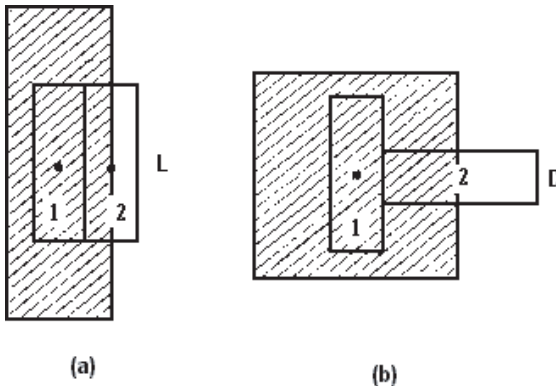
Figure 2.2.   Schematic for excluded volume (shadowed area) of the rod 1: (a) parallel to the neighbor rod 2; (b) perpendicular to the neighbor rod 2.

2.1.2.   The excluded volume

The second virial coefficient β_1 is actually the excluded volume of the a_i molecule to another rod with orientation a_j. According to the definition, the exclusion volume is the volume occupied by one molecule in which the mass centers of other molecules are not allowed to touch. For cylindrical rods with length L and diameter D, the exclusion volume is schematically shown in Figure 2.2. In this figure the two particular cases are depicted, *i.e.*, two cylinders are parallel or perpendicular to each other. β_1 is dependent on the shape of the rigid rods. The expression for cylinders can be approximately expressed by

$$\beta_1(\mathbf{a}_i, \mathbf{a}_j) = -2L^2 D |\sin \gamma|, \qquad (2.21)$$

γ is the angle that a_i makes with respect to a_j.

The third virial coefficient $\beta_2(\boldsymbol{a}_i, \boldsymbol{a}_j, \boldsymbol{a}_k)$ can be neglected if

$$\frac{\rho_c \beta_2}{\beta_1} << 1,$$

where ρ_c is the minimum concentration for forming the liquid crystal state, *i.e.*,

$$\frac{\rho_c \beta_2}{\beta_1} \sim \frac{\rho_c L^3 D^3 \ln(L/D)}{L^2 D} \sim \rho_c L D^2 \sim \phi_c << 1,$$

where ϕ_c is the volume fraction of rigid rods as $\rho = \rho_c$. It is shown that the Onsager approach is valid when the solution is dilute, *i.e.*, ϕ_c is much less than unity.

In order to obtain the maximum $Z(\{N_\alpha\})$, we minimize Equation 2.19 with respect to the orientation distribution function while retaining the normalization condition 2.20. The Euler–Lagrange equation is

$$1 + \lambda + \ln f(\Omega) + \rho \int f(\Omega')V^{ex}(\Omega - \Omega')d\Omega' = 0, \qquad (2.22)$$

where λ is an unknown multiple. Equation 2.22 and the normalization 2.20 together give the orientation distribution function $f(\Omega)$ at the equilibrium state. The orientation distribution $f(\Omega)$ will be discussed later in this section.

2.1.3.   The equilibrium of liquid crystals

According to Equation 2.19 the free energy of the system is written as

$$F = Nk_BT \left[\ln(A\rho) + \int f(\Omega) \ln f(\Omega)d\Omega \right.$$
$$\left. + \left(\frac{\rho}{2}\right) \int\int d\Omega d\Omega' f(\Omega)f(\Omega')V^{ex}(\Omega - \Omega') \right]. \qquad (2.23)$$

The first term is the contribution of translation, the second term results from entropy reduction due to the orientational order of rigid rods, and the third term is the second virial term. The higher virial terms are neglected.

From the free energy (see Equation 2.23), the equation of state at equilibrium and the chemical potential can be determined accordingly. For instance, when the free energy is differentiated with respect to volume V, $P = -\partial F/\partial V$, the pressure–volume relationship shown in Figure 2.3 is obtained. The ordinate is the reduced pressure PV_0/k_BT (V_0 is the volume of rod) and the abscissa is the reduced volume V/NV_0 (or the reciprocal of volume fraction of rods in solution). In a system of axial ratio 10, the change of density at the transition is 0.15 while the order parameter jumps by 0.7361.

By means of the Maxwell equal area rule, the dashed line in the figure is replaced by an equal pressure solid line. The regime of low pressure and low density is the isotropic phase while the regime of high pressure and high density corresponds to the anisotropic phase — nematic liquid crystal phase. The order parameter is determined by

$$S = \int f(\Omega)P_2(\cos\theta)d\Omega. \qquad (2.24)$$
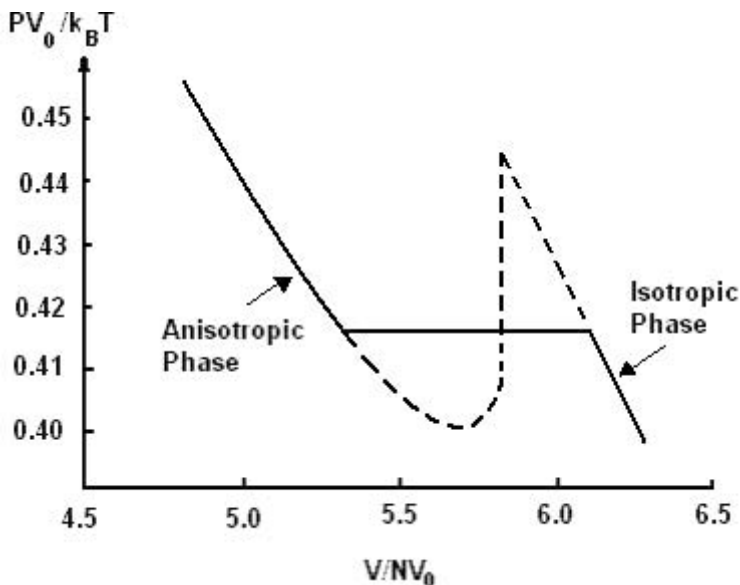
Figure 2.3.   The pressure *vs.* volume of Onsager rigid rod system. (Modified from Onsager, 1949.)

When the isotropic–nematic transition occurs the concentration of rods changes abruptly and the order parameter jumps from zero to a value S_c.

The conclusions are dependent on the shape of rigid rods and hence the second virial coefficient. Thus, the concentration difference and the critical order parameter differ at the nematic — isotropic transition for different shapes of rods.

For simplicity, Onsager suggested that the orientation distribution function $f(\Omega)$ has the form as follows

$$f(\Omega) = \frac{\alpha}{4\pi} \frac{ch(\alpha \cos \theta)}{sh\alpha}, \qquad (2.25)$$

where α is the variational parameter. At the phase transition, the osmotic pressure and chemical potential are equal for the two phases. The results associated with the phase transition are

(1) The nematic to isotropic transition of rigid rods in solution is of the first order. If the axial ratio L/D is great, the concentration of rods $\phi \sim D/L << 1$, even at the $N - I$ transition, meets the condition of the second virial approximation.

(2) When the N − I transition occurs, the critical volume fractions in the nematic and isotropic phase are respectively

$$\phi_I = 3.34\frac{D}{L},$$
$$\phi_N = 4.49\frac{D}{L}. \tag{2.26}$$

For $\phi < \phi_I$, the solution is in the isotropic phase; for $\phi > \phi_N$ the solution is in the nematic phase; for $\phi_N > \phi > \phi_I$ the nematic and isotropic phases coexist.

(3) At the nematic to isotropic transition the critical order parameter $S_c = 0.84$.

The numerical solution of Equation 2.22 gives the critical volume fractions in the two phases and the critical order parameters at the N − I transition are respectively

$$\phi_I = 3.290\frac{D}{L};$$
$$\phi_N = 4.191\frac{D}{L}; \tag{2.27}$$
$$S_c = 0.792.$$

It has been shown that Onsager's approximation (Equation 2.25) on the orientational distribution function works well (error is within 7%).

The Onsager theory first examined the theoretical basis of long rigid rods' forming of a liquid crystal phase: the steric repulsion and the long molecular shape are essential to forming the liquid crystal phase. The theory successfully explains the nematic to isotropic transition of very long rigid polymers, such as the PBLG in dioxane water and the two-phase coexistence. It was found that as the concentration of a solution of tobacco mosaic virus (Bawden & Pirie, 1937; Bernal & Fankuchen, 1941) approaches a critical value, biphasic coexistence occurs. One of the two phases is an isotropic phase of low concentration, while the other is the nematic phase of higher concentration. The Onsager theory has played an important role in the development of liquid crystalline polymers.

It can be easily extended to disc-like molecules (de Gennes, 1973) that form a liquid crystal phase because of their anisotropic shape. The Onsager theory has also been extended to treat the poly-disperse polymer system (Parsons, 1979) and semi-rigid chain systems (Lekkerkeker *et al.*, 1984).

The contribution from Russian scientists is worthy of special mention. We will introduce their theory later.

It should be pointed out that to meet the second virial approximation, molecules must have a large L/D so that at the transition the solution is dilute. For molecules of axial ratio less than 10 the theory does not work well. In addition, the Onsager value of the density difference at the nematic — isotropic transition is greater than the experimental data.

Introducing higher virial terms may extend the Onsager theory to concentrated solutions (Khokhlov & Semenov, 1981).

The Flory theory discussed in the next section is another important theory on rigid liquid crystalline polymers. Because of its clear picture of the lattice model and the incorporation of the Onsager theory, it has become a basic method for the theoretical study of liquid crystalline polymers. As a result of the constant efforts of Flory and his co-workers, the theory has been applied to binary and poly-disperse systems and also includes the "soft" interactions.

2.2.   FLORY THEORY FOR RIGID — ROD LIQUID CRYSTALLINE POLYMERS

2.2.1.   Partition function of a rigid rod solution

Flory (1956, 1984) adopted the lattice model. The Flory theory starts with the partition function of systems consisting of rigid rods and solvent molecules.

Assume the long axis of the rigid rods makes an angle ψ with respect to the director of the system and the director is along one principal axis of the cubic lattice. Divide each rod into x basic units of equal width. Each basic unit occupies one cell in the lattice. x is actually the axial ratio of the rods. For simplicity, suppose that the dimension of a solvent molecule is compatible to the size of a cell lattice. In this section we adopt the same assignations as Flory. These may be different from those used in the preceding section by Onsager.

In order to put a rod into the lattice, a postulate is made, which suggests that each rigid rod be divided into y sub-particles as shown in Figure 2.4b

$$y = x \sin \theta. \tag{2.28}$$

Each sub-particle has x/y basic unit and its long axis is along the director. If a particle is perfectly aligned along the director, y is zero. As a
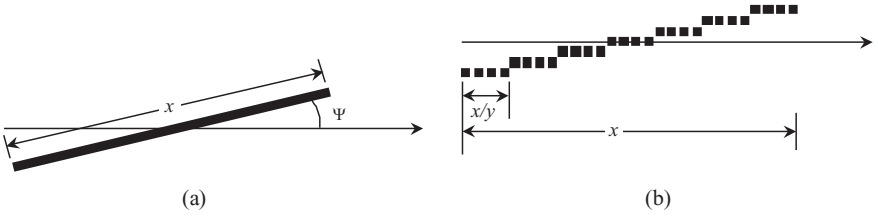
Figure 2.4.   A rigid rod in the Flory lattice. (a) a rod making an angle Ψ to the director; (b) the rod divided into y sub-particles.

particle is aligned off the director the value of y increases. Therefore, y can be regarded as a measure of a rod's deviation off the director. y is called the off-orientation degree or disorder degree.

Assume that the total number of cells in the system is n_0 and $(j-1)$ rods have been placed in the lattice. They have occupied $x(j-1)$ lattice cells and hence $n_0 - x(j-1)$ lattice cells remain unoccupied. In this case, there are ν_j ways to put the j-th rod into the lattice

$$\nu_j = [n - x(j-1)]N_j^{(x-y_j)}P_j^{(y_j-1)}, \qquad (2.29)$$

where y_j is the number of the sub-particles of the rod; the first term represents the number of ways of putting the first basic unit of the first sub-particle into the lattice which is the number of unoccupied cells. P_j is the ways of putting the first unit of remaining $(y-1)$ sub-particles; N_j is the number of ways of placing the remaining $(x-y_j)$ units entering into the lattice.

First we will work out P_j. Once the first sub-particle's position is determined each of other sub-particles must be the closest neighbor to the preceding sub-particle shown in Figure 2.4. In addition, the first unit must be immediately next to the last unit of the preceding sub-particle. The probability of such an arrangement is the volume fraction of unoccupied cells in the system, so that

$$P_j = \frac{[n - x(j-1)]}{n}. \qquad (2.30)$$

All units of each sub-particle must be in same row of the cell. Once the first unit has been put into the lattice (the cell must be unoccupied and is allowed to put in) each of remaining units must be positioned immediately next to preceding unit (the cell must be unoccupied). There are two possibilities: the cell may be unoccupied and is allowed to enter in; the other possibility is that it has been occupied by the first unit of a sub-particle

of another rod and is not allowed to enter in. The possibility N_j of emptiness for the cell is the fraction of empty cells in both empty cells and total number of sub-particles. Thus N_j is

$$
\begin{aligned}
N_j &= \frac{[n - x(j-1)]}{[n - x(j-1) - \bar{y}(j-1)]} \\
&= \frac{[n - x(j-1)]}{[n - (x - \bar{y})(j-1)]},
\end{aligned}
\tag{2.31}
$$

where $\bar{y}$ is the average of y of the $(j-1)$ rods already in the system, $\bar{y}(j-1)$ is the total number of sub-particles already in the lattice, *i.e.*, the total number of the first unit of all the sub-particles.

Substitute P_j and N_j to Equation 2.29 one obtains

$$
\begin{aligned}
\nu_j &= [n - x(j-1)]N_j^{(x-y_j)}P_j^{(y_j-1)} \\
&= \frac{[n - x(j-1)]^x}{\{[n - (x - \bar{y})(j-1)]^{(x-y_j)}n^{(y_j-1)}\}} \\
&\approx \frac{[n - x(j-1)]![n - (x - \bar{y})j]!}{(n - xj)![n - (x - \bar{y})(j-1)]!n^{(\bar{y}_j-1)}}.
\end{aligned}
\tag{2.32}
$$

Assume there are n_p identical rigid rods in the system and the contribution of the n_p rods to the partition function of the system can be written as

$$
Z_{comb} = \frac{1}{n_p!}\prod_{j=1}^{n_p}\nu_j,
\tag{2.33}
$$

where the factor of $(1/n_p!)$ is introduced to avoid repeatedly counting identical rods. Substituting Equation 2.32 into Equation 2.33 gives

$$
Z_{comb} = \frac{(n_s + \bar{y}n_p)!}{n_s!n_p!n^{n_p(\bar{y}-1)}},
\tag{2.34}
$$

where $n_s = n - xn_p$ is the number of empty cells left in the system which are occupied by solvent molecules.

It is shown that both the numerator and denominator in Equation 2.34 increases as the off-orientation degree $\bar{y}$ increases, but the denominator increases more rapidly. As a result, Z_{comb} decreases with increasing $\bar{y}$. It illustrates that if the disorder of configuration of rods in the system increases, the excluded volume occupied by each rod increases and the space

in which rods can move freely decreases. Therefore, the collision between particles increases and the entropy decreases, reducing the stability of the system. Inversely, if $\bar{y}$ decreases, the degree of orientation along the director becomes high, hence Z_{comb} becomes great and the contribution to the energy reduction accordingly becomes important.

In fact, the above-mentioned equation is valid only for the perfectly ordered case, *i.e.*, the rods are all aligned in parallel. This illustrates that the Flory theory works well for concentrated solutions.

Another contribution to the total partition function of the system arises from the orientation, *i.e.*, Z_{orient}

$$Z_{orient} = \prod_y \left(\frac{\omega_y n_p}{n_{py}} \right)^{n_{py}}, \tag{2.35}$$

where n_{py} is the number of rods with off-orientation degree y, ω_y is the solid angle fraction associated with $\bar{y}$, and n_{py}/n_p represents the orientation distribution function. The average of y is given by

$$\bar{y} = \sum_y \frac{y n_{py}}{n_p} \tag{2.36}$$

It is illustrated from Equation 2.35 that if the system is in a perfectly ordered state, $y = 1$; thus $n_{py} = n_p$, Z_{orient} becomes very small. Otherwise, the system is in disorder ($\bar{y} = x$) then $\omega_y = n_{py}/n_p$ and $Z_{orient} = 1$.

According to the Flory's (1956) approximation, when the orientational order is high, n_{py}/n_p is important only in the range $\theta \ll \theta'$. Assume that n_{py}/n_p is uniform within the range. When $\theta > \theta'$, n_{py}/n_p is zero. In the range $\theta \le \theta'$ the solid angle becomes approximately $(\bar{y}/x)^2$. Therefore,

$$Z_{orient} \approx (\bar{y}/x)^{2n_p}. \tag{2.37}$$

The fact that the orientational partition function Z_{orient} increases as $\bar{y}$ increases can be understood. Suppose the next neighbor of each cell in a lattice is six. If the orientation is random each basic unit of a particle has five ways and hence the particle of x units has $5x$ ways to enter into the lattice and thus the contribution to the entropy of the system is $k_B x \ln 5$. In the perfectly ordered state, after the first unit is put into the lattice the remaining units enter the lattice via the same direction. The contribution to the system entropy is about zero, and thus is not favored, taking only the orientational entropy into account. Therefore, the fundamental reason

for rigid rods to form a liquid crystal phase must be attributed to the steric repulsion effect between the rods. Consequently, the partition function is given by

$$Z = Z_{comb} Z_{orient} = \frac{(n_s + \bar{y}n_p)! \, (\bar{y}/x)^{2n_p}}{n_s! n_p! n^{n_p(\bar{y}-1)}}. \tag{2.38}$$

The equation describes the dependence of the partition function on n_p (the number or concentration of rods), x (the axial ratio or degree of polymerization of rods), and $\bar{y}$ (the averaged off-orientation degree). From the partition function one can find the critical concentrations of phase separation of the underlying system as a function of the axial ratio and other quantities which are of interest.

2.2.2.   Formation of the liquid crystal phase

From the partition function in Equation 2.38 the free energy can be obtained as

$$\frac{F}{k_B T} = -\ln Z = n_s \ln(1 - \phi) + n_p \ln\left(\frac{\phi}{x}\right) + n_p(\bar{y} - 1)$$

$$- (n_s + \bar{y}n_p) \ln\left[1 - \phi\left(\frac{1 - \bar{y}}{x}\right)\right] - 2n_p \ln\left(\frac{\bar{y}}{x}\right). \tag{2.39}$$

For the isotropic system $y = x$ and Equation 2.39 becomes

$$\frac{F}{k_B T} = n_s \ln(1 - \phi) + n_p \ln\left(\frac{\phi}{x}\right) + n_p(\bar{y} - 1), \tag{2.40}$$

where

$$\phi = \frac{x n_p}{n}$$

$$1 - \phi = \frac{n_s}{n}$$

are the volume fractions of solvents and rods, respectively.

The relation of the partition function and off-orientation degree $\bar{y}$ in Equation 2.39 is depicted in Figure 2.5 where $x = 100$. Each curve corresponds to a different volume fraction.

As shown in Figure 2.5, for the volume fraction of rods less than critical value ϕ^* (here $\phi^* = 0.0784$) *e.g.*, $\phi = 0.060$, Z increases monotonously with increasing y. In other words, the more disorder the higher Z.
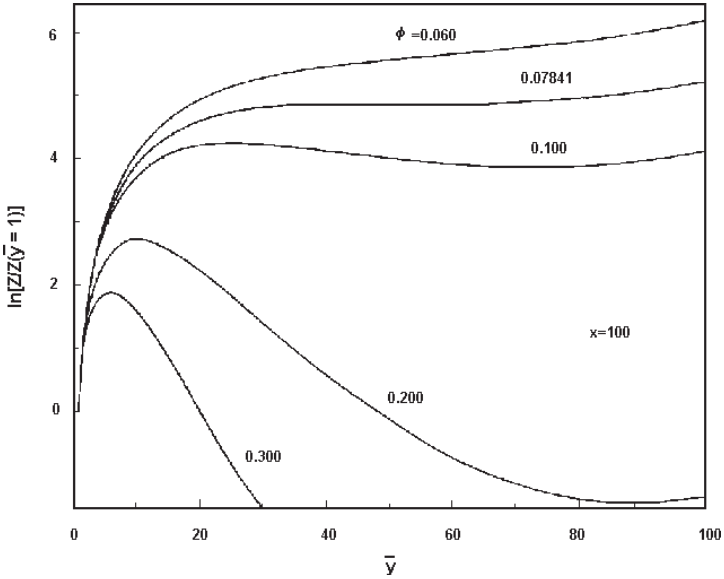
Figure 2.5.   The partition function *vs.* off-orientation degree of a rod system of axial ratio $x = 100$. (Modified from Flory, 1956.)

As $\phi > \phi^*$ there is a maximum Z_{max} with $\bar{y}$. If Z_{max} is greater than Z_0, the value for $\bar{y} = x$, then Z_{max} gives the equilibrium state; otherwise, it is the meta-equilibrium state.

Another conclusion from Figure 2.5 is that the $\bar{y}$ value at $Z = Z_{max}$ is much less than $x/2$, even for $\phi = \phi^*$. As ϕ increases, $\bar{y}$ at $Z = Z_{max}$ decreases. It is illustrated that when the system transforms from the disordered state ($\bar{y} = x$) to the liquid crystal state, $\bar{y}$ changes abruptly to $x/2$.

If ϕ and x are great enough, there are two extremes in Z. The maximal value is associated with the stable (or meta-stable) states, in which $\bar{y}$ is less than that at the minimum Z. Differentiate F in Equation 2.39 with respect to $\bar{y}$ and make $\mathrm{d}(-\ln Z)/\mathrm{d}\bar{y}$ equal to zero. The $\bar{y}$ for the two extremes are given by

$$\phi = \left[\frac{x}{(x - \bar{y})}\right]\left[1 - \exp\left(\frac{-2}{\bar{y}}\right)\right]. \tag{2.41}$$

There are two solutions for $\bar{y}$. The smaller solution corresponds to the stable or meta-stable state in which Z is at a maximum, as shown in Figure 2.5. The dependence of ϕ on $\bar{y}$ can be obtained numerically.

To obtain the critical value of ϕ^* when the system starts to appear in the meta-stable state, *i.e.*, the minimum value of ϕ for the existence of liquid crystal state, let

$$\frac{d\phi}{d\bar{y}} = 0$$

and ϕ^* is given implicitly by

$$x = y^* + y^{*2} \frac{[\exp(2/y^*) - 1]}{2}, \tag{2.42}$$

where y^* is the value at $\phi = \phi^*$, or

$$\phi^* = 1 - \left(1 - \frac{2}{y^*}\right) \exp\left(\frac{-2}{y^*}\right) \tag{2.43}$$

Substituting 2.42 into 2.41 Flory *et al.*, in their 1956 approximation, obtained the critical ϕ^* as the function of the axial ratio x

$$\phi^* \approx \frac{8}{x}\left(1 - \frac{2}{x}\right). \tag{2.44}$$

If $x > 10$, the error of the approximation in the above equation is less than 2%. It is concluded from Equation 2.44 that the larger the axial ratio of rods x, the less is ϕ^*.

Equation 2.44 is the well-known Flory formula which is widely used in the study of liquid crystalline polymers. It should be pointed out that ϕ^* is only the minimal solution of Equation 2.41 at which the partition function first shows a maximum. At this volume fraction ϕ^*, Z_{max} is actually less than the Z at the disordered state ($\bar{y} = x$). The system is at a meta-stable state only when the volume fraction further increases to a greater value in which the system is indeed at a stable state.

It is shown in Equation 2.43 that as ϕ^* increases up to $\phi^* = 1$, *i.e.*, the neat polymer system, $y^* = 2$. Substituting $y^* = 2$ into Equation 2.42 the axial ratio is

$$x = 2e = 5.44,$$

which is approximately the minimum axial ratio of rods that the systems are able to show a liquid crystal phase.

2.2.3.   Two phase equilibrium

According to the above analyses, when the concentration of rods in the solvent increases beyond ϕ^*, phase separation occurs, and the biphasic

coexistence of liquid crystal and isotropic phases appears. The chemical potentials of each component must be equal at the coexistence of two phases, *i.e.*,

$$\mu_s = \mu'_s$$
$$\mu_p = \mu'_p, \tag{2.45}$$

where the subscript "s" is designated for the solvent while p is for the rigid rods, and μ and μ' are the chemical potentials at the isotropic and liquid crystal phase, respectively.

According to Equation 2.38, the derivative of $(-\ln Z)$ with respect to the volume fraction n_s of the solvent gives

$$\frac{(\mu'_s - \mu^0_s)}{RT} = \ln(1 - \phi') + \frac{\phi'(\bar{y} - 1)}{x} - \ln\left[1 - \phi'\left(1 - \frac{\bar{y}}{x}\right)\right]. \tag{2.46}$$

At equilibrium $d(-\ln Z)/d\bar{y} = 0$. Replace the last term by $2/\bar{y}$ from Equation 2.41 and thus Equation 2.46 becomes

$$\frac{(\mu'_s - \mu^0_s)}{RT} = \ln(1 - \phi') + \frac{\phi'(\bar{y} - 1)}{x} + \frac{2}{\bar{y}}. \tag{2.47}$$

The chemical potential for solvents in the isotropic phase is

$$\frac{(\mu_s - \mu^0_s)}{RT} = \ln(1 - \phi) + \phi\left(1 - \frac{1}{x}\right). \tag{2.48}$$

Similarly, the chemical potential of rods in the liquid crystal and in the isotropic phase are given respectively by

$$\frac{(\mu'_p - \mu^0_p)}{RT} = \ln\left(\frac{\phi'}{x}\right) + \phi'(\bar{y} - 1) + 2 - 2\ln\left(\frac{\bar{y}}{x}\right) \tag{2.49}$$

and

$$\frac{(\mu_p - \mu^0_p)}{RT} = \ln\left(\frac{\phi}{x}\right) + \phi(x - 1). \tag{2.50}$$

The equilibrium state of coexistence of two phases is governed by the following set of equations

$$\ln(1 - \phi') + \frac{\phi'(\bar{y} - 1)}{x} + \frac{2}{\bar{y}} = \ln(1 - \phi) + \phi\left(1 - \frac{1}{x}\right)$$
$$\ln\left(\frac{\phi'}{x}\right) + \phi'(\bar{y} - 1) + 2 - 2\ln\left(\frac{\bar{y}}{x}\right) = \ln\left(\frac{\phi}{x}\right) + \phi(x - 1). \tag{2.51}$$
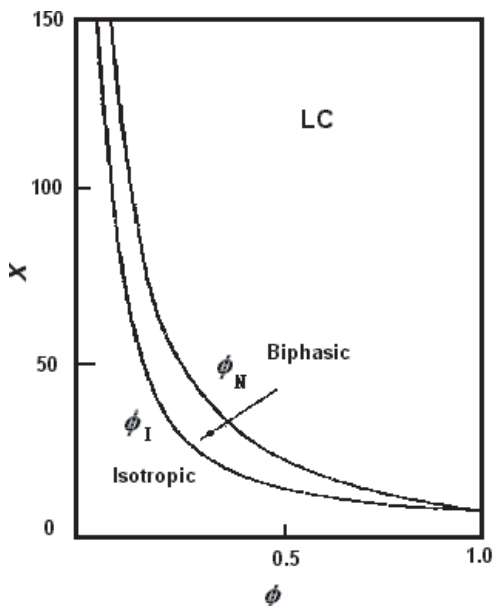
Figure 2.6.   Phase diagrams for various rod axial ratios. (From Flory & Ronca, 1979a.)

and Equation 2.43, where ϕ' and ϕ are the volume fraction of rods in the liquid crystal and isotropic phase, respectively.

For various axial ratios x of the rods the numerical solutions of the above set of equations are summarized in Figure 2.6.

The following important conclusions can be obtained from Figure 2.6:

(1) Those rigid molecules capable of showing a stable liquid crystal phase must have the axial ratio greater than $x = 6.7$. This value is somewhat greater than the estimated value of $x = 5.44$. We have emphasized that the estimate of the minimum axial ratio for forming a liquid crystal phase ($x = 5.44$) is that at which the partition function starts to take a maximum.

(2) At the equilibrium state, the volume fraction of rods in the two phases decreases as the axial ratio x increases. The volume fraction of the liquid crystal phase is slightly greater than that of the isotropic phase, the ratio between these two critical volume fractions increases with increasing x, but is always less than 1.56.

For enough large x, the critical volume fractions are respectively

$$\phi = \frac{8}{x}, \quad \phi^* = \frac{12.5}{x}.$$
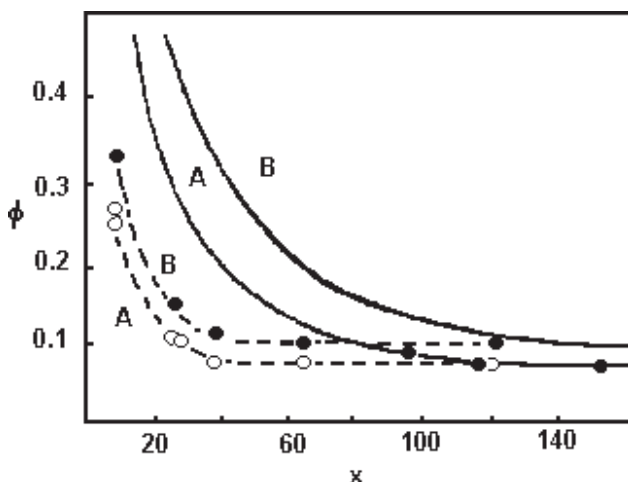
Figure 2.7.   Critical volume fraction *vs.* axial ratio. (Modified from Flory, 1961. Reproduced by permission of John Wiley & Sons, Inc.)

(3) $\bar{y}/x$ increases smoothly as x increases, however, the variation is not great. The value of $\bar{y}/x$ is very small which illustrates that the ordering in the liquid crystal phase is very high.

An experiment was carried out for PBLG to verify the theory. PBLG molecules in solution adopt an extended α-helical conformation so that they are rigid rods. In Figure 2.7, the critical volume fractions of PBLG in solvents (Flory, 1961) were depicted as a function of the axial ratio. The curve A is for ϕ at which the liquid crystal phase starts to appear while the curve B is for ϕ' at which the isotropic phase completely disappears and the system becomes entirely a liquid crystal. The solid curve is the theoretical expectation while the dashed line is the experimental result. Both are in good agreement.

2.2.4.   Effect of "soft" interaction between molecules

Later Flory further took the two "soft" interactions between the molecules into account. The anisotropic interaction is associated with molecular orientations while the isotropic one is irrelevant of the molecular orientation. In fact, the anisotropic interaction was the basis of another well-known theory in liquid crystals — Maier–Saupe theory (Maier & Saupe, 1959). Flory successfully captured the essence of the theory.

First we introduce the isotropic interaction which results from the mixing of rods and solvents. The previous theory, without the mixing contribution to entropy, is only applicable to an athermal system. If there is a mixing entropy contribution, the free energy in Equation 2.39 is implemented by a term $\chi \phi n_s$, where χ is the Flory–Huggins interaction parameter. Flory called the mixing term the isotropic "soft" interaction to distinguish it from the steric interaction of rods.

At the coexistence of the two phases the chemical potentials of the rods and solvents in both the liquid crystals phase and isotropic phase must be equal and thus the following set of equations for ϕ, ϕ' and $\bar{y}$ holds

$$\ln(1 - \phi') + \frac{\phi'(\bar{y} - 1)}{x} + \frac{2}{\bar{y}} + \chi \phi'^2 = \ln(1 - \phi) + \phi\left(1 - \frac{1}{x}\right) + \chi \phi^2$$

$$\ln\left(\frac{\phi'}{x}\right) + \phi'(\bar{y} - 1) + 2 - 2\ln\left(\frac{\bar{y}}{x}\right) + \chi x(1 - \phi')^2$$

$$= \ln\left(\frac{\phi}{x}\right) + \phi(x - 1) + \chi x(1 - \phi)^2. \tag{2.52}$$

Figure 2.8 shows the numerical result of the rod/solvent system for the rod axial ratio $x = 100$.

The ordinate is the Flory–Huggins parameter χ and the abscissa is the volume fraction of rigid rods. For negative χ, the two phase equilibrium is basically independent of χ. A positive χ has a significant effect on the two-phase equilibrium. The diagram can be divided into three regions: in Region I the concentration is small and the system is in a single isotropic phase; in Region II the system is in the liquid crystal phase; and in Region III both the liquid crystal and isotropic phases coexist. For χ less than, say, 0.07, the region of biphasic coexistence is narrow, $\phi^{**}/\phi^* = 1.5$. For χ greater than 0.07 the volume fraction difference between the two phases becomes larger.

Figure 2.9 shows the experimental results of the PBLG/dimethyl formamide(DMF)-methanol system (Nakajama *et al.*, 1968). The axial ratios were 150 and 350, respectively, and the χ value was controlled by varying the concentration of methanol. The more methanol the greater is χ. It was shown that for small concentrations of methanol, the biphasic range is narrow. As the volume fraction of methanol increases (up to 0.10–0.12) the biphasic range becomes wider.
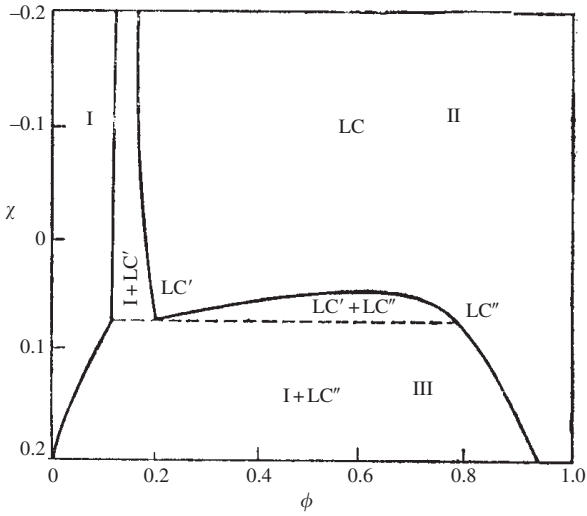
Figure 2.8.   Phase diagram for rod axial ratio of 100. (From Flory, 1956.)
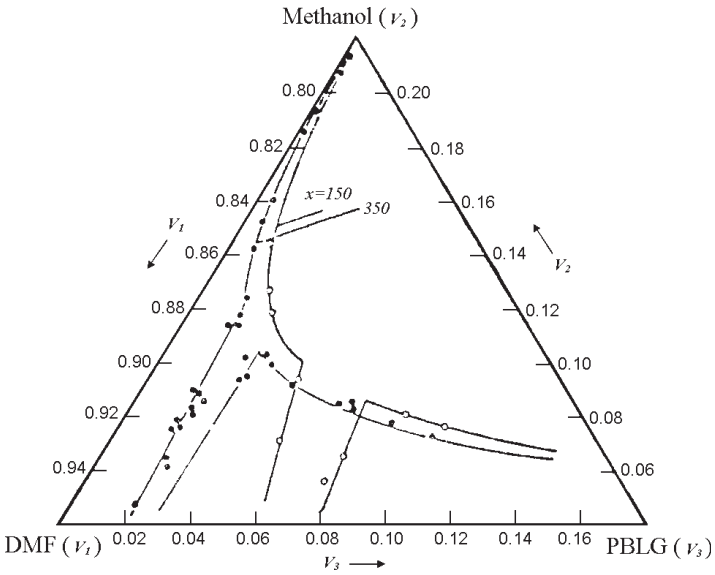
Figure 2.9. Experimental phase diagram of PBLG/dimethyl formamide(DMF)-methanol system. (Modified from Nakajama *et al.*, 1968.)
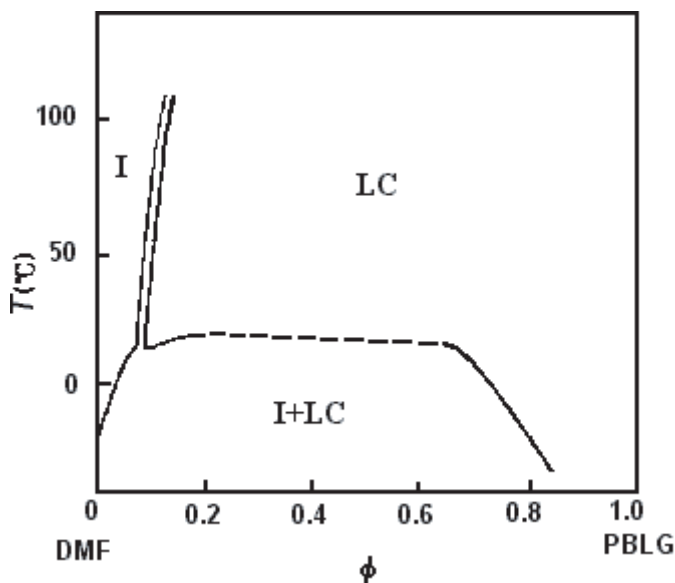
Figure 2.10.   The phase equilibrium *vs.* temperature. (From Miller *et al.*, 1974.)

The value of χ varies with the temperature, *i.e.*, χ decreases as the temperature increases. Wee & Miller (1971) examined the phase equilibrium as a function of temperature. The results are shown in Figure 2.10. For temperatures below $35\,°C$ the phase diagram is basically the same as the Flory theory; while at higher temperatures, the curve deflects to a high concentration regime. This phenomenon was observed in a system of cellulose derivatives (Navard *et al.*, 1981).

Warner and Flory (1980) found that the introduction of the anisotropic attractive force predicts this effect. This anisotropic interaction associated with molecular orientation is expressed by

$$-\left(\frac{1}{2}\right)\left(\frac{xn_p\phi S^2 T^*}{T}\right),\tag{2.53}$$

where S is the order parameter and T^* is the characteristic temperature which is a function of the anisotropy of the longitudinal and transverse electric susceptibilities

$$k_B T^* \propto r^{-6}(\Delta\alpha)^2,$$

where r is the distance of neighboring rods.

2.2.5.   **Semi-rigid chains**

The completely extended chain is not essential for formatting a liquid crystal phase. In fact, most liquid crystalline polymers are semi-rigid chains, having more or less flexibility. The structural distortion during the polymerization and the flexible parts (introduced in polymer synthesis for the purpose of reducing the melting point and to improve solubility), *etc.*, all reduce the rigidity of the polymer chains while retaining the liquid crystal phase. Flory (1978) pointed out that the above theory is applicable to the semi-rigid chains in terms of the Kuhn length *vs.* the repeated length.

The axial ratio of the Kuhn segment can be expressed by

$$x_k = \frac{l_k}{D} = \left[\frac{\langle r^2 \rangle_0}{n} \right] \left(\frac{\rho N_A}{l_u M_u} \right)^{1/2}, \tag{2.54}$$

where l_k is the Kuhn length; $\langle r^2 \rangle_0$ is the mean square end-to-end distance

$$\langle r^2 \rangle_0 = n_k l_k^2 = (n l_u) l_k, \tag{2.55}$$

where n_k is number of Kuhn segments along a chain, $n_k l_k$ is the extended length of the chain, n is the number of repeated units of a real chain, l_u is the projection of a repeated unit onto the extended chain. D is the diameter of chain and

$$D = \left(\frac{M_u}{\rho N_A l_u} \right)^{1/2}, \tag{2.56}$$

where M_u is the molecular mass of a repeat unit; ρ is the density of the polymer and N_A is Avogadro's constant.

The conformational distortions give rise to some flexibility of the molecules of cellulose derivatives. Tanner and Berry (1974) measured the mean square end-to-end distance of diacetate cellulose in trifluoroacetic acid

$$\frac{\langle r^2 \rangle_0}{n} \approx 1100 \, \text{Å} \quad (n \to \infty).$$

Assuming $\rho = 1.3 \, \text{g/cm}^3$, $l_u = 5.2 \, \text{Å}$, $M_u = 265$, one obtains the Kuhn length and the critical volume fraction as

$$x_k = 26, \quad \phi^* = 0.284.$$

Table 2.1. Comparison of theory and experimental data of various cellulose derivative solutions. (From Flory, 1978.)

Derivative	Solvent	ϕ^*(theory)	ϕ^*(experiments)
diacetate cellulose	acetone	0.284	0.33
	dimethyl formamide	0.284	0.37
	dioxane**	0.284	0.35
	m-cresol	0.284	0.28
	trifluoroacetic acid	0.284	0.25
ethyl cellulose	acetate	0.32	0.39
	dichloroacetate	0.32	0.28
hydroxypropyl cellulose	water	0.38	0.33, 0.37, 0.30
	methanol	0.38	0.33
	ethanol	0.38	0.37, 0.39
	acetate	0.38	0.27
	dimethylacetylamide	0.38	0.32, 0.35

For ethyl cellulose, assume $\rho = 1.3\,\mathrm{g/cm}^3$, $l_\mathrm{k} = 180\,\text{Å}$ and one obtains

$$x_k = 23 \quad \text{and} \quad \phi^* = 0.32.$$

For hydroxypropyl cellulose $\rho = 1.2\,\mathrm{g/cm}^3$, $l_\mathrm{k} = 180\,\text{Å}$:

$$x_k = 19, \quad \phi^* = 0.38.$$

Table 2.1 summarizes the above calculations and compares them with the experimental data. Good agreement was found.

2.2.6.   Discussion of the Flory theory

Equation 2.28 was suggested in Flory's 1956 approximation which is actually valid for a two-dimensional lattice. As shown in Figure 2.11, y is the projection of a rod's length onto the plane (X–Y) perpendicular to the director in a three-dimensional lattice. But one would find that the system shows some orientational order at all concentrations even though for isotropic phase.

To overcome the contradiction, Flory and Ronca (1979) made the following improvement for the three-dimensional lattice

$$y = x \sin\theta(|\sin\phi| + |\cos\phi|) \tag{2.57}$$
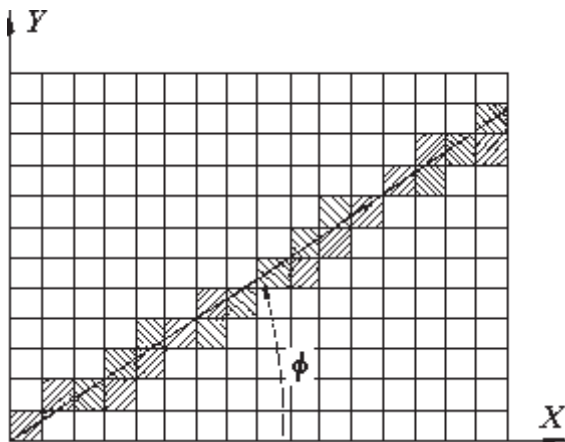
Figure 2.11.   The Projection of a rod on X–Y plane. (From Flory & Ronca, 1979a)

where ϕ is the azimuthal angle of the rod's projection onto the x axis. For a uniaxial nematic phase, the system is independent of ϕ. Averaging over ϕ

$$y = (4/\pi)x \sin\theta. \tag{2.58}$$

It is more reasonable to adopt Equation 2.58 instead of Equation 2.28.

It was pointed out that the approximation form in Equation 2.37 used for Z_{orient} (valid only for high degrees of orientation) leads to the incorrect result that an isotropic phase can exist in a solution of rods in an external orienting field.

Free energy resulting from the orientational distribution was precisely defined in the Onsager model (Equation 2.19) instead of Equation 2.35

$$F_{orient} = k_B T n_p \int f(\Omega) \ln f(\Omega) d\Omega, \tag{2.59}$$

where the orientational function of rods $f(\boldsymbol{n})$, similar to the function already applied in the Onsager model.

Hence the off-orientational degree is expressed by

$$\bar{y} = \left(\frac{4}{\pi}\right) x \int \sin\theta f(\Omega) d\Omega. \tag{2.60}$$

In this modified Flory model, the liquid crystal–isotropic transition of rods in a solution occurs at

$$\phi_I = 7.89\frac{D}{L},$$
$$\phi_N = 11.57\frac{D}{L}, \tag{2.61}$$
$$S_c = 0.92.$$

Only a minor change was found.

No matter which Equation, 2.28 or 2.58, is used, y is zero if θ is zero. However, for perfectly oriented rods parallel to the z axis, y should be 1 in the lattice. The theory has omitted orientations with $y < 1$. Because x is generally large, the above approximation does not cause a significant error. Only for a small x regime does a modification become important.

For the isotropic phase, one has $\bar{y} = x$, which implies that y may take values greater than x. This is forbidden in the lattice model. Fortunately, we apply here the Flory–Huggins model for the isotropic phase and we do not need to use the quantity y. In the liquid crystal phase $y < x$ and the lattice model holds.

It is worth pointing out that some assumptions of the Flory theory are valid only in a perfectly ordered phase, *i.e.*, the Flory theory is more applicable in the case of high order and of large concentration.

2.3. COMPARISON OF THE ONSAGER AND FLORY THEORIES

The Onsager and Flory theories are both statistical theories on rigid rod liquid crystalline polymers, but the former is a virial approximation while the latter is a lattice model. The first is more applicable to dilute solutions while the latter works especially well for high concentrations and a highly ordered phase. These theories with experiments, especially critical volume fractions ϕ_i and critical order parameter S_c at nematic–isotropic transition are made below.

The Onsager theory points out that liquid crystalline polymers enter from the liquid crystal phase to the isotropic phase at the volume fraction

$$\phi_I = \frac{3.3}{x} \tag{2.62}$$
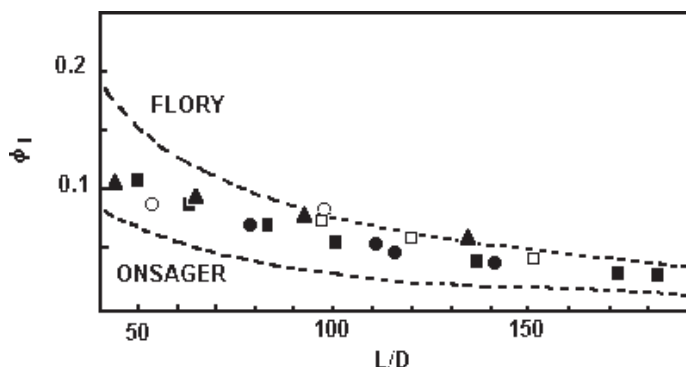
Figure 2.12.   Critical volume fraction *vs.* axial ratio: comparisons of Onsager and Flory theories with experimental data. (Modified from Ciferri, 1991. Reproduced by permission of John Wiley & Sons, Inc.)

while Flory predicts that the critical volume fraction is

$$\phi_I = \frac{8}{x}\left(1 - \frac{2}{x}\right). \tag{2.63}$$

These two predictions are depicted in Figure 2.12 together with some experimental data. In this figure, the dashed lines are the expectations from the Onsager and Flory theories. The points are for PBLG (molecular diameter $D = 15.6\,\text{Å}$ in m-cresol (Hermans, 1962), marked "□" and in dioxane, "○" (Robinnov *et al.*, 1958). In addition, the data of PBA ($D = 5\,\text{Å}$ in DMAC (+3% LiCl) (•) (Bruzone, 1986) and in H_2SO_4 (■) (Kwolek *et al.*, 1977) and schizophylian ($D = 16.7\,\text{Å}$) dissolved in H_2O (▲) (Itou *et al.*, 1985) were compared in Figure 2.12.

It is shown that the predictions of the Onsager theory are smaller than that of the experimental data. This discrepancy is due to the second virial approximation. Adopting higher terms of virial coefficients may improve the predictions.

Meanwhile, Flory predicts a higher critical volume fraction. It is thought that the Flory lattice model is comparatively simple, even though the addition of the soft interactions does not change this shortcoming.

The real liquid crystalline polymers exhibit finite flexibility. This kind of polymer was studied extensively by Khokhlov and his co-workers. Assume that the semiflexible chain has the total contour length L, and Kuhn length l and diameter D, and $L \gg l \gg D$. Analogous to the Onsager model, the free energy of the polymer in solution is composed of the conformational

contribution F_{conf} and the steric interaction F_{ster}. Khokhlov and Semenov (1982) defined F_{ster} and F_{conf} for the semiflexble polymers as

$$F_{ster} = NT\frac{4}{\pi}\frac{L\phi}{D}\iint f(\Omega_1)f(\Omega_2)2l^2D|\sin\gamma|d\Omega_1 d\Omega_2 \qquad (2.64)$$

and

$$F_{conf} = NT\frac{L}{l}\int[(\nabla_n f)^2/4f]d\Omega. \qquad (2.65)$$

They obtain the following quantities at the N–I transition

$$\phi_I = 10.48\frac{D}{l},$$
$$\phi_N = 11.39\frac{D}{l}, \qquad (2.66)$$
$$S_c = 0.49.$$

It has been illustrated that the jump of the order parameter at the transition is smaller in semiflexible polymers.

When dealing with semiflexible polymers with $L \sim l$ they reported the results (Khokhlov & Semenov, 1982; Odijk, 1986)

$$\phi_I = \frac{D}{L}\frac{3.34 + 11.3\left(\frac{L}{l}\right) + 4.06\left(\frac{L}{l}\right)^2}{1 + 0.387\left(\frac{L}{l}\right)},$$

$$\ln\left(1 - \frac{\phi_N}{\phi_I}\right) = -\frac{1.07 + 14.4\left(\frac{L}{l}\right) + 84.1\left(\frac{L}{l}\right)^2}{1 + 34.5\left(\frac{L}{l}\right)^2}, \qquad (2.67)$$

$$\ln S_c = \frac{D}{L}\frac{0.166 + 3.56\left(\frac{L}{l}\right) + 15.9\left(\frac{L}{l}\right)^2}{1 + 22.5\left(\frac{L}{l}\right)^2}.$$

It is shown that only very rigid or very short polymers behave like rigid chains.

For flexible chains the ratio of the Kuhn length or the persistence length to the molecular diameter (l/D) plays the same role that the axial ratio of molecules (L/D) does in the rigid rods. Figure 2.13 shows the expectations of Onsager and Flory theories (dashed lines) and the experimental data:

hydroxypropylcellulose (HPC) ($D = 10.4$ Å) dissolved in DMAc denoted as HPC/DMAc (Conio *et al.*, 1988);
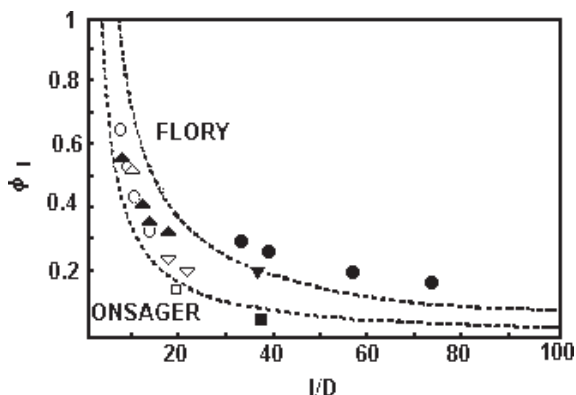
Figure 2.13.   Critical volume fraction *vs.* ratio of persistence length to molecular diameter (l/D): comparisons of the Onsager and Flory theories with experimental data. (Modified from Ciferri, 1991. Reproduced by permission of John Wiley & Sons, Inc.)

poly(n-hexyl isocyanate) (PHIC) ($D = 10.3$ Å)/1-CN (Bianchi *et al.*, 1987);

PHIC/toluene (Krigbaum *et al.*, 1985);

acetoxypropylcellulose (APC)/DCM (Conio *et al.*, 1984);

APC ($D = 12.0$ Å)/DMPh (Laivins & Gray, 1986);

HPC/DCAc (Aden *et al.*, 1984);

cellulose acetate (CA) ($D = 8.1$ Å)/DMAc (Bianchi *et al.*, 1986);

cellulose ($D = 5.8$ Å)/DMAc (McCormick *et al.*, 1985).

Most experimental data fall between the two theoretical expectations with the Flory model representing the upper limit and the Onsager limit representing the lower limit. The two theories are in reasonable agreement with experimental data if the uncertainty of the molecular diameter D and Kuhn length l is taken into account.

A comparison of the theoretical expectations of worm-like liquid crystalline polymers and experimental data is made in Figure 2.14. The abscissa is the ratio of total length to persistence length L/l; the ordinate is the critical volume fraction in the unit of the ratio of molecular diameter to persistence length. The theoretical expectation is taken from Khokhlov *et al.*'s theory (Khokhlov & Semenov, 1982; Odijk, 1986) on the worm-like chains.
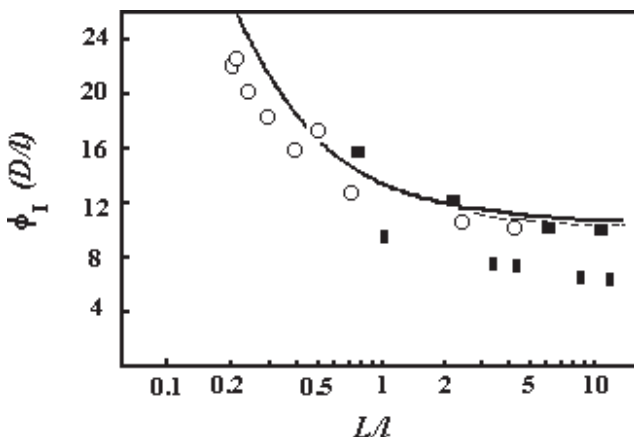
Figure 2.14. Critical volume fraction (in the unit of D/l) *vs.* the total length (in the unit of l): the curve for Khokhlov theory (Equation 2.67); the data taken from experimental data. (Modified from Ciferri, 1991. Reproduced by permission of John Wiley & Sons, Inc.)

The experimental data are from the following solutions: PHIC($D = 12.5\,\text{Å}$)/toluene, $l = 750\,\text{Å}$, PHIC/DMC, $l = 370\,\text{Å}$ at room temperature (Conio *et al.*, 1984) and PHIC/toluene at $25\,^\circ\text{C}$ (Itou & Teramoto, 1984). It can be seen that the theoretical prediction of the worm-like chain is in good agreement with experiments. The diagram illustrates the relationship of the critical volume fraction and molecular length or molecular weight to the formation of a liquid crystal phase.

Another important parameter is the critical order parameter S_c at the nematic-isotropic transition. The predictions of the Flory and Onsager theories for rigid rods are in good agreement with the experimental data of PBLG/PMF ($30\,^\circ\text{C}$) (Abe & Yamazaki, 1989) and PBA/DMAc +3% LiCl (Sartirana *et al.*, 1986). The order parameter of PBLG was measured by means of NMR on a deuteriated sample; while that for PBA was investigated via the dichroism ratio using polarizing IR spectroscopy. The Onsager theory seems to be in better agreement with the experiments. The worm-like chains allows continuous conformational deviations and thus significantly reduces the order parameter.

In summary, the Flory theory is appropriate in dealing with critical volume fractions while the Onsager theory is better in predicting the order parameter at transition.

2.4.   MAIER-SAUPE MEAN FIELD APPROACH

2.4.1.   Maier-Saupe mean field theory for small molecular mass liquid crystals

Liquid crystalline polymers can be regarded as a long chain with rods connected in sequence, each rod being, in some sense, equivalent to a small molecular mass liquid crystal. This is the so-called freely-jointed-rod chain, the simplest model of polymers. It is understood that the constituent units — small molecular mass liquid crystals play an essential role in liquid crystalline polymers. Here, we introduce an important theory for small molecular mass liquid crystal — the Maier–Saupe mean field theory (Maier & Saupe, 1959, 1960).

In contrast to the Onsager and Flory theories, the Maier–Saupe theory no longer takes into account molecular steric effects as the basic interaction but instead proposes that the van der Waals interactions between molecules are the basis for forming a liquid crystal phase. The van der Waals interaction depends on molecular orientations. The Maier–Saupe theory adopts a rather simple mathematical treatment and can easily take into account the relationship of system properties to temperature. This theory has been successfully applied to a thermotropic system of small molecular mass liquid crystal.

In this system, a molecule is subjected to the van der Waals attractions of other molecules in the system which is related to the relative orientations of the pair molecules. Suppose the Z axis is the reference direction. Then, the potential for each molecule is a function of orientation

$$U_i = -a\langle P_2(\cos\theta_{ij})\rangle_j \ P_2(\cos\theta_i), \tag{2.68}$$

where θ_i is the angle of the molecular long axis made with respect to the Z axis, θ_{ij} is the angle molecule j interacting with molecule i makes with respect to the Z axis. $P_2 = 3x^2/2 - \frac{1}{2}$ is the second Legend polynomial. The bracket denotes the statistical average over all the molecules in the system and according to the definition the averaged quantity is actually the order parameter.

Therefore, the mean field potential of a molecule is given by

$$U = -aSP_2(\cos\theta), \tag{2.69}$$

where a is the constant of a van der Waals type interactions which is associated with the mean distance r between the molecules, being proportional

to r^{-6}. The coupling constant a depends on the molecular properties. For the nematic phase, which has no positional order and is uniaxially symmetrical, the potential U is independent of the position of the molecular masses and the azimuthal of the molecular orientations.

The orientational distribution function is thus expressed by

$$f(\Omega) = \frac{\exp(-\beta U)}{Z} = \frac{\exp[\beta a S P_2(\cos\theta)]}{\int \exp[\beta a S P_2(\cos\theta)]d\Omega}, \qquad (2.70)$$

where the denominator, Z, is the partition function. The order parameter S can be evaluated in terms of the orientational function

$$S = \frac{\int_{-1}^{1}[P_2(\cos\theta)]\exp[\beta a S P_2(\cos\theta)]\sin\theta\,d\theta}{\int_{-1}^{1}\exp[\beta a S P_2(\cos\theta)]\sin\theta\,d\theta} \qquad (2.71)$$

Equation 2.71 is the self-consistency equation for S. S depends on the combination $k_B T/a$ only, shown in Figure 2.15, and thus is a function of temperature and the coupling constant a. As $k_B T/a = 0.22019$, a nematic to isotropic transition occurs. The temperature T_c is the N–I transition temperature at which S jumps from 0.4289 to zero.
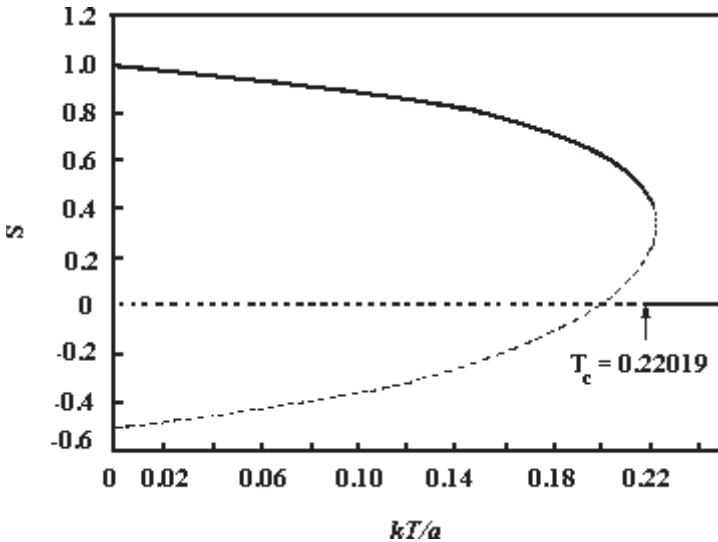
Figure 2.15. The order parameter *vs.* reduced temperature for small molecular mass liquid crystals. (Modified from Maier & Saupe, 1959.)

The free energy in the nematic phase is

$$\frac{F}{Nk_BT} = \ln \int_{-1}^{1} \exp[\beta a S P_2(\cos\theta)] \sin\theta \, d\theta + \frac{aS^2}{2}. \qquad (2.72)$$

The last term avoids double counting of the pair interaction in the mean field theory.

At the transition, the free energy of both nematic and isotropic phases are equal.

The latent change at the N–I transition is

$$\frac{\Delta E(T_c)}{N} = \frac{aS_c^2}{2T_c} = 3.47 \, \text{J/mol. K}. \qquad (2.73)$$

It is illustrated that the N–I transition is of first order. Experimentally, the latent entropies of small molecular mass liquid crystals, $\Delta E(T_c)$, are very diverse, ranging from 1.25 to 7.55 J/mol. K. Most fall in the range of 2.50–3.35 J/mol. K. The Maier–Saupe prediction for the latent entropy at transition is in reasonable agreement with experiments.

It is worthwhile to point out that the Maier–Saupe theory has been successful in analyzing the behavior of small molecular mass liquid crystals at transition, such as the temperature change of the order parameter. The jump of the order parameter at transition, $S_c = 0.43$ is in reasonable agreement with most experiments. The Onsager and Flory theories, which take into account the steric effects predict a higher critical order parameter.

2.4.2.   Freely-jointed-rod chains

In a very crude sense, liquid crystalline polymers can be regarded as a freely-jointed-rod chain, shown in Figure 2.16. The freely-jointed-rod chain consists of a series of repeated segments of length l_0. Each segment is able to rotate freely. It is assumed that the freely-jointed-rod chain is a replica of its small molecular mass liquid crystal counterpart in the liquid crystalline properties.

2.4.2.1.   Liquid crystallinity

The application of the Maier–Saupe theory to the polymer system results in the nematic to isotropic (N–I) transition temperature, T_c, the order

parameter, S_c, and the latent entropy of each repeated segment, $\Delta E(T_c)/N$, at the transition as follows

$$\frac{k_B T_c}{p} = 0.2202,$$

$$S_c = 0.4289, \qquad (2.74)$$

$$\frac{\Delta E(T_c)}{N} = 0.42\text{R},$$

where N is the degree of polymerization. R is the Gas constant.

2.4.2.2. Polymer conformations

Molecular conformation is an important subject of concern in liquid crystalline polymers. It is also the basic subject of polymer science. The mean square end-to-end distance or the radius of gyration is often used to characterize the size of a polymer molecule. According to the definition, the end-to-end distance is the sum of each rod's vectors in sequence

$$\boldsymbol{R} = \boldsymbol{l}_1 + \boldsymbol{l}_2 + \cdots + \boldsymbol{l}_N = \sum_i^N \boldsymbol{l}_i. \qquad (2.75)$$

The statistical mean over all possible conformations is zero, so that only the mean square $\langle R^2 \rangle$ (or mean square root) is meaningful. The radius of gyration is used often and is defined as follows

$$R_g^2 = \sum_i^N \frac{m_i r_i^2}{M}, \qquad (2.76)$$

where $\boldsymbol{r}$ is the position vector of the i-th segment from the mass center of the polymer. The mean square end-to-end distance is related to the radius of gyration for a homogeneous, long random walk chain by

$$R_g^2 = \frac{\langle R^2 \rangle}{6}. \qquad (2.77)$$

The conformation of a freely-jointed-rod chain in the nematic liquid crystal is anisotropic and its end-to-end distance component along the z axis is evaluated as follows

$$\langle R_z^2 \rangle = \left\langle \left(\sum_i^N l_{iz} \right)^2 \right\rangle = \sum_i^N \langle l_{iz}^2 \rangle + \sum_{i,j}^N \langle l_{iz} l_{jz} \rangle = N \langle l_{iz}^2 \rangle$$

$$= N l^2 \langle \cos^2 \theta \rangle = \frac{N l^2 (2S + 1)}{3}, \qquad (2.78)$$

where the summation $\sum_{i,j}^{N} \langle l_{iz} l_{jz} \rangle$ is zero as the projections of each rod onto the z axis cancel each other.

Similarly, the end-to-end distance component along the x or y axis is

$$\langle R_x^2 \rangle = \langle R_y^2 \rangle = N l_0^2 \frac{(1-S)}{3}, \tag{2.79}$$

where $\langle \sin^2 \phi \rangle = \frac{1}{2}$. S is always positive so that the conformation of liquid crystalline polymers is of a prolate shape. In the isotropic phase $S = 0$ and the components of end-to-end distance are all equal, *i.e.*, $Nl^2/3$.

It is understood that the extension of a freely-jointed-rod chain along the director is due to the preferred orientation of each segment. The maximum $\langle R_z^2 \rangle$ is less than Nl^2, which is a result of random walk. In other words, a freely-jointed rod chain cannot produce the rod-like conformation expected for liquid crystalline polymers at low temperature.

2.4.3.   Elastically-jointed-rod chains

As is expected, at low temperatures liquid crystalline polymers have, to a great extent, a rod-like conformation. This is not predicted by a freely-jointed-rod chain.

To overcome this shortcoming Warner and Wang (1992c) proposed the theory of elastically-jointed-rod chains in which any deviations of consecutive rods' orientation causes an energy penalty.

The jointed-rod chain is one-dimensional system of a series of repeated segments and we naturally apply the Transfer matrix technique in the Ising model to obtain the partition function for both the freely-jointed-rods and the elastically-jointed-rods. We will not go into the details of this model but instead will show some results derived from the model.

Wang (1995a) calculated the N–I transition temperature, the critical order parameter and the latent entropy at transition according to the model

$$\frac{k_B T_c}{p} = 0.541,$$

$$S_c = 0.500, \tag{2.80}$$

$$\frac{\Delta E(T_c)}{N} = 0.25R.$$

It is noted that the same conclusions are not reached by using previous results derived from the Maier–Saupe method. The transfer matrix

approach predicts higher transition temperatures and less latent entropy at transition. One reason is the simplicity of the discrete orientation approximation in the transfer matrix approach. The difference may also result from the fact that the Maier–Saupe method is actually specified for small molecular mass liquid crystals and does not take into account that connections of consecutive segments reduce the system entropy. Experimentally, the N–I transition temperature increases as the degree of polymerization increases. The higher T_c prediction for a freely-jointed-rod chain of liquid crystalline polymers is expected from the same argument. Meanwhile, the latent entropy at transition is reasonably less than that of the Maier–Saupe results.

For the elastically-jointed-rod chain, the nematic mean field energy is expressed as

$$U_n = -\sum_i pSP_2(\mathbf{n}_i), \tag{2.81}$$

where p is the Maier–Saupe coefficient of one monomer and n_i denotes the orientation of the i-th segment. In addition, there is an elastic energy associated with the bending of the successive rods,

$$U_B = \sum_i \frac{q}{2}(\mathbf{n}_{i+1} - \mathbf{n}_i)^2, \tag{2.82}$$

where, q is the bend elasticity.

Thus the Hamiltonian of a polymer is expressed as

$$H_i = \sum_i \left[-pSP_2(\mathbf{n}_i) + \frac{q}{2}(\mathbf{n}_{i+1} - \mathbf{n}_i)^2 \right]. \tag{2.83}$$

In principle, n_i can be any orientation in three-dimensional space. For simplicity, we limit the orientation of each segment to six directions, *i.e.*, the three orthogonal axes in a cubic lattice. The six orientations are: $n = 1$ for pointing up, $n = -1$ for pointing down and $n = 0$ for four transverse directions, rightward, leftward, forwards and backward, the degeneracy being four, as shown in Figure 2.16.

Split the Maier–Saupe potential into two terms and express the partition function as

$$Z = \sum_{n_i} \prod_i \exp \left\{ \frac{a}{2}[P_2(n_{i+1}) + P_2(n_i)] - \frac{b}{2}(n_{i+1} - n_i)^2 \right\}, \tag{2.84}$$

where $a = \beta pS$ and $b = \beta q$. b is actually the ratio of persistence length to repeated unit length, l/l_0. We assume that b is constant. The summation $\sum$ is made over all possible orientations of each segment while the
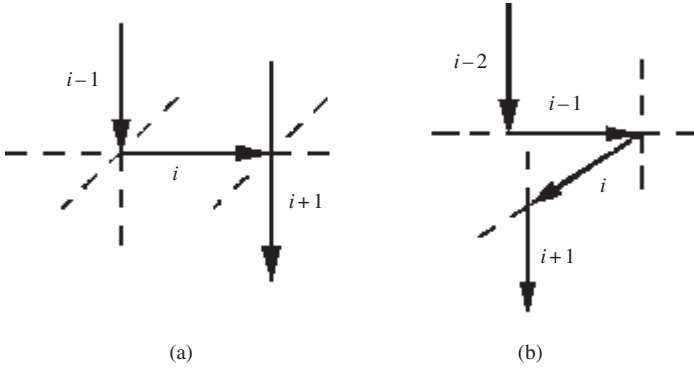
Figure 2.16.   The discrete orientations of rods in Warner and Wang's model (1992c).

multiplication $\prod$ is the product over all segments along the chain. To meet the requirement of the transverse matrix method, we assume $n_{N+1} = n_1$. Because there are many segments in a chain the assumption does not affect the results. The partition function can be further written as a matrix form

$$Z = \cdots M^{(i-1)}_{\xi\eta} M^{(i)}_{\eta\zeta} M^{(i+1)}_{\zeta\delta} \cdots , \qquad (2.85)$$

where the repeated subscript $\eta\eta, \xi\xi, \ldots$ indicates the summation over all orientations of n and the superscript i is the index for the respective segment. The 6×6 matrix $\boldsymbol{M}$ is

$$M^{(i)}_{\eta\zeta} = \left\langle n^{(i)}_\eta \,|\exp[-\beta H(n_i, n_{i+1})]|\, n^{(i+1)}_\xi \right\rangle . \qquad (2.86)$$

The operator $H(n_i, n_{i+1})$, given by Equation 2.83, on $|n>$ generates the Boltzmann factor of Equation 2.86. The degeneracy $g = 4$ makes it possible to project the 6×6 matrix $\boldsymbol{M}$ to a 3×3 one. This deduction significantly simplifies the underlying problem and allows one to have analytic solutions of the eigenvalues of the matrix.

The transfer matrix $\boldsymbol{M}$ of 3×3 is accordingly expressed as

$$M = \begin{pmatrix} e^a & 2e^{a/4-b/2} & e^{a-b/2} \\ 2e^{a/4-b/2} & (1+2e^{-b/2}+e^{-2b})e^{a/2} & 2e^{a/4-b/2} \\ e^{a-2b} & 2e^{a/4-b/2} & e^a \end{pmatrix} , \qquad (2.87)$$

where $a = pS/k_BT$, $b = q/k_BT$. b is actually associated with the chain rigidity. The coefficients of the matrix elements result from the degeneracy.

Because each matrix is the same and thus the partition function is the trace of the product of the N matrices, M^N

$$Z = \text{Tr } M^N = \sum_{j=1}^{3} \lambda_j^N, \qquad (2.88)$$

where Tr denotes the trace and λ_i is the i-th eigenvalue of the matrix. The trace of N-power of matrix, M^N is the sum of the N-power of all eigenvalues. Because N is very large, Z is dominated by the largest eigenvalue, λ_{max}. The free energy of a nematic polymer is associated with the largest eigenvalue, λ_{max}, of the matrix $\boldsymbol{M}$

$$\frac{F}{Nk_BT} = -\ln\lambda_{max} + \frac{T'p^2}{2}, \qquad (2.89)$$

where $T' \equiv k_BT/p$ is the reduced temperature.

Substituting λ_{max} into the equation, we obtain the free energy which is a function of the nematic coupling a, the chain rigidity (l/l_0) and the temperature T. The transition temperature can be obtained from the form of free energy. The form of free energy is rather complicated. We apply the Landau-de Gennes theory to analyze it.

Landau used a very simple form of free energy to describe systems such as the para-magnetic system where the magnetic polarization M is the order parameter. The idea has been extended by de Gennes (1973) to deal with nematic liquid crystals. The free energy is given in the extended Landau-de Gennes form as

$$F = a(T - T^*)S^2 - BS^3 + CS^4, \qquad (2.90)$$

where a, B and C are positive coefficients. Figure 2.17 depicts the relationship of free energy and the order parameter S for various temperatures. When temperature is high, the isotropic state is stable. If the temperature is low, the minimum free energy exists at a non-zero order parameter, *i.e.*, the nematic phase is stable. When the temperature is between T' and T'' there are two minimums of free energy. The one with zero free energy corresponds to the isotropic phase while the other corresponds to the nematic phase. T' is the limit of temperature at which the super-cooled isotropic phase exists while T'' is the limit at which the nematic phase completely vanishes. There is a temperature at which the two minima have the same free energy for the nematic to isotropic transition. At the N–I transition, the order parameter jumps from zero in the isotropic phase to a finite value
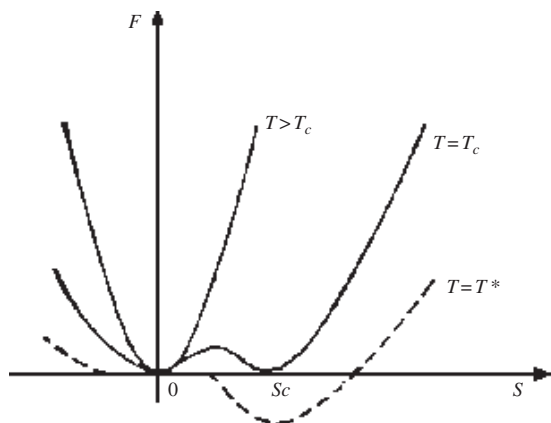
Figure 2.17.   Free energy *vs.* order parameter S for various temperatures according to Landau–de Gennes theory.

of the nematic phase. This is the first order phase transition. At temperature T' where the quadratic term vanishes, *i.e.*, $T' = T^*$, is the pseudo second phase transition temperature. In fact, the N–I transition is a weak first order transition. We quantitatively analyze the problem below.

The stable state of the system is given by

$$2a(T - T^*)S - 3BS^2 + 4CS^3 = 0. \qquad (2.91)$$

This is a cubic equation. One solution $S = 0$ is for the isotropic phase. The second solution is for the nematic phase which is a function of temperature

$$S = \frac{3}{8}\left[1 + \sqrt{1 + \frac{32a(T - T^*)C}{9B^2}}\right]. \qquad (2.92)$$

The third solution corresponds to the maximum free energy at which the system is not stable.

At the N–I transition, the free energy is the same for both isotropic and nematic phases with different order parameters, 0 and S_c. Thus the N–I transition temperature is obtained as

$$T_c = T^* + \frac{B^2}{(4aC)}. \qquad (2.93)$$

The first term in the formula is the pseudo second order phase transition temperature T^*. The coefficient B is not great, therefore the second term is not significant. The difference of T_c and T^* is small, experimentally only a few degrees difference.

Expanding the free energy in Equation 2.89 to the fourth power gives the Landau–de Gennes form. One can evaluate the thermodynamic properties accordingly.

In the elastically-jointed-rod chain, the mean square end-to-end distance along the director tends to be a rod as q approaches infinity or T is very small, *i.e.*,

$$\langle R_z^2 \rangle \to N^2 l_0^2 \quad \text{as} \quad b \to \infty. \tag{2.94}$$

2.4.4. Discrete and continuum chain models

If we take the limit of the rod length $l_0 \to 0$ and the number of rods $N \to \infty$ such that the polymer length is kept constant $L = Nl_0$, we have an integral instead of a summation:

$$L = \sum_i h_i \to \int_0^L ds, \tag{2.95}$$

where h_i is the length of each segment along the jointed-rods and s is the contour length of a point along a continuous chain. The discrete elastically-jointed-rod chain thus evolves into a continuous elastic chain or the worm chain. In this case, the bending elastic energy becomes

$$U_{el} \to \sum_i h \frac{1}{2} qh \left(\frac{\theta_{i+1} - \theta_i}{h} \right)^2 \to \frac{1}{2} \int_0^L ds \varepsilon \left(\frac{d\theta}{ds} \right)^2, \tag{2.96}$$

where the elastic constant $\varepsilon = ql_0$ as $q \to \infty$ and $l_0 \to 0$. Meanwhile, the nematic part, U_{nem}, becomes

$$U_{nem} \to -\sum_i h \frac{p}{h} SP_2(\cos \theta_i) \to -\int_0^L ds v SP_2(\cos \theta(s)), \tag{2.97}$$

where $v = p/l_0$ as $l_0 \to 0$ and $p \to 0$. v is the nematic coupling constant per unit length.

These two parts constitutes the energy for a worm-like nematic polymer. The first part (Equation 2.96) demands a slow reversal as a chain evolves and favors parallel alignment, but the second term (Equation 2.97) prefers both anti-parallel and parallel alignments, and a rapid reversal of

orientations. A natural scale of length ξ emerges to balance the two effects. In terms of the parameters p and q of the discrete chain

$$\xi = \sqrt{\frac{q}{pS}} \qquad (2.98)$$

or in terms of v and ε of the worm chain

$$\xi = \sqrt{\frac{\varepsilon}{vS}}. \qquad (2.99)$$

If $\xi < l_0$, it becomes the case of the discrete picture and jointed-rods are applicable. If $\xi > l_0$, however, the elastically discrete polymer evolves into a worm chain, *i.e.*, an elastically homogeneous chain. The orientation change can then take place over a length comparable to l_0. With this continuum of allowed orientational states, the worm chain accurately represents the angular entropy of the real polymer.

2.5.   WORM CHAIN MODEL OF LIQUID CRYSTALLINE POLYMERS

2.5.1.   Path integral description for polymers

The path integral technique was first proposed by Feynmann (Feynmann & Hibbs, 1965). The purpose of this technique was to deal with questions in quantum mechanics. It has been applied to the study of the statistical mechanics of polymer systems (Kreed, 1972; Doi & Edwards, 1986) and liquid crystalline polymers as well (Jahnig, 1981; Warner *et al.,* 1985; Wang & Warner, 1986). The path integrals relate the configurations of a polymer chain to the paths of a particle when the particle is undergoing Brownian or diffusive motion.

The path integral for a jointed-chain polymer, with a step length c, is given by

$$G(\boldsymbol{R}, \boldsymbol{R}'; L) = \int_{r(0)=\boldsymbol{R}}^{r(L)=\boldsymbol{R}'} D[\boldsymbol{r}(s)]$$

$$\times \exp\left\{-\int_0^L ds \left[\frac{3}{2c}\dot{\boldsymbol{r}}^2(s) + U(\boldsymbol{r}(s))\right]\right\} \qquad (2.100)$$

which is also described by the differential equation

$$\left[\frac{\partial}{\partial s} - \frac{c}{6}\nabla_{\boldsymbol{r}}^2 + U(\boldsymbol{r})\right] G(\mathbf{R}, \mathbf{R}'; L) = \delta(\mathbf{R} - \mathbf{R}')\delta(L), \qquad (2.101)$$

where $D_t = c/6$ is the translational diffusion coefficient. $G(\boldsymbol{R}, \boldsymbol{R}'; L)$ is the Green function for the diffusion equation or propagator, and $\delta(\boldsymbol{R} - \boldsymbol{R}')$ the Dirac delta function.

If the chain is worm-like, the bending of the chain will cost the energy

$$U_{el} = \int_0^L \frac{\varepsilon}{2}\left[\frac{d\boldsymbol{u}(s)}{ds}\right]^2 ds, \qquad (2.102)$$

where ε is the bending constant, $\boldsymbol{u}$ is the tangent along the chain at contour length s, $\boldsymbol{u} \equiv \dot{r} = \partial r/\partial s$, and is a unit vector.

This elastic energy give rise to the Boltzmann factor of Equation 2.100, therefore the path integral becomes the case of a worm-like chain, $\dot{\boldsymbol{u}} \equiv \partial \boldsymbol{u}/\partial s$,

$$G(\boldsymbol{R}, \boldsymbol{R}'; \boldsymbol{U}, \boldsymbol{U}'; L) = \int_{\boldsymbol{r}(0)=\boldsymbol{R}}^{\boldsymbol{r}(L)=\boldsymbol{R}'} D[\boldsymbol{r}(s)]$$

$$\times \int_{\boldsymbol{u}(0)=U}^{\boldsymbol{u}(L)=U'} D[\boldsymbol{u}(s)]\delta\left[\boldsymbol{R} - \int_0^L ds\,\boldsymbol{u}(s)\right]$$

$$\times \exp\left\{-\int_0^L ds\left[\frac{3}{2c}\boldsymbol{u}^2(s) + \frac{\beta\varepsilon}{2}\dot{\boldsymbol{u}}^2(s)\right]\right\} \qquad (2.103)$$

where

$$\boldsymbol{R} = \int_0^L \boldsymbol{u}(s)ds = \boldsymbol{r}(L) - \boldsymbol{r}(0). \qquad (2.104)$$

The unit vector $\boldsymbol{u}$, enables Equation 2.103 to be rewritten as, by taking $\int D[R(s)]$,

$$G(\boldsymbol{U}, \boldsymbol{U}'; L) = \int_{\boldsymbol{u}(0)=U}^{\boldsymbol{u}(L)=U'} D[\boldsymbol{u}(s)] \exp\left[-\int_0^L ds\frac{\beta\varepsilon}{2}\dot{\boldsymbol{u}}^2(s)\right], \qquad (2.105)$$

where the uninteresting term $\exp(-3L/2c)$ is absorbed into the normalization factor.

Analogous to Equation 2.101, G satisfies the diffusion equation

$$\left[\frac{\partial}{\partial s} - \frac{1}{2\beta\varepsilon}\nabla_{\mathbf{u}}^2\right] G(\mathbf{U}, \mathbf{U}'; L) = \delta(\mathbf{U} - \mathbf{U}')\delta(L), \qquad (2.106)$$

where $1/(2\beta\varepsilon)$ is a rotational diffusion constant which we denote by D_r, or D below. The Green function G can be expressed as an infinite series in the eigen-functions $Y_{lm}(\theta, \phi)$, the Spherical harmonics. θ and ϕ are the polar and azimuthal angles that $\boldsymbol{u}$ makes with respect to a reference direction, *e.g.*, the z axis.

Having sketched the concepts of the path integral approach in conventional polymers, we now shift to the nematic liquid crystalline polymers. In the smectic phase of polymers, the positional order term is expected to become important (Renz & Warner 1986).

We are concerned here only with polymers in their nematic phase with no positional potential and with a uniaxial system. The path integral for nematic polymers is given by (Warner *et al.,* 1985)

$$Z = \int D[u(s)] \exp\left\{\beta a S \int ds P_2(\cos\theta) - (\beta\varepsilon/2) \int ds \left[\frac{du(s)}{ds}\right]^2\right\}.$$
$$(2.107)$$

Note that the path integral in Equation 2.107 is in fact the same as that for diffusion of a point on the surface of a unit sphere with diffusion constant $D = 1/(2\beta\varepsilon)$. The reciprocal of this diffusion constant is actually the persistence length l. In the presence of a potential $-vSP_2(\cos\theta)$, Equation 2.107 reduces to a "Schrodinger type" differential function:

$$\left[\frac{\partial}{\partial s} - D\nabla_{\boldsymbol{u}}^2 - \beta v S P_2\right] G(\mathbf{U}, \mathbf{U}'; s, s') = \delta(\mathbf{U} - \mathbf{U}')\delta(s - s'). \qquad (2.108)$$

If we relax the unit vector condition of $\boldsymbol{u}$, we can obtain an analytical solution to the differential equation. The relaxation of this condition allows the use of the Wiener integral in the case.

Unfortunately, this does not give a good description of a polymer. It fails to reproduce rod-like behavior when an isotropic chain is short (Freed, 1972).

The green function G can be expressed in the Spheroidal wave functions, $Sp_n(z)$, *i.e.*,

$$G(z, z'; s, s') = \sum_{n=0}^{\infty} \frac{2n+1}{2} Sp_n(z) Sp_n(z') \exp(-\lambda_n D|s - s'|), \qquad (2.109)$$

where $z = \cos\theta$ and $\lambda_n = (2/3)\Delta^2$ are the eigenvalues where

$$\Delta^2 = -3v\varepsilon S\beta^2 = \frac{-3S}{T'^2}$$

with $T' = k_B T/\sqrt{v\varepsilon}$, the reduced temperature. G is Markovian.

The partition function is the integral of G over all orientations

$$Z = \iint dz\, dz'\, G(z, z'; L)$$
$$= \sum_{n=0}^{\infty} \frac{2n+1}{2} \left[\int dz\, Sp_n(z) \right]^2 \exp\left(\frac{-\lambda_n L}{l} \right). \qquad (2.110)$$

If the chain is reasonably long, compared to the persistence length, only the ground state where $n = 0$ is dominant and taken into account. Therefore, the free energy is expressed by

$$F = \lambda_0 + \frac{S^2}{(T')^2}. \qquad (2.111)$$

2.5.2. Anisotropic conformation

In the isotropic phase, differential Equation 2.106 is simplified to the Legendre equation with eigenfunctions, the Legendre polynomials $P_n(\cos\theta)$ and the eigenvalues $n(n+1)$.

The mean square end-to-end distance component parallel to the director is given by

$$\langle R_z^2 \rangle = \int_0^L \int_0^L ds\, ds' \langle \cos\theta \cos\theta' \rangle$$
$$= \frac{1}{3} \int_0^L \int_0^L ds\, ds' \exp\left[\frac{-(\lambda_1 - \lambda_0)|s - s'|}{l} \right]$$
$$= \frac{[Ll - l^2 \frac{(1-e^{-2L/l})}{2}]}{3}. \qquad (2.112)$$

The three components of the mean square end-to-end distances are the same.

If the chain is long enough, the chain conformation is of random walk

$$\langle \mathbf{R}^2 \rangle = Ll \qquad (2.113)$$

and the step length is the persistence length l.

If L/l is very small then

$$\langle \mathbf{R}^2 \rangle = L^2. \tag{2.114}$$

The chain becomes a rod.

For nematic polymers, their conformation is no longer spherical, but a prolate ellipsoid. The mean square end-to-end distance of the chain at its nematic phase is anisotropic.

For large L/l, the components parallel and perpendicular to the director are given respectively by

$$\langle R_z^2 \rangle = \frac{3}{4} \frac{Ll}{\lambda_1 - \lambda_0} \left[\int_{-1}^{1} Sp_0(z) Sp_1(z) z \, dz \right]^2, \tag{2.115}$$

$$\langle R_x^2 \rangle = \langle R_y^2 \rangle = \frac{3}{8} \frac{Ll}{\lambda_1^1 - \lambda_0} \left[\int_{-1}^{1} Sp_0(z) Sp_1^1(z) \sqrt{1 - z^2} \, dz \right]^2, \tag{2.116}$$

where Sp_1^1 and λ_1^1 are the eigenfunction and eigenvalue, respectively, of the first rank Spheroidal wave equation. The two mean square end-to-end distance components *vs.* the intermediate parameter $-\Delta^2$ are shown in Figure 2.18. The abscissa is normalized by the value in the isotropic phase.
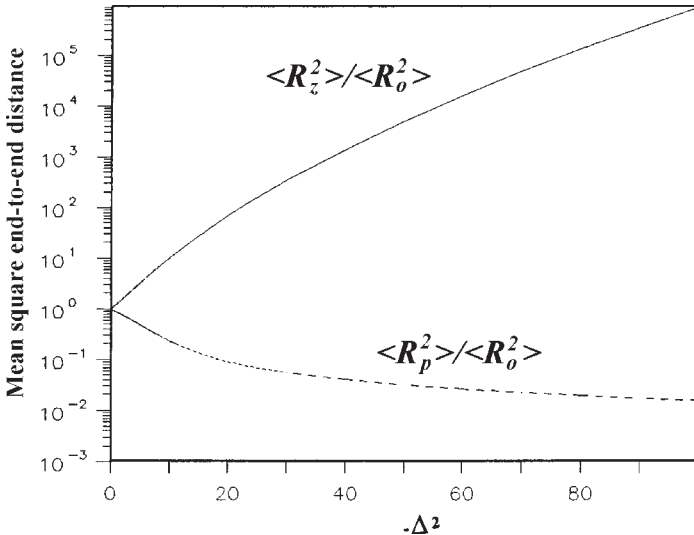
Figure 2.18.   The mean square end-to-end distance of worm chains *vs.* $-\Delta^2$. (From Wang, 1997.)

As polymers enter from the isotropic phase into the nematic phase, $-\Delta^2$ jumps from zero to a finite value of about 7. The corresponding ratio of the mean square root of the end-to-end distance component parallel to the director is about 3.

2.5.3.   Order parameter

In terms of the Spheroidal wave function, the order parameter may be re-expressed as

$$S = \int_0^1 [Sp_0(z)]^2 P_2(z) dz. \tag{2.117}$$

$Sp_0(z)$ is a function of Δ^2, hence, S and T'. Thus, the equation is self-consistent.

The nematic-isotropic transition occurs when the free energies of the nematic and the isotropic phases are equal, *i.e.*,

$$\lambda_0 + \frac{S^2}{(T')^2} = 0, \tag{2.118}$$

where λ_0 is the eigenvalue of the ground state of the Spheroidal wave function.

The S vs. T' relationship (Wang & Warner, 1986) is similar to the well-known Maier-Sauipe shape, the temperature scale being $T' = k_B T/\sqrt{\nu\varepsilon}$ instead of $T' = k_B T/p$. The order parameter decreases as T' increases until the critical temperature $T'_c = 0.388$. The order parameter discontinually jumps from 0.356 to zero. Because T' is the reduced temperature the transition temperature T'_c is a function of the geometric mean of ν and ε. The greater v, the higher T'_c. The more ε, the more stable the nematic phase. These conclusions are consistent with experiments. It was found that the critical order parameter for the semi-flexible liquid crytalline polymers ranges from 0.3 to 0.45.

2.5.4.   Dependence of N–I transition on polymer chain length

It is worth pointing out that after expanding the free energy in the Landau–de Gennes form and taking into account the entropic contribution of the free ends of the chain (contrary to circle polymers) and the $n = 2$ term in
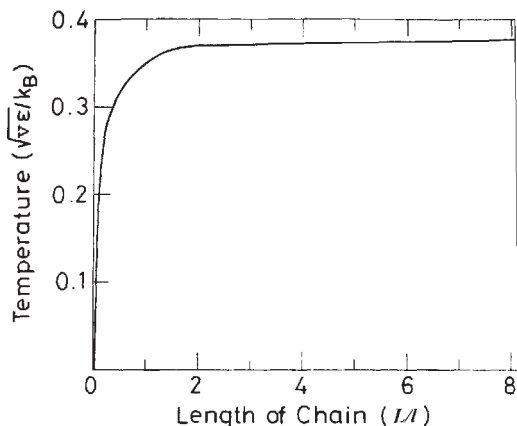
Figure 2.19.   N–I transition temperature T_c against the chain length L. (From Wang & Warner, 1986.)

Equation 2.110, we obtain the analytical expression for the pseudo-second-phase-transition temperature (Wang, 1995a)

$$T'^* = \frac{2}{15}\left[1 - l/6L(1 - e^{-\frac{6L}{l}})\right],\qquad(2.119)$$

which is reminiscent of the numerical calculation of the N–I transition temperature *vs.* the chain length or the degree of polymerization, shown in Figure 2.19.

The N–I transition temperature, or the pseudo-second-phase-transition temperature, increases as the chain length increases and then saturates to a finite value when L/l is greater than, *e.g.*, about 1.5. Griffin *et al.* (1989) and Blumstein *et al.* (1984) found that for a monomer, dimer, oligomer as well as a polymer with the same building units displaying a nematic phase, the transition temperature increases with an increasing degree of polymerization and then rapidly saturates, as shown in Figure 2.20. Good agreement was found for the above theory and experimental data.

2.5.5.   Latent entropy at transition

Ignoring the temperature dependence of ε, as justified by Jahnig (1979), the latent entropy ΔE for a repeat unit at the transition (Wang & Warner, 1986) is

$$\frac{\Delta E(T_c)}{N} = 1.69R\left(\frac{l_0}{l}\right),\qquad(2.120)$$
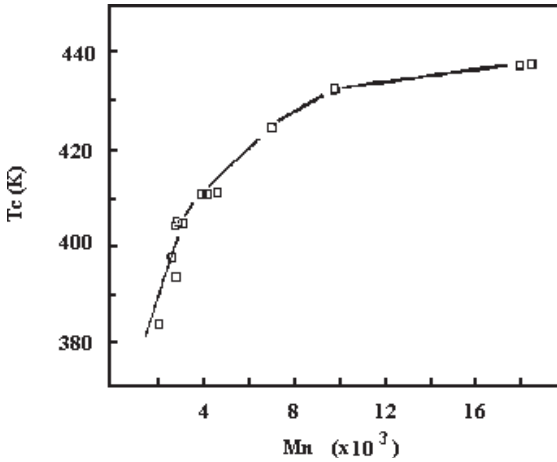
Figure 2.20. N–I transition temperature T_c against the molecular weight. (From Blumstein *et al.* 1984.)

where N is the degree of polymerization and l_0 and l are lengths of the repeat unit and persistence length.

It is known that the persistence length is normally about 2–10 times that of the repeat units for polymers, depending on the real structure of polymers. It is seen that the latent entropy is no longer a universal value, as in the Maier–Saupe theory. Some experimental results has been reviewed by Luckhurst (1986).

The worm chain in a possible polar nematic phase was discussed as well (Wang & Lam, 1992). The dipolar interaction was taken into account in addition to the quadrupolar interaction. It results in the complexity of the phase diagram.

2.6. MAIN CHAIN LIQUID CRYSTALLINE POLYMERS WITH SPACERS

2.6.1. Molecularly non-homogeneous liquid crystalline polymers

Most main chain liquid crystalline polymers are composed of mesogenic units linked by spacers with varying degrees of flexibility, such as repeated methylene, oxyethylene, or siloxane groups, *etc.*, in order to reduce the
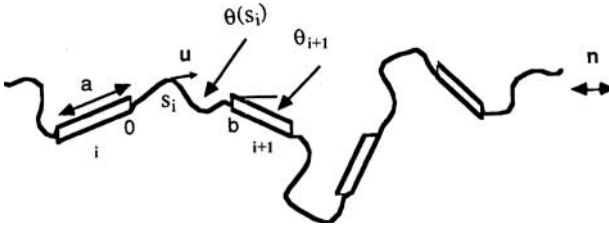
Figure 2.21.   Schematic of liquid crystalline polymers with spacers where i denotes the *i*-th segments (the *i*-th spacer and the *i*-th rod).

mesomorphic temperature of liquid crystalline polymers and to be able to process them. The participation of flexible spacers dramatically changes the properties of liquid crystalline polymers. These properties depend not only on the mesogenic units but also on the type of flexible spacers. The theoretical basis for these liquid crystalline polymers has been studied by, for example, Matheson & Flory (1981), Yurasova & Semenov (1991) and Wang & Warner (1992a,b).

Flexible spacers are constrained by the mesogenic units to which they are linked in order to have some orientational order. In turn, they affect the order of the mesogenic units which are not decoupled. It is also expected that the spacers have an order that differs from that of the mesogenic units.

The liquid crystalline polymer with spacers is schematically shown in Figure 2.21. In this polymer, the mesogenic units are modeled as rigid rods in a quadrupolar potential while the spacers are regarded as a worm chain according to the Spheroidal approach. The physical linkage is examined. Meanwhile, the molecular parameters such as the self and cross couplings between the rods and spacers (denoted by constants v_a, v_b and v_{ab}), the lengths of the two components, a and b, and the persistence length of spacer l, are also taken into account. In all that follows, the subscripts A and B denote rod and spacer segments, respectively.

The partition function Z of a polymer chain of this kind results from summing over all orientational angles θ_i for the rods and over all choices of the contours of chains, $\boldsymbol{u}(\theta)$ or $\theta(s)$, for the worm spacers:

$$z = \int \prod_{i=1}^{N} \exp[\beta_v U_A P_2(z_0^i)] \prod_{i=1}^{N-1} \delta(z_b^i - z_0^{i+1})$$

$$\times \prod_{i=1}^{N} [Sp_0(z_0^i) Sp_0(z_b^i) \exp\left(\frac{-\lambda_0 b}{l}\right) dz_0^i dz_b^i]. \qquad (2.121)$$

The Dirac delta functions, δ, ensure that the ends of spacers, B, have the same orientation as the consecutive A rods to which they are attached. U_A and U_B are the linear transformations of ϕS_a and $(1 - \phi)S_b$, S_a and S_b are the orders of A and B components, respectively, the tranformation matrix being associated with the self and cross couplings:

$$\begin{pmatrix} U_A \\ U_B \end{pmatrix} = \begin{pmatrix} v_a & v_{ab} \\ v_{ab} & v_b \end{pmatrix} \begin{pmatrix} \phi S_a \\ (1-\phi)S_b \end{pmatrix}.$$

The volume fractions of rods and worms, ϕ and $(1 - \phi)$, as prefactors in each term are due to the dilutions of each component.

Performing the summation over the rod's direction, the partition function becomes, for large N

$$Z = \exp\left(\frac{\lambda_0 N b}{l}\right) \left\{ \int \exp[\beta v U_A P_2(z)[Sp_0(z)]^2 dz \right\}^N. \qquad (2.122)$$

We are now able to evaluate the order parameters of rods and spacers *vs.* temperature (Figure 2.22), the transition temperature as a function of the molecular parameters, such as the geometrical lengths a, b and l (it has the length dimension but is actually the rigidity of the worm spacers), and the coupling constants v_a, v_b and v_{ab}, shown in Figure 2.23(a–e). In these figures, the transition temperature T_{red} is relative to the N–I transition temperature of the pure rods, *i.e.*, $T_0 = 0.22 v_a/k_B$.
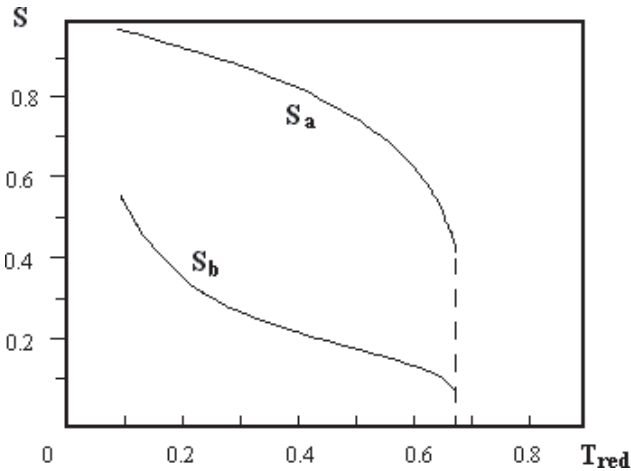
Figure 2.22. The order parameters S *vs.* reduced temperature T_{red}. (From Wang & Warner, 1992a.)
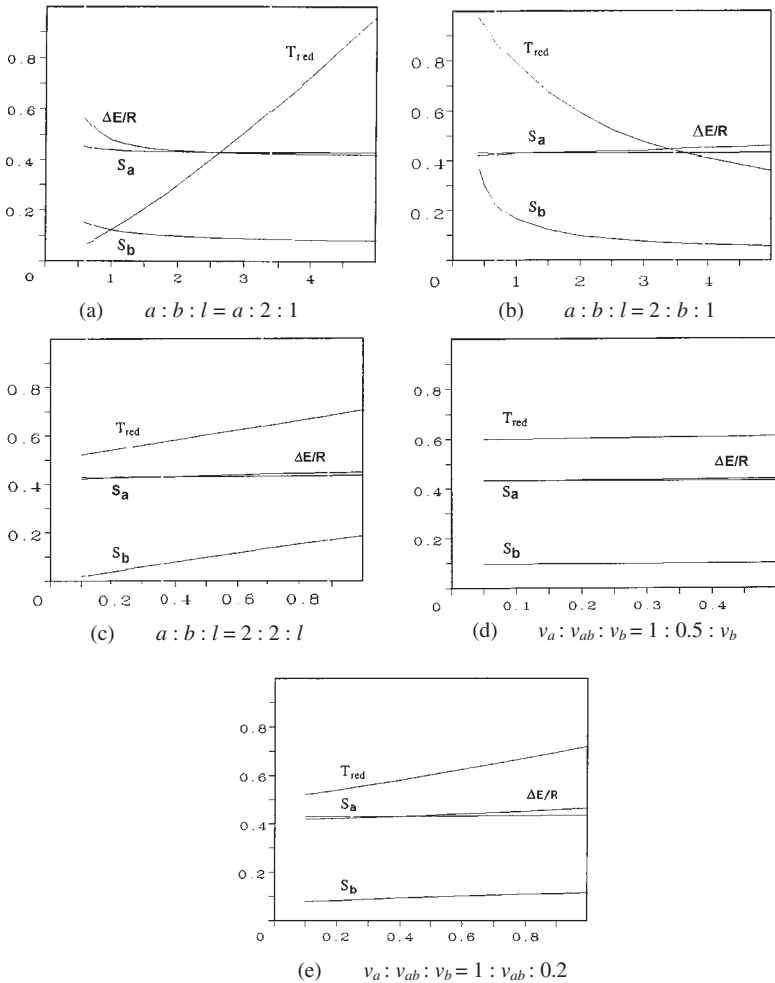
Figure 2.23.   The transition temperature against the molecular parameters: (a) rod's length a; (b) spacer's length b; (c) persistence length of spacer l; (d) self coupling constant of spacers v_b; (e) cross coupling constant v_{ab}. (From Wang & Warner, 1992a.)

The following conclusions can be obtained from these plots. The transition temperature T_c increases significantly as v_a increases, and increases at an intermediate speed with v_{ab}, but is weakly dependent on v_b. T_c increases as the length of the rods a and the persistence length l of the worm spacers increase, while T_c decreases with increasing spacer length, b. The order of mesogenic units is generally greater than that of spacers.
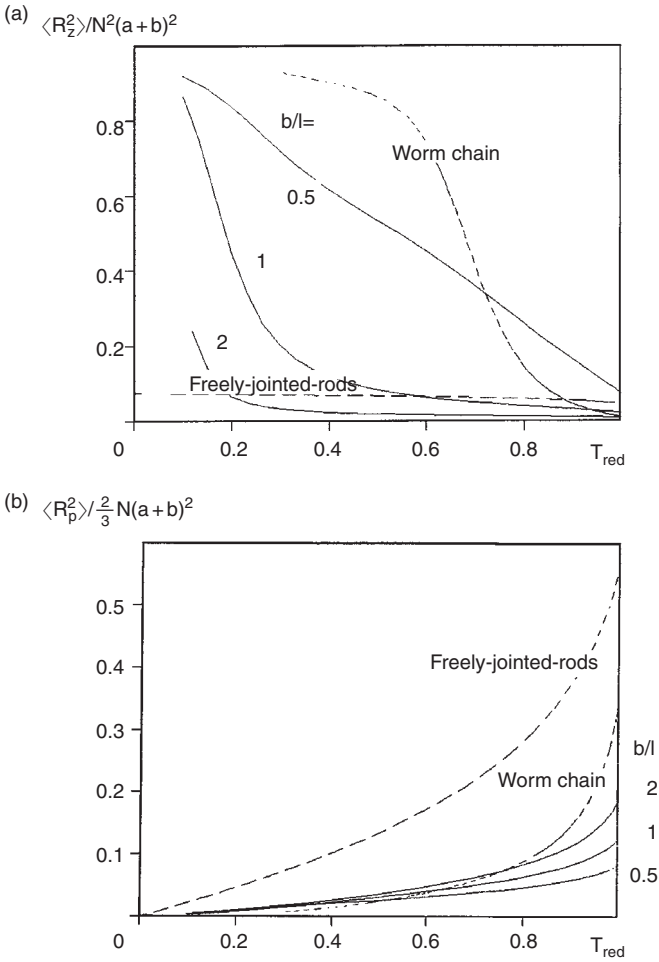
Figure 2.24. The mean square end-to-end distance (a) $< R_z^2 >$ and (b) $< R_p^2 >$ against the reduced temperature T_{red}. (From Wang & Warner, 1992a.)

The latter's order is enhanced by the former. Experiments are being carried out on polymers with deuterated spacers, and/or deuterated mesogenic groups. The results of such experiments can be used to test the theory.

In Figure 2.24(a,b), the mean square end-to-end distance components along and perpendicular to the director are plotted respectively against the temperature relative to the transition temperature of the pure rods. In order to emphasize their features, we apply different vertical scales for $\langle R_z^2 \rangle$ and $\langle R_p^2 \rangle$, the former is reduced by $N^2(a+b)^2$, the value in perfect order; while

the latter is relative to the random walk value in the isotropic phase. For comparison, the mean square end-to-end distance of both the freely-jointed-rod chain and worm chain is plotted in the same figures. $\langle R_z^2 \rangle$ and $\langle R_p^2 \rangle$ are no longer universal curves, depending on the molecular parameters.

One of the advantages is that this non-homogeneous model connects the statistical properties of main chain liquid crystalline polymers to their molecular parameters.

2.6.2.   Pseudo-second-order-phase-transition temperature

For simplicity, assume that v_{ab} is the geometrical mean of v_a and v_b, *i.e.*, the Berthelot law, and extend the free energy derived from Equation 2.122 in the power series of S_a and S_b. The zero determinant of the quadratic coefficients gives the pseudo-second-phase-transition temperature as follows (Wang, 1995a)

$$k_B T^* = \left(\frac{3a^2 v_a + blv_b + 2al\sqrt{v_a v_b}}{15(a+b)} \right). \qquad (2.123)$$

In the second-order approximation of the free energy, above $T*$, S_a and S_b are both zero. Below $T*$, the order parameters are non-zero. At $T*$, the quadratic terms vanish. This formula illustrates the pseudo-second-phase-transition temperature *vs.* the molecular parameters that shows the same shapes as those of the numerical calculations of the N–I transition temperature T_c, mentioned above.

2.6.3.   Hinge effect

On the basis of this argument, we may be able to deal with the hinge effect, *i.e.*, the effect of the orientational deviation α of the conjunctive mesogen and spacer on the phase transition. The picture is depicted in Figure 2.25.

The free energy becomes dependent on the deviation α, *i.e.*,

$$\frac{F}{Nk_BT} = \frac{\beta(v_a U_A S_a + v_b U_B S_b)}{2} + \frac{\lambda_0 b}{l} - \left(\frac{1}{2\pi}\right)^2 \iint d\phi d\phi'$$
$$\times \int \exp[\beta v U_A P_2(\cos\theta)] S p_0(\cos\theta) S p_0(\cos\gamma) d\theta, \qquad (2.124)$$
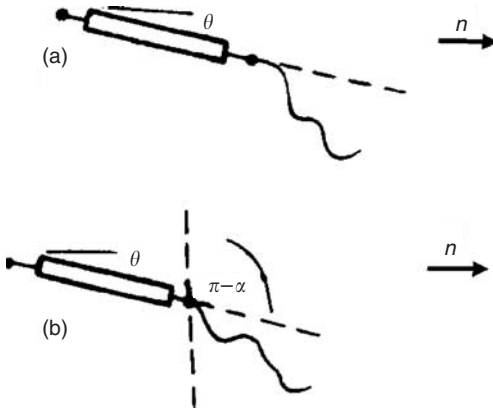
Figure 2.25.   Schematic of the hinge effect of the main chain liquid crystalline polymers. (From Wang, 1995b.)

where γ is the angle of the spacer at the conjunction to the director which is associated with the mesogenic rod's orientation θ, the deviation angle α and their azimuthal angles ϕ and ϕ'

$$\cos \gamma = \cos \theta \cos \alpha + \sin \theta \sin \alpha \cos(\phi - \phi'). \qquad (2.125)$$

If the Spheroidal wave function $Sp_0(\cos \theta)$ is expanded in terms of the Legendre polynomials as

$$Sp_0(\cos \theta) = \sum_{n=0}^{\infty} a_n P_n(\cos \theta) \qquad (2.126)$$

and the integral of $Sp_0(\cos \gamma)$ over ϕ and ϕ' in Equation 2.124 gives

$$\left(\frac{1}{2\pi}\right)^2 \int \int d\phi d\phi' Sp_0(\cos \gamma) = \sum_{n=0}^{\infty} a_n P_n(\cos \theta) P_n(\cos \alpha) \qquad (2.127)$$

then the pseudo-second-phase-transition temperature can be deduced. The transition resulting from the hinged case is

$$\frac{T^*(\alpha) - T^*(0)}{T^*(0)} = -\frac{\sin^2 \alpha}{4} \frac{l^2 v_b + 6al\sqrt{v_a v_b}}{3a^2 v_a + bl v_b + 2al\sqrt{v_a v_b}}, \qquad (2.128)$$

where $T^*(0)$ and $T^*(\alpha)$ are for non-hinged and hinged cases, respectively. The difference is proportional to the square of $\sin \alpha$. For example, as

$a = b = l$ and $v_b/v_a = 0.1, \alpha = 45°$, the left hand side of Equation 2.128 is $-1/15$. If the transition temperature of the non-hinged $T^*(0) = 180\,°C$, the hinged temperature will be $150\,°C$.

The well known even-odd effect in liquid crystals may be attributed to the hinge effect. For liquid crystalline polymers with the even carbon atoms in their spacers, the overall contribution of even $-CH_2-CH_2-$ bonds makes the conjunctions bent. The odd counterparts do not have such an effect. Thus, the transitions for even ones are lower than those of odd ones. This hinge effect offers an explanation for the even-odd effect.

2.7.   SIDE CHAIN LIQUID CRYSTALLINE POLYMERS

In this section, we are concerned with another kind of liquid crystalline polymer – side chain liquid crystalline polymers. According to the ways in which the side chains are connected to the backbone, they are classified into two main categories—the end-on side chain liquid crystalline polymers (Ringsdorf & Schneller, 1981) in which the side chains are terminally attached to backbone, and the side-on (laterally attached) side chain liquid crystalline polymers (Hessel & Finkelmann, 1985). Recently, shoulderly attached liquid crystalline polymers (Gray *et al.*, 1989) were synthesized in which the side chain attachment is off-set from the center of the side chain. There is a kind of side chain liquid crystalline polymers where both backbones and side chains are comprised of mesogenic groups, *i.e.*, the combined liquid crystalline polymers. More recently, a co-polymer (Dumon *et al.*, 1995) combining end-on mesogenic groups and side-on chromophores was prepared which exhibits a liquid crystal phase. We will limit ourselves to the end-on side chain nematic polymers in this discussion.

2.7.1.   Model

A model presented by Wang & Warner (1987) quantitatively describes the statistical mechanics of side chain nematic polymers with a semi-flexible backbone and stiff mesogenic side chains. In general, side chains and backbones have different orders, the former denoted by S_A and the latter denoted by S_B, respectively. The phase types, phase diagrams and backbone conformations in each phase is dependent on the competition of side chains of various lengths, x, and backbone of various stiffness, ε. Mesogenic

side chains prefer to align parallel to each other because of anisotropic interactions, characterized by v_a, while the backbones behave like worm chains, characterized by ε and v_b. In addition, there is the hinge elasticity v_f, which forces side chains and backbones to be perpendicular, and the van der Waals attraction v_c, compelling two parts to be parallel.

The side chains are regularly attached to the backbone with the gap n. Assuming the cross-sections of the side chains and backbones are equal, the maximum possible value of the volume fraction is $\phi = x/(x+1)$. ϕ varies at fixed x by changing n, or equally at fixed n by changing x, or equally by changing x and n together. The lengths of backbones L and side chains x are all relative to the cross-section d and these lengths are equivalent to the number of cells with dimension d in the lattice.

In terms of the above five interaction constants $(v_a, v_b, v_c, v_f$ and $\varepsilon)$, we can write the mean field potential of a side chain as

$$U_S = -\{\phi v_a x S_A + [(1-\phi)v_c x - v_f]S_B\}P_2(z). \qquad (2.129)$$

Meanwhile the nematic energy of a backbone is given by

$$U_B = -\{(1-\phi)v_b S_B + [\phi v_c - v_f/n]S_A\} \int_0^L ds P_2[u_z(s)]. \qquad (2.130)$$

2.7.2.   Phase classification of side chain nematic polymers

According to the competition of all the interactions in the side chain nematic polymers, there are three uniaxial nematic phases: N_I, N_{II}, N_{III}. The three phases, each having a special conformation, may transform each other when the free energies are equal. These phases are shown in Figure 2.26 with the director pointing upward.

In the N_I phase, $S_A > 0$, but $S_B < 0$. The conformation of the backbone chain is discus-like, *i.e.*, is oblate shape, in which the mean square end-to-end distance along the director, $\langle R_Z^2 \rangle$ is less than the perpendicular component $\langle R_P^2 \rangle$. In the smectic phase the anisotropy of two components is greater than that in the nematic phase. At the extreme case the backbone is surpassed in a plane, which was predicted by Renz & Warner (1986) to exist in smectic polymers where backbones become confined between smectic layers formed by side chains, and has been seen by Moussa *et al.* (1987). In the extreme case, the backbone becomes a two-dimensional random walk when $S_B = -\frac{1}{2}$ and $S_A = 1$.
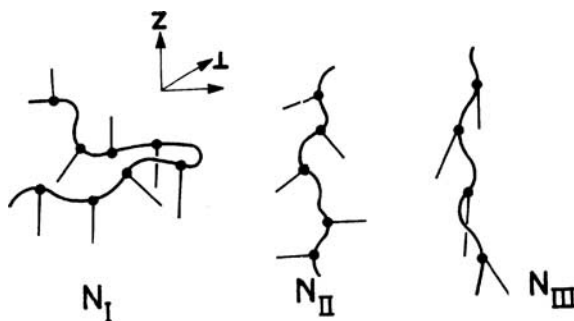
Figure 2.26.   The three nematic phases of side chain nematic polymers: N_I, N_{II}, N_{III}. (From Wang & Warner, 1987.)

In the N_{II} phase, $S_A < 0$, but $S_B > 0$, the conformation is bottle brush-like.

In the N_{III} phase, both S_A and S_B are positive.

In the latter two phases backbones have the spindle-like conformation, *i.e.*, the prolate shape with $\langle R_Z^2 \rangle > \langle R_P^2 \rangle$, the characteristic of main chain liquid crystalline polymers. Important means of investigating the conformations of side chain liquid crystalline polymers include small angle neutron scattering from deuterium-labeled chains (Kirst & Ohm, 1985), or small angle X-ray scattering on side chain liquid crystalline polymers in a small molecular mass liquid crystal solvent (Mattossi *et al.*, 1986), deuterium nuclear resonance (Boeffel *et al.*, 1986), the stress- or electro-optical measurements on crosslinked side chain liquid crystalline polymers (Mitchell *et al.*, 1992), *etc.* Actually, the nematic (or smectic modifications) phases of the side chain liquid crystalline polymers have been substantially observed by experiments.

2.7.3.   Order parameter and phase transitions

Figure 2.27(a) is an example of order parameters *vs.* temperature in which the length of the side chain is $x = 5$ and the volume fraction of the side chains is $\phi = 0.5$. Figure 2.27(b) shows S *vs.* T for $x = 3$ and $\phi = 0.4$, where T_0 is the N–I transition temperature of a neat backbone system. There are N_{III}, N_I and I phases in the former case while N_{II}, N_I and I phases are in the latter.
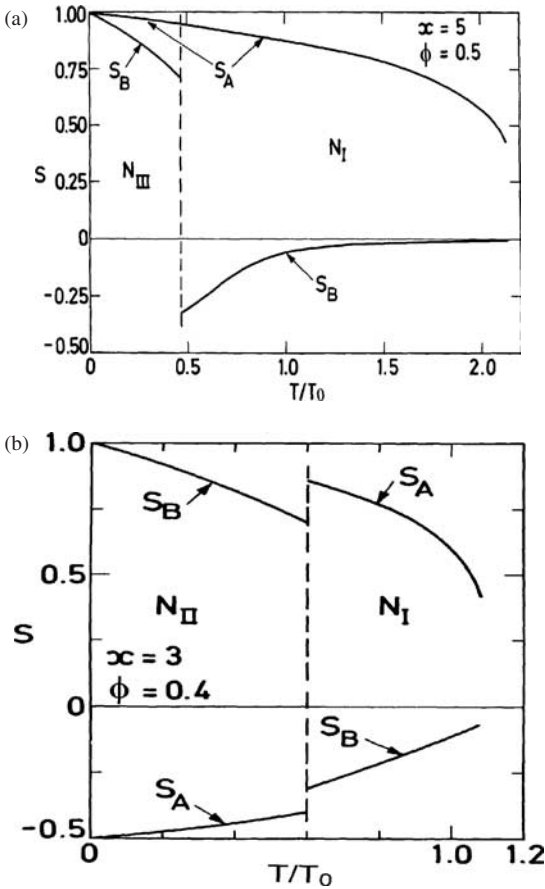
Figure 2.27. Orders *vs.* temperature of side chain nematic polymers (a) $x = 5$, $\phi = 0.5$ and (b) $x = 3, \phi = 0.4$. (From Wang & Warner, 1987.)

Experimental results of the order parameter S_A of side groups of side chain liquid crystalline polymers are shown in Figure 2.28, where the chemical formulae of the side group polymers are
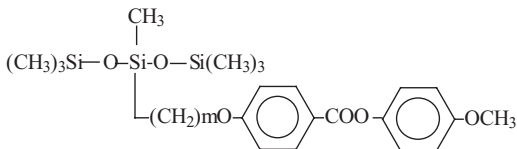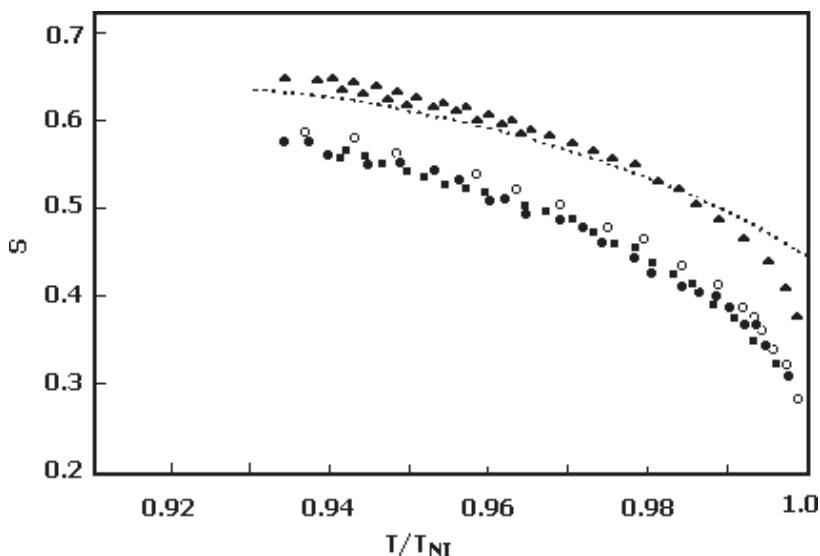
Figure 2.28.   Order parameter of side groups of side chain liquid crystalline polymers and small molecular mass liquid crystal *vs.* temperature. (Modified from Finkelmann, 1991. Reproduced by permission of John Wiley & Sons, Inc.)

where m = 3, marked by "●"; m = 4, by "○"; m = 6, by "■". The order parameter data of the counterpart small molecular mass liquid crystal, marked by "▲", is drawn in the same figure.

The phase diagram for a system of $x = 5$ and $\phi = 0.5$ is plotted in Figure 2.29 where the relative ratio of the coupling constants $v_a : v_b : v_c : v_f : \varepsilon/d = 3 : 2 : 1 : 3 : 2$. If all parameters are kept constant but v_c increased by a factor 2, N_{II} phase disappears while the N_{III} phase comes out, see Figure 2.29.

The phase diagram of the side chain systems depends on the interactions and dimensions of the backbone and side chains. Generally, a high volume fraction ϕ favors the N_I phase as the side chain effect becomes important; otherwise the N_{II} and N_{III} phases appear, likely owing to the presence of the backbone. S_A is positive for the N_I and N_{III} phases which have opposite S_B. Either N_I or N_{III} phase is likely to appear, depending on the value of $(\phi v_c - v_f/n)$. Large $(\phi v_c - v_f/n)$ favors the N_{III} phase; otherwise the N_I phase is likely to appear. The length of the side groups is important in determining the phase diagram as well. Longer side chain favors the N_{III} phase, otherwise the N_{II} phase is favored, see Figure 2.29. v_a and ϕ, v_b and $(1 - \phi)$ play a similar role in the competition. A high v_c favors the N_{III}
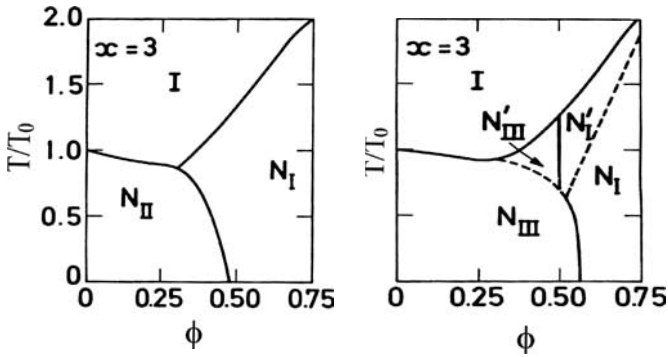
Figure 2.29.   Phase diagrams of side chain nematic polymers: $v_a : v_b : v_c : v_f : \varepsilon/d = 3 : 2 : 1 : 3 : 2$ and $v_a : v_b : v_c : v_f : \varepsilon/d = 3 : 2 : 2 : 3 : 2$. (From Wang & Warner, 1987.)

phase. For a small v_c, the effect of v_f becomes important and the N_{II} phase is likely to appear, as shown in Figure 2.29.

2.7.4.   Conformations

The backbones in the N_{II} and N_{III} phases are prolate, the same as that of main chain liquid crystalline polymers. In the N_I phase, the backbone is oblate.

If the side chain liquid crystalline polymers goes into the smectic A phase from the nematic phase, the backbone chain is confined between two successive smectic layers, occasionally jumping into the neighboring layer gap. See Figure 2.30 where the cylinders denote side groups and thick lines represent backbones. The mean square end-to-end distances parallel and perpendicular to the director differs more than that in the nematic phase.

The components of the mean square end-to-end distance were given in the last section. If the temperature is low and $|\Delta^2|$ is much greater than zero, the mean square end-to-end distance in the N_{II} and N_{III} phases have the forms

$$\langle R_z^2 \rangle = L^2 \left(1 - \frac{1}{|\Delta|} \right),$$

$$\langle R_p^2 \rangle = \frac{Ll}{|\Delta|}. \tag{2.131}$$
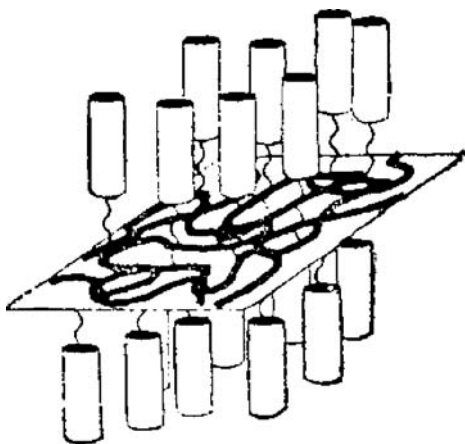
Figure 2.30.   Backbone of side chain liquid crystalline polymer confined between smectic layers. (From Finkelmann, 1991. Reproduced by permission of John Wiley & Sons, Inc.)

The conformation is rod-like in the direction along the director, while in the N_I phase both conformations along the two principal directions, expressed in the following equation, are random walks. In the z direction it is greatly depressed, as seen from the following equations

$$\langle R_z^2 \rangle = \frac{Ll}{2\Delta^2} \left(1 + \frac{1}{2\Delta} \right),$$

$$\langle R_p^2 \rangle = 2Ll \left(1 - \frac{3}{2\Delta} \right).$$

$$(2.132)$$

2.8.   LIQUID CRYSTALLINE NETWORKS

Liquid crystalline polymers can be crosslinked to form a network, or an elastomer, while retaining liquid crystallinity. This section is devoted to both the liquid crystallinity and the rubber elasticity of the crosslinked polymers.

Figure 2.31 is an example of a liquid crystalline polymer network which is the crosslinked product of crosslinkable liquid crystalline polymers and the crosslinking agents.

de Gennes suggested a free energy of the Landau–de Gennes form and discussed qualitatively the properties of nematic networks, such as the
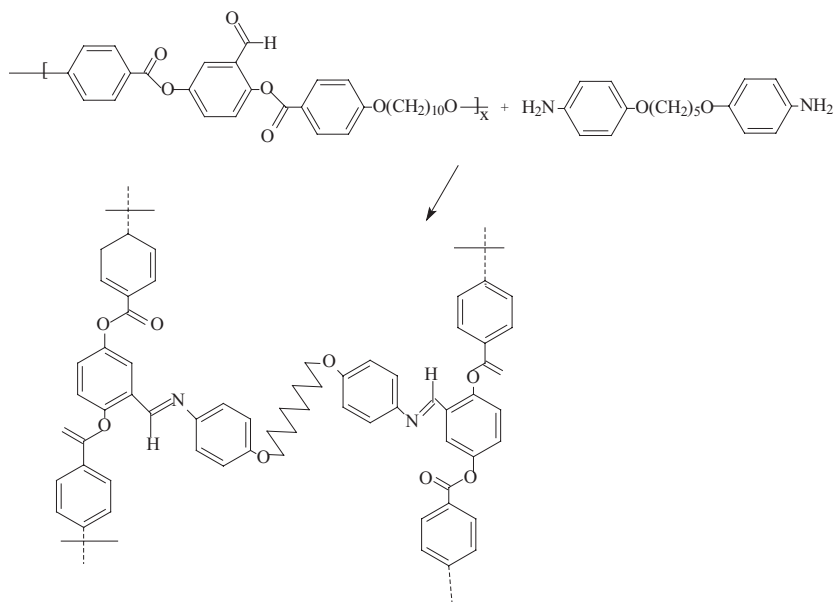
Figure 2.31.   An example of forming a liquid crystalline polymer network. (From Sirigu, 1993.)

discontinuous stress-strain relation, *etc.* (de Gennes, 1975). Several other models have been presented to attack this subject (Jarry & Monnerie, 1979; Deloche & Samulski, 1981; Abramchuk & Khokhlov, 1988; Warner *et al.*, 1988; Warner & Wang, 1991). Warner and Wang (1991) started from the anisotropic Gaussion chain and applied the worm chain model to envisage the properties of nematic networks.

2.8.1.   Conventional networks

In order to emphasize the additional phenomena resulting from liquid crystallinity, we adopt the following postulates of a classical polymer network (Treloar, 1975):

(1) The strands between crosslinks are long enough so that they remain essentially Gaussian, though anisotropic in the nematic network;
(2) The strand chains in the network deform affinely with the bulk deformation due to the constraint of crosslinks;

(3) The free energy of the network is the sum of that of each strand's chains.

Thus, the probability of R, the end-to-end vector of a strand of a polymer network, is given by

$$P(R) = (2\pi l_0 L)^{-\frac{3}{2}} \exp\left[-\frac{3R^2}{2l_0 L}\right], \qquad (2.133)$$

where l_0 is the persistence length in the isotropic phase. The mean square end-to-end distance of the undeformed sample is

$$\langle \mathbf{R}_0^2 \rangle = L l_0. \qquad (2.134)$$

The three orthogonal components of the mean square end-to-end distance are equal.

According to the affine deformation postulate for the bulk deformation $\boldsymbol{\lambda}$, a symmetrical rank two tensor, the end-to-end distance vector deforms from $\boldsymbol{R}_0$ to

$$\boldsymbol{R} = \boldsymbol{\lambda}\boldsymbol{R}_0. \qquad (2.135)$$

Define the extension ratio along the extension direction, Z axis, by $\lambda = \lambda_z$, then

$$\lambda_x = \lambda_y = \lambda^{-\frac{1}{2}}. \qquad (2.136)$$

Accordingly, the elastic free energy of a strand chain of a network with the deformed span $\boldsymbol{R}$ is given by

$$F_{el} = -Nk_B T \ln P(\mathbf{R}) = \frac{1}{2}Nk_B T\left(\lambda^2 + \frac{2}{\lambda}\right), \qquad (2.137)$$

where P is the probability of $\boldsymbol{R}$. Here we apply the third assumption, *i.e.*, the total free energy is the sum of all the strands of network. We omit the irrelevant terms of λ.

The external stress energy adds an energy term

$$F_{ext} = -\sigma \ln \lambda. \qquad (2.138)$$

The equilibrium deformation λ can be obtained by minimizing the total energy and thus

$$\sigma = Nk_B T\left(\lambda^2 - \frac{1}{\lambda}\right). \qquad (2.139)$$

If the deformation is not great, it is usually helpful to define an extension deformation, e, rather than use the deformation λ, *i.e.*, $\lambda = 1 + e$. As e is small $\lambda^2 - 1/\lambda \approx 3e$ and then

$$\sigma = 3Nk_B Te. \qquad (2.140)$$

The Young's modulus for the isotropic networks is

$$E = 3Nk_BT \tag{2.141}$$

and we can deduce the Poison's ratio from the impressibility condition

$$\delta = \tfrac{1}{2}. \tag{2.142}$$

2.8.2.   Model of liquid crystal networks

Now we return to liquid crystal networks. In addition to the above three postulates, we further assume: (4) The total free energy of the network is comprised of elastic, nematic and external stress contributions, *i.e.*,

$$F = F_{nem} + F_{el} + F_{ext}. \tag{2.143}$$

The nematic networks are composed of strands whose conformation is uniaxial with two end-to-end distance components not all being equal which read

$$\langle R_z^2 \rangle = l_z \frac{L}{3}, \quad \langle R_p^2 \rangle = l_p \frac{L}{3}, \tag{2.144}$$

where L is the contour length of a strand. Two distinct persistence lengths l_z and l_p are different from the isotropic value l_i.

Under the Gaussian assumption, the probability of the end-to-end distance vector being $\boldsymbol{R}$ is

$$P(\boldsymbol{R}) = (2\pi l_0 L)^{-3/2} \left(\frac{l_0^3}{l_z l_p^2} \right)^{\frac{1}{2}} \exp\left[-\left(\frac{3R_z^2}{2l_z L} + \frac{3R_p^2}{l_p L} \right) \right]. \tag{2.145}$$

For uniaxial deformations, two distinct principal extension ratios λ_z and λ_p, along and perpendicular to the director respectively, satisfy the relation $\lambda_z \cdot \lambda_p^2 = 1$ because of the incompressibility of rubbers.

If the chains are crosslinked in the isotropic state and P_0 is an isotropic Gaussian distribution, the additional elastic free energy of a strand of the network with deformed span $\boldsymbol{R}$ is given by (denoting λ_z by λ)

$$\frac{F_{el}}{k_BT} = \frac{1}{2} \left(\lambda^2 \frac{l_i}{l_z} + \frac{2}{\lambda} \frac{l_i}{l_p} \right) - \frac{1}{2} \ln \left(\frac{l_i^3}{l_z l_p^2} \right). \tag{2.146}$$

The nematic contribution to free energy is

$$\frac{F_{nem}}{k_B T} = N \frac{L}{l} \left(\lambda_0 + \frac{S^2}{T'^2} \right), \tag{2.147}$$

where $T' = k_B T / \sqrt{v\varepsilon}$.

Without the external stress, the nematic network has to deform to minimize free energy and thus the optimum deformation λ_m is

$$\lambda_m = \left(\frac{l_z}{l_p} \right)^{\frac{1}{3}} \tag{2.148}$$

The l_z and l_p are functions of temperature and thus λ_m is dependent on temperature. λ_m differs from the natural extension of the strand, $(l_z/l_0)^{\frac{1}{2}}$, which results from the confinement of crosslinks. The elastic free energy can thus be reduced, if assuming $w = l_i (l_z l_p^2)^{-1/3}$

$$\frac{F_{el}}{k_B T} = \frac{3}{2} N(w - \ln w). \tag{2.149}$$

The external stress energy adds an energy term

$$F_{ext} = -\sigma \ln \lambda. \tag{2.150}$$

The total free energy of the system in the absence of external stress is the sum of the elastic term (Equation 2.149) and the nematic contribution (Equation 2.147).

We are dealing with only a single domain sample. To achieve a single domain sample, the following techniques may work:

(1) Crosslinking polymers in a single domain liquid crystal phase, as demonstrated by the Mitchell group (Legge *et al.*, 1991);
(2) Crosslinking polymers under an external field. To achieve good effect, crosslinking may occur in two steps: first crosslink lightly and then apply a stress while completing the whole crosslinking process. This technique was applied by the Finkelmann group (Schatzle *et al.,* 1989).

The order parameter of nematic networks is obtained as a function of temperature and the crosslink density. For nematic networks crosslinked at the isotropic phase, the nematic to isotropic transition is lower than that of the constituent nematic polymers which are the same length as the strands in the networks, while the transition temperature increases for the

nematic network crosslinked at the liquid crystal phase. Mitchell *et al.*'s experiments demonstrate this effect (Legge *et al.*, 1991). The difference of the N–I transition temperature between the nematic networks and the counterpart nematic polymers is insignificant as long as the concentration of the crosslink agent is low enough. The reason for the small difference is that the conformation of the network strands differ from the crosslink-free nematic polymers by a factor of $w^{-1/2}$, which is not far from unity at the transition.

2.8.3. Relation of stress and strain

Small molecular mass liquid crystals do not respond to extension and shear stress. Liquid crystalline polymers may exhibit a high elastic state at some temperature due to the entanglements. However, the liquid crystalline network itself is an elastomer, showing rubber elasticity. In the presence of external stress, liquid crystalline networks deform remarkably and then relax back after the release of stress. The elasticity of liquid crystalline networks is more complicated than the conventional network, such as the stress induced phase transition, the discontinuous stress-strain relationship and the non-linear stress optical effect, *etc.*

The stress–strain relationship of nematic networks is given by

$$\frac{\sigma}{Nk_BT} = \lambda^2 \frac{l_i}{l_z} - \frac{1}{\lambda}\frac{l_i}{l_p}. \tag{2.151}$$

This relationship is shown in Figure 2.32(a) where reduced stress $\sigma^* \equiv \sigma/Nk_BT$, and curves are drawn for various reduced temperature T/T_c. This is in good agreement with the experimental data (Schatzle *et al.*, 1989), shown in Figure 2.32(b).

It is shown that the elasticity of the nematic networks is catalogued into three temperature ranges:

(1) $T \gg T_c$, *e.g.*, $T/T_{c'} = 1.5$, the network is in the isotropic phase. This curve is actually the same as that for the conventional networks.
(2) $T \ll T_c$, the polymer network is in the nematic phase. The free stress nematic networks display significant extension, *i.e.*, a natural anisotropic shape. The extension increases as stress persists.
(3) $T \geq T_c$, *e.g.*, $T/T_{c'} = 1.02$, an external stress induces a phase transition accompanied by spontaneous extension. The discontinuous stress-strain relationship and an associated critical point are observed.
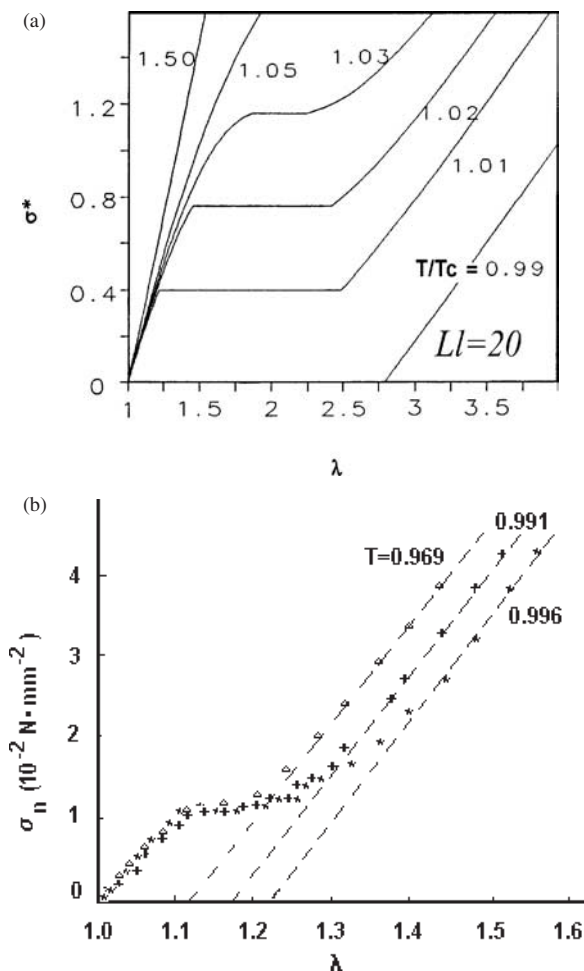
Figure 2.32.   Stress–strain relations of the nematic networks ($\sigma^* \equiv \sigma/Nk_BT$) for various temperatures (a) (From Warner & Wang, 1991); and experimental stress–strain relations of the nematic networks (b) (Modified from Schatzle *et al.*, 1989.)

Disagreement between classical network theory and experimental data occurs. The entanglement effect was thought to be responsible for the deviation. According to the classical network theory, the stress–strain relationship should follow Equation 2.139. The plot of the reduced force, $\sigma^*/(\lambda^2 - 1/\lambda)$, against the reciprocal strain, $1/\lambda$, should be constant, *i.e.*, unity. But experiments show that the reduced force is a function of the extension ratio λ. Figure 2.33 shows the typical experimental data of PDMS
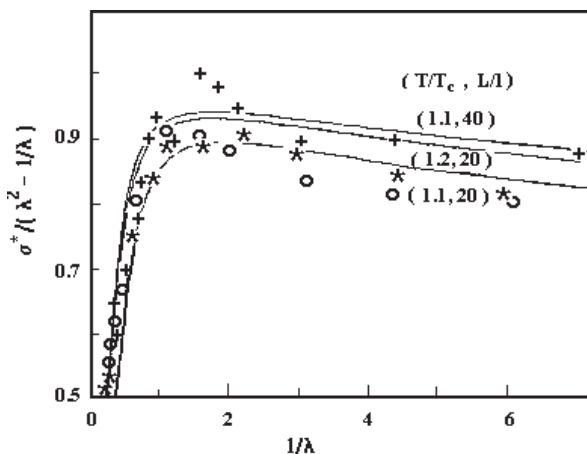
Figure 2.33. The reduced force, $\sigma^*/(\lambda^2 - 1/\lambda)$, against reciprocal strain, $1/\lambda$. (Modified from Warner & Wang, 1991.)

with 3% DCP ($\star$) and 2% DCP ($+$) (Pak & Flory, 1979), and natural rubbers ($\circ$) (Rivin & Saunders, 1951). $1/\lambda < 1$ is the case of extension, while $1/\lambda > 1$ means compression. The solid lines in the figure are theoretical predictions for $L/l = 20, 40$ and $T/T_{c'} = 1.1$ and 1.2. The polymer network is in fact in the isotropic phase and is far from the nematic-isotropic transition. For instance, for a network with a transition temperature $T_c = -23\,^\circ\mathrm{C}, T/T_c = 1.02$ means $T = 27\,^\circ\mathrm{C}$. The curve apparently deviates from a straight line and is in agreement with experimental data.

This demonstrates that liquid crystallinity is not exhibited by many polymer networks because their liquid crystal to isotropic transitions are too low to be observed. But the residual liquid crystallinity affects the stress-strain relationship at higher temperatures. These results form a deviation from classical rubber elasticity theory.

We have only dealt with the main chain nematic networks so far. Actually many liquid crystalline networks are formed by crosslinking the backbones of side chain liquid crystalline polymers. The side chain nematic polymers have three nematic phases and their backbones have either prolate or oblate conformations, depending on their phase. It is expected that the rubber elasticity of a side chain nematic polymer network is more complex. For instance, the stress-induced N_I–N_{III} phase transition is predicted as the network shape transforms from oblate to prolate. Liquid crystalline networks have a bright potential in industry.

2.9.   LIQUID CRYSTAL NETWORK GELS

The swelling of a nematogenic network by either an isotropic or nematic solvent is more complex than that of a classical network. In the swelling case, the volume conserving constraints need not be applied, as the volume fraction of the network is able to change by solvent exchange. The change in the degree of swelling thereby offers alternative routes to lower the free energy. As we know, the unique feature of nematic polymers is that molecules change their shape, in contrast to simple nematic rods. Shape changes of the constituent polymers of a network mean that the network too changes its shape. This is further reflected in its macroscopic properties. The nematic behavior couples to volume change and makes swelling of these networks more complex than the swelling of isotropic networks.

For simplicity, we restrict our consideration to nematic polymers of prolate shape. This includes (i) main chain nematic polymers and (ii) side chain nematic polymers, but in such a way that they preferentially align with the backbone, thus giving the features of (i). This has been called the N_{III} phase. The other prolate possibility in the N_{II} phase is that the backbone takes a prolate shape while the side chains are forced to have oblate symmetry. We shall only discuss the nematic polymers of (i), but the method and the conclusions are quite general.

There are three combinations of the two components of nematic network gels: (1) an isotropic network swollen by a nematic solvent, reminiscent of the polymer dispersed liquid crystal systems (PDLC). This case (1) was discussed by Brochard (1979) and Ballauff (1991); (2) a nematic network swollen by an isotropic solvent was actually studied experimentally by Carudo *et al.* (1992) and theoretically by Warner and Wang (1992a); (3) both components can order at a temperature above the glass transition. Actually the first two systems are special cases of the last one which has been experimentally investigated (Zentel, 1986; Barnes *et al.*, 1989; Kishi *et al.*, 1994) and theoretically studied (Wang & Warner, 1997).

We now start the case (2) to focus on the new effects of nematic gels, and then discuss the general case (3).

2.9.1.   Nematogetic network swollen by isotropic solvent

The free energy per site of gels consists of three parts

$$F = F_{mix} + F_{el} + F_{nem}, \tag{2.152}$$

where the free energy of mixing has the Flory-Huggins form

$$\frac{F_{mix}}{k_B T} = (1 - \phi) \ln(1 - \phi) + \chi \phi (1 - \phi) \tag{2.153}$$

with ϕ the network volume fraction. For simplicity χ is assumed to be temperature-independent. Therefore, the shape of the phase diagram of the conventional isotropic gels is expected to be temperature independent accordingly.

The elongations of the gel, are λ_z and λ_p, and are related to the swelling by

$$\lambda_z \lambda_p^2 = \frac{1}{\phi}. \tag{2.154}$$

We can retain λ_z and ϕ as variables, writing λ for λ_z, by taking $\lambda_p^2 = 1/\lambda \phi$.

The elastic free energy is thus written as

$$\frac{F_{el}}{k_B T} = \frac{\phi}{2L} \left[\left(\lambda^2 \frac{l_i}{l_z} + \frac{2}{\lambda \phi} \frac{l_i}{l_p} \right) - \ln \left(\frac{l_i^3}{l_z l_p^2} \right) \right], \tag{2.155}$$

which depends on the current state of nematic order of the network, S. In all that follows we shall define l_i, l_z and l_p to be the number of sites associated with these persistence lengths.

The equilibrium elongation of the gel, λ_m, is

$$\lambda_m = \left(\frac{l_z}{l_p \phi} \right)^{\frac{1}{3}}, \tag{2.156}$$

and the elastic free energy becomes:

$$\frac{F_{el}}{k_B T} = \left(\frac{3}{2L} \right) [\phi^{\frac{1}{3}} w(S) - \ln w(S)]. \tag{2.157}$$

The nematic contribution to the free energy is

$$\frac{F_{nem}}{k_B T} = \frac{\phi}{l_0} \left(\lambda_0 + \frac{\phi S^2}{T'^2} \right), \tag{2.158}$$

where the ϕ terms account for the reduction of the energy per site and the dilution of the relevant nematic interaction. The nematic free energy F_{nem} is the function of the combination $\Delta^2 = -3\phi S/T'^2$ and $T' = k_B T/\sqrt{a\varepsilon}$. In these units, $T'_c = 0.388$, the N–I transition temperature in the undiluted network.

The extent of solvent up-take is governed by the equality of the chemical potential (μ) of the solvent in the gel, either with μ for the solvent reservoir (for gel/solvent equilibrium), or with μ for solvent in another gel phase (for gel/gel equilibrium). The chemical potential is defined as

$$\mu = F - \phi \left(\frac{dF}{d\phi} \right) \tag{2.159}$$

which yields

$$\frac{\mu}{k_B T} = \phi + \ln(1 - \phi) + \chi \phi^2 + \frac{w(S)\phi^{\frac{1}{3}}}{L}. \tag{2.160}$$

The gel/gel equilibrium requires the common tangent condition on the $F - \phi$ plot which is satisfied both by equal chemical potential, and by equal exchange potential, *i.e.*, $\partial F / \partial \phi$. The numerical solutions of the phase diagram are shown below.

We employ the convention of upper case N and I to denote the nematic and the isotropic phases of a gel, and the lower case n and i for the phases of the neat solvent. Moreover, we adopt the convention that in A–B coexisting phases, the first letter denotes the less concentrated of the coexisting phases.

At low temperatures the nematic gel coexists with excess solvent, *i.e.*, the i–N biphasic coexistence. Above the triple point T_t', excess solvent coexists with an isotropic gel, *i.e.*, the i–I coexistence. Also, above this temperature, the isotropic and the nematic phases of a gel can coexist, *i.e.*, I–N phases. Beyond the phase gap, a single nematic phase exists. The I–N region terminates at the $\phi = 1$ axis. This is at $T_{ni}^{(x)}$, the N–I transition temperature of the undiluted network which, in turn, is close to T_{ni}, the transition temperature of the uncrosslinked polymer melt from which the network derives. The nematic order is not expected for any ϕ for T' above $T_{ni}^{(x)}$. This is the limit of stability for even the undiluted case.

2.9.2.   Nematogetic network swollen by nematic solvent

The addition of a nematic solvent yields more complex possibilities, dependent on the relationship between $T_{ni}^{(s)}$ of the solvent and $T_{ni}^{(x)}$ of the network. Because the solvent can also order, at temperature $T_{ni}^{(s)}$ in the neat state, the nematic tendencies of the solvent prevent it from acting directly to destroy the nematic state of the network it is swelling.

It is possible to envisage three regimes of relative nematicity for the network and solvent: (a) $T_{ni}^{(s)} \ll T_{ni}^{(x)}$, (b) $T_{ni}^{(s)} \cong T_{ni}^{(x)}$ (with various delicate cases we treat below) and (c) $T_{ni}^{(s)} \gg T_{ni}^{(x)}$. Additionally, the magnitude of the nematic cross coupling between the solvent and the network polymers will be discussed. All of the above cases will be discussed, illustrating the qualitative features that emerge by presenting representative phase diagrams that correspond to the various choices of the nematic coupling constants.

An extreme case of (c) where $T_{ni}^{(x)} = 0$ has been treated by Ballauff (1992). As T is lowered below $T_{ni}^{(s)}$, the network rapidly de-swells as isotropic chains are highly incompatible with a nematic solvent. By giving the chains some (variable) degree of nematicity, we allow for the possibility that they can order in response rather than de-mix.

The total free energy of the nematic gel still consists of mixing, elastic and nematic parts; with the nematic energy resulting from both the network and solvent. For greater simplicity, the network chains are to be treated as freely-jointed rod chains instead of the worm chains, with each segment behaving like a Maier–Saupe rod similar to that of the solvent. The qualitative features of the phase diagrams should not be changed by adopting this simplification.

A qualitative understanding of why new phase equilibria are possible can be seen from a plot of the free energy of nematic gels with such a common tangent drawn in, see Figure 2.34.
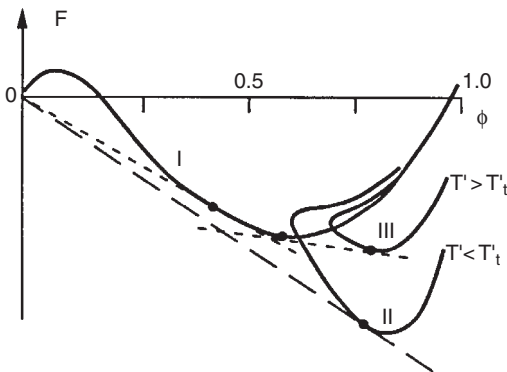
Figure 2.34.   The free energy of nematic gels *vs.* volume fraction where $T_{ni}^{(s)} = 0$. (I) isotropic gel; (II) and (III) nematic gel. T_t' is the i–I–N triple-point temperature. (From Warner & Wang, 1992a.)

In Figure 2.34 where $T_{ni}^{(s)} = 0$, the N branch of the free energy is defined only to a lowest ϕ since the nematogetic network is diluted with a non-nematic solvent. If we dilute with a nematic solvent it is possible for the nematic branch of F to extend all the way to $\phi = 0$ if $T < T_{ni}^{(s)}$. If $T_{ni}^{(s)} > T > T_{ni}^{(x)}$, the nematic branch of F may extend from $\phi = 0$ to a maximum with $\phi < 1$. How far it can be extended depends partly on how much greater T is than $T_{ni}^{(x)}$ as well as on the cross-coupling v_c.

The precise structure of the phase diagram depends on the relative strengths of the couplings, more precisely on the coupling matrix $\begin{pmatrix} v_a & v_c \\ v_c & v_b \end{pmatrix}$. We will now consider a variety of representative examples of self and cross couplings and their effect on the phase diagrams.

First of all, we will treat the simple case where $\det(\mathbf{v}) = 0$, *i.e.*, v_c is the geometrical mean of the self couplings and, except for unusual molecules, it approximates the order of that expected for a van der Waals mediated nematic interactions. Next, we will deal with more unusual behavior where $\det(\mathbf{v}) < 0$ and $\det(\mathbf{v}) > 0$, respectively.

In all that follows we shall reduce all coupling constants by v_a, that is when (v_a, v_b, v_c) are quoted they will be quoted as $(1, v_b/v_a, v_c/v_a)$. Temperatures will be reduced by the transition temperature of pure solvents which is at $T_{red} = 0.22 v_a / k_B T$. As a result, in this reduction scheme, the neat solvent has its transition at $T = 1$.

Phase diagram with $\det(\boldsymbol{v}) = 0$

Figure 2.35(a) shows the phase diagram for $v_c = 1.1$ and thus $v_b = 1.21$, that is where the network is a stronger nematic than the solvent. The strand length $L = 10$ and the isotropic Flory-Huggins parameter $\chi = 0.4$, correspond to a good solvent. These values will be used through out this section.

It is shown qualitatively, as in Figure 2.35(a), that the I–N phase coexistence extends downwards from the transition at $T = 1.21$ of the neat network. There is a triple point i–I–N.

If the network is less nematic than the solvent with $v_c = 0.9$ and thus $v_b = 0.81$. Now the N–I coexistence extends upward from the neat network's transition at $T = 0.81$. Diluting with such a solvent stabilizes the nematic phase of the network against a temperature increase. The triple point is now n-N–I, instead and from this point upwards to $T = 1$, there is n-I coexistence. The vertical phase "chimney" (i–I) extends above $T = 1$. Figure 2.35(b) shows the opposite limit.
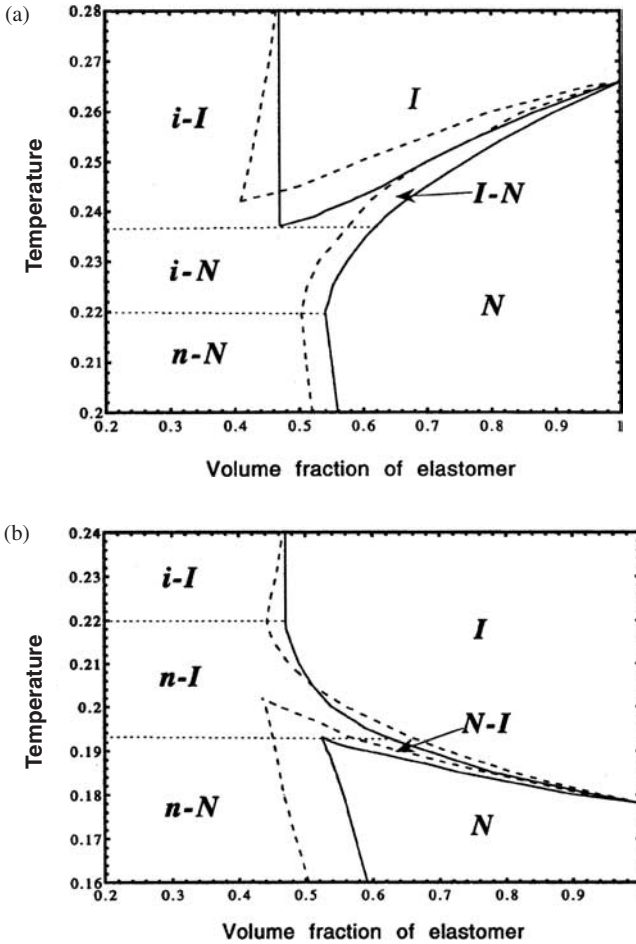
Figure 2.35. The phase diagrams of nematic gels (a) $v_c = 1.1, v_b = 1.21$ and (b) $v_c = 0.9, v_b = 0.81$. (From Wang & Warner, 1997.)

Phase diagram with $\det(\boldsymbol{v}) < 0$

Figure 2.36 is a phase diagram for $v_b = 1.1$ and $v_c = 1.2$, *i.e.*, $\det(\boldsymbol{v}) < 0$. This is where the network is more strongly nematic than the pure solvent. Since $v_c > v_b$, dilution initially stabilizes the nematic phase of the network. Thus, N–I coexistence initially extends upwards from $T = 1.1$, $\phi = 1.0$ (the N–I transition of the neat network) as in Figure 2.36(b). As dilution
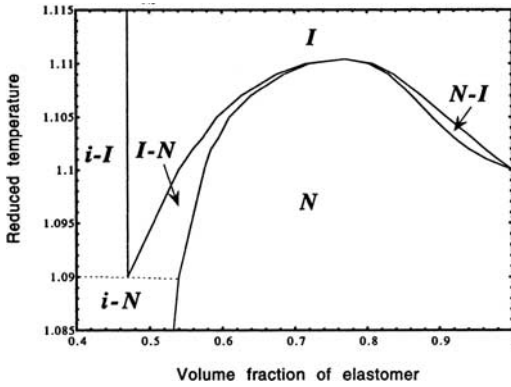
Figure 2.36.   The phase diagram of nematic gels where $\det(\boldsymbol{v}) < 0$ and $v_b = 1.1, v_c = 1.2$. (From Wang & Warner, 1997.)
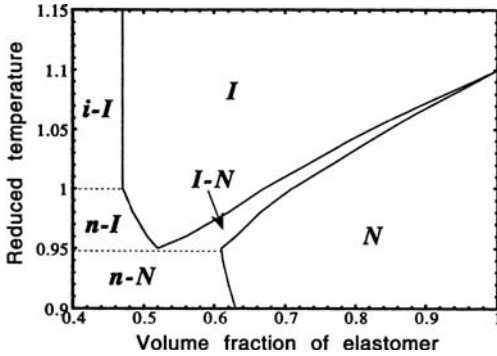
Figure 2.37.   The phase diagram of nematic gels where $\det(\boldsymbol{v}) > 0$ and $v_b = 1.1, v_c = 0.9$. (From Wang & Warner, 1997.)

continues, the trend is reversed and the coexistence extends downwards as I–N, more appropriate to when $v_a < v_b$ (as found in Figure 2.34 and is truly the case here). The triple point region is therefore as in Figure 2.36. The reversal point on dilution occurs at a special value of ϕ where the N–I and I–N phase gaps each shrink to points and merge with each other. This azeotropic phenomenon is discussed by Brochard *et al.* (1979). It mimics a pure phase since heating the N gel at this volume fraction yields an I gel at the same volume fraction.

Phase diagram with $\det(\boldsymbol{v}) > 0$

Figure 2.37 shows the case where the cross coupling is relative weaker, namely $v_c^2 < v_a v_b$, this is where $\det(\boldsymbol{v}) > 0$.

The values chosen for the couplings are $v_b = 1.1$ and $v_c = 0.9$. One sees from Figure 2.37 that the central region of the diagram, from the vertical chimney to the triple point now slopes downward, reflecting the loss of nematic stability in intermediate regions of ϕ where the weakness of v_c is most felt. Since v_c is also less than v_b, dilution from $\phi = 1$ causes a reduction in the nematic phase stability, requiring lower temperatures, and thus causing the phase gap to extend downward from T_{ni}.

2.9.3. The shift of phase equilibria under the presence of force

In the presence of an applied force, that is, a fixed nominal stress σ, the phase diagrams change accordingly, as shown by dotted curves in Figure 2.35(a) and (b). For simplicity we deal only with the stress applied along the director and adopt the reduced nominal stress $\sigma* = \sigma L/v_a$. It is known that strain imposed at an angle to the director in a neat nematic network is more complicated and can cause nematic rotational and mechanical instabilities (Mitchell *et al.*, 1993), and the formation of striped states (Kundler & Finkelmann, 1995). In Figure 2.35(a) and (b), the applied longitudinal stress is shown to stabilize the nematic phase, shifting phase lines to higher temperatures. The shift in $T_{ni}^{(x)}$ for the neat network does occur but is too small to display on the figures. This is known from earlier studies of the effect of stress on the transitions of neat networks (Warner & Wang, 1991, 1992b). The stress is more effective when acting on swollen networks, since it competes with the osmotic modulus of the network to up-take solvent, osmotic moduli being $\sim k_B T$ per unit volume, and the elastic moduli being $\sim k_B T/L$ per unit volume, as in the reduction of σ to σ^*. The low temperature limits of this behavior are particularly sensitive to the application of stress.

Nematic gels are very interesting systems, thus deserving further study. Actually, these systems are being studied experimentally for applications. Examples are: polymer dispersed liquid crystal displays are sometimes dispersed not in a polymer, but in a polymer network. Displays by means of the polymer stabilized cholesteric texture change, are also achieved in crosslinked systems. In addition, the chiral smectic phase has been obtained in such systems as well. Other types of liquid crystal gels have been applied or are expected to be applied in such devices.

This page intentionally left blank

Chapter 3

Molecular Engineering of Liquid Crystalline Polymers

3.1. INTRODUCTION

The molecular theories introduced in Chapter 2 are the principal guidelines for any successful molecular design of liquid crystalline polymers. According to the theories, rigid molecules with an anisotropic shape, rod-like in particular, are able to form nematic phases even if no soft interactions are included in the consideration. Thermal stability (characterizable by T_i, the clearing temperature) of the liquid crystal phase is a function of the axial ratio of the molecules. Those molecules with higher length-to-diameter ratios will result in nematic phases of a higher clearing temperature. When the ratio is large enough, the nematic phase is always more stable than the isotropic liquid phase and the clearing temperature will be infinite. Different theoretical treatments have reached the same conclusion, although they have resulted in different critical axial ratios. In the literature of polymeric liquid crystals, the most cited value for the critical axial ratio of rigid rods is 6.4, given by Flory.

Actual molecules always have certain flexible elements and are not as rigid as a true rod. Taking the rod-like poly(1,4-phenylene) as one example,

$\langle 3.1 \rangle$
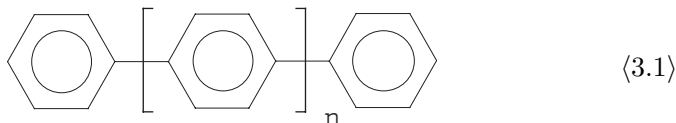
rotation of phenylene rings about the interphenylene bonds, together with vibrations of the bonds, have brought about flexibility of the molecule even

though a rod-like shape has persisted. The formability of a liquid crystal phase and the phase transition temperatures of the homologous compounds of poly(1,4-phenylene) are characterized and shown in Table 3.1.

Two conclusions may be drawn from the data in Table 3.1. First, only the homologues with sufficiently large values of length-to-diameter ratio can form a liquid crystal phase. Secondly, both the melting point and the clearing temperature of the liquid crystal phase increase very fast with an increasing degree of polymerization (n + 2). The compound with only six 1,4-phenylene units and an axial ratio of 5.5 has a melting point of 438 °C and a clearing temperature of 565 °C, which is already too high a temperature for organic molecules to survive. It is therefore not practical to synthesize liquid crystal forming polymers by the simple linking-together of rigid structures into rod-like molecules, even if certain flexible elements are present.

By inserting in between every two phenylene rings a linking unit with a certain flexibility, such as an ester group, the flexibility of the molecules will be increased. For example, if an ester group is used as the linking unit, it will not only allow the crankshaft type movements in the molecule, but also serve as a separation between the phenylene rings and thus reduce the hindrance for a free rotation of the rings. As a result, poly(4-hydroxybenzoic acid), PHA, with the following formula does have much lower transition temperatures than poly-phenylenes as shown in Table 3.2. Specifically, the compound with n = 3 has a melting point of 220 °C and a clearing temperature of 464 °C. The calculated axial ratio l/d is 6.4. In comparison, this compound has slightly higher axial ratio but much lower transition temperatures than the poly(1,4-phenylene) with n + 2 = 6 (l/d = 5.5, m.p.

Table 3.1.   The Axial ratio and Phase Transition Temperature of Poly(1,4-phenylene)s*.

n + 2	Axial Ratio, l/d	Melt. Point, °C	Clearing Point, °C
1	1.0	5.4	non-liquid-crystalline
2	2.0	70.5	non-liquid-crystalline
3	3.0	213	non-liquid-crystalline
4	3.9	320	non-liquid-crystalline
5	4.8	388	418
6	5.5	438	565

* Source: Irvine and Flory, 1984.

Table 3.2. Axial ratio and Transition Temperature of Poly(4-hydroxybenzoic acid)[*].

n	Axial Ratio, l/d	Melt.Point, °C	Clearing Point, °C
1	3.8	132	100 monotropic
2	5.1	176	254
3	6.4	220	464
13	19	415	
100		600	

[*] Source: Ballauff and Flory, 1984; Economy, *et al.* 1988.

$438\,°C$, $Ti = 565\ °C$. Table 3.1). Thus, PHA can have a higher degree of polymerization than poly(1,4-phenylene) before the transition temperatures become infinite. However, studies on PHA have shown that its melting point is already higher than its decomposition temperature if the degree of polymerization reaches only such a low value as 13 (Table 3.2).

$$\langle 3.2 \rangle$$
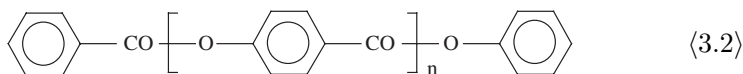
In Table 3.2, the compound with n = 1 has a monotropic liquid crystalline phase. In the literature of liquid crystals a monotropic phase is a metastable phase which forms only in the process of cooling but not when the sample is heating. On the other hand, if a liquid crystalline phase forms not only in the process of cooling but also in the process of heating, the phase is termed enantiotropic. For example, a nematic phase is monotropic if the melting point, Tm, of the sample is higher than the clearing temperature, Ti, of the liquid crystal phase. It is enantiotropic if Ti is higher than Tm.

It is worthwhile pointing out that the critical axial ratio 6.4 given by Flory's theory is based on assumptions that include zero free volume and zero net interaction energy between the rods (Chapter 2). By increasing the free volume, for example, the ratio will be increased accordingly. It is thus also understandable that the critical axial ratio will become larger when the temperature is increased. On the other hand, no actual system will meet these assumptions to any perfection. In addition, the flexibility of an actual molecule such as poly(1,4-phenylene) and PHA will increase with increasing temperature. In other words, the axial ratio of a molecule is not a constant,

but a function of temperature. The actual axial value of a compound will deviate from what was calculated for a standard condition, and will become lower and lower with the increase of experimental temperature. Therefore, no direct comparison may be made between the critical axial ratio given by the theory and the axial ratio of an actual compound for evaluation of the liquid crystalline properties of the compound.

We have shown that polymers formed by the simple linking together of rigid rod-like mesogenic units, such as poly(1,4-phenylene) and poly(4-hydroxybenzoic acid) formed by linking together the phenylene rings with single bonds or ester units, have melting temperatures so high that no liquid crystalline phase can actually exist above melting. To achieve liquid crystallinity, the melting point of the polymers has to be decreased. The most convenient way to achieve this is to mix the rod-like polymer with a solvent. Blades (1973, 1975) discovered that with sulfuric acid the high molecular weight poly(1,4-phenylene terephthamide) is able to form crystalline solvates with finite melting temperatures. The solvate formed with about one mole polymer and 10 moles of sulfuric acid melts and forms the lyotropic liquid crystalline phase at $70\,^{\circ}$C, a very convenient temperature for processing. Other rod-like polymers may form solvates also. Poly(γ-benzy-L-glutamate), for example, forms crystal solvates with DMF. Watanabe *et al.* (1981) found the melting point of the solvates increases with the increasing of the polymer content. The lyotropic liquid crystal phase can form only when the polymer content is higher than $18\,\mathrm{wt}\%$. Papkov (1982) has given a phase diagram for the two-component system of a rigid rod polymer and a solvent. According to this researcher, with the addition of a solvent to the polymer, a two-phase system (crystal C + crystal-solvate CS) is first formed. A single CS phase, then the second two-phase system of CS and the isotropic liquid phase will form with the further addition of the solvent. Thus in principle, liquid crystals of rigid rod-like polymers can be obtained by solvent incorporation and formation of crystal solvates with finite melting points. As a matter of fact, lyotropic liquid crystal phases are achieved not only with poly(1,4-phenylene terephthamide) (PPTA) and Poly(γ-benzy-L-glutamate), but also with such rigid rod-like polymers as poly(1,4-phenylene benzo-bis-thiazole) (PBT) and poly(1,4-phenylene benzo-bis-oxazole) (PBO). PPTA, PBT and PBO are important lyotropic liquid crystal polymers that result in materials with very high tensile strength and modulus.

Unfortunately, because of the very low mixing entropy, not many of the rigid rod-like high polymers have sufficient solubility and form solvates. For example, among many others, poly(1,4-phenylene) and

poly(4-hydroxybenzoic acid) hardly dissolve in any solvent. Therefore, these high-melting polymers are not able to form any liquid crystalline phase, neither thermotropic nor lyotropic, if no substantial chemical modifications of the molecules are made. It has been indeed the focus of molecular engineering in this scientific area to design and synthesize polymers with desirable liquid crystallinity in desirable temperature regions. To achieve the goal, two principal ideas have been developed. The first is to disrupt the chain sequence of mesogenic units by inserting into the chain, different structural moieties, so as to incorporate in the chain certain irregularity and flexibility. The result of this practice are main-chain type liquid crystalline polymers. The second idea is to use the mesogenic units individually as side groups attached to the main chain of the polymer molecules, resulting in side-group type liquid crystalline polymers. Depending on the extent of disruption in the sequence of mesogenic units, main-chain type liquid crystalline polymers of very different properties can be synthesized. The polymers can still be rather rigid and have very high, but acceptable melting temperatures if only rigid moieties are used as the disruptions. Copolyesters of 4-hydroxybenzoic acid (HBA) with 6-hydroxy-2-naphthalic acid (HNA), and copolyesters of HBA with terephthalic acid (TA) and biphenol, are famous examples of these polymers. Properties of these copolyesters will be further discussed in Section 3.3 and Chapter 5. On the other hand, main-chain type liquid crystalline polymers can be very flexible with very low melting points if flexible spacers are frequently incorporated along the chain. By comparison, side-group type liquid crystalline polymers usually are flexible polymers with low Tg or low melting temperatures because the rigid mesogenic units with only limited length-to-diameter ratio are used only as individual side groups (Section 3.4). However, side-group type liquid crystalline polymers can have properties similar to that of rigid or semi-rigid main-chain type liquid crystalline polymers if unusual molecular designs are adopted (Section 3.5). Naturally, different molecular designs result in different polymer properties and different applications. Liquid crystalline polymers with higher chain rigidity and melting points may find applications as high-strength, high-modulus, and heat-resistant materials (Chapter 5). Those with very low chain rigidity and transition temperatures may be used in display or information process devices (Chapter 6).

Liquid crystalline polymers have been classified in a variety of ways according to the style of incorporation of mesogenic units in the molecules. The most basic types are shown in Figure 3.1, in which the squares are representative of mesogenic units. Mesogenic units are structural moieties with sufficient rigidity and are mostly in the shape of straight rods. Other

Main-Chain Type:
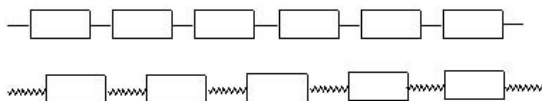
Side-Group Type with End-on Attachment:
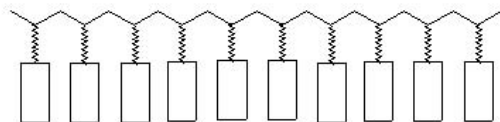
Side-Group Type with Side-on Attachment:
(Mesogen-Jacketed Liquid Crystal Polymers)
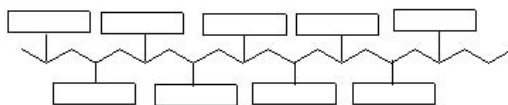
Molecular Shish-Kebab:
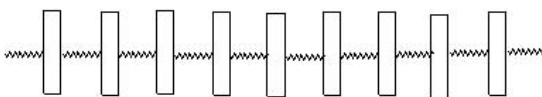
Figure 3.1.   Basic types of liquid crystalline polymers.

anisotropic shapes such as discotic and bowl-like ones are rare but can also be found in certain liquid crystalline polymers. It is commonly believed that mesogenic units are essential to the formation of the liquid crystal phase. Liquid crystalline polymers without mesogenic units are rare and will be discussed in Section 3.6.

3.2.   LOW MASS LIQUID CRYSTALLINE COMPOUNDS AND MESOGENIC UNITS

By and large, mesogenic units make up most of the principal components in a liquid crystalline polymer. The structure and property of mesogenic units are of primary importance in determining properties of a polymer. It is thus very instructive to have a brief study of the structure and its influence on the property of mesogenic units with low mass liquid crystalline compounds as models and references.

Gray (1961) has had a good account for the structure and properties of low molecular mass liquid crystals. In this section we discuss only a few structural elements having the most impact on the properties of liquid crystals. The structural elements include those imposing on molecules, the "side-steps", the kinks, the flexible spacers, the bulky substituents, and others. The discussion starts with poly(1,4-phenylene)s as the parent or reference molecules.

3.2.1.   Poly(1,4-phenylene)s

Most, if not all, the liquid crystal compounds have the 1,4-phenylene unit in the molecules. This structural brick has all the most desirable characteristics for liquid crystals: stiffness, polarizability, and linear orientation. The simplest, although very difficult at the same time, construction of a liquid crystal with this moiety is the synthesis of poly(1,4-phenylene)s, ⟨3.1⟩. In Table 3.1 the number of the phenylene rings and the length-to-diameter ratio are related with the liquid crystallinity of these compounds.

Conformational analysis of ⟨3.1⟩ has reached the conclusion (Laupretre and Noel, 1991) that the most stable conformations of the molecules are linear and rod-like. Because of the steric interactions between the hydrogen atoms of the neighboring phenylene rings, in solution and in the melt state, the coplanar forms have higher energy than the forms with two neighboring rings rotating from each other by an angle of approximately 20–25 degrees. Therefore, the molecules are expected to be more rod-like than coplanar or plate-like in the liquid crystalline phases. On the other hand, the flexibility of these molecules stems basically from only the hindered rotation of the rings. The flexibility is thus very limited. In other words, poly(1,4-phenylene)s can be characterized as rigid and rod-like molecules.

As shown in Table 3.1, poly(1,4-phenylene) becomes liquid-crystal-forming when five rings are present and the molecular rod is sufficiently long. The property of this polymer is most predictable by the Flory theory because of its rod-like nature.

3.2.2.   Incorporation of "side-steps"

In the literature of liquid crystals, "side-steps" have been used to describe the structural moieties that will change the shape of a rod-like molecule

into a stairlike one. The side-step units may include $-COO-$, $-CH=N-$, $-N=N(O)-$, trans $-CH=CH-$, $-CONH-$, and 2,6-naphthalene. The molecule will depart one step aside at such units, but a linear contour of the molecule can be maintained (Figure 3.2).

In such molecules, the crank-shaft type movements shown by Figure 3.3 are possible, rendering the molecules with significant flexibility.

Poly(4-hydroxybenzoic acid), $\langle 3.2 \rangle$, is an example of these molecules. In this case, the ester groups serve as side-steps. Because of the steric repulsion, the two phenylene rings on the two ends of $-COO-$ tend to take the trans-configuration relative to the $CO-O$ bond. The phenylene ring attached directly to the carbon atom in $-COO-$ takes approximately a coplanar configuration with the COO plane. The other ring attached to the oxygen in $-COO-$, on the other hand, deviates from the coplanarity with the COO plane by an angle of about 67 degrees (Laupretre and Noel, 1991), required by the steric interactions between the hydrogen at the ortho position on this ring and the oxygen of the carbonyl. We see in this example the combination of linearity with side-steps and the combination of coplanarity with non-coplanarity in the molecule. With these characteristics, poly(4-hydroxybenzoic acid)s have on the one hand sufficient linearity and rigidity of the rod-like nature for formation of liquid crystalline phases, they have on the other hand much higher flexibility than the corresponding poly(1,4-phenylene)s. With a comparison between the data in Tables 3.1 and 3.2, one finds immediately the much lower phase transition temperatures of the former than of the latter. With five phenylene rings, for example, the axial ratio of the poly(4-hydroxybenzoic acid) was 6.4, higher than the value 4.8 for the poly(1,4-phenylene). Both the compounds form a nematic liquid crystalline phase. However, because of the higher flexibility, the melting point and the isotropization temperature of the liquid crystal phase for the former are $220\,°C$ and $464\,°C$ respectively, much lower than that for
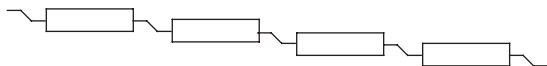
Figure 3.2.   "Side-steps" incorporated in a liquid crystal molecule.
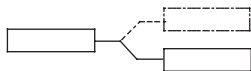
Figure 3.3.   "Crank-shaft" movement created at the side-steps.

the latter. Poly(4-hydroxybenzoic acid) with a sufficiently high molecular weight (n ∼ 100) has been synthesized and processed to products of very high mechanical properties (Chapter 5). Because of the unique character, the availability, and the high polymerizability, 4-hydroxybenzoic acid has become one of the most popular monomers used in the synthesis of liquid crystalline polymers.

The side-step linkages other than −COO− are also found in liquid crystals. Among them, the amide linkage −CONH− was not used until very recently in low mass liquid crystals. Amide linkages are to bring about strong hydrogen bonding and very high melting temperature for the compounds. By lateral substitution with suitable substituents, e.g., Br and nitro-, on the phenylene ring, Zhou, Zhang and coworkers (1995) were able to synthesize thermotropic liquid crystals with the following general formula ⟨3.3⟩:

$$\langle 3.3 \rangle$$
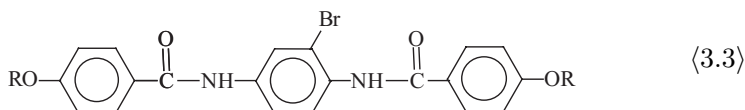
In this case, lateral substitution plays an important role in weakening hydrogen bonding and significantly depresses the melting temperature of the compound. As a result, the potential of this type of rod-like molecule to form liquid crystal phases is revealed. In Table 3.3 are shown the liquid crystalline property of a few of the 2-bromo-1,4–bis(4-alkoxybenzamido)benzene.

Table 3.3.   Liquid crystallinity of ⟨3.3⟩.

	R	Heating	(cooling)
1	Methoxy	K 232-233 N 239-240 I	(I 237-238 N)
2	Ethoxy	K 233-234 N 245-247 I	(I 243-242 N)
3	n-Octoxy	K 165-166 S 190-191 N 192 I	(I 192 N 190 S 165 K)
4	R1 = ethoxy R2 = cyano	K 234-235 N 269-270 I	(I 269-267 N)

Note: compound 4 is the unsymmetrically substituted homologue:
2-bromo-1-(4-ethoxybenzamido)-4-(4-cyanobenzamido)benzene.

3.2.3.   Incorporation of kinked elements

The most significant consequence of the incorporation of kinked elements in the molecules is the destruction of the linearity and the shortened length of the rod-like structural sequence of the molecules. Naturally, the type and the amount of the kinked elements have to be carefully decided in the molecular engineering of liquid crystals. For example, Vorlander (1923) studied the influence of different $-X-$ elements in the following molecules $\langle 3.4 \rangle$:

$$R-\bigcirc-CH{=}N-\bigcirc-X-\bigcirc-N{=}CH-\bigcirc-R \qquad \langle 3.4 \rangle$$

If in $\langle 3.4 \rangle$ the central linking unit $-X-$ is none, the molecules will have a linear rod-like shape with a length to diameter ratio somewhat larger than five. All the compounds, including those with R either being an H, a methyl, or a methoxy group, were found to be able to form a stable liquid crystal phase. On the other hand, if $-X-$ is $-O-$, or $-S-$, or $-HCH-$ unit, a kinked structure is introduced (Figure 3.4):

The molecule becomes two short rods linked by the kink. The linearity is destroyed. The compounds are no longer liquid crystals. In contrast, if $-X-$ is $-Hg-$, the linearity of the molecules can be maintained because the bond angle at $-Hg-$ is 180°. The mercury derivatives are all liquid crystals with the following data for phase-transition temperatures: for R = H, $Tm = 18$ °C, $Ti = 22$ °C; for R = methyl, $Tm = 217$ °C, $Ti = 229$ °C; for R = methoxy, $Tm = 209$ °C, $Ti = 285$ °C.

Kinked units such as $-O-$ also served as separators between two phenylene rings. As a result, the rotation of the rings about the linking unit becomes less hindered. Studies on the conformations for diphenyl ether, diphenyl sulfide, diphenylmethane, and diphenyl ketone have reached the conclusion that these molecules all have very low energy barriers for internal rotations. According to the summary of Laupretre and Noel (1991), a large portion of conformation space lies in the 1 kcal/mol region in these molecules. Besides, the energy barrier between any of the low-energy regions is also very small. In other words, the molecules are flexible and can easily
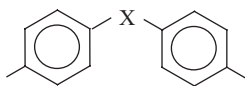
Figure 3.4.   Kinked structure destroys chain linearity.

go from one conformation to any other. However, there are also kinks that are much more rigid. The rigid kinked units often found in liquid crystal polymers are 2,2-diphenylpropane as well as 1,2-and 1,3-phenylenes.

3.2.4.   Incorporation of flexible spacers

Some of the kinked units discussed in the previous section, such as $-O-$ and $-S-$, are simple examples of flexible spacers that space the mesogenic units into separate structural sequences of smaller length-to-diameter ratios. Other segments often used as flexible spacers include oligomeric polymethylenes, polyoxyethylenes, polysiloxanes, and so forth. The following series of molecules, $\langle 3.5 \rangle$ with n = 1–8, make up one of the oldest examples of the flexible spacer concept in the molecular design of liquid crystals (Vorlander, 1927):

$$\langle 3.5 \rangle$$
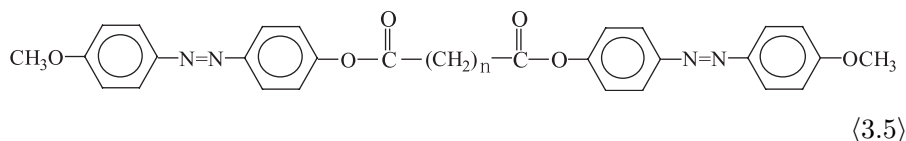
All the compounds in the series $\langle 3.5 \rangle$ form nematic liquid crystals, of which the clearing temperature decreases in an odd–even manner with the number n of the methylene unit in the spacer. Later studies have repeatedly confirmed this odd–even effect in different series of liquid crystals. Not only does the clearing temperature change in this way, the enthalpy, entropy and the molecular order parameter all have similar changes with the number of chain atoms in the spacer. Usually, the homologue with an even number of chain atoms in the space has a higher value of these parameters than that of the two neighboring homologues with odd numbers. It is believed that the spacers of even numbers of chain atoms are able to approximately maintain the linear shape of the molecules, while those with odd number atoms are not. This concept has frequent applications in the design of polymeric liquid crystals, and will be discussed further in the corresponding section.

3.2.5.   Terminal or end-on substitution

Terminal substitution is another factor having significant impact on the properties of liquid crystals. Taking the following homologues of hydroxybenzoate, $\langle 3.6 \rangle$ and $\langle 3.7 \rangle$, as examples, these two compounds have the

same chemical structure as rod-like cores but are different in terminal sub-stitutions. Compound $\langle 3.6 \rangle$ has no substituents at the ends. It melts at $132\,°C$ and does not form a liquid crystalline phase. In contrast, $\langle 3.7 \rangle$ has two alkyls as end groups. It has a lower melting point $(114\,°C)$ and is able to form a stable nematic phase in the temperature range from $114\,°C$ to $231\,°C$.

$$\langle 3.6 \rangle$$

$$\langle 3.7 \rangle$$
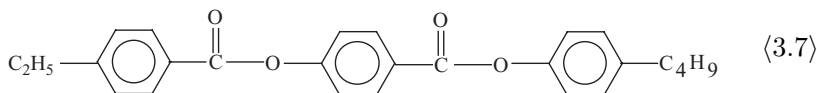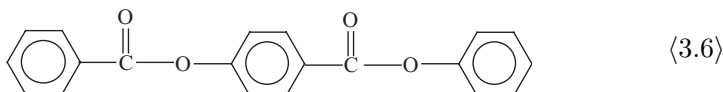
The comparison of the following two compounds, $\langle 3.8 \rangle$ and $\langle 3.9 \rangle$, is even more remarkable. In this case, only a small end methoxy substitution changes the nature of the compound from non-liquid crystalline to liquid crystalline. $\langle 3.8 \rangle$ melts at $162\,°C$ and no liquid crystal phase will be formed. On the other hand, $\langle 3.9 \rangle$ melts at a somewhat lower temperature $(157\,°C)$ forming a nematic phase with the clearing point of $165\,°C$.

$$\langle 3.8 \rangle$$

$$\langle 3.9 \rangle$$
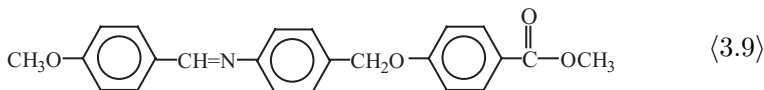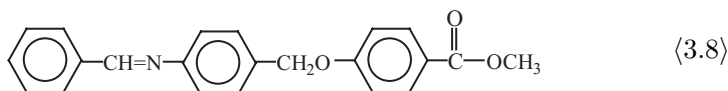
We see in these examples that great effect can be created by substitutions on the two ends of the mesogenic cores. The consequence includes not only the formability of liquid crystal phases and transition temperatures, but also the types of the liquid crystalline phase. It is well known that substitution on the end with longer linear alkyls and alkoxyls favor the formation of smectic phases. One example for this remark has been given in Table 3.3. In the design of liquid crystal polymers, especially in the cases of side-group type and molecular shish-kebabs, the concept of end-substitution has been fully utilized.

3.2.6.   Lateral or side-on substitution

The most significant consequence of lateral substitution on the mesogenic cores of a liquid crystal compound is the increase of diameter and the decrease of the length-to-diameter ratio. In addition, in comparison with the unsubstituted parent molecules, the molecular interactions will not be as strong and the packing of the molecules in both the crystal and the liquid crystal phases will not be as dense and compact. All these factors have negative effects on the thermal stability of the liquid crystal phase. Nevertheless, lateral substitution can bring down the melting point to a large extent, so large in cases as to be able to reveal the potential of a compound to form a liquid crystal phase. In Section 3.2.2 we have given one such example, ⟨3.3⟩, in which the lateral substitution of a bromo or nitro group on the central phenylene ring of the molecules has changed the non-liquid crystalline parent compounds into liquid crystals.

Another interesting example is 1,4-phenylene dibenzoate ⟨3.10⟩ and its vinyl substituted homologue 2-vinyl-1,4-phenylene dibenzoate ⟨3.11⟩ (Zhou *et al.*, 1993):

⟨3.10⟩

⟨3.11⟩
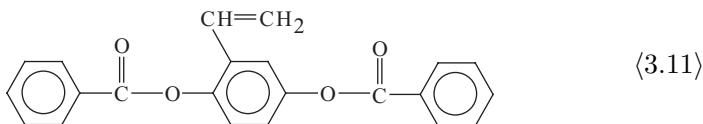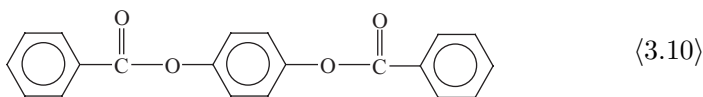
1,4-phenylene dibenzoate is a rod-like molecule with a length-to-diameter ratio of about 3.8. It should have the potential of liquid crystal forming. Ballauff and Flory (1984) reported that the compound ⟨3.6⟩ had a latent liquid crystal phase with a clearing temperature of about 100 °C. The two compounds ⟨3.6⟩ and ⟨3.10⟩ are very much alike in molecular structure. They all have three phenyl rings separated by two ester linkages. The only difference in them is the orientation of the ester groups, with two −CO−O− in ⟨3.6⟩ but one −CO−O− and one −O−CO− in ⟨3.10⟩. It is therefore reasonable to expect that ⟨3.10⟩ has a very similar potential as ⟨3.6⟩ to form a liquid crystal phase of very similar thermal stability and clearing point. However, ⟨3.10⟩ has a very stable crystalline state with a melting temperature as high as 207 °C, so far above the clearing point of

its latent liquid crystal phase that no such phase can be possibly observed. The substitution on the central ring with a bulky vinyl group gives the compound ⟨3.11⟩. To the researcher's pleasant surprise, by this substitution the melting point has been depressed to 88 °C, a value well below the clearing point of the latent liquid crystal of the parent molecule. A nematic liquid crystalline phase is indeed formed, the clearing point of which is 95, lower but very close to the prediction of Ballauff and Flory.

It is also interesting to mention that the compound ⟨3.11⟩ is the first published example that has lateral but no terminal substitutions and yet forms a liquid crystal phase. By and large, the studies on substitution effect have shown that while the terminal substitutions are favorable to the thermal stability and the formation of a liquid crystal phase, the lateral substitutions are not. The larger the lateral substitution, the more harm it can do to the thermal stability of the liquid crystalline phase. A typical and very convincing example for this idea is given by homologues of the well known para-substituted azoxyanisole ⟨3.12⟩:

$$CH_3O-\bigcirc-N{=}N(O)-\bigcirc-OCH_3 \hspace{2cm} \langle 3.12 \rangle$$
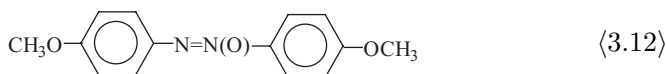
Para-azoxyanisole is the terminally substituted homologue. It melts at 118 °C and forms a nematic phase. The clearing temperature is 135 °C. However, its laterally substituted meta- and ortho-forms both are non-liquid crystals. The meta-form melts at 51 °C, the ortho-form melts at 80 °C.

In addition to the negative effect the lateral substitution may have on the thermal stability of a liquid crystal phase, one more important aspect has to be considered, for liquid crystal polymers especially when high strength and high modulus material are the goals. Thus, *e.g.*, if a fibre is made of the polymer, the tensile strength is a function of the number of polymer chains per unit cross section. Obviously, the lateral substitution and thickening of the chains will result in a lower strength. Besides, crystallinity can be affected to a great extent. A lower crystallinity often means a lower mechanical property and a lower heat deflection temperature. All the negative aspects have to be taken into consideration when lateral substitution is used to bring down the melting points.

In this section we have discussed several structural aspects of liquid crystal compounds. However, these are not the only aspects that have a significant impact on the formation and property of liquid crystals. For

successful molecular engineering, an integrated analysis of these and certain other factors are required. In polymer systems, the molecular weight is of special importance and is accounted for in Section 3.3.

3.3.   MOLECULAR WEIGHT AND MOLECULAR WEIGHT DISTRIBUTION

Polymers, including liquid crystal polymers, distinguish themselves from low mass compounds by their high molecular weight and the existence of a distribution of molecular weights. In contrast to low mass compounds, polymers usually have limited solubility, slow chain motion and high viscosity, extensive chain entanglements, slow relaxation process, retarded and non-equilibrium phase transitions, less perfect crystallization and a lower degree of crystallinities, as well as the existence of the glassy state and glass transitions. Thus, a thermotropic liquid crystal polymer may be non-crystalline and forms a liquid crystal phase in the temperature region above Tg (the glass transition temperature) and below Ti (the isotropization temperature). On the other hand, the polymer may be a semi-crystalline two-phase system that has such a sequence of the transition processes: the two-phase state (amorphous plus crystalline) transfers at Tg to the second two-phase state (liquid crystalline plus crystalline) that transfers at the melting temperature Tm to the one-phase liquid crystalline state that in the end transfers at Ti to the one-phase isotropic liquid state. This is actually a simplified picture of the process. For example, above the glass transition there may also be a crystallization process. Yet because of the distribution of molecular weights and other reasons, the melting as well as the isotropization process are usually not sharp, but happen in a broad temperature range in which at least two phases coexist. The situation becomes even more intricate if the structure and property of each phase and the multiphase state are to be considered. The consequence brought about by high molecular weights and by the molecular weight distributions are profound but only a few remarks are made in this short account.

For lyotropic liquid crystals, the relationships between the chain length (molecular weight) and the formability of liquid crystals have been formulated. According to Onsager and Flory (Chapter 2), for any solutions of rigid rods there is a critical concentration ν' (the volume fraction of rods in the solution) determined by the length-to-diameter ratio (L/d) of the rods

[Equations (3.1) and (3.2)].

$$\text{Onsager: } \nu' = \frac{3.29}{(L/d)} \qquad \nu'' = \frac{4.19}{(L/d)}. \tag{3.1}$$

$$\text{Flory: } \quad \nu' = \frac{7.89}{(L/d)} \qquad \nu'' = \frac{11.57}{(L/d)}. \tag{3.2}$$

Above ν', the solution separates into isotropic and anisotropic phases. If the concentration is further increased to above the value ν'', the solution becomes a single liquid crystal phase. The longer the rods, the lower the ν' and ν'' values. On the other hand, if dilution is made for the liquid crystalline solutions of rigid rods, the solution of longer rods will transfer into the isotropic liquid at a higher dilution. In other words, the rods with higher length-to-diameter ratios are predicted by the theories to have higher formability of a more stable lyotropic liquid crystal phase. In order to have a better fit with experimental data for polymers of a different nature, some modified forms of the original Onsager and Flory theories have been derived. For the worm-like chains, for example, the KSO theory (Odijk, 1986) gives the following form (Equation 3.3) to correlate ν' with the chain length L, diameter d, and persistence length q:

$$\nu' = \frac{d}{2q} \left[\frac{3.34 + 11.3\left(\frac{L}{2q}\right) + 4.06\left(\frac{L}{2q}\right)^2}{\left(\frac{L}{2q}\right)\left(1 + 0.387\left(\frac{L}{2q}\right)\right)} \right]. \tag{3.3}$$

The experimental data of ν' for several polymer systems have been compared with the calculated values of the KSO theory. The two are found to be in very good agreement (e.g., Ciferri and Marsano, 1987).

For thermotropic systems, such parameters as the temperature of phase transitions, the enthalpy and entropy changes at the transitions, as well as the order parameter of the liquid crystal phase are all affected by molecular weight. In general, these parameters all increase with molecular weight until leveling off when the molecular weight becomes high enough. This is true for both the main-chain type and the side-group type liquid crystal polymers.

Portugall *et al.* (1982) noticed that the phase transition temperature and enthalpy of the following side-group type liquid crystal polymer, ⟨3.13⟩, were dependent on the degree of polymerization n. The polymer was non-crystalline. If n = 13, the glass transition temperature was 53 °C, the clearing point of the liquid crystal phase was 100 °C, the enthalpy of

the isotropization was 0.6 kJ/mol; If n = 41, the corresponding parameters increased to 59 °C, 114 °C, and 0.6 kJ/mol respectively. These parameters were found to increase to 62 °C, 116 °C, and 0.9 kJ/mol with the further increase in the degree of polymerization to n = 114.

$$-\left(CH_2-CH\right)_n \\ \quad | \\ COO-CH_2CH_2-O-\langle\bigcirc\rangle-COO-\langle\bigcirc\rangle-OCH_3 \qquad \langle 3.13\rangle$$
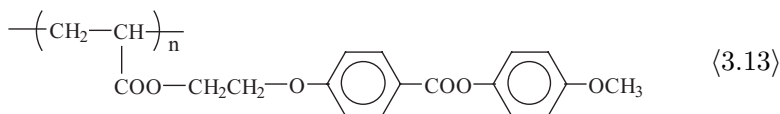
Stevens *et al.* (1984) carried out a more detailed study on the effect of molecular weight. Several side-group type polymers, ⟨3.14⟩, with polysiloxane backbones and flexible spacers of different number of methylene units were studied:

$$(CH_3)_3\,Si-O-\left[\begin{array}{c} CH_3 \\ | \\ Si-O \\ | \\ CH_2-(CH_2)_{m-2}-CH_2-O-\langle\bigcirc\rangle-COO-\langle\bigcirc\rangle-OCH_3 \end{array}\right]_n Si(CH_3)_3 \qquad \langle 3.14\rangle$$
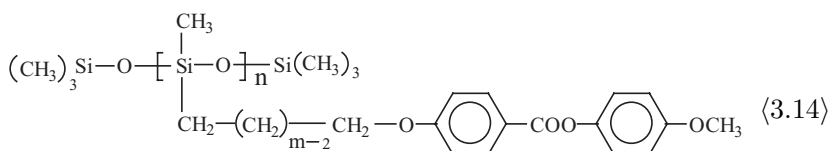
$$m = 3-6.$$

The degree of polymerization of these polymers varied from n = 1 to n = 100.

A few conclusions were obtained from this study. For all four systems with m = 3 to 6, the properties change most significantly when the degree of polymerization increases from 1 to 10. For example, for the polymer of m = 3, the monomer and the dimer do not form liquid crystals. The trimer forms a nematic liquid crystalline phase between the glass transition ($Tg = 270\,°\mathrm{K}$) and isotropization ($Ti = 285\,°\mathrm{K}$). The mesophase is stable within this temperature interval. With the further increase of n to 10, both Tg and Ti shift to higher temperatures, but the latter increases much faster than the former so that the temperature range of the stable liquid crystalline phase also increases with n. Above n = 10, the transition temperatures increase only slightly until stable values are reached at approximately n = 100. For the polymer of m = 3 and n = 95, Tg and Ti were found to be 290 °K and 356 °K respectively. The other polymers with different m have similar behavior. However, the polymer with the longest spacer in the series, m = 6, forms a smectic phase in addition to a nematic phase. The influence the flexible spacer has on the property of the side-group type liquid crystalline polymers will be discussed in Section 3.5. Stevens and coworkers

proposed that the increase in thermal stability of the mesophase with molecular weight was attributed to progressively denser packing of the mesogenic side groups of the oligomers with a growing degree of polymerization. This effect is macroscopically seen in a decrease of specific volume at the phase transformation temperature with a degree of polymerization.

Another interesting phenomenon found by Stevens *et al.* is the monotropic mesophase formed by the dimer and trimer of the polymer with m = 6. The dimer has a monotropic nematic phase, the trimer has a monotropic smectic phase. These metastable monotropic phases become stable enantiotropic phases with the increase of n by 1. At about the same time, Blumstein *et al.* (1984) found the low mass model compound of a main-chain type liquid crystalline polymer was monotropic while the mesophase of the polymer was enantiotropic.

Zhou *et al.* (1986) studied the transformation of monotropic to enantiotropic mesophase of the main-chain type liquid crystalline polymer, $\langle 3.15 \rangle$, in terms of the molecular weight effect.

$$-O-(CH_2)_{10}-O-\overset{\overset{\displaystyle O}{\|}}{C}-\!\!\bigcirc\!\!-\overset{\overset{\displaystyle O}{\|}}{C}-O-\!\!\bigcirc\!\!-O-\overset{\overset{\displaystyle O}{\|}}{C}-\!\!\bigcirc\!\!-\overset{\overset{\displaystyle O}{\|}}{C}- \qquad \langle 3.15 \rangle$$
$$\underset{\text{CHO}}{}$$
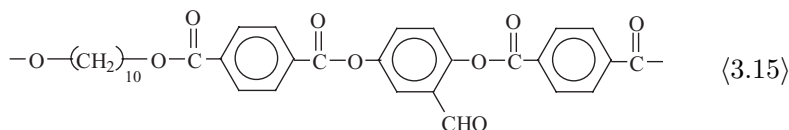
Some of the results are shown in Table 3.4.

In this study, the inherent viscosity was used as the measure of molecular weight. We see in Table 3.4 that the transition temperatures, especially Ti change with molecular weight in a relatively wide range of molecular weights. The first three samples with inherent viscosity lower than $0.19\,\mathrm{dl/g}$ are monotropic liquid crystals. They form liquid crystals only in the course of cooling from an isotropic liquid state. It is so because the melting point is higher than the clearing temperature of the latent mesophase. It is only possible for a polymer to transform from monotropic to enantiotropic if the isotropization temperature increases faster than the melting point with increasing molecular weight. This is the case for the polymer in consideration. When the viscosity has increased from 0.14 to 0.20, the increase in Tm is from $144\,°\mathrm{C}$ to $159\,°\mathrm{C}$. At the same time, the increase in Ti has been from below $144\,°$ to $160\,°\mathrm{C}$. Ti increases faster than Tm and starts to surpass the latter at the viscosity of $0.197\,\mathrm{dl/g}$. Care was taken to determine Ti for the samples just starting to show the enantiotopic property. Thus the samples were heated to $200\,°\mathrm{C}$, a temperature well above Ti so as to guarantee an isotropic liquid phase. Taking advantage of the large extent

Table 3.4.   Inherent viscosity and phase transition temperatures of polymer $\langle 3.15 \rangle$.

Viscosity	Tm	Ti	Ti–Tm	Tlc	Tc	Tlc–Tc	Remark
0.140	144	—	0	139	107	32	monotropic
0.150	139	—	0	122	—	—	monotropic
0.158	144	—	0	129	102	17	monotropic
0.197	159	160	1	160	112	48	transitive
0.198	158	161	3	160	119	41	transitive
0.254	156	167	11	163	102	61	enantiotropic
0.301	160	170	10	169	103	66	enantiotropic
0.355	158	176	18	174	102	72	enantiotropic
0.474	159	180	21	173	102	71	enantiotropic
0.596	155	180	25	172	102	70	enantiotropic
0.712	153	176	24	167	103	70	enantiotropic

Note: The inherent viscosity is in dl/g; Tm: melting point; Ti: isotropization temperature; Tlc: isotropic liquid to liquid crystal transformation temperature in cooling; Tc: crystallization temperature. All the Ts are the peak temperatures in the DSC curves and are all in °C.

of super cooling, the samples were quickly cooled to $130\,°C$, a temperature much lower than Tlc but sufficiently higher than Tc, so that the samples were in the metastable mesophase. As soon as the mesophase was obtained, the samples were heated up to find Ti. The determinations were carried out by DSC and by polarizing microscopy. Both the techniques have given the same result.

In Table 3.4, one is able to see the increasingly higher thermal stability of the liquid crystal phase with the increase of molecular weight. While Tm is about the same for polymers of viscosity higher than $0.2\,$dl/g, Ti keeps increasing until above $0.35\,$dl/g. As a result, the temperature range (Ti–Tm) of the mesophase is also broadened.

From this study, we see that the influence of increasing molecular weight is stronger on the mesophase than on the crystalline phase. The melting point of the crystal stops increasing much earlier than the clearing point of the mesophase. The reason for this result is still to be deduced, but one hint is given below. For thermotropic liquid crystalline polymers, it has been found that the thickness of the crystal lamella increases with increasing molecular weight until a thickness of about $100\,$nm is reached. Crystals of thinner lamellae have a lower thermal stability and a lower melting temperature. Since the finite value of lamella thickness is about

100 nm and the polymer chain in the crystalline state is oriented along the thickness of the lamella, only a few tens of the repeating units can be accommodated by the thickness. Thus in principle, a perfect lamella of 100 nm thick can be formed by a polymer with a degree of polymerization of only a few tens. If no chain ends are included inside the lamella, only thinner lamellae are formed by polymers of lower molecular weights. If chain end inclusion is allowed in the lamella, lamella with more defects will result from samples of lower molecular weight. On the other hand, for samples of high degrees of polymerization, extensive chain folding may occur, otherwise the polymer chain has to travel through two or more lamellae. Nevertheless, the limited low value of lamella thickness gives reason for the fast attainment of the limited melting point of the polymer crystals.

In order to study the general applicability of the above principle for the transformation of the monotropic liquid crystals to the enantiotropic ones by increasing the molecular weight of the monotropic liquid crystal polymers, the polymer, $\langle 3.16 \rangle$, reported by Ober *et al.* (1983), was restudied (Duan *et al.* 1987).

$$-\overset{\overset{\displaystyle O}{\|}}{C}-\!\!\!\!\bigcirc\!\!\!\!-O-\overset{\overset{\displaystyle O}{\|}}{C}-\!\!\!\!\bigcirc\!\!\!\!-\overset{\overset{\displaystyle O}{\|}}{C}-O-(CH_2)_{10}-O- \qquad \langle 3.16 \rangle$$
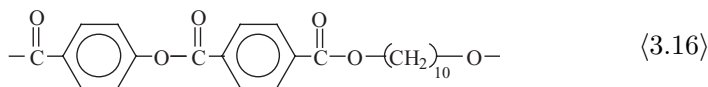
According to Ober *et al.*, the polymer with an intrinsic viscosity of 0.17 dl/g is monotropic. In this restudy, a sample with a viscosity of 0.30 dl/g was obtained. The sample melts at 148 °C and forms a nematic phase. The clearing point of the liquid crystal is 170 °C. The sample was fractionated to obtain three fractions with viscosity of 0.14, 0.39 and 0.61 dl/g respectively. In agreement with Ober *et al.*, the sample of the lowest intrinsic viscosity (0.14 dl/g) is monotropic, melts at 140 °C and forms the liquid crystal phase only in the circle of cooling. However, the fractions with higher viscosity are all enantiotropic liquid crystals. The one of 0.39 dl/g melts at 149 °C, the clearing temperature of the liquid crystal phase is 159 °C. The fraction of the highest viscosity also melts at 149 °C, but the clearing point is somewhat higher (164 °C).

At about the same time, Percec and Nave (1987) also found that the transformation of the monotropic liquid crystalline polymers to the enantiotropic ones could be achieved by increasing molecular weight. The polymer studied by these authors has the following structural formula

$(\langle 3.17\rangle)$:

$$-\text{O}-\phenyl-\underset{\underset{\text{CH}_3}{|}}{\text{C}}=\text{CH}-\phenyl-\text{O}+\text{CH}_2\overset{}{\underset{11}{)}} \qquad \langle 3.17\rangle$$
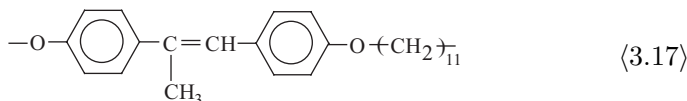
Some of the results for the polymer $\langle 3.17\rangle$ are shown in Table 3.5.

As shown in Table 3.5, the low molecular weight polymer of Mn 1100 is non-liquid-crystalline. The sample of Mn 3500 is monotropic while those with Mn of 10200 and higher are enantiotropic. The thermal stability of the mesophase increases with increasing molecular weight as shown by the higher clearing temperature Ti of the sample with higher molecular weight. Percec *et al.* (1989) also studied the effect of molecular weight in side-group type liquid crystal polymers. The similar monotropic to enantiotropic transformation was found in these systems. The crystallization of side groups was considered to be responsible for the transformation in these cases. The polymer with a higher molecular weight has a lower crystallizability of the side groups. In contrast, the crystallization of the main-chain type polymers seems not to be affected in such a way by the molecular weight. In the latter case, samples with higher molecular weights have a higher melting point in the region of low molecular weights.

The principle of the monotropic to enantiotropic transformation by increasing molecular weight has been demonstrated by the above examples. However, for a full understanding of this phenomenon, further studies are required. For the main-chain type liquid crystal polymers with alternating sequences of the rod-like and the flexible segments, Kohlhammer *et al.* (1989) have found that the orientational order of the flexible segments is higher in the samples of higher molecular weights. In other words, the contribution by the flexible segments to liquid crystalline ordering is higher in

Table 3.5. Phase property and molecular weight of the polymer $\langle 3.17\rangle^*$.

Mn	Mw	Tm	Ti	Tlc	Tc	Remark
1100	2300	101.5	–	–	89.8	non l.c.
3500	6700	117.9	–	111.5	97.5	monotropic
6700	10200	121.6	134.0	129.7	104.8	enantiotropic
10900	15200	124.0	147.9	143.6	107.5	enantiotropic
29400	92300	126.2	152.0	139.0	93.3	enantiotropic

* Source: Percec and Nave (1987).

samples of higher molecular weights. This and related findings have rendered partial explanations for the molecular weight effect on the stability of the polymeric liquid crystal phase.

Very few reports have been given on the effect of molecular weight distribution. In the restudy on Ober's polymer mentioned above in this section, we see also the influence of the molecular weight distribution on the thermal stability of the liquid crystal phase. The unfractionated sample has a broader molecular weight distribution and a broader temperature range of the nematic phase (148 °C to 170 °C). On the other hand, the fractionated sample with a little higher viscosity (0.39) has narrower distribution and a narrower temperature range of the mesophase (149 °C to 159 °C). However, in another study on a side group type liquid crystalline polymethacrylate, the two samples with very close values of molecular weight ($Mn = 9860$ and 10300) but significantly different molecular weight distributions ($Mw/Mn = 4.21$ and 1.70) were found to have the same Tg (= 206 °C) and the same Ti (= 344 °C).

For polymers, not only is the thermal stability of the mesophases important, the consequence of molecular weight and its distribution on the process and application properties is also of primary significance. For instance, higher polymers result in higher melt viscosity and slower response to applied physical fields. Thus, for certain applications where fast responses are essential, high molecular weight liquid crystals may not have any superiority. On the other hand, higher molecular weight polymers usually result in superior mechanical properties. It is known that, e.g., the strength of the fiber spun from 2-phenyl-1,4-phenylene terephthalate with the molecular weight of 5000 is 0.6 Gpa, only about one sixth of that with a molecular weight of 40000, or that from the polymer of m.wt. 30000 is only one third of the one from m.wt. 300000 (Jackson, 1988). High molecular weight is thus required for polymers used as high-strength and high-modulus materials. However, things are more complicated even in this case. In a study on the copolymers from 2,6-naphthalenedicarboxylic acid (20 mol%), terephthalic acid (20 mol%), 1,4-phenylene diacetate (40 mol%) and 4-acetoxybenzoic acid (60 mol%), Jackson (1992) found that the tensile strength and flexural properties of the injection-molded liquid crystalline polymer first increased with molecular weight as would have been expected, but decreased markedly when the absolute molecular weight was over 40000. Light scattering data indicate that this polymer behaves as a rigid rod at lower molecular weights. It becomes worm-like and forms chain entanglements at the higher molecular weights. The measurement of the Hermans orientation factors through

wide angle X-ray diffraction of the samples resulted in a higher value (0.51) for the sample having the highest tensile strength and a lower value (0.40) for that having the highest molecular weight ($\sim$65000). Thus the reduction in tensile strength can be explained by the reduction in molecular orientation because of the increased extent of entanglement in samples of the highest molecular weight.

In summary, the nature and property of a polymer can be varied simply by the variation of molecular weight. Most significantly, some polymers may change from non-liquid-crystalline to monotropic liquid crystalline and to enantiotropic liquid crystalline with the increase in molecular weights. The phase transition temperatures also increase with molecular weight at lower values, especially where the isotropization process is concerned. Therefore, no reliable analysis for the structure-property relationship can be made for any liquid crystalline polymer if there is no reliable information on its molecular weight. At the same time, no reliable comparison on the structure and property can be made for two polymers if the molecular weights are not high enough and if the property is still a function of the molecular weight. In the literature of the side-group type liquid crystal polymers, there have been some suggestions that the property becomes stable when the degree of polymerization is higher than 10, others suggest that the d.p. value must be over 200 before the property is stabilized. Keeping in mind the effect imposed by molecular weight, our discussion in the following sections will be in principle based on data for polymers having sufficiently high molecular weights.

3.4. MAIN CHAIN LIQUID CRYSTALLINE POLYMERS

As discussed in Section 3.1, the rod like main chain type polymers can form only lyotropic liquid crystals on the condition that a solvent with sufficient solubility is present. In order to obtain liquid crystalline melts of the polymers, effective structural modification has to be made, so as to reduce the structural regularity and rigidity of the molecular chains. The polymers with higher irregularity and flexibility will have lower crystallinity and a lower melting point. The general approach of molecular modification include the introduction of the substituents, the side-step moieties, the kinked units, the flexible segments, as well as the copolymerization of different structural units. Utilization of two or more of the methods has become the common practice so that the crystallinity and melting point can be brought down sufficiently.

Taking poly(1,4-phenylene terephthalate) as an example, the basic constitutions of this polymer is the regularly positioned 1,4-phenylene rings and the ester linkages. Because of the very high structural regularity and lack of flexible elements, it is highly crystalline with no melting before decomposition. Thus no mesophase is formed on heating to melt the sample. The most convenient and very effective way to bring down the melting temperature has been the introduction of a substituent group on one of the two rings in the repeating unit as demonstrated by the polymers ⟨3.18⟩ (Jackson and Kuhfuss, 1976) and ⟨3.19⟩ (Payet, 1979):

m.p. 370°C   ⟨3.18⟩

m.p. 343°C   ⟨3.19⟩
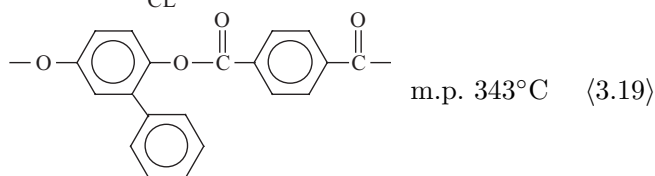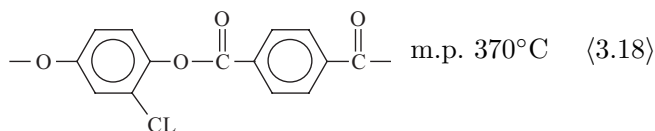
In these two cases substitution of an H of the ring with a chlorine atom or a phenyl group resulted in a remarkable decrease in the melting point. Both polymers are thermotropic liquid crystals and are melt. Because of the larger size of the phenyl substituent, polymer ⟨3.19⟩ has an even lower melting point and can be melt-spun to form high strength fibers. A simple substitution such as that in ⟨3.18⟩ and ⟨3.19⟩, not only has the consequence of broadening the molecule and separating the neighboring chains, but also brings in certain irregularities for the chain. One type of the irregularities is shown by ⟨3.20⟩ where two types of incorporation of the phenyl substituted 1,4-phenylene moieties are demonstrated for the polymer ⟨3.19⟩. Obviously in the chain there is a distribution of these two types of bonding. In other words, this polymer, though generally considered to be a homopolymer, is actually a random copolymer consisting the two different building blocks. The substitution thus has a higher efficiency in decreasing crystallinity and transition temperature than one might have realized if only the broadening and separation effects are considered.

⟨3.20⟩
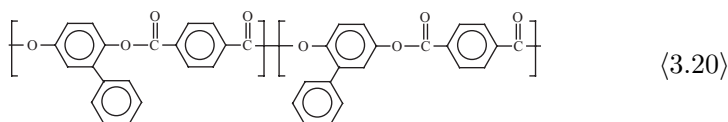
The effectiveness of random copolymerization in depressing crystallization and melting point can be further demonstrated by the polymer ⟨3.21⟩ (Jackson & Kuhfuss, 1982). In comparison to the polymer ⟨3.19⟩, the polymer ⟨3.21⟩ has an even lower melting point (330 °C) even though the extent of the substitution is lower by 25%.

⟨3.21⟩
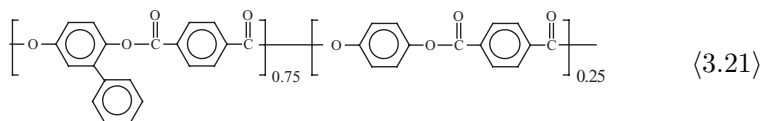
Similarly, copolymerization of a certain amount of 4-hydroxybenzoic acid (HBA) with phenyl-1,4-hydroquinone and terephthalic acid also gives rise to a remarkable decrease in the melting point. The general structural formula and the melting points of the copolymers with different HBA content are given respectively by ⟨3.22⟩ and Table 3.6. In this particular case, the incorporation of 20 mol % of HBA into the polymer ⟨3.19⟩ has resulted in a polymer with a melting point as low as 229.

⟨3.22⟩
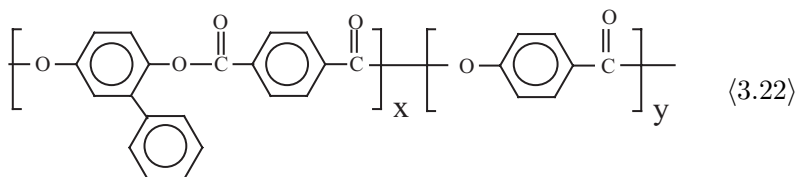
It is interesting to make a comparison of the polymer ⟨3.19⟩ with ⟨3.23⟩ shown below. The only difference in structure of these two polymers is that in ⟨3.19⟩ the phenyl substituent is on the

m.p. 278°C ⟨3.23⟩
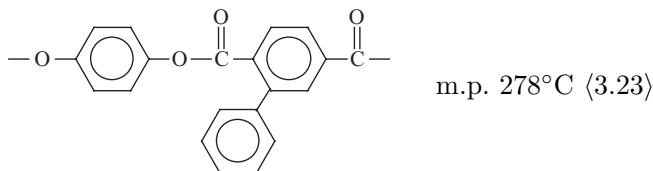
hydroquinone moiety while in ⟨3.23⟩ (Harris, 1981) the substitution is on the terephthalic moiety. However, the difference in melting point of the two is a remarkable 343 °C to 278 °C. Because of the very high similarity in

Table 3.6.   Melting point and composition of polymer $\langle 3.22\rangle$*.

y (mol %)	0	5	10	20	30	50	60	70	100
m.p. (°C)	343	335	317	229	309	325	373	379	~600

* Source: Jackson *et al.* 1980.

molecular structure of the two, we can expect a very high similarity for the two in chain thickness and chain irregularity. Thus there must be other reasons for such a high difference in the melting property of the two. For one thing, the sample of $\langle 3.23\rangle$ has a somewhat lower intrinsic viscosity (0.51) than the sample of $\langle 3.19\rangle$ (1.03), for the other, substitution on the phenylene ring of terephthalic moiety will interfere with the coplanarity between the ring and the two ester groups. As discussed by Laupretre and Noel (1991), the ring in terephthlic moiety takes the coplanar conformation with the ester groups as the lowest energy form, while the lowest energy conformation in 1,4-hydroquinone diesters is not coplanar but has its plane of the phenylene ring and the plane of the ester group rotated from one another by an angle of approximately 60 degrees. Thus, the substitution on the ring of hydroquinone moiety in $\langle 3.19\rangle$ should have only minor interference with the already non-coplanar conformation, but the substitution on the ring of terephthalic moiety in $\langle 3.23\rangle$ should have changed the conformation from a coplanar one to a non-coplanar one because of the steric interactions between the bulky substituent and the ester group. This non-coplanarity caused by the bulky substitution on the terephthalic moiety may have explained the relatively lower melting point of this ($\langle 3.23\rangle$) and other polymers of phenylterephthalic acid. The following polymer $\langle 3.24\rangle$ serves as one more example to show the effect (Harris, 1981). This polymer has a very similar intrinsic viscosity (0.99) as that (1.03) of $\langle 3.19\rangle$, but has a much lower melting point (270 °C compaired with 343 °C) regardless of the presence of the longer rod-like moiety biphenyl.

m.p. 270°C $\langle 3.24\rangle$
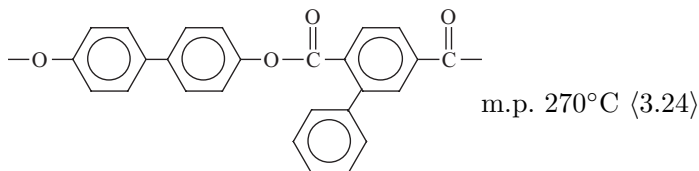
Zhou and Lenz (1983) and Zhou *et al.* (1985) discussed the substitution effect from the point of view of steric and polar effects. However, from above discussions one sees a more intricate picture. A full understanding of the effect demands further study. Nevertheless, substitution is so effective that a lot of studies have used this concept in the molecular engineering of liquid crystalline polymers in order to have desired phase properties.

Back to copolymerization. Even though such monomers as 4-hydroxybenzoic acid (HBA), monomer pairs as 1,4-hydroquinone (HQ) and terephthalic acid (TA) or 4,4′-dihydroxybiphenyl (BP) and terephthalic acid can result in only unmeltable rigid polymers, their copolymerizations have resulted in meltable polymers. The melting points of the HBA-HQ-TA copolymers were reported to be around 400 (Inai *et al.*, 1982), that of the HBA-BP-TA was also only 380 °C–420 °C. Based on the latter together with isophthalic acid, the products "Xydar" and "Ekonol" have been commercialized as high strength high modulus and flame resistant materials. The heat deflection temperature (HDT) of these materials is in the range of 317 °C–355 °C (at 1.82 MPa). The excellent mechanical and thermal properties have qualified these thermotropic liquid crystalline aromatic polyesters for advanced engineering materials (Suenaga, 1990).

Another famous type of liquid crystalline aromatic polyesters are those copolymers based on 6-hydroxy-2-naphthoic acid (HNA) and 4-hydroxybenzoic acid (HBA). These polymers have been commercialized by Hoechst-Celanese as "Vectra". The incorporation of 2,6-naphthalylene moieties brings into the polymer chains with "side-steps" and with the crank-shaft movements (Figures 3.2 and 3.3). As mentioned in Section 3.2.2, this type of structural modification will result in less chain rigidity. Calundann (1979) had a systematic study on the relationship of property and the ratio of HNA/HBA in the copolymers prepared from the melt polycondensations of 4-acetoxybenzoic acid and 6-acetoxy-2-naphthoic acid. The result is shown in Table 3.7. Although the homopolymers of these two monomers are both crystalline with melting points over 400 °C, the copolyesters all have a much lower melting point and can be processed by melt spinning at about 310 °C.

Table 3.7.   Melting point of HNA/HBA copolyesters*.

HNA/HBA	0/100	25/75	30/70	40/60	50/50	60/40	100/0
m.p. °C	~600	302	275	245	260	263	~440

* Source: Calundann (1979).

The effectiveness of 2,6-naphthalene moiety in depressing melting temperature is also demonstrated by copolymers containing 2,6-dioxynaphthalene or 2,6-naphthoyl units. It was reported, *e.g.*, the melting point of the polymer of terephthalic acid and 2,6-dihydroxynaphthalene was only 210 °C (Harris, 1981); that of the copolymer of 2 mol 4-hydroxybenzoic acid with 1 mol of 2,6-dihydroxy-naphthalene and 1 mol of terephthalic acid was 285 (Calundann, 1980); that of the copolymer of 1 mol hydroquinone, 1 mol of 2,6-naphthoic acid and 3 mol 4-hydroxybenzoic acid was 325 °C–340 °C; and that of 1 mol 2,6-naphthoic acid, 1 mol 4,4′-dihydroxybiphenyl, 3 mol 4-hydroxybenzoic acid was 385 °C–390 °C (Calundann, 1978).

As shown by the above examples, with the substitution and incorporation of side-step moieties such as 2,6-naphthalene side-steps the melting point of the fully aromatic polyesters can be depressed to below 400 °C. But because of the high degree of chain rigidity of the fully aromatic polymers, the clearing point of the liquid crystalline phase of these copolyesters is not observable before decomposition takes place. In order to further increase the chain flexibility and realize the clearing temperature of the liquid crystalline phase, flexible aliphatic or siloxane segments are often used in the practice of molecular engineering of liquid crystalline polymers. The flexible element may be applied as substituent on the aromatic rings as in the polymers ⟨3.25⟩ reported by Berger and Ballauff (1988):

$$\langle 3.25 \rangle$$
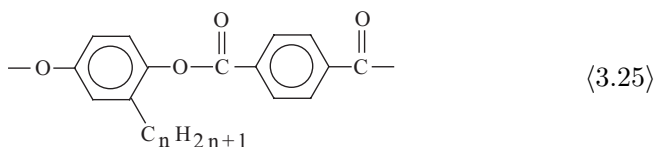
The unsubstituted parent polymer does not melt without decomposition. The methyl-substituted polymer, n = 1 in ⟨3.25⟩, melts at 381 °C. With longer alkyl substitution, the melting point will be decreased to a larger extent. When n is 10, the polymer melts in the range of 250 °C–310 °C and begins to show the clearing point of the liquid crystal phase ($Ti \sim 400$ °C). The clearing point will decrease with a longer alkyl substituent, but the temperature range of the liquid crystal phase will also narrow because the extent of depression of the melting point is not as large as Ti. The polymer is no longer liquid crystalline when n is 16 and larger.

The other and most popular way is to copolymerize the flexible segment into the polymer main chains. De Gennes (1975) predicted that incorporation of both a rigid and a flexible segment in the repeating unit should afford semi-flexible polymers exhibiting thermotropic liquid crystallinity,

and allow control of the transition temperatures. Studies on the main-chain type liquid crystalline polymers with flexible segments along the chain (Figure 3.1) have been active and extensively reviewed by Ober *et al.* (1984) and by Sirigu (1991). Accordingly, we will make only a few remarks on the three principal structural elements of the polymers, namely the mesogenic units, the flexible segments, and the way in which the mesogenic units and the flexible segments are connected.

In Table 3.8, the structure and property are shown for a few polymers with different mesogenic units and/or different connecting groups but all with decamethylene as flexible segments. These polymers are so selected that the influence of the structure of mesogenic units and of the way of connecting may be demonstrated.

The mesogenic units in polymer ⟨3.26⟩ are of the type based on conformational isomerism (Percec, 1988, and Section 3.7). Although they take the extended linear shape as one of their lowest energy conformations and thus are capable of forming liquid crystalline phases, they are rather flexible in comparison with what is mostly used in liquid crystalline polymers such as the one in polymer ⟨3.27⟩. The calculated length of the extended shape of the two mesogenic units in ⟨3.26⟩ and ⟨3.27⟩ is almost the same (∼1.8 nm). However, because of the significant difference in rigidity of the two types of mesogenic units, polymer ⟨3.26⟩ has a much lower phase transition temperatures than ⟨3.27⟩. In addition, the mesophase of the latter is nematic, that of the former is smectic. The reason for the difference in the type of liquid crystalline phase has not been analyzed in literature. We believe that the polymer ⟨3.27⟩ also has the potential of forming a smectic phase with a similar or somewhat higher thermal stability than that of ⟨3.26⟩. However, because the melting point (237) of ⟨3.27⟩ is significantly higher than the clearing point (211) of the smectic phase of ⟨3.26⟩, it may also be higher than the transition temperature of the latent smectic phase of ⟨3.27⟩. The high melting temperature might have prevented polymer ⟨3.27⟩ from forming a smectic phase.

The polymer ⟨3.29⟩ is obtained if the central 1,4-phenylene moiety in ⟨3.27⟩ is replaced by 4,4′-biphenylene that is as rigid but longer than the former. Such a replacement increases the length and the length-to-diameter ratio of the mesogenic unit. More stable mesophase and higher mesophase transition temperatures can be expected (Section 3.1). As a matter of fact, not only are the melting and the clearing temperatures of the mesophase are higher for ⟨3.29⟩ than ⟨3.27⟩, the temperature range of the mesophase is also broader for the former by 39 °C.

The substitution effect on liquid crystals has been discussed for low mass and fully aromatic polymers. The comparison of ⟨3.28⟩ with ⟨3.27⟩ shows the effect of substitution in mesogenic units on the properties of polymers with flexible segments in main chains. Again, the substituted polymer has a lower melting point, a lower clearing temperature, and a narrower temperature

Table 3.8.   Property of polymers with mesogenic units separated by flexible decamethylene segments.
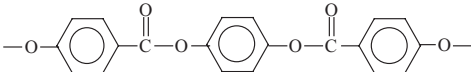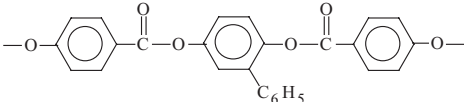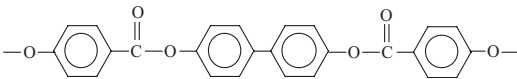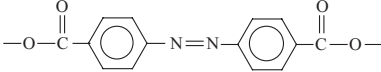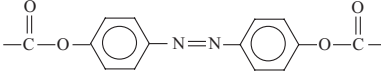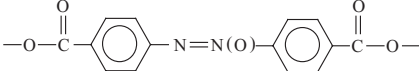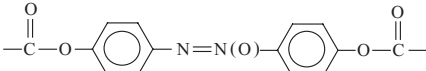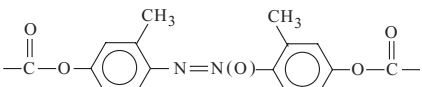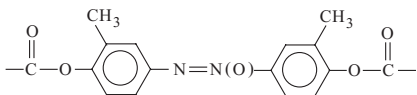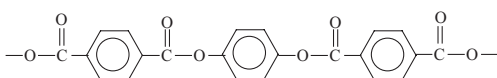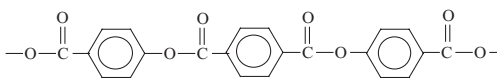
	Mesogenic moiety together with the connecting group	Transition, °C
⟨3.26⟩	—O—⟨◯⟩—O—CH₂—⟨◯⟩—CH₂—O—⟨◯⟩—O—	C 195 S 211 I (Josson *et al.*, 1989)
⟨3.27⟩	—O—⟨◯⟩—C(O)—O—⟨◯⟩—O—C(O)—⟨◯⟩—O—	C 237 N 294 I (Antoun *et al.*, 1981)
⟨3.28⟩	—O—⟨◯⟩—C(O)—O—⟨◯⟩(C₆H₅)—O—C(O)—⟨◯⟩—O—	C 151 N 168 I (Jo *et al.*, 1982)
⟨3.29⟩	—O—⟨◯⟩—C(O)—O—⟨◯⟩—⟨◯⟩—O—C(O)—⟨◯⟩—O—	C 258 N 354 I (Van Luyen *et al.*, 1980)
⟨3.30⟩	—O—C(O)—⟨◯⟩—N=N—⟨◯⟩—C(O)—O—	C 210 I (Iimura *et al.*, 1981)
⟨3.31⟩	—C(O)—O—⟨◯⟩—N=N—⟨◯⟩—O—C(O)—	C 225 N 245 I (Iimura *et al.*, 1981)
⟨3.32⟩	—O—C(O)—⟨◯⟩—N=N(O)—⟨◯⟩—C(O)—O—	C 200 I (Iimura *et al.*, 1981)
⟨3.33⟩	—C(O)—O—⟨◯⟩—N=N(O)—⟨◯⟩—O—C(O)—	C 216 N 265 I (Blumstein *et al.*, 1982)
⟨3.34⟩	—C(O)—O—⟨◯⟩(CH₃)—N=N(O)—⟨◯⟩(CH₃)—O—C(O)—	C 118 N 162.5 I (Blumstein *et al.*, 1982)

Table 3.8.   *Continued*

Mesogenic moiety together with the connecting group	Transition, °C
⟨3.35⟩	C 196 N 218 I (Blumstein *et al.*, 1982)
⟨3.36⟩	C 231 N 265 I (Zhou and Lenz, 1983)
⟨3.37⟩	C 220 S 267 I (Ober *et al.*, 1983)

range of the mesophase. The same is seen for the polymers ⟨3.33⟩, ⟨3.34⟩ and ⟨3.35⟩. The two methyl substituted polymers have lower mesophase transition temperatures and narrower mesophase ranges than the parent polymer ⟨3.33⟩.

In addition, the comparison between ⟨3.34⟩ and ⟨3.35⟩ shows the importance of the position of substitution in the mesophase stability of the polymers. The methyl substitutions in ⟨3.34⟩ are at the 2-and 2′-positions relative to the central azoxy group, while that in ⟨3.35⟩ are at the 3-, and 3′-positions. Because the 2,2′-substitutions are in the vicinity of azoxy and thus have stronger steric interactions with the azoxy group, they should have deviated the two phenylene rings from coplanarity with azoxy to a larger extent than the 3,3′-substitutions should have. Thus, the melting and clearing temperatures as well as the mesophase range of the 2,2′-disubstituted polymer ⟨3.34⟩ are significantly lower and narrower than those of the 3,3′-disubstituted ⟨3.35⟩. Recall the properties of the low mass compound ⟨3.12⟩ and its 2,2′ -(ortho-) and 3,3′-(meta-) isomers.

Another interesting result is obtained when the way of connecting the mesogenic units and the flexible segments is varied. This is shown by the polymer pairs of ⟨3.30⟩ and ⟨3.31⟩, and ⟨3.32⟩ and ⟨3.33⟩. The end phenylene rings of the mesogenic units are connected to the flexible segments through −O− or through −CO− (Figure 3.5):

A large number of studies show that the former way of connection helps the formation of the nematic mesophase. For instance, of the four polymers, ⟨3.30⟩ to ⟨3.33⟩, the two with the connection through −O− are liquid crystalline; the other two with the −CO− connection are
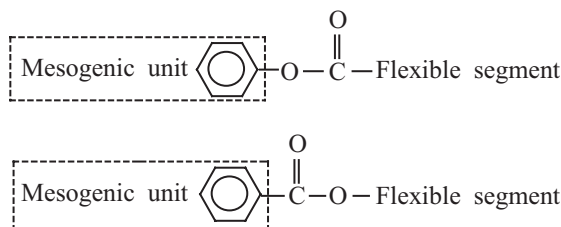
Figure 3.5.   Mesogenic unit attached through $-O-$ (top) or $-CO-$ to flexible segment.

non-liquid-crystalline even though their melting points are lower than that of the former two. Conformational analysis has been used to rationalize the result in terms of the population of extended chain conformers. Yoon and Bruckner (1985) stated that the distribution of chain sequence extension depends strongly on the specific groups or atoms connected at the ends of the two parts. When the linear rigid mesogenic units are attached to flexible segments (polymethylene) through $-O-$ (or $-O-CO-$), the chains have a higher population of highly extended conformers than when the attachment is through $-CO-O-$. This is especially so when flexible segments have an even numbers of chain atoms. With the first type of attachment, chains having even-numbered methylene units in a flexible polymethylene segment exhibit a significant population of highly extended conformers that allow nearly parallel alignment of rigid units along the major extension axis. Chains with odd-numbered methylenes attached in the same way offer few conformers in which the polymer as a whole is highly extended. With the second type of attachment, the difference in the population of extended conformers for even- and odd-numbered methylenes is less significant. Giving an example, in Table 3.9 the odd-even effect of a polymethylene segment on the nematic-to-isotropic transition of the polymer ⟨3.38⟩ (Buglione *et al.*, 1983) is demonstrated. Even though the phase transition temperature and the enthalpy have a tendency of decreasing with a lengthening of the flexible segment, the clearing temperature and the enthalpy of isotropization are higher for polymers with even-numbered methylene units than for the two neighboring polymers having odd-numbered methylenes.

$$\langle 3.38\rangle$$
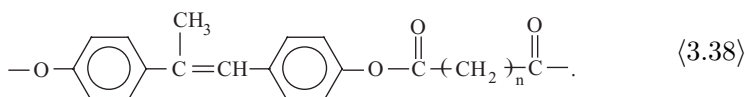
Table 3.9. Odd-even effect in liquid crystalline property of ⟨3.38⟩*.

n	6	7	8	9	10	11	12
Ti, K	575	503	528	479	498	452	464
ΔH, kJ/mol	9.59	2.72	8.66	3.18	7.37	3.39	6.57

* Source: Buglione *et al.*, 1983

The result of conformational analysis has received support from NMR studies. Kohlhammer *et al.* (1989) studied the orientational order parameter of the structural elements of polymers with a mesogenic unit attached through $-O-$ to a flexible segment. They found that the flexible segment between two mesogenic units has a significant degree of orientational order along the direction of mesogenic units. In polymers having even-numbered methylene units there is not only a higher degree of order in the flexible segment than in those with odd-numbered methylenes, but also a higher degree of orientation in the whole molecule. Besides, there is an order gradient of methylene units in the flexible segment, with the methylene nearest to the mesogenic unit having the highest order of orientation. Thus, flexible segments not only impart flexibility to polymers, but also play an active role in the orientation of the molecules. Obviously, flexible segments other than polymethylenes can be applied in the engineering of liquid crystalline polymers. Among others, oligomeric polysiloxanes and polyethers have been used as flexible segments for synthesizing polymers of somewhat different liquid crystalline properties. The use of flexible segments with chiral carbons to prepare polymers having chiral mesophase was also reported (e.g., Van Luyen *et al.*, 1980).

As is for low mass liquid crystals, incorporation of "kinked" moieties will result in destructive effects on the liquid crystallinity of polymers (Figure 3.4). 2,2-diphenylpropane, diphenylmethane, diphenyl ether, diphenyl ketone, 1,2-phenylene, 1,3-phenylene, and 1,2-naphthalene are examples of kinked moieties used in the modification of liquid crystalline polymers. They are very effective in destroying the linearity of rigid rods. Polymers with kinked units have less crystallinity and lower phase transition temperatures. Appropriate use of kinked units is thus of help from case to case. However, the type and amount of kinked units should be carefully determined so as to maintain desirable liquid crystallinity.

The last but not the least important point to be emphasized is the structural stability of the main-chain type polymers especially when a large

majority of the polymers are copolyesters. Post-polymerization and trans-esterification reactions may take place during characterization and process. Lenz and Feichtinger (1979) found that extensive transesterifications and structural rearrangements occurred in the melt of a thermotropic liquid crystalline copolyester of 4-hydroxybenzoic. The rigid moieties tended to bind together and form longer sequences of 4-oxybenzoic units. As a result, the originally random copolymer became at last a block copolymer with the loss of meltability and thermotropic liquid crystallinity. On the other hand, a post-polymerization experiment described by Zhou *et al.* (1989) doubled the molecular weight of a polyester in 90 minutes. The melting point and clearing temperature of its liquid crystal phase also increased significantly. The temperature range of the liquid crystal phase was broadened by 22 °C.

3.5. LIQUID CRYSTALLINE POLYMERS OF THE SIDE-GROUP TYPE WITH END-ON ATTACHMENT

These types of liquid crystalline polymers have mesogenic moieties as side groups or as a component part of side groups (Figure 3.1). They are tra-ditionally named "side chain liquid crystal polymers." Because the side groups may not take the form of chains, we are advised to use the present name. Excellent reviews on this subject are given collectively by the book "Side chain liquid crystal polymers" edited by McArdle (1989). For molec-ular engineering, the readers are best referred to the chapters contributed by Percec and Pugh (1989) and by Gray (1989).

In side group type liquid crystalline polymers, mesogenic units attach to the main chain in two basic ways, *i.e.*, by end attachment (end-on) or by side attachment (side-on). Most polymers studied are of the end-on type. The side-on type is relatively new and only a few systems have been studied. However, because the latter polymers have displayed unusual structure and property, they are discussed separately in Section 3.6.

3.5.1. Synthesis

While main-chain type liquid crystalline polymers are made by step-wise polymerizations, side-group type polymers have been synthesized by both step and chain polymerizations of monomers with desired mesogenic side groups. In addition, mesogenic side groups can be introduced to polymers

by a variety of polymer reactions. The concepts of self-assembly and supramolecular interactions between polymers and low mass mesogenic compounds are also applied for the formation of mesogenic side groups (Kumar *et al.*, 1992). These approaches are outlined by Figure 3.6.

Examples of vinyl monomers for addition polymerization include acrylates, methacrylates, vinyl ethers and styrene derivatives. Radical, ionic, and group-transfer polymerizations are possible according to polymerizability of the monomers. Living polymerization is difficult because mesogenic monomers often contain bonds such as benzoate ester, which are easily attacked by growing ends. Cyclic and condensation monomers are less

By addition polymerization

(e.g. Finkelmann *et al.*, 1978):

g 95 N 105 I

By ring-opening polymerization

(e.g. Akiyama *et al.*, 1993):

g 0 S$_E$ 123 S$_B$ 177 S$_A$ 219 I
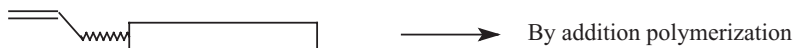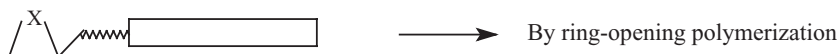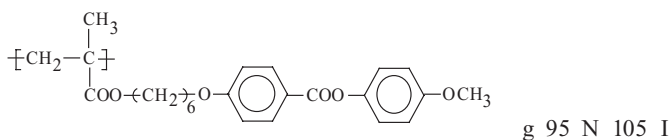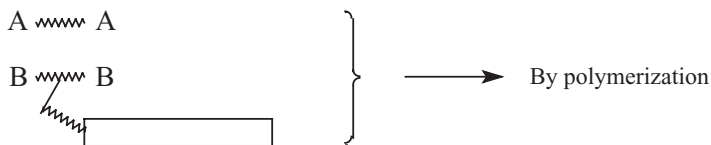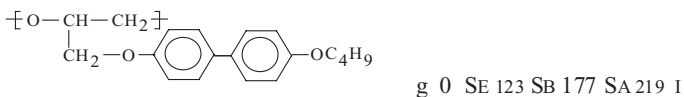
By polymerization

(e.g. Engel *et al.*, 1985):
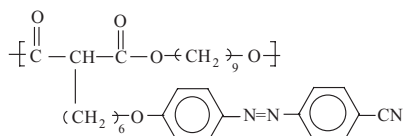
g 10 N 64 I
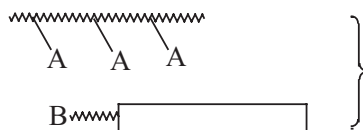
By polymer reaction

(e.g. Frenzel, 1981):
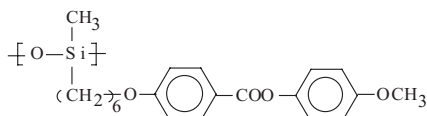
g 5 S 46 N 108 I
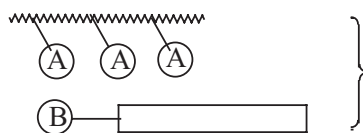
By supramolecular
interactions such as
H-bonding

(e.g. Kumar *et al.*, 1992):
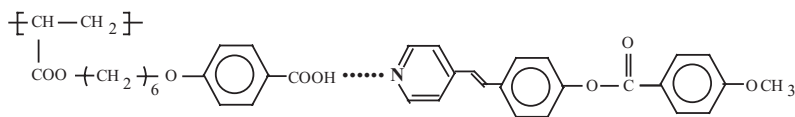
Figure 3.6. Polymerizations and polymer reactions for synthesis of side–group type liquid crystalline polymers.

studied, but have included epoxides, cyclic siloxanes, malonate derivatives, diols and others. Polymer reactions often found in the synthesis of side-group type liquid crystalline polymers are esterification and Si—H addition (hydrosilylation). Special attention has to be paid to the approach of polymer reactions because the reactions are usually not in perfect control.

Polymer reactions often cannot go to 100% completion and various side reactions may be involved. At worst the side reactions may be so extensive that no desirable product is formed (Chen and Ma, 1988).

Although the same polymer may be synthesized by two or more different approaches, the product can be somehow different in a chain structure including a different molecular weight and distribution, a different stereochemistry and a different extent of irregularity along the chains. Special attention must be paid when polymer reactions are applied for the synthesis of polymers. Two factors worthy of consideration, the extent of reaction and formation of isomers, are demonstrated by the two polymer examples ⟨3.39⟩ and ⟨3.40⟩.

Polymer ⟨3.39⟩ was synthesized by Piercourt *et al.* (1992) with polymer reactions:

$$\left[O-CH_2-CH\right] \quad + \quad Na^+ \ {}^-O-\!\!\!\bigcirc\!\!\!-\!\!\!\bigcirc\!\!\!-CN \quad \longrightarrow$$

$$\left[O-CH_2-CH\right]\left[O-CH_2-CH\right]$$

with CH_2-CL and $CH_2-O-\!\!\!\bigcirc\!\!\!-\!\!\!\bigcirc\!\!\!-CN$

⟨3.39⟩
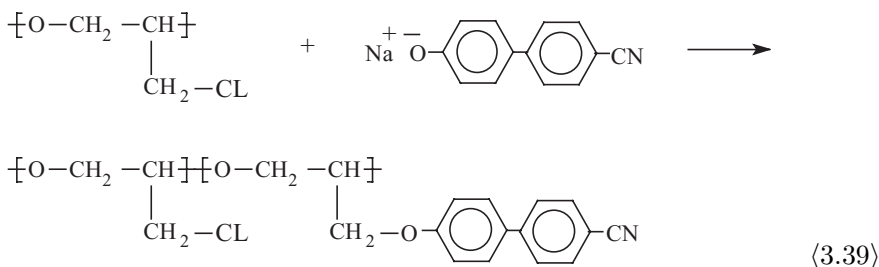
Because of the difficulty in carrying the reaction out to completion, these researchers were not able to obtain a 100% substituted product. However, they obtained a series of polymers with different extents of reaction. The liquid crystalline property and phase transition temperatures are shown in Table 3.10. The polymers with a molar content of mesogenic units in the total side groups equal to and less than 40% are non-liquid-crystalline. Liquid crystallinity increased with the content of mesogenic side groups. The higher the content, the higher the clearing temperature of the nematic

Table 3.10.　Degree of substitution and the properties of polymer ⟨3.39⟩*.

Degree of substn. %	0	25.5	40	65	74	83	91
Glass transition, °C	−26.5	10	26	66.6	79.5	83	86
Clearing point, °C	non-l.c.	non-l.c.	non-l.c.	105	133.5	143	153.5

* Source: Piercourt *et al.* (1992).

phase and the broader the temperature range of the mesophase. Thus, together with the properties, the extent of reaction has to be carefully characterized.

Liquid crystalline polysiloxanes are usually synthesized by hydrosilylation reactions between polysiloxanes containing reactive Si−H groups and vinyl compounds with mesogenic units. Gray (1989) and Percec and Pugh (1989) have discussed the problems and side reactions in hydrosilylation reactions, including incompletion, catalyzed migration of double bonds and production of isomeric products, the danger of cross-linking involving side groups, and product contamination by residual alkenes. The synthesis is further complicated by the possible coexistence of the α-addition and the β-addition as shown by Figure 3.7.

Even though the addition of silicon hydrides to vinyl compounds often takes the form of β-addition, exceptions do exist. For example, the reaction of methyldichlorosilane and styrene catalyzed by chloroplatinic acid or Pt/C yielded 53% β-addition and 33% α-addition product (Ryan and Speier, 1959). For polysiloxanes, Huang and Wu (1992) studied the synthesis of polymer $\langle 3.40 \rangle$ using NMR analysis. The result showed that at 50 °C using chloroplatinic acid as catalyst, the product was actually a copolymer with isomeric structures, 58% of which were from β-addition ($\langle 3.40 \rangle$), the other 42% were from the α-addition $\langle 3.41 \rangle$.

$$\begin{array}{c} CH_3 \\ | \\ \left[\!\!\left[\, O\!-\!S\,i \,\right]\!\!\right] \\ | \\ H \end{array} \quad + \quad CH_2\!=\!CH\!-\!CH_2\!-\!O\!-\!\bigcirc\!-\!COO\!-\!\bigcirc\!-\!OCH_3$$

$$\xrightarrow{\hspace{1cm}} \begin{array}{c} CH_3 \\ | \\ \left[\!\!\left[\, O\!-\!S\,i \,\right]\!\!\right] \\ | \\ (CH_2)_3\!-\!O\!-\!\bigcirc\!-\!COO\!-\!\bigcirc\!-\!OCH_3 \end{array} \qquad \langle 3.40 \rangle$$

$$\begin{array}{c} CH_3 \\ | \\ \left[\!\!\left[\, O\!-\!S\,i \,\right]\!\!\right] \\ | \\ CH_3\!-\!CH\!-\!CH_2\!-\!O\!-\!\bigcirc\!-\!COO\!-\!\bigcirc\!-\!OCH_3 \end{array} \qquad \langle 3.41 \rangle$$
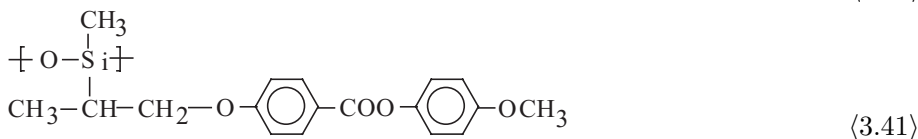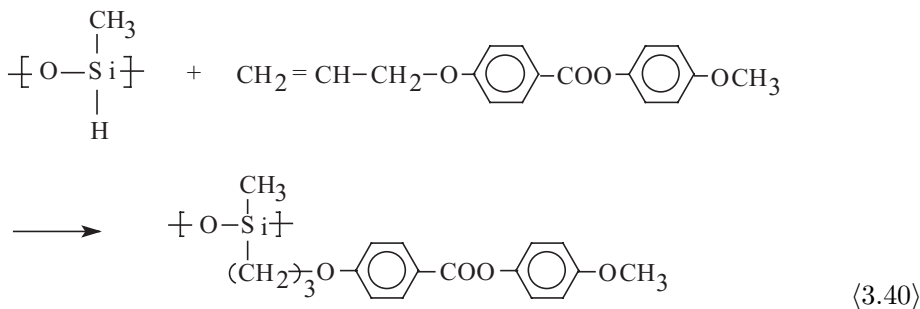
Different catalyst and reaction conditions may result in different molecular structures with various percentages of α-and β-additions. Thus, even if the reaction went to a 100% completion, the product would still be a

α - ADDITION:

$$\begin{CD} \cdots \end{CD}$$
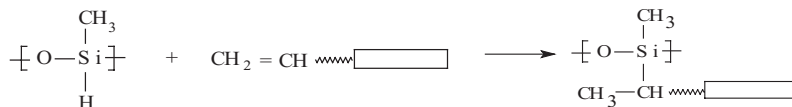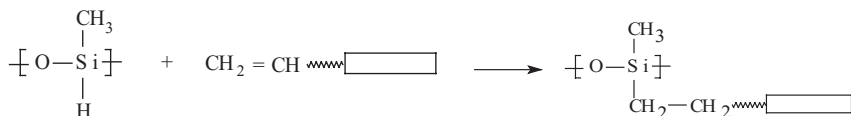
β - ADDITION:

Figure 3.7.   α- and β-addition of hydrosilylation.

copolymer of different contents with the two structural units distributed in a certain way along the molecular chains. Different properties should be expected.

3.5.2.   Structure and properties

The property of a side group type liquid crystalline polymer is determined by its three principal structural components, namely the main-chain backbone, the mesogenic unit, and the connecting moiety. As is the case for most polymers, if a flexible main chain and rigid mesogens are combined together through linking units, two contradictory tendencies of molecular movements and organizations are present: while the main chain tends to take three dimensional random coil conformations, mesogenic units tend to organize with an orientational order. If the first tendency is overwhelming, no mesophase is formed. Otherwise the main chain will yield to formation of the ordered phase. In order to diminish the interference of the random movement of the main chain on the mesophase organization of the side groups, Finkelmann *et al.* (1978a) introduced the concept of a flexible spacer that is a flexible segment connecting the main chain and the mesogenic unit and serves to decouple the two movements. With intermediation by the spacers, liquid crystalline phases are favorably formed. According to Shibaev and Platé (1984), flexible spacers were successfully used in the synthesis of side group type polymers at Moscow State University as early as 1973. On the other hand, if both the main chain and side groups are mesogenic, three

nematic phases are speculated by Wang and Warner (1987). Depending on the sign (positive or negative) of the order parameters of the two, the nematic phase can be N_I $(+,-)$, N_{II} $(-,+)$ or N_{III} $(+,+)$. Whether or not a mesophase is formed and the type of the mesophase is determined by the relative tendency or strength of the three components in forming or interfering in the order of the mesophase.

If no flexible segments are used to connect a non-mesogenic main chain with mesogenic groups, main chain flexibility seems to be essential for the formation of a mesophase. Taking polymethacrylates and polyacrylates as examples, the main chain of the former is less flexible than that of the latter as can be justified by the glass transition temperatures. Thus, if the mesogenic moiety is not very strong in the tendency of the mesophase formation, there is more of a chance for the more flexible polyacrylates to form a liquid crystalline phase. The effect may be demonstrated by poly(biphenyl acrylate), $\langle 3.42 \rangle$ (Bresci *et al.*, 1980), and poly(biphenyl methacrylate), $\langle 3.43 \rangle$ (Maganini *et al.*, 1974). The biphenyl group is a weak mesogenic unit. More flexible main chains are more desirable for the formation of a liquid crystalline phase. The polyacrylate has a lower glass transition temperature and does form a smectic phase, but the less flexible polymethacrylate does not.

$$\text{(g 110 S 280 I)}. \quad \langle 3.42 \rangle$$

$$\text{(g 170 I)}. \quad \langle 3.43 \rangle$$
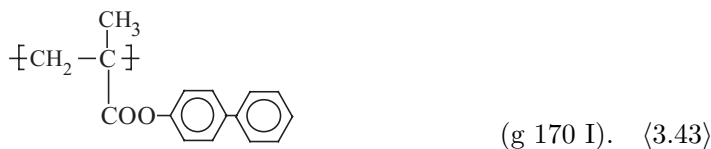
The same was observed for the following two polymers $\langle 3.44 \rangle$ and $\langle 3.45 \rangle$ with the mesogenic units of a schiff base structure (Frosini *et al.*, 1981). The polyacrylate is a smectic liquid crystal from 93 °C to 258 °C. The polymethacrylate does not form any liquid crystalline phase.

$$\text{(g 93 S 258 I)}. \quad \langle 3.44 \rangle$$

$$\begin{array}{c} \text{CH}_3 \\ | \\ +\text{CH}_2-\text{C}+ \\ | \\ \text{COO}-\bigcirc-\text{CH=N}-\bigcirc \end{array}$$

(g 163 I).   ⟨3.45⟩
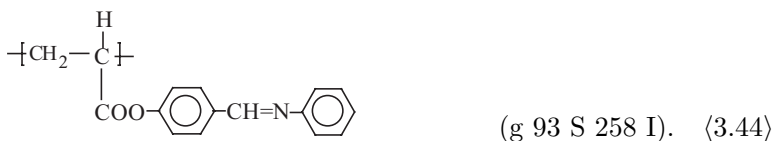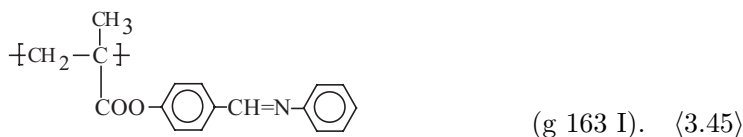
On the other hand, if the mesogenic unit is modified so as to have a stronger tendency to form the liquid crystalline phase (Section 3.2), the polymer will have more of a chance to form more stable liquid crystals. This is well demonstrated by homologues of the above mentioned two non-liquid-crystalline polymethacrylates ⟨3.43⟩ and ⟨3.45⟩. According to Alimoglu *et al.* (1984), substitution of $-$CN groups at the ends of biphenyl units in ⟨3.43⟩ resulted in poly[4-(p-cyanophenyl)phenyl methacrylate] that showed a smectic phase above Tg, the clearing point of which is 240 °C. If the substitution is not by cyano but by $-$OCH$_3$ the resulted poly[4-(p-methoxyphenyl)phenyl methacrylate] is also smectic (Ti = 255 °C; Duran *et al.*, 1987a). The same is true with polymer ⟨3.45⟩. For example, the ethoxy substituted homologue poly[4-(p-ethoxyphenylimino)methylphenyl methacrylate] (⟨3.46⟩) forms a smectic phase with the transitions: g 198 S 284 I (Frosini *et al.*, 1981). However, even though both the polyacrylate and polymethacrylate are liquid crystalline, the more flexible polyacrylate has a broader temperature range for the mesophase as shown by a comparison of the polymers ⟨3.46⟩ and ⟨3.47⟩.

$$\begin{array}{c} \text{CH}_3 \\ | \\ +\text{CH}_2-\text{C}+ \\ | \\ \text{COO}-\bigcirc-\text{CH=N}-\bigcirc-\text{OC}_2\text{H}_5 \end{array}$$

(g 198 S 284 I).   ⟨3.46⟩

$$\begin{array}{c} \text{H} \\ | \\ +\text{CH}_2-\text{C}+ \\ | \\ \text{COO}-\bigcirc-\text{CH=N}-\bigcirc-\text{OC}_2\text{H}_5 \end{array}$$

(g 88 S 268 I).   ⟨3.47⟩
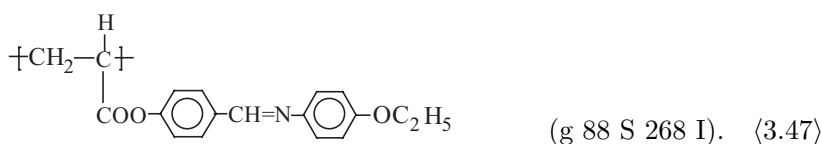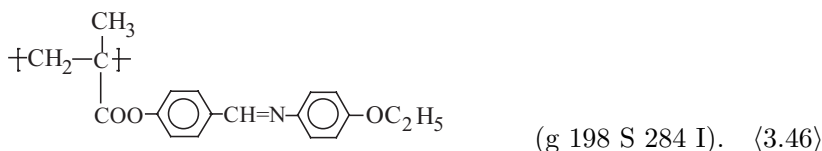
We have discussed the influence of the flexibility of the polymer backbone on the mesophase formation by examples of polyacrylates and polymethacrylates. More flexible polymers should have a stronger tendency to form more stable mesophases. Nevertheless, smectic liquid crystalline phases are the most common mesophases formed, if they do indeed form, by polymers in which no flexible spacers are used to connect main chain and

mesogenic units (Finkelmann and Rehage, 1984). The reason for the preferred formation of smectic rather than nematic phase is not yet completely understood.

In order to decouple the interactions between main chain and mesogenic units and systematically realize the liquid crystalline phase, especially the nematic phase, Finkelmann *et al.* (1978a) introduced the concept of decoupling by flexible segments such as oligomeric polymethylenes, polyoxyethylenes and polysiloxanes. The concept has since been repeatedly proven to be correct. Following this model, numerous liquid crystalline polymers were synthesized. Naturally, the structure and property of the spacer will determine its effectiveness in decoupling and in helping the formation of liquid crystals. A few representative polymers are shown in Table 3.11.

As shown by the examples in Table 3.11, regardless of the type of polymer backbones, introduction of flexible spacers does help the formation

Table 3.11.   Representative side-group type liquid crystalline polymers and phase transitions.

Polysiloxanes ⟨3.48⟩

$+O-\underset{\underset{(CH_2)_n}{|}}{\overset{\overset{CH_3}{|}}{Si}}+$ —O—⟨O⟩—COO—⟨O⟩—OCH$_3$

n	Phase transitions				
3	g	15	N	61	I
4	g	15	N	95	I
5	K	87	N	115	I
6	K	52	N	112	I

(Finkelmann and Rehage, 1980; Finkelmann *et al.*, 1981)

Polymethacrylates ⟨3.49⟩

$+CH_2-\underset{\underset{COO-(CH_2)_n}{|}}{\overset{\overset{CH_3}{|}}{C}}+$ —O—⟨O⟩—⟨O⟩—OCH$_3$

n	Phase transitions						
0					S	255	I
2		g	120	N	152	I	
6		K	119	S	136	I	
11	g	54	Sc	87	S$_A$	142	I

(Finkelmann *et al.*, 1978b; Hsu *et al.*, 1987; Duran *et al.*, 1987b)

Polyacrylates ⟨3.50⟩

$+CH_2-\underset{\underset{COO-(CH_2)_n}{|}}{\overset{\overset{H}{|}}{C}}+$ —O—⟨O⟩—⟨O⟩—CN

n	Phase transitions						
2		g	84	K	114	I	
3		g	54	S$_A$	82	I	
4		g	42	N	229	I	
5	g	35	S$_A$	120	N	124	I
11	g	25	S$_C$	30	S$_A$	145	I

(Dubois *et al.*, 1986; Kostromin *et al.*, 1984)

of the liquid crystalline phase especially the nematic phase. Oligomeric polymethylenes have been the most applied and effective spacers. Other spacers including oligomeric polyoxyethylenes and polysiloxanes are usually less effective and thus are used less often. Polymethylene is non-polar and has little interaction with mesogenic groups that are always polar. On the other hand, if polar spacers such as oligomeric polyoxyethylenes are used, there may be certain undesired interactions between spacers and mesogenic groups (Percec and Pugh, 1989). For polymethylene, the length is critical in determining the type and thermal stability of the mesophase formed by the polymer. Very short and very long spacers favor the formation of smectic phases. The nematic phase is favored by spacers of intermediate length depending on the type and property of the main chain.

Investigations on comb like polymers by Platé and Shibaev (1980) with non-branched oligomeric polymethylene segments as the teeth, showed that for polymethylenes with a degree of polymerization greater than 8, the teeth crystallized independently of the main chain conformation. Consequently, it was speculated that if mesogenic molecules were linked to the ends of teeth longer than 8 methylene units, they would take a liquid crystalline order without influence from the main chain conformation. This speculation has in fact born the idea of complete decoupling by long flexible spacers. However, studies on low molecular mass compounds and their polymeric counterparts have demonstrated clearly that liquid crystalline properties are always affected by polymerization no matter how long a polymethylene is used as the spacer (Shibaev and Platé, 1984). In particular, the temperature range of the polymeric mesophase is always broader than that of the low molar compound, with that of the polyacrylate even broader than that of the polymethacrylate. Decoupling is never complete. The influence of the structure and nature of the main chain is always there on properties of mesophase formed by the polymers. In Table 3.12, three groups of examples, each with the same spacer and mesogenic units, are given to show the influence of different main chains. Again we see the general trend that the mesophase is broader and more stable for the polymer of less flexibility.

Using such techniques as ^{2}H-NMR and 2D-^{13}C-MAS-NMR, Spiess and coworkers (Böeffel and Spiess, 1989) have been able to determine the molecular order of the different parts of the molecule. The decrease of order from the mesogenic group to the polymer chain was found. For example, in the glassy state with a frozen-in molecular order of the liquid crystalline phase, the order parameters for the polymer $\langle 3.52 \rangle$ (Table 3.12) were found to be 0.88, 0.52 and 0.25 respectively for the mesogenic unit, the spacer, and

Table 3.12.   Influence of main chain structure on liquid crystalline property.

Flexible spacer and mesogenic unit	$-(CH_2)_6-O-\bigcirc-COO-\bigcirc-OCH_3$	
Polymethacrylate ($\langle 3.51 \rangle$)	g 95 N 105 I	(Wendorff *et al.*, 1978)
Polyacrylate ($\langle 3.52 \rangle$)	g 60 S 98 N 125 I	(Ringsdorf and Schneller, 1981)
Polysiloxane ($\langle 3.53 \rangle$)	K 52 N 112 I	(Finkelmann and Rehage, 1980)
Flexible spacer and mesogenic unit	$-(CH_2)_6-O-\bigcirc-COO-\bigcirc-CN$	
Polymethacrylate ($\langle 3.54 \rangle$)	g 60 N 110 I	(Davidson *et al.*, 1985)
Polyacrylate ($\langle 3.55 \rangle$)	g 33 N 133 I	(LeBarny *et al.*, 1986)
Polysiloxane ($\langle 3.56 \rangle$)	g 55 S 185 I	(Gemmell *et al.*, 1985)
Flexible spacer and mesogenic unit	$-(CH_2)_6-O-\bigcirc-\bigcirc-CN$	
Polymethacrylate ($\langle 3.57 \rangle$)	g 55 S 100 I	(Shibaev and Platé, 1985)
Polyacrylate ($\langle 3.58 \rangle$)	g 32 Nrc 80 S_A	
	S_A 124 N 132 I	(Dubois *et al.*, 1986)
Polysiloxane ($\langle 3.59 \rangle$)	g 14 S_A 166 I	(Gemmell *et al.*, 1985)

the main chain. The main chain was no longer a random coil. A considerable degree of mesogenic order was transferred via the spacer to the main chain. No gradient in the order parameter was observed for the spacer carbons. The gradient from the spacer to the acrylic carbo, next to the polymer chain, was also not very much (from 0.52 to 0.45). On the other hand, there was a strong decrease in order parameter across the bond linking the main chain and the side group (from 0.25 to 0.45), suggesting the importance of rotation about that bond for the decoupling. In addition, the relative alignment of the mesogenic unit and the main chain is different for different polymers. For polyacrylates, a parallel orientation of these two parts is preferred because nematic-like interactions between the spacer and the polymer chain exist. For polymethacrylate the repulsive forces between the spacer and the polymer chain are dominant and a perpendicular orientation is preferred. As stated by these authors, the studies have on the one hand confirmed the spacer concept, while on the other hand shown its limitations. Decoupling is partial, the molecular conformation and the liquid crystalline properties are related not only to the mesogenic unit but also to such structural parameters as spacer length and the flexibility of polymer backbones.

The ease of forming the smectic mesophase by this class of side-group type liquid crystalline polymers has rendered a great possibility in synthesizing polymeric chiral smectic materials useful in non-linear optics, transducers, pyroelectric detectors and display devices (Chapter 6). The first polymer forming a chiral smectic-C phase was synthesized by Shibaev *et al.* (1984). It has a polymethacrylate main chain, a long polymethylene spacer, and a mesogenic unit attached at the end with a chiral moiety (polymer ⟨3.60⟩). Since then, a lot of polymers with chiral mesophases have been synthesized and studied (Le Barny and Dubois, 1989).

$$\text{g } 20\text{–}30 \text{ S}_C{}^* \text{ } 73\text{-}75 \text{ S}_A \text{ } 83\text{–}85 \text{ I.} \qquad \langle 3.60 \rangle$$
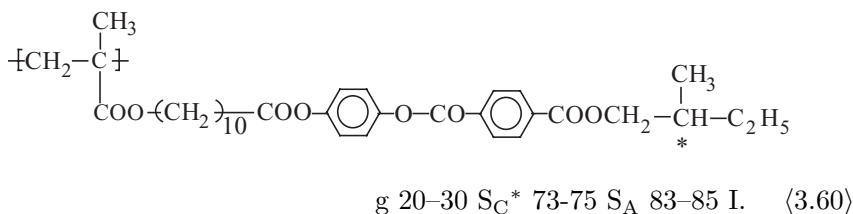
It is worthy to note at this point that the polymerization of mesogenic monomers with chiral moieties does not necessarily result in polymers with the chiral liquid crystalline phase. For example, Finkelmann (1982) reported that homopolymers of chiral monomers yielded only smectic mesophases. On the other hand, copolymerization of chiral monomers with different spacers or of a chiral monomer and a nematic monomer has been proven effective and convenient for synthesizing chiral liquid crystalline polymers.

Other attempts at synthesizing chiral smectic polymers have reached the conclusion that no general conclusion can be made so far as for what molecular structure will yield the desired phase. Again, all the structural elements including the main chain, the spacer, and the mesogenic unit are playing a part. Nevertheless, a longer spacer and more flexible main chain seem to favor the chiral S_C phase (Le Barny and Dubois, 1989).

3.6.   LIQUID CRYSTALLINE POLYMERS OF THE SIDE-GROUP TYPE WITH SIDE-ON ATTACHMENT AND "MESOGEN-JACKETED LIQUID CRYSTAL POLYMERS"

We have emphasized in Section 3.5, the concept of coupling between motions of main chain and side groups in side-group type liquid crystal

polymers. Decoupling is achieved by the insertion of the flexible segment so that systematic realization of the liquid crystal phase is possible. With this "coupling-decoupling" concept, one should be able to obtain not only the side-group type liquid crystal polymers as described in a previous section, but also those with side-on attachment. The first report on the synthesis of the new type of side-group liquid crystalline polymers is by Hessel and Finkelmann (1985, 1987), in which the polymers have the following general structure:

$$\text{~}-CH_2-\underset{\underset{\underset{\underset{(CH_2)_{11}}{O}}{C=O}}{\overset{CH_3}{|}}}{C}-\text{~}$$

R—⟨◯⟩—COO—⟨◯⟩—OOC—⟨◯⟩—R   ⟨3.61⟩
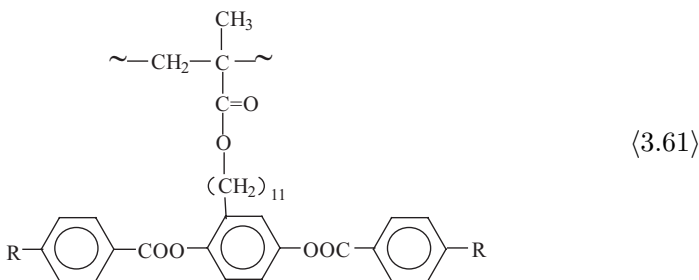
Indeed, with a long decoupling spacer, all the polymers form a nematic phase. The transition temperatures (in °C) of polymers ⟨3.61⟩ with different R in the mesogenic unit are shown in Table 3.13.

At about the same time, Zhou *et al.* (1987) also designed and synthesized polymers with mesogenic units attached laterally to main chains. However, as these authors have pointed out, with the new way of attachment at the waist position or the gravity center of mesogenic units, motions of the main chain will create only a minor moment on the mesogenic units. As a result, the process and degree of molecular orientation of the mesogenic units will be less influenced by or less coupled with the main chain. The decoupling spacer is thus no longer a requisite for the realization of the liquid crystal phase of such polymers. In addition, if no spacer or only a very short spacer is used, the mesogenic units would form a dense "jacket" around each chain backbone because of their high population in and around the backbone and because they are both bulky and rigid. This situation is imaginable if one thinks of the fact that there is a mesogenic long rod of approximately 2 nm being directly attached to each repeating unit of only 0.25 nm long. Because of steric requirements, the jacket will force the main chain to extend and to show much higher rigidity than otherwise, showing a "jacket effect." With the above considerations, two concepts, the "mesogen-jacketed liquid crystal polymers (MJLCP)" and the "rigid side-group type liquid crystal polymers," have been proposed by Zhou *et al.* (1987, 1989,

1993, 1996). MJLCP distinguishes itself from other main classes of liquid crystal polymers (Figure 3.1) by having chemical structures similar to conventional side-group type liquid crystalline polymers but chain properties similar to rigid or semi-rigid main-chain type liquid crystalline polymers. Shown below are a few examples of the molecular design of MJLCPs:

Poly-2,5-bis[(4-R-substituted)benzoyloxy]styrene:

$$\sim\!\!-CH_2-CH-\!\!\sim$$

R—〇—COO—〇—OOC—〇—R $\qquad$ ⟨PE-R⟩

Poly-2,5-bis[(4-R-substituted)benzamido]styrene:

$$\sim\!\!-CH_2-CH-\!\!\sim$$

R—〇—CNH—〇—NHC—〇—R $\qquad$ ⟨PA-R⟩
$\quad\quad\quad\;\overset{\|}{O}\quad\quad\quad\quad\quad\overset{\|}{O}$
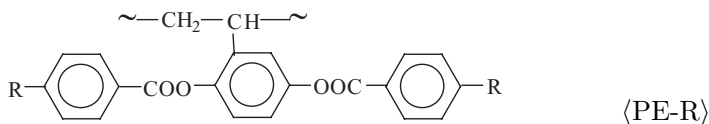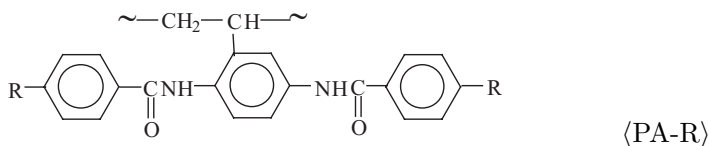
Poly-3-vinyl-{2,6-bis(4-R-substituted)phenyl}benzo-[1,2-d;4,5-d']bisthiazole:

$$\sim\!\!-CH_2-CH-\!\!\sim$$

R—〇—C(N,S)benzobisthiazole C—〇—R $\qquad$ ⟨PBTA-R⟩
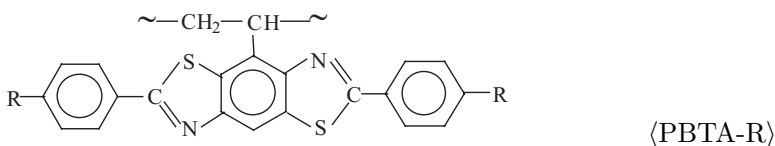
Other designs are possible. Among the above three polymers, ⟨PE-R⟩ and ⟨PA-R⟩ are the most studied while ⟨PBTA-R⟩ is still to be synthesized (Zhou *et al.*, 1987; 1989; 1993; 1996). Poly-2,5-bis[(4-R-substituted)benzoyloxy]styrenes, ⟨PE-R⟩, and Poly-2,5-bis[(4-R-substituted)benzamido]styrene, ⟨PA-R⟩ have been synthesized by radical chain polymerizations of corresponding monomers. Table 3.14 shows some of the characterization results for some of the ⟨PE-R⟩ polymers.

Although the mesogenic substituent on the vinyl group is bulky and rigid, high molecular weights have been achieved in the syntheses. For the high polymerizability of these monomers, we have the following plausible explanation: the nematic interaction among monomer molecules has brought vinyl groups close to a favorable position relative to each other. As reference, for a single crystal of a few of the monomers, WAXS has revealed

Table 3.13.   Phase property of polymers
⟨3.61⟩ and monomers

R	Monomer	Polymer
CH_3O-	K 63 (N 23) I	g 38 N 62 I
C_2H_5O-	K 92 I	g 34 N 82 I
$n-C_3H_7O-$	K 71 (N 26) I	g 26 N 58 I
$n-C_4H_9O-$	K 69 (N 41) I	g 19 N 67 I
$n-C_5H_{11}O-$	K 52 (N 29) I	g 10 N 51 I
$n-C_6H_{13}O-$	K 49 (N 45) I	g 5 N 60 I
$n-C_7H_{15}O-$	K 46 (N 36) I	g 1 N 48 I
$n-C_8H_{17}O-$	K 54 (N 48) I	g -2 N 61 I
$n-C_3H_7$	K 38 (N -20) I	g 12 I

Table 3.14.   Molecular weights and Tg of PE-R as well as phase transition property
of monomers.

PE-R	R	Mn $(\times 10^{-4})$	Mw $(\times 10^{-4})$	Mw/Mn	Tg^* $(°C)$	Property of monomers (in °C)
PE-H	H	5.4	10	1.9	170	K 88 N 95 I
PE-OC$_1$	OCH$_3$	13	30	2.3	160	K 184 N 195 I
PE-OC$_2$	OC$_2$H$_5$	4.5	9.5	2.1	130	K 150 N 168 I
PE-OC$_4$	OC$_4$H$_9$	24	88	3.7	80	K 109 S 130 N 167 I
PE-CN	CN	**	**	**	200	K 216 N 257 I
PE-C$_1$	CH$_3$	7.7	22	2.9	172	K 123 N 128 I
PE-C$_2$	C$_2$H$_5$	6.8	17	2.5	160	K 106 (N 102) I ***
PE-C$_4$	C$_4$H$_9$	2.8	8.6	3.0	130	K 44 S 98 I

* Above Tg, all the polymers have a nematic phase which is thermally very stable;
** It is not soluble in THF, intrinsic viscosity was given as 1.1 g/dl in DMF;
*** Monotropic.

that the molecules are parallel aligned and the distance between any two
vinyl carbons of two neighboring molecules is small.

All the ⟨PE-R⟩ polymers are non-crystalline as revealed by X-ray anal-
ysis. There is only a very diffuse halo at 20 degrees and a diffuse peak
at 5.5 degrees for two corresponding respectively to the lateral pack-
ing of the chains and to the length of the side groups (16 Å, calculated
from $d = \lambda/2\sin\theta$). The glass transition temperatures are also shown in
Table 3.14. At temperatures above Tg, the polymers all have a nematic
phase. These mesophases are very stable and no isotropization tempera-
ture has ever been observed before decomposition starts to occur at about

300 °C or higher. Two remarkable differences between MJLCPs and conventional side chain liquid crystal polymers are noticed. First, MJLCPs favor the formation of the nematic phase rather than the smectic phases. This is not only true for systems with no spacers as PE-R described here, it is also true even if flexible spacers are used to connect the main chain and the mesogens so long as the attachment is at the waist or nearby positions of the mesogens (e.g., polymers ⟨3.61⟩ shown in Table 3.13; ⟨3.62⟩ and ⟨3.63⟩ shown below; Hessel and Finkelmann, 1987; Keller *et al.*, 1988; Gray *et al.*, 1991). For conventional side-group liquid crystalline polymers, it is well known that they often form smectic phases, in addition to nematics, especially when no spacers or relatively long spacers are used (McArdle, 1989). Secondly, the nematic phases of PE-R are so stable that no clearing point or isotropization temperature (Ti) can be observed before thermal decomposition of the molecular structure occurs (Zhou *et al.*, 1989; 1993; Xu *et al.*, 1993). On the other hand, nematic phases of conventional side-group liquid crystalline polymers scarcely have Ti higher than 150 °C. By contrast, the thermal stability of MJLCPs is similar to many of the main chain type liquid crystal polymers, especially many of the semi-rigid or rigid aromatic polyesters. It is also interesting to mention the fact that semi-rigid and rigid aromatic polyesters form essentially only nematic liquid crystal phases. Therefore, we are able to notice here the first similarity between the properties of MJLCPs and the main chain type liquid crystal polymers.

At this point, we would like to mention again that the polymer PE-H in Table 3.14, poly-2,5-di(benzoyloxy)styrene, was first synthesized some 40 years ago as a precursor of an electron exchange polymer (Ezrin *et al.*, 1953). In this study we were lucky to have found that this polymer is liquid crystalline at temperatures above its glass transition (Table 3.14). To our knowledge PE-H is probably the oldest thermotropic liquid crystalline polymer ever synthesized by chemists.

It is also interesting to mention that in molecules of PE-H the side group moiety, hydroquinone dibenzoate, is on its own not a liquid crystal. A question thus arises if one recalls that for liquid crystal formation of conventional side-chain type polymers it is the ordering of mesogenic side groups and not the ordering of the main chains that is principally concerned, even though the conformations of the main chains do change in accordance with the ordering of the side groups. What are the principal ordering elements for the formation of the liquid crystalline phase of MJLCPs? Are they the side groups as in the cases of conventional side-group type liquid crystalline

polymers? Or are they the rigid molecular segments as in the cases of main chain type liquid crystalline polymers describable by the worm-like or Kuhn chains? We are not able to answer this question for certain at this moment, but we would rather believe that it is the ordering of the rigid molecular segments which have the principal responsibility for the formation of the liquid crystalline phase of MJLCPs. In other words, we intend to believe that MJLCPs are worm-like and can be described by Kuhn chains (Kratky and Porod, 1949). Chain properies of MJLCPs have been studied from the view points of morphology (Zhou *et al.*, 1993; Xu *et al.*, 1993) and solution behavior (Wan *et al.*, 1994; Zhou *et al.*, 1996).

It is well known that rigid and semi-rigid main-chain type liquid crystal polymers, both lyotropic and thermotropic, can form banded textures by shear or elongational flow in their liquid crystal state (Dobb *et al.*, 1977; Chen *et al.*, 1987). In the oriented liquid crystal specimens, the polymer molecules are packed in a parallel alignment to form fibrils. The fibrils travel parallel in a regular zigzag manner, resulting in the unique alternating light and dark pattern when being observed on a polarizing microscope, thus the name "banded texture." No such textures have ever been observed for flexible chain polymer molecules including that of conventional side-group type liquid crystal polymers having mesogenic groups attached longitudinally (end-on) to flexible backbones. Thus, the rigidity of mesogen-jacketed liquid crystal polymers may also be demonstrated by the morphological study of oriented liquid crystal films. Studies on the PE-R series of MJLCPs have revealed that all the polymers indeed form banded textures when they are in nematic phases (Zhou *et al.*, 1993). Besides, their banded textures have been found to be thermally very stable, and remain almost unchanged in a wide temperature range (Xu *et al.*, 1993).

In studies on banded textures of main-chain type liquid crystal polymers, a contraction effect has been proposed to explain the mechanism of band formation (Xu *et al.*, 1993). Thus, the rigid or semi-rigid molecules of liquid crystalline polymers are packed in parallel in the form of fibrils under shear along the shearing direction. Formation of the banded textures after shear cessation is not the result of the free thermal relaxation of individual molecules, but the result of contraction and zigzag rearrangement of the fibrils as a whole along the orientation direction. The elastic energy stored during shearing may have provided the driving force for contraction, but the high stability of the parallel alignment of neighboring molecules due to the very limited molecular motion of these polymers is a necessary condition for formation of the bands. By contrast, in the case of flexible chain

polymers, molecules may also assume a parallel orientation under shearing, however, the orientational relaxation takes place easily as a result of the fast thermal motions of individual molecules. The external elastic force may even accelerate this process. As a result, no regular banded textures should be expected for flexible polymers.

The morphological studies have given clear evidence for a rather high degree of chain rigidity of MJLCPs. The very high capability of forming banded textures represents another similarity of properties of MJLCPs and the main chain type liquid crystal polymers. It is also interesting to mention the fact that this study has offered the first examples of side chain type liquid crystal polymers (though not of the conventional type) that form banded textures.

Chain rigidity of polymer molecules can also be evaluated by studies of solution properties. According to Kratky and Porod (1949), the persistence length of a polymer molecule in a good solvent characterizes the chain stiffness of the polymer. Theoretical studies and experimental evaluations of persistence lengths of a variety of polymer molecules have given values in the order of 1 nm for the flexible or Gaussian chains, 10 nm for semi-rigid chains, and higher than 10 nm for rigid chains. Among liquid crystal polymers, lyotropic ones usually have higher rigidity than thermotropic aromatic polyesters which in turn are much stiffer than side-group type liquid crystalline polymers. There have been reports on the persistence lengths of liquid crystalline polymers (Brelsford and Krigbaum, 1991). For example, a typical value of 30 nm has been found for poly-(1,4-phenylene teraphthamide), PPTA, in sulfuric acid. For thermotropic aromatic polyesters the persistence length data are also available. The value for a fully aromatic copolyester composed of 4-hydroxybenzoic acid, terephthalic acid, 2,6-naphthalene dicarboxylic acid, and 1,4- hydroquinone with the molar ratio of $6:2:2:4$ has been reported to be 12 nm (Jackson, 1992); that for an aromatic terephthalic acid copolyester in tetrachloroethane is 9 nm (Tsvetkov *et al.*, 1984). Thus, in order to evaluate persistence length and chain stiffness of MJLCPs, a typical polymer sample, poly-2,5-bis[(4-methoxybenzoyl)oxy]styrene, PE-OC$_1$ in Table 3.14, was studied (Wan *et al.*, 1995). By repeated fractionation precipitation with DMF as the solvent and methanol as the precipitant, nine fractions were obtained. The fractions were studied by GPC, DSC, viscometry and static light scattering (with a Photal DLS-700 Dynamic Light Scattering Spectro-photometer) techniques. The experimental temperature was 25 °C and THF was used as the solvent. From the results and by a procedure of Bohdanecky (1983), the

Table 3.15.   Representative values of persistence length for typical polymers*.

Flexible polymers	Lyotropic LCP	Main-chain type LCP	Mesogen-jacketed LCP
Nylon- 6,6 $\sim$1 nm PET $\sim$5 nm	PPTA $\sim$30 nm	HBA/HNA $\sim$6–9 nm	PE-OC$_1$ $\sim$12 nm

* PPTA, poly(phenylene terephthamide);
HBA/HNA, copolyester of 4-hydroxybenoic acid and 6-hydroxy-2-naphthalic acid.

persistence length q of this polymer was evaluated to be 11.5 nm–13.5 nm. This is much higher than what a flexible polymer would have, and is in the range of values for rigid or semi-rigid polymers such as liquid crystalline aromatic copolyesters. The comparison is shown in Table 3.15. Besides, the exponential parameter of the Mark-Houwink-Sakurada equation for PE-OC$_1$ was found to be 0.82, again a value significantly higher than that for flexible polymers. Both the persistence length and the parameter have indicated that the molecules of this MJLCP are rather rigid and can be described as worm-like chains. The chain rigidity of this MJLCP is similar to that of the main-chain type liquid crystal aromatic copolyesters, but quite different from that of conventional side-group type liquid crystalline polymers.

Liquid crystal polymers with sufficient high persistence length and sufficient solubility may form lyotropic phases (Flory, 1984). Examples of the lyotropic liquid crystal polymers include PPTA, polybenzothiazole, polybenzoxazole, and poly(benzyl glutamate). MJLCPs such as PE-R and PA-R all have good solubility in normal solvents such as DMF and DMSO. Those in the PE-R series have been shown to have high values of persistence length and chain rigidity similar to that of liquid crystalline aromatic polyesters. On the other hand, the PA-R polymers have been expected to have even higher stiffness than the PE-R polymers (evaluation of the persistence length of PA-R is on the way). Therefore it would be interesting to study the possibility of the formation of lyotropic phases of both PE-R and PA-R types of MJLCPs.

We have found that in dry DMF, the PA-R polymers indeed form lyotropic solutions with a strong light scattering effect. The preliminary studies for PA-OC$_1$(R is methoxy in PA-R) have shown that the scattering is observable at concentrations of about 0.2 wt%. It becomes stronger

and stronger when the concentration increases to about 4 wt% when a gel is formed. The scattering of the gels is significantly weaker than the lyotropic solutions at concentrations of about 0.5 wt% and higher. Upon centrifugation, the solutions separate into two phases. The top phase is isotropic with no observable light scattering while the bottom phase scatters light strongly. The lyotropic phase also has thermotropic properties. The temperature at which the liquid crystal to the isotropic liquid phase transition occurs for the solution of 0.20 wt% is 75 °C, that for the solution of 0.51 wt% is 90 °C, showing a very strong dependence on the concentration of the solutions. The transitions are reversible.

PE-R solutions were also made to study the lyotropic phase. No solutions with concentrations up to 50 wt % have been observed to scatter lights. However, both the powder samples (obtained from solutions by the addition of precipitant methanol and drying in a vacuum) and the film samples (casted from solutions by the evaporation of the solvent at ambient temperatures) are strongly birefringent when observed on a polarizing microscope. This is true not only for PE-R but also true for PA-R polymers. Because both PE-n and PA-n polymers are non-crystalline, the birefringence must be a result of mesophase ordering formed during the precipitation or solvent evaporation. In other words, a mesophase is formed in the course of the preparation of the samples. Careful studies have found that with the process of concentration of solutions of MJLCPs, a nematic phase with typical threaded and schlierene defects is developed (Zhou *et al.*, 1996). With such evidence for formation of lyotropic liquid crystals, the similarity in the property of MJLCPs with rigid and semi-rigid main chain type liquid crystal polymers is further demonstrated.

Experimental supports for the concept of MJLCPs were also given by other research groups. Side chain type liquid crystal polymers with mesogenic units laterally substituted on the main chains have also been studied by Keller *et al.* (1988), Gray *et al.* (1991), Pugh and Schrock (1993). Mesogenic units used by Finkelmann (polymer ⟨3.61⟩) and by Keller (polymer ⟨3.62⟩) were the same as or very similar to what we have used in polymers PE-R. However, flexible spacers with different length and structure were used in their polymers. Finkelmann's polymers are polymethacrylates, while Keller's are polysiloxanes. Gray also used polysiloxanes as polymer backbones and polymethylene segments as flexible spacers, but the attachment of the mesogens to the backbone is not at the waist but at the shoulder position of the mesogens (polymer ⟨3.63⟩). In spite of these differences in

molecular structure, the polymers all form nematic liquid crystal phases, same as our PE-R and PA-R polymers.

$$\langle 3.62\rangle$$

$$\langle 3.63\rangle$$

$$\langle 3.64\rangle$$
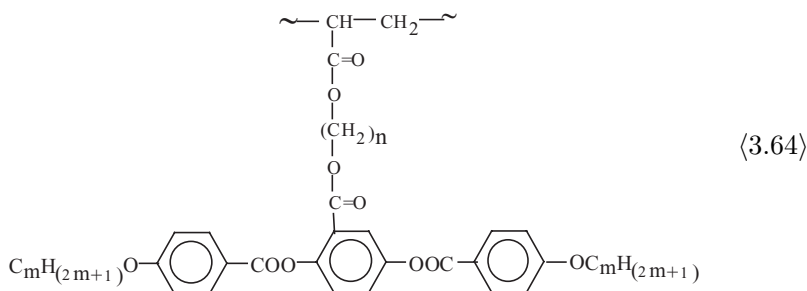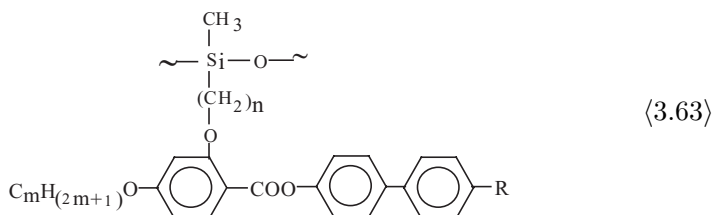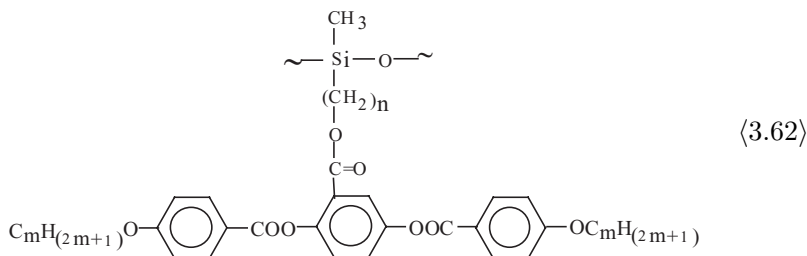
   With small angle neutron scattering, Hardouin and co-workers (1991) have been able to study the global shape of the polymer molecules in the nematic phase and the jacket effect imposed by mesogenic units on the molecular shape and property of the polymers. The polymers include those with mesogenic units laterally attached through flexible spacers of different length (polymer $\langle 3.62\rangle$), those with different degrees of substitution of such mesogens in copolymers, and those having different degrees of polymerization. Because of the mesogenic jacket, according to these authors, these polymers all have a strong tendency of chain extension. The highly prolated chain conformations are adopted in the nematic phase. Typical values of four or larger for the ratio of the apparent quadratic sizes parallel $(R_{\parallel})$ and perpendicular $(R_{\perp})$ to the magnetic field were found for the polymers. The results contrast significantly with those for conventional side

Table 3.16.   Phase transition and size ratio of a few side-on type polymers.

Polymer	D.P.	Phase transition	$R_\parallel/R_\perp$
$\langle 3.62 \rangle$,		(From: Hardouin *et al.*, 1992)	
n = 4, m = 4	70	g 36 N 130 I	4
n = 4, m = 4	35	g 39 N 129 I	6
$\langle 3.63 \rangle$, R = OC_5H_{11};		(From: Gray *et al.*, 1991)	
m = 8, n = 5	–	g 9.3 N 65.5 I	–
m = 8, n = 11	–	g 8.3 N 57.1 I	–
$\langle 3.64 \rangle$,		(From: Leroux *et al.*, 1993)	
m = 4, n = 4	–	g 40 N 116 I	6.0
m = 4, n = 6	–	g 28 N 105 I	4.5

chain type polymers. Conventional side chain type liquid crystalline polymers often take the oblate rather than the prolate chain conformations with quadratic size ratios smaller than 1. However, the jacket effect does vary for different molecules. In general, the jacket effect is stronger for polymers that have higher degrees of mesogenic substitution (Leroux *et al.*, 1994), shorter spacers (Leroux *et al.*, 1993), and lower degrees of polymerization (Hardouin *et al.*, 1992). As examples, Table 3.16 shows phase transition temperatures and the ratio $(R_\parallel/R_\perp)$ of a few polymers.

Polymers studied by these groups all have flexible spacers, meaning the mesogenic jacket effect is smaller than it is in PE-R and PA-R polymers in which no spacers are incorporated. As a matter of fact, all the polymers with flexible spacers have lower glass transition (40 °C or lower) and lower isotropization temperatures (below 130 °C). By contrast, PE-R polymers have Tg from ~80 °C to ~200 °C depending on the type of R groups at the two ends of the mesogenic units. As mentioned earlier, the PE-R polymers have very stable nematic phases. On the other hand, the PA-R polymers have even higher glass transitions, so high that no definite value can be obtained before slow thermal decomposition starts.

In summary, polymers with rigid mesogenic units as side groups attached through the waist or nearby positions to the main chain, form a new class of liquid crystal polymers. The chain conformation and property of this class of polymers depend strongly on the presence of a flexible spacer between the main chain and mesogenic units. In the polymers where no spacer or only very short spacers are used as are in the cases of PE-R and PA-R polymers, the rigid and bulky mesogenic units would form a dense "jacket" around the main chain, thus the term "Mesogen-Jacketed Liquid Crystal

Polymers." The mesogenic jacket of a MJLCP will impose on the main chain a strong jacket effect and force the main chain to take extended conformations. The chain is thus stiffened and may be described by Kratky-Porod's worm-like chains. If longer flexible spacers are used, there will be much more space for the mesogenic units to pack in, the density of the mesogenic units in the space around the chain will be smaller, and the jacket will be looser. As a result, a weaker jacket effect should be expected. MJLCPs have shown chain conformation and properties of rigid or semi-rigid polymers, including a high tendency (if not exclusive) of nematic phase formation, formation of nematic banded textures, high values of chain persistence length, and formation of lyotropic liquid crystalline phases. While in chemistry the MJLCPs are similar to conventional side-group type liquid crystal polymers by using mesogenic units as side groups, the similarity in the physical aspects of MJLCPs and main-chain type liquid crystalline polymers is remarkable.

3.7.   LIQUID CRYSTALLINE POLYMERS WITHOUT MESOGENIC UNITS

We have in previous sections discussed the molecular structure of a variety of liquid crystal polymers, including main-chain type, side-group type, and mesogen-jacketed type polymers. Others such as the shish-kebab type (Figure 3.1) molecules are possible, but will not be discussed further. These polymers are so classified because they all have mesogenic units present in a certain relation with the chain backbone. Mesogenic units are mostly rod-like in shape. Other shapes such as the cross or X-shaped, the T-shaped, the Π-shaped, the dish-like, and bowl-like mesogenic units are all imaginable and have invited certain interests. A question arises: are mesogenic units a requisite for polymers having a liquid crystalline property? The answer is "no." We give an explanation in this section.

A liquid crystalline phase is a phase in which molecules or components of molecules take a parallel alignment with thermal fluctuation and with certain transitional disorder. Thus in principle, most linear polymers and even branched or slightly crosslinked polymers can fit in with a liquid crystalline phase. Taking polyethylene as an example, the lowest energy conformation of this polymer is the extended trans form. Suppose that the extended chains or chain segments of PE align in parallel fashion leaving

certain transitional disorder, it is a liquid crystalline phase of polyethylene. However, two more things have to be considered: the thermal stability of the extended chain conformation which is a function of chain rigidity, and the realization and maintenance of transitional disorder which is related to crystallizability. Polyethylene is flexible with a glass transition temperature as low as $-120\,°C$. $C-C$ bonds in PE are flexible with a very low energy barrier for rotation. Thus if the polymer is in its non-crystalline state, extensive motions of bonds and chain segments should have already taken place at the most commonly used experimental temperatures which are much higher than Tg. It is thus impossible to maintain the required parallel alignment at such temperatures well above Tg and in normal experimental conditions of pressure. The flexibility is of course a function of temperature. If the temperature is significantly lowered down to the vicinity of, but above Tg, it would be possible to maintain parallel alignment. However, PE is a highly crystallizable polymer with a melting point at about $137\,°C$. If the temperature is decreased to about $130\,°C$, extensive crystallization will take place. Other flexible polymers behave similarly. As a result, no liquid crystal phase can form through the simple control of the temperature of such polymers.

It is well known that pressure can have a similar result as temperature. Imposition of higher pressure will restrict molecular motion and crystallization. Bassett and Turner predicted and found a new phase of PE at a sufficiently high pressure and temperature (Bassett, 1981). According to Bassett, polyethylene samples form a smectic-B phase before crystallization take place if they are being cooled down from melt at a sufficiently high pressure. The process is reversible. In Figure 3.8 are three DTA traces of such a sample at three pressures. It is interesting to notice that if the melting is at a pressure not high enough, the crystal will melt directly into an isotropic liquid (Figure 3.8a). The S_B phase can form only at a sufficiently high pressure (Figure 3.8b and c). The higher the pressure, the wider the temperature range of the S_B phase.

Joining in Bassett, Rastogi *et al.* (1991) have found that poly(4-methyl-1-pentene), also flexible, forms a nematic liquid crystal either when pressure is changed at a constant temperature, or when temperature is changed at a constant high pressure. The phase transition process is reversible. However, because the density of the crystal phase is unusually lower than the noncrystalline phase, the transition of crystal-to-nematic liquid crystal occurs at a high pressure when temperature is decreased rather than increased. Nevertheless, the nematic phase does exist in this flexible aliphatic polymer.
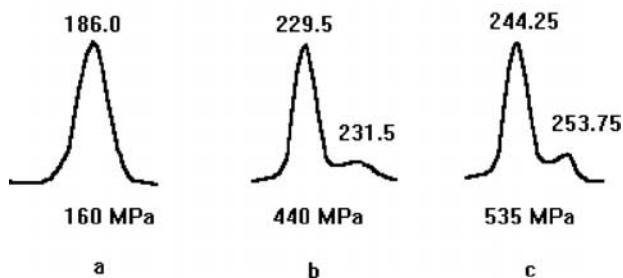
Figure 3.8.   DTA traces of anabarically crystallized (at $500\,\text{MPa}$) samples of 5×10^4 molecular mass polyethylene melting at three pressures. Transition temperatures are in °C. After Bassett (1981)

Thus we see that such flexible aliphatic polymers as polyethylene and poly(4-methyl-1-pentene) indeed form a liquid crystalline phase.

Liquid crystals formed through pressure change have been named barotropic. Barotropic behavior is observed not only for flexible polymers, it is also rather popular for conventional thermotropic liquid crystalline compounds and polymers. It has been reported by several research groups (*e.g.*, Herrmann *et al.*, 1983; Chandrasekhar and Shashidhar, 1979; Stevens *et al.*, 1984). As an example, Hsiao *et al.* (1988) claimed that for the aromatic copolymer of 4-hydroxybenzoic acid (20 mol %), hydroquinone (40 mol %) and 1,3-phthalic acid (40 mol %), not only would the temperature range of the liquid crystalline phase formed at normal pressure increase with increasing pressure, it would also form a new liquid crystal phase at high pressure.

In addition to barotropic liquid crystals of flexible polymers, there are also a few reports on the observation of the liquid crystalline phase of polymers containing no mesogenic units of rigid rods. Aharoni (1988), for example, was very lucky to have found a series of the following polymers that form a thermotropic liquid crystal phase.

$$\left(CH_2\right)_x \overset{\displaystyle O}{\underset{\displaystyle \|}{C}}-NH-\!\!\left\langle\bigcirc\right\rangle\!\!-\overset{\displaystyle O}{\underset{\displaystyle \|}{C}}-O\left(CH_2\right)_y O-\overset{\displaystyle O}{\underset{\displaystyle \|}{C}}-\!\!\left\langle\bigcirc\right\rangle\!\!-NH-\overset{\displaystyle O}{\underset{\displaystyle \|}{C}}- \qquad \langle 3.65\rangle$$
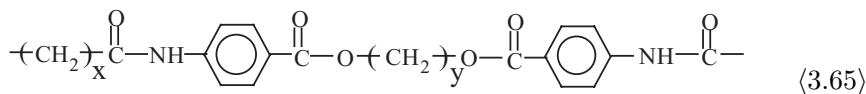
In $\langle 3.65 \rangle$ there is more of an aliphatic component than an aromatic one. Phenylene rings are each isolated by aliphatic components. No mesogenic units of rigid-rods are present in the molecule. However, the thermotropic liquid crystalline phase was observed for many of the polymers although

the liquid crystallinity is very sensitive to changes in the structure of $\langle 3.65 \rangle$. According to Aharoni, the polymers having $1 \leq x \leq 20$ and $3 \leq y \leq 9$ all are thermotropic liquid crystal, with those of $10 \leq x \leq 14$ and $y = 3$ or 5 having the most stable liquid crystalline phase. The specific combination of ester and amide groups shown in $\langle 3.65 \rangle$ is subtle for liquid crystallinity. Aharoni found that the change of amide with ester could completely destroy the liquid crystallinity, and vice versa. Of $\langle 3.65 \rangle$, the molecular chains are linear. The chain segments when taking extended conformations, are not contradictable with the formation of the liquid crystalline phase. The exact combination of structural moieties as shown by $\langle 3.65 \rangle$ may have brought about the chain rigidity just requested for stabilization of the liquid crystal phase at temperatures above melting. Too many amide groups may have raised the melting point too much. On the other hand, too many ester groups may have made the chain too flexible. Thus, replacement of the ester groups in $\langle 3.65 \rangle$ with more flexible ether linkages was found by the same author to destroy liquid crystallinity completely.

The gap present between the polymers having mesogenic units of rigid rods and those having no mesogenic units may have bridged by the concept of "flexible rodlike mesogenic units" proposed by Percec and coworkers (Percec and Yourd, 1988; Percec and Tsuda, 1991). In this case, two conformational isomers of certain structural moieties delicately designed are in equilibrium with each other (Figure 3.9).

One of the isomeric forms is rodlike and plays the role of mesogenic units in the formation of the liquid crystalline order. Because the rodlike form is the form of lower potential, a decrease in temperature results in a higher percentage of the rods. The mesophase is thus more stable at a lower temperature. However, crystallization is again a critical problem to be considered. In order to depress crystallization and melting point to a sufficient extent, substitution together with copolymerization of two repeating units has been successfully applied by Percec such as in the following structure:

$\langle 3.66 \rangle$
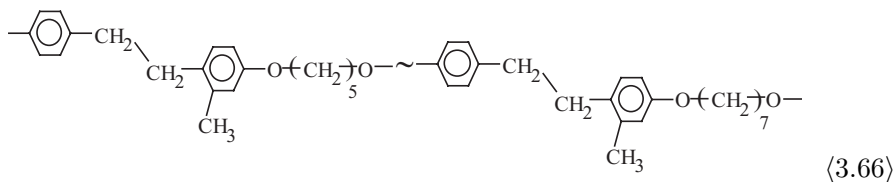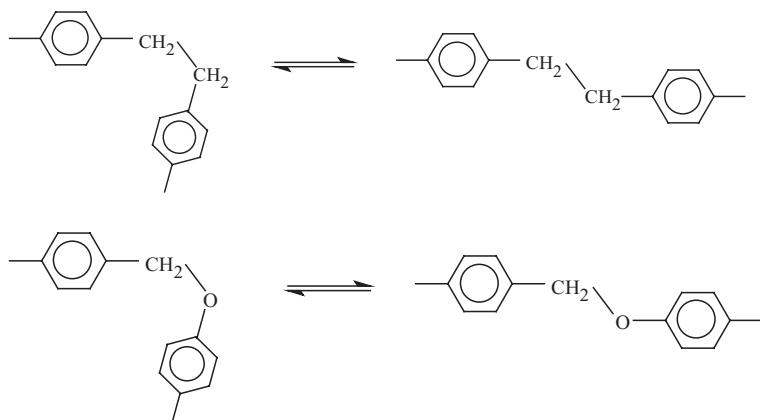
Figure 3.9.   Flexible rodlike mesogenic units proposed by Percec and coworkers.

According to Percec and coworkers, the copolymer ⟨3.66⟩ is non-crystalline with a glass transition temperature of 14 °C. In the temperature range between 14 °C and 55 °C, it is smectic. Above 55 °C it is nematic and then transfers into the isotropic liquid phase at 68 °C. The isotropization temperature is low, with the temperature range of the mesophase being only 13 degrees. The relatively low stability of the liquid crystal phase of this polymer can be attributed to the significant flexibility of flexible rodlike mesogenic units. Interestingly, if the polymer is annealed at a temperature within the temperature range of its nematic phase, the nematic phase will slowly transfer into a smectic phase. Percec reported the finding and explained it as a result of shifting the equilibrium of the two conformers to the rodlike side. A higher percentage of the trans isomer is necessary for the formation of the smectic phase which has a higher degree of molecular ordering than the nematic phase. The equilibrium process is slow. A long time annealing is needed for it to reach the equilibrium.

At about the same time of the findings of Percec, Josson *et al.* (1989) synthesized a series of polymers with following general structure:

$$-O-⟨\text{O}⟩-O-CH_2-⟨\text{O}⟩-CH_2-O-⟨\text{O}⟩-O(CH_2)_n- \qquad ⟨3.67⟩$$
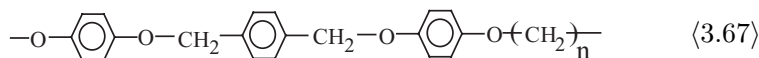
In ⟨3.67⟩, n = 7–12. The polymers have a smectic phase. The temperatures of the transitions from crystal to smectic phase (T_{CS}) and from smectic to isotropic liquid (T_{SI}) are shown in Table 3.17. The structure of

Table 3.17.   Phase transition of polymers $\langle 3.67 \rangle^*$.

n	7	8	9	10	11	12
T_{CS} (K)	466	473	460	468	452	463
T_{SI} (K)	480	493	473	484	466	480

* Source: Josson *et al.* (1989).

the mesogenic unit in $\langle 3.67 \rangle$ is longer than, but rather similar with what was shown in Figure 3.9. This mesogenic unit can thus be included in the category of "flexible rodlike mesogenic units." However, because it is much longer than that in $\langle 3.66 \rangle$, the transition temperatures and thermal stability of $\langle 3.67 \rangle$ are higher than that of $\langle 3.66 \rangle$.

This page intentionally left blank

Chapter 4

Characterization of Liquid Crystalline Polymers

A complete characterization of liquid crystalline polymers should include at least two aspects: the characterization of the molecular structure and that of the condensed state structure. Since the first characterization is nothing more than what is practiced for non-liquid-crystalline polymers, we will restrict the discussion to only a short introduction of methods mostly used in the characterization of the presence and the main types of polymeric liquid crystal phases. The methods include the mostly used polarizing optical microscopy (POM, Section 4.1), differential scanning calorimetry (DSC, Section 4.2) and X-ray diffraction (Section 4.3). The less frequently used methods such as miscibility studies, infrared spectroscopy and NMR spectroscopy will also be discussed briefly (Section 4.4).

Before we leave for the discussion on individual methods, a few points important for any smooth characterization should be emphasized. The first is the purity of the sample. Polymer samples are often obtained from solutions. Since a large portion of liquid crystalline polymers dissolve only in polar and high boiling solvents, there is often a danger of sample contamination by solvents. As a typical example, shown in Figure 4.1 are two DSC heating curves of two samples of the same polymer which is thermotropically liquid crystalline. The polymer was synthesized in the author's laboratory. The original sample was obtained by precipitation in methanol of the polymer from its tetrachloroethane (TCE) solution and dried in vacuum at $40\,°C$–$50\,°C$ for two days. Its DSC heating curve is shown on the top of Figure 4.1. There were three endothermic peaks respectfully centered at $90\,°C$, $156\,°C$, and $185\,°C$, suggesting three phase transitions. This result, however, did not agree with the POM observations that indicated only the
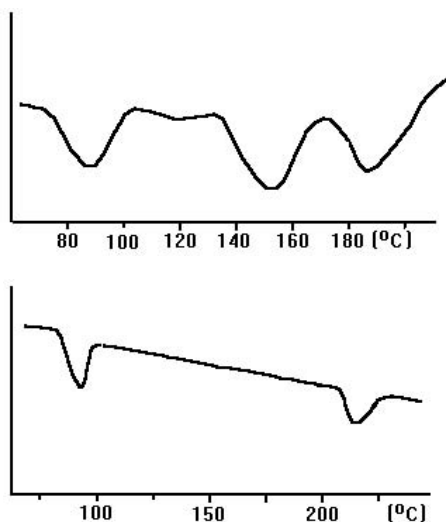
Figure 4.1. DSC heating curves of a liquid crystalline polyester. Top: sample contaminated with solvent; Bottom: pure sample.

presence of one melting process as well as one isotropization of its nematic phase. The X-ray diffraction studies suggested also only one nematic phase at temperatures above the melting and below the isotropization. Since the second endothermic peak at $156\,°C$ was very close to the boiling point of the solvent TCE, this peak was considered to be a result of TCE contamination. In order to clarify the result, the sample was further purified by careful re-dissolution with the lower boiling THF and re-precipitation from methanol. The drying was carried out in vacuum at $50\,°C$ for one week. The result is the bottom curve of Figure 4.1. Now the DSC result agrees very well with the POM observations. The polymer melts at $92\,°C$, forming a nematic phase which in turn transfers at $219\,°C$ to an isotropic liquid. The example shows that solvent contamination can be misleading to such a degree that special attention should be called upon. The example has also emphasized the necessity of using more than one technique for reliable characterizations.

Secondly, thermotropic liquid crystalline polymers are characterized in a temperature range that is often too high to keep the molecular structure unchanged. The post-polymerization and decomposition are two possible results of a prolonged study of a polymeric liquid crystalline phase. There have been reports on liquid crystalline phases observable only

for the first heating of the virgin samples. These have been referred to as "monotropic" liquid crystals by some reporters. However, the decomposition and other undesirable reactions are often the cause of these observations. A monotropic phase has Ti lower than Tm, that is thermotropically metastable and is observed only in the process of cooling and not during the heating.

More often, the post-polymerization and the increment of molecular weight can occur during the characterization of condensation polymers. In addition, changes in chain structure or the sequence distribution along the chain can occur through transesterification or alike reactions. This is the case especially when the polymer is a copolyester obtained from condensation polymerization and no end-capping has been made. Because the properties depend on the sequence distribution as well as on the molecular weight particularly at low values, the melting and liquid crystal phase transition temperatures may vary during repeated testing of a sample. One typical experiment (Zhou *et al.*, 1989) has shown that the molecular weight of a copolyester doubled within half an hour at $200\,^{\circ}\mathrm{C}$. This increase resulted in some 30 degrees of increment of clearing temperature of the nematic phase.

Finally, the history at experimental temperature may cause changes in the structure of the condensed state of a sample. We have introduced in Section 3.7 the interesting finding by Percec and coworkers of the nematic-to-smectic transformation after annealing of a liquid crystalline copolyether. Taking this as an unusual finding, it is then often the case that the crystallinity and the melting point will change because of the annealing. We will come back to this point in Section 4.2 for a further discussion.

4.1.   POLARIZING OPTICAL MICROSCOPY (POM)

Polarizing optical microscopy is often the method of first choice. It was with POM that the textures of liquid crystals were observed and the classification of liquid crystals was first made according to these observations. In this field, two books are recommended: *The Textures of Liquid Crystals* by Demus and Richter (1978) and *Smectic Liquid Crystals — Textures and Structures* by Gray and Goodby (1984). While the latter provides readers with a practical and useful experimental guideline to the textures and classification of smectic liquid crystals of different polymorphic types together with as many as 124 reference photographs of typical textures, the former

emphasizes the effects of structural disclinations upon the texture and the origins of these in local deformations of or discontinuities in the arrangement of the molecules. The two books are thus complementary. On the other hand for identification of the mesophases exhibited by thermotropic liquid crystalline polymers, an excellent account was given by Noel (1985). In this section, the optical principle of POM in the characterization of liquid crystals is briefly introduced, followed by typical texture observations for polymeric liquid crystals.

4.1.1.   Optical basics for POM

When light of a given wavelength λ_a, that is when a monochromatic light travels from air into a liquid crystal, the wavelength will change to a new value. The refractive index n is the ratio of the two wavelengths. Because liquid crystals (with exceptions of the D- and Blue phases) are optically anisotropic, the behavior of light in liquid crystals depends on the direction of the travelling. Liquid crystals may be uniaxial (*e.g.*, the uniaxial nematic and S_A, S_B) or biaxial (*e.g.*, S_C and the very rare biaxial nematic). Because the uniaxial phases are the most often observed polymeric liquid crystals, and because the learning of the optical principle for the uniaxial is also the base for the understanding of biaxial phases, the emphasis of the following discussion is on this type of liquid crystals.

In a uniaxial liquid crystal, the light decomposes into two components namely the ordinary rays with λ_o and the extraordinary rays with λ_e. While the wavelength of the ordinary ray λ_o does not depend on direction, that of the extraordinary ray λ_e is direction-dependent. If the refractive index of the extraordinary ray n_e is larger than that of the ordinary ray n_o, the liquid crystal is positive. Otherwise it is negative. In other words, the birefringence ($\Delta n = n_e - n_o$) of a positive liquid crystal is positive. That of a negative liquid crystal is negative. Because λ_e and thus n_e depends on the direction of travelling the birefringence is direction-dependent.

The behavior of light travelling in a uniaxial liquid crystal may be analyzed with help of the wave surface figure. The wave surface figure is the geometrical figure formed by the wave front of a monochromatic light emitted from a point source. Because ordinary rays travel with the same velocity in all directions, their wave surface is a sphere. In contrast, the wave surface of extraordinary rays is an ellipsoid of rotation. In Figure 4.2 are two principal sections of the wave surfaces. Figure 4.2(a) is for the positive uniaxial
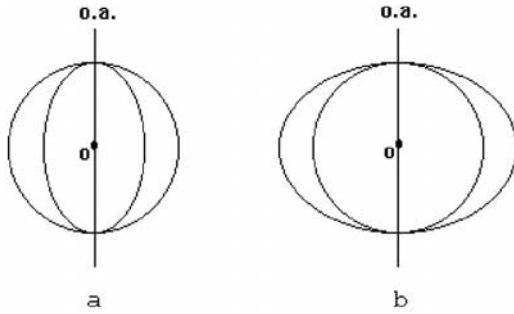
Figure 4.2.   Principal sections of the wave surfaces. **o** is the point source, **o.a.** is the optic axis. (a) positive uniaxial liquid crystal, (b) negative uniaxial liquid crystal.
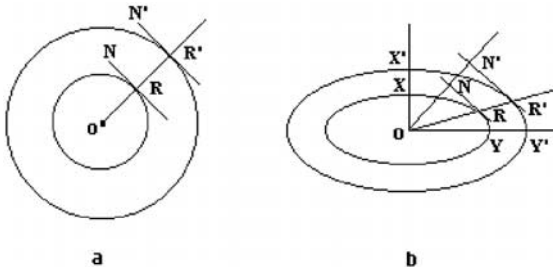
Figure 4.3.   Wave fronts and wave directions of the ordinary (a) and the extraordinary (b) rays.

liquid crystals, in which the ordinary rays are faster than the extraordinary rays except along the optic axis where the two have the same velocity. For a negative uniaxial liquid crystal, the extraordinary rays are faster than the ordinary rays. The two wave surfaces are related as shown in Figure 4.2(b).

Figure 4.3 illustrates wave fronts and wave directions of ordinary and extraordinary rays. For the ordinary rays Figure 4.3(a), the wave surface is spherical so that the wave front at any point (for example wave front RN at point R) is perpendicular to the ray (OR) which meets the surface at that point (R), so that the wave direction (the direction in which the wave front travels) and the ray direction are the same (along the ORR′ direction). This is not the case for extraordinary rays. As shown in Figure 4.3(b), the wave front (the tangent plane RN at R and the tangent plane R′ N′ at R′) is not perpendicular to the ray direction (ORR′). They are perpendicular to each other only when the rays are traveling along the axis directions of the ellipsoid of rotation (OYY′ or OXX′). Therefore, the wave direction (ONN′)

is normally different from the ray direction (ORR'). The velocity of the wave front, or the wave velocity is also different from the ray velocity. When a ray starting from O reaches the point R, its wave front reaches the point N. With OR representing the velocity of the ray, ON is then the velocity of wave front of the ray. The extraordinary refractive index (n_e) is defined to be the velocity of the ray in air divided by the velocity of its wave front in the liquid crystal. This definition of refractive index also holds for ordinary rays. For with ordinary rays the wave front direction and the ray direction coincide, so that it is immaterial whether the velocity of the ray or the velocity of its wave front is used in the definition. In Figure 4.3(b) one sees the fact that the extraordinary rays starting from the same point O but traveling along different directions (OY, OR, OX etc.) should have different wave-front velocities (OY for the ray OY, ON for the ray OR, OX for the ray OX). The extraordinary refractive index is therefore direction-dependent. If the radii of the figure represent velocities of the light with respect to its velocity in air, the refractive indices are given by the reciprocals of the lengths of the lines representing the wave normal. Thus, the refractive index of the extraordinary ray along OR is represented by 1/ON, whilst those for the extraordinary rays along OX and OY are represented respectively by 1/OX and 1/OY, because OX and OY are also the lengths of the two wave normals. The rays along OX have the highest refractive index (n_{max}) that along OY has the lowest value (n_{min}). Rays along other directions such as OR have intermediate values. In a positive uniaxial liquid crystal phase, the ordinary rays have refractive index equal to n_{min}. In a negative uniaxial liquid crystal phase the refractive index of ordinary rays is equal to n_{max}.

In studies of the optical properties of the liquid crystal phase the microscope may be arranged for orthoscopic observations between crossed polars, or it may be arranged for conoscopic observations. These two arrangements are shown in Figure 4.4.

In Figure 4.4, the letters represent respectively the following principal components of a polarizing microscope: P the polarizer, D the substage iris, C the condenser, S the graduated rotable stage, O the objective, L a slot for compensator, A the analyzer, B the Bertrand lens for conoscopic observations, and E the eyepiece. In orthoscopic observations (Figure 4.4(a)), the polarization effects together with the image of the sample X is observed. Rays emanating from a given point on the sample are brought to a focus at the focal plane of the upper lens of the eyepiece. In conoscopic observations (Figure 4.4(b)), on the other hand, it is not the image of the sample but the
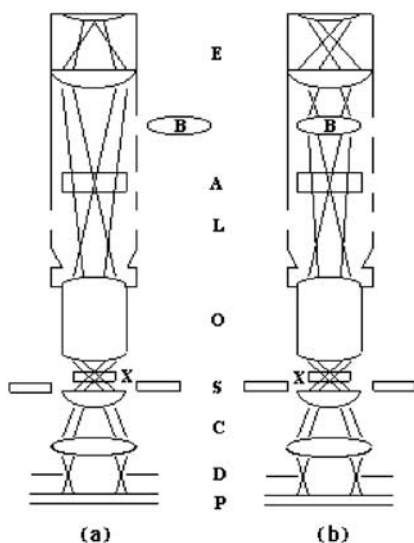
Figure 4.4.   Polarizing microscope for orthoscopic (a) and conoscopic (b) observations.

interference figure (also referred to as the direction image) that is observed through the eyepiece when the Bertrand lens is inserted. In this case the parallel rays which have passed through the sample in any given direction are brought to a focus of the upper lens of the eyepiece. In practice, the sample X is placed on the stage as a thin film or it becomes so on the stage.

4.1.2.   Orthoscopic observation

Orthoscopic examination with crossed polars is carried out first of all to determine the isotropism or the anisotropism of a sample. The polarization colors, the defects and variation in molecular orientation, and the orientation pattern or "texture" of liquid crystals are observed in this examination. With a heating stage the temperature of phase transition is also determined. In addition, with use of a compensator, the determination of vibration directions of the ordinary and extraordinary rays, the determination of relative retardation and birefringence are possible. In this section, the optical basics for orthoscopic observations are briefly outlined. The description of textures frequently observed for polymeric liquid crystals is given in Section 4.1.4.
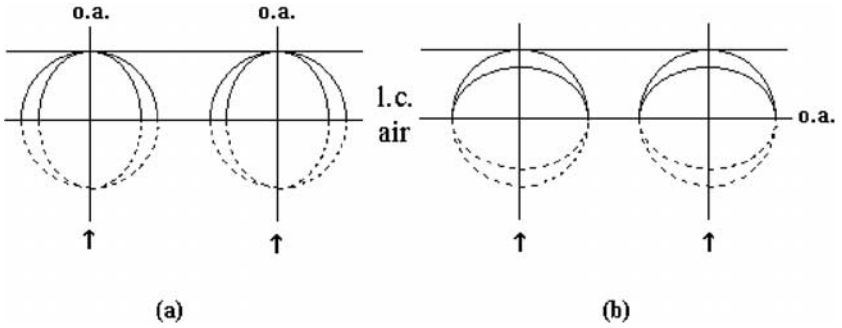
Figure 4.5.   Perpendicular incidence on positive uniaxial liquid crystal films. **o.a.** is the optical axis. (a) rays incident along optical axis, (b) rays incident perpendicular to optical axis.

In orthoscopic observations parallel rays are required because the optical property of liquid crystals is direction-dependent. Often a low-power, low aperture objective lens is used so that most of the light will travel through the sample in the same direction or nearly so. Otherwise the substage iris (D in Figure 4.4) is closed accordingly so that a sufficient approximation of the parallel condition is achieved.

Take a positive uniaxial liquid crystal as an example. If the sample is so arranged that its optical axis is perpendicular to the sample surface (Figure 4.5(a)), the incident rays normal to the surface will pass through the sample along the direction of the axis. There will be no birefringence because all rays have the same velocity. Liquid crystals with such an orientation have been given the name "homeotropic". We will soon show that the liquid crystal of homeotropic orientation will extinguish and remain dark on rotation when being examined between two crossed polars.

In Figure 4.5(b), the optical axis is in the surface plane ("homogeneous" alignment). The incidence is perpendicular to the axis. In this case, the light travels through the sample as the extraordinary and the ordinary rays. In a positive liquid crystal, the ordinary rays are faster, having wave front ahead of that of the extraordinary rays. The extraordinary ray along the direction normal to the optical axis is the slowest with the refractive index equal to n_{max}. On the other hand in a negative sample (not shown in the figure), the extraordinary ray is the fastest in this direction with the smallest refractive index that is equal to n_{min}.

In most cases, the axis is obliquely oriented with respect to the sample surface. This is shown by Figure 4.6. AB/CD are rays perpendicularly
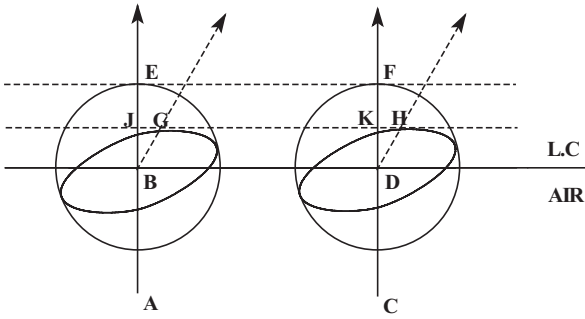
Figure 4.6.   The axis of the positive uniaxial liquid crystal obliques from the surface. The rays AB/CD enter the sample in the direction perpendicular to the surface.

illuminating at an instant on the sample surface BD with wave front BD on the surface. The rays will then decompose into two components. The ordinary rays will travel through the sample with the direction BE/DF, the same as it has been before entering the sample. The extraordinary rays will deviate from that direction as shown in the figure by BG/DH. In the positive liquid crystal, the extraordinary rays are slower than the ordinary rays. The wave front of the former (GH in the figure) at any instant lags behind that of the latter (EF). However, the wave direction BJ/DK of the extraordinary rays is the same as the wave front BE/DF of the ordinary rays. In other words, the wave direction of the ordinary rays and that of the extraordinary rays are both the same as the direction of incidence regardless of the relative orientation of the optic axis with the surface plane.

In a uniaxial liquid crystal, the ordinary and extraordinary rays are both polarized. The following rules determine the vibration directions of the two:

(1) Vibration direction is parallel to the wave front for both the rays;
(2) An ordinary ray always vibrates at right angles to the plane containing the ray and the optic axis;
(3) An extraordinary ray always vibrates in the plane containing the ray and the optic axis. Obviously the vibration direction of the ordinary and that of the extraordinary rays are perpendicular to each other.

These rules are illustrated in Figure 4.7 showing a principal section of a positive uniaxial wave surface figure. OX is the axis. OS is an ordinary ray of which the vibration direction is at a right angle to the principal section (that is the plane SOX) and at a right angle to the ray. This is represented
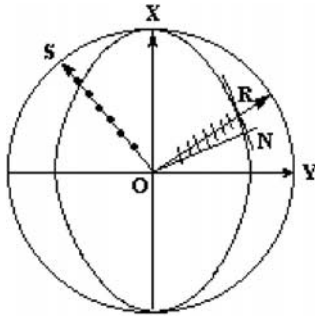
Figure 4.7.   Vibration directions of the ordinary and the extraordinary rays in a positive uniaxial liquid crystal. OX is optic axis.
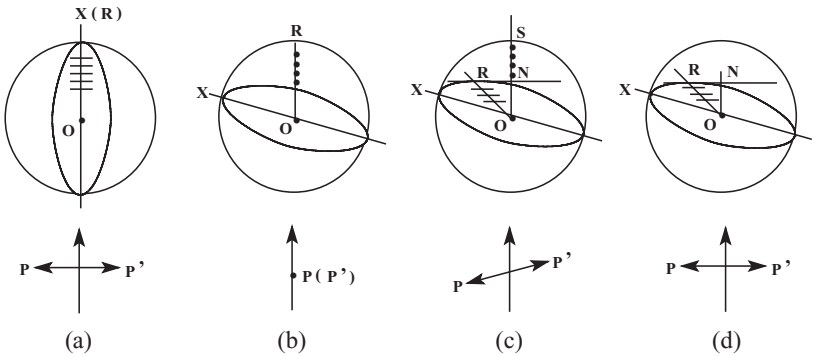
Figure 4.8.   Linear-polarized light passing through a positive uniaxial liquid crystal.

by dark spots on OS. OR is an extraordinary ray. The vibration direction of OR is in the plane ROX and parallel to the wave front RN. This is denoted with strokes across OR, which are perpendicular to the wave normal ON.

In studies of liquid crystals with POM, a polarizer is used (Figure 4.4) so that the source light is linear-polarized with vibration direction determined by the polarizer. If PP′ is the vibration direction of the entering light, the result will depend on the relative orientation of PP′ with the axis and principal section of the liquid crystal. In Figure 4.8, a few cases for a positive uniaxial liquid crystal are shown. When the incident is parallel to the optic axis (Figure 4.8(a)), the refracted light will vibrate in the same direction as PP′. The light emerging from the liquid crystal will also vibrate in this direction. Thus, if a second polarizer (the analyzer) is used on the detecting side as shown in Figure 4.4 and if the vibration direction of the analyzer (AA′, not showing in Figure 4.8) is at a right angle to
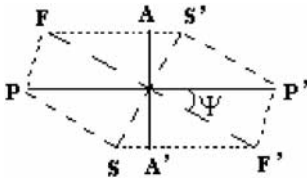
Malus' equation:

$$I = \sin^2 \Phi \sin^2 (2\Psi)$$
$$\Phi = (\pi / \lambda) d \Delta n$$

Figure 4.9.

PP′, there will be no light passing through the analyzer. Rotation of the sample stage results in no difference. The sample is thus extinct and forms a homeotropic texture (dark). In most cases, the optic axis is oblique to incident direction (Figures 4.8(b), 4.8(c), 4.8(d)). If in addition, the PP′ is in the direction perpendicular to the principal section (represented with bold dots in Figure 4.8(b)), PP′ coincides with the vibration direction of the ordinary ray resulting in no extraordinary component. The light coming out from the sample will vibrate in the same direction as PP′. Again no light will pass through the analyzer. If the sample stage is rotated for an angle so that the relative orientation is such as shown in Figure 4.8(c), neither the ordinary rays nor the extraordinary rays will vibrate in the direction PP′. The light decomposes in the sample into ordinary and extraordinary rays. Generally in this case there will be light passing through AA′ (see discussion below with Figure 4.9 and the Malus' equation), a birefringent image of the sample is seen through the eyepiece of the microscope. With further rotation of the stage, a position as shown in Figure 4.8(d) is reached, which is 90 degrees relative to the position showing in Figure 4.8(b). PP′ is now parallel to the principal section. The vibration direction of the extraordinary ray coincides with PP′. The light coming out from the sample is the extraordinary ray that is unable to pass through the analyzer. Again only an extinct image is observed. The relationship represented by Figures 4.8(b), 4.9(c) and 4.9(d) will remain with rotation of the stage. Thus the sample will extinguish once for every rotation of 90 degrees. The rotation effect can be used to distinguish extinct images of liquid crystals from that of an isotropic sample. For the latter the rotation of the stage makes no difference and the image remains dark. On the other hand the homeotropic liquid crystal and the isotropic liquid may be conveniently distinguished by making disturbance in the sample with a press on the cover glass. The press will disturb the molecular orientation of the liquid crystal resulting in an observable birefringence. The distinguishing can also be achieved with conoscopic observation (Section 4.1.3).

The above analysis may be summarized with Figure 4.9 and Malus' equation which relates the intensity I of the light detectable by POM. In the equation, d is the thickness of the sample, $d\Delta n$ is the relative retardation, and the angle Ψ is defined by Figure 4.9. PP′ and AA′ are the vibration directions of the polarizer and analyzer. FF′ is the vibration direction of the faster ray (ordinary ray in a positive uniaxial liquid crystal). SS′ is that of the slower ray (extraordinary ray in a positive sample). Thus, if $d\Delta n$ is by chance equal to $m\lambda$ (m is zero or integral number), the intensity will be null independent of the angle Ψ even if it is $45\,°$. The angle $45\,°$ is what makes the second sinusoid in the equation the highest value. On the other hand, if $d\Delta n$ happens to be $(m + 1/2)\lambda$, the intensity will be the highest when Ψ is $45\,°$.

In most characterizations the incident light is practically white rather than monochromic. This often makes the image of a liquid crystal very colorful. For example, if $d\Delta n$ is 400 nm, that is λ of the violet band, the violet band will be extinguished. The color showing will be the compensative orange. If $d\Delta n$ is 700 nm (about λ of the red), the color will be blue. Obviously, the observed color of interference relates to the thickness and the birefringence of the sample. With an increase of the thickness the color will become more and more faint because of the increased overlapping of the extinguished bands. The thickness is practically 10–100 microns in most POM studies.

4.1.3.   Conoscopic observation

In conoscopic observations (Figure 4.4(b)), it is not the image of the sample but the interference figure that is observed through the eyepiece when the Bertrand lens is inserted. In this case the parallel rays which have passed through the sample in any given direction are brought to a focus of the upper lens of the eyepiece. Conoscopic observations are used to determine the uniaxial or biaxial character of liquid crystals. A homeotropic liquid crystal which is extinct under orthoscopic examinations can be differentiated from isotropic liquids with conoscopic studies. The positive or negative nature of the sample may be determined by this technique also.

While in orthoscopic studies the parallel incident lights are desirable, in conoscopic examinations high-aperture condenser and objective are used so that a wide-angle cone of light is allowed to pass through the sample. The cone is composed of bundles of parallel rays along different directions.
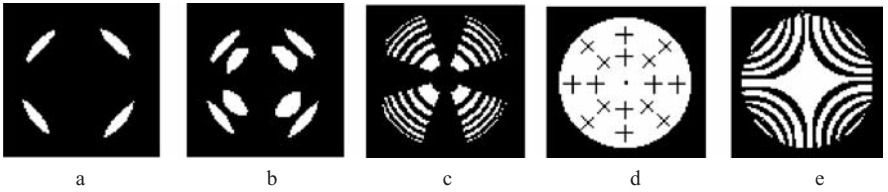
Figure 4.10.   Interference figures of a uniaxial liquid crystal: a, b, c for the homeotropic phase with increased thickness from a to c; d shows vibration directions for different parts of these figures. e represents interference figure of the homogeneous phase.

Each bundle of the parallel rays passing through and emerging from the sample is brought to a focal point in the upper focal plane of the objective (Figure 4.4(b)). Parallel rays with different incident angles will suffer different birefringence and have to pass through different thicknesses of the sample. For a thin film of a uniaxial liquid crystal of uniform thickness, for example, if the optic axis is perpendicular to the surface, the parallel rays along the axis direction will suffer no birefringence. Other parallel rays incident along directions oblique to the axis will suffer birefringence. The larger the angle is made by the axis and the incident direction, the higher the birefringence is and the longer distance the light has to travel in the sample. Thus a larger retardation $d\Delta n$ is created. If monochromatic light is used, concentric fringes of a sequence of alternate dark and bright rings will form on the focal plane. As discussed in Section 4.1.2, dark rings are formed where the retardation $d\Delta n$ is equal to $m\lambda$. On the other hand, if $d\Delta n$ is $(m + 1/2)\lambda$, the ring will be the brightest. In addition, there is no light passing through the analyzer along directions where the vibration of refracted light is parallel to that of the polars. A dark cross is formed. In Figure 4.10, a, b, and c demonstrate interference figures of a uniaxial liquid crystal with axis perpendicular to the surface. Figure 4.10(d) shows vibration directions for different parts of these figures. As discussed before, the light incident along a non-axial direction is decomposed by the sample into two components. The ordinary ray vibrates in the direction normal to the plane containing the ray and the axis, whilst the extraordinary ray vibrates in this plane and normal to the vibration direction of the ordinary ray. Thus as shown in Figure 4.10(d), the extraordinary rays vibrate in directions of the radials, the ordinary rays vibrate tangentially. Obviously extinction occurs along the vibration directions of the two polars, and the figure will remain the same when the stage is rotated. From Figure 4.10(a)
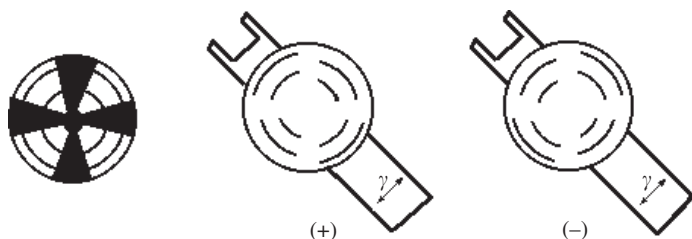
Figure 4.11.   Determination of optical sign by conoscopic examination with insertion of a compensator.

to 4.10(c), the thickness of the sample is increased. With this increase, more and more fringe rings of equal retardation are observed. Note also that the interval is smaller when the angle between the axis and the direction of the incident rays is increased. The interval between the two out-most rings is the smallest as shown in Figure 4.10(c). This is so since both d and Δn and thus $d\Delta n$ becomes greater and greater when the emergent rays are more inclined to the optic axis. Figure 4.10(e) shows an interference figure of a homogeneous phase in which the optic axis is in the plane of the sample and is about $45\,^{\circ}$ to the vibration directions of the polarizer and the analyzer. The figure changes with rotation of the stage. When the axis coincides with one of the vibration directions of the polars, a dark cross is observed.

Biaxial liquid crystals result in much different interference figures dependent on how the specimen is cut relative to the two axes. For example, if it is cut perpendicular to one of the axes, the figure-8-like fringes of equal retardation may be observed. Thus the uniaxial and biaxial liquid crystals may be differentiated. Since biaxial liquid crystals are very rare in polymers, no further discussion is given.

As having been shown in Figure 4.10(d), the extraordinary rays vibrate in the directions of the radials, the ordinary rays vibrate tangentially. If the liquid crystal is positive, the ordinary ray is faster than the extraordinary ray. If it is negative, the ordinary ray is the slower. Thus, by insertion of a compensator (the slow direction γ: SW-NE) the optical sign can be determined. With uniaxial positive liquid crystals the phase difference is increased in the first and third quadrant. The interference fringes move inwards towards the center of the figure in these two quadrants (Figure 4.11, center). On the other hand, if it is negative, the phase difference is decreased and the fringes move outwards in these two quadrants (Figure 4.11, right).

4.1.4.   Textures of polymeric liquid crystals

Texture or the orientation pattern refers to the picture observed in orthoscopic observation of a liquid crystal film, which is a combination of sample image and polarizing effect. Defects of material and orientation as well as interference colors are shown in texture. An ideal monodomain of a uniform thickness and orientation ("liquid single crystal") gives out only the contour of the domain in certain monotonic color. The texture of a liquid single crystal is termed the "homogeneous texture" and is a result of perfect orientation. A liquid single crystal of homeotropic orientation will be extinct between crossed polars and will remain such with rotation of the sample stage. The liquid single crystals with other orientations will change in color with rotation of the stage.

Often there is a variety of defects in liquid crystals (Chapter 1). This is so particularly in polymeric liquid crystals because in polymers the molecular structures are often very complex and the melt viscosity is very high. The complexity in molecular structure often prevents perfect orientation or even results in phase separation. For example in a side-group type polymer the non-mesogenic main chain segment may not join the mesogenic side groups in orientation. In a main-chain type polymer containing flexible or nonlinear segments the molecular orientation in the liquid crystal phase is also imperfect. On the other hand because of the often very high viscosity of polymer melts, the molecular motions of polymer segments have a high activation energy and are slow in comparing with that of low mass liquid crystals. Much longer experimental time is needed for the formation of a polymer liquid crystal in thermodynamic equilibrium. Thus while a low mass liquid crystal enters its liquid crystal phase as soon as it melts, a period of time may have to be waited for a polymer sample to finish this process.

Nevertheless in polymeric liquid crystals the same types of orientational defects and thus the same types of textures as present in the low mass counterparts have been observed. The textures often formed by polymers are the threaded texture, the schlieren texture and the focal conic texture of smectics. As is for low mass liquid crystals, the texture is a consequence of defects (disclinations and dislocations, refer to Chapter 1) present in the liquid crystal and is characteristic of a specific type of the phase. The texture examination has become a very useful tool in the determination of the type and nature of the polymeric liquid crystals.
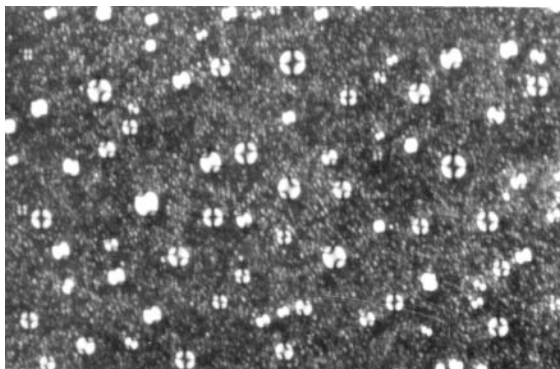
Figure 4.12.   Nematic droplets separated from an isotropic melt of a polymer.

The texture of polymeric nematics. The most often observed textures for polymeric nematic liquid crystals are nematic droplets, schlieren textures, and threaded textures. When a nematic polymer sample is slowly cooled down from its isotropic melt to its liquid-crystallization temperature T_{lc}, the nematic phase often starts to form in the form of birefringent droplets (Figure 4.12). With time or/and slightly lowering temperature the number and size of the droplets grow. Two droplets may combine to form a larger droplet. The droplets will disappear and finally be replaced by a continuous nematic phase with a schlieren texture and/or a threaded texture. Dependant on the state of molecular orientation the droplet may have a dark cross in center when a spherical symmetry of orientation is present, or it has other forms of extinction when spherical symmetry is absent. An example of nematic droplets of a polymer is given by Figure 4.12.

The polymeric and the low mass nematic droplets are the same in appearance. However, because of the much higher viscosity and because of the presence of molecular weight distribution, the following has been observed for polymers: 1, while the super-cooling of the isotropic phase is only to a small extent (often one or two degrees) for low mass liquid crystals, that for a polymer may be small but can also be very large. Ten even twenty degrees of super-cooling is not unusual for polymers. The number of the droplets increases fast in low mass samples, the increase is relatively slow in polymers with a lowering temperature. 2, the droplets formed earlier have a higher thermal stability. In other words, in the course of heating, the nematic-to-isotropic phase transition (N/I) takes place in a wide-range of temperature. The droplets originally formed in the earlier stage during

cooling will disappear at higher temperatures during heating. These observations may be explained in terms of the effect imposed by molecular weight. The property of liquid crystalline polymers is molecular weight dependent (Chapter 3). The nematic phase of a higher molecular weight polymer has a higher thermal stability and a higher clearing temperature. Yet the polymers are often widely dispersed in molecular weight. Thus a molecular weight fractionation may occur during cooling from an isotropic melt. The droplets formed earlier may contain more high mass molecules, that formed in the last may contain more of the low mass molecules. Obviously, if the sample is monodispersed in molecular weight, a much sharper transition at N/I will be observed. An excellent account for this and structural effect on supercooling at N/I transition has been given by Blumstein *et al.* (1985).

A schlieren texture is often observed for polymeric nematics. This texture is characterized by point singularities from which two ($s = \pm 1/2$) or four dark ($s = \pm 1$) brushes radiate. A representative photomicrograph of the texture is given in Figure 4.13. In this nematic a schlieren texture is observable for both the singularities of two and four brushes.

According to Nehring and Saupe (1972), the strength s of a singularity is determined by the number of the brushes $s = \pm 1/4$ (number of the brushes). The value is positive if the brushes rotate in the same direction as the polars. Otherwise it is negative. This is demonstrated by Figure 4.14. In the center part of each picture in the figure there are two singularities each with four

Figure 4.13.   Photomicrograph of the schlieren texture of a polymeric nematic phase.
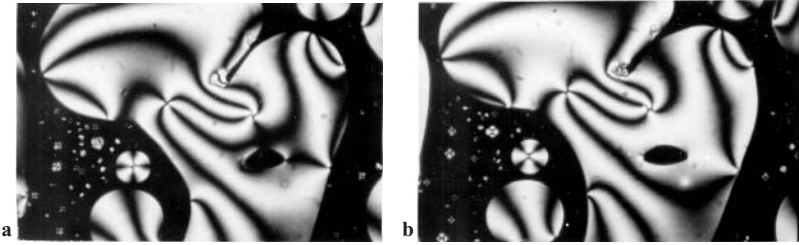
Figure 4.14.   Rotation of the brushes with rotation of the crossed polars. **b** was obtained after the two polars were rotated anticlockwise for 45° relative to their positions for **a**. The dark cross showing in the spherulite positioned south-west of the center of the picture disclosed the vibration directions of the two polars.

brushes ($s = \pm 1$). The vibration directions of the two crossed polars for the picture are disclosed by the dark cross in the spherulite southwest of the center of the picture. For Figure 4.14(a) the vibrations are in the west–east and north-south directions. For Figure 4.14(b) the polars have been rotated anticlockwise relative to the positions for Figure 4.14(a) by 45°. The brushes of the left singularity is rotated in the same direction as the polars so that the sign determined is positive and $s = +1$. On the other hand, $s = -1$ was determined in the same way for the right singularity. Any two singularities with one or more common brushes have the opposite sign of strength. The degree of rotation of the brushes (ϕ) and that of the polars (β) have a relation defined by $\phi = \beta/s$. Thus, if the polars have rotated 2π in the anticlockwise sense, the brushes of the singularity of $s = -1$ should have rotated clockwise by 2π, while that of $s = +1$ should have rotated anticlockwise by 2π. This relationship remains when the rotation is made on the polars but not on the sample stage. If the rotation is made on the stage by an angle of β while keeping the polars stationary, the relationship becomes $\phi = \beta(s - 1)/s$. For example, if the stage has been rotated by $\beta = \pi$, the brushes of the singularity of $s = -1$ should have rotated by $\phi = 2\pi$. On the other hand, rotation of the stage will bring about no rotation of the brushes of the singularity with $s = +1$.

In a nematic phase, the strength of disclination may have values that are half-numbered or whole-numbered. However because the disclination energy is proportional to s^2 (Nehring and Saupe, 1972), it is rare to observe singularities with $|s| > 1$. In studies of a series of nematic polymers with "two-dimensional mesogenic units" Zhou and coworkers (1993) have been
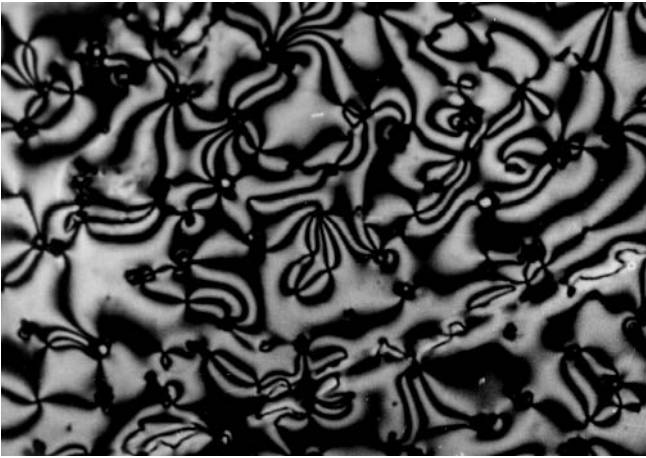
Figure 4.15.   A nematic texture showing singularities of high strength. The sample is a nematic polymer with two-dimensional type mesogenic units.

able to observe singularities with $|s| = 3/2$, 2, and 5/2. The unique "two-dimensional" architecture of the mesogenic units may have brought in a high energy for splay distortion and "escape" so that the high strength singularities are significantly stabilized. Figure 4.15 shows such a nematic texture with high strength disclinations.

Disclination in smectic phases may also show up in the form of schlieren textures. It was believed that only the whole-numbered singularities are present in these phases. However more recent work has shown that certain smectic C_A phases can also give schlieren textures with half-numbered singularities (Watanabe *et al.*, 1989; 1992; Niori *et al.*, 1995). Other methods such as X-ray scattering may be needed for an unambiguous characterization of the phase.

Nematic schlieren texture also show up in the form of "inversion walls" (Nehring and Saupe, 1972). This happens when the preferred orientation is along the surface and has a change of 180° in crossing the region of a wall. In the center of the wall a change of 90° in orientation is achieved. Thus, if the sample is examined under crossed polars, it is observable that a dark line is sandwiched between two bright lines, or the opposite. With every rotation by 90° of the polars the dark and the bright lines interchange. Figure 4.16 shows the texture of a domain full of inversion walls (inversion lines) of a nematic polymer with two-dimensional mesogenic units. For the bottom picture in the figure the polars have rotated by 90° relative to that for the
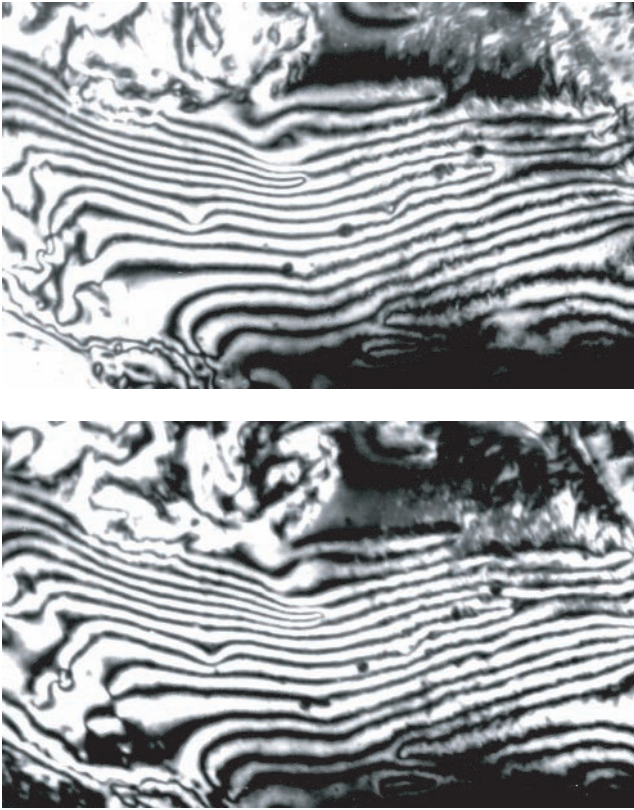
Figure 4.16.   A domain full of inversion walls. From top to bottom the polars have rotated by 90°. The sample is a nematic polymer with the two-dimensional type mesogenic units.

top. The dark spots may be used as reference for an easier examination of the two pictures. The dark line with a dark spot in the top picture turns bright after the polars have rotated by 90° as shown in the bottom picture.

The threaded texture is also often observed for nematics especially when a thicker film is examined. In this texture disclination lines show up as dark lines swimming in the sample with thermal motion. The lines are observable without polars (Figure 4.17) but the thread contrast will be higher when crossed polars are used. Because of the stopless molecular reorientation with thermal motion in the sample the old dark lines may disappear and new ones may form. In cases when the two ends are anchored on the surfaces the ends will stay where they have been but the thread may swing about.
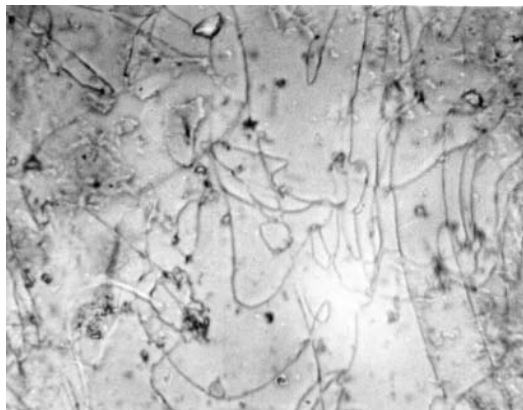
Figure 4.17.   Threads in a polymeric nematic phase.
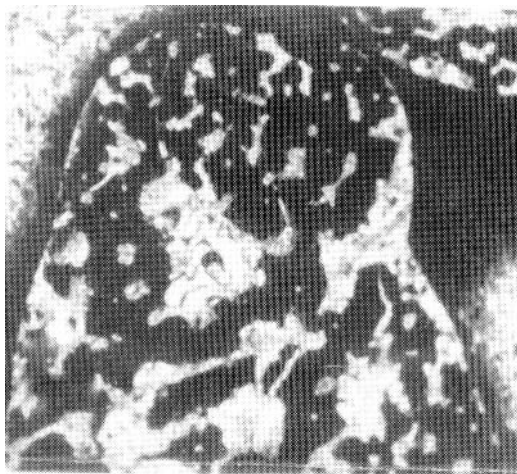
Figure 4.18.   A polymeric nematic droplet with both homeotropic and non-homeotropic alignment.

It is possible (although rare) for a nematic phase to show homeotropic alignment even if no foreign field is applied and no surface treatment is intentionally made on the glass slide and the cover slip. However on this condition the alignment is often not perfect so that domains with other alignments coexist with the homeotropic domain. Therefore, with ortho-scopic examination a dark field contaminated with bright domains of threaded or schlieren texture may be obtained (Figure 4.18). Noel and

Figure 4.19.   Banded texture of a mesogen-jacketed liquid crystalline polymer. The shearing direction is perpendicular to the direction of the parallel bands.

coworkers (Noel, 1985) found that a more perfect homeotropic alignment was achieved by the simple treatment of glass slides with boiling chromic sulfuric acid, acetone and methanol and rinsing with hot distilled water. Films thus prepared appear completely dark when viewed orthoscopically but form conoscopic interference patterns as outlined by Figure 4.10. On the other hand, planar alignment may be obtained by using freshly cleaved mica surfaces or by directed oblique evaporation of silicon monoxide on glass surfaces.

A unique optical phenomenon observable for the nematic phase of polymers with significant chain rigidity is the formation of a "banded texture" (Figure 4.19) composed of parallel bands of alternate brightness (Dobb *et al.*, 1977; Chen *et al.*, 1987; Xu *et al.*, 1993). This texture has not been observed for low mass liquid crystals but often found for oriented thermotropic or lyotropic liquid-crystalline main-chain type polymers with sufficient chain rigidity. In the oriented liquid crystal specimens the polymer molecules are packed in a parallel alignment to form fibrils. The fibrils travel parallelly in a regular zigzag manner, resulting in the unique alternating light and dark pattern when being observed on a polarizing microscope. A contraction effect has been proposed to explain the mechanism of band formation. Thus, the rigid or semi-rigid molecules of liquid crystalline polymers are packed in parallel in the form of fibrils under shear along the shearing direction. The formation of the banded textures after

shear cessation is not the result of free thermal relaxation of individual molecules, but the result of contraction and zigzag rearrangement of the fibrils as a whole along the orientation direction. The elastic energy stored during shearing may have provided the driving force for contraction, but the high stability of the parallel alignment of neighboring molecules due to very limited molecular motion of these polymers is a necessary condition for formation of the bands. By contrast, in the case of flexible chain polymers, molecules may also assume a parallel orientation under shearing. However, the orientational relaxation takes place easily as a result of the fast thermal motions of individual molecules. The external elastic force may even accelerate this process. As a result, no regular banded textures should be expected for flexible polymers. Figure 4.19 is a photomicrograph of the banded texture given by a mesogen-jacketed liquid crystal polymer ("MJLCP", Zhou *et al.*, 1987; 1996). The polymer is the first side-chain type polymer that forms a banded texture. This result shows that the polymer has a chain rigidity comparable with main-chain type liquid crystalline polymers although its molecular structure is more like a side-chain type polymer.

The texture of polymeric smectic. As discussed in Chapter 1 there are many subcategories of smectic phases. The identification of a smectic phase by POM becomes more difficult with less certainty when the order of molecular packing in the phase is increased. Other techniques such as WAXS are often used together with POM for conclusive identification of smectics (Gray and Goodby, 1984). Because of the complexity in the molecular structure of liquid crystalline polymers there are fewer types of polymeric smectics. The polymeric smectics most often observed are the less ordered types A and C.

The often observed textures for S_A are the focal-conic fan texture and the homeotropic texture. When the molecular orientation is homeotropic, the optic axis is perpendicular to the film surface so that the preparation appears black (pseudoisotropic) on a crossed polarizing microscope. As with the homeotropic nematics, the homeotropic S_A phase can be differentiated from the true isotropic phase by conoscopic observations. Further more, if the cover slip of the homeotropic S_A preparation is slightly moved, the orientation is disturbed resulting in "oily streaks" in form of bright bands. The homeotropic S_A phase may thus be distinguished from the homeotropic nematic phase.
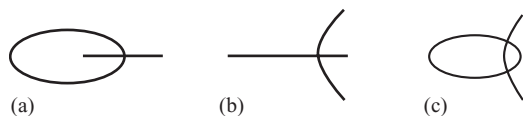
Figure 4.20.   Defects in the form of ellipses and hyperbolae in confocal relationship:
(a) the elliptical defect is in the plane of the sample film; (b) the elliptical defect is
normal to the film plane; (c) other cases.

The S_C phase cannot form a homeotropic texture because it is biaxial with tilted alignment. The often observed textures of the S_C phase are the schlieren texture and the focal-conic texture with the former preferred. According to the theory of Nehring and Saupe (1972), the schlieren textures formed by smectic phases only have the whole-numbered singularities. So far only the singularities with four brushes or with a strength of $s = \pm 1$ has been observed for polymeric S_C. Recently, Watanabe and coworkers (Watanabe *et al.*, 1989; 1992; Niori *et al.*, 1995) reported the formation of a new smectic phase, S_{CA}, that could form schlieren texture with singularities of $s = \pm 1/2$. The polymers studied by these researchers are of the main-chain type but have flexible spacers of odd-numbered methylene units. Thus the layered structure with opposite tilt direction of the director of the mesogenic units in two consecutive layers is formed. Interestingly, the S_{CA} could form not only the schlieren texture with half-numbered singularities but also the extinguished homeotropic texture because the phase is uniaxial.

The formation of focal-conic textures is characteristic of smectic phases (Gray and Goodby, 1984). These textures are the result of smectic layers arranged in Dupin cyclides (Friedel, 1922). The common defects included in these arrangements have the form of ellipses and hyperbolae in certain confocal relationship. Dependent on the direction of observation relative to the defects, the dark lines shown in Figure 4.20 may be observed in focal-conic domains.

Figure 4.21 shows a focal-conic fan texture of a smectic A phase in which is observable some defects represented by Figure 4.20(b). While S_A forms the fan-like focal-conic textures, the focal-conics formed by the S_C phase are often broken and less distinct. In addition, as stated above, S_A is uniaxial but S_C is biaxial. S_A may take a homeotropic alignment with the axis normal to the sample plane and extinct on POM with crossed polars. The two smectic phases are therefore distinguishable with POM. Nevertheless, it is desirable to include WAXS studies in order to identify the two with assurance (Section 4.3).

Figure 4.21.   Focal-conic fan texture of a smectic A phase.

The texture of polymeric chiral liquid crystalline phases. The chiral liquid crystalline phases include the chiral smectics and the chiral nematic or cholesteric phase. Poly(γ-benzyl-L-glutamate) and derivatives of cellulose are popular examples of polymers that form a chiral mesophase. Side-chain type copolymers of two chiral monomers with flexible spacers of different lengths and copolymers of one chiral and the other non-chiral mesogenic monomers may also form a cholesteric phase (Finkelmann *et al.*, 1978; 1980). In addition, a polymeric nematic phase may be transformed to a cholesteric phase by dissolving in a chiral compound (Fayolle *et al.*, 1979). The first polymer that formed a chiral smectic C phase was reported by Shibaev *et al.* (1984). It has the sequence of phase transition of g 20–30 S_C^* 73–75 S_A 83–85 I with the S_C^* phase at the lower temperature side of S_A. More examples of S_C^* polymers are given by Le Barny and Dubois (1989).

Studies on low and high mass cholesteric phases have shown that the compound may form a focal-conic texture if no displacement is made on the cover slip when the sample is heated up or cooled down to the cholesteric phase. The focal-conic texture is similar to that of a smectic A, but the particles are usually too small to identify except for rare preparations. If the cover slip is displaced the focal-conic texture will give way to a homeotropic one with the optic axis normal to the plane of the preparation. The cholesteric homeotropic film reflects vivid colors having wavelength λ decided by the De Vries (1951) expression: $\lambda = pn$ where p is the pitch

and n the refractive index. This property makes the texture distinguishable from that of the homeotropic nematic or smectic A phase.

Another and more characteristic texture observable of the cholesteric phase is the Grandjean planar texture with a series of regularly spaced bands separated by sharp lines. This was observed by F. Grandjean (1921) when a wedge-shaped split between two sheets of fresh mica (or clean glass slides) was used as the cell for examination under crossed polars. Under such conditions the cholesteric phase formed on cooling a homeotropic planar texture with visible bands.

According to De Vries (1951), the periodic bands are the result of the progressively changing thickness of the film in the wedge-shaped split and the surface effect on orientation of the molecules. When the thickness of the wedge is equivalent to a whole number of half turns of the helicoid the mesophase structure is not disturbed by the surface, while in the interval sections the molecular twisting will be disturbed by the orienting effect of the surface. The succession of disturbed and undisturbed sections (planes) of the phase would give rise to an observable image of alternating bands. Thus the plane texture will not occur in a preparation with parallel surfaces.

The texture with parallel and equally spaced bands is also observed in the lyotropic cholesteric phase. In studies on the birefringent phase of PBLG solution, Robinson (1956) observed the formation of the alternately spaced dark and bright bands. The spacing between adjacent dark and bright bands had a value of $1-100\,\mu m$ depending on the solvent and concentration. The spacing was so large that the reflected lights are in region of infrared thus no visible cholesteric colors were observed. The formation of this characteristic texture was accounted for by a helical structure of the cholesteric phase. The spacing of the bands is equal to a half pitch of the phase. In the middle of a dark band the director of molecular rods is in the homeotropic orientation (the same as the viewing direction), while in the middle of a bright band the director has twisted for 90 degrees from that in the neighboring dark bands. Obviously one will see no bands if the view is along the axis of twist. This is different from that in the observation of Grandjean plane texture for which the view is along the axis of the twist.

The $S_C{}^*$ phase exhibits four textures including the pseudo-homeotropic texture, the petal texture, the focal-conic texture and the lined texture (Gray and Goodby, 1984). The last occurs when the layer planes are not parallel to the surface. The lined appearance may be similar to what have been discussed for the cholesteric phase, but can also occur as being superimposed on the focal-conics. Examples of such lined and focal-conic

textures have been given by Fayolle *et al.* (1979) for the S_C* phase of a two-component system obtained by the addition of a chiral compound to the S_C phase of a homopolyester. The lines or bands are equally spaced with the spacing directly related to the pitch of the smectic screw.

4.2.   DIFFERENTIAL THERMAL ANALYSIS (DTA) AND DIFFERENTIAL SCANNING CALORIMETRY (DSC)

Both DTA and DSC detect thermal behavior including the glass transition and various phase transitions. In DTA the temperature difference (ΔT) between a reference sample and a test sample is measured when the two are heated at a constant rate. The reference is stable and no chemical or physical changes would occur in the interesting range of temperatures. Thus the rate of temperature change in the reference is not disturbed. On the other hand, if there is any physical or chemical change that happened in the test sample the rate of temperature change is disturbed. An endothermic change, for example the isotropization of a liquid crystal phase, will stop the temperature from rising until the process is finished. When such a change occurs, a negative ΔT is observed. In differential scanning calorimetry (DSC), the sample is not heated at a constant rate, but a definite quantity of heat is either added to (for an endothermic change in the test sample) or taken away (for an exothermic process) from the test sample so that no temperature difference will be created between the test and the reference. DSC is preferred over DTA as not only the temperature but also the heat is measured for transitions in the test sample during DSC studies. Nonetheless, neither DTA nor DSC alone can tell the nature of a change. In other words, neither of the two can decide, for example, whether an endothermic change is the melting or the isotropization of a mesophase or the transition from one mesophase to the other. Other characterization methods especially POM (polarizing optical microscopy) discussed in the previous section should also be applied for the identification of any such event.

Figure 4.22 is a representative DSC of a semi-crystalline polyester ($\langle 4.1 \rangle$) that has a nematic phase above melting. The polymer has a glass transition at 315 °K as shown by the jump in the heating curve (A). The endothermal melting peak is at 434 °K with an enthalpy of 17 kJ/mol and an entropy of $\sim$2.2 J°K^{-1} mol^{-1}. There is another endothermal peak at 467 °K with an enthalpy of 3.2 kJ/mol and an entropy of $\sim$0.38 J°K^{-1} mol^{-1}.
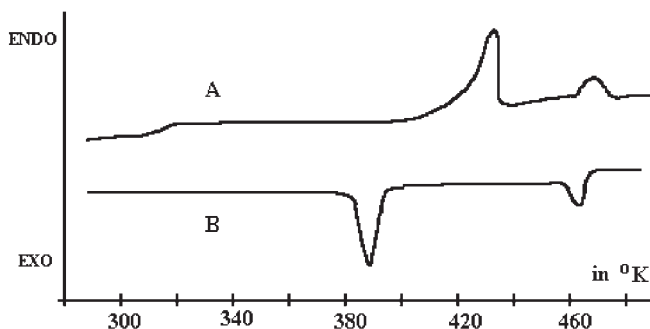
Figure 4.22.   DSC thermograms of a semi-crystalline polyester, $\langle 4.1 \rangle$, that has a nematic phase above melting: (A) is the heating curve, (B) is the cooling curve.

$$\langle 4.1 \rangle$$
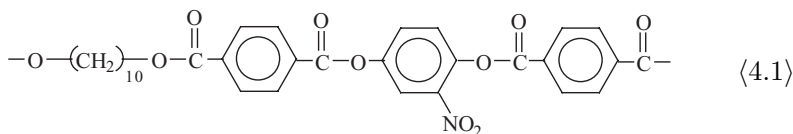
The nature of the two endothermal processes has been revealed by study with POM: that at $434\,°$K is the melting of the crystals and the formation of a nematic phase, while at $467\,°$K is the isotropization of the mesophase. If the polymer is cooled down from its isotropic liquid state the curve (B) is obtained. In the cooling process the first exothermal peak occurs at $463\,°$K which is the formation of the nematic phase as revealed by POM. The second exothermal peak is centered at $387\,°$K corresponding to the crystallization of nematic polymer. The jump in (B) of the glass transition is not as clear as in the heating curve. This is understandable because the glass transition is not a genuine thermodynamic transition.

One sees in the above example that the supercooling of the isotropic liquid phase is significant ($467 - 463 = 4$ degrees), but it is much smaller than that for the nematic phase ($434 - 387 = 47$ degrees). Significant degrees of supercoolings are often observed for polymers but that for low mass systems are often much smaller. There have been suggestions that the transition is liquid-crystallization if the supercooling is no larger than 0.6 degrees, otherwise it is crystallization. The suggestion does not apply in polymer systems because much higher viscosities and much slower molecular motions are involved in polymers than in low mass liquid crystals. In addition, the transition peaks of polymers are usually much broader than that of low mass

compounds. This can be interpreted by the presence of molecular weight distribution and/or irregularities in the polymer chains.

After a survey of existing data, Wunderlich *et al.* (1988) pointed out that the nematic phases of different types of compounds have entropies of isotropization with the following values: $2 \pm 1 \, \mathrm{J\,K^{-1}\,mol^{-1}}$ for low mass liquid crystals, $7 \pm 5 \, \mathrm{J\,K^{-1}\,mol^{-1}}$ for side-group type liquid crystal polymers, and $15 \pm 7 \, \mathrm{J\,K^{-1}\,mol^{-1}}$ for main-chain type liquid crystalline polymers. The value for the above polymer sample $\langle 4.1 \rangle$ is very small ($0.38 \, \mathrm{J\,K^{-1}\,mol^{-1}}$) suggesting that a rather small degree of order is present in such a polymeric mesophase. In this particular case the polymer has a nitro-substituent on each mesogenic unit. Lateral substitution would decrease the aspect ratio of the rod-like mesogenic unit and play the role of separating neighboring mesogenic units from each other. The liquid crystal phase is thus not as stable as when no substitution is present (Zhou *et al.*, 1985).

Many liquid-crystalline polymers are semi-crystalline and have only one mesophase that is nematic. The DSC thermograms of such polymers are very similar in appearance with Figure 4.22. Many other polymers are non-crystalline but have one and only one mesophase. The DSC will then show a glass transition and a transition from the mesophase to the isotropic liquid phase. Yet many other polymers may have more than one liquid crystalline phase so that their DSC curves should also include the transitions from one mesophase to another. DSC is obviously a very useful and very convenient technique for the characterization of liquid crystalline polymers. Nevertheless, the following points should be emphasized in order to interpret the DSC results with less ambiguity.

(1) Although liquid crystalline polymers with no crystallinity often give rise to DSC curves showing the glass transition jump as well as the endothermic peak(s) for the mesophase(s) (*e.g.*, Finkelmann, 1982), there are exceptions. If for instance the mesophase formed after the glass transition is so stable that the latent transition temperature is beyond that for chemical decomposition, there will only be in the DSC heating curve at most a glass transition jump. Examples may be given by the "mesogen-jacketed liquid crystal polymers" (Zhou *et al.*, 1996) represented by $\langle 4.2 \rangle$ below:

$$\mathrm{R} - \bigcirc - CO - O - \bigcirc - O - CO - \bigcirc - R \qquad \langle 4.2 \rangle$$
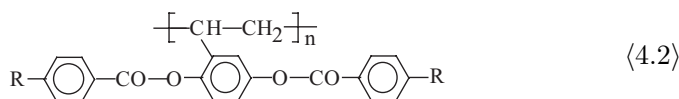
The polymers in the $\langle 4.2 \rangle$ series with different R groups all are non-crystalline but each form a nematic phase when heated to above Tg. The nematic phase is thermally very stable so that no endothermic isotropization transition is shown in the curve. Instead the signals for chemical decomposition will occur if the heating is continued to $300\,°C$ or above depending on R. In such cases the characterization of the mesophase relies more on POM and X-ray scattering.
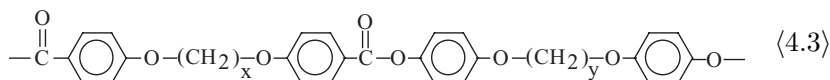
More recently in the study of another series of mesogen-jacketed liquid crystalline polymers we found (Zhang *et al.*, 1996) that the frozen-in nematic order (formed from evaporation of the solvent or when precipitated from solution) in the non-crystalline polymers will disappear when they are heated up to the temperature region of the glass transition. The DSC curves of these polymers shows again only the glass transition, however instead of a jump a broad endothermic peak appears. Obviously in such cases the glass transition and the transition of the nematic-to-amorphous are superimposed.

(2) The glass transition may appear as an endothermic peak rather than a jump in the curve. It is thus necessary to distinguish the glass transition from the melting and other endothermic phase transitions. The endothermic peak at glass transition is believed to be a result of annealing or storage of the sample at temperatures below Tg (Volkenstein and Sharonov, 1961; Qian *et al.*, 1989).

Cheng *et al.* (1990) carried out isothermal annealing experiments below Tg of a series of the main-chain type liquid crystalline poly(azomethine)s. The samples had been quenched rapidly from their nematic or isotropic states before the annealing experiment. A jump was observed in the DSC heating curves of the samples without annealing. However, they were able to observe an endothermic peak of glass transition after only a short time of annealing. For example, with the polymer having the Tg of $318\,°K$, the annealing at $295\,°K$ for $0.75\,h$ had led to a small endothermic peak. With increasing annealing time, the peak temperature shifts to a higher location and the enthalpy of the peak increases. According to the authors the enthalpy could reach a value of $0.891\,kJ\,mol^{-1}$ after an infinite time of annealing. The results are well interpreted by the enthalpy relaxation theory proposed by Kovacs *et al.* (1979).

(3) Like other crystalline polymers, liquid crystalline polymers can also exhibit multiple melting peaks when studied with DSC. Multi-melting is common to crystalline polymers including single crystals of polyethylene. For example, Bair *et al.* (1967) found the single crystals of PE grown

at 85 °K in xylene showed multiple melting peaks in its DSC heating (10 degrees per minute) curve. These peaks have been related to the lamellar thickening process. The multiple melting behavior of PET, nylon and many other polymers have also been studied and interpreted (*e.g.*, Sweet and Bell, 1973). The two melting endotherms of PET are believed to be the existence of two interconvertible forms of crystals which differ from each other in terms of crystal size and perfection. The smaller and less perfect crystals melt at a lower temperature and recrystallize to form the more perfect and larger form which melts at a higher temperature. This idea has been supported by DSC studies at different heating rates. At a lower heating rate the recrystallization would take place to a higher extent so that the second endotherm becomes larger. The multi-melting behavior is popular in crystallizable polymers although the reason for each case may be different.

$$-\overset{\overset{\displaystyle O}{\|}}{C}-\langle\!\bigcirc\!\rangle-O-(CH_2)_{\overline{x}}O-\langle\!\bigcirc\!\rangle-\overset{\overset{\displaystyle O}{\|}}{C}-O-\langle\!\bigcirc\!\rangle-O-(CH_2)_{\overline{y}}O-\langle\!\bigcirc\!\rangle-O-\qquad\langle 4.3\rangle$$

The multiple-melting behavior is also observed for liquid crystalline polymers. For example, Griffin and Havens (1981) found that many polymers of $\langle 4.3\rangle$ with different x and y showed multiple endotherms on melting to the nematic phase. The lower-temperature endotherm represents the transition to the nematic phase of the polymer which recrystallizes to the higher-temperature form as soon as it melts during the DSC scan. Increased heating time with a slower scan speed increased the relative amount of material which could recrystallize to a more stable crystalline form. As the result the relative sizes of the two endotherms changed with the scan rate. For the polymer with x = 5 and y = 10 in $\langle 4.3\rangle$, the two endotherms are of approximately equal size at a heating rate of 40 degrees per minute, while at lower heating rates the higher-temperature endotherm is larger.

(4) Not only does the melting process depend on the thermal history of the sample, the isotropization of the polymeric nematic phase is also history-dependent. Feijoo and coworkers (1988; 1990) are apparently the first to have studied in detail the effect on the isotropization of the thermal treatment. According to these researchers the establishment of thermodynamic equilibrium in the nematic phase was not as quick as has been commonly believed, for both the nematic and the isotropic phases are fluid states. They found that the heat and temperature of isotropization of the polymeric nematic phase were remarkably affected by the preceding

thermal treatment. For a polymer with a nematic phase of Ti = 162 °C, the annealing in the isotropic phase (190 °C) for two minutes had brought the Ti down to 158 °C which is four degrees lower than the original. The enthalpy of isotropization for the annealed sample was only 57% of the original. On the other hand, if the above-annealed sample was cooled to 120 °C and annealed at this temperature (in its nematic phase) for two minutes the Ti would recover its original value. Ti was found to increase further with a longer time of annealing in the nematic phase. The equilibrium value of Ti = 172 °C was achieved only after a few hours of annealing. One comes to the conclusion after these studies that there is present, a residual nematic order in the isotropic phase after the isotropization, and there is present, a residual disorder in the nematic phase after the transition of isotropic-to-nematic phase. To erase the memory of the order or disorder requires several minutes or several hours. The measured Ti for the samples of the same polymer but with different thermal history may scatter about for as wide as ten degrees and more.

(5) Special attention is drawn to the phenomenon of the monotropic liquid crystalline phase. The monotropic phase is metastable and comes to existence only when its related phase has a sufficient extent of super-cooling. For instance, a crystalline polymer melts at T_{C-I} to form only an isotropic liquid, but when the isotropic liquid is cooled a nematic phase is formed before crystallization starts. Such a nematic phase is monotropic. In its DSC heating curve there is only an endothermic melting peak at T_{C-I} but there are two exothermal peaks in the cooling curve. The higher-temperature exotherm is of the formation of the nematic phase (T_{I-N}) while the lower one is of the crystallization (T_{N-C}). If T_{N-C} is sufficiently lower than T_{I-N} it should be possible to cool the sample to a temperature which is below T_{I-N} but above T_{N-C}. The monotropic nematic phase is obtained. The isotropization temperature T_{N-I} of the phase is then measured by heating in DSC. The few transition temperatures should have the sequence of $T_{C-I} \geq T_{N-I} \geq T_{I-N} > T_{N-C}$ which are shown in Figure 4.23.
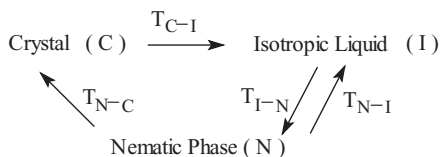
Figure 4.23.   A crystalline compound which exhibits a monotropic nematic phase.
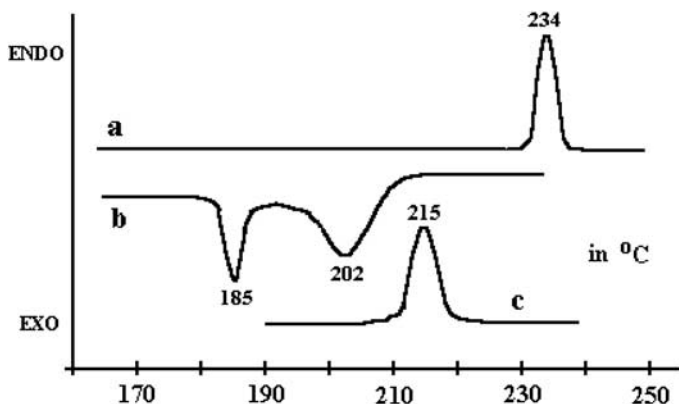
Figure 4.24. DSC thermograms of the polymer ⟨4.4⟩.

⟨4.4⟩
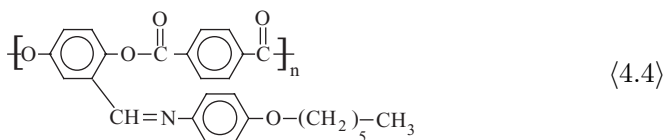
An example of the monotropic nematic polymer ⟨4.4⟩ was given by Zhang *et al.* (1993). In the DSC heating curve (curve **a** in Figure 4.24) of the powder sample of ⟨4.4⟩ there was only an endothermic melting peak at 234 °C(T_{C-I}). No liquid crystalline phase was formed upon the melting. However, in the cooling (from 250 °C to 150 °C) curve (curve **b** in Figure 4.24) there were two exothermic peaks, one at 202 °C, the other at 185 °C. The POM examination revealed the formation of a nematic phase at 202 °C (T_{I-N}) which solidified at 185 °C(T_{N-C}). The crystallization temperature was lower than the melting point by 49 °C, so large that the nematic phase was allowed to form in the course. If the solidified sample was heated up for the second time to 250 °C the result that is the same as that of the first heating was obtained, showing only an endothermic transition of the crystal-to-isotropic liquid at 234 °C. Thanks to the sufficiently broad gap between the T_{I-N} and T_{N-C} the authors were able to cool the sample to its nematic phase at 190 °C yet with no crystallization taking place. The nematic phase was then heated up and the isotropization temperature (T_{N-I}) of this monotropic phase was found to be 215 °C (curve **c**

in Figure 4.24). Therefore the following sequence of phase transitions was observed for this monotropic-nematic polymer:

$$
\text{Crystal (C)} \xrightarrow{\;234\,^{\circ}\text{C}\;} \text{Isotropic Liquid (I)}
$$

185 °C 202 °C 215 °C

Nematic Phase (N)

Interestingly, if in a sample there coexist a crystalline phase and a monotropic-nematic phase, on heating of the two-phase sample there should give rise to a DSC curve which shows a peak of N–I transition on *the lower temperature side* of the melting temperature because T_{N-I} is lower than T_{C-I}. Such a DSC curve (Figure 4.25) was indeed observed when we were studying a low mass monotropic-nematic compound $\langle 4.5 \rangle$.
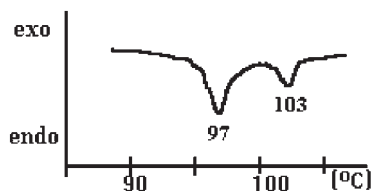
$$
C_2H_5 \text{—} \bigcirc \text{—} \overset{\overset{\displaystyle O}{\|}}{C} \text{—} O \text{—} \bigcirc \text{—} O \text{—} \overset{\overset{\displaystyle O}{\|}}{C} \text{—} \bigcirc \text{—} C_2H_5
$$

$$
\text{CH}=\text{CH}_2
$$

$\langle 4.5 \rangle$

The compound $\langle 4.5 \rangle$ melts at 105 °C. On cooling the isotropic melt it forms a monotropic-nematic phase. The isotropization temperature of the nematic phase is 98 °C as determined with DSC by the method described above. The crystallization was found to be the fastest at 57 °C. In order to obtain a biphasic sample and a DSC heating curve showing not only the melting endotherm but also the isotropization endotherm which is at the lower temperature side of the melting, the following procedure was carried out. The sample at 120 °C (isotropic) was quickly cooled to 60 °C and annealed for 1 minute at this temperature. It was then heated to 120 °C. It was by chance and indeed very fortunate to us that the DSC curve shown in Figure 4.25 was obtained. The endotherm at 97 °C is the isotropization of the residual nematic phase (T_{N-I}), while the one at 103 °C is the melting (T_{C-I}) of the crystals formed during the annealing.

4.3. X-RAY DIFFRACTION

When fast electrons impinge on matter, electrons are ejected from the inner shell (say, the K shell) of an atom of the target material. The resultant

Figure 4.25.   DSC heating curve of a biphasic sample of $\langle 4.5 \rangle$ showing $T_{N-I} = 97\,^{\circ}\mathrm{C}, T_{C-I} = 103\,^{\circ}\mathrm{C}$.

vacancy will be filled by an electron falling from a higher energy shell (L, M, *etc.*). Since the energy levels of the different shells are quantized, a coherent ray is emitted in the form of an X-ray photon with energy equal to the difference in energy levels of the two shells. The X-rays resulting from the fall of electrons from the L and M shells into the K shell are known as Kα and Kβ radiations. The Kα radiation of Cu has a wavelength of 0.154 nm. It is most frequently used in X-ray diffraction studies on polymers and liquid crystals. The information obtainable from X-ray diffraction studies includes degree of crystallinity, crystal lattice, crystal size, molecular orientation, and varieties of structural defects. For liquid crystals, it is widely used to identify a smectic phase from a crystal, a nematic liquid, and other smectic phases.

X-rays are diffracted at crystal planes since the distance between the planes is comparable to the wavelength of the X-ray. The X-ray diffraction conditions may be illustrated by Figure 4.26.

As depicted in Figure 4.26, the path difference between waves reflected by the two-neighboring lattice planes is $2d_{hkl} \sin \theta$. If the path difference is equal to the wavelength of the X-ray used, or some integral multiple of it, the reflected beams are in phase and a constructive interference is formed between the reflected beams. Therefore, if $2d_{hkl} \sin \theta = n\lambda$, an intense diffracted wave is produced in the direction **S** which is defined by θ. The intensity decreases abruptly with any deviation from the critical value of θ because of destructive interference. In polymers the reflection with the strongest intensity is frequently found for $n = 1$, that is, $2d_{hkl} \sin \theta = \lambda$.

The reflection condition can also be expressed in terms of the reciprocal lattice which is defined as follows. If **a**, **b**, **c** are the primitive translations of the real crystal lattice, and $\mathbf{a}^*$, $\mathbf{b}^*$, $\mathbf{c}^*$ are those of the reciprocal lattice, then $\mathbf{a}^*$ is perpendicular to both **b** and **c**; $\mathbf{b}^*$ is perpendicular to both **a** and **c**; $\mathbf{c}^*$ is perpendicular to both **a** and **b**. These mutually perpendicular
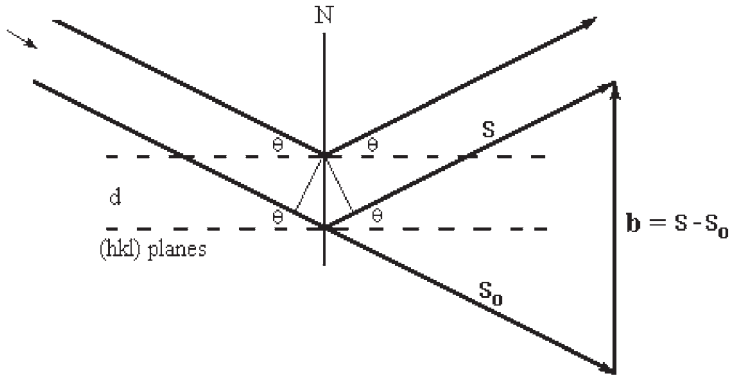
Figure 4.26.   The incident ($\mathbf{S_o}$ is the unit vector of the incident wave-normal) and diffracted ("reflected", $\mathbf{S}$ is the unit vector of the reflected wave-normal) X-ray beams on two parallels crystal lattice planes (*hkl*) separated by a distance d_{hkl}. The vector $\mathbf{b} = \mathbf{S} - \mathbf{S_0}$ is normal to the lattice plane (*hkl*) with $|\mathbf{b}| = |\mathbf{s} - \mathbf{s_0}| = 2\sin\theta$.

relations are expressed in vector notations as below:

$$\mathbf{a}^* \cdot \mathbf{b} = \mathbf{a}^* \cdot \mathbf{c} = \mathbf{b}^* \cdot \mathbf{a} = \mathbf{b}^* \cdot \mathbf{c} = \mathbf{c}^* \cdot \mathbf{a} = \mathbf{c}^* \cdot \mathbf{b} = 0$$

The magnitudes of the reciprocal vectors are the reciprocal of the spacing of the corresponding planes in the real lattice, i.e., $\mathbf{a}^* \cdot \mathbf{a} = \mathbf{b}^* \cdot \mathbf{b} = \mathbf{c}^* \cdot \mathbf{c} = 1$. It means that $|\mathbf{a}^*|$ is the reciprocal of the spacing of the a planes of the real crystal lattice; $|\mathbf{b}^*|$ is the reciprocal of the spacing of the b planes of the real crystal lattice; and $|\mathbf{c}^*|$ is the reciprocal of the spacing of the c planes of the real crystal lattice. Thus, as shown in Figure 4.27, if PO is the vector of length $1/\lambda$ in the direction of the incident wave-normal ($\mathbf{S_o}/\lambda$), and PQ the vector ($\mathbf{S}/\lambda$) of the diffracted wave in the direction of a maximum diffraction, OQ must be the vector ($\mathbf{b}/\lambda$) normal to one of the lattice planes (*hkl*) with a magnitude of $(2/\lambda)\sin\theta$. When the Bragg condition $2d_{hkl}\sin\theta = \lambda$ is fulfilled, $(2/\lambda)\sin\theta$ is equal to $1/d_{hkl}$. OQ is therefore in the direction of a vector in the reciprocal lattice, and is equal to the vector in magnitude $(1/d_{hkl})$. If the vector PO is drawn so that O lies at the origin of the reciprocal lattice, Q must lie at another point (h, k, l) of this lattice. In other words, if a sphere is drawn with P as the center and $1/\lambda$ as the radius, both the origin O and another point Q of the reciprocal lattice must lie on the sphere. Otherwise there will be no diffraction.

For certain orientations of the crystal relative to the direction of the incident X-rays, there will be no reciprocal lattice points lying on the surface of the diffraction sphere, and therefore no diffraction from the crystal planes.
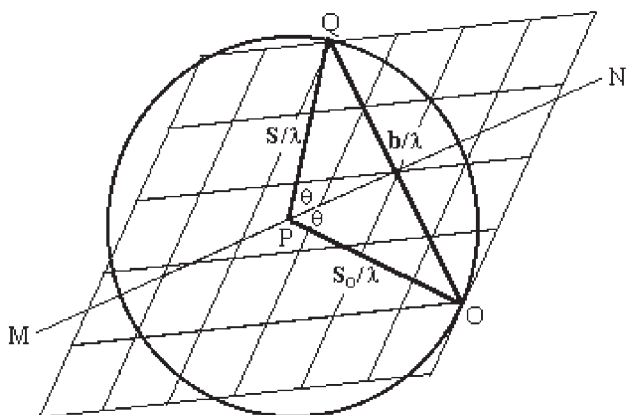
Figure 4.27.   The reciprocal lattice and the sphere of reflection. O is the origin of the lattice. P is the center of the sphere. PO is the incident vector with a magnitude of $1/\lambda$. Q is another point of the lattice. A maximum diffraction arises in the direction PQ if Q lies on the sphere. The vector OQ is normal to the real lattice plane MN represented by the reciprocal point Q; The magnitude of OQ is the reciprocal of the spacing d_{hkl} of the crystal lattice planes (hkl).

In this case a change in the direction of the incident X-rays (corresponding to a rotation of the entire reciprocal lattice about its origin O) will usually bring a lattice point into coincidence with the surface of the sphere of reflection, so that the condition of diffraction is satisfied. On the other hand, for finely powdered crystalline specimens, specimens consisting of small crystals, and crystalline polymer samples in which small crystalline regions are randomly distributed, the parallel planes of the different crystallites are randomly skewed relative to one another. A monochromatic primary ray will find enough particles to yield all the reflection positions that fulfill the diffraction condition. A system of coaxial cones of diffracted X-rays with a common apex at the center of the sample is obtained (Figure 4.28). Each cone has the half angle 2θ that satisfies the diffraction condition. A vertical section of this system of cones on a photographic plane film gives a series of concentric circles. The diffraction angle θ is calculated from the sample-to-film distance and the distance from the diffraction spot to the center of the film (Figure 4.30, below). It is apparent that an unoriented liquid crystal will also give such a type of diffraction pattern.

The case often applied in polymers and liquid crystals is that when a uniaxial orientation is adopted such as in oriented fibers and a monodomain of the nematic phase. The reciprocal lattice points in such systems are
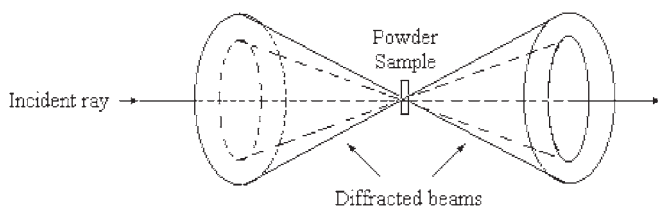
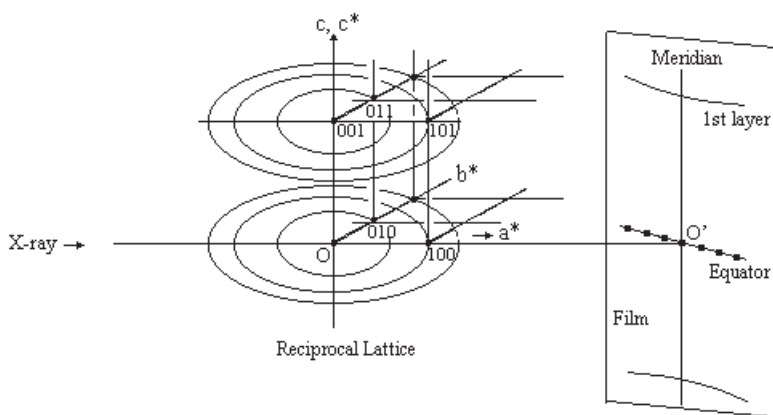Figure 4.28.   X-ray diffraction by crystal powders.

Figure 4.29.   Diffraction from a uniaxially oriented specimen.

arranged in concentric circles around the fiber axis (the c-axis, or the orientation director of the liquid crystal phase) as shown in Figure 4.29. The diffraction pattern obtained with an incident X-ray beam normal to the fiber axis is of the same type as the rotation photograph of a single crystal. Since the reciprocal lattice is in the form of concentric circles, the intersection with the diffraction sphere (not shown in the figure) and thus the diffraction always occurs.

It should be noted that any defects and imperfection in structure and orientation would give rise to rather coarse points and doughnut-shaped zones in the reciprocal lattice rather than clearly defined points and circles. This is the case for oriented liquid crystals and polymer fibers. Diffused diffraction patterns are therefore obtained for these specimens.

There have been excellent reviews on X-ray diffraction in studying structures of low- and high mass liquid crystals (*e.g.*, Wendorff, 1978;
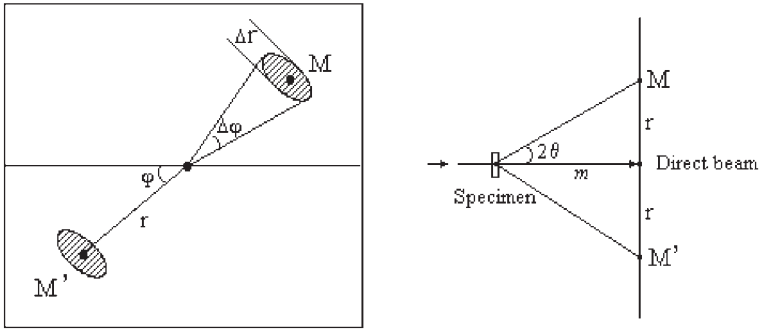
Figure 4.30.   The radial (r) and azimuthal (φ) positions of two diffraction maxima M and M′; Δr and $\Delta\varphi$ respectively is the radial width and azimuthal width.

Shibaev and Plate, 1984; 1985; De Vries, 1985; Noel, 1985; Azaroff, 1987; Noel, 1989). For powder samples of low mass liquid crystals, the X-ray diffraction pattern can be divided into inner rings (inner maxima) at small angles ($2\theta \sim 3°$) and outer rings (outer maxima) at large angles ($2\theta \sim 20°$). With an increasing of the degree of molecular orientation, the rings will decay into arcs with decreasing azimuthal width. The location and size of the diffraction maxima are described by the radial and azimuthal positions as well as the radial and azimuthal widths (Figure 4.30). The radial position refers to the distance r of the maximum to the center of the X-ray diffraction pattern; the azimuthal position refers to the angle φ made by a reference line through the center and the line from the maximum to the center.

From the radial position one can obtain the angle between the diffracted beam and the incident beam (Figure 4.30, right). This angle is related to the average distance between the long axes of adjacent molecules if the angle 2θ is about 20° (outer maxima). It is related to the molecular length or layer thickness if 2θ is only a few degrees (inner maxima). The radial width of the diffraction maxima is related to the regularity of the molecular packing. The more constant is the spacing between adjacent molecules (or layers), the smaller is the radial width of the outer (or inner) maxima. Thus, no Bragg diffraction is obtained for a nematic phase because of the lack of positional order. The X-ray pattern of a nematic phase (Figure 4.31(a)) is characterized by only the diffused inner (corresponding to molecular length) and outer (corresponding to average lateral spacing between molecules) rings. The intermolecular spacing can be estimated from the radial position of the outer ring using the equation $2d \sin\theta = 1.117\lambda$ based on the
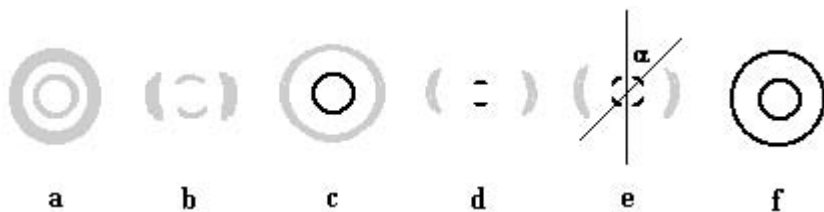
Figure 4.31.   Schematic X-ray diffraction patterns of liquid crystalline phases (**a**) unoriented nematic; (**b**) oriented nematic; (**c**) unoriented smectic A or C; (**d**) oriented smectic A; (**e**) oriented smectic C; (**f**) unoriented smectic B phase.

assumption of a disordered packing of the molecules around the c axis (De Vries, 1970). The radial position of the diffused inner ring is related to molecular length (De Vries, 1985) of the nematogens. Although it is difficult (if not impossible) to differentiate a nematic phase with an isotropic phase by X-ray diffraction of unoriented samples, a sharp decrease of about 0.01 nm in the spacing has been observed at the I/N transition (e.g., Yoon *et al.*, 1996). In addition, a nematic sample can be preferentially oriented along the direction of the meridian so that the outer maxima are split into two crescents symmetrical about the equator (Figure 4.31(b)). The azimuthal width of the crescents allows one to calculate the orientational order parameter (De Vries, 1985). The isotropic phase and the nematic phase can thus be identified using X-ray diffractometry. The diffraction pattern of the cholesteric phase is very similar to that of the nematic phase. The formation of cybotactic clusters (De Vries, 1970; Maret and Blumstein, 1982) in the nematic (or cholesteric) phase close to the nematic-smectic (or cholesteric-smectic) transition leads to an increase of the intensity of the inner ring, indicating that a layered structure of smectic phase is about to develop.

The diffraction patterns of the unoriented smectic A and C phases are similar and characterized by one or more sharp Bragg reflections in small angles and a diffuse outer ring (Figure 4.31(c)). The sharp inner reflection rings are due to the smectic layers. From the radial position of these rings the layer thickness is calculated by using Bragg equation. The average tilt angle of the molecular director relative to the layer normal may be obtained by comparing the Bragg spacing with the calculated length of the molecular rods. A smectic C phase may be suggested when the tilted angle is large. The outer ring is due to the disordered lateral arrangement of the molecules within the layer, which is diffused but less so than that of

the nematic phase. The average intermolecular distance (d) in these phases may be estimated from the radial position of the outer ring with the formula $2d \sin \theta = 1.1547\lambda$ (De Vries, 1985).

The two most often observed smectic phases A and C are well distinguished with X-ray studies on oriented samples. While the diffused outer rings of the two have both decayed into two crescents symmetrical about the equator, the small angle reflections of the oriented A phase are lying on the meridian (Figure 4.31(d)); that of the C phase are disposed along axes on either side of the meridian (Figure 4.31(e)). The tilted angle relative to layer normal is obtained from the angle α made by this axis and the meridian. In a smectic B phase all the distances between nearest-neighbor molecules in the layer are equal, so that there is one and only one sharp outer ring (Figure 4.31(f)) in addition to the sharp inner ring for its layered structure. On the other hand, there are two different nearest-neighbor distances in the smectic-E layers. Two sharp outer rings are observed (De Vries, 1975).

The picture of liquid crystal is complicated by many more types and sub-categories of each basic type (Chapter 1), so are the X-ray diffraction patterns of these phases. The drawings shown in Figure 4.31 are only schematic. For more detailed information the readers are referred to the cited reviews and the literature on recent developments.
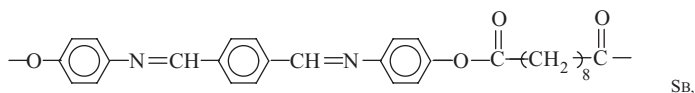
The X-ray diffraction of polymeric liquid crystal systems and their low mass counterparts are the same in principle, but the diffraction results for the polymers are often less ideal and more difficult to interpret. In practice the oriented specimens are often preferred over the unoriented samples for an unambiguous determination. X-ray diffraction is nearly always used together with texture observations using a polarizing optical microscope. Miscibility tests are also used in some cases for confirmation. For smectic phases with higher translational and orientational orders, X-ray diffraction is the most useful (if not the only) technique for unmistakable characterization. A few examples are cited below. The details of each characterization of the various polymeric smectic phases were described by individual authors.
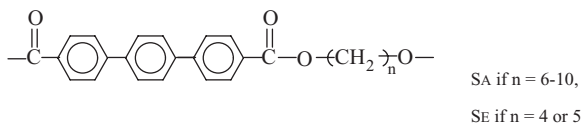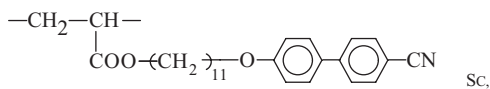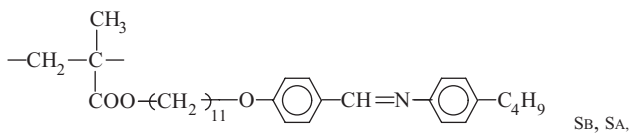
Ober *et al.* (1983):
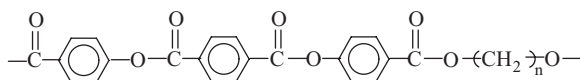
S_A if n is 10 or 12,

S_C if n is 9

Blumstein *et al.* (1982):

$$-O-\!\!\bigcirc\!\!-N\!=\!CH-\!\!\bigcirc\!\!-CH\!=\!N-\!\!\bigcirc\!\!-O-\overset{\overset{O}{\|}}{C}\!\!-\!(CH_2)_8\!-\overset{\overset{O}{\|}}{C}-$$

S$_B$,

Noel and Navard (1991):

$$-\overset{\overset{O}{\|}}{C}-\!\!\bigcirc\!\!-\!\!\bigcirc\!\!-\!\!\bigcirc\!\!-\overset{\overset{O}{\|}}{C}\!\!-O-(CH_2)_n-O-$$

S$_A$ if n = 6-10,

S$_E$ if n = 4 or 5

Shibaev *et al.* (1984):

$$-CH_2-\overset{\overset{CH_3}{|}}{\underset{COO-(CH_2)_{10}-COO-\bigcirc\!\!-\bigcirc\!\!-CN}{C}}-$$

S$_A$,

$$-CH_2-\overset{\overset{CH_3}{|}}{\underset{COO-(CH_2)_{11}-O-\bigcirc\!\!-CH\!=\!N-\bigcirc\!\!-C_4H_9}{C}}-$$

S$_B$, S$_A$,

$$-CH_2-\underset{COO-(CH_2)_{11}-O-\bigcirc\!\!-\bigcirc\!\!-CN}{CH}-$$

S$_C$,

Freidzon *et al.* (1986):

$$-CH_2-\underset{COO-(CH_2)_5-COO-\bigcirc\!\!-COO-\bigcirc\!\!-OC_3H_7}{CH}-$$

S$_F$, S$_G$, S$_C$,
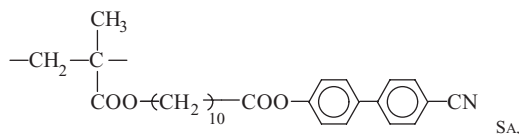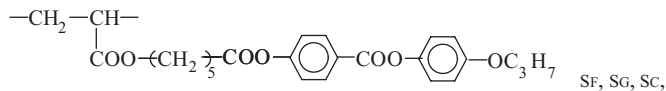
Yoon *et al.* (1996):
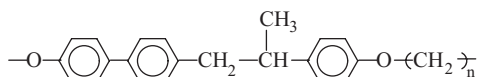
SF and SG if n = 4-20

SH if n = 4, 6, 8, 10-20.

4.4. OTHER METHODS

In addition to what has been briefly introduced in the previous three sections, methods including miscibility testing, IR dichroism, NMR, and small-angle neutron scattering among others are also used to identify the phase type or to probe the information of molecular orientation in the mesophase. The use of these techniques is briefly demonstrated in this section. No detailed account is given. The readers are referred to the cited original literature or monographs on the subject.

4.4.1. Miscibility testing

Studies on 180 binary systems of 120 substances by Sackmann and coworkers have led to the empirical "rule of selective miscibility" (Sackmann and Demus, 1965): All liquid crystalline states which exhibit an uninterrupted series of mixed crystals in binary systems without contradiction can be marked with the same symbol. On the other hand, the liquid crystalline states having the same symbol exhibit in no case an uninterrupted series of mixed crystals with the liquid crystalline states of another symbol. Therefore, the nature of a mesophase can be determined by establishing its isomorphy with a known mesophase of a reference compound. The applicability of this empirical rule has been repeatedly justified in low mass systems. For instance, Sackmann and Demus (1973) have observed in only one case a heterogeneous region between two modifications of the same type. In contrast, in over 100 cases these researchers have observed heterogeneous regions between modifications of different types.

This empirical rule has been applied to mixtures composed of well-known model liquid crystals with polymeric liquid crystals in order to identify the type of mesophase of the polymers (Nyitrai *et al.*, 1977; Millaud *et al.*, 1978;

Noel *et al.*, 1978; Fayolle *et al.*, 1979; Ringsdorf *et al.*, 1982; Finkelmann *et al.*, 1982; Benthack-Thoms and Finkelmann, 1985; Sigaud *et al.*, 1987). The Kofler's contact method (Kofler and Kofler, 1954) was used in the studies so that the phase diagram was composed in a relatively short time. Thus, at temperatures of its isotropic phase a small amount of the polymer is put between a glass slide and a cover slip. The model compound is then introduced by capillary action such that the polymer and the model compound are in contact. The preparation contains the complete possible concentration range which begins at the model compound and ends with the polymer. By changing the temperature one can determine the temperature of each transition which occurs in the contact zone between the two pure substances. The contact method is limited because the gradient in concentration in the contact zone is unknown. Consequently the preparations of well-defined compositions are also examined to complete the phase diagram and fix the concentration position of the transitions. As one example, the phase diagram of terephthal-bis(4-n-butylaniline) and the polymer prepared from di-n-propyl-p-terphenyl-4,4′-carboxylate and an aliphatic diol was obtained by Fayolle *et al.* (1979) to confirm the smectic C phase of the polymer.

Nevertheless, the rule of selective miscibility must be applied with caution. The highly viscous nature of polymeric mesophases could possibly prevent the mixing of the mesophase of polymers and certain model compounds. Therefore, while the miscibility of model compounds with a polymer may be used to identify the type of mesophase, the lack of compatibility does not necessarily suggest that the mesophases are not the same. Some model compounds and polymers with the same mesophase may even be inherently incompatible. As a result, some judgment is required in order to make both the proper choice of the model compound and the correct assignment of the mesophase when using this technique.

### 4.4.2.   Infrared dichroism

The detailed information about molecular orientation in oriented film specimens can be obtained from IR dichroism measurements (Hu *et al.*, 1985; Wu *et al.*, 1986). Light is absorbed when the direction of oscillation of its electrical vector has a component along the direction of oscillation of the absorbing group. The intensity of the absorption band of an oriented polymer thus depends on the direction of the electrical vector of the incident ray

relative to the direction of orientation. Consequently, the absorption will be different according to the direction of oscillation of the incident polarized light. Thus the order parameter, S, can be determined from the ratio of absorptions or the dichroic ratio R according to the following equations (Zbinden, 1964):

$$R = \frac{A_\parallel}{A_\perp} = \frac{\ln(I_0/I_\parallel)}{\ln(I_0/I_\perp)} \quad \text{and} \quad S = \frac{2(R-1)}{(R+2)(3\cos^2\alpha - 1)},$$

where I_0 is the intensity of the incident light; $I_\parallel$ and $I_\perp$ are the intensities of the transmitted light parallel and at right angles to the direction of elongation, respectively; α is the angle made by the axis of orientation and the transition moment of the absorbing group. If the transition moment is parallel to the orientation axis, α is zero and $S = (R-1)/(R+2)$; If it is perpendicular to the axis, $S = 2(1-R)/(R+2)$.

Using this technique Wen and coworkers (Wen *et al.*, 1988) studied the molecular orientation in the nematic phase of the liquid crystalline polyester with following repeating units:
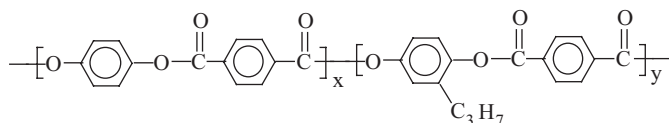
From the dichroic ratio R of the phenyl ring C$-$H out-of-plane bending bands (870 and 720 cm^{-1}), the transition moment of which is perpendicular to the long axis of the chain and the mesogenic units, the order parameter was found to be 0.45.

IR dichroism is also used to obtain the orientation of mesogenic units relative to the main chain in side-chain type liquid crystalline polymers. One example was given by Xu *et al.* (1993). The polymer studied by them was a mesogen-jacketed liquid crystalline polymer shown below:
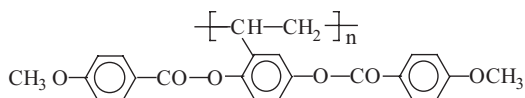
In this study two IR bands, 2905 cm^{-1} and 2939 cm^{-1} were used to discuss the orientation of the main-chain axis of the polymer molecules. They were

assigned to the C−H stretching of the main chain with transition moments perpendicular to the axis of the main chain. Taking AS as the absorption for radiations polarized in the shear direction and AL as the absorption in the lateral direction, the ratio AS/AL was found to be always less than unity for these two bands. This implies that in the oriented specimens the main chains of the molecules tend to orient in the shear direction. On the other hand, among the bands related to the mesogenic side groups, all (e.g., phenyl ring C−H in-plane bending and C−O stretching) that has a transition moment parallel or approximately parallel to the mesogen axis has the ratio AS/AL less than unity. All (e.g., phenyl ring C−H out-of-plane bending and C=O stretching) that has a transition moment perpendicular to the mesogen axis has a ratio greater than unity. From these observations it was supposed that the mesogenic side groups tended to be packed perpendicularly around the main chain in the nematic phase of this MJLCP.

4.4.3.   NMR study

NMR is a powerful technique for the study of the orientation in liquid crystalline polymers (Boeffel and Spiess, 1989). The magnetic dipole-dipole interaction of a pair of protons held in rigid orientation in a magnetic field was treated first by Pake (1948), who showed that splitting of the proton resonance into a doublet should occur in ^{1}H-NMR absorption. One recent example making use of this phenomenon in the study of orientation was given by Klein and coworkers (1996). The Hoechst-Celanese random copolyester formed from 73 mole % of 4-hydroxybenzoic acid (HBA) and 27 mole % of 2-hydroxy-6-naphthoic acid (HNA) was studied in this work. The specimen 73M was a monofilament of about 1 mm diameter from melt extrusion at 300 °C followed by annealing for 4 h at 250 °C and 15 h at 280 °C. The specimen 73R was in the form of cylindrical rod of about 5 mm by injection molding into a mould maintained at 100 °C. The proton NMR spectra were recorded on a Chemagnetics CMX 200 system at 200 MHz. The observed Pake doublet splitting, Δf, is due to the dipolar interaction between the nearest neighbor protons on the phenyl ring of the HBA component, which (in kHz) is related to the measure of orientation by the following equation (Harris, 1986):

$$\Delta f = \left(\frac{\mu_0}{4\pi}\right)\frac{3\gamma^2\hbar}{4\pi\gamma^3}(\cos^2\theta - 1),$$

where γ is the gyromagnetic ratio, r is the distance between the two protons, and θ is the angle between the inter-proton vector and the magnetic field. Taking 0.234 nm for r from molecular modeling we have:

$$\Delta f = 12.5(\cos \theta^2 - 1)\text{kHz}.$$

Because the observed Δf for the 73M specimen in the parallel and perpendicular orientations was approximately 25 and 13 kHz respectively, it can be concluded that in this specimen the polymer chain axis is highly aligned with the fiber axis. Similar result was obtained for the 73R specimen.

For completely protonated liquid crystals the ^{1}H-NMR spectra are, unfortunately, often extremely complex because of the multiplicity of dipole-dipole interactions possible (Rowell *et al.*, 1965). In these cases, selectively deuterated compounds are used to simplify the spectra. The splitting can then be easily assigned to specific dipole-dipole interactions. On the other hand, deuteron magnetic resonance spectroscopy, ^{2}H-NMR, is attractive since the quadrupole splittings are large and uncomplicated. To a good approximation for the C−D bond, the magnitude of the splitting observed for a nematic liquid crystal is given by

$$H^* = H_0 \pm \frac{3}{8}\left(\frac{e^2 qQ}{\mu_D}\right)(3\cos^2 \theta - 1),$$

where $(e^2 qQ/\mu D)$ is the quadrupole coupling constant, θ is the angle between the magnetic field and the C−D bond under examination. A precise treatment on this subject has been given by Boeffel and Spiess (1989). In this excellent review of B and S, the utilization of the two-dimensional magic angle spinning NMR, ^{13}C-MAS-NMR, is also well discussed.

4.4.4.   Small-angle neutron scattering

While the IR dichroism and NMR studies can give information about the conformation at individual bonds, the small-angle neutron scattering (SANS) measures the global conformation of the polymers (Cotton *et al.*, 1974). SANS has been successfully utilized, for example by Hardouin and coworkers (Hardouin *et al.*, 1991; Leroux *et al.*, 1993), to establish the evolution with the temperature of the global shape of some mesogen-jacketed liquid crystalline polymers from isotropic to the nematic phase. A pseudo-binary system of fully protonated polymer (P4,4,4) with the same polymer

selectively deuterated on the aliphatic tails was used. The weight ratio of the two isotopic isomers was 50/50 for the maximum scattered coherent intensity:
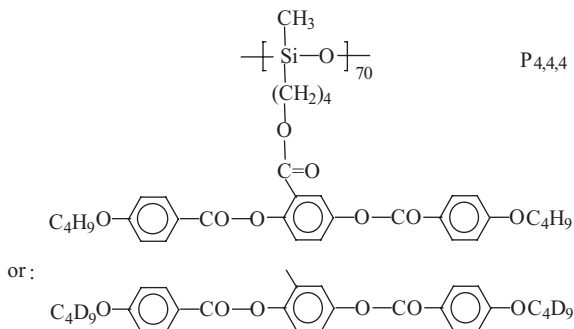
The experiments were performed with the spectrometer "PAXY" on the Orphee reactor of the Laboratoire Leon Brillouin in Saclay. The sample was placed in the oven at a temperature regulated to $0.2°C$. A magnetic field of $1.4\,T$ was applied to obtain a uniform orientation along the direction of the magnetic field in the nematic phase. The incident wavelength used was $\lambda = 1\,nm$ and the distance between the detector and the sample was $2\,m$. The range of scattering wave vector q studied was $0.0008\,nm < q < 0.01\,nm$. The scattering intensity $I_{(q)}$ was obtained with a two-dimensional multidetector and the spectra were recorded in the XY-plane perpendicular to the beam. In the limit of small scattering wave vectors the scattering intensity $I_{(q)}$ can be expressed as:

$$I^{-1}(q_{\parallel}) = I^{-1}(0)(1 + q_{\parallel}^2 R_{\parallel}^2) \quad \text{for} \quad q_{\parallel} R_{\parallel} \leq 1,$$
$$I^{-1}(q_{\perp}) = I^{-1}(0)(1 + q_{\perp}^2 R_{\perp}^2) \quad \text{for} \quad q_{\perp} R_{\perp} \leq 1,$$
$$I^{-1}(q) = I^{-1}(0)(1 + q^2 R_g^2/3) \quad \text{for the isotropic phase,}$$

where $R_{\parallel}$ and $R_{\perp}$ are the apparent quadratic size of the polymer backbone parallel and perpendicular to the magnetic field. From the linearity in the plot of I^{-1} against q^2, $R_{\parallel}$ and $R_{\perp}$ are deduced. This study of Hardouin and coworkers has shown that with the cooling down from the isotropic state an anisotropy of the polymer shape appears in the nematic phase which increases on cooling further. Far enough from the I–N transition, a large extension of the dimension parallel to the magnetic field gives rise to a high value for the anisotropy of $R_{\parallel}/R_{\perp} \approx 4$. Thus, the polymer backbone has a prolate conformation in the nematic state. Using this technique, they

have been able to evaluate the jacket effect of structural parameters such as the degree of polymerization and the length of the flexible spacer. In contrast, the shape anisotropy in the nematic phase of conventional end-on type side-chain liquid crystalline polymers is small. For example, Kirste and Ohm (1985) found by using SANS that in the nematic phase the radii of gyration of the following polymer showed only a small ratio of $1:1.25$ with the shorter dimension parallel to the magnetic field:
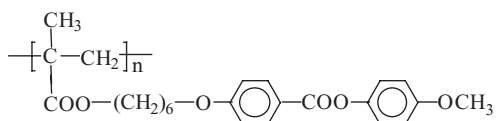
This page intentionally left blank

Chapter 5

Liquid Crystalline Polymers as High Performance Fiber and Structural Materials

5.1. INTRODUCTION

Organic polymers can be used as structural materials because they may be as strong as inorganic materials such as iron and steel. Polyethylene is a well-known example. Polyethylene with the simple chemical structure of $-(CH_2CH_2)_n-$, has been found to show mechanical properties dependent on processing and morphology. In certain diluted (say 0.001 to 0.01 percent in xylene) conditions PE may form single crystals (Keller, 1957) from which a strong mat can be prepared. In most cases PE is melt-processed resulting in the very complex semicrystalline morphology of spherulites with chain-folded lamellae and interlamellar links (Hoffman *et al.*, 1976). Such PE samples often show moderate mechanical properties useful in applications such as film, foil, bottles, tubing, and coatings. With vigorous stirring of a high molecular weight PE solution (0.1 to 1 percent), "shish kebabs" are formed. They are very strong (stronger than steel based on weight) because the "shish" is formed of extended chains along the length of the shish (Pennings and Kiel, 1965; Pennings *et al.*, 1970). The more recently developed "gel-spinning" (Smith and Lemstra, 1979) of PE has resulted in fibers (*e.g.*, "Spectra") with extended-chains and very high tensile strength (up to ∼5 GPa) and modulus (up to ∼220 GPa).

   With a polymer the condition of processing and thus the morphology has a remarkable effect on the properties of polymeric materials as shown by the above examples. However, the highest tensile strength and modulus are possible only when the polymer molecules are the most extended and assembled in fibril form, and when the chains are aligned along the long

axis of the fibril. In such conditions the molecular response to stretching will be bond extension and bond angle distortion. Both the processes have very high activation energy.

Theoretical studies have suggested that organic polymers can be very strong if the chains are perfectly oriented and fully extended. The strength and modulus values can reach 10 to 30 GPa and 100 to 300 GPa respectively. Prevorsek (1988) believes for PE the theoretical maximum strength of ∼50–55 GPa is the most probable. However, even for the strongest PE fibers prepared so far by most advanced technologies the tensile strength is only about one tenth of the predicted value. Varieties of defects including chain-end aggregation, the presence of fractions with insufficient molecular weight, and imperfect orientation, are responsible for the lower strength. Efforts in this direction have been rewarding.

Main-chain type liquid crystalline polymers (MC-LCP) are characterized by a strong tendency of self-orientation along the chain axis. It should be much easier for an MC-LCP than for a non-liquid-crystalline polymer such as PE to achieved a high degree of chain orientation. MC-LCP's are thus very promising polymers for preparing high-strength high-modulus fibers. Another favorable property of MC-LCP's is their high Tg and melting point, making these materials more heat-resistant and applicable in higher temperatures than PE and other flexible polymers. In the following sections, MC-LCP's for high-strength high-modulus fiber and structural materials are discussed. Research and development in this area have been very active. Significant progress is seen every year with industrial success and numerous patents and academic papers. Our discussion is only introductory as the title of the book has suggested. The selection of literature material is also based on such considerations. According to Yang (1989) a high strength fiber may be defined to have elongation at break smaller than 5% and initial modulus greater than 300 gpd or 264 dN/tex. The tenacity should be greater than 15 gpd or 13.2 dN/tex assuming a linear stress-strain relationship for the fiber. The conversion factor for fiber tenacity and modulus is: 1 (gpd) = 0.08826 ρ (GPa) where ρ is the fiber density in g/cm^3. For instance if a Kevlar fiber discussed in next section has a modulus of 950 gpd, the value is 120 in GPa, for its density ρ is 1.44 g/cm^3.

5.2.   LIQUID CRYSTALLINE AROMATIC POLYAMIDES

The polymers in this category are best represented by poly(1,4-benzamide) (PBA) and poly(*p*-phenylene terephthalamide) (PPD-T) prepared in high

molecular weight in the early 1960's by Kwolek and coworkers (Kwolek *et al.*, 1962). Kwolek was also the first to report the formation of liquid crystalline solutions of such aromatic polyamides. Each of these polyamides begins to form a liquid crystalline phase above a critical concentration (~5 to 10 wt-%) dependent on polymer molecular weight and the solvent. The fibers spun from liquid crystalline solutions of PBA or PPD-T both showed high-strength and high-modulus. However because of the lower production price, "Kevlar" fiber commercialized by Du Pont Co. is largely based on PPD-T.
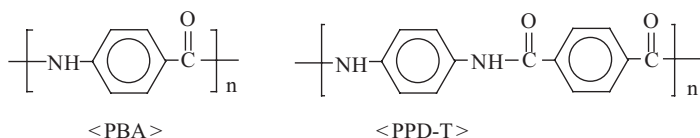
PBA and PPD-T can be prepared by low-temperature (often below $50\,^{\circ}\mathrm{C}$) polycondensation of 4-aminobenzoyl chloride hydrochloride (Kwolek *et al.*, 1977) or between 1,4-phenylene diamine and terephthaloyl chloride (Bair *et al.*, 1977) in a suitable amide solvent such as N,N-dimethylacetamide (DMAc), tetramethyl urea (TMU) and N-methyl-2-pyrrolidone (NMP). The weakly basic dialkylamide solvent also plays the role of an acid acceptor. In many instances, a few percent of inorganic salt is combined with the amide solvent to increase the polymer solubility. According to Morgan (1977), the discovery of the value of salts as aids in the synthesis of aromatic chain polyamides was made in a backhanded way in preparations of poly(1,3-phenylene isophthalamide). A high molecular weight polymer was obtained when the diamine monomer was used in its dihydrochloride form together with triethylamine for activation of the monomer and neutralization of HCl. If, instead, pure free diamine was used, only low polymers were obtained. The difference was traced to the extra by-product salt (triethylamine hydrochloride) which promoted solvation and dissolution of the polymer and prevented the premature precipitation of the product. Other salts including LiCl, $\mathrm{Li_2CO_3}$ and $\mathrm{CaCl_2}$ have since been discovered as effective and used widely. Naturally, the variation in the solvent composition and polymer concentration has a significant influence on the molecular weight of the products. For example for preparation of PPD-T in DMAc-salt, $\mathrm{CaCl_2}$ (0.15–$0.2\,\mathrm{mol/L}$) and $\mathrm{MgCl_2}$ ($0.10\,\mathrm{mol/L}$) are the two that resulted in polymers of inherent viscosity higher than $1.2\,\mathrm{dL/g}$. Lower

molecular weights were obtained with other salts or different salt contents (Pedorov *et al.*, 1970). On the other hand, Akzo (1979) found with NMP containing 14% $CaCl_2$ the inherent viscosity of PPD-T can reach 5.05 dL/g. Lower viscosity was observed for higher or lower $CaCl_2$ content.

For fiber production, the inherent viscosity of PPD-T is normally in excess of 4 dL/g. The molecular weight is in the order of 20,000 which corresponds to a degree of polymerization of 80. A higher tenacity and higher modulus are obtained for the polymer with higher molecular weight. The Mark-Houwink equation for PPD-T in 96% H_2SO_4 was determined (Aspin and Strazielle, 1977) to be:

$$[\eta] = 8 \times 10^{-3} M_W^{1.09}$$

while Parkov (1977) suggested a higher exponent of 1.7. Irrespective of the difference, the exponent parameter higher than 1.0 has indicated that the chain of PPD-T is rather stiff (Bohdanecky and Kovar, 1982). The chain rigidity and extended chain conformations of these polymers are also characterized with the high values of persistence length q in dilute solution. While the flexible aliphatic polyamide-6,6 has a very low value for q, in the order of 1 nm, the q for the extended-chain PBA and PPD-T is 40 times higher (Kwolek *et al.*, 1988).

For preparation of PBA or PPD-T fibers with the highest possible strength and modulus, the solution and spinning process must be optimized. The solution concentration must be significantly higher than the critical concentration so that a single liquid crystalline phase is obtained. This effect was well demonstrated by Kwolek (1977) for PBA with an inherent viscosity of 2.1 dL/g using tetramethylurea-LiCl (6.5 wt-% of the salt) as the solvent. If the polymer concentration is 4.6 wt-%, no liquid crystalline phase was separated and the as-extruded filaments showed a tenacity of 4.4 gpd and an initial modulus of 182 gpd. The properties were much better (8.5 gpd and 330 gpd respectively) if the concentration was increased to 5.8% when a small amount of the liquid crystalline phase was separated. When the concentration is increased further to 6.7%, a large amount of the anisotropic phase was separated while the tenacity and initial modulus increased to 9.7 gpd and 424 gpd respectively. The strength and modulus were more than doubled when the dope was anisotropic than when it was isotropic. The enhanced molecular orientation in the liquid crystalline dope was responsible for the enhanced tenacity and modulus. The orientation angle reported by the same authors had decreased from 33 degrees (for the isotropic dope) to 20 then 16 degrees (for the more concentrated dopes).

It is desirable to have the dope concentration as high as possible, both for better mechanical properties and for lower production cost. Blades (1973, 1975) found that PPD-T and sulfuric acid could form a complex crystal with a very high content (20 wt-% or higher) of PPD-T. The complex crystal melts above ∼70 °C to form an anisotropic dope. The fiber spin can thus be carried out in a very desirable concentration that is higher than normally used. Another breakthrough made by this researcher was the invention of the "dry-jet wet spinning" process, in which fiber spinning occurs in an air gap and is followed by coagulation. This process is most effective for polyamides with high chain stiffness such as PPD-T. Polymers with relatively low chain rigidity can be spun by the ordinary wet spinning method followed by drawing. The dry-jet wet spinning process has the advantage of being free from the danger of freezing inside the spinneret which may happen in an ordinary wet spinning process. The fiber spun by dry-jet wet spinning has a higher degree of molecular orientation. The fiber tenacity (T) and modulus (M) were reported to be significantly higher while elongation to break (E) was lower by the dry-jet process than by the wet-jet process. For PPD-T, the values of $T = 26$ gpd, $M = 750$ gpd and $E = 3.7\%$ for the dry-jet process were in contrast to that of $T = 7.0$ gpd, $M = 173$ gpd and $E = 9.1\%$ for the wet-jet wet spinning process. PPD-T has been processed in various conditions to meet different needs. In Table 5.1 the

Table 5.1. Yarn properties of representative Kevlar aramid fiber[*].

Property	Kevlar 29	Kevlar 49	Kevlar 149
Tensile strength, in MPa (gpd)	2,930 (23)	2,930 (23)	2,345 (18)
Elongation, in %	3.6	2.5	1.45
Initial modulus, in GPa (gpd)	67 (525)	114 (900)	141 (1,110)
Secant modulus to 1% elongation; in GPa		116	156
Denier	1,140	1,140	1,140
Density; in g/cc	1.44	1.44	1.47
Equilibrium moisture regain, 25 °C, 65% RH; in %	4.3	4.3	1.0–1.5
Creep rate/log time; Load: 40%–58% ultimate T. Str.; in %	0.052	0.020	0.011
Melting point	none	none	none
Shrinkage after 250 °C exposure; in %		<0.09	
Coefficient of thermal expansion (longitudinal); in m/m/°C		-4.25×10^{-6}	-1.96×10^{-6}

[*] Source: *Liquid Crystalline Polymers* by National Materials Advisory Board, Washington, DC, 1990.

properties of a few classes of Kevlar aramid fibers are given. The property difference results from different processing conditions. Specifically, the heat treatment of spun fibers under tension at high temperatures (150–550 °C) for a short period of time has been applied successfully to enhance fiber properties. For instance, Kevlar 49 is a hot-drawn version of Kevlar 29. The enhancement in physical properties is not only achieved by heat treatment at tension of dry fibers, it is also observed for fibers containing solvent. In one example, wet PPD-T fibers containing 100% sulfuric acid were stretched within drawable limits and then dried at above 300 °C. Fibers thus produced had a tenacity of 23 gpd (same as Kevlar 49) and an initial modulus of 1,500 gpd (even greater than that of Kevlar 149) (Asahi Chem., 1977). In general, heat treatment at tension increases the strength and most probably the modulus of fibers.

The increase in properties by heat treatment is attributed to the increased orientation and crystallization of the polymer chains. X-ray studies have shown that Kevlar fibers are highly crystalline with polymer chains parallelly oriented along the fiber axis. A centered monoclinic (pseudo-orthorhombic) unit cell was proposed by Northolt and Van Aartsen (1973). According to Tashiro *et al.* (1977), the unit cell has the dimensions of $a = 7.87$ Å, $b = 5.18$ Å and $c = 12.9$ Å. The orientation angles of the molecular chains with respect to the c axis are approximately 6° for the 1,4-diaminophenylene segment and ∼14° for the terephthaloyl segment. The amide groups are assumed to be coplanar and oriented nearly parallel to the (100) planes. The characteristic distance between two neighboring amide groups from adjacent polymer chains is only 3 Å, so close that strong hydrogen bonding exists. In addition, since the amide bonds are preferentially in the trans configuration with considerable double bond character, the rotational activation energy of the carbon–nitrogen bond is large (approximately 22 kilocalories per mole as compared to 2–4 kilocalories per mole for a simple carbon–nitrogen single bond). The rigid rodlike character of the polymer chain is hence significantly enhanced. However, the difference in processing does bring about changes in the structure of Kevlar fibers. For instance, Blades found the apparent crystallite size (A.C.S.) for Kevlar 49 fiber was above 58 Å which was larger than the value 52 Å of the Kevlar 29 fiber. On the other hand, the axial crystal orientation measurement by the azimuthal X-ray diffraction of PPD-T fibers has given the orientation angle of 12° or less for Kevlar 49 and larger values for Kevlar 29. These results indicate that in Kevlar 49 the crystallites are close to perfect and better oriented along the fiber axis. According to Kwolek *et al.* (1988),

Kevlar 149 has a substantially higher degree of crystallinity and larger crystal size than for Kevlar 49. The unit cell dimensions for the two also differ significantly. In addition, while there are present skin-core structure in both Kevlar 29 and Kevlar 49 fibers, there is no definable difference between the skin and core for Kevlar 149.

The success of "Kevlar" has since greatly animated research on liquid crystalline polymers in general and the search for new polymers that show similar properties to the Kevlar polymer in particular. Numerous polymer compositions have been tested. In Table 5.2 are selected examples of copolyamides that have similar properties to Kevlar and have the two monomeric units of PPD-T together with a third monomer. The data in Table 5.2 also demonstrate the importance of processing conditions on product properties. The comparison of examples 15 and 16 shows that a higher dope concentration would result in higher fiber properties. This result is similar to that reported by Kwolek (1977). On the other hand the examples from 14 to 20 all show that the significantly higher strength, higher modulus and lower elongation are obtained after proper heat-treatment of the as spun fibers.

Besides Kevlar fibers commercialized by Du Pont, fibers with comparable properties based on PPD-T are also produced in other trade names, for example "Twaron" by Akzo, "Terlon" by Russia. For example, a Twaron aramid T-1000A fiber has a tensile strength of 22 gpd, an elongation at break of 3.3% and an initial modulus of 630 gpd (Source: *Liquid Crystalline Polymers* by National Materials Advisory Board, Washington, DC, 1990). The properties of a "Terlon" fiber are 190 sN/tex for tensile strength, 2.5% for elongation at break, and 150 GPa for modulus (Volokhina and Kudryavtsev, 1988).

A class of related copolymers (8 to 13 in Table 5.2) interesting from the view point of chemistry and properties are the copolymers (produced as "Technora" by Teijin Ltd.) based on 1,4-phenylenediamine, terephthaloyl chloride and the third monomer 3, 4′-diaminodiphenylether (Ozawa *et al.*, 1978). The polymerization can be carried out at 0 °C–80 °C in an amide solvent (NMP or DMAc) with a small amount of salt ($CaCl_2$ or LiCl). The incorporation of 3, 4′-diaminodiphenylether moieties in the chain makes the polymer less rigid than PPD-T and it has a slightly lower decomposition temperature (500 °C as compared to 550 °C for PPD-T). However, as shown in Figure 5.1, except for side-steps the polymer can take a fully extended linear chain conformation because of the unique 3, 4′-disubstitution of the diphenylether unit. If the two substitutions are in

Table 5.2. Selected copolyamides for high-strength high-modulus fibers form 1,4-phenylenediamine, terephthaloyl chloride and a third monomer.

No	The third monomer (III)	Mol-% of (III)	η_{inh} (dL/g)	$T/E/M^*$	Ref.
1	Cl–CO–CH=CH–CO–Cl	20	4.3	24/5.7/680	Blades, 1973
2	Chloroterephthaloyl chloride	5.0	5.5	23/4.2/580	ibid.
3	t-Hexahydroterephthaloyl chloride	25	4.3	22/4.5/ 540	ibid.
4	4, 4′-Diaminodiphenyl ether	5.0	4.3	24/6.2/520	ibid.
5	4, 4′-Dichloroformylbiphenyl	10	6.5	26/6.4/620	ibid.
6	1,2-Di-*p*-chloroformylphenylethane	10	3.2	22/3.6/730	ibid.
7	4-Aminobenzoic acid	25	5.4	32/5.4/800	ibid.
8	3, 4′-Diaminodiphenyl ether	20	2.0	22/4.5/590	Ozawa *et al.*, 1978
9	ibid.	30	2.5	25/4.6/620	ibid.
10	ibid.	40	2.6	26/4.5/640	ibid.
11	ibid.	50	2.8	27/5.0/620	ibid.
12	ibid.	60	2.5	25/4.7/616	ibid.
13	ibid.	70	2.6	23/5.2/585	ibid.
14	5-Amino-2-(*p*-aminophenyl)-benzoxazole	35	6.1	A: 20/8/700 H: 29/3/1,050	Nakagawa *et al.*, 1977
15	5-Amino-2-(*p*-aminophenyl) benzo-thiazole (spin dope: 12% in H$_2$SO$_4$)	50	6.4	A: 17/9.1/680 H: 21/3.5/980	ibid.
16	5-Amino-2-(*p*-aminophenyl) benzo-thiazole (spin dope: 16% in H$_2$SO$_4$)	ibid.	ibid.	A: 21/8.5/720 H: 30/2.5/1,150	ibid.
17	4, 4′-Diamino-5, 5′-dimethyl-2, 2′-bi-phenylsolfone; dope: 20% in H$_2$SO$_4$	10	4.9	A: 23/5.5/460 H: 31/3.3/875	Kaneda *et al.*, 1983
18	ibid.	20	5.7	A: 24/5.3/490 H: 36/3.7/807	ibid.
19	4, 4′-Diamino-2, 2′-bi-phenylsolfone Spin dope: 20% in H$_2$SO$_4$	10	5.0	A: 22/5.2/481 H: 30/2.8/1,018	Kaneda *et al.*, 1981
20	ibid.; Spin dope: 22% in H$_2$SO$_4$	20	6.1	A: 26/4.9/525 H: 37/3.9/971	ibid.

* Fiber property: T—tenacity in gpd; E—elongation in %; M—modulus in gpd; A—as spun; H—heat treated.
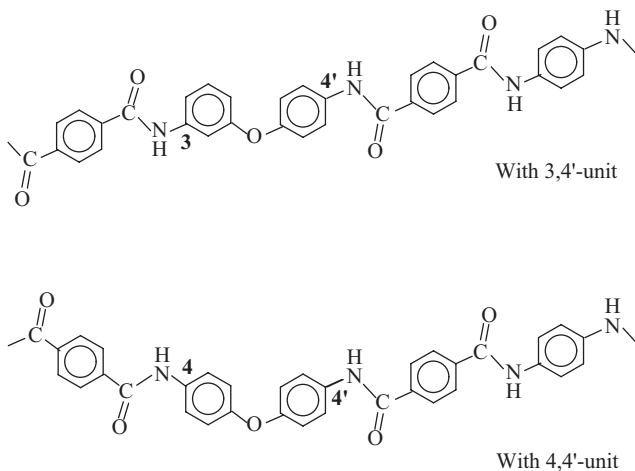
Figure 5.1.   "Technora" copolymer containing $3, 4'$-diphenylether units and related $4, 4'$-copolymer.

other positions such as $4, 4'$- or $3, 3'$–the linearity of the chain desirable for high-strength high modulus fibers will be destroyed. Because of the higher flexibility and solubility, the "Technora" polymer can be spun by the ordinary wet spinning method. However, a high draw ratio of six to ten times is required for the fiber to develop a highly oriented structure so as to have high strength and high modulus. In contrast, the postdrawing is not a necessary step for the dry-jet wet spun PPD-T fiber to show high properties. The typical tensile properties of Technora multifilament yarns are 25 gpd tenacity, 570 gpd tensile modulus, and 4.4% elongation at break.

We have shown that with the advanced processing technology of the dry-jet wet spin and heat-treatment, the lyotropic liquid crystalline polyamides form fibers of excellent tensile properties. The tenacity of 23 gpd of Kevlar yarn is more than five times that of steel wire and more than twice that of high-tech spun nylon, polyester, or glass fibers. The initial modulus of Kevlar is about twice that of steel wire or fiber glass, four times that of high tenacity polyester, and nine times that of high tenacity nylon. The high values of tensile properties are the result of the unusually high degree of orientation of the extended polymer chains along the fiber axis. The high degree of uniaxial orientation of the highly extended chain, however, is not always desirable for property and application. For instance, it is difficult if not impossible to process films of high and isotropic physical properties from

these anisotropic polymers that have a strong tendency to orient along the elongational flow. Even for fibers, the extended chain structure is not desirable for axial compression. Except for the relatively weak van der Waals force and hydrogen bonding there is little strong intermolecular bonding such as chain entanglements. The lateral connection among the microfibrils is also weak. The fibers tend to split into microfibrils when bent or when under compression. Deteresa *et al.* (1982, 1984) reported that the compressive strength of Kevlar 49 was only one fifth (0.7 GPa) of the tensile strength (3.4 GPa). The compressive strain to break or yield was also only one fifth of the tensile value. These researchers also found that after applying ∼3% axial compression the fibers would lose ∼10% tensile strength. The limited compressive properties limit the application of liquid crystalline polymers (discussed in this and the following sections) as structural materials when a high compressive property is essential.

The proposed end applications of Kevlar (Yang, 1989) and related fibers include ballistic and fire protective apparel, hard armors, reinforced tires and rubber goods, various forms of composites, filament wound pressure vessels, marine ropes, optical cables and industrial gloves. Almost all of them utilize the high tensile properties and high heat-resistance.

5.3. LIQUID CRYSTALLINE AROMATIC HETEROCYCLIC POLYMERS

The most important development in lyotropic liquid crystalline polymers after Kevlar is probably the synthesis of poly{[benzo(1,2-d:4,5-d′) bisthiazole-2,6-diyl]-1,4-phenylene}, or for short, poly(*p*-phenylene benzo-bisthiazole) ("PBT"; Wolfe and Loo, 1980; Wolfe *et al.*, 1981), and the closely related poly{[benzo(1,2-d:5,4-d′)bisoxazole-2,6-diyl]-1,4-phenylene} or poly(*p*-phenylene benzobisoxazole) ("PBO"; Helminiak and Arnold, 1977; Wolfe and Arnold, 1981). Both PBT and PBO are lyotropic liquid crystalline and can be spun into fibers with mechanical properties even superior to that of Kevlar fibers. The molecular structures of these polymers are shown in Figure 5.2.

The success of this class of polymers was the result of a research program sponsored by the U.S. Air Force and has since been a paragon of molecular engineering for new structural materials having low density, high strength, high modulus and superior thermal resistance (Helminiak, 1979). The molecular structures shown in Figure 5.2 are wholly aromatic

$X = O$ (PBO) $X = S$ (PBT)
S (cis-PBT)   O (trans-PBO)
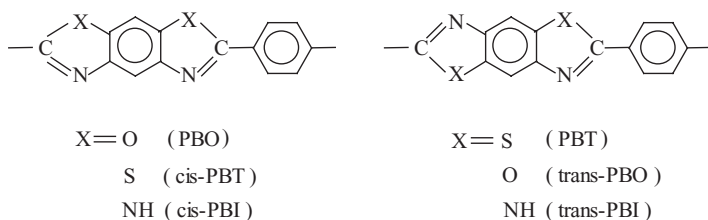NH (cis-PBI)   NH (trans-PBI)

Figure 5.2. Repeating units of PBO, PBT and the closely related polymers.

with fused heterocyclic rings. They were expected to show excellent thermal and thermooxidative stability as concluded from the intensive study on heat-resistant polymers since late 1950s. A large number of polybenzoxazoles (Imai *et al.*, 1965; Korshak, 1969) and polybenzimidazoles (Vogel and Marvel, 1961; Jones, 1968) was synthesized and reported to have very good heat-resistance. Among them was poly($2, 2'$-*m*-phenylene-$5, 5'$-benzimidazole) which was first synthesized by Vogel and Marvel and commercialized by Celanese Fibers Co. as Celanese PBI. PBI fiber has very good thermal stability. It was found to lose its breaking strength only above $300\,°C$ in air. However, because of its meta-substitution and non-linear shape, this polymer does not offer high strength and high modulus. The tensile properties of PBI fibers are in the range of conventional textile fibers. The fiber tenacity is a few grams per denier, the initial modulus is in the order of $100\,gpd$–$200\,gpd$. In contrast, the polymer molecules in Figure 5.2 are linear and rod-like. It is the characteristic shape required for the formation of lyotropic liquid crystalline phase (Onsager, 1949; Flory, 1956). In addition, it was demonstrated by Kevlar that strong fibers were spun from lyotropic liquid crystalline solutions of rod-like polymers. With these and other considerations the aromatic heterocyclic polymers with rod-like configuration and many modified structures were carefully examined.

Most specifically, the polybenzimidazole, trans-PBI shown in Figure 5.2 with X = NH, was prepared by melt polymerization of 1,2,4,5-tetraaminobenzene and terephthalic acid as early as 1961 (Vogel and Marvel, 1961). The molecular weight was low ($0.8\,dL/g$). Later, by modified polymerization reactions Kover and Arnold (1976) were able to obtain the same polymer with high molecular weight. The polymer gave a liquid crystalline solution in methane sulfonic acid or polyphosphoric acid. However, because of its high level of moisture absorption this polymer was eliminated from further development as a structural material

(Wolfe *et al.*, 1981). On the other hand, trans-PBO was ruled out because the polycondensation did not proceed below the temperature of monomer decomposition. Wolfe and coworkers also attempted the synthesis of cis-PBT through polycondensation of 4,6-diamino-1,3-benzenedithiol dihydrochloride and terephthalic acid. This attempt was not successful, for only low molecular weight polymer was obtained. Nevertheless, high molecular weight PBT and PBO were prepared and spun to high-strength high-modulus fibers (Wolfe and Loo, 1980; Wolfe and Sybert, 1985; 1987).

PBT was prepared (Wolfe *et al.*, 1981) in polyphosphoric acid by the reaction of terephthalic acid (TA) and 2,5-diamino-1,4-benzenedithiol dihydrochloride (DABDT). The monomer DABDT was better prepared under argon by the addition of the dipotassium salt of 2,5-diamino-1,4-benzenedithiol into a large volume of 6 N HCl. The resulting solid was collected by filtration and transferred immediately into a large volume of dilute HCl. Concentrated HCl was then added slowly to give large hexagonal prisms of DABDT. The monomer prepared in this manner gave PBT prepared on a large scale with intrinsic viscosities between 18 dL/g and 30 dL/g. With other methods, the average crystal size of the monomer was too small, giving a greater chance of contamination and making the control of dehydrochlorination for large scale production more difficult. For polymerization, an 85% polyphosphoric acid (PPA) was freshly prepared by heating 1.52 times excess weight of P_2O_5 with 86% H_3PO_4 at 150 °C for 5 hours to 8 hours. The monomer DABDT was first activated by dehydrochlorination with PPA at room temperature for 24 hours under a stream of argon, followed by heating to 70 °C. The complete dehydrochlorination is essential to obtain the monomer in a reactive form. The reaction temperature should be controlled to ≤100 °C, otherwise a side reaction with the evolution of H_2S occurs. A stoichiometric amount of terephthalic acid of suitable particle size was then added to the reactor. Additional PPA was also added to adjust the polymer concentration to the desired value (5% to 10%). The mixture was heated to 150 °C to dissolve terephthalic acid, and then to 175 °C–185 °C for 24 hr–48 hr. The resulting polymerization mixture was precipitated in water, and washed successively with water, ammonium hydroxide, and water. The polymer was generally of very high molecular weight with intrinsic viscosity as high as 30 dL/g with a weight-average of molecular weight of ∼40,000. The conditions summarized by Wolfe and coworkers for high molecular weight PBT included the use of high purity DABDT, the use of terephthalic acid of small particle size, the complete

activation of DABDT with PPA below 100 °C and a sufficient reaction time at an appropriate temperature (160 °C–200 °C).

The synthesis of high molecular weight PBO seems more difficult probably because the diamino-dihydroxybenzene monomer had insufficient purity, or because this monomer is less reactive than the diaminobenzenedithiol used for PBT. A third factor that should be considered is the solubility of the resulting polymer. PBO is less soluble in its polymerization mixture than in the case of PBT. The earlier preparations by Wolfe and Arnold (1981) using reactions of terephthalic acid and 4,6-diamino-1,3-benzenediol dihydrochloride (DABDO) in PPA, and that by Choe and Kim (1981) by using terephthaloyl chloride for TA, all resulted in PBO of only low or moderate molecular weight with intrinsic viscosities below 10 dL/g. The insufficient molecular weight made the fiber-spinning more difficult and the fiber property was for the best 4.8 gpd tenacity, 0.7% elongation, and 711 gpd modulus after heat-treatment (Choe and Kim, 1981).

Two significant developments in the preparation of PBO may be mentioned briefly. One was the modification of the monomer synthesis by Lysenko (1986; 1988; Harris *et al.*, 1990). BABDO had been synthesized starting from nitration of resorcinol diacetate with fuming nitric acid. The yield of the desired isomer 4,6-dinitroresorcinol was only 30%. Repeated recrystallization was necessary in order to wash out other products such as 2,4-dinitroresorcinol, 2,4,6-trinitroresorcinol, as well as the mononitro-resorcinol isomers. The purified 4,6-isomer was then reduced in dilute HCl by catalytic hydrogenation to give the monomer. In Lysenko's method, 1,2,3-trichlorobenzene was used as the starting material. The 2-position was protected by Cl from nitration. 4,6-dinitro-1,2,3-trichlorobenzene was the principal product which upon hydrolysis with $NaOH/CH_3OH$ gave 2-chloro-4,6-dinitroresorcinol. The latter was transferred to the desired monomer by catalytic hydrogenation of the 2-chloro as well as the two nitro groups. This method is superior to the previous one by giving a higher total yield of the monomer with higher purity. Other progress was made for polymerization by Wolfe and Sybert (1985, 1987). In short, the improvement was made by the controlled continuous addition of P_2O_5 so that the content of this compound was kept at ∼82% to the end of the process. The high content of P_2O_5 let to the high extent of dehydration required for the high degree of polymerization. In addition the polymer was more soluble in this system so that no precipitation of the polymer with insufficient molecular weight occurred. With this process PBO with intrinsic viscosity as high as 42 dL/g

was obtained. The high molecular weight PBO showed very good spinnability resulting in as-spun fibers of very high tenacity (3 GPa) and very high modulus (300 GPa). After heat-treatment the properties were even better, 3.4 GPa ($\sim$25 gpd) and 400 GPa ($\sim$3,000 gpd) respectively.

PBT and PBO fibers were spun from their liquid crystalline solution using the dry-jet wet spinning process. For instance, PBO fibers may be prepared by spinning of 13 wt-%–17 wt-% PBO/PPA solution at 60 °C to 90 °C. The as-spun fibers were then heat-treated under tension at $\sim$500 °C for 60 seconds. As for the preparation of Kevlar fibers, the heat-treatment under tension is the key to achieving the highest-possible property of PBT and PBO fibers. Allen *et al.* (1985) studied the effects of heat-treatment in a nitrogen atmosphere on PBT fibers. The variables include the temperature, the tension, and the time taken for the as-spun fiber samples for the study to be made by dry-jet wet spinning of a PBT with an inherent viscosity of 14 dL/g. The tensile modulus of the as spun fiber was 150 GPa. Its tensile strength was 1.6 GPa. The tensile mechanical properties were doubled to 300 GPa and 3 GPa by the most suitable heat-treatment. To achieve these values, temperatures of 630 °C–680 °C with a duration time of under one minute were required. The tensions applied were in the range of 150 MPa–200 MPa. To interpret the significant improvement in property by heat-treatment, Allen and coworkers studied the structure change using wide-angle X-ray diffraction. They found the crystallite size perpendicular to the fiber axis increased from approximately 2 nm in as-spun fibers to 10 nm–12 nm in fibers after heat-treatment. Fiber tensile strength was found to increase with this increase in the extent of the lateral molecular order. With measurement of the azimuthal spread of the major equatorial reflections of the fibers, they also found that a higher applied tension during heat treatment had led to a higher overall molecular orientation with respect to the fiber axis. For example, the azimuthal spreads of the two major equatorial reflections were 12.5°, 7.3° and 5.5° respectively for three samples heat-treated at 640 °C in nitrogen for 8 seconds under different tensions (0, 32 and 190 MPa). The Herman's orientation factor f was 0.93, 0.98 and 0.99 while the value for the as-spun fiber was 0.87. This increase in axial orientation is associated with significant increases in both tensile modulus and tensile strength. Thus the primary factors affecting the tensile properties by heat-treatment are the increase of overall axial molecular orientation combined with increases in the extent and perfection of the lateral molecular order in the fiber. In Table 5.3 are typical tensile properties of PBT and PBO fibers.

Table 5.3.   Properties of PBT and PBO fibers*.

Fiber type	Density	Tenacity	Modulus
PBT	1.58	25 gpd (3.5 GPa)	2,200 gpd (307 GPa)
PBO	1.51	26 gpd (3.4 GPa)	2,600 gpd (344 GPa)

* Source: Yang, 1989.

As shown in the table, PBO fibers can have higher tensile properties than PBT. This has been interpreted by the higher coplanarity between the 1,4-phenylene ring and the plane of the heterocyclic moiety present in PBO than in PBT. From conformational analysis, Welsh (1987) and coworkers found that for PBO the lowest energy conformation was coplanar, the same as concluded by Bondi (1964) on model compounds. On the other hand for PBT, the calculation showed that the phenylene ring plane and the fused heterocyclic ring formed an angle of approximately $20°$ for the lowest energy conformation. This nonplanarity is attributable to the large van der Waals radius ($1.85\,\text{Å}$) of the S atom in contrast to the smaller value ($1.40\,\text{Å}$) of O in PBO. Since the van der Waals radius of H atom is $\sim 1.15\,\text{Å}$, the separation of the S and its neighboring H on the *p*-phenylene ring must be larger than $3.00\,\text{Å}$. If a coplane conformation was adopted between *p*-phenylene ring and the fused heterocyclic moiety, the separation would be only $2.66\,\text{Å}$ which is much less than the requested value. The repulsion of the H and S forces the two planes to rotate apart from each other while keeping the highest possible coplanarity favorable for a larger degree of conjugation. This difference in the degree of coplanarity has two notable results: that there must be higher conjugation along the whole chain and that the packing density must be higher in PBO than in PBT. The two are factors making the material stronger. However, the density values (1.58 to 1.51) shown in Table 5.3 seemed to be contradictive to the proposed higher packing density in PBO. This was explained by the higher molecular mass of the repeat unit in PBT (266 dalton) than in PBO (234 dalton). This is acceptable because the ratio of the two mass values is 1.14 which is higher than the density ratio 1.04.

5.4.   THERMOTROPIC LIQUID CRYSTALLINE POLYMERS

The polymers discussed in the previous two sections are all lyotropic type liquid crystals and cannot be melt-processed because they have no melt

point or a melting point well above decomposition temperature. They are processed from liquid crystalline solutions in strong acids into strong fibers which may be used as reinforcing component in composites. In contrast, a thermotropic liquid crystalline polymer may be melt-processed from its ordered melt phase into not only strong fibers but also self-reinforcing plastics, films and sheets of strong mechanical property. These polymers have a common feature of a high degree of linearity and rigidity in molecular structure. Thus building blocks such as the linear and aromatic 1,4-phenylene and $4,4'$-biphenylene are widely used. However, for achieving the thermotropic liquid crystallinity and melt-processibility, other monomeric units with somewhat less linearity and higher flexibility are needed. 2,6-Naphthalene is widely used because it offers a "side-walk" to decrease the melting temperature while retaining the aromatic character and linear contour of the molecules. The concepts of lateral substitution and copolymerization are widely applied in molecular design for the same reason. A relatively smaller amount of the non-linear monomeric units, such as $4,4'$-diphenylether and 1,3-or 1,2-phenylene, is often copolymerized in the chains to provide processibility. In certain cases the aliphatic units such as alkylene and 1,4-cyclohexylene are used for the purpose. On the other hand, in order to realize the thermotropic liquid-crystallinity the amide linkages present in the lyotropic liquid crystalline aramid polymers are replaced or partly replaced by the ester, azomethine, or other linkages that show no or weaker hydrogen-bonding. The structure-property relationship of liquid crystalline polymer molecules is outlined in Chapter 3.

Although a lot of molecular structures give rise to thermotropic liquid crystallinity, the aromatic ester type polymers and copolymers are the only ones which have been successfully prepared as structural materials. These aromatic polyesters have been classified into three types, as shown in Figure 5.3, based on their molecular composition and thermomechanical property (Suenaga, 1990). Type-1 has the highest heat-deflection temperature (HDT) of $\sim 300\,^{\circ}$C and above under a load of $18.6\,\text{kg/cm}^{-2}$. Its molecular composition is characterized by having 1,4-biphenylene moieties as represented by "Xydar" of Amoco (Dartco) and "Ekonol" of Sumitomo. The HDT of the Type-2 is in the range of $180\,^{\circ}$C–$240\,^{\circ}$C under the load $18.6\,\text{kg/cm}^2$. Its characteristic structural moiety is 2,6-naphthalene. The representative product "Vectra" of Hoechst-Celanese Type-3 is semi-aromatic with a high of p-hydroxybenzoic acid moiety (HBA) content and a smaller portion ($\sim 40\,\text{mol-\%}$ or less) of poly(ethylene terephthalate). It is normally considered as HBA modified PET, although there
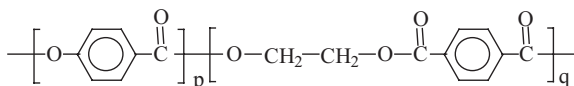
Type-1 ("Xydar","Ekonol")
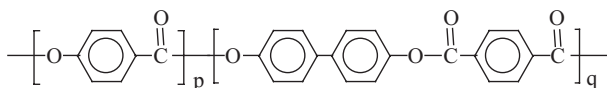
Type-2 ("Vectra","Vectran")
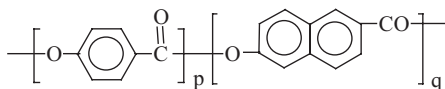
Type-3 ("X7G", "Rodrun")

(other structural moieties, such as isophthalic for type-1, may be also incorporated)

Figure 5.3.   Representative structures of three types of thermotropic copolyesters.

are fewer PET moieties than HBA. The HDT of Type-3 is ∼170 °C under $18.6 \, kg/cm^{-2}$. Unitika commercialized this PET/HBA copolymer as "Rodrun". All these copolymers have a common structural moiety of HBA because this monomer is already mass-produced. The three types of thermotropic polymers applicable for structural materials are discussed briefly in the following subsections.

5.4.1.   Type-1 copolyesters

The homopolymer of HBA was first successfully prepared in 1963 by Economy and coworkers at Carborundum Co. (Economy, 1989). The goal was to prepare new types of high temperature polymers that were processible by techniques such as compression sintering developed at Carborundum rather than by expensive solution processes normally used for high temperature polymers. By carefully designed polymerizations of phenyl 4-hydroxybenzoate, they were able to synthesize poly(4-hydroxybenzoate). The product was very stable in air even up to 400 °C and could be compression sintered at 400 °C under 10,000 psi to yield specimens with a flexural

strength of 74 MPa and flexural modulus of 6,896 MPa. By high energy rate forging of the polymer preheated to 300 °C they obtained fused specimens that showed an even higher flexural modulus of ∼16 GPa. X-ray diffraction analysis of the fused sample showed a high degree of orientation. This high stiffness PHBA became available commercially under the trade name "Ekonol" in 1970. It was later found (Economy *et al.*, 1988) to form a nematic phase at ∼445 °C.

The undesirable side of the PHBA is its poor processibility. It is not processible by more convenient methods such as injection molding. Economy and coworkers then decided to modify PHBA by copolymerization with another *p*-aromatic ester. The copolymers should have an aromatic nature and rod-like shapes so that excellent mechanical properties and high temperature resistance could be obtained. However, sufficient structural defects should also be introduced into the copolymers to depress the melting point to well below 440 °C for better processibility. After preparation and evaluation of a large number of systems they found that 4, 4′-biphenylene terephthalate provided the best combination of desired properties. By 1972, they were able to make two copolymers (Figure 5.3, type 1) of desirable properties. These polymers are commercially available as Ekkcel I-2000 (the injection molding grade with a p/q of 2/1) and Ekkcel C-1000 (the compression molding grade with a p/q of 1/2). The properties of the two are adopted from Economy (1989) in Table 5.4.

The injection molding grade Ekkcel I-2000 was licensed to Dart Kraft and was sold under the trade name "Xydar". However, the melting point

Table 5.4.   Properties of two Type-1 copolyesters*.

Properties	Ekkcel C-1000 (p/q = 1/2)	Ekkcel I-2000 (p/q = 2/1)
Specific gravity, g/cm³	1.35	1.40
Tensile strength, psi	10,000 (69 MPa)	14,000 (97 MPa)
Tensile modulus, psi	190,000 (1.3 GPa)	350,000 (2.4 GPa)
Elongation, %	7–9	8
Flexural strength, psi		
at 23 °C	15,000 (100 MPa)	17,000 (120 MPa)
at 260 °C	5,000 (34 MPa)	4,000 (28 MPa)
Flexural modulus, psi		
at 23 °C	460,000 (3.2 GPa)	700,000 (4.8 GPa)
at 260 °C	125,000 (0.86 GPa)	235,000 (1.6 GPa)
HDT at	300 °C	293 °C
265 psi (18.6 kg/cm²)		

* Source: Economy, 1989.

Table 5.5.   Properties of the Ekonol and Kevlar fibers*.

	Kevlar 49	Ekonol fiber
Density, g/cm^3	1.45	1.40
Tensile strength, psi	400,000 (2,758 MPa; 22 gpd)	550,000 (3,793 MPa; 31 gpd)
Tensile modulus, psi	20 × 10^6 (138 GPa; 1,078 gpd)	24 × 10^6 (165 GPa; 1,339 gpd)
Elongation, %	2.7	3.0
Moisture absorption, %	2.0	0.01

* Source: Economy, 1989.

of this liquid crystalline copolyester is still too high ($\sim$421 °C) for melt spinning. In order to further depress the melting point, Cottis *et al.* (1975, 1976) modified the copolymer with isophthalic acid and obtained melt spun filaments that displayed high tensile properties. In one example the fibers were spun at 350 °C–400 °C and then heated in air at 320 °C to increase the molecular weight by chain extension. The resulting fiber had a tenacity of 6 gpd and tensile modulus of 420 gpd. After drawing of $\sim$10% in air at 400 °C the tenacity increased to 13 gpd, the modulus increased to 840 gpd. This is the first report of polyester fibers that have such impressive high tensile properties. The process was further advanced to achieve even higher properties by Sumitomo Chemical Co. The fibers based on the copolymers of 4-hydroxybenzoic acid, 4, 4′-biphenol (BP), terephthalic acid (TA) and isophthalic acid (IA), were commercialized under the name "Ekonol" in 1985. The properties of Ekonol fibers are impressive and comparable with that of Kevlar 49 fibers as shown in Table 5.5 (Economy, 1989). Ekonol fibers may be used for ropes, cables, composite, and protective apparel.

Naturally, the fiber properties vary with polymer composition as well as process conditions. Two examples that show the effect of these variables are given in Table 5.6. As would be expected, the increase in the amount of the non-linear structural component of isophthalic acid decreased the strength and modulus. Other structural modifications such as replacing TA with phenyl substituted terephthalic acid (Harris, 1983), replacing TA with hexahydroterephthalic acid (East and Calundann, 1982), and using 6-hydroxy-2-naphthalic acid (HNA) as the fourth monomer copolymerized together with HBA, TA, and BP (Calundann *et al.*, 1984) were also examined. Most interestingly, the HNA (5 mol-%) modified copolyester could be extruded at 345 °C to form strong fibers. The as-spun fiber had a tenacity of 7.2 gpd and a modulus of 597 gpd. The tenacity increased by more than three times to 27.2 gpd, while the modulus was doubled to 1079 gpd

Table 5.6.   Effect of polymer composition and heat treatment on Ekonol fibers*.

HBA : BP : TA : IA Molar ratio	Extrusion °C	Heat treatment °C	hr	Strength gpd	Elongation %	Modulus gpd
12 : 4 : 3 : 1	350	As spun fiber		5.5	1.4	410
		320	2	30.8	2.7	1,420
		310	2	27.3	2.6	1,190
		270	2	21.5	2.3	1,320
12 : 4 : 2.2 : 1.8	340	As spun fiber		4.4	1.1	383
		320	2	26.0	3.6	1,030
		300	2	26.2	2.7	1,100

* Source: Ueno *et al.*, 1985.

after heat treatment at 300 °C for 8 hours. At the same time, the elongation at break of 1.33% of the as-spun fiber also increased to a value of 2.57%. This is in contrast to Kevlar and other lyotropic polymer fibers discussed in previous sections. For these fibers the heat treatment resulted in a decrease of elongation at break when the strength and modulus were increased (Table 5.2). The property enhancement by heat treatment of as-spun fibers of polyesters is also shown in Table 5.6. The high temperature treatment must have provided a certain degree of molecular mobility for post-polycondensation as well as perfection of crystal order. The resultant higher molecular weight and higher degree of molecular order made the fiber stronger. It has therefore become a necessary step in preparation of high-strength high-modulus aromatic polyester fibers that the as-spun fibers are heat treated at elevated temperatures. Eskridge and Louis (1984) discovered that the heat treatment time was reduced substantially by coating the as-spun fibers with a small amount of inorganic salts.

5.4.2.   Type-2 copolyesters

Type-2 copolyesters were synthesized by melt polycondensation of 4-acetoxybenzoic acid (HBA) and 6-acetoxy-2-naphthoic acid (HNA) (Calundann, 1979). While the 4-acetoxybenzoic acid tends to form P(HBA) blocks in certain cases such as in the copolymers of HBA/BP/TA/IA discussed in the previous section, and in HBA/PET copolymers to be discussed in the next section, a random distribution is readily achieved in HBA/HNA copolymers because the two monomers have about the same reactivity toward copolymerization. As shown in Figure 5.3, the 2,6-naphthalene

moieties offer the "side-walk" type defects along the chain. The melting temperature of the copolymers is decreased while the aromatic character and the linear contour of the molecules remain. The copolymers of HBA with HNA should have not only good thermal and mechanical properties, but also much better processibility than the homopolymer of HBA. HNA is thus widely used in the molecular engineering of high performance structural polymers.

2,6-Naphthalene monomers other than HNA, including 2,6-dihydroxynaphthalene (DHN) and 2,6-naphthadioic acid (NDA), play the same rule as HNA and are used in many cases. For example, the acetate of DHN was copolymerized with TA and HBA with a molar ratio of $1:1:2$ to give a copolymer which melts at $285\,°C$ (Calundann, 1980). When the molar ratio was changed to $1:1:3$ the melting point was found to be $298\,°C$–$305\,°C$. On the other hand, NDA was copolymerized with 1,4-hydroquinone (HQ) and HBA (Calundann, 1978). The product with $1:1:3$ of NDA:HQ:HBA melts at $325\,°C$–$340\,°C$. The melting point of the copolymer from a more rigid unit $4,4'$-dihydroxybiphenyl (HBP) rather than HQ with the same NDA : HBP : HBA molar ratio of $1:1:3$ is also below $400\,°C$ ($385\,°C$–$395\,°C$). However, it is obviously much easier to achieve a stoichiometric feed of the functional groups when HNA is used than when a pair of the diol (DHN) and diacid (NDA) monomers is used. High molecular weight polymers should be obtained with less difficulty by using HNA. In addition, because the substitutions on the naphthalene ring in HNA are asymmetric, the melting point can be decreased with high efficiency by using a small amount of HNA. Thus, the studies in this category have been mostly on the HBA/HNA copolymers. The HBA/HNA copolymers have been commercialized as Vectra resins and Vectran fibers by Hoechst Celanese with success.

Data given in Table 5.7 shows the effect of polymer composition and heat treatment on the tensile properties of HBA/HNA fibers. The copolymers with approximately a molar ratio of 3/1 of HBA/HNA seem to give the best balance of properties after heat treatment. The properties of a representative Vectran fibers are shown in Table 5.8.

As shown in Table 5.7, the heat treatment resulted in the higher tensile properties of the fibers. However, Muramatsu and Krigbaum (1986) found that the fiber properties were dependent on the spin temperature and the draw ratio. The heat treatment improved the fiber properties only if the draw ratio was high. For instance, the initial modulus for HBA/42HNA ("42" is the mol-% of HNA moieties) fibers spun at $260\,°C$ or $280\,°C$

Table 5.7.   Fiber properties of HBA/HNA copolymers*.

HBA:HNA molar ratio	Inh. visc. dL/g	Melt. point °C	Extrusion Temp.	Heat treat. °C	hr	Strength gpd	Elongation. %	Modulus gpd
75:25	5.7	302	310	as-spun		12.1	2.8	541
				250	90	20	5	550
70:30	4.3	275		as-spun		9.1	2.5	490
				250	40	14	3.0	485
60:40	3.0	245		as-spun		9.2	2.2	597
50:50	3.5	260		as-spun		10.1	2.6	513
				250	90	15.6	4.0	500
40:60	2.8	263		as-spun		7.2	1.3	742

* Source: Calundann, 1979.

Table 5.8.   Properties of a Hoechst Celanese Vectran HS Yarn*.

Density	$1.4 \, \mathrm{g/cm^3}$
Melting temperature	327 °C–331 °C
Tensile strength	20 gpd–25 gpd; 2.472 GPa–3.09 GPa
Elongation	2.2%–2.5%
Initial modulus	680 gpd–840 gpd; 84 GPa–104 GPa
HDT ($18.6 \, \mathrm{kg/cm^2}$)	180–240

* Source: *Liquid Crystalline Polymers* edited by National Materials Advisory Board, Washington, DC, 1990.

(which is well above the melting point of 247 °C found by DSC measurement) increased strongly at low spin draw ratios and reached a plateau value of ∼425 gpd at a spin draw ratio of 135. The initial modulus of fibers spun at 250 °C increased more slowly with spin draw ratio and reached a much lower plateau value of ∼220 gpd at a spin draw ratio of 60. On the other hand, heat treatment of the fibers increased the molecular weight, the degree of crystallinity, and the melting temperature of the crystals. For example, the heat treatment at 231 °C of the fiber spun at 260 °C with the draw ratio of 5.8 increased the inherent viscosity from 7.5 dL/g to 11.3 dL/g in 26 hr. The viscosity for the fiber spun at the same temperature but with a higher draw ratio of 68 increased to 10 dL/g in a shorter 10 hr. The melting temperatures of the two heat-treated samples both increased to 268 °C.

However, the fiber with spin draw ratio of 5.8 did not exhibit any improvement in mechanical properties. In contrast, the initial modulus and breaking tenacity of the fiber with a spin draw ratio of 68 improved significantly after heat treatment. In order to improve the mechanical properties of the fibers a spin draw ratio larger than 45 was found to be needed for this material. These findings show that the improvement in mechanical properties upon heat treatment cannot be explained solely by an increase of polymer molecular weight or by an improvement of crystal perfection. The initial degree of molecular orientation must also be taken into consideration. At sufficiently high draw ratios the chains are nearly fully extended and parallel with a much reduced number of chain entanglements. The heat treatment of these highly oriented fibers can bring about an improvement in the lateral packing of the chains.

A combination of the type-1 and type-2 polymers resulted in the following copolyesters (Calundann *et al.*, 1984) that were spun to as-spun and heat-treated fibers of excellent mechanical properties as demonstrated in Table 5.9:
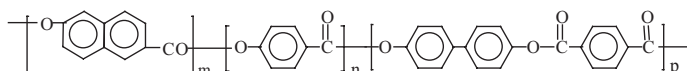
Table 5.9.   Fiber properties of copolyesters $\langle 5.1 \rangle^*$.

Molar ratio m : n : p	Inh. visc. dL/g	Extrusion temp. (°C)	Heat treatment Temp. (°C)	Time (hr)	Tenacity gpd	Elongation %	Modulus gpd
10 : 50 : 20	5.53	330	as-spun fiber		7.9	1.5	605
			280	15	22.5	3.1	758
5 : 45 : 25	8.6	375	as-spun fiber		4.9	1.0	550
			300	8	8.5	1.07	740
5 : 55 : 20	5.8	345	as-spun fiber		7.2	1.33	597
			300	8	27.2	2.57	1,079
5 : 65 : 15	8.1	360	as-spun fiber		8.4	1.54	621
			350	8	24.8	2.38	1,077
5 : 60 : 17.5	7.04	345	as-spun fiber		8.3	1.48	606
			300	8	25.8	2.6	952

* Source: Calundann *et al.*, 1984.

Table 5.10. Properties of injection-molded PET/HBA copolyesters with varied HBA mol-%[*].

HBA mol-%	0	30	40	60	80
Cylinder temperature (°C)	275	250	250	260	340
Inherent viscosity before	0.76	0.59	0.54	0.67	insoluble
(After) molding	(0.62)	(0.54)	(0.54)	(0.62)	
Tensile strength (MPa)	55	117	197	232	240
Elongation to break (%)	240	12	10	20	24
Flexural modulus (GPa)	2.3	4.0	7.65	12.5	9.65
HDT (load: 18.6 kg/cm^2) (°C)	66	73	71	64	154

[*] Source: Jackson and Kuhfuss, 1976.

5.4.3.   Type-3 copolyesters

The PET/HBA copolyester is probably the polymer first reported to show thermotropic liquid crystallinity. In 1971 when Jackson and coworkers tried to modify PET to improve its thermo-mechanical properties, the propionate of HBA was copolymerized with PET. In this study they found that at HBA levels of 35 mol-% and higher, the reaction mixture turned from clear to turbid as the polymerization progressed. The shear opalescence was also observed (Jackson, 1989). According to Jackson, these phenomena were not recognized to be the liquid crystal nature of the polymers at the time, but later suspected and demonstrated to be so by McFarlane and Nicely in 1973. In the famous paper of Jackson and Kuhfuss (1976), a number of the unique properties of thermotropic liquid crystal polymers were discussed. These included the very low melt viscosities, the very high tensile and flexural properties of injection-molded bars, the anisotropic physical properties of injection-molded plaques depending upon the direction and degree of orientation of the polymer chains, and an essentially zero coefficient of linear thermal expansion in the direction of polymer orientation. Typical properties of injection-molded PET/HBA copolymers with varied HBA mol-% (Table 5.10) showed that the liquid crystalline PET/40-HBA, PET/60-HBA and PET/80-HBA did have much higher tensile strengths and flexural moduli than the non-liquid crystalline PET/30-HBA which was in turn stronger than the injection-molded PET.

The melt-processibility, superb mechanical property, and the relatively low cost of production make the liquid crystalline PET/HBA copolyesters very attractive. However because of the tendency toward homopolymerization of the acyl ester of 4-hydroxybenzoic acid to form

poly(4-oxybenzoyl) blocks in the melt-transesterification, the control of the segment distribution of the copolyesters is difficult. This is especially so when a high content of HBA is required. For example, Economy (1989) and coworkers found that PET/60-HBA samples contained a chloroform soluble fraction and an insoluble fraction. Yet the ratio and composition of the two fractions were different for different batches of the samples. For one batch the soluble portion was 17% with an average composition of 56/44 PET/HBA which was rich in PET. For another batch the soluble portion was 28% which was made of 50/50 PET/HBA. Thus the apparent composition was only an average of at least two fractions of different copolymers. Meesiri *et al.* found there were two glass transitions of PET/HBA copolyesters. One was at ∼80 °C for the PET-rich segments. It was essentially independent of the apparent composition up to 63 mol-% HBA. The other was at ∼167 °C for polymers of 30–100 mol-% HBA. This high glass transition was attributed to a separate phase. In contrast to the constant glass transition temperature, the melting temperature of the copolyesters changed with HBA content. The PET/60-HBA had the lowest melting point of ∼200 °C, while the melting point of the homopolymer of HBA was found to be 345 °C. However, according to Economy *et al.* (1988), the transition at 340 °C was the transition from crystals to plastic-crystals which transformed to a nematic phase at about 445 °C.

One significant result of the nonuniform distribution of PET and HBA segments in the copolyester chains is the low HDT as shown in Table 5.10. The HDT for the copolymer containing 60 mol-% HBA (PET/60-HBA) was only 64 °C which was about the same as that of PET. Obviously this low value was attributed to the presence of PET-rich phase. Another result is the presence of highly melting particles which may come out unmelted during process leading to structural defects and lower properties.

The high tendency to homopolymerization of the 4-acetoxybenzoic acid relative to transesterification is responsible for the nonuniform distribution. In order to obtain copolymers with HBA units randomly distributed along the chains, the monomer 4-acetoxybenzoic acid may be added in portions rather than in a singla batch. Unitika (Suenaga and Okada, 1989) advanced the production process so that the HBA and PET moieties are uniformly distributed in the copolymers. With the advanced process the resins ("Rodrun LC-5000") showed almost 100% solubility in a hot (150 °C–160 °C) 50/50 mixed solvent of tetrachloroethane and phenol, while that produced by the old (Jackson and Kuhfuss, 1973) method has an insoluble residue of about 30 wt-%. The ^{13}C-NMR spectra also showed that

the chains in LC-5000 were more random than the old type. WAXD analysis showed a much higher orientation in the extruded fibers of LC-5000. The HDT and mechanical properties of the LC-5000 fibers were found to be superior to the old type with the same composition (Table 5.11). The resin was proposed to be used as thermal endurance injection grade. Naturally, the fiber properties are dependent on composition as well as processing conditions. Recently Mehta and Deopura (1993) reported that the higher extrusion temperature and the higher draw-down ratio were favorable for a higher initial modulus and tensile strength as shown in Table 5.12.

Table 5.11. Typical properties of fibers of LC-5000 and conventional PET/HBA*.

Property	Conventional PET/HBA	Rodrun LC-5000
Tensile strength, kg/cm^2	1,000 ($\sim$100 MPa)	2,200 ($\sim$220 MPa)
Elongation at break, %	7.5	4.5
Flexural strength, kg/cm^2	1,150 ($\sim$110 MPa)	1,450 ($\sim$140 MPa)
Flexural modulus, kg/cm^2	60,000 ($\sim$5.9 GPa)	100,000 ($\sim$9.8 GPa)
Izod impact strength, kg/cm^2	18	40
HDT (load: 18.6 kg/cm^2), °C	145	170

* Source: Suenaga, 1990.

Table 5.12. Effect of extrusion temperature and draw-down ratio on mechanical properties of as-spun fibers of PET/60HBA and PET/80HBA*.

Extrusion temp. °C	PET/60 HBA Draw-down ratio (V_0 = 1.02 m/min)	Modulus GPa	Strength MPa	PET/80 HBA Draw-down ratio (V_0 = 1.06 m/min)	Modulus GPa	Strength MPa
255	196.6	6.98	131	189.2	20.8	250
265	196.6	7.34	137	189.2	21.5	256
275	55.6	6.1	133			
	72.5	6.6	136			
	106.3	7.4	139	102.6	21.6	252
	196.6	*8.5*	*148*	*189.2*	*22.3*	*268*
	373.6	10.9	158	361.2	25.8	310
	415.5	12.0	175	400.3	26.7	315
285	196.6	8.36	150	189.2	23.6	274

* Source: Mehta and Deopura, 1993; PET/60HBA and PET/80HBA contain 60 mol-% and 80 mol-% respectively.

The highest modulus and tensile strength obtained in this study were 26.7 GPa and 315 MPa for the fiber of PET/80HBA spun at 275 °C and a draw-down ratio of 400.3. The properties of the copolymer with 80 mol-% HBA were always higher than that of the copolymer with 60 mol-% HBA.

5.5.   COMPOSITES REINFORCED BY LIQUID CRYSTALLINE POLYMERS

Composites are multiphase materials of two or more components with different physical and chemical properties. The history of polymer composites is almost as old as the history of polymers. The success of the phenol-formaldehyde resin achieved in the beginning of this century by L. H. Baekeland was largely based on the addition of an inert filler (wood powder or asbestos) into the resin, together with an advanced curing process of heat and pressure. While the heat and pressure allowed the curing reaction to be completed in a short time without the gassing, bubbling and distortion, the inert filler improved strength, reduced shrinkage, and moderated the curing reaction. The inert filler was also the cheaper component so that the cost of production was reduced. Properties and cost have since been the two major concerns in production of polymeric composites. Glass and graphite (carbon) fibers have been widely used as fillers in polymer composites for structural applications. The high-strength high-modulus liquid crystalline polymer fibers can be used as well in this field. The lower density (thus higher specific mechanical property) and the high heat resistance make liquid crystalline polymer fibers very attractive. In Table 5.13 are representative data of epoxy composites reinforced by liquid crystalline polymer and graphite fibers. The tensile properties of the liquid crystalline polymer reinforced composites are good, but the compressive strength is much poorer than the graphite fiber composite. The poor compressive properties of liquid crystalline polymer fibers have limited their utilization in composites. However, the liquid crystalline polymer fibers were found to be very valuable in hybrid composite containing graphite fibers. The excellent compressive tensile properties of the carbon fiber combined with the inherent damage tolerance of the liquid crystalline polymer fibers make a desirable system.

It has been concluded that in fiber reinforced composites the aspect ratio L/D of the fiber is one of the most important parameters in controlling the uniaxial modulus and ultimate tensile strength (Kardos and Raisoni, 1975).

Table 5.13. Properties of unidirectional epoxy composite*.

Property	Heat treated PBT	Kevlar 49	H.S Graphite
Tensile strength	1,900 MPa	1,380 MPa	2,100 MPa
modulus	190 GPa	75.8 GPa	150 GPa
strain	1.0%	1.8%	1.5%
In-plane shear strength	35 MPa		69 MPa
In-plane shear modulus	1.4 GPa		4.8 GPa
Compressive strength	200 MPa	275 MPa	1,400 MPa
Modulus	190 GPa	75.8 GPa	125 GPa
Strain	0.12%	0.4%	1.1%
Flexural strength	410 MPa		1,600 MPa
Modulus	140 GPa		120 GPa

* Fiber loading 60%.
Source: *Liquid Crystalline Polymers* edited by National Materials Advisory
Board, Washington, DC, 1990.

L and D are the length and diameter of the fiber. Increasing the ratio by increasing the length or decreasing the diameter of the fiber can increase the modulus of the composite up to two orders of magnitude. Following this reasoning, the concept of the molecular composite was proposed at almost the same time by Helminiak *et al.* (1980; Husman *et al.*, 1979) and by Takayanagi *et al.* (1980). In these composites the reinforcing fibers are replaced by extended rod-like high polymer molecules which have the highest aspect ratio if they are dispersed in the matrix on the molecular level. An extended rod-like molecule of PBT with a molecular weight of 30,000 would have a length-to-diameter ratio of ~300. However if ten chains of these molecules coagulated to form a microfibril of 5 nm in diameter the ratio could decrease at the most by 90%. A successful dispersion at the molecular level is the key to a successful preparation of molecular composite with high reinforcing effect. Another significant advantage of the molecular composite over a macroscopic fiber reinforcing composite is that there will be no failure caused by a difference in the thermal expansion coefficients or by poor interfacial adhesion.

The composite systems studied by Takayanagi *et al.* (1980) used the polyaramides poly(*p*-phenylene terephthamide), PPDT, or poly-*p*-benzamide (PBA) as the reinforcing component with nylon 6 or nylon 66 as the ductile matrix polymer. Block copolymers of one of the aromatic polyamides with one of the nylon polymers were also evaluated. The blends were prepared by extruding the sulfuric acid solutions of polymers into a

Table 5.14. Properties of composites of PPTA/nylon 6*.

Sample	Mol. Wt. of PPTA	PPTA/Nylon	Young's modulus	Yield stress	Ultimate strength	Elongation at break
Nylon 6		0/100	0.91 GPa	24 MPa	51 MPa	5.3%
Composite	980	5/95	1.45 GPa	40 MPa	52 MPa	2.7%
Composite	4,500	5/95	1.59 GPa	46 MPa	54 MPa	1.6%
Composite	12,300	5/95	1.67 GPa	58 MPa	59 MPa	0.6%
Oriented (drawn at 170 °C to three times its original length):						
Nylon 6		0/100	1.18 GPa		220 MPa	28%
Composite	34,000	3/97	3.35 GPa		340 MPa	20%

* Source: Takayanagi *et al.*, 1980.

large amount of water and washed with water and methanol. For mechanical property measurements the specimens were prepared by compressing at an appropriate temperature (240 °C for that of nylon 6 and 290 °C for the blends of nylon 66) and quenched in ice-water. Electron microscopy revealed that the rod-like molecules were dispersed in the matrix in the form of microfibrils. The diameter is in the range of 15 nm to 30 nm depending on the molecular weight of the rod-like polymer. The PPTA molecules of lower molecular weight (4,500 by viscosity-average) formed a thinner microfibril (∼15 nm in diameter) than that (∼30 nm) of the higher molecular weight (34,000). The diameters are much smaller (1 µm–10 µm) than that of macroscopic fibers used in composites. Significant reinforcement was achieved by the microfibrils as shown in Table 5.14. PPTA of higher molecular weight resulted in a higher reinforcement. The Young's modulus of nylon 6 was almost doubled by blending in only 5% of the high molecular weight PPTA. The oriented sample with 3% of PPTA was found to show a modulus of 3.35 GPa and a strength of 340 MPa. The calculated value for the ultimate strength of the microfibrils of PPTA in the oriented composite was 4.2 GPa if an additive rule was applied. This calculation suggested that the tensile property of PPTA was fully developed in the composite.

Although the reinforcement by aromatic polyamides was remarkable, the composites prepared by these researchers were not molecular. As mentioned above, the molecules were coagulated into microfibrils of 15 µm–30 nm in thickness. Using the Halpin-Tsai equation modified by Nielsen (1975) and the modulus values of $E_1 = 0.91$ GPa and $E_2 = 182$ GPa for nylon 6 and PPTA as well as the observed modulus of the composites, the calculated L/D ratio was 15 for low molecular weight PPTA and 25 for high molecular

weight PPTA in the composites. These ratio values are much smaller than that of single PPTA chains if the chains are fully extended. A higher degree of dispersion of PPTA in the matrix should result in stronger reinforcement.

The method used by Helminiak *et al.* (1980) in their attempts to prepare molecular composites resulted in much thinner microfibrils or molecular bundles. This method was based on Flory's treatment on ternary systems consisting of a rod-like polymer, a conventional random coil like polymer and a solvent (Flory, 1978). According to this treatment there is a critical concentration C_{cr} below which the system is a single isotropic phase consisting of rods randomly dispersed in the coils. If phase separation can be avoided on solidification by rapid coagulation such that the rod/coil mixture is frozen to overcome the unfavorable thermodynamic driving force for phase separation, a molecular composite is obtained. On the other hand, if the concentration is above C_{cr}, phase separation occurs resulting in a rod-rich phase along with a coil-rich phase. The molecular composite is not possible with the two-phase solution. Thus, in the study of the molecular composites of the rigid-rod polymer poly-*p*-phenylenebenzobisthiazole (PBT) and the flexible-coil polymer poly-2,5(6)-benzimidazole (ABPBI), the work was started off with the determination of C_{cr} (Hwang *et al.*, 1983). This was done by slowly titrating the originally biphasic, stir-opalescent solution of known concentration with solvent until a point was reached at which the solution became isotropic and stir-opalescence ceased. The coil polymer ABPBI used in this study had a very high molecular weight (100,000 g/mol). A high solution viscosity and a high degree of entanglement were achieved to protect the blend from phase separation during solidification. C_{cr} was found to change with the molecular weight of PBT and the ratio of PBT/ABPBI in methanesulfonic acid solvent containing 2.5 vol-% of chlorosulfonic acid. With the PBT of 41,000 g/mol and the ratio PBT/ABPBI of 30/70, the critical concentration at room temperature was found to be 3.05 wt-%. The composite fibers were prepared from a solution of 2.5 wt-% (which was below C_{cr}) by extruding through a single-hole spinneret into a water coagulating bath at room temperature. The partially coagulated solution was subsequently drawn to a ratio of 3.4 in a water bath and might be neutralized with NH_4OH to leach out all the residual acids. The neutralized samples were further washed with running deionized water. The bulk specimens were then air dried at ambient conditions. The heat treatment at various temperatures with a further draw ratio of 1.20 was also carried out for comparison. Thus, while the pure ABPBI fiber obtained after neutralization with NH_4OH and heat-treated

at 543 °C was the best to show a Young's modulus of 39.7 GPa, a tensile strength of 1,176 MPa, and an elongation to break of 5.70%, the best composite fiber processed at the same condition showed a Young's modulus of 120 GPa, a tensile strength of 1,363 MPa, and an elongation at break of 1.61%. The high modulus displayed by the 30/70 PBT/ABPBI composite fiber suggested that the modulus (310 GPa) of the reinforcing PBT was about fully utilized in the composite. Using the observed $E_c = 120$ GPa and $E_m = 39.7$ GPa, and assuming $E_f = 310$ GPa, $V_f = 0.3$, the reinforcement efficiency factor calculated from the equation $E_c = f E_f V_f + E_m(1 - V_f)$ was $f = 0.99$. On the other hand, the morphology and structure studies using scanning electron microscopy and wide-angle x-ray diffraction techniques showed no phase segregation in the as-spun fibers of the composites. A molecular level composite was obtained.

In a more detailed study by Krause *et al.* (1986), the heat-treated fiber and film processed from an optically homogeneous solution (C < C$_{cr}$) of 30/70 PBT/ABPBI exhibited no large-scale phase separation. The fiber and film contained crystallites of both PBT and ABPBI with lateral dimensions no larger than 3 nm which were well oriented in the fiber and planar isotropically oriented in the film. The PBT homopolymer was dispersed in the matrix at the molecular level in ordered regions at a scale no larger than 3 nm, resulting in a rigid-rod molecular composite. However, if the solution was more concentrated with C > C$_{cr}$ the resulted fiber and film contained brittle, 100 nm–4,000 nm long ellipsoidal particles which were phase-separated from the surrounding matrix material. The particles in such a film were larger (2,000 nm–4,000 nm) than that in the fiber (100 nm–200 nm). The shearing on the phase-separated domains during fiber spinning broke the particles and reduced their size. Because of the phase separation and to a lesser extent the lower degree of orientation, the fiber and film prepared from the concentrated solution showed much lower mechanical properties as shown in Table 5.15.

Although the concept of the molecular composite was demonstrated by the work on PBT/ABPBI, the resulted composite was not melt-processible since the melting points (if there is one) of the two component polymers are well above 800 °C. Efforts were then put on systems with a thermoplastic polymer as the matrix. One such system was PBT/nylon 66 (Chuah *et al.*, 1987). Thus, the PBT/nylon 66 in different ratio was dissolved in methane sulphonic acid to make 2 wt-%–3 wt-% (<C$_{cr}$) solutions. They were processed by extrusion and rapid coagulation into thin films. The films were optically clear and did not show gross phase separation in

Table 5.15.   Mechanical properties of the PBT/ABPBI molecular composites in comparison with the phase-separated composites*.

Fiber or film	Modulus	Tensile strength	Elongation at break
PBT fiber	310 GPa	3,000 MPa	1.1%
ABPBI fiber	36 GPa	1,100 MPa	5.2%
PBT/ABPBI (30/70) fiber			
From C > C_{cr}	11 GPa	310 MPa	13%
From C < C_{cr}	120 GPa	1,300 MPa	1.4%
PBT/ABPBI (30/70) film			
From C > C_{cr}	1.1 GPa	35 MPa	5.6%
From C < C_{cr}	88 GPa	920 MPa	2.4%

* Source: Krause *et al.*, 1986.

microscopy studies. However, the molecular composite did undergo heat induced phase separation when heated to the nylon melting temperature (260 °C). For instance the as-processed 70/30 PBT/nylon 66 specimen showed no domain features in the back scattering SEM micrograph. After heating to 280 °C for one and one half hours, distinct phase separated PBT-rich domains 2 μm–7 μm in size appeared as bright areas in the micrograph. Further studies showed the thermally induced phase separation could occur at temperatures well below the peak melting but much higher than the nylon glass transition. Partial melting was needed. Segmental motion alone at Tg was not sufficient to cause phase separation. The result indicated that even though a thermally moldable molecular composite was prepared by using thermoplastic polymers as the matrix, phase separation would occur if the material was melt-processed. Compression molding at lower temperatures was useful to make laminated articles of the thermoplastic molecular composites. Otherwise the hydrated molecular composite was consolidated by a hot press into desired specimens under pressure and temperature in a closed mold (Wang *et al.*, 1988). In one experiment, the pressure was increased in 30 minutes to 45 MPa; the temperature was then increased in 30 minutes to 175 °C. The specimen was kept at this temperature and pressure for 30 more minutes. It was then dried in vacuum at 100 °C for 24 hr, and heat-treated at 175 °C for 24 hr. The specimen thus prepared showed much higher mechanical properties than the matrix polymer. The reinforcement efficiency factor was 0.5–0.7 for the rod polymer PBT.

The phase separation of a molecular composite was also observed in PBT/ABPBI blends by Hwang *et al.* (1983). The phenomenon of a

thermotropic liquid crystalline composite had been studied by Nakai *et al.* (1986). Obviously in such physical blends of rigid rod/flexible coil polymers there is a thermodynamic driving force for phase separation (Flory, 1978). Molecular composites can be obtained only through solutions below a C_{cr} which is as low as only a few percent. Yet, the higher is the molecular weight of the rod molecule, the lower is the value of the critical concentration. These inherent difficulties make the process impractical. Efforts have since been made in searching for new systems such as the chemically bonded composites of ABA or AB block copolymers of the rod and the coil polymers (Takayanagi and Goto, 1984; Tsai *et al.*, 1985; Chang and Lee, 1996). The covalent bond was expected to force the two components to be in close proximity. As a matter of fact, *e.g.*, Tsai and coworkers (1985) did find that there were no discernible aggregates of PBT in the vacuum cast films of the block copolymer ABPBI/PBT/ABPBI. This was in contrast to the extensive phase separation found in the vacuum cast films of the physically blended PBT/ABPBI composites (Hwang *et al.*, 1983). However, there is again a critical concentration of phase separation for these block copolymers due to inherent thermodynamic immiscibility of the rod and coil components. Although the mechanical properties of the specimens prepared from these molecular composites were found to be improved, the phase-separated rigid-rod/thermoplastic blend is by and large no better in properties than a corresponding macroscopic fiber reinforcing composite (Hwang and Helminiak, 1989). Enhanced and desirable properties may only be realized in a true molecular composite. One approach to producing a true molecular composite is to make the rod and coil components thermodynamically miscible by introducing attractive interaction such as hydrogen bonding (Painter *et al.*, 1991) and ionic interaction.

Some recent examples demonstrating the molecular dispersion of rod polymer molecules in coil polymer matrices due to ionic interactions were given by Parker *et al.* (1996). These systems were based on three types of ionic PPTA's (Figure 5.4) and polar polymers, such as poly(4-vinylpyridine) (PVP), poly(vinyl chloride) (PVC), poly(ethylene oxide) (PEO), and poly(styrene-co-acrylonitrile) (S-AN). Due to the ionic-dipole interactions the rod-coil polymer pairs formed molecular composites as revealed by optical clarity, polarized microscopy, Tg measurements, as well as TEM observations. More significantly the molecular composites based on amorphous matrix polymers (*e.g.*, PVP) were all transparent and showed no phase separation upon heating. Therefore they are melt-processable. As would expected, the mechanical properties of the molecular composites were
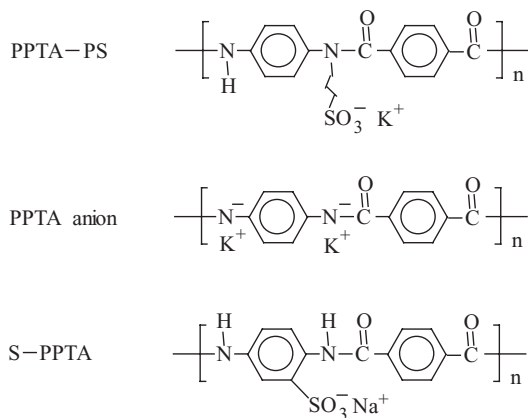
Figure 5.4.   Chemical structures of ionic PPTA's (Parker *et al.*, 1996).

significantly higher than that of the matrix polymers. An addition of only 2 wt-% of PPTA anion to PVP was found to have enhanced the modulus by 50%. The tensile strength and ductility of the composite were also much higher. These results have demonstrated the enhanced miscibility by strong interactions for the formation of stable dispersion in molecular composites. However, the introduction of ionic groups will have side effects on the properties of the material. For instance, the moisture uptake will be high which in turn will affect the dimensional stability and physical properties of the material.

While the reinforcing effect of liquid crystalline polymers can be realized through the molecular composites as discussed above, the most attractive approach to most researchers is through the formation of "in situ" composites in which the thermotropic liquid crystalline polymer molecules orient to form reinforcing microfibrils during melt-processing. Joseph *et al.* (1983, 1985) and Siegmann *et al.* (1985) are among the first to apply the concept of "self-reinforcement" (Menges and Hahn, 1981) of thermotropic liquid crystalline polymers (TLCP) in blends of thermoplastic polymers with TLCP. Joseph and coworkers studied the blends of PET/60HBA with PET. The injection molded specimens had a skin-core structure. The TLCP appeared in the skin as oriented macroscopic rod-like domains. The bending modulus in the direction of flow of the blend with 50 wt-% of PET/60HBA was three times higher than that of the pure PET injection molded under similar conditions. Siegmann *et al.* reported the in situ formation of LCP

fibrils in the injection molded blends of a thermotropic liquid crystalline copolyester (HNA/HBA) with an amorphous polyamide (PA). In this study, the injection temperature was 295 °C–300 °C which was above the melting temperature of the liquid crystalline polymer. They found that both the elastic modulus and ultimate tensile strength first increased linearly with increasing liquid crystalline polymer content and then continued to increase at a lower rate; simultaneously, the ultimate elongation sharply decreased. The higher modulus LCP particles dispersed in the polyamide matrix acted as reinforcing components. The morphology of the blends was studied using scanning electron microscopy. The etched surfaces of a 10/90 LCP/PA blend and a 15/85 blend revealed ellipsoidal LCP domains embedded in the PA matrix. The 25/75 blend had a morphology that contained both particulate and fabrillar LCP structures with various elongated fibrils or rod-like structures. The etched surface of a 50/50 LCP/PA showed rod-like or fibrillar structures. Thus the blends consisted of two phases, the structure of which was composition dependent. At low liquid crystalline polymer content the liquid crystalline polymer was dispersed as ellipsoidal particles; at high content it formed rodlike structures or fibrils. A core-shell structure was also observed for the injection molded blends. The core sections had lower orientation and lower modulus and strength but a higher elongation than those of the whole specimens. The concentration condition for fibril formation observed in this study was in contrast to that reported by Isayev and Modic (1987) on a different blend system with two naphthalene-moiety-based liquid crystalline polymers and polycarbonate. In the latter experiment the fiber in matrix morphology was found to be achievable only at low (<10%) concentrations of the liquid crystalline polymer phase.

Kiss (1987) is probably the first to actually use the term "in situ composite" to describe the blends of TLCP and thermoplastics where the reinforcing component comes into existence during molding or extrusion. According to Kiss, since the thermotropic liquid crystalline polymers form fibers extremely readily in melt-processing, they would form fibrous domains or inclusions in a matrix polymer when melt blended. Given the inherent strength and stiffness of the thermotropic polymers, these fibrous inclusions would then act as a reinforcement like the chopped glass fibers or "meltable chopped glass fibers". The idea was verified by experiments on melt-processed blends of the naphthalene-moiety-based thermotropic polyesters (liquid crystalline polymer polyester) or a polyesteramide of Celenese Corp. The isotropic components were thermoplastic polymers including polyether sulfone (PES), poly(chlorotrifluoro-ethylene) (Aclon),

Table 5.16.   Properties of injection-molded minitensile bars of in situ composites[*].

Material	Tensile strength	Elongation	Tensile modulus	Flex strength	Flex modulus
PES	63.6 MPa	122%	2.50 GPa	101.9 MPa	2.58 GPa
LCP polyester	235.1 MPa	3.8%	13.1 GPa	159.9 MPa	9.38 GPa
LCP polyesteramide	385.4 MPa	1.68%	26.2 GPa	237.1 MPa	15.0 GPa
PES/LCP polyester	125.5 MPa	3.8%	4.99 GPa	125.1 MPa	4.11 GPa
PES/LCP polyesteramide	172.4 MPa	2.6%	8.82 GPa	157.2 MPa	6.78 GPa
PES/Glass fiber	140 MPa	3%	1.24 GPa	190 MPa	8.4 GPa
Aclon	27.0 MPa	21.7%	1.70 GPa	52.4 MPa	2.75 GPa
Aclon/LCP polyester	70.3 MPa	2.5%	5.24 GPa	83.4 MPa	3.83 GPa
Ardel	71.0 MPa	155%	1.52 GPa	67.2 MPa	1.76 GPa
Ardel/LCP polyester	102 MPa	5.3%	4.27 GPa	100.6 MPa	3.32 GPa
Lexan	66.9 MPa	100%	2.32 GPa	93.1 MPa	2.47 GPa
Lexan/LCP polyester	121 MPa	3.49%	5.72 GPa	132 MPa	4.54 GPa
Ultem	91.0 MPa	59%	3.05 GPa	141 MPa	3.34 GPa
Ultem/LCP polyester	129 MPa	4.3%	5.15 GPa	156 MPa	4.78 GPa
Ultem/LCP polyesteramide	95.8 MPa	1.54%	7.45 GPa	103 MPa	6.18 GPa

[*] LCP content (or the glass fiber) in composite is 30 wt-%.
Source: Kiss, 1987.

polyacrylate Ardel, polycarbonate Lexan, polyetherimide Ultem, and so on. Four types of blending equipment were used and, to a first approximation, there was no difference for different techniques. In Table 5.16 are representative results showing liquid crystalline polymer reinforcement in injection-molded minitensile bars of in situ composites. By inclusion of 30 wt-% of liquid crystalline polymer the tensile and flex modulus were significant increased by 100%–300%. The increase in tensile and flex strength was somewhat less significant by 30%–100%. The extruded strands showed similar properties. Some of the injection-molded blends gave strengths over 130 MPa and moduli over 6 GPa which was well in the property range of glass-filled engineering resins. In comparison, glass fibers are much cheaper than liquid crystalline polymers; but with liquid crystalline polymer, the processing is much easier with significantly lower viscosity and little wear on the processing equipment.

The morphology of the fracture surfaces of both the extruded and injection-molded specimens was studied via scanning electron microscopy (SEM). Although there were many morphologies across the fracture surfaces, highly elongated liquid crystalline polymer domains parallel to the flow direction were observed for both the extruded and molded specimens.

In order to determine what conditions were necessary for the development of a fibrillar morphology of the liquid crystalline polymer in blends, Blizard and Baird (1987) prepared blends of polycarbonate (PC) and nylon 66 with the liquid crystalline polymer PET/60HBA under different processing conditions. The morphology of the blends was then examined using SEM. They showed that in shear fields as generated in a cone and plate rheometer, fibrils of the liquid crystalline polymer could not be generated under isothermal conditions even at as high as 10,000 strain units. However, extensional flow fields such as those that exist at the entrance to the capillary, promoted the formation of fibrils of the LCP phase.

At about the same time, Weiss *et al.* (1987) studied the blends of polystyrene and a thermotropic LCP with flexible chain segments at LCP concentrations below 10 wt-%. The LCP was immiscible with PS. When an extensional component of flow was present during processing, the LCP forms an elongated fibrous phase oriented in the flow direction. The reinforcing LCP phase was observed to consist of fibrils having high aspect ratios of 20–150. The mechanical properties were improved by the fibrils; for example, at a liquid crystalline polymer concentration of 4.5 wt-%, the modulus increased by 40% vs. pure PS. In addition, a reduction in viscosity at higher shear rates was also reported. Thus, the liquid crystalline polymer was demonstrated to function as both a processing aid and a reinforcing filler.

The undesirable side of the self-reinforced or in situ composites of liquid crystalline polymer is the anisotropy of mechanical properties of the product. While the property in the flow direction is high, the property in the direction transverse to flow is usually much inferior. For example (Menges and Hahn, 1981), the molded liquid crystalline polymer PET/60HBA showed an ultimate tensile strength of 107 MPa in the flow direction but only 28.4 MPa in the direction perpendicular to the flow. The flexural modulus was 11.8 GPa and 1.67 GPa respectively in the two directions. The notched izod impact strength is also anisotropic — 317 Jm in the flow direction and 31.4 Jm in the transverse. Another problem met in an injection molded article is the poor property in the weldline regions. Kiss (1987) carried out a weldline study for isotropic polymers and for in situ composites by using an ASTM standard tensile bar gated from both ends. This produced the most severe weldline possible when the flows from both gates impinged at the center of the specimen. The comparison was made in Table 5.17. While the isotropic polymers usually have a good retention of strength and modulus in weldlines, the strength is poor in weldline regions in the specimens of the in situ composites.

Table 5.17.   Comparison of normal and weldline bars*.

Material	Specimen	Tensile strength	Elongation	Tensile modulus
PES	Normal	56.1 MPa	19.6%	2.65 GPa
	Weldline	60.5 MPa	9.68%	2.61 GPa
PES/LCP polyesteramide	Normal	88.9 MPa	1.45%	7.45 GPa
	Weldline	10.3 MPa	0.19%	6.07 GPa
Ardel	Normal	40.1 MPa	4.27%	1.87 GPa
	Weldline	28.7 MPa	1.44%	2.19 GPa
Ardel/LCP polyester	Normal	73.1 MPa	2.72%	3.87 GPa
	Weldline	18.6 MPa	0.61%	3.27 GPa
Ardel/LCP polyesteramide	Normal	76.2 MPa	1.69%	5.59 GPa
	Weldline	32.3 MPa	1.25%	3.06 GPa
Lexan	Normal	58.9 MPa	97%	2.34 GPa
	Weldline	45.2 MPa	36%	2.28 GPa
Lexan/LCP polyester	Normal	80.0 MPa	3.4%	3.89 GPa
	Weldline	32.3 MPa	1.25%	2.92 GPa
Lexan/LCP polyesteramide	Normal	120 MPa	1.99%	8.07 GPa
	Weldline	29.6 MPa	0.71%	4.38 GPa

* Source: Kiss, 1987.

There has been a great challenge in material design to fully utilize the superior properties of liquid crystalline polymers while limiting the inferior influence to the lowest possible extent. Significant progress has been made in recent years. These include a better understanding of the processing–structure–property relationship, the development of advanced mixing techniques, and application studies. A recent review was given by Isayev (1996). Some statements in this review are cited below. Rheological studies have suggested that the most important parameter governing the fibrillation is the viscosity ratio of thermoplastic to liquid crystalline polymer. Most results indicate that the fibrillation is enhanced as the viscosity ratio of liquid crystalline polymer to thermoplastic becomes less than unity. The fibrillation is also affected by the type of deformation. The prevailing opinion is that the elongational flow causes more extensive fibrillation than shear flow. Concentration of liquid crystalline polymer also plays a significant role in fibrillation. There are many cases where liquid crystalline polymer fibrils are found in blends at low concentrations. In many others a strong fibrillation was observed at a high concentration of liquid crystalline polymer. Apparently, the effect of the concentration on fibrillation in blends depends on the nature of components. The fibrillation is also dependent on mixing techniques. The dual-extruder mixing

method has a significant advantage over the blending in a single screw extruder with respect to formation of the in situ fibers and accordingly with respect to mechanical properties. In particular, single screw extruder blends showed a skin-core fibril-droplet structure, while the dual extruder blends indicated continuous liquid crystalline polymer fibers. The interfacial interaction between components is another important factor for composites with good mechanical properties. This can be realized by the proper choice of the components for blending with liquid crystalline polymer. The interactions between electron donor and acceptor groups, or hydrogen bonding between the two components may be utilized. In addition, a compatibilizer may be used to improve interaction at the interface between the components. The possible areas of applications of liquid crystalline polymer blends described in the recent literature include the manufacture of high barrier containers and films, electronic and electrical components, tubing and light-weight structures, health care and industrial and consumer goods.

This page intentionally left blank

Chapter 6

Physical Properties and Applications of Liquid Crystalline Polymers
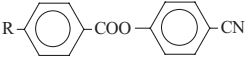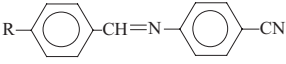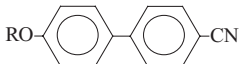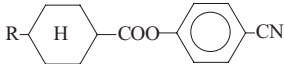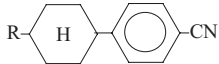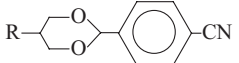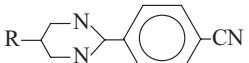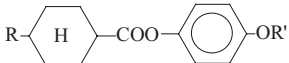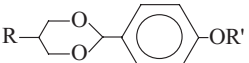
6.1. ELASTIC PROPERTIES OF LIQUID CRYSTALLINE POLYMERS

According to the elastic continuum theory of liquid crystals which was introduced in Chapter 1, the three kinds of deformations can be described by three elastic constants, K_{11}(splay), K_{22}(twist) and K_{33}(bend). In the case of small molecular mass liquid crystals, the three constants are mainly determined by the chemical composition of the liquid crystalline molecules. Among them, K_{22} is the smallest while the other two are approximately close. All three elastic constants are of the order of 10^{-12} N. The elastic constants of some important liquid crystals are listed in Table 6.1. Each kind of liquid crystals is a mixture of R5-pentyl and R6-hexyl homologues in the ratio of $40:60$. The data are obtained at the temperature of $T = T_c - 10\,^\circ\text{C}$ where T_c is the clear temperature.

For liquid crystalline polymers, the elastic constants are determined not only by the chemical composition but also by the degree of polymerization, *i.e.*, the length of the molecular chain. One main aim of this section is to address the effects of molecular chain length on the elastic constants of liquid crystalline polymers. Figure 6.1 shows the three typical deformations of nematic liquid crystalline polymers. The length and flexibility of liquid crystalline polymers make the elastic constants of liquid crystalline polymers quite different from those of monomer liquid crystals.

de Gennes (1977) argued that a splay deformation is unlikely to occur in the rod-like liquid crystalline polymers because of the difficulty of maintaining the splay configuration while keeping the molecules from conflicting and overlapping. The molecular chain ends of liquid crystalline polymers in

Table 6.1.   Elastic constants $K_{11}(\times 10^{-12}\,\mathrm{N})$ of some important liquid crystals.

Chemical composition	K_{11}	K_{22}	K_{33}
R—〇—COO—〇—CN	6.05	3.62	10.10
R—〇—CH=N—〇—CN	6.25	3.16	8.70
R—〇〇—CN	6.70	3.60	9.00
RO—〇〇—CN	5.15	3.10	6.40
R—(H)—COO—〇—CN	5.50	3.16	8.50
R—(H)—〇—CN	6.75	3.30	10.50
R—(O,O)—〇—CN	4.90	3.14	7.00
R—(N,N)—〇—CN	7.00	3.86	8.10
R—(H)—COO—〇—OR'	6.20	3.43	7.95
R—(O,O)—〇—OR'	7.95	3.89	6.75

the splay-deformed domain have to be segregated, as shown in Figure 6.2, otherwise, a gradient of density must accompany the splay deformation

$$\nabla \cdot \mathbf{n} = -\mathbf{n} \cdot \frac{\nabla \rho}{\rho}, \tag{6.1}$$

where ρ is the density of rod-like liquid crystalline polymer chains penetrating the plane normal to the directors. As a result the density in
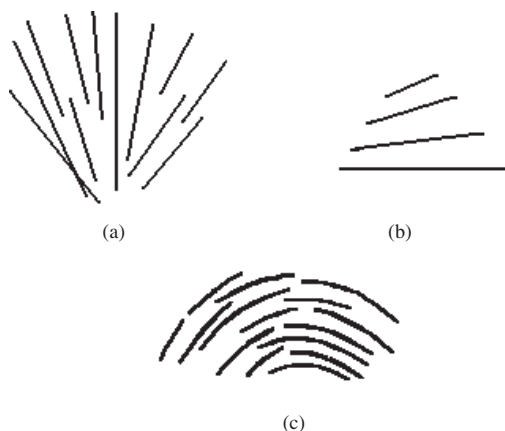
Figure 6.1.   Three typical deformations in rod-like liquid crystalline polymers. (a) splay; (b) twist; (c) bend. (Modified from Donald and Windle, 1992.)
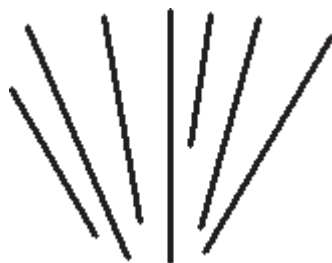
Figure 6.2.   The segregation of molecular terminals in the splay-deformed domain of rod-like liquid crystalline polymers.

the deformed zone should be lower than those in the undeformed area, and a gradient of density should occur. Apparently, this is unlikely to happen in a bulk material.

In the case of very long rigid rods it is very difficult for the bend deformation to appear, shown in Figure 6.3. This is due to the steric overlap effect. However, a real liquid crystalline polymer chain is somewhat flexible, which makes bend deformation possible. This is the case for those liquid crystalline polymers with flexible spacers in their main chains. Even for those not having flexible spacers in their main chains, a bend configuration can also exist so long as their persistence length is smaller than the bend radius.

Concerning the twist deformation, shown in Figure 6.1(b), the parallel molecules are arranged in parallel planes but are twisted in these successive
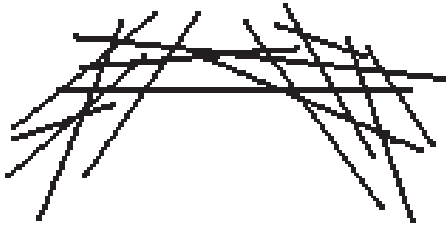
Figure 6.3.   The bend deformation is difficult to form because of steric overlap.

planes. In fact, liquid crystalline polymer molecules do not always stay within planes, but often stretch out to the nearby planes in which the molecules have slightly different orientations. This effect tends to destroy the typical twist configuration and becomes frequent due to the flexibility.

The above qualitative description illustrates that the molecular length has an important effect on the elastic constants of liquid crystalline polymers.

Priest (1973) and Straley (1973), in terms of the classical virial expansion, the Onsager theory (referred to in Section 2.1) and the curvature moduli theory, derived the elastic constants of rigid liquid crystalline polymers. The free energy varies according to the change of the excluded volume of the rods due to the deformation. The numerical calculation of elastic constants (Lee, 1987) are shown in Table 6.2.

The three elastic constants are reduced by $k_B T/D$ (D is the diameter of the rod). They are the functions of the dimensionless parameter $Q = \phi L/D$ with ϕ the volume fraction of the liquid crystalline polymers and L the molecular length. It is shown in the Table 6.2 that the three elastic constants increase as Q and the order parameter S increase. Among them the bend elastic constant K_{33} varies dramatically, and finally becomes infinite as S approaches unity in the perfectly ordered state.

Assume that the degree of the ordering of liquid crystalline polymers is high and the orientational distribution function is simply Gaussian, Odijk (1986) developed the analytical formulae for elastic constants

$$\frac{K_{11}}{\frac{k_B T}{D}} \approx \frac{3K_{22}}{\frac{k_B T}{D}} = \frac{7}{8\pi}\phi\frac{L}{D},$$

$$\frac{K_{33}}{\frac{k_B T}{D}} = \frac{4}{3\pi^2}\left(\phi\frac{L}{D}\right)^3.$$

$$(6.2)$$

K_{11} and K_{22} are the linear functions of Q while K_{33} varies with Q^3.

Table 6.2. The relationship of elastic constants $K_{ii}(k_B T/D)$ and $Q = \phi L/D$ or S. (From Lee, 1987.)

Q	S	K_{11}	K_{22}	K_{33}
3.60	0.598	0.465	0.155	1.558
3.70	0.656	0.552	0.184	2.115
3.80	0.697	0.623	0.208	2.740
3.90	0.729	0.684	0.228	3.334
4.00	0.755	0.739	0.246	3.948
4.20	0.794	0.838	0.279	5.251
4.50	0.835	0.967	0.322	7.429
4.75	0.859	1.065	0.355	9.477
5.00	0.859	1.156	0.385	11.76
5.25	0.892	1.244	0.415	14.29
5.50	0.904	1.328	0.443	17.09
6.00	0.923	1.490	0.497	23.55
6.50	0.936	1.646	0.549	31.24
7.00	0.946	1.798	0.599	40.29
7.50	0.953	1.948	0.649	50.80

Experimental work is preliminary. The ratios $K_{33}/K_{22} = 43$ and $K_{11}/K_{22} = 2.5$ for TMV (Hurd *et al.*, 1985), and $K_{33}/K_{22} = 13$ for PBLG (Taratuta *et al.*, 1985) are not too far away from the theory.

In the case of concentrated solutions or melts of liquid crystalline polymers, the Onsager theory and hence the above arguments are not applicable. It is also not applicable to the rather flexible liquid crystalline polymers.

If the semi-flexible liquid crystalline polymers are well stretched along the director and thus the order parameter is high, the underlying equations are valid and can demonstrate qualitatively the effect of chain flexibility on the splay elastic constant.

In fact, the flexibility (or rigidity) of polymer chains affects the elastic constants. The molecular bend elasticity ε is a measure of the flexibility of liquid crystalline polymers and the persistence length is associated with the chain flexibility by

$$l = \frac{\varepsilon}{k_B T}. \tag{6.3}$$

A large l represents a rigid chain.

To strictly analyze the conformational distribution of liquid crystalline polymers and accordingly, to calculate the elastic constants are very difficult. Odijk (1985) derived the elastic constants for semi-flexible

liquid crystalline polymers

$$\frac{K_{11}}{\frac{k_B T}{D}} \approx \frac{3K_{22}}{\frac{k_B T}{D}} \approx 3\left(\phi\frac{l}{D}\right)^{1/3}$$

$$\frac{K_{33}}{\frac{k_B T}{D}} \approx \phi\frac{l}{D}.$$

(6.4)

It is found that the elastic constant ratio (K_{11}/K_{33}) is small in the rod-like systems, and becomes further smaller as the chain length L increases. The ratio is larger in semi-flexible chains, and increases proportionally as the chain length increases.

K_{11} is usually greater than K_{33} for thermotropic liquid crystalline polymers. Two neighboring splay deformations tend to compensate each other. This effect tends to lower K_{11}.

Several experiments were carried out to investigate the elastic constants of nematic polymers. They were essentially in agreement with the theory. But the available data are insufficient for checking theoretical predictions. Systematic and careful experiments are required to investigate the relationship of elastic constants to the flexibility and molecular length. We will introduce some measurement techniques and experimental data for elastic constants.

The elastic constants of liquid crystalline polymers can be measured in terms of the Frederiks transitions under the presence of a magnetic or electric field. Raleigh light scattering is also a method for measuring the elastic constants. Those techniques successfully applied to small molecular mass liquid crystals may not be applicable to liquid crystalline polymers. This is why very few experimental data of elastic constants are available for liquid crystalline polymers.

The rigid polymers PBLG in solution is an exception which has been well studied. There have been a few experimental data on the elastic constants, especially on the twist elastic constants.

PBLG is a para-magnetic material with positive magnetic susceptibility anisotropy χ_a. It exhibits the cholesteric phase in various solutions with a helical pitch ranging from ten to tens of microns. The unwinding effect is an approach to measure the twist elastic constant K_{22}.

A sheet of cholesteric liquid crystal (pitch is P_0) is sandwiched between two glass plates with the gap d being ten microns. The helical axis of cholesteric liquid crystals in the absence of a magnetic field is defined along the Z axis, shown in Figure 6.4, and θ is the deformation angle between
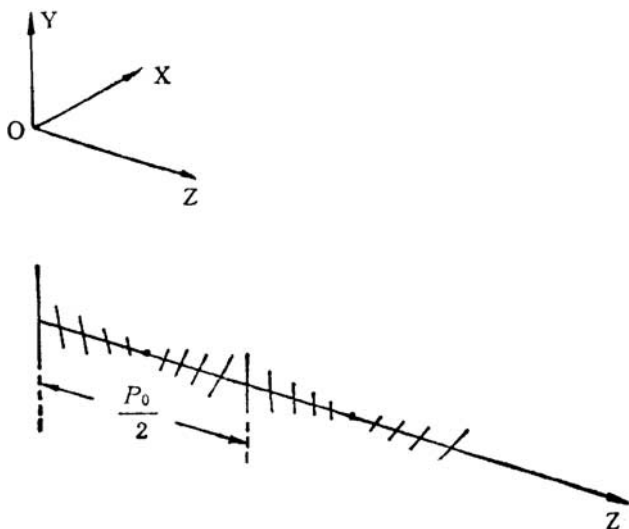
Figure 6.4.   Cholesteric liquid crystals: unwind effect.

the director and the X axis. The director is then written as

$$n_1 = \sin\theta(z),$$
$$n_2 = \cos\theta(z),$$
$$n_3 = 0.$$

If a magnetic field H is applied along the Y axis, the cholesteric liquid crystal has only the twist deformation.

The free energy per unit cell area F is accordingly

$$F = \frac{1}{2}\int_0^d \left[K_{22}\left(\frac{d\theta}{dz} + \frac{2\pi}{P_0}\right)^2 - \chi_a H^2 \sin^2\theta \right] dz, \qquad (6.5)$$

where $\chi_a = \chi_\parallel - \chi_\perp$ is the magnetic susceptibility anisotropy of the cholesteric liquid crystals. The equilibrium Euler-Lagrange equation is thus

$$\varsigma^2 \frac{d^2\theta}{dz^2} + \sin\theta\cos\theta = 0, \qquad (6.6)$$

where the magnetic coherence length

$$\varsigma = (K_{22}/\chi_a H^2)^{\frac{1}{2}}. \qquad (6.7)$$

The primary integral gives

$$\left(\varsigma \frac{d\theta}{dz}\right)^2 + \sin^2\theta = k^{-2}, \tag{6.8}$$

where $k^2 < 1$ and k^{-2} is the integral constant. The further integral gives the relation of θ and z as

$$\frac{1}{k}\frac{z}{\varsigma} = \int_0^\theta \frac{d\theta'}{(1 - k^2 \sin^2\theta')^{\frac{1}{2}}} = F(\theta, k), \tag{6.9}$$

where $F(\theta, k)$ is the elliptic integral of the first kind. In the absence of a magnetic field, no deformation occurs and the twist angle is a linear function of z. But as a magnetic field is applied, the dependence of θ on z is no longer a linear function. The Elliptic integral of the first kind $F(\theta, k)$ is a periodic function with the period $4K(k)$ where $K(k) \equiv F(\pi/2, k)$, the complete elliptic integral of the first kind. Thus the helical pitch P for a magnetic field H is

$$P = 4k\varsigma K(k) \tag{6.10}$$

and the integral constant k is expressed implicitly by

$$\frac{E(k)}{k} = \pi^2 \varsigma P_0, \tag{6.11}$$

where $E(k) = \int_0^{\pi/2}(1 - k^2 \sin^2\theta)^{\frac{1}{2}} d\theta$, is the complete elliptic integral of the second kind. Substituting it into Equation 6.10 then yields the ratio of the current to intrinsic helical pitch as

$$P/P_0 = \left(\frac{2}{\pi}\right)^2 K(k)E(k) \tag{6.12}$$

If k is small, the ratio is rewritten approximately as

$$\frac{P}{P_0} \approx 1 + \frac{1}{32}\left(\frac{P_0}{\varsigma}\right)^4. \tag{6.13}$$

It is noted that for a small magnetic field, the helical pitch increases slowly until $k^2 = 1$ at which one has $E(k) = 1$ and $K(k) \to \infty$ and then

$$P/P_0 \to \infty. \tag{6.14}$$
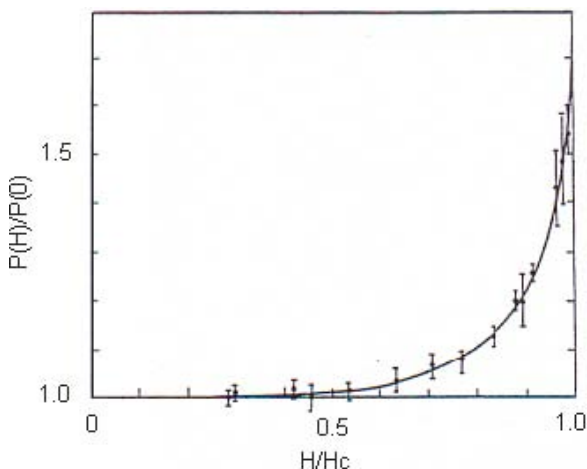
Figure 6.5. The pitch P/P_0 *vs.* magnetic field H/H_c for 20% PBLG solution in dioxane. (Modified from Duke and DuPre, 1974b.)

The cholesteric liquid crystal then becomes a nematic. The critical magnetic field H_c is then given by

$$H_c = \frac{\pi^2}{2P_0}\sqrt{\frac{K_{22}}{\chi_a}}. \tag{6.15}$$

Figure 6.5 shows the dependence of P/P_0 of 20% PBLG solution in dioxane on the reduced magnetic field H/H_c (Duke and DuPre, 1974a). P_0 is 30 microns. As H/H_c is greater than 0.7, P/P_0 increases rapidly. At H_c, the cholesteric-nematic transition occurs. For a 20% solution of PBLG of molecular weight 310,000 in dioxane, H_c is 5.06 kG (Duke and DuPre, 1974b). The solid curve is the theoretical prediction and the circles are the experimental data. A good agreement was found between the theory and experiments.

The twist elastic constant of lyotropic liquid crystalline polymers, e.g., PBLG, depends on the molecular weight and on solvent as well. Table 6.3 lists the value of pitch, threshold magnetic field and twist constant for various solvents (DuPre, 1982; Parthasarathy *et al.*, 1988) where PBLG molecular weight being 310,000. If the molecular weight of PBLG increases to 550,000, the twist constant is one order of magnitude higher for PBLG solution in dichloromethane, *i.e.*, 58.2×10^{-12} N. Recently, DuPre group (1988) carefully measured the twist constant of PBLG in various solvents.

Table 6.3. The pitch, magnetic threshold, magnetic susceptibility anisotropy and twist constant of PBLG(Mn = 310,000) at three kinds of solvents. (From DuPre, 1982.)

Solvent	P_0 (μm)	H_c (kG)	K_{22}/χ_a	χ_a (10^{-8} esu/cm^3)	K_{22} (10^{-12} N)
dioxane	30	5.06	9.6	$0.64 + 0.07$	0.62
trichloromethane	42	6.87	33.7	$0.64 + 0.09$	2.1
dichloromethane	80	5.23	72.3	$0.74 + 0.05$	5.4

Table 6.4. Data of K_{22}/χ_a of PBLG (Mn = 150,000) solutions. (From Parthasarathy *et al.*, 1988.)

Solvent	K_{22}/χ_a
cyclohexanone	4.7
dioxane	9.5
dioxane/60% trifluoro-acetyl fluoride	14.4
pyridine	20.0
nitrobenzene	18.1
metatoly	22.0

The results are listed in Table 6.4, the molecular weight of PBLG being 150,000, and the equivalent molecular length is 1000 Å.

The twist elastic constant of PBLG is a function of the concentration in solution, seen from Figure 6.6(a), and of the temperature, shown in Figure 6.6(b). It is demonstrated that K_{22} is approximately proportional to the concentration in solution as the theory predicts and decreases as temperature increases and thus the order parameter decreases.

Three kinds of Frederiks transitions can be used to measure the three elastic constants of nematic polymers. The magnetic threshold fields H_{ci} are functions of $K_{ii} (i = 1, 2, 3)$ respectively,

$$H_{c,i} = \frac{\pi}{d}\sqrt{\frac{K_{ii}}{\chi_a}}. \tag{6.16}$$

When the applied magnetic field is beyond the threshold, the deformation of the liquid crystal (the director field) increases with an increasing field.

The deformation of the director can be probed by optical transmission, electric capacitance, conoscopic pattern, *etc.* The experimental set-up
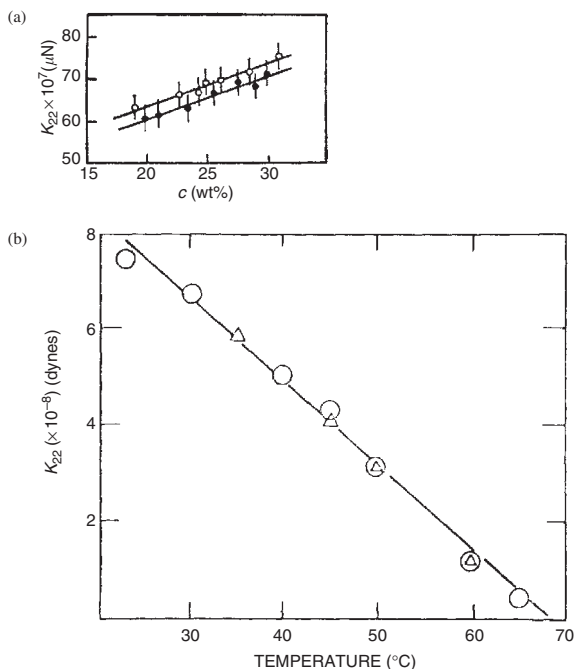
Figure 6.6.   Twist constant of PBLG in dioxane is plotted against (a) concentration at 20 °C (○) and 25 °C (●), (From DuPre and Duke, 1975), and (b) temperature for up (○) and down (△). (From DuPre and Samulski, 1978.)

to measure the transmission of the liquid crystal cell against the applied magnetic field is shown in Figure 6.7.

The optical intensity is associated with the optical path shift δ of the liquid crystal sheet by

$$I = I_0 \sin^2 \left(\frac{\delta}{2}\right) \tag{6.17}$$

and

$$\delta = \frac{\pi}{\lambda} \int_0^d (n_o - n_e)dz, \tag{6.18}$$

where

$$n = n_o n_e (n_e^2 \sin^2 \theta + n_o^2 \cos^2 \theta)^{-\frac{1}{2}} \tag{6.19}$$
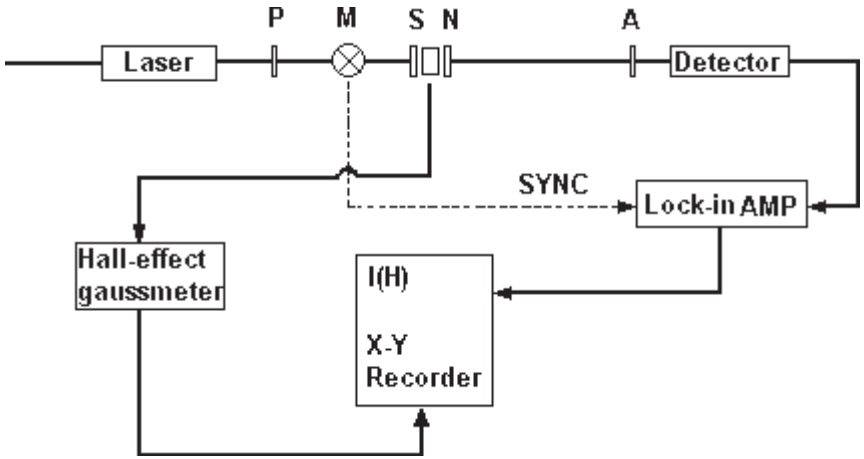
Figure 6.7.   Experimental set-up to measure transmission of liquid crystal cell against applied magnetic field. (Modified from DuPre, 1982.)

and λ is the wavelength of light and I_0 is the incident beam intensity, θ is the deformation angle, n_o and n_e are the refractive indices of ordinary and extraordinary light, respectively. The optical path shift for the first kind of Frederiks transition is derived according to Equation (1.20) of Chapter 1 as

$$
\delta = \frac{2\pi n_o d}{\lambda}
$$
$$
\times \left\{ 1 - \frac{2H_c}{\pi H} \int_0^d d\chi \left[\frac{1 + \alpha \sin^2 \theta_m \sin^2 \chi}{(1 - \sin^2 \theta_m \sin^2 \chi)(1 + \beta \sin^2 \theta_m \sin^2 \chi)} \right]^{\frac{1}{2}} \right\},
$$
$$
(6.20)
$$

where $\alpha = K_{11}/K_{33}$, $\beta = n_o^2/n_e^2 - 1$, θ_m is the tilt angle of the director at the middle of a cell, and $\sin \theta = \sin \theta_m \sin \chi$.

The transmission *vs.* magnetic field H/H_c is plotted in Figure 6.8, where $K_{11} = 5.19 \times 10^{-12}$ N, $K_{33} = 6.49 \times 10^{-12}$ N. Four curves are drawn
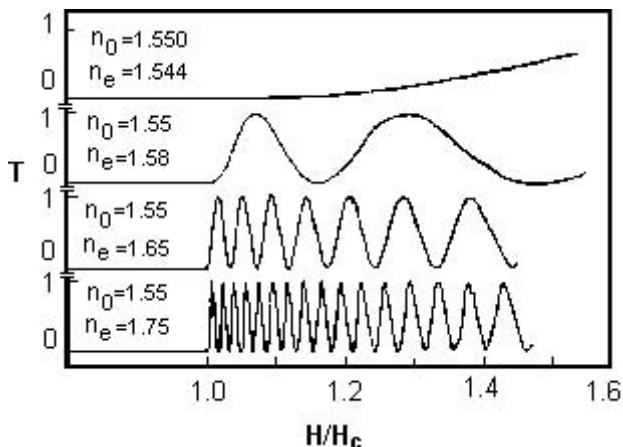
Figure 6.8.   The transmission *vs.* magnetic field H/H_c. (From DuPre, 1982.)

for various values of n_e and n_o (DuPre, 1982). For very small values of liquid crystal birefringence, the magnetic threshold field is not well defined. Instead the derivative dI/dH displays the threshold clearly. PBLG solution is a cholesteric liquid crystal, the pitch about ten microns. If the cell thickness is less than the pitch, one may use the strong boundary anchoring on glass plates and hence PBLG is, in fact, a nematic.

The Raleigh light scattering, another important approach to measure elastic constants and viscosities simultaneously, is applicable to liquid crystalline polymers as well.

The long wavelength fluctuation of the liquid crystal director causes the Raleigh light scattering which depends on the configuration of the director. The fluctuation is related to the elastic constants. By carefully designing the configuration of the liquid crystal cell, the Raleigh scattering can be especially associated with one elastic constant. Therefore, Raleigh scattering can be utilized to measure the elastic constants of liquid crystals. de Gennes (1973) wrote the differential scattering cross-section of liquid crystals as

$$\frac{d\sigma}{d\Omega} = \left(\frac{\pi\varepsilon_a}{\lambda^2}\right)^2 \sum_{\alpha=1,2} \left\langle |\delta n_\alpha(\mathbf{q})|^2 \right\rangle (i_\alpha f_z + i_z f_\alpha)^2, \qquad (6.21)$$
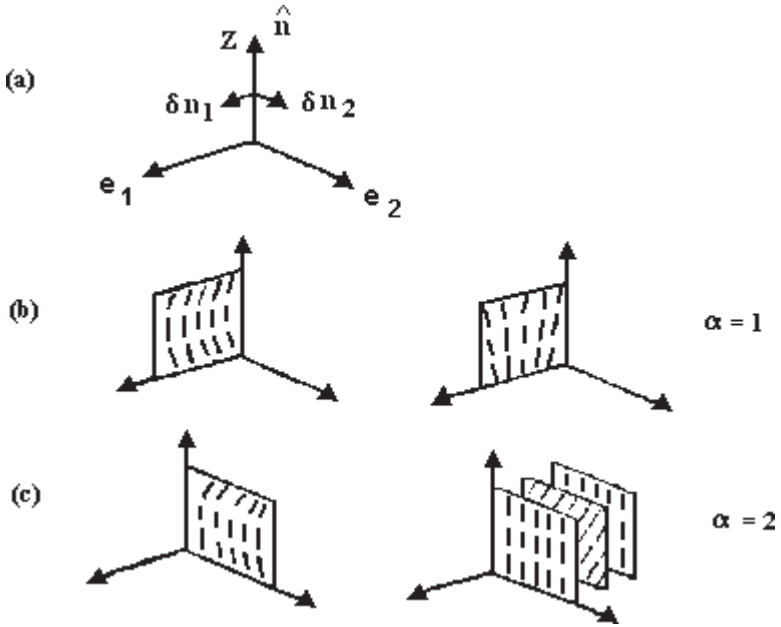
Figure 6.9.   The director fluctuation causes light scattering: (a) two independent fluctuation modes δn_1 and δn_2; (b) two components in δn_1: splay and bend and (c) two components of δn_2: bend and twist. (Modified from DuPre, 1982.)

where α represent two independent modes, $\alpha = 1$ is the mixture of splay and bend deformations, shown in Figure 6.9(b), while $\alpha = 2$ is the overlap of twist and bend deformations, shown in Figure 6.9(c). $\mathbf{q}$ is the scattering vector, $\boldsymbol{i}$ and $\boldsymbol{f}$ are the polarization direction of incident and scattering light, respectively. The averages of the Fourier components of the director fluctuation are

$$\left\langle |\delta n_\alpha(\mathbf{q})|^2 \right\rangle = \frac{V k_B T}{(K_\alpha q_\perp^2 + K_{33} q_{//}^2)} \quad (\alpha = 1, 2). \tag{6.22}$$

By carefully designing the polarization of the incident beam and the configuration of the liquid crystal, the elastic constant ratio and the ratio of an elastic constant to a viscosity can be derived from the scattering data (scattering intensity and relaxation time).

It is noted that the viscosity of liquid crystalline polymers which is much higher than the small molecular mass liquid crystals, affects the amplitude of the director fluctuation, *i.e.*, the overdamped effect. Thus, the scattering

beam intensity is usually not very strong. In addition, the small birefringence of lyotropic liquid crystalline polymers such as PBLG solution causes further weaker scattering. Fortunately, advanced instruments have been applied to improve the measurements.

Meyer's group (Taratuta *et al.*, 1985) designed an experiment in which the liquid crystalline polymers were sandwiched between two glass hemispheres with the director normal to the scattering plane and the incident beam polarization parallel to both the director and scattering plane. By adjusting the sample, the scattering amplitude associated with splay deformation is $\cos^2(\theta_s/2)/K_{11}q^2$ (θ_s is the scattering angle) while the twist deformation is responsible for the term $\sin^2(\theta_s/2)/K_{22}q^2$. The relaxation time is given by

$$\frac{1}{\tau_\alpha(q)} = \frac{K_\alpha(q)}{\eta_\alpha(q)}, \tag{6.23}$$

where η_1 and η_2 are the viscosities of liquid crystals which are actually a combination of the conventional intrinsic viscosities. The correspondent elastic constants are designated as $K_\alpha(\alpha = 1, 2)$. The viscosity of liquid crystalline polymers will be discussed in detail in the coming section.

In the second experiment, the geometry is the same as the first one but for rotating the sample along the surface normal so that the director is parallel to the scattering vector. Thus the scattering arises from a pure bend deformation, which is proportional to $\cos^2(\theta_s/2)/K_{33}q^2$. The sample is switched between the two geometrical configurations while recording data. The ratio of scattering amplitudes of the two measurements is expressed by

$$\frac{K_{33}}{K_{11}} + \frac{K_{33}}{K_{22}} tg^2 \left(\frac{\theta_s}{2}\right). \tag{6.24}$$

By varying the scattering angle one can evaluate elasticity ratios K_{33}/K_{11} and K_{33}/K_{22}, and accordingly K_{11}/K_{22}. Tables 6.5 and 6.6 list the elasticity ratio of PBG at the volume fractions $\phi = 0.16$ and 0.20 against the average molecular weight and the degree of polymerization (Lee and Meyer, 1988, 1990).

These data demonstrate that K_{11} and K_{33} are roughly the same and are all are greater than K_{22} by an order of magnitude. K_{33}/K_{11} increases initially with an increasing degree of polymerization and then decreases. Assuming K_{22} constant, K_{11} is approximately proportional to L/D while K_{33} increases initially and then saturates at about $L/D = 50$. The persistence length of PBG falls in the range of about $q/D = 50$–100. For a

Table 6.5.   The dependence of elastic constant ratios of nematic PBG solution on the average molecular weight and degree of polymerization ($\phi \approx 0.16$).

Sample	Molecular weight ($M_W \times 10^{-4}$)	Degree of polymerization	Volume fraction	K_{33}/K_{11}	K_{33}/K_{22}	K_{11}/K_{22}
1-1	7.0	320	0.159	0.84	10.7	12.5
1-2	8.5	390	0.158	1.14	16.5	14.5
1-3	9.2	420	0.157	1.32	19.9	14.8
1-4	11.0	500	0.155	1.44	23.1	16.1
1-5	12.7	580	0.156	1.43	24.0	17.2
1-6	15.8	720	0.154	1.21	25.3	22.4
1-7	16.5	750	0.152	1.14	25.4	23.2
1-8	19.0	870	0.158	0.97	26.7	26.6
1-9	21.0	1,000	0.154	0.83	27.3	31.2

Table 6.6.   The dependence of elastic constant ratios of nematic PBG solution on the average molecular weight and degree of polymerization ($\phi \approx 0.2$).

Sample	Molecular weight ($M_W \times 10^{-4}$)	Degree of polymerization	Volume fraction	K_{33}/K_{11}	K_{33}/K_{22}	K_{11}/K_{22}
2-1	7.0	320	0.203	1.05	17.8	12.5
2-2	8.5	390	0.196	1.38	21.7	18.4
2-3	12.7	580	0.202	1.41	22.2	22.2

chain length of PBG greater than this range, the chain is no longer rod-like, therefore, the semi-flexible chain model is more appropriate to address the behavior of the polymer chain.

6.2.   VISCOSITY AND RHEOLOGY OF LIQUID CRYSTALLINE POLYMERS

The phenomenological hydrodynamics for small molecular mass liquid crystals which were developed in analog to conventional fluids was, at the early stage, addressed by Ericksen (1960) and Leslie (1966, 1968). The hydrodynamics of the conventional fluids deals with the profile of the velocity field of fluid $v(x_i) = v_i (i = 1,2,3)$. The distortion of velocity field results in

viscous stress σ_{ij}, which is proportional to the velocity distortion A_{ij}, the coefficient being the viscous coefficient η

$$\sigma_{ij} = \eta A_{ij}, \tag{6.25}$$

where

$$A_{ij} = \frac{1}{2}\left(\frac{\partial v_i}{\partial x_j} + \frac{\partial v_j}{\partial x_i}\right). \tag{6.26}$$

σ_{ij} is a symmetrical tensor so that no momentum in the conventional isotropic fluid exists.

There is an orientational order in the liquid crystals which are anisotropic fluids. The director field $\boldsymbol{n}(\boldsymbol{r})$ or its components n_i affect the hydrodynamic behavior, so that σ_{ij} is dependent on the distortion of the director field as well. For convenience, we designate a vector $\boldsymbol{N}$ for the angular velocity of liquid crystal directors with respect to the background fluid, *i.e.*,

$$\boldsymbol{N} = \dot{\boldsymbol{n}} - \boldsymbol{w} \times \boldsymbol{n}, \tag{6.27}$$

where $\dot{\boldsymbol{n}}$ is the derivative of $\boldsymbol{n}$ over time, $\boldsymbol{w}$ is the vortex strength which is proportional to the curl of $\boldsymbol{v}$

$$\boldsymbol{w} = \boldsymbol{\nabla} \times \frac{\boldsymbol{v}}{2}. \tag{6.28}$$

The viscous stress of liquid crystals is defined as the Ericksen–Leslie stress tensor and is related to $\boldsymbol{A}$, $\boldsymbol{n}$ and $\boldsymbol{\omega}$ or $\boldsymbol{N}$:

$$\sigma_{ij} = \alpha_1 n_i(n_k A_{ke} n_e)n_j + \alpha_2 n_i N_j + \alpha_3 n_j N_i + \alpha_4 A_{ij}$$
$$+ \alpha_5 n_i n_k A_{kj} + \alpha_6 n_j n_k A_{ki}, \tag{6.29}$$

where the six coefficients $\alpha_\mu(\mu = 1\text{--}6)$ are called the Leslie coefficients. Parodi obtained the following relation (1970) according to the Onsager reciprocal relation

$$\alpha_2 + \alpha_3 = \alpha_6 - \alpha_5. \tag{6.30}$$

Consequently only five independent coefficients actually exist in the nematic liquid crystals. The viscosity tensor is no longer symmetrical and hence a viscous moment appears

$$\Gamma_i = \varepsilon_{ijk}\sigma_{jk}, \tag{6.31}$$
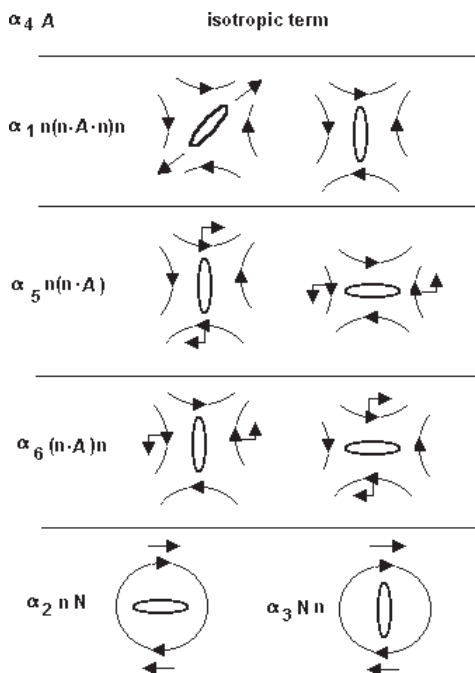
Figure 6.10.   Physical meaning of the α terms of Ericksen–Leslie coefficients. (Modified from Dubois–Violette *et al.*, 1978.)

where ε_{ijk} is a non-symmetrical pseudo three-rank unit tensor, and is null as two of three subscripts are equal so that it has only six non-zero components.

Figure 6.10 schematically shows the physical meaning of the six terms of the Ericksen–Leslie stress tensor. The correspondent flow fields and the viscous moments are depicted. It is seen that α_4 is the term arisen from the conventional fluid. α_1 is symmetrical, representing an extension effect caused by a non-rotation flow, which produces a viscous stress while being without moment. α_2 and α_3 terms arises from rotation flow which produces a moment. α_5 and α_6 terms are non-symmetrical, same as α_2 and α_3, but they are associated with the stress and moment resulting from non-rotational flow.

The Ericksen–Leslie theory is valid for the polymeric liquid crystals if the velocity gradient is small. The theory was applied to examine the director tumbling in liquid crystals and the associated effects. It is concluded
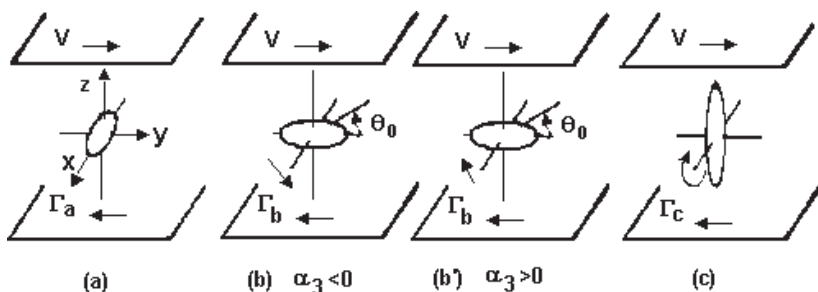
Figure 6.11. Three typical cases of simple shear flow of liquid crystals. (Modified from Dubois–Violette *et al.*, 1978.)

that when α_3 is positive the system will have director tumbling and for negative α_3, the tumbling will be suppressed with only the shear aligning occurring. The molecular orientation makes an angle with respect to the shear direction, known as the Leslie angle. The singular behavior in the first normal stress difference is predicted according to the theory.

The methods of measuring the shear flow of conventional fluids can be applied to measure the viscous coefficients of liquid crystals. Figure 6.11 shows three typical cases of simple shear flow. In all the configurations, liquid crystals molecules are arranged parallel to the surface of the glass plate. The glass plates are slid slowly to produce a shear flow while measure the viscosity. The viscosity depends on the shear direction. There are two cases with the opposite α_3 signs and thus different directions of moment. The three special viscous coefficients are related to the Leslie coefficients via the following formulae

$$\text{as } \boldsymbol{n}//X \text{ axis} \quad \eta_a = \frac{\alpha_4}{2}, \tag{6.32a}$$

$$\text{as } \boldsymbol{n}//Y \text{ axis} \quad \eta_b = \frac{(\alpha_3 + \alpha_4 + \alpha_6)}{2}, \tag{6.32b}$$

$$\text{as } \boldsymbol{n}//Z \text{ axis} \quad \eta_c = \frac{(\alpha_4 + \alpha_5 - \alpha_2)}{2}. \tag{6.32c}$$

The above three viscous coefficients are defined as the Miesowicz viscous coefficients.

In the case of the three Fredericks deformations, the correspondent viscosities are associated with the known viscosities by

$$\eta_{twist} = \alpha_3 - \alpha_2,$$

$$\eta_{splay} = \eta_{twist} - \frac{(\eta_c - \eta_b - \eta_{twist})^2}{4\eta_b},$$

$$\eta_{bend} = \eta_{twist} - \frac{(\eta_c - \eta_b - \eta_{twist})^2}{4\eta_c}.$$
(6.33)

The hydrodynamics of the liquid crystalline polymer is described by the Ericksen–Leslie theory but liquid crystalline polymers have their polymeric characteristics, such as the viscosity's dependence on the molecular length.

Doi first proposed the generalized dynamic equations for the concentrated solution of rod-like polymers. Such constitutive equations can be derived from the molecular theory developed by Doi and Edwards (1986). The basis for the molecular theory is the Smoluchowski equation or Fokker–Planck equation in thermodynamics with the mean field approximation of molecular interaction.

The detail of the Doi theory can be refered to in the book by Doi and Edwards "The Theory of Polymer Dynamics" (1986) in which the Leslie coefficients are related to the order parameter and the isotropic viscosity $\bar{\eta}$ as follows

$$\alpha_1 = -2\bar{\eta}S^2,$$

$$\alpha_2 = \frac{-2\bar{\eta}S(1 + 2S)}{(2 + S)},$$

$$\alpha_3 = \frac{-2\bar{\eta}S(1 - S)}{(2 + S)},$$

$$\alpha_4 = \frac{2\bar{\eta}(1 - S)}{3},$$

$$\alpha_5 = 2\bar{\eta}S,$$

$$\alpha_6 = 0,$$
(6.34)

and

$$\bar{\eta} = \rho k_B \frac{T}{2} D^*,$$
(6.35)

where ρ is the concentration of liquid crystalline polymers and D^* the effective rotational diffusion coefficient of the molecules.
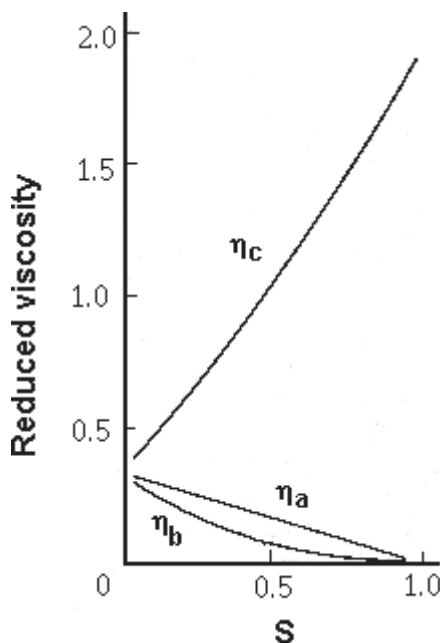
Figure 6.12. Miesowicz coefficients of liquid crystalline polymers against order para-
meter. (From Doi and Edwards, 1986.)

In reality, it is difficult to measure the six Leslie coefficients. However,
it may be easier to measure the Miesowicz viscous coefficients which are
related to the order parameter and $\bar{\eta}$

$$\eta_a = \bar{\eta} \, \frac{(1-S)}{3},$$

$$\eta_b = 2\bar{\eta} \, \frac{(1-S)^2}{3(2+S)}, \qquad (6.36)$$

$$\eta_c = 2\bar{\eta} \, \frac{(1+2S)^2}{3(2+S)}.$$

The relations are shown in Figure 6.12 where the Miesowicz viscous
coefficients are plotted as a function of the order parameter of long rods in
solution. The Doi and Edwards theory gives the order parameter *vs.* the
concentration shown in Figure 6.13, in which the order parameter starts at
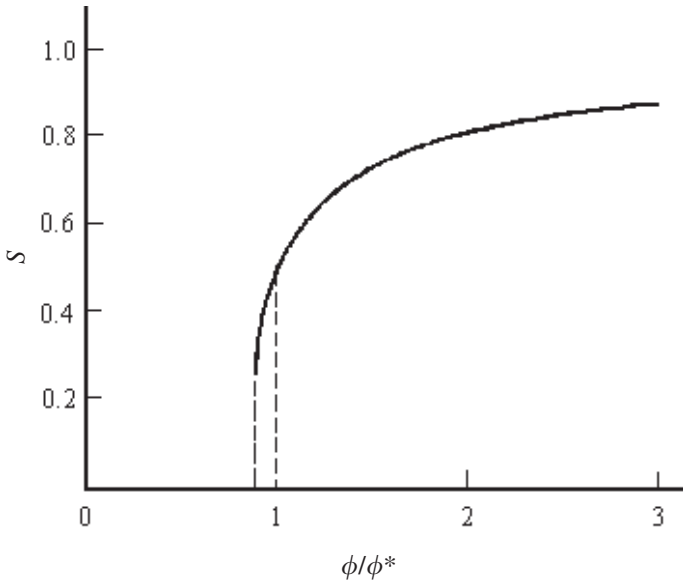
Figure 6.13.   Order parameter *vs.* reduced concentration of lyotropic liquid crystalline polymers. (From Doi & Edwards, 1986.)

$\frac{1}{4}$ of the reduced concentration $\phi/\phi^* = \frac{8}{9}$ and then gradually approaches unity.

Lee (1988) further connected the viscosities of liquid crystalline polymers (in the unit of $\bar{\eta}$) with concentration and molecular length as Equation (6.37), where λ is a constant less than unity which is associated with the stability of simple shear flow, μ is a dimensionless parameter associated with the interaction in the fluid, $R = \langle P_4(\boldsymbol{a} \cdot \boldsymbol{n}) \rangle$ is the second order parameter where $\boldsymbol{a}$ is the molecular long axis and P_4 is the fourth rank Legendre polynomial.

$$\alpha_1 = -(2 - \mu)R,$$

$$\alpha_2 = -\left(1 + \frac{1}{\lambda}\right)S,$$

$$\alpha_3 = -\left(1 - \frac{1}{\lambda}\right)S, \tag{6.37}$$

$$\alpha_4 = \left(\frac{2}{105}\right)[7(3 + \mu) - 5(3 + 2\mu)S - 3(2 - \mu)R],$$

$$\alpha_5 = \left(\frac{2}{7}\right)[(5+\mu)S + (2-\mu)R],$$

$$\alpha_6 = -\left(\frac{2}{7}\right)(2-\mu)(S-R).$$

In analog to the approach used by Odijk when dealing with elastic constants, Lee (1988) took the orientation distribution function approximately as Gaussian. When the system is highly ordered, the asymptotic expression can be deduced for viscosities of liquid crystalline polymers, e.g., the Miesowicz viscosities (in the unit of $\bar{\eta}$) are expressed by

$$\eta_a = \frac{\pi}{Q},$$

$$\eta_b = \frac{\mu\pi}{Q}, \tag{6.38}$$

$$\eta_c = 8Q + \frac{\pi(3+2\mu)}{2Q},$$

and the viscosities associated with the three Fredericks distortions (in the unit of $\bar{\eta}$) are

$$\eta_{splay} = 8Q + \frac{\pi(11\mu - 8)}{2\mu Q},$$

$$\eta_{twist} = 8Q + \frac{11\pi}{2Q}, \tag{6.39}$$

$$\eta_{bend} = \frac{\pi\mu}{Q},$$

where $Q = \phi L/D$.

Kuzuu and Doi (1983, 1984) derived the six coefficients (in the unit of $\bar{\eta}$) in the limit of low flow rates for prolate molecules

$$\alpha_1 = -2R[K(a)]^2,$$

$$\alpha_2 = -\left(1 + \frac{1}{\lambda}\right)SK(a),$$

$$\alpha_3 = -\left(1 - \frac{1}{\lambda}\right)SK(a), \tag{6.40}$$

$$\alpha_4 = \frac{2}{35}(7 - 5S - 2R)[K(a)]^2,$$

$$\alpha_5 = \left[\frac{1}{7}K(a)(3S + 4R) + S\right] K(a),$$

$$\alpha_6 = \left[\frac{1}{7}K(a)(3S + 4R) - S\right] K(a),$$

where $K(a)$ is the function of the axial ratio $a \equiv L/D$.

$$K(a) = \frac{a^2 - 1}{a^2 + 1}. \tag{6.41}$$

The quantity $K(a)$ is near unity for the physical range of a. The tumbling parameter, λ, in a simple sheering flow is related to the flow alignment, or Leslie angle θ by

$$tg\theta = \sqrt{\frac{\lambda - 1}{\lambda + 1}}. \tag{6.42}$$

Larson (1995) simplified the above expression for λ in terms of S, R and L/D:

$$\lambda = K(a)\frac{(15S + 48R + 42)}{105S}. \tag{6.43}$$

Meyer (1982) predicted that as the length of the chain approaches infinity, the Leslie coefficients α_1 and α_2 should tend to $-\infty$ and α_3 tends to ∞, while α_4, α_5 and α_6 are of finite values. The Miesowicz viscosities η_a and η_b are finite while η_c tends to infinity because the velocity is perpendicular to the director and the shear flow.

Table 6.7 lists expressions of Kuzuu & Doi (1983, 1984) and Lee (1988) at the infinite long chain limit. Meyer's prediction is listed for comparison. From Table 6.7 one can estimate the applicability of the theories.

Table 6.7 reveals that Lee's calculation, based on Doi's argument, is in better agreement with Meyer's predictions.

Table 6.7. Comparison of theories on viscosities of liquid crystal with infinite long chain. (From Lee and Meyer, 1991.)

Viscosity ratio	Reference (Kuzuu & Doi, 1983, 1984) $(Q \to \infty)$	Reference (Lee, 1988) $(Q \to \infty)$	Meyer's prediction (1982) $(L \to \infty)$
η_a/η_b	$\propto Q^2$	$1/\mu$	finite
η_a/η_c	$\pi/8Q^2$	$\pi/8Q^2$	0
η_b/η_c	$\propto 1/Q^4$	$\pi\mu/8Q^2$	0
$\eta_{splay}/\eta_{twist}$	const$-$const$/Q^2$	$1 - \pi/2\mu Q^2$	finite
η_{twist}/η_c	$1 + \pi/2Q^2$	$1 + \pi(4 - \mu)/8Q^2$	finite
η_{bend}/η_{twist}	$\propto 1/Q^4$	$\pi\mu/8Q^2$	0

Table 6.8. The viscosities of PBG at volume fraction of $\phi = 0.16$ (1-X) and $\phi = 0.20$ (2-X) as functions of the degree of polymerization (the latter is about $10 \times L/D$) (From Lee and Meyer, 1988; 1990.)

Sample	Degree of polymerization	$\eta_{\text{splay}}/\eta_{\text{twist}}$	$\eta_{\text{twist}}/\eta_{\text{bend}}$	η_{twist} (P)	η_{bend} (P)	$\eta_{\text{c}}/\eta_{\text{b}}$
1-1	320	0.85	108	27	0.25	92
1-2	390	0.88	136	39	0.28	120
1-3	420	0.92	140	49	0.35	129
1-4	500	0.94	170	70	0.41	160
1-5	580	0.97	148	86	0.58	144
1-6	720	0.99	187	141	0.77	185
1-7	750	1.00	203	173	0.85	203
1-8	870	1.00	254	223	0.88	254
1-9	1,000	1.00	311	274	0.88	311
2-1	320	0.92	166	45	0.27	158
2-2	390	0.93	207	71	0.34	193
2-3	580	1.00	254	139	0.55	254

Unfortunately, there are very few discussions about the viscosity behavior for semi-flexible liquid crystalline polymers. Semenov (1988) calculated the viscosities of worm-like chains and found that α_3/α_2 of this liquid crystalline polymers is always positive and decreases as the order parameter increases. The conclusion is different from that of rod systems.

There are a few approaches to measuring viscosities of liquid crystalline polymers. In addition to the classical means such as the capillary method, the rotating cone-plate and the shear, the supersonic shear decay method, NMR method, and Raleigh light scattering approach have been applied. Table 6.8 lists the viscosity ratio as a function of the degree of polymerization for PBG at the volume fraction of $\phi = 0.16$ and 0.2, which were measured by the Raleigh scattering method (Lee and Meyer, 1988; 1990).

It is illustrated that the experimental data of PBG are in agreement with theoretical predictions, especially in good agreement with Lee's calculation. $\eta_{\text{splay}}/\eta_{\text{twist}}$ approaches to unity as the degree of polymerization increases while $\eta_{\text{twist}}/\eta_{\text{bend}}$ and $\eta_{\text{c}}/\eta_{\text{b}}$ increases drastically with an increasing degree of polymerization. When the volume fraction increases from 0.16 to 0.20, the $\eta_{\text{splay}}/\eta_{\text{twist}}$ approaches to unity more rapidly while the others increase approximately quadratically. All of these are the conclusion of the Meyer-Lee results. Another experiment was carried out for chain length, $L/D \approx 30$, by varying the volume fraction. It was found that η_{twist} and η_{c} are proportional to ϕ^2, η_{a} is proportional to ϕ, while η_{b} is approximately independent of ϕ.

Table 6.9.   The comparison of experiments and theories on viscosities of PBG and TMV. (From Lee and Meyer, 1991.)

Viscosity ratio	PBG	TMV	Meyer (1982)	Kuzuu/Doi (1983, 1984)	Lee (1988)
$\eta_{\mathrm{splay}}/\eta_{\mathrm{twist}}$	0.85–1.00	—	1	finite	1
$\eta_{\mathrm{bend}}/\eta_{\mathrm{twist}}$	<0.01	0.007	0	0	0
$\eta_{\mathrm{b}}/\eta_{\mathrm{c}}$	$\leq$0.01	0.002	0	0	0
$\eta_{\mathrm{twist}}/\eta_{\mathrm{c}}$	$\approx$1	0.95	1	1	1

The experimental data (Lee and Meyer, 1991) on the viscosities of PBG and tobacco mosaic virus (TMV) were compared with the theories, as shown in the Table 6.9. A good agreement was found between them for both PBG and TMV.

In general, liquid crystalline polymers do not exist in the form of a single domain and instead exist in the form of poly-domains with the domain size of about a few microns. Liquid crystalline polymers are macroscopically isotropic despite the molecules that are roughly parallel to each other in each domain. Therefore, many physical properties of liquid crystalline polymers such as mechanical performance are visually isotropic.

The apparent viscosity of typical thermotropic liquid crystals is plotted as a function of temperature in Figure 6.14 (Porter and Johnson, 1967). As a material enters from the isotropic into the liquid crystal phase, the viscosity decreases significantly. This phenomenon is, in fact, observed in the lyotropic liquid crystalline polymers. Figure 6.15 shows the viscosity dependence on the concentration of solution of poly(para-benzamide)/N,N-dimethylacetamide/LiCl (Baird, 1978). The viscosity in the isotropic phase increases with increasing concentration of poly(para-benzamide). However, in the liquid crystal phase, the viscosity decreases abruptly, in the same way as the small molecular mass liquid crystals. The higher the molecular weight of liquid crystalline polymers, the lower the concentration for the liquid crystalline polymers to enter into the liquid crystal phase and the higher the maximum viscosity in the liquid crystal phase. It is believed that as the system becomes a liquid crystal, the director will align along the shear direction and thus the viscosity is reduced rapidly. Moreover, the fact that viscosity decreases with increasing shear rate supports such a view point. The last phenomena illustrates that liquid crystalline polymers are not a Newtonian fluid at high shear rates.
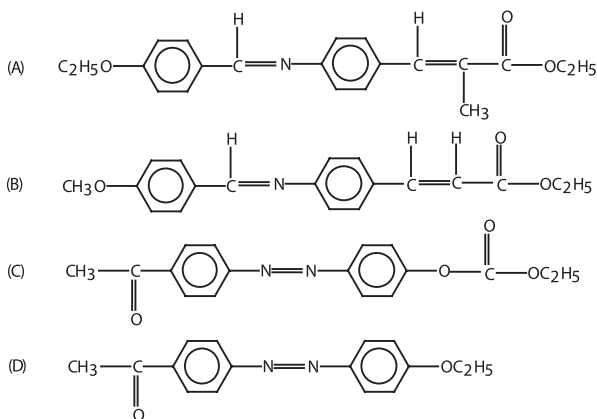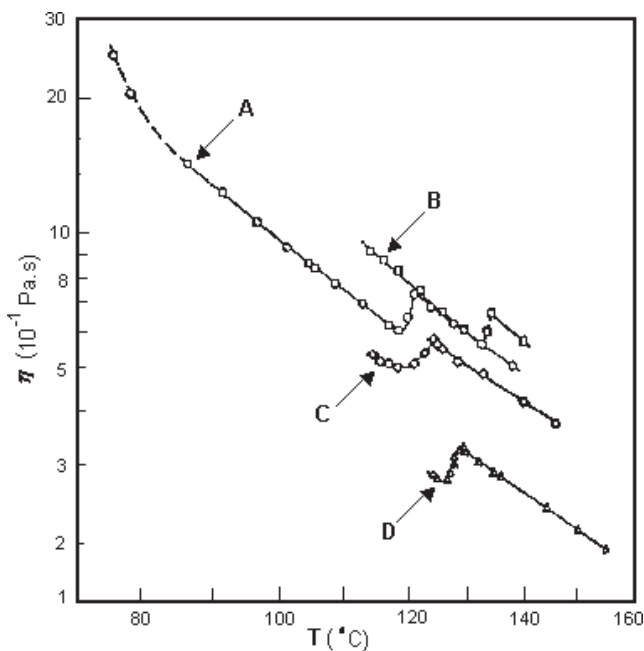
Figure 6.14. The temperature dependence of viscosity of liquid crystals. (Modified from Porter and Johnson, 1967.)

As elaborated above, the Ericksen–Leslie theory takes into account only the first rank effect of the velocity gradient of liquid crystalline polymers. If the amplitude of the velocity gradient is high enough, these theories are no longer valid and the steady viscosity of liquid crystalline polymers
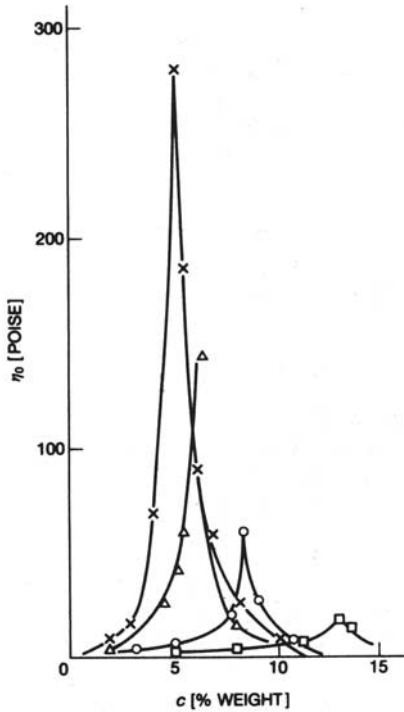
Figure 6.15.   The concentration dependence of the viscosity at 20 °C for solutions of poly(para-benzamide) of various molecular weights in N,N-dimenthylacetamide/LiCl: □ 10900; ○ 16000; △ 23800; ×69000. (From Papkov *et al.*, 1974. Reproduced by permission of John Wiley & Son, Inc.)

becomes a function of shear rate γ, which decreases with increasing shear rate. It is known as the shear thinning effect. A higher shear rate forces the liquid crystalline polymer molecules to be reoriented along the shear direction and thus the multiple domains with various director directions become gradually concise so that whole sample has a global macroscopic orientation. In consequence, the viscosity decreases.

Doi (1982) predicted the dependence of the viscosity of liquid crystalline polymers solution as a function of shear rate and concentration, as shown in Figure 6.16. This prediction is qualitatively in agreement with experimental data for liquid crystalline polymers in solutions. The data on PBG is plotted in Figure 6.17 (Kiss and Porter, 1980a,b).

The low viscosity and the shear thinning effect of liquid crystalline polymers are advantageous for application. For instance, the filling of molded
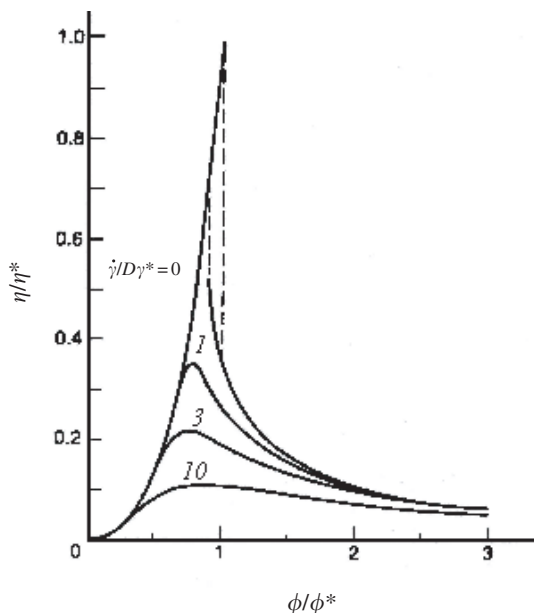
Figure 6.16.   Steady viscosity of liquid crystalline polymers as a function of concentration and shear rate. (From Doi, 1982.)
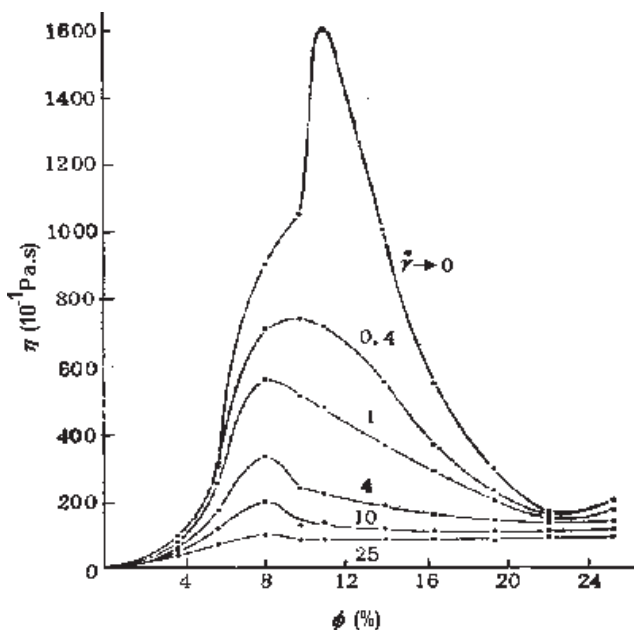
Figure 6.17.   The viscosity of PBG solution ($Mn = 350,000$) as a function of concentration and shear rate. (From Kiss and Porter, 1980a,b. Reproduced by permission of John Wiley & Sons, Inc.)
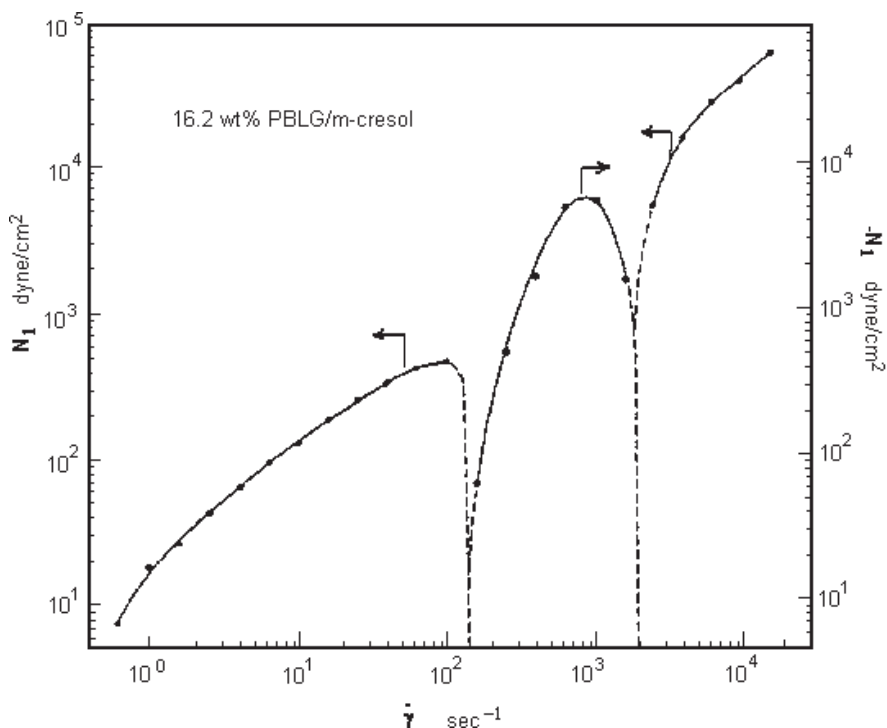
Figure 6.18.   The first normal stress difference *vs.* the shear rate. (From Kiss and Porter, 1980a.)

plastic products becomes convenient and the molded shape is sharper and better.

A more detailed study verified that PBLG/m-cresol solution and thermotropic copolyester under shear rate exhibits negative first normal stress difference, *i.e.*, the difference between normal stresses parallel and perpendicular to the flow direction, as shown in Figure 6.18.

The negative first normal stress difference under a medium shear rate, characterized by liquid crystalline polymers, makes the material avoid the Barus effect—a typical property of conventional polymer melt or concentrated solution, *i.e.*, when a polymer spins out from a hole, or capillary, or slit, their diameter or thickness will be greater than the mold size. The liquid crystalline polymers with the spin expansion effect have an advantage in material processing. This phenomenon is verified by the Ericksen-Leslie theory. On the contrary, the first normal stress difference for the normal polymers is always positive.

In the period after the flow of liquid crystalline polymers stops, the sample releases to the original multiple domains. This process is often accompanied by the appearance of regular banded textures normal to the shear direction and with a gap of a few microns between them. Inside the banded texture, the director fluctuates continuously along the original shear direction and then gradually relaxes back to the disordered multiple domains. If the liquid crystalline polymers cools down or the solvents are removed before the relaxation is completed, the resultant sample becomes an anisotropic solid with a unified macroscopic orientation. The effect constitutes the basis for liquid crystalline spinning. The high strength fiber Kevlar is manufactured in such a way.

When compared with lyotropic liquid crystalline polymers, the viscosity theory associated with thermotropic liquid crystalline polymers is far less studied except for a very few works done in theory (de Gennes, 1982) and experiment (Martins *et al.*, 1986). More work should be carried out in this respect.

6.3. CHOLESTERIC LIQUID CRYSTALLINE POLYMERS

6.3.1. Optical properties of cholesteric liquid crystals

As mentioned in Chapter 1, cholesteric liquid crystals have a helical structure. The helical structure results in unique optical properties, such as selective reflection, circular dichroism, drastic optical activity, and electro-optic effects.

Selective reflection

A sheet of cholesteric liquid crystals is sandwiched between two glass plates separated by a gap of tens microns. The cholesteric liquid crystals on two glass plates are homogeneously aligned to form the planar texture. The cell displays a bright color. The color varies according to the view angle and temperature. This is an important characteristic of cholesteric liquid crystals—selective reflection.

The effect of the selective reflection doesn't result from the interference of a thin film, but from the Bragg-like reflection.

Assume a to be the lattice gap of a crystal, usually a few Å. When an incident X-ray impacts the sample, the well-known Bragg reflection occurs.

The first order reflection is given by the formula

$$\lambda = 2a \sin \beta, \tag{6.44}$$

where β is the incident angle and λ is the wavelength of X-ray.

The natural pitch P of cholesteric liquid crystals is in general in the order of 10^2 nm, comparable with the visible band of light. The Bragg reflection from cholesteric liquid crystal occurs at the wavelength

$$\lambda = P\bar{n} \sin \beta, \tag{6.45}$$

where the average refractive index is $\bar{n} = (n_o + n_e)/2$. The band width is

$$\Delta\lambda = |n_e - n_o| P \sin \beta. \tag{6.46}$$

Circular dichroism

When circular polarized light in the band of selective reflection impacts a cholesteric liquid crystal of left-handed helix which is in the planar texture, the right circular polarized light goes through without reflection. However, the left circular polarized light is all reflected. The result is the so-called circular dichroism. If the incident light is a linear polarized light, then half of the light is transmitted while the other half is reflected because natural light consists of two circular polarized lights with opposite senses of handedness and equal intensity.

This reveals that the selective reflection arises from the structural period, and the circular dichroism is attributed to the helical structure.

Optical activity

Many media exhibit optical activity which depends on wavelength, *i.e.*, optical rotation dispersion. Quartz is an example.

Cholesteric liquid crystals have more optical activity than conventional crystals do. The optical rotation power is a function of wavelength, cholesteric pitch, and birefringence, *i.e.*,

$$R = -\frac{\pi(\Delta n)^2 P}{4\lambda^2 \left(1 - \dfrac{\lambda^2}{P^2 \bar{n}^2}\right)}, \tag{6.47}$$

where the negative sign means the optical rotation has the opposite sense to that of the helix of cholesteric liquid crystals. For typical values, the optical

power is about 10,000 °/mm. For comparison, the optical rotation power of quartz at the same light wavelength is only 21.7 °/mm. The difference is as large as 500 times!

Dependence of cholesteric pitch on temperature and external field

The pitch P is the most important parameter of cholesteric liquid crystals. The physical properties of cholesteric liquid crystals are associated with P, such as selective reflection, optical rotation dispersion, circular dichroism, *etc.* The helical pitch is sensitive to the temperature and external field, for example, electric and magnetic field, chemical environment, pressure or radiation, *etc.*

The reflective wavelength of cholesteric liquid crystals varies according to temperature. Such an effect has been made useful in thermography. It has been applied in the diagnosis of cancers by displaying the skin temperature distribution. It has also been applied to test faults in integrated circuits. The applications also include thermometers and temperature warning indicators and non-destructive detection.

As explained in Section 6.1, the pitch increases with an increasing electric or magnetic field until it reaches a threshold at which the helical structure is unwounded.

In order to achieve cholesteric liquid crystals with various pitch, one can mix two cholesteric liquid crystals at a certain ratio, each having a different natural pitch, or mix a cholesteric liquid crystal with a nematic material.

Electro-optic effects

Cholesteric liquid crystals show many electro-optic effects. Among them the cholesteric-nematic phase transition effect is the most interesting one which was addressed in the early part of this chapter. Others are the square grid effect, storage effects and color effects, *etc.*

(1) *Square grid effect*: Before the electric field becomes great enough to cause the cholesteric–nematic phase transition, a periodic deformation may appear in cholesteric liquid crystals. The layer undulation occurs in two orthogonal directions so that a square pattern is observed. This effect is more likely to happen for cholesteric liquid crystals of large pitch (about microns).

(2) *Storage effects*: Two modes of storage effects exist. One is the negative mode in which cholesteric liquid crystals, doped with a small amount of conducting impurity, are negative in dielectric anisotropy. This is caused by the turbulence of the liquid crystal director field and is called conductive-mode display. The other storage effect is the positive mode. The cholesteric liquid crystals have a positive dielectric anisotropy. It is a dielectric-type display. The current interest — the polymer stabilized cholesteric liquid crystals (Doane *et al.*, 1995) is based on this display mode.

Both displayed images can be kept for days' or months' long without the presence of an electric field. From the energy consumption point of view, such storage effects have a great advantage for displays. In addition, the display of such kind has a wide view angle which is an important feature for information board displays.

In the above applications, cholesteric liquid crystals need to be sealed between two glass plates or in the form of micro encapsulates. However, cholesteric liquid crystalline polymers can easily form thin films or be coated on substrates.

6.3.2.   Lyotropic cholesteric liquid crystalline polymers

To form cholesteric liquid crystalline polymers, one either polymerizes cholesteric monomers or mixes low molecular mass cholesteric liquid crystals with polymers. In the latter case, two components may be mixed homogeneously or in such a way that the polymers act as a matrix while the small molecular mass cholesteric liquid crystals are in droplets, known as the polymer-dispersed liquid crystals (PDLC) (Doane *et al.*, 1988) or the nematic curvilinear aligned phase (NCAP) (Fergason, 1985). In addition, there are many polymers in nature exhibiting the cholesteric phase such as PBLG, cellulose, DNA, *etc.*

The rod-like PBLG is the most well studied cholesteric liquid crystalline polymer, which is a kind of poly-peptides forming α-helices, shown in Figure 6.19. In such a structure, the neighboring twist sites are connected by hydrogen bonds in every four peptide bonds between the neighboring –C=O– and –NH–. The side chains $-CH_2CH_2-COOCH_2C_6H_5$ extend out radically. It exhibits the cholesteric phase in solutions, *i.e.*, lyotropic liquid crystalline polymers. The solvents can be dioxane, dichloromethane, trichloromethane, *etc.*
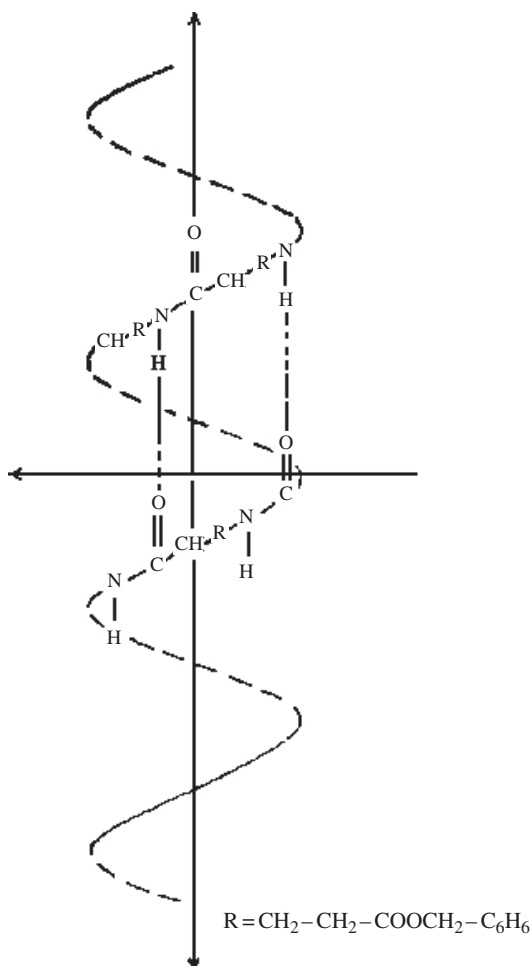
Figure 6.19.   The α-helical structure of PBLG molecule. (From Brown and Wolken, 1979.)

PBLG solution shows the finger-print texture, seen in Figure 6.20. A pair of neighboring dark-bright stripes corresponds to a half period of the helix, $P/2$, which is about a few microns. It is a practical means of estimating the pitch of cholesteric liquid crystals.

Pitch as a function of concentration

The more concentrated cholesteric polymers in solution have small pitch. No satisfactory theory has been presented to describe the relationship between
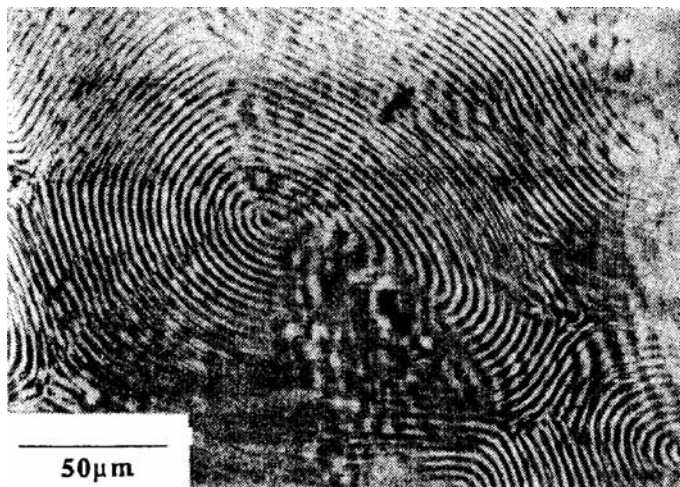
Figure 6.20. The finger-print texture of PBLG solution (20% PBLG in dichloromethane, $Mn = 40000$). (From Ritter, 1986.)

pitch and concentration. Figure 6.21 plots the pitch of PBLG in dioxane (Onagi *et al.*, 1980) and hydroxypropyl-cellulose in water (Robinson, 1955, 1961).

Pitch as a function of temperature

The molecular chirality does not necessarily decide the chirality of cholesteric liquid crystalline polymers because the sample's chirality also depends on the solvent. PBLG is itself a right-hand molecule. It indeed forms a right-handed chiral liquid crystalline polymer in dioxane or trichloromethane, while it forms the left-handed polymer in chloromethylene and chloroethylene. In Figure 6.22, the reciprocal of pitch is plotted against temperature for PBLG in dioxane and dichloroethylene mixture with concentration $c = 0.1$ vol%. With an increasing concentration of dichloroethylene, the cholesteric liquid crystalline polymer changes gradually from right-handed to left-handed. In a median value for concentration of dichloroethylene, 60% at $T = 50°C$, the helix is completely unwounded. It is found that $1/P$ is approximately linear in proportion to temperature. As temperature increases, the pitch increases until the helical sense reverses and then decreases (Uematsu, 1984). It was found that the pitch
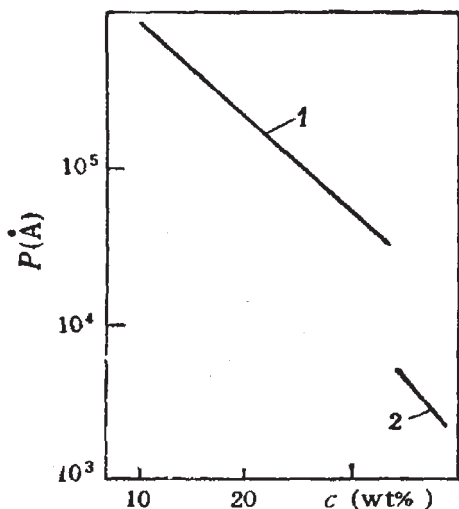
Figure 6.21. The pitch as a function of concentration (1) PBLG in dioxane; (2) hydroxypropyl-cellulose in H$_2$O. (From Onagi *et al.*, 1980; Robinson, 1955, 1961; Freidon, Y. S. and Shibaev, V. P., 1993.)
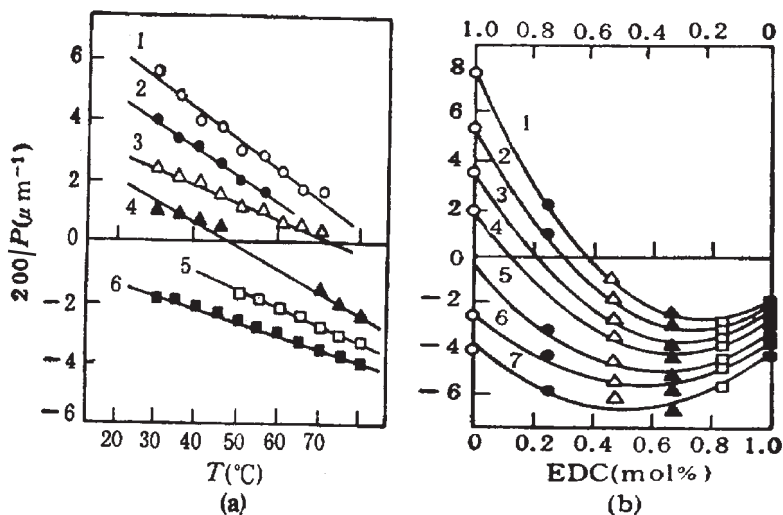
Figure 6.22. The reciprocal of pitch *vs.* (a) temperature for PBLG with concentration $c = 0.15$ vol% in a mixture of dioxane and dichloroethylene and (b) dichloroethylene concentration for PBLG in a mixture of m-cresol and dichloroethylene. The curves, 1–6 in (a) and 1–7 in (b) correspond to 0, 20, 40, 60, 80, 100% dichloroethylene in the solvent mixture (a) and 20, 30, 40, 50, 60, 70, 80°C (b). (From Uematsu, 1984.)

dependence on temperature is sometimes rather complicated. For instance, for the poly(penzyl-L-glutamate) (PPLG) in trichloromethane solvent, $1/P$ decreases with increasing temperature until a temperature at which $1/P$ approaches to zero and then $1/P$ increases as the temperature increases. But for most substitutes of the poly(L-glutamate) in the same solvent $1/P$ is essentially proportional to the temperature. Attempts were made to address the pitch behavior with temperature. One model proposed the following formula (Kimura *et al.*, 1979, 1982).

$$\frac{1}{P} = \frac{12\Delta}{\pi^2 LD}\left(1 - \frac{T}{T_N}\right)cf(c), \tag{6.48}$$

where Δ is a parameter proportional to side chain length, T_N is the temperature at which the chirality starts to reverse, *i.e.* when $P = \infty, f(c)$ is a function of concentration of cholesteric liquid crystalline polymers.

Pitch on side chains of poly-peptides

Experiments were carried out on poly-peptides with various side chain length in a solvent. The substitution of poly-peptides affects the pitch (Yoshida, 1972). Usually, the larger substitute has the greater pitch. The pitch varies with the substitutes of poly(L-glutamate) in such sequences

$$-CH_2-\text{⟨◯⟩} > -(CH_2)_5-CH_3 > -(CH_2)_4-CH_3 > -(CH_2)_3-CH_3$$
$$> -\text{⟨◯⟩} > -(CH_2)_2-CH_3 > -CH_2-CH_3 > -CH_3$$
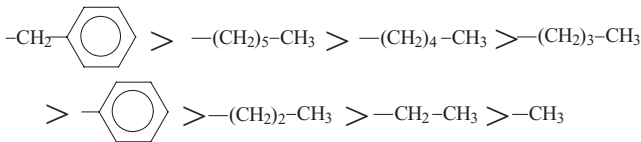
It is found from experiments that after the solvent is evaporated or removed, the solidified poly-peptides remain in its chiral structure with an expanded pitch. The pitch in the solidified poly-peptides is associated with the original solvent. In Figure 6.23, the dichroism is plotted against the central wavelength of selective reflection for poly(methzyl-L-glutamate) (PMLG). The samples were originally dissolved in (1) dichloroethane or (2) dichloroethane/dimethyl formamide or (3) trichloromethane/dimethyl formamide, and then were solidified after the solvents were removed.

It is demonstrated that the original chiral structure in the cholesteric phase is frozen-in after the solvent is removed.

An interesting experiment was performed (Tsutsui and Tanaka, 1980, 1981). PBLG and PLG was placed in the solvent propenoic acid and
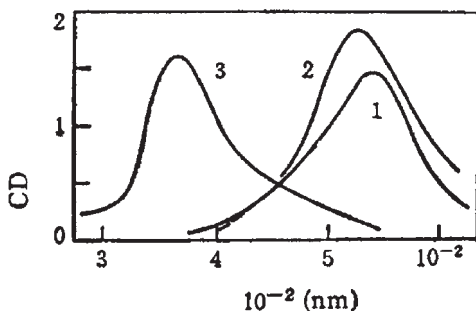
Figure 6.23. The circular dichroism (in relative unit) spectra of PMLG films dried from solutions of the polymer in (1) dichloroethane; (2) dichloroethane/dimethyl formamide, and (3) chloroform/dimethyl formamide. (From Uematsu and Uematsu, 1984.)
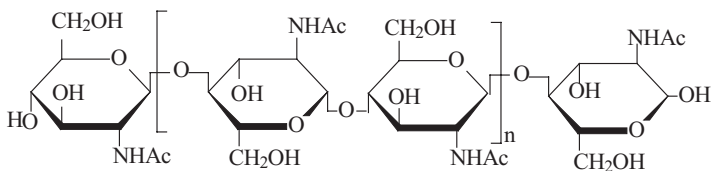
Figure 6.24. The chemical formula of the cellulose.

methacrylic acid, or other solvents, and then the solvent was polymerized. The cholesteric structure remains in the new polymer/polymer solution. The thin film of the sample was transparent, displaying a color.

Other important lyotropic cholesteric liquid crystalline polymer are the cellulose esters. Cellulose is a natural polymer. Their chemical formula is shown in Figure 6.24.

The derivatives of cellulose esters exhibit the lyotropic cholesteric phase in many solvents. Cellulose is less rigid than PBG. The persistence length of PBG is about $2000\,\text{Å}$ while the latter is between 130 and $330\,\text{Å}$, depending on the chemical formula of the substitute and the solvent. The cellulose derivatives are cheap in cost and easy to process, and hence were studied extensively. Among the derivatives, hydroxypropyl cellulose (HPC) is one of most well studied.

The chemical structure of HPC is as follows
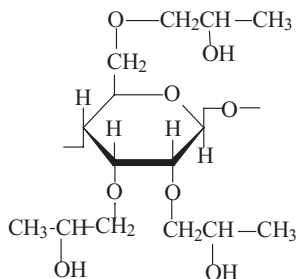
Its helical pitch decreases with increasing concentration in solution. In acid solvents the pitch is small.

It is observed from experiments that HPC exhibits thermotropic cholesteric liquid crystal characteristics as well (Tsvetkov, 1989).

Biological cholesteric liquid crystalline polymers

A lot of biological polymers exhibit cholesteric liquid crystal characteristics as pointed out first by Robinson *et al.* (1958). The notable examples are RNA and DNA. The well-known double helical structure, shown in Figure 6.25, makes them rod-like in conformation.

Some viruses such as the tobacco mosaic virus (TMV) can form lyotropic cholesteric liquid crystals. TMV contains 94% protein and 6% RNA. In TMV the proteins and RNA are stacked regularly, see Figure 6.26. It looks like a long rod of average length 300 nm and of diameter 15 nm. The molecular mass is as high as 4×10^7.

The cholesteric-like structure has been found in many biological bodies. The report on these discoveries is scattered, mainly based on optical rotation observations and chiral structure. For example, the wings and shells of some insects can rotate incident light and selectively reflect one circular polarized light (Shimamura *et al.*, 1981). Very few experiments on these materials are available because of the difficulty in extracting and separating the effective materials from biological bodies.

It is worth pointing out that the existence of cholesteric liquid crystalline polymers are far more common than one can imagine.
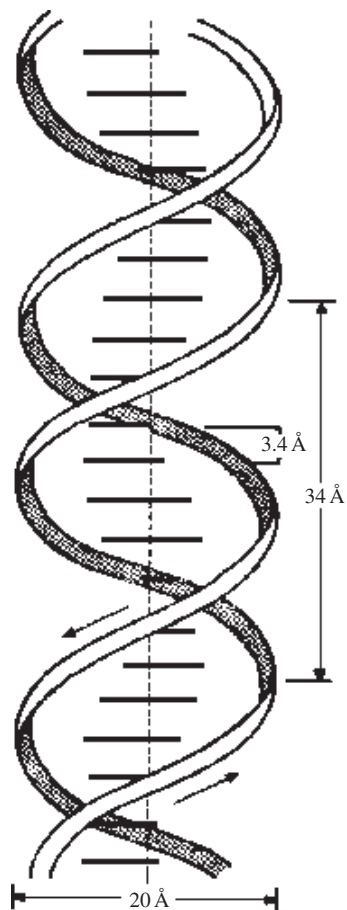
Figure 6.25. The well-known double helical structure of DNA. (Modified from Etkin, 1973.)
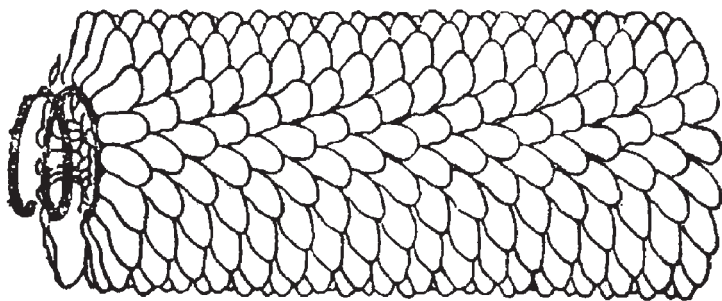
Figure 6.26. The structural schematic of TMV. (From Wu *et al.*, 1988.)

6.3.3. Thermotropic cholesteric liquid crystalline polymers

In addition to the above mentioned lyotropic cholesteric liquid crystalline polymers composed of rigid polymers, there is a diversity of thermotropic cholesteric liquid crystalline polymers which consist of a flexible chain incorporated with a mesogenic and chiral units. The thermotropic cholesteric liquid crystalline polymers are classified into two categories: main chain and side chain.

6.3.3.1. *Main chain cholesteric liquid crystalline polymers*

In main chain cholesteric liquid crystalline polymers, the mesogenic groups and flexible spacers are linked alternatively. The flexible units contain asymmetrical carbon atoms which enable the polymers to possess chirality and thus form cholesteric liquid crystals. By varying the ratio of chiral to non-chiral parts, the cholesteric temperature range and pitch can be changed. The cholesteric range depends on the mol fraction of the polymers. A typical main chain cholesteric liquid crystalline polymer is shown in Figure 6.27.

D-3-methyl-glyoxal is a common chiral spacer. In addition, D-butane-1, 3-diphenol, L-propane-1, 2-diphenol, and their dimers and trimers are used as the chiral spacers in cholesteric liquid crystalline polymers as well.

Mesogenic group M	Chiral spacer (A) and its mole fraction (x)	Linear spacer (B) and its mole fraction ($1-x$)

$x = 0.5$	K	(150)	Ch	(230)	I
$x = 0.4$	K	(160)	Ch	(230)	I
$x = 0.3$	K	(165)	Ch	(220)	I
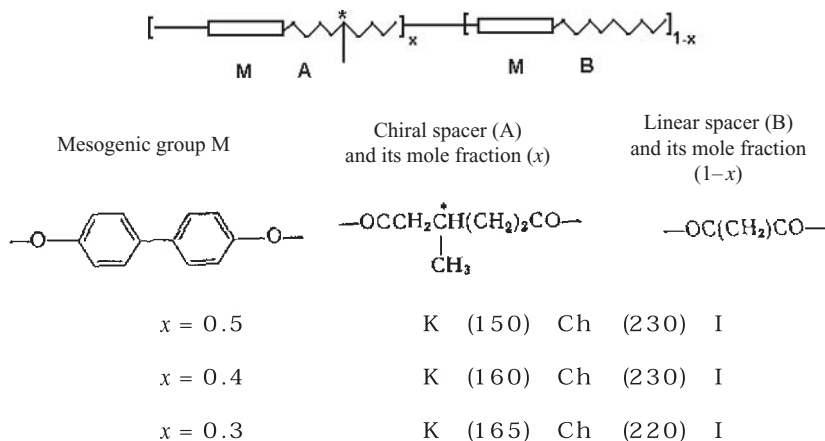
Figure 6.27. A typical main chain cholesteric liquid crystalline polymer. (From Watanabe and Krigbaum, 1985.)

6.3.3.2. Side chain cholesteric liquid crystalline polymers

In the side chain liquid crystalline polymers the nematogenic side groups and chiral side groups are attached respectively to a polymer backbone to form a copolymer. They exhibit the cholesteric phase. A typical example is shown below. One is the homopolymer (shown in Figure 6.28) and the other is the copolymer (Figure 6.29).

$$-[CH_2=C-CH_2]-$$
$$\qquad\qquad |$$
$$\qquad\qquad COO-(CH_2)n-COO-Chol$$

and

$$
\begin{array}{lllllllll}
n = 5 & G & (85) & S_A & (190) & Ch & (210) & I \\
n = 10 & G & (60) & S_A & (124) & Ch & (158) & I \\
n = 14 & G & (50) & S_{A1} & (54) & S_{A2} & (153) & I \\
\end{array}
$$

Figure 6.28. The side chain cholesteric homopolymers. (From Chiellini *et al.*, 1983.)

x	T_g	T_c
12	132	260
16	125	245
24	117	238

Figure 6.29. The side chain cholesteric copolymers. (From Freidzon *et al.*, 1980.)

High viscosity is the main drawback for cholesteric liquid crystalline polymers in applications. However, cholesteric polymers have their advantages. They may exhibit the memory effect. These polymers make processing and handling easily. Therefore, cholesteric liquid crystalline polymers have become the new materials for optical filters, temperature indicators, *etc.* The Merck product with the trade name Transmax is actually associated with the cholesteric liquid crystalline polymers.

Ueno *et al.* (1986) synthesized polysiloxane cholesteric copolymers. The polysiloxane in a solvent was coated on the biphthalate polyethylene (PET), a black substrate, making the helical axis perpendicular to the substrate. The cholesteric liquid crystal was in the Granjean texture. The displayed information was written by an Argon ion laser and the cholesteric polymers were thus heated up into an isotropic state. When cooled down, the helical axes were randomly distributed and thus the sample was opaque. The rest of such polymers remained in the Granjean texture and displayed a bright color because of the selective reflection. If one observed through a circular polarizer of the same sense as the cholesteric polymers, the scattering light was blocked. Consequently, a black image was displayed on a color background. If observed through a circular polariser of the opposite sense, a white image was displayed on a black background.

The polysiloxane cholesteric polymers doped by diphenyl ketone were used as an optical storage material (Pinsl *et al.*, 1987). The display was based on the convertible photo-reaction. The information was written by a semiconductor laser of wavelength $\lambda = 800$ nm. The storage density of 1.33×10^9 bytes/cm^2 was achieved. The image can be kept up to two or three months.

Table 6.10.   Liquid crystalline polymers C6M and chiral molecules CB15 (28 wt%): pitch and reflective peak wavelength as functions of polymerization temperature before and after the removal of CB15. (From Hikmet *et al.*, 1993.)

$T/\,^\circ$C	λ_{max}/nm with CB15	P/nm with CB15	λ_{max}/nm after removal of CB15	P/nm after removal of CB15
30	543	337	380	236
40	551	343	422	263
50	583	362	433	269
60	598	372	449	281
70	606	378	462	288

Recently, Hikmet *et al.* (1993) mixed liquid crystals C6M

$$\text{CH}_2=\text{CH}-\text{COO}-(\text{CH}_2)_6\text{O}-\!\!\!\bigcirc\!\!\!-\text{COO}-\!\!\!\bigcirc\!\!\!-\text{OOC}-\!\!\!\bigcirc\!\!\!-(\text{CH}_2)_6-\text{OOC}-\text{CH}=\text{CH}_2$$
$$\underset{\text{CH}_3}{}$$
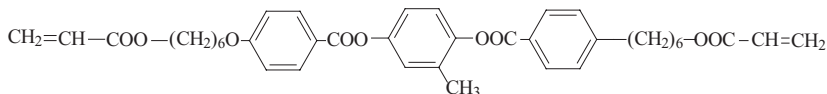
together with chiral molecule CB15 (no reacting unit)

$$\text{CH}_3-\text{CH}_2-\text{C}^*\text{H}(\text{CH}_3)-\text{CH}_2-\!\!\!\bigcirc\!\!\!\bigcirc\!\!\!-\text{C}\!\equiv\!\text{N}$$
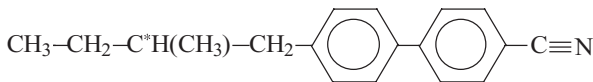
Then the liquid crystalline monomers were polymerized under an ultraviolet irradiation. The system became a cholesteric gel. After heating the sample and removing the chiral molecules CB15, the helical structure remained. In Table 6.10, the cholesteric pitch P and reflective peak wavelength $\lambda_{\max}$ are listed as a function of temperature at which polymerization occurs. The CB15 weighed 28% in the original mixture before the removal.

6.4. NON-LINEAR OPTICAL LIQUID CRYSTALLINE POLYMERS

The liquid crystalline polymer's potential application in non-linear optics has been the interest of research since the material appeared, as reviewed by Dubois *et al.* (1993).

As an infrared YAG laser beam of wavelength $1.06\,\mu\text{m}$ impacts a non-linear optical (NLO) medium, a green light of $\lambda = 0.53\,\mu\text{m}$ is observed. This is the second harmonic generation (SHG) effect. The medium is the NLO sample. In addition to the second harmonic generation, the NLO effects include the Pockel effect, the Kerr effect, the third harmonic generation and the four-wave mixing.

In the presence of an electric or optical field, the component of polarization in the sample can be expressed as (the convention summation is applied)

$$P_i = \chi_{ij}^{(1)}E_j + \chi_{ijk}^{(2)}E_jE_k + \chi_{ijkl}^{(3)}E_jE_kE_l + \cdots , \qquad (6.49)$$

where $\chi_{ij}^{(1)}$ is the linear susceptibility. It is related with the refractive index as $\chi_{ij}^{(1)} = n_{ij}^2 - 1$; $\chi^{(2)}$ and $\chi^{(3)}$ are the third and fourth rank tensors, and are termed as the second and the third NLO susceptibilities, respectively. In general, $\chi^{(3)}$ is less than $\chi^{(2)}$. E_i is the i-th Cartesian component of

the electric field of the laser beam. The non-zero $\chi^{(2)}$ and $\chi^{(3)}$ affect the refractive index of the media. The NLO effects associated with $\chi^{(2)}$ are the Pockel effect, the second harmonic generation, *etc.*; and those related with $\chi^{(3)}$ are the Kerr effect, the third harmonic generation, *etc.*.

In order to achieve high NLO coefficients $\chi^{(2)}$ and $\chi^{(3)}$, the medium must follow two criteria: the constituent blocks must have high NLO polarizabilities, depending on the chemical structure; and the medium must have the appropriate symmetry. For those possessing the center-symmetry, $\chi^{(2)}$ vanishes. Among them are amorphous and isotropic materials. However, these media may have non-zero $\chi^{(3)}$. In the presence of an electric field, some of these materials may change from center-symmetrical to non-center symmetrical.

The high molecular NLO polarizability is a basic requirement. For an independent molecule under an electric field the molecular electric moment (the i-th component) is as follows

$$\mu_i = \alpha_{ij}E_j + \beta_{ijk}E_jE_k + \gamma_{ijkl}E_jE_kE_l + \cdots , \qquad (6.50)$$

where α, β and γ are the molecular polarizabilities of the individual molecule.

The relation between the molecular polarizabilities to the bulk susceptibilities depends on the molecular density, N, and the local internal field factor F. Particularly, it relates to the molecular orientation. For example, the second NLO coefficient is expressed as

$$\chi^{(2)}_{IJK} = NF\beta_{ijk}\langle\cos\theta_{Ii}\cos\theta_{Jj}\cos\theta_{Kk}\rangle, \qquad (6.51)$$

where θ_{Ii} is the angle between the i-th component of molecular polarization and the I-th component of bulk polarization. The bracket designates the statistical average over all the molecules. Similarly, the relationship for the third NLO coefficient is expressed as

$$\chi^{(3)} \propto \gamma\langle\cos^4\theta\rangle. \qquad (6.52)$$

The three typical molecular configurations and the associated second and third NLO polarization coefficient summary are shown in Figure 6.30. Those with the center symmetry have no second NLO property. However, they may have a non-zero value if an electric field destroys the up and down symmetry of molecular orientation.
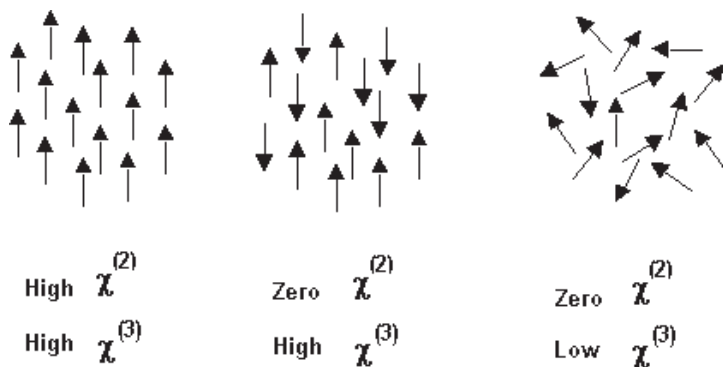
Figure 6.30. The NLO coefficients for different molecular orientation configurations. (Modified from Donald and Windle, 1992.)

Table 6.11. The second NLO coefficients of several important NLO inorganic materials and the organic crystal MNA (The Chemical Rubber Company, 1971) (unit: 10^{-12} m/V).

Material	Tensor element/ijk	$\chi_P^{(2)}$	$\chi_D^{(2)}$
quartz	111	1.37	0.8
KDP(KH$_2$PO$_4$)	321	21.6	0.94
zinc oxide	333	26.3	14
LiNbO$_3$	333	410	82
MNA	333	540	500

The third NLO susceptibility may not be zero even though the molecular orientation is completely randomly distributed, *i.e.*, in an isotropic state. The highly ordered phase usually has a high value for the third NLO coefficient. For example, the highly ordered nematic phase has a third NLO coefficient five times that in the isotropic phase.

The NLO materials used so far are mainly inorganic materials, such as quartz, KDP, zinc oxide, LiNbO$_3$, *etc.* The ions in these inorganic materials are responsible for the NLO properties. The ions have a great mass so that the NLO coefficients of these NLO materials are small at high frequency. Table 6.11 lists elements of the NLO tensors of the Pockel effect and of the second harmonic generation for some widely used NLO materials, $\chi_P^{(2)}$ and $\chi_D^{(2)}$.

The second harmonic generation (SHG) works usually at a much higher frequency than the Pockel effect does so that the ion contribution to SHG is usually very small. Consequently, $\chi_D^{(2)}$ of inorganic crystals is less than $\chi_P^{(2)}$. Table 6.11 also lists the values of the organic crystal MNA, *i.e.*, 2-methyl-4-nitroaniline, whose $\chi_D^{(2)}$ and $\chi_P^{(2)}$ are high and approximately the same. It demonstrates that electron polarization in the organic material dominates. In addition, organic materials have advantages such as a high optical damage threshold, fast response, and easy processing.

In order to achieve high second NLO coefficients, a concept of the following conjugate molecules was proposed:

$$donor - conjugate\ electron\ system - acceptor$$

donors:

$$O^{(-)} > N\genfrac{}{}{0pt}{}{Me}{Me} > NH_2 > OCH_3 > CH_3$$

acceptors:

$$N_2^{(+)} > NO_2 > COCH_3 > CHO > CN$$
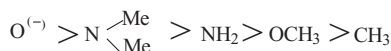
Molecules must meet the following structural requirements:

(1) Molecules must possess large permanent dipole moments. Donor and acceptor units are placed at opposite terminals;
(2) Electrons move easily along the long axis;
(3) Long, linear molecular shape.

The liquid crystals, in fact, meet the above requirements: large molecular length, linear molecular configuration and with polar terminals. Unfortunately, low molecular mass liquid crystals have difficulty in maintaining the non-center symmetry after electrical polarization. Moreover, it is difficult to process the low molecular mass liquid crystal materials. Apparently, polymers are good candidates in these respects.

The organic materials with the appropriate second NLO coefficient are classified as three different kinds:

(1) Organic crystals,
(2) Langimur-Blogette films,
(3) Polymer films.

It is difficult to grow a good organic crystal film and a Langimur-Blogette film of up to 1 micron thickness. However, polymers have a wide choice and can be tailored to meet the above requirements. The polymers may be side chain liquid crystalline polymers, ferroelectric liquid crystalline polymers and amorphous polymers. Among them the side chain liquid crystalline polymers have drawn more attention.

The processing steps are as follows. First, deposit a film of one micron thickness of the material on a substrate by means of dip or spin-coating. Then, apply an electric field at temperatures greater than the glass temperature. Finally, cool down the sample to room temperature under the presence of a d.c. electric field. The pole procedure is shown in Figure 6.31, where T_g and T_p are the polarization and glass temperatures, respectively.

Main chain liquid crystals are not easily polarized. They are unable to keep the uniform orientation for a long period because the molecule incorporated by NLO groups is generally very long. In addition, the response time is very great. Therefore, the main chain liquid crystals are not appropriate for producing a reasonable second NLO effect. However, PBLG is an exception. In solution, PBLG is in the cholesteric phase and can be poled under an electric field of medium scale. PBLG has a high dipole moment and high second NLO susceptibility β. For a PBLG of molecular weight 500,000, β can be as high as 500×10^{-30} esu, which is much greater than conventional NLO active small molecules such as DANS
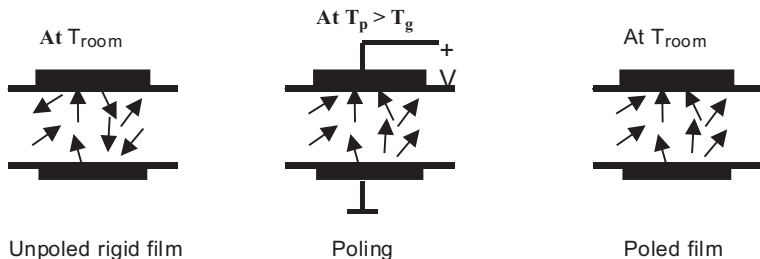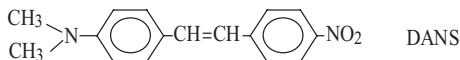
Figure 6.31.   The schematic of the pole procedure, where T_g and T_p are the polarization and glass temperature, respectively. (Modified from Dubois, 1993.)

whose β is about 60×10^{-30} esu ($\lambda = 1.9\,\mu$ m). The consequent second NLO coefficient $\chi^{(2)}$ of PBLG can reach up to 10^{-7} esu (Levine and Bethea, 1976).

The side chain polymeric liquid crystal (as host) is doped with NLO active small molecules (as guest). In the matrix of side chain polymeric liquid crystals, the NLO active molecules are aligned along the director. The system is then poled and processed. Meredish *et al.* (1982) adopted a side chain polymeric liquid crystal as the host and DANS as the dopant, as shown in Figure 6.32. The pole field is $1.3\,$KV/mm. The resultant second NLO coefficient reached 6×10^{-9} esu. The glass temperature of the polymers is low ($T_g < 50\,^{\circ}$C) thus the orientation is not good enough.

This method has a disadvantage. The dissolution of the NLO active guest in a side chain liquid crystalline polymer is usually poor so that the concentration of the NLO active component in the system is limited and thus $\chi^{(2)}$ is accordingly low.

To overcome the drawback, copolymers are proposed for the NLO purpose. In a side chain liquid crystalline polymer some side mesogenic groups are replaced by NLO active groups. In this method, the concentration of
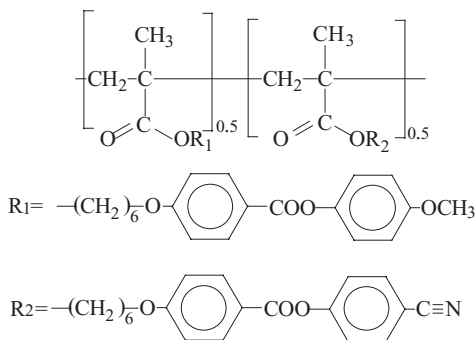
phase transition: G (37 °C) N (101 °C) I

The dye molecule (guest)

DANS $\lambda = 425$ nm $\beta = 4.5 \times 10^{-28}$ esu

Figure 6.32.   The host (side chain polymeric liquid crystal)—guest (DANS) system. (Modified from Meredish *et al.*, 1982.)

NLO active groups can be tailored and controlled. Moreover, the orientation of NLO active groups in the copolymer form are better than in the guest–host mode. The NLO coefficient d_{33} of a side chain polymeric liquid crystal is plotted as a function of restore time in Figure 6.33 (Singer *et al.*, 1988). $d_{33}(6 \times 3)$ is another expression of the second NLO coefficient $\chi_{ijk}^{(2)}$. The side chain polymeric liquid crystal is PMMA. DCV is the NLO active unit either as the side groups in copolymer DCM-PMMA or as the guest in the guest–host system DCV/PMMA. The chemical formula of DCV is shown in Figure 6.33. It is demonstrated that d_{33} of the copolymer is almost unchanged after one month's restore time while d_{33} in guest–host mixture is reduced by 70%.

$\chi^{(2)}$ of copolymers increases as the concentration of NLO active side groups increases, see Figure 6.34.
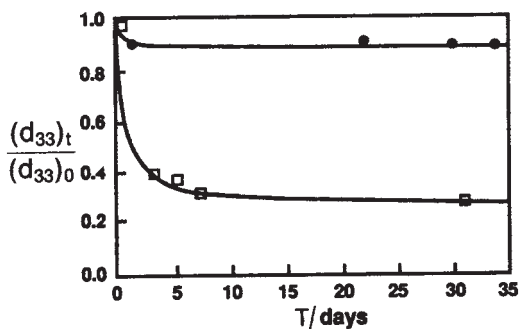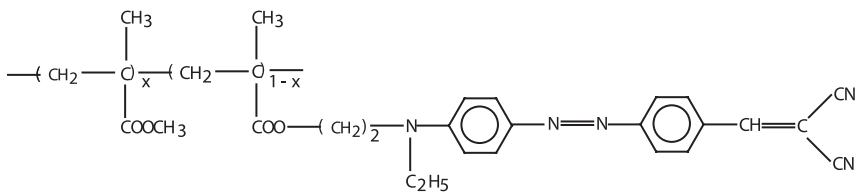
Figure 6.33.   The NLO coefficient d_{33} of a side chain liquid crystalline polymer PMMA as a function of restore time. (Modified from Singer *et al.*, 1988.)
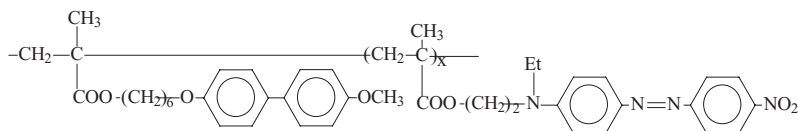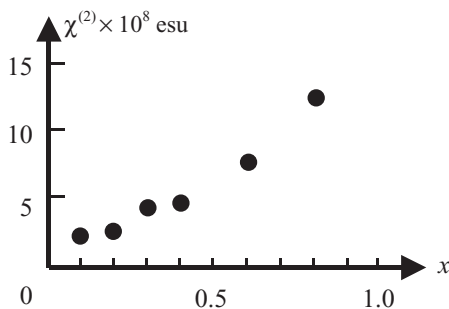
Figure 6.34. $\chi^{(2)}$ of copolymer as a function of concentration of NLO active side groups. (From Koide *et al.*, 1991. Reproduced by permission of Taylor & Francis, <http://www.tandf.co.uk/journals/tf/02678292.html>)

Griffin synthesized a side chain polymeric liquid crystal in which side group mesogens are NLO active themselves (Griffin *et al.*, 1988), shown below
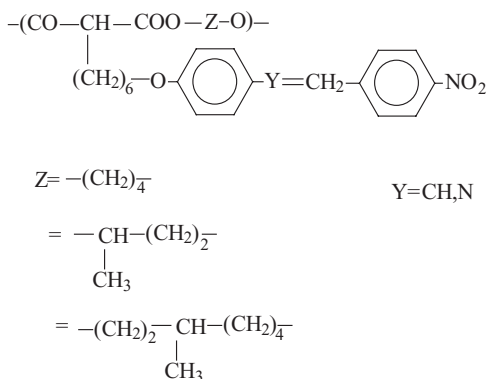
The material exhibits low transparency because its glass transition temperature T_g is low. Therefore, after the electric poling, the molecular orientation is not satisfactory and thus the sample scatters light. Recently, a side chain polymeric liquid crystal with high T_g was synthesized and the performance got improved. Mclulloch and Beiley (1991) achieved d_{33} of 19×10^{-7} esu ($\lambda = 1.31 \, \mu m$).

Amorphous side chain polymers with NLO active side groups have an appropriate second NLO coefficient. But further study revealed that these side chain polymers if in the liquid crystal phases have better NLO behavior. For the side chain polymer shown below, $\chi^{(2)} = 8 \times 10^{-9}$ esu in a liquid crystal phase which is greater than the value in the amorphous phase by a factor 1.5. The poling field in both cases is 15 KV/mm (Amano *et al.*, 1990).
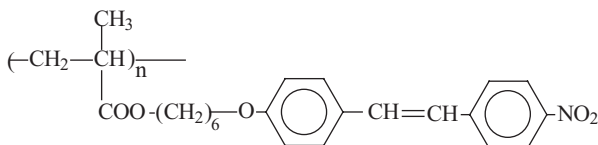
McCulloch *et al.* (1991) and Koide *et al.* (1990) observed such phenomena as well in the side chain copolymers.

The orientation of side chain polymeric liquid crystals after the poling is not ideal and the defects appear often. Two techniques were proposed to deal with these problems:

(1) As we know, the small molecular mass liquid crystals are easy to align. Therefore, one may align monomers first and then polymerize them (Broer *et al.*, 1989; Stamatoff *et al.*, 1990). Consequently, a good aligned sample is obtained. But this technique is not suitable for a large sample in which the internal stress due to the density change during the polymerization results in defects.
(2) Apply the concept of liquid crystal networks: crosslink the backbone of NLO side chain liquid crystalline polymers when they are in the liquid crystal phase. In the presence of a mechanical force the resultant sample may be well aligned because of the interaction between the network strands and the side groups. The mechanical effect is equivalent to the electric or magnetic field. The re-orientation response of the liquid crystal is a quadratic function of the applied electric field, but it is linearly proportional to the mechanical stress. Thus, the mechanical stress is more effective in aligning the liquid crystals and is expected to produce less defects and hence to promote the transparency of the sample.

Hirschmann *et al.* (1991) synthesized a smectic liquid crystal network whose side chains contain NLO active groups. After the poling with the

electric field 19 V/micron, the second NLO coefficients $\chi_{333}^{(2)} = 2.2 \times 10^{-7}$ esu and $\chi_{311}^{(2)} = 0.14 \times 10^{-7}$ esu were achieved. The study is in an early stage and further improvement of the NLO performance is expected.

Ferroelectric side chain liquid crystalline polymers have been synthesized recently. Because of their non-central symmetry they don't need to be poled. This has led to the recent active research efforts in the field of ferroelectric side chain liquid crystalline polymers (Guglielminetti *et al.,* 1990; Spassky *et al.*, 1989; Kapitza *et al.*, 1986).

In general, the ways to promote the third NLO coefficient is consistent with the methods that promote the second NLO coefficients. For the former, it is not necessary to pole samples. The molecule does not necessarily have to have a non-symmetrically electronic structure. According to recent calculation by Medrano (1989) the molecules with donor (or acceptor) groups at their terminal exhibit high molecular NLO polarizability γ and hence a high third NLO coefficient $\chi^{(3)}$.

Prasad (1988) further demonstrated that γ increases remarkably with the increase of the molecular length n. The relation of γ and n of the para-acetylene ($C_n H_{n+2}$) is shown in Figure 6.35 in which γ increases exponentially with n. Therefore, the long molecular shape and the linear conjugated system are still the essential requirements for a high $\chi^{(3)}$. Apparently, liquid crystals are a good candidate.

The rigid main chain liquid crystalline polymers PBO, the molecular formula being
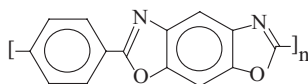
and PBTZ with the molecular formula
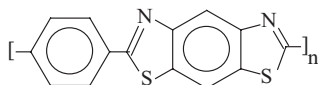
are two interesting materials of this type (Ulrich, 1988). PBO/PBTZ in solution such as the diazomethane is a lyotropic liquid crystal. Removal of the solvent after being aligned, led to the $\chi^{(3)}$ of the mixture reaching up to 10^{-10} esu.
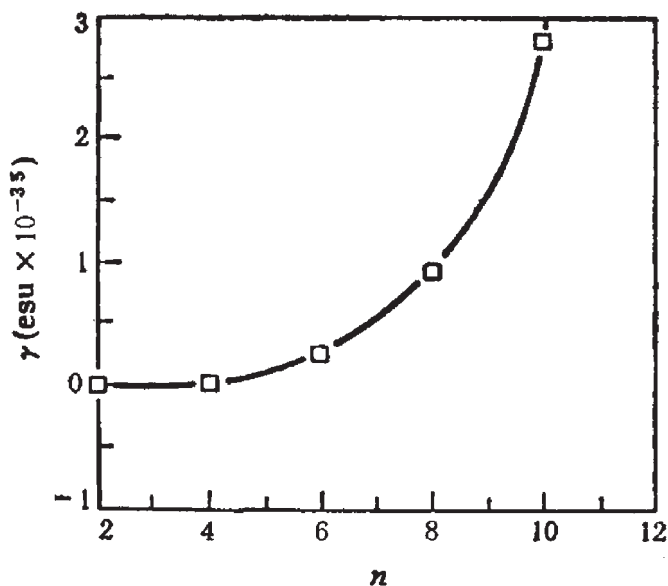
Figure 6.35. The relation of the third molecular NLO polarizability γ and n for para-acetylene. (From Prasad, 1988.)

Liquid crystalline polymers can be applied in the electro-optic modulator. Materials for such an application must be able to vary their refractive index according to the electric (optical) field, *i.e.*,

$$\frac{1}{n_{ij}^2} = \left(\frac{1}{n_{ij}^2}\right)_0 + \gamma_{ijk}E_k + S_{ijkl}E_kE_l + \cdots, \qquad (6.53)$$

where $(1/n_{ij}^2)_0$ is the refractive index in the absence of electric field, γ_{ijk} and S_{ijkl} are the Pockel coefficients and the Kerr coefficients, respectively. Typically, the components of S are less than the elements of γ. The Pockel coefficients γ_{ijk} are proportional to the second NLO coefficients, $\chi_{ijk}^{(2)}$, the relation is given by the following equation

$$\chi_{ijk}^{(2)}(-\omega, \omega, 0) = -\frac{1}{2}\frac{1}{n_{ii}^2(\omega)n_{jj}^2(0)}\gamma_{ijk}(-\omega, \omega, 0), \qquad (6.54)$$

where γ_{33} and d_{33} are compared in Figure 6.36 (Dubois *et al.*, 1993). It is demonstrated that Equation (6.52) is in agreement with experimental data. $\gamma_{ij}(6 \times 3$ tensor) is an another expression of $\gamma_{ijk}(3 \times 3 \times 3$ tensor).
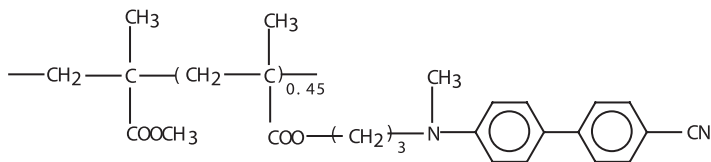
	d_{33}	γ_{33}			(pm/V)
Wavelength/micron	1.06	1.32	1.06	0.83	0.6328
Experimental	12	3.99	6.03	6.16	6.12
Calculated	10	4.6	4.9	5.6	7.5

Figure 6.36.   The comparison of the Pockel coefficient γ_{33} and the second NLO coefficient d_{33}. (Modified from Dubois *et al.*, 1993.)
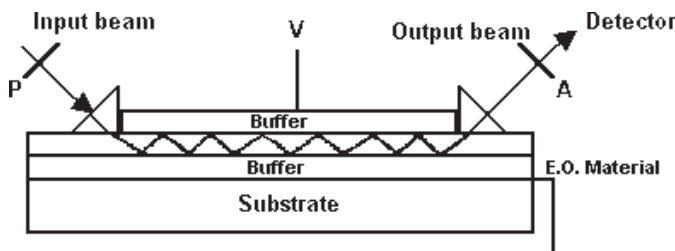
Figure 6.37.   The schematic structure of a planar optical opto-electric modulator. (Modified from Dubois, 1990.)

   In Figure 6.37 the structure of a planar optical opto-electric modulator is schematically depicted. It consists of three spin-coated layers on a silicon wafer: two are light-buffer layers and a poled side chain polymeric liquid crystal layer, the polarization being perpendicular to the plane. In such a configuration, the electric field of light propagating along the optical wave-guide is parallel to the director of the liquid crystals.

   Dubois (1990) constructed an opto-electric modulator in terms of a liquid crystalline polymer, for which the wavelength $\lambda = 1.3$ microns and the modulation frequency $f = 1\,\text{GHz}$.

6.5.   FERROELECTRIC LIQUID CRYSTALLINE POLYMERS

The chiral smectic C liquid crystal phase, S_C*, was mentioned in Chapter 1. In this phase, molecules are arranged in layers and are tilted by an angle θ with respect to the normal to the layers. θ is a function of temperature. Traveling along the normal of the smectic layers the azimuthal angle of molecular tilt directions vary to form a helix. There is a C_2 symmetry axis in each layer. When the helix is unwound due to, *e.g.*, the anchoring effect, these C_2 axes of all smectic layers point to a common direction, *e.g.*, pointing up. Thus the sample exhibits a macroscopic polarization, see Figure 6.38.

Such a homogeneous alignment can be maintained by an electric field, the spontaneous polarization of the unwound ferroelectric liquid crystals being along the electric field. Reversing the electric field, the ferroelectric liquid crystal molecules switch their spontaneous polarization from up to down, *i.e.*, their orientation jump from $+\theta$ to $-\theta$. The magnitude of the tilt angle θ is kept unchanged but the tilt azimuthal becomes the opposite.

By appropriately installing two polarizers on two surfaces of the cell the bright/dark states can be obtained by changing the polarity of the applied voltage. The response of the liquid crystal cells is much faster than other liquid crystal displays. The response time is inversely proportional to the spontaneous polarization P_s and applied electric field E, and is linear in proportion to viscous coefficient η. It is typically tens of microseconds. In comparison, the relaxation time is generally tens of milliseconds for other liquid crystal displays. The ferroelectric liquid crystal display exhibits the
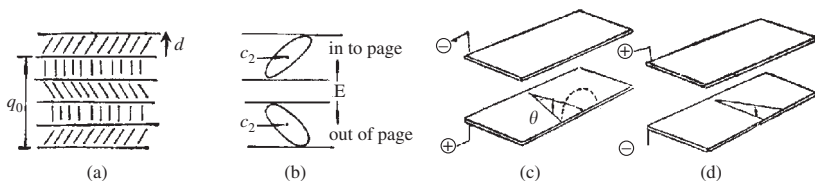
Figure 6.38.   The chiral smectic C phase (a and b) and the ferroelectric liquid crystal display (c and d).

fastest liquid crystal electro-optic effect so far and hence has attracted great attention.

Two of the important ferroelectric liquid crystal are

$$C_6H_{13}O-\text{⟨○⟩}-CH{=}N-\text{⟨○⟩}-CH{=}CH-COOCH_2\overset{*}{C}HC_2H_5$$
$$\underset{Cl}{|}$$

with the transitions being

$$K \quad 60 \quad S_H* \quad 64 \quad S_C* \quad 78 \quad S_A \quad 135 \quad I$$

and

$$C_{10}H_{21}O-\text{⟨○⟩}-CH{=}N-\text{⟨○⟩}-CH{=}CH-COOCH_2\overset{*}{C}HC_2H_5$$
$$\underset{CH_3}{|}$$

with the transitions being

$$K \quad 76 \quad S_C* \quad 95 \quad S_A* \quad 117 \quad I$$
$$\vdash\!\!\!-\!\!\!-\!\!\!-\!\!\!- S_H \quad 63 \!\!-\!\!\!-\!\!\!-\!\!\!-\!\!\!-\!\!\dashv$$
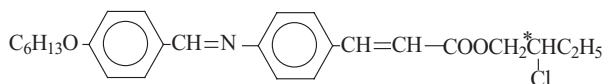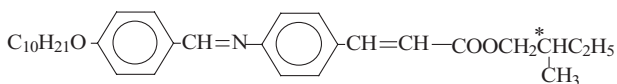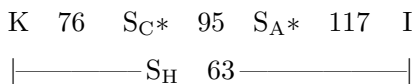
In the last few years the anti-ferroelectric liquid crystal $S_{CA}*$ was discovered by Chandani *et al.* (1988, 1989) in MHPOBC

$$C_8H_{17}O-\text{⟨○⟩}-\text{⟨○⟩}-COO-\text{⟨○⟩}-COO\overset{*}{C}HC_6H_{13}$$
$$\underset{CH_3}{|}$$
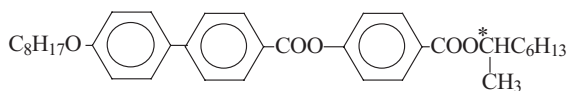
In the anti-ferroelectric liquid crystal molecules are aligned in layers and the layers are grouped in pairs. The molecules in one layer of each pair are tilted in an azimuthal direction opposite to those in the other, as shown in Figure 6.39. Moving along the layers' normal, the tilt azimuthal of molecules in layers varies to form a double helical structure with two helices differing by a phase shift of π. In the anti-ferroelectric liquid crystal, the number of layers with opposite tilt angle is almost the same, there is not any macroscopic spontaneous polarization in the anti-ferroelectric liquid crystal even if the helix is unwound by any reason. Since the anti-ferroelectric liquid crystal has been discovered great interest has been paid to it.
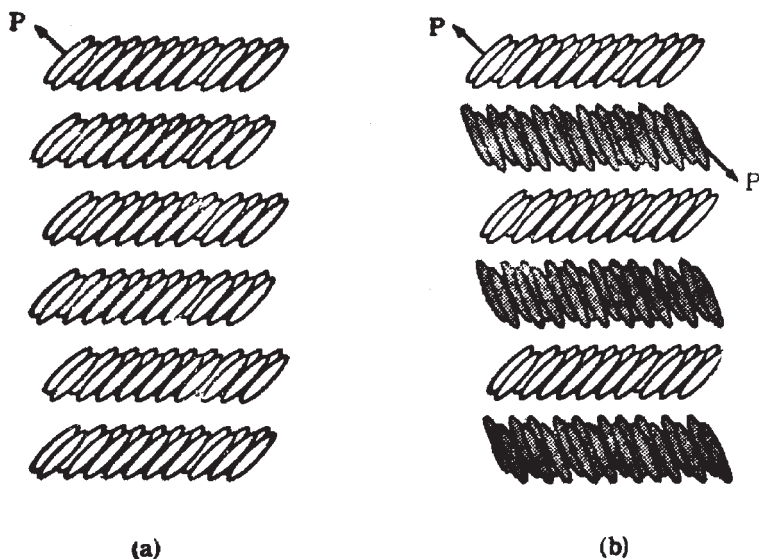
Figure 6.39.   The molecular packing of unwound samples: (a) ferroelectric and (b) anti-ferroelectric liquid crystals. (From Goodby *et al.*, 1993.)

Compared with conventional ferroelectric liquid crystals, anti-ferro-electric liquid crystals have the following advantages:

(1) It has an electric threshold between electrically induced ferroelectric to anti-ferroelectric transition and hence it is suitable for multiplexing liquid crystal displays.
(2) It shows three opto-electric states and exhibits double hysteresis in the electric-optic curve. Thus, it can display an image with a gray level and can be easily driven.

Assume a side chain liquid crystal polymer, consisting of a flexible backbone and mesogenic side groups, is able to form the $S_{C}*$ phase and its glass transition is below the ambient temperature, such a side chain liquid crystal polymer will be expected to show ferroelectricity. The side groups are packed in a way similar to small molecular mass ferroelectric liquid crystals. The backbone is suppressed between layers, occasionally penetrating into them. The conformation of the backbone is discus-like.

Introduce the chiral center into one end of the side groups and one may obtain a cholesteric liquid crystalline polymer. If both mesogenic units

Table 6.12.   The phase transitions of small molecular mass liquid crystals: L1, L2 and L3.

Sample	K		S_1		S_C*		S_A		Ch		I
L1	*	52			*	105	*	130			*
L2	*	42			*	100	*	130	*	132	*
L3	*	40	*	46	*	101	*	118			*

*S_1 is an unknown smectic phase.

and chiral monomers in a liquid crystalline copolymer, as side groups, are alternatively attached to the backbone, the liquid crystalline polymer may exhibit the cholesteric phase. Such a polymer may show a ferroelectric phase S_C*.

Shibaev *et al.* (1984) first synthesized a ferroelectric side chain polymeric liquid crystal. In the following years a lot of liquid crystalline polymers of such kind were synthesized. In early research studies techniques used to understand polymers and whether they showed the liquid crystal phase were limited so that the conclusion was ambiguous. It was only in 1988 when Uchida *et al.* (1988) measured the spontaneous polarization and the tilt angle that people became convinced that this side chain polymer in the literature (Shibaev *et al.*, 1984) is indeed a ferroelectric liquid crystal.

The following three molecules show the ferroelectric liquid crystal phase S_C* (Sekiya *et al.*, 1993). Their phase transitions are listed in Table 6.12.

L_1: $C_{10}H_{21}O$ —⬡— COO —⬡—⬡— COO$\overset{*}{C}$H$(CH_3)C_3H_7$

L_2: $C_{10}H_{21}O$ —⬡— COO —⬡—⬡— COO$\overset{*}{C}$H$(CH_3)COOC_2H_5$

L_3: $C_{10}H_{21}O$ —⬡— COO —⬡—⬡— COO$\overset{*}{C}$H$(CH_3)C_6H_{13}$
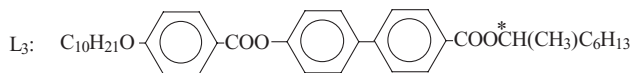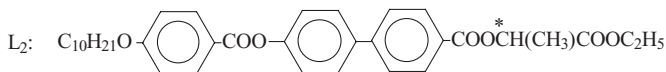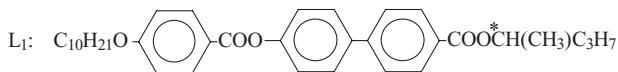
The side chain polysiloxane liquid crystalline polymers P1, P2 and P3 composed of the above three ferroelectric liquid crystals as the side groups exhibit the ferroelectric liquid crystal phase, their chemical formulae being respectively.

Table 6.13. The phase transitions of side chain polymeric liquid crystals: P1, P2 and P3. (From Sekiya *et al.*, 1993.)

Sample	G		S_C*		S_A		I
P1	*	30	*	130	*	107	*
P2	*	23	*	132	*	148	*
P3	*	22	*	122	*	152	*

P1: $-(OCH_2CH)_{\overline{n}}-$
$(CH_2)_{10}O$-⬡-COO-⬡-⬡-$COO\overset{*}{C}H(CH_3)C_3H_7$

P2: $-(OCH_2CH)_{\overline{n}}-$
$(CH_2)_{10}O$-⬡-COO-⬡-⬡-$COOCH(CH_3)COOC_2H_5$

P3: $-(OCH_2CH)_{\overline{n}}-$
$(CH_2)_{10}O$-⬡-COO-⬡-⬡-$COO\overset{*}{C}H(CH_3)C_6H_{13}$
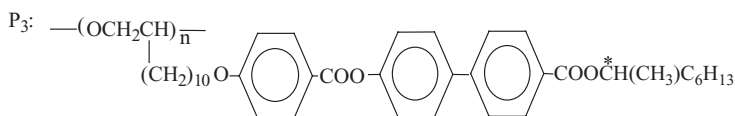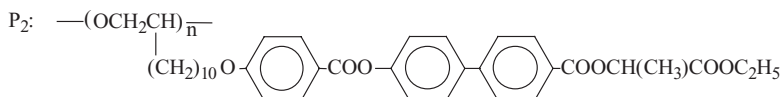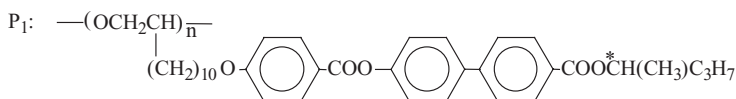
The phase transitions of the three side chain polymeric liquid crystals are listed in Table 6.13.

The three side chain polymeric liquid crystals have approximately the same molecular weight, for P1: $Mn = 4,600$; P2: 4,700 and P3: 4,900.

It is observed that compared with the constituent small molecular mass liquid crystal monomers the side chain polymeric liquid crystals have a wider S_C* temperature range, its upper limit going up while its lower limit goes down.

It has been found experimentally that the spontaneous polarization P_s of side chain liquid crystalline polymers is more or less the same as that of small molecular mass liquid crystals, *i.e.*, so far as the chemical formula of the side group of a side chain liquid crystalline polymer is the same as that of a small molecular mass liquid crystal. This phenomenon illustrates that either the side groups in the side chain liquid crystalline polymer or the small molecular mass ferroelectric liquid crystal in their S_C* phase are aligned in same way. The dependence of P_s on temperature for the three small molecular mass ferroelectric liquid crystals L1, L2 and L3 and their polymer counterparts P1, P2 and P3 are depicted in Figure 6.40.
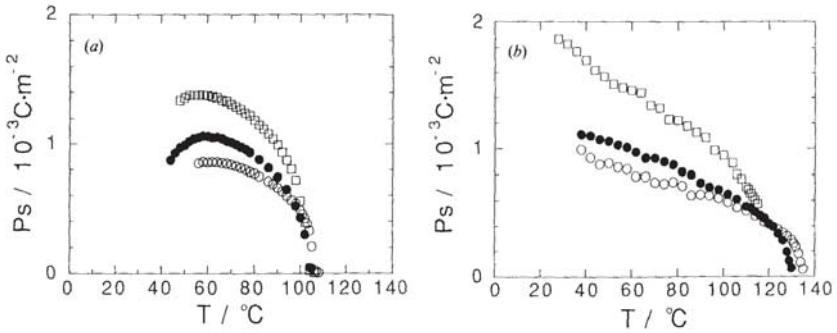
Figure 6.40.   The dependence of P_s on temperature for (a) the small molecular mass ferroelectric liquid crystals L1, L2 and L3 and (b) their polymer counterparts P1, P2 and P3. (From Sekiya *et al.*, 1993. Reproduced by permission of Taylor & Francis, <http://www.tandf.co.uk/journals/tf/02678292.html>)

The data were obtained by Sekiya *et al.* (1993) in terms of the triangle-waveform method (Miyasato *et al.*, 1983). They used a liquid crystal film of 7 microns thick. The peak value of the applied triangle-wave voltage was 20 KV/mm with frequency being 50–100 Hz for small molecular mass ferroelectric liquid crystals and 0.02–2 Hz for ferroelectric liquid crystalline polymers. It is observed from the experiments that P_s varies according to the chemical formulae for the small molecular mass ferroelectric liquid crystals, L1 (○) < L2 (●) < L3 (□); for the side chain liquid crystalline polymers, the sequence is the same; P1 (○) < P2 (●) < P3 (□). The tilt angle for both small molecular mass ferroelectric liquid crystals and side chain ferroelectric liquid crystalline polymers were measured. They were approximately same, see Figure 6.41. It is further illustrated that the molecular arrangement in both materials are essentially the same.

The backbone affects the dynamic behavior of the ferroelectric liquid crystalline polymer. Sandwiching the two kinds of ferroelectric liquid crystals between two ITO-coated glass plates of 1.5 microns gap respectively, one constructs a SSFLC (surface stabilized ferroelectric liquid crystal) cell. The switch time between two optical states τ is determined by

$$\tau = \frac{\eta}{P_{sE}}. \tag{6.55}$$

Measuring τ, P_s and the applied electric field E, the apparent rotational viscosity of ferroelectric liquid crystals is obtained.

τ for small molecular mass ferroelectric liquid crystals L1–L3 ranges between 1 and 10^3 microseconds, and for side chain ferroelectric liquid
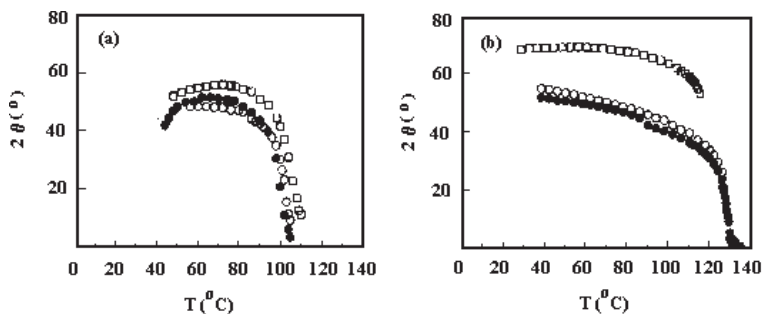
Figure 6.41. The dependence of the tilt angle 2θ on temperature for (a) the small molecular mass ferroelectric liquid crystals L1, L2 and L3 and (b) their polymer counterparts P1, P2 and P3. (From Sekiya *et al.*, 1993. Reproduced by permission of Taylor & Francis, <http://www.tandf.co.uk/journals/tf/02678292.html>)
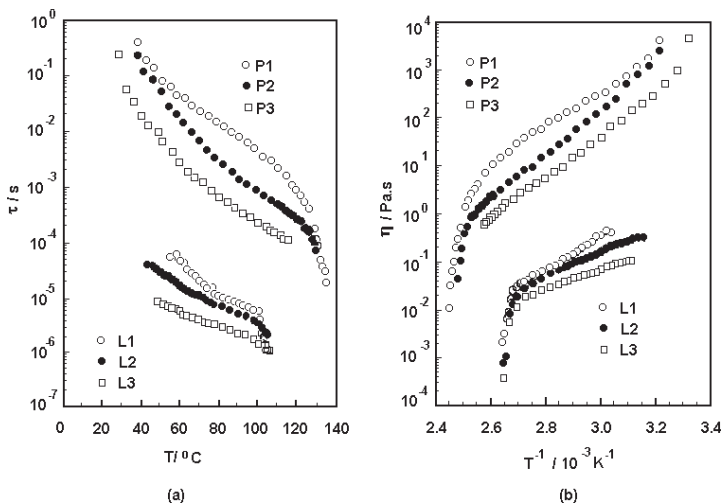
Figure 6.42. The switch time τ (a) and the rotational viscosity η (b) *vs.* temperature for small molecular mass (L1–L3) and polymeric (P1–P3) ferroelectric liquid crystals. (Modified from Sekiya *et al.*, 1993. Reproduced by permission of Taylor & Francis, <http://www.tandf.co.uk/journals/tf/02678292.html>)

crystalline polymers P1–P3 τ is mainly in the range of 1–10^3 milliseconds. The difference is about 10^2–10^3 times! This is shown in Figure 6.42(a). Substituting the values for P_s and E the rotational viscosities are obtained and shown in Figure 6.42(b). The viscosity difference is about 10^2–10^3 times, similar to that of the relaxation time. The difference results from the effect of the backbone of the side chain ferroelectric liquid crystalline polymer.

(a)   (b)
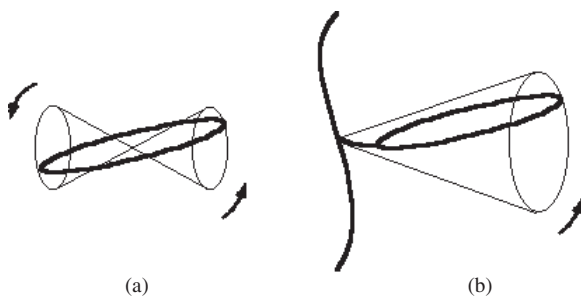
Figure 6.43.   The molecular movement during the polarization inversion for (a) small molecular mass and (b) polymeric ferroelectric liquid crystals. (Modified from Sekiya *et al.*, 1993.)

For the small molecular mass ferroelectric liquid crystal when reversing the polarity of the applied electric voltage the molecules rotate locally while their molecular mass centers don't necessarily move accordingly. But for side chain ferroelectric liquid crystalline polymers, as one of the side group ends is confined to backbone, shown in Figure 6.43, the polarity reversion must be accompanied by the movement of their mass centers, which causes a backflow in order to re-distribute the mass centers. Moreover, the side groups may collide with each other. The effect results in the displacement of the backbone. The above effects increase the difficulty of re-orientation and hence increase the viscosity.

Endo *et al.* (1992) measured the optical transmission and the polarity-reverse current during the polarity reversion of a side chain ferroelectric liquid crystalline polymer. It was found that both parameters reached peak values at the same time. It was concluded that the rigid core of the side groups responsible for birefringence moves simultaneously with the dipole moment reversion and the latter contributes to the polarity reversion current. The FTIR experiment suggested that the backbone moves when the polarity is reversed.

The liquid crystalline polymer in the experiment is
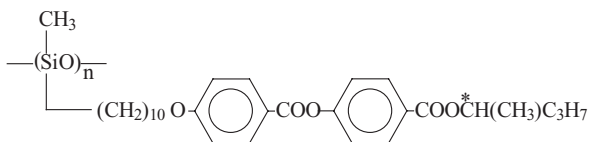
its phase transition being

$$G \quad 37 \quad S_{C^*} \quad 87 \quad S_A \quad 117 \quad I.$$
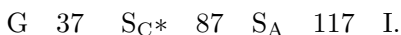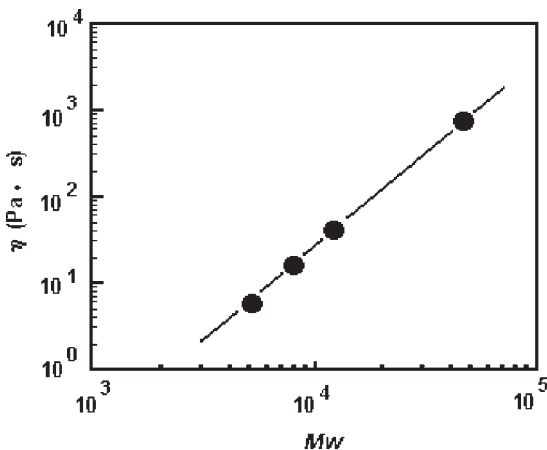
Figure 6.44.   The relation of rotational viscosity η and molecular weight Mw at $600\,°C$. (Modified from Endo *et al.*, 1992.)

The molecule contains Si–O bonds. FTIR suggested that the Si–O bonds move when the side groups move. Hence, ferroelectric liquid crystalline polymers have higher rotational viscosities than small molecular mass ferroelectric liquid crystals. In Figure 6.44 the relation of rotational viscosity η and molecular weight Mw at $600\,°C$ is plotted. η increases as Mw increases and the quadratic law is observed.

Boemlburg *et al.* (1991) first discovered the anti-ferroelectric liquid crystal phase in the chiral side chain liquid crystalline polymer, $S_{CA}*$ phase. Several other research groups followed with more such side chain liquid crystalline polymers. Boemlburg *et al.* (1992) reported an anti-ferroelectric liquid crystal in the molecule
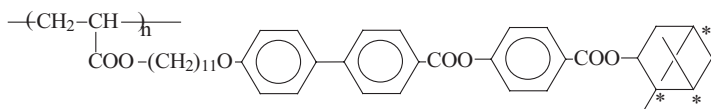
Scherwsky *et al.* (1989) first utilized a SSFLC display in terms of the ferroelectric liquid crystalline polymer. The polymer SSFLC display is fabricated on the ITO-coated plastic substrate. The display was $15 \times 40\,\mathrm{cm}^2$ in area and had 100×300 pixels (Lagerwell, 1993). The display doesn't need the orientation layer which is essential in the conventional liquid crystal displays in order to anchor the liquid crystal molecules. By lightly bending the

flexible substrates, liquid crystal molecules sandwiched between two substrates suffer a uniform shear stress and thus are aligned uniformly. Such a display has a good anti-shock capability. This advantage is very important because the conventional small molecular mass ferroelectric liquid crystal display is vulnerable to shock.

If some of the side groups are substituted by dyes or fluorescent molecules, the display may work without polarizers. It is expected that large screen ferroelectric liquid crystalline polymer displays will come out in the near future.

6.6.   APPLICATIONS OF LIQUID CRYSTALLINE POLYMERS IN INFORMATION STORAGE

In principle, liquid crystalline polymers can be applied in displays. Unfortunately, the response of them to the external fields isn't satisfactory because their viscosity is greater than the small molecular mass liquid crystals by a few orders of magnitude. In fact, only when the temperature is near the glass transition temperature, can the response be measured in seconds. Apparently, this is far from the real requirement. One may mix the liquid crystalline polymer with small molecular mass liquid crystal for such a purpose, but the mixture doesn't show an advantage over the small molecular mass liquid crystal displays. The ferroelectric liquid crystalline polymer is an exception. It works with a very fast effect and can achieve a display with a response time of a few milliseconds or a few tens of milliseconds.

On the other hand, liquid crystalline polymers applied to optical information storage has attracted great attention. The liquid crystalline polymer is applied mainly in terms of the thermo-optical effect. The backbone of liquid crystalline polymer can be polysiloxane, polyacrylate, or polyesters. In order to enhance the absorption coefficient for the writing laser beam, the dyes may be either dissolved into the liquid crystalline polymer in the guest-host model or attached to the backbone of the liquid crystalline polymer to form a copolymer. The nematic, cholesteric and smectic liquid crystalline polymers are all be able to be utilized in optical information storage.

6.6.1.   Nematic liquid crystalline polymers

Figure 6.45 is a schematic of optical information storage which applied a nematic liquid crystalline polymer with a glass transition T_{g}, less than
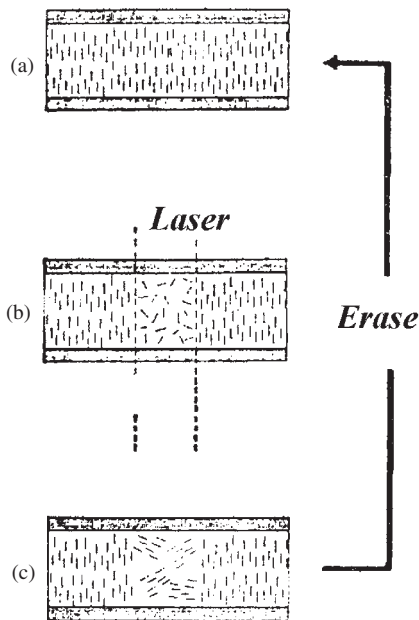
Figure 6.45.   The schematic of optical information storage by nematic polymer.

the ambient temperature and the clear point T_c, greater than the ambient temperature. For example, Shibaev group applied polyacrylate (Kostromin *et al.*, 1982)
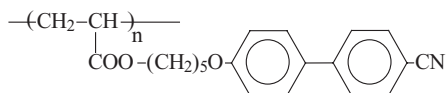
where $T_c = 106\,^\circ\mathrm{C}$ and the degree of polymerization is about 150. When the polymer is cooled down from the isotropic to the nematic in the presence of an electric field, the molecules are aligned perpendicular to the glass plates, see Figure 6.45(a), and hence the cell is transparent. When an area irradiated by a laser beam is heated up beyond the isotropic phase and then cooled down to the ambient temperature, shown in Figure 6.45(b), the area is no longer in the homeotropic alignment but in the multi-domains instead. This multi-domain state, shown in Figure 6.45(c), causes a strong scattering and the area becomes opaque. A dark image displays on the bright background. The image can be maintained or stored for a long time. The image can be erased by re-heating the whole sample up to the isotropic state,

returning the sample back to bright state. The process takes a few seconds. The drive voltage is about 10 volts. The image may be erased selectively by the laser beam. The writing or storage image may be projected by a read-up light onto a large screen.

Inversely, a bright image can be displayed on a dark background. The background corresponds to the multi-domains. The image is written by a laser beam. By applying an electric field while the area irradiated is cooled down one obtains the homeotropic alignment, *i.e.*, a bright state.

6.6.2.   Smectic liquid crystalline polymers

The smectic liquid crystalline polymers can be utilized (Coles and Simon, 1985) in optical information storage as well. The sample used was smectic polysiloxane with side groups cyano-biphenyl units. Its chemical formulae and phase transition are shown in Figure 6.46. The average degree of polymerization is 50 and the molecular weight $Mn = 2.0 \times 10^4$. The thickness of the liquid crystalline polymer is 30 microns. An Ar^+-laser beam of $25\,\mathrm{mW}$ ($\lambda = 514.5\,\mathrm{nm}$) is converged from a $1.5\,\mathrm{mm}$ diameter beam to 20 microns after going through a $50\,\mathrm{mm}$ converging lens. The converged beam illuminates liquid crystalline polymers at a speed of 5 cm/sec. The

Figure 6.46.   The chemical formulae and phase transition of the side chain smectic polymer utilized in thermo-electric effect. (From Coles and Simon, 1985.)

response area is only 5 microns in width, much less than the diameter of the laser beam. The definition of the storage image depends on the intensity and the scan speed. Enough illumination is required to make the sample transform from the smectic to the isotropic state. By optimizing experimental conditions, the panel of 1 to 2 micron definition and $1,000:1$ contrast was achieved.

6.6.3. Cholesteric liquid crystalline polymers

Ueno *et al.* applied cholesteric polysiloxane copolymer in optical information storage, using the configuration depicted in Figure 6.47. The polymer is in the cholesteric state, its glass transition is $T_g = 25\,°C$ and $T_c = 150\,°C$. Varying the cholesterol group concentration in the copolymer, the pitch can be adjusted and accordingly the reflective band is chosen in the visible band, e.g., at $\lambda_{max} = 585\,nm$, yellow-green. The liquid crystalline polymer is coated on a black PET of thickness 100 microns in order to enhance the efficiency of heating and thus to increase the contrast. By appropriate treatment, a planar texture cholesteric liquid crystalline polymer of thickness 20 microns was achieved, the helical axis being normal to the substrate. The display screen is greater than an A4-format sheet.

Ueno's group studied the erasable cholesteric optical information storage display. They used the semiconductor pulse laser (power 18 mW) instead. A definition of 1.5 microns was achieved.
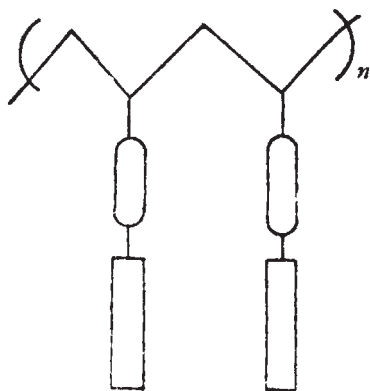
Figure 6.47.   A cholesteric polysiloxane copolymer applied in the optical information storage application.
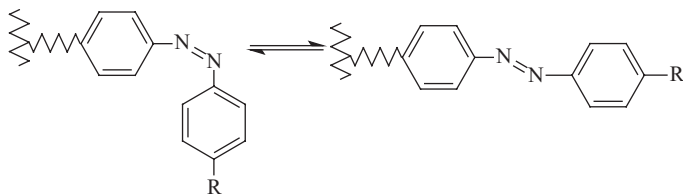
Figure 6.48.   The para-trans transition of azobenzene molecule.

6.6.4.   Photo-isomeric change

Eich *et al.* (1987) developed an effect to utilize an optical information storage effect which is totally different from the above thermo-optical effect. Under illumination by a laser beam the azobenzene undergoes the para-trans transition, shown in Figure 6.48. If azobenzene units are attached to the backbone of side chain liquid crystalline polymers the azobenzene units in the presence of an electric field are aligned uniformly. The trans-configuration is not stable and will relax back to the para configuration under light irradiation or thermal effect. The azobenzene units don't relax back to exactly the original position but a deformation occurs. Accordingly a birefringence change occurs. The effect can be enhanced by applying a polarized light because the optical axis of the azobenzene units prefers to align themselves to be perpendicular to the polarization direction.

Eich *et al.* (1987) applied 70 mol % mesogenic group — cyano-phenylbenzoate and 30 mol % azobenzene as the side group to form a polyacrylate copolymer. The sample cell is homeotropically aligned. Under the illumination of a laser beam the azobenzene accordingly undergoes the para-trans isomeric change, and thus the local orientation is changed. In such way the holographic recording is then utilized by this liquid crystalline polymer film. The thickness of the liquid crystalline polymer is 10 microns, the glass transition temperature is $T_g = 30\,^{\circ}\mathrm{C}$ and the nematic to isotropic transition is $T_c = 103\,^{\circ}\mathrm{C}$. The definition of the holograph strips reached 300 lines/mm, the recording content is about $1\,\mathrm{Gbit/cm^2}$. The holography can be kept for a few weeks. Heating the sample erases the storage image.

The side chain liquid crystalline polymer as storage display has such advantages as easy erasure, long working life, high contrast and reliable storage, *etc.* The molecular features can be tailored. The future of its application is expected to be bright.

References

Abramchuk, S.S. and Kokhlov, A.R., 1988, *Chem.*, **297**, 1069.

Aharoni, S.M., 1980, *Polymer*, **21**, 1413.

—— 1988, *Macromolecules*, **21**, 1941.

Akiyama, E., Nagase, Y. and Koide, N., 1993, *Makromol. Chem., Rapid Commun.*, **14**, 251.

Akzo, N.V., 1979, *Br.Pat.*, 1,547,802.

Alimoglu, A.K., Ledwith, A., Gemmell, P.A., Gray, G.W. and Lacy, D., 1984, *Polymer*, **25**, 1342.

Allen, S.R., Farris, R.J. and Thomas, E.L., 1985, *J. Materials Sci.*, **20**, 2727; 4583.

Amano, M., Kaino, T., Yamamoto, F. and Takeuchi, Y., 1990, *Mol. Cryst. Liq. Cryst.*, **182**, 81.

Antoun, S., Lenz, R.W. and Jin, J.I., 1981, *Journal of Polymer Science, Polymer Chemistry Edition*, **19**, 1901.

April, E.N., 1975, *Nature*, **257**, 139.

—— 1975, *J. Mechanochem. Cell Motil.*, **3**, 111.

Asada, T., Muramatsu, H., Watanabe, R. and Onoge, S., 1980, *Macromolecules*, **13**, 867.

Asahi Chem. Ind. Co., Ltd., 1977, *Jap. Pat. Appl.*, 12325; 12326.

Aspin, M. and Strazielle, C., 1977, *Polymer*, **18**, 591.

Aubourg, P., Huignard, J.P., Hareng, M. and Mullen, R. A., 1982, *Appl. Optics*, **21**, 3706.

Azaroff, L.V., 1987, *Mol. Cryst. Liq. Cryst.*, **145**, 31.

Bair, H.E., Salovey, R. and Huseby, T.W., 1967, *Polymer*, **8**, 9.

Bair, T.I., Morgan, P.W. and Killian, F.L., 1977, *Macromolecules*, **10**, 1396.

Baird, D.G., 1978, in *Liquid Crystalline Order in Polymers*, ed. A. Blumstein, New York: Academic Press.

Ballauff, M., 1991, *Mol. Cryst. Liq. Cryst.*, **196**, 47.

Ballauff, M. and Flory, P.J., 1984, *Ber Bundsenges. Phys. Chem.*, **88**, 530.

Barnes, N.R., Davis, F.J. and Mitchell, G.R., 1989, *Mol. Cryst. Liq. Cryst.*, **168**, 13.

Bassett, D.C., 1981, *Principles of Polymer Morphology*, Cambridge: Cambridge University Press.

Bawden, F.C. and Pirie, N.W., 1937, *Proc. Roy. Soc.*, **B123**, 274.

Benthack-Thoms, H. and Finkelmann, H., 1985, *Makromol. Chem.*, **186**, 1895.

Benthack, H., Finkelmann, H. and Rehage, G., 1981, *Intl. Symp. Macromol. 27th, Abstr. Commun.*, **2**, 961.

Berger, K. and Ballauff, M., 1988, *Mol. Cryst. Liq. Cryst.*, **157**, 109.

Blades, H., 1973, *U.S.Pat.*, 3,767,756.

—— 1975, *U.S.Pat.*, 3,869,429.

Blizard, K.G. and Baird, D.G., 1987, *Polymer Engineering and Science*, **27**, 653.

Blumstein, A., *et al.*, 1982, *J. Polym. Sci., Polym. Phys. Ed.*, **20**, 87.

Blumstein, A., Sivaramakrishnan, K.N., Blumstein, R.B. and Clough, S.B., 1982, *Polymer*, **23**, 47.

Blumstein, A., Vilasagar, S., Ponrathnan, S., Clough, S.B. and Blumstein, R.B., 1982, *J. Polym. Sci., Polym. Phys. Ed.*, **20**, 877.

Blumstein, R.B., Thomas, D., Gauthier, M.M., Asrar, J. and Blumstein, A., 1985, in *Polymeric Liquid Crystals*, ed. A. Blumstein, New York: Plenum.

Blumstein, R.B., *et al.*, 1984, *Macromolecules*, **17**, 177.

Boeffel, C. and Spiess, H.W., 1989, in *Side Chain Liquid Crystal Polymers*, ed. C.B. McArdle, New York: Blackie & Son.

Boeffel, L., *et al.*, 1986, *Makromol. Chem. Rapid Commun.*, **7**, 777.

Bohdanecky, M., 1983, *Macromolecules*, **16**, 1483.

Bohdanecky, M. and Kovar, J., 1982, In *Viscosity of Polymer Solutions*, ed. A.D. Jenkins, New York: Elsevier.

Bomelburg, J. and Heppke, G., 1992, 14th International Liquid Crystal Conference, Abstracts, Pisa, 202.

Bomelburg, J., Heppke, G. and Hollidt, J., 1991, *Macromol. Chem., Rapid Commun.*, **12**, 483.

Bondi, A., 1964, *J. Phys. Chem.*, **18**, 441.

Bouligand, Y., 1978, in *Liquid-Crystalline Order in Polymers*, ed. A. Blumstein, New York: Academic Press.

Bouligand, Y. and Kleman, M., 1970, *J. Phys. (Paris)*, **31**, 1041.

Brelsford, G.L. and Krigbaum, W.R., 1991, in *Liquid Crystallinity in Polymers*, ed. A. Ciferri, New York: VCH.

Bresci, V., Frosini, A., Lupinacci, D. and Magagnini, P. L., 1980, *Makromol. Chem., Rapid Commun.*, **1**, 183.

Brochard, F.J., 1979, *J. Phys. (Paris)*, **40**, 1049.

Broer, D.J., Hikmet, R.A.M. and Challa, G., 1989, *Makromol. Chem.*, **190**, 3201.

Brown, G.H. and Wolken, J.J., 1979, *Liquid Crystals and Biological Structures*, New York: Academic Press.

Buglione, J.A., Iannelli, P., Roviello, A. and Sirigu, A., 1983, *Gazz. Chim. Ital.*, **113**, 193.

Calundann, G.W., 1978, *U.S.Pat.*, 4,067,852.

—— 1979, *U.S.Pat.*, 4,161,470; *Ger.Pat.*, 052,844,817; *Br.Pat.Appl.*, 2,006,242A.

—— 1980, *U.S.Pat.*, 4,184,996.

Calundann, G.W., Charbonneau, L.F. and Bericewicz, B.C., 1984, *U.S.Pat.*, 4,473,682.

Caruso, U., Centore, R., Roviello, A. and Sirigu, A., 1992, *Macromolecules*, **25**, 129.

Chaikin, P.M. and Lubensky, T.C., 1995, *Principles of Condensed Matter Physics*, Cambridge: Cambridge University Press.

Chandani, A.D.L., *et al.*, 1988, *Jpn. J. Appl. Phys.*, **27**, L729.

—— 1989, *Jpn. J. Appl. Phys.*, **28**, L1265.

Chandrasekhar, S., 1977, *Pramana*, **9**, 471.

Chandrasekhar, S. and Ranganath, G.S., 1986, *Advances in Physics*, **35**, 507.

Chandrasekhar, S. and Shashidhar, R., 1979, *Advances in Liquid Crystals*, **4**, 83.

Chang, K.Y. and Lee, Y.D., 1996, in *Liquid-Crystalline Polymer Systems*, ed. A.I. Isayev, T. Kyu and S.Z.D. Cheng, Washington, DC: ACS.

Chapoy, L.L., 1985, in *Recent Advances in Liquid Crystalline Polymers*, ed. L.L. Chapoy, London: Elsevier.

Chapoy, L.L. and Biddle, D., 1983, *J. Polym. Sci., Polym. Lett. Ed.*, **21**, 621.

Chapoy, L.L. and Munck, D.K., 1983, *J. Phys. (Paris)*, **44**, c3-697.

Chapoy, L.L., *et al.*, 1983, *Macromolecules*, **16**, 181.

Chemical Rubber Company, 1971, *Handbook of Lasers*, Cleveland.

Chen, S., Jin, Y., Hu, S. and Xu, M., 1987, *Polym. Commun.*, **28**, 208.

Chen, S. and Ma, Y.F., 1988, *Macromolecules*, **21**, 904.

Cheng, S.D.D., Janimak, J.J., Lipinski, T.M., Sridhar, K., Huang, X.Y. and Harris, F.W., 1990, *Polymer*, **31**, 1122.

Chiellini, E., Galli, G., Malanga, C. and Spassky, N., 1983, *Polym. Bull.*, **9**, 336.

Choe, E.W. and Kim, S.N., 1981, *Macromolecules*, **14**, 920.

Chuah, H.H., Kyu, T. and Helminiak, T.E., 1987, *Polymer*, **28**, 2130.

Ciferri, A., 1991, in *Liquid Crystallinity in Polymers: Principles and Fundamental Properties.*, ed. A. Ciferri, New York: VCH.

Ciferri, A. and Marsano, E., 1987, *Gazz. Chim. Ital.*, **117**, 567.

Clark, N.A. and Lagerwall, S.T., 1980, *Appl. Phys. Lett.*, **36**, 899.

Coles, H.J. and Simon, R., 1985, in *Polymeric Liquid Crystals*, ed., A. Blumstein, New York: Plenum.

Collings, P.J., 1990, *Liquid Crystals: Nature's Delicate Phase of Matter*, Bristol: Adam Hilger.

Cottis, S.G., Economy, J. and Wohrer, L.C., 1975, *Jap.Kokai*, 50-;43223.

—— 1976, *U.S.Pat.*, 3,975,487.

Cotton, J.P., Decker, D., Benoit, H., Farnoux, B., Higgins, J., Jannink, G., Des Cloizeaux, J. and Picot, C., 1974, *Macromolecules*, **75**, 863.

Daniell, J.F. and Davson, H., 1935, *J. Cell. Comp. Physiol.*, **5**, 495.

Davidson, P., Keller, P. and Levelut, A.M., 1985, *J. Phys.*, **46**, 939.

de Gennes, P.G., 1973, *The Physics of Liquid Crystals*, Oxford: Oxford University Press.

—— 1975, *C. R. Acad. Sci. Ser.* **B281**, 101.

—— 1977, *Mol. Cryst. Liq. Cryst. Lett.*, **34**, 177.

—— 1982, in *Polymer Liquid Crystals*, ed. A. Ciferri, W.R. Krigbaum and R.B. Meyer, New York: Academic Press.

Deloche, B. and Samulski, E.T., 1981, *Macromolecules*, **14**, 575.

Demus, D., 1957, *Freiburger Arbeitstagung Flussigkristalle*, No. 1.

Demus, D., Kunicke, G., Neelson, J. and Sackmann, H., 1968, *Z. Naturforsch.* **23a**, 84.

Demus, D., *et al.*, 1984, *Advances in Liquid Crystals*, **6**, 1.

Demus, D. and Richter, L., 1978, *The Textures of Liquid Crystals*, Leipzig: Verlag Chemic Weinhein.

Deteresa, S.J., Farris, R.J. and Porter, R.S., 1982, *Polymer Composite*, **3(2)**, 57.

Deteresa, S.J., Allen, S.R., Farris, R.J. and Porter, R. S., 1984, *J. Materials Sci.*, **19**, 57.

De Vries, Hl., 1951, *Acta Cryst.*, **4**, 219.

——1970, *Mol. Cryst. Liq. Cryst.*, **10**, 31; 219.

——1975, *Pramana*, suppl. **1**, 93.

——1985, *Mol. Cryst. Liq. Cryst.*, **131**, 125.

Doane, J.W., Goldmme, A., West, J.L., Whitehead, J.B. Jr. and Wu, B.G., 1988, *Mol. Cryst. Liq. Cryst.*, **165**, 511.

Doane, J.W., Yang, D.K. and Pfeiffer, M., 1995, in *Macromolecular Symposia*, **96**, ed. X.J. Wang, Zug: Huthig & Wepf Verlag.

Dobb, M.G., Johnson, D.J. and Saville, D.P., 1977, *J. Polym. Sci., Polym. Phys. Ed.*, **15**, 2201.

Doi, M., 1981, *Polym. Sci., Polym. Phys. Ed.*, **19**, 229.

——1982, *J. Polym. Sci. Phys. Ed.*, **20**, 1963; unpublished work.

Doi, M. and Edwards, S.F., 1986, *The Theory of Polymer Dynamics*, Oxford: Clarendon Press.

Donald, A.M. and Windle, A.H., 1992, *Liquid Crystal Polymers: Fundamentals and Principles*, Cambridge: Cambridge University Press.

Duan, X.Q., Liu, Y.L., Liu H.B. and Zhou, Q.F., 1987, *Science Bulletin (China)*, **20**, 1562.

Dubois, J.C., 1990, in *Organic Conjugated Materials for Optoelectronic and Applications*, ed. J.L. Bredas, Kluwer: Academic Press.

Dubois, J.C., Decobert, G., LeBarny, P., Esselin, S., Friedrich, C. and Noel, C., 1986, *Mol. Cryst. Liq. Cryst.*, **137**, 349.

Dubois, J.C., *et al.*, 1993, *Liquid Crystals*, **14**, 197.

Dubois-Violette, E., Durand, G., Guyon, E., Manneville, P. and Pieranski, P., 1978, *Liquid Crystals*, ed. L. Liebert, New York: Academic Press.

Duke, R.W. and DuPre, D.B., 1974a, *Macromolecules*, **7**, 374.

——1974b, *J. Chem. Phys.*, **60**, 2759.

Dumon, M., Zentel, R., Kulinna, C. and Siesler, H.W., 1995, *Liquid Crystals*, **18**, 903.

DuPre, D.B., 1982, in *Polymer Liquid Crystals*, ed. A. Ciferri, W.R. Krigbaum and R.B. Meyer, New York: Academic Press.

DuPre, D.B. and Duke, R., 1975, *J. Chem. Phys.*, **63**, 143.

DuPre, D.B. and Samulski, E.T., 1978, in *Liquid Crystals: The Fourth State of Matter*, ed. F. Saeva, New York: Dekker.

Duran, R., Guillon, D., Gramain, A. and Skoulios, A., 1987a, *Makromol. Chem., Rapid Commun.*, **8**, 181.

——1987b, *Makromol. Chem., Rapid Commun.*, **8**, 321.

East, A.J. and Calundann, G.W., 1982, *U.S.Pat.*, 4,318, 842.

Economy, J., 1989, *Mol. Cryst. Liq. Cryst.*, **169**, 1.

Economy. J., Volksen, W., Viney, C., Geiss, R., Siemens, R. and Karis, T., 1988, *Macromolecules*, **21**, 2777.

Eich, M. and Wendorff, J., 1985, *Makromol. Chem.*, **186**, 2639.

——1987, *Makromol. Chem., Rapid Commun.*, **8**, 467.

Eich, M., Wendorff, J., Beck, B. and Ringsdorf, H., 1987, *Makromol. Chem., Rapid Commun.*, **8**, 59.

Endo, H., Hachiya, S., Sekiya, T. and Kawasaki, K., 1992, *Liquid Crystals*, **12**, 147.

Ericksen, J.L., 1960, *Arch. Ration. Mech. Anal.*, **4**, 231.

Eskridge, C.H. and Louise, R.R., 1984, *U.S.Pat.*, 4,424,184.

Etherington, G., Leadbetter, A.J., Wang, X.J., Gray, G. W. and Tajbakhsh, A., 1986, *Liquid Crystals*, **1**, 209.

Etherington, G., Langley, A.J., Leadbetter, A.J and Wang, X.J., 1987, *Liquid Crystals*, **3**, 685.

Etkin, W., 1973, *Bioscience*, **23**, 653.

Ezrin, M., Updegraff, I.H. and Cassidy, H.G., 1953, *J. Am. Chem. Soc.*, **75**, 1610.

Fayolle, B., Noel, C. and Billard, J., 1979, *J. Phys. (Paris)*, **40**, C3–485.

Feijoo, J.L., Ungar, G., Owen, A.J., Keller, A. and Percec, V., 1988, *Mol. Cryst. Liq. Cryst.*, **155**, 487.

Feijoo, J.L., Ungar, G., Keller, A. and Percec, V., 1990, *Polymer*, **31**, 2019.

Fergason, J.L., 1985, SID International Symposium, *Digest of Technical Papers*, 210.

Feynmann, R.P. and Hibbs, A.R., 1965, *Quantum Mechanics and Path Integrals*, NewYork: McGraw Hill.

Finkelmann, H., 1982, in *Polymer Liquid Crystals*, ed. A. Ciferri, W.R. Krigbaum and R.B. Meyer, New York: Academic Press.

——1991, in *Liquid Crystallinity in Polymers: Principles and Fundamental Properties*, ed. A. Ciferri, New York: VCH.

Finkelmann, H. and Rehage, G., 1980, *Makromol. Chem., Rapid Commun.*, **1**, 733.

——1984, in *Liquid Crystal Polymers II/III*, ed. M. Gordon, Berlin: Springer-Verlag.

Finkelmann, H., Kock, H. and Rehage, G., 1981, *Makromol. Chem.*, **2**, 317.

——1982, *Mol. Cryst. Liq. Cryst.*, **89**, 23.

Finkelmann, H., Ringsdorf, H. and Wendorff, J.H., 1978, *Macromol. Chem.*, **179**, 273.

Finkelmann, H., Ringsdorf, H., Siol, W. and Wendorff, J.H., 1978, *Makromol. Chem.*, **179**, 829.

Finkelmann, H., Happ, M., Portugall, M. and Ringsdorf, H., 1978, *Makromol. Chem.*, **179**, 2541.

Flory, P.J., 1956, *Proc. Roy. Soc.*, **A234**, 73.

——1961, *J. Polym. Sci.*, **49**, 105.

——1978, *Macromolecules*, **11**, 1138; 1141.

——1984, *Adv. Polym. Sci.*, **59**, 1.

Flory, P.J. and Ronca, G., 1979a, *Mol. Cryst. Liq. Cryst.*, **54**, 311.

——1979b, *Mol. Cryst. Liq. Cryst.*, **54**, 289.

Frank, F.C., 1958, *Discuss. Faraday Soc.*, **25**, 19.

Freden, S., Lonberg, F. and Meyer, R.B., 1983, *J. Phys. (Paris)*, **46**, 903.

Frederiks, V. and Zolina, V., 1933, *Trans. Faraday Soc.*, **29**, 919.

Freed, K., 1972, in *Advances in Chemical Physics*, ed. I. Prigogine and S.A. Rice, vol. XXII, New York: Willy-Interscience.

Freidzon, Y.S., Shibaev, V.P., Kharitonov, A.V. and Plate, N.A., 1980, in *Advances in Liquid Crystal Research and Applications*, Oxford: Pergamon.

Freidzon, Y.S., Boiko, N.I., Shibaev, V.P., Tsukruk, V. V., Shilov, V.V. and Lipatov, Y.S., 1986, *Polymer Commun.*, **27**, 190.

Freidzon, Y.S. and Shibaev, V. P., 1993, in *Liquid-Crystal Polymers*, ed. N. Plate, translated by S. C. Schnur, New York: Plenum.

Frenzel, J., 1981, Ph.D. Thesis, Tech. Univ. Clausthal, Clausthal-Zellerfeld.

Friedel, G., 1922, *Ann. Physique*, **18**, 273.

Frosini, A., Levita, G., Lupinacci, D. and Magagnini, P.L., 1981, *Mol. Cryst. Liq. Cryst.*, **66**, 21.

Garito, A.F., Singer, K.D. and Teng, C.C., in *Molecular Optical Properties of Organic and Polymeric Materials*, ed. D.J. Williams, ACS Symp. Ser. **233**, Washington DC: ACS.

Gemmell, P.A., Gray, G.W. and Lacey, D., 1985, *Mol. Cryst. Liq. Cryst.*, **122**, 205.

Goodby, J. and Gray, G.W., 1980, Unpublished results.

Goodby, J., Nishiyama, I., Slaney, A.J., Booth, C.J. and Toyne, K.J., 1993, *Liquid Crystals*, **14**, 37.

Goodby, J., Waugh, M.A., Stein, S.M., Chin, E., Pindak, R. and Patel, J.S., 1988, *Nature*, **337**, 449.

—— 1989, *J. Am. Chem. Soc.*, **111**, 8119.

Grandjean, F., 1921, *Compt. Rend*, **172**, 71.

Gray, G.W., 1961, *Molecular Structure and the Properties of Liquid Crystals*, London: Academic Press.

—— 1989, in *Side Chain Liquid Crystal Polymers*, ed. C.B. McArdle, New York: Blackie and Son.

Gray, G.W. and Goodby, J.W.G., 1984, *Smectic Liquid Crystals: Textures and Structures*, Glasgow: Leonard Hill.

Gray, G.W., Hill, J.S. and Lacey, D., 1991, *Mol. Cryst. Liq. Cryst.*, **197**, 43.

Gray, G.W., Jones, B. and Marson, F., 1957, *J. Chem, Soc.*, 393.

Griffin, A.C. and Havens, S.J., 1981, *J. Polym. Sci., Polym. Phys. Ed.*, **19**, 951.

Griffin, A.C., Bhatti, A.M. and Hung, R.S.L., 1988, *Mol. Cryst. Liq. Cryst.*, **155**, 129.

Griffin, A.C., Sullivan, S.L. and Hughes, W.E., 1989, *Liquid Crystals*, **4**, 677.

Grosberg, A.Y. and Zhestkov, A.V., 1986, *Polym. Sci. USSR*, **28**, 97.

Guglielminetti, J.M., Decobert, D. and Dubois, J.C., 1986, *Polym. Bull.*, **16**, 411.

Hardouin, F., Mery, S., Achard, M.F., Noirez, L. and Keller, P., 1991, *J. Phys. II (Paris)*, **1**, 511.

Harris, J.F., 1981, *U.S.Pat.*, 4,294,955.

—— 1983, *U.S.Pat.*, 4,391,966.

Harris, R.K., 1986, *Nuclear Magnetic Resonance Spectroscopy*, Avon: Longman.

Harris, W.J., Kleiss, L.R., Liu, M.B., Lysenko, Z. and Rosenberg, S., 1990, *Eur.Pat.Appl.*, EP 393,559.

Helminiak, T.E., 1979, *Prepr., Am. Chem. Soc., Div. Org. Coat. Plat.*, **40**, 475.

Helminiak, T.E. and Arnold, F.E., 1977, *U.S.Pat.*, 4,051,108.

Helminiak, T.E., Benner, C.L., Arnold, F.E. and Husman, G.E., 1980, *U.S.Pat.*, 4,207,407.

Hermans, J. Jr., 1962, *J. Coll. Sci.*, **17**, 638.

Herrmann, J., Kleinhans, H.D. and Schneider, G.M., 1983, *J. Chim. Phys., Phys,-Chim. Biol.*, **80**, 111.

Hessel, F. and Finkelmann, H., 1985, *Polym. Bull.*, **14**, 375.

—— 1987, *Makromol. Chem.*, **188**, 1597.

Hessel, V. and Finkelmann, H., 1985, *Polym. Bull.*, **14**, 3751.

Hikmet, R.A.M. and Zwerver, B.H., 1993, *Liquid Crystals*, **13**, 561.

Hirschmann, H., Velasco, D., Reinecke, H. and Finkelmann, H., 1991, *J. Phys.*, **24**, 559.

Hobdell, J. and Windel, A., 1995, *Liquid Crystals*, **19**, 401.

Hoffman, J.D., Davis, G.T. and Lauritzen, Jr., J.I, 1976, in *Treatise on Solid State Chemistry*, ed. N.B. Hannay, New York: Plenum.

Hsiao, B.S., Shaw, M.T. and Samulski, E.T., 1988, *Macromolecules*, **21**, 543.

Hsu, C.S., Rodriguez-Parada, J.M. and Percec, V., 1987, *Makromol. Chem.*, **188**, 1017.

Hu, S.R., Xu, M., Li, J.C., Qian, B.G., Wang, X.Y. and Lenz, R.W., 1985, *J. Polym. Sci., Polym. Phys. Ed.*, **23**, 2387.

Huang, J.H. and Wu, R.J., 1992, *Polymerica Sinica*, **6**, 742.

Husman, G.E., Helminiak, T.E., Adams, D.W. and Benner, C.L., 1979, *Am. Chem. Soc., Div. Org. Coat. Chem.*, **40**, 797.

Hwang, W.F. and Helminiak, T.E., 1989, in *The Material Science and Engineering of Rigid-Rod Polymers*, ed. W.W. Adams, R.K. Eby and D.E. McLemore, Pittsburgh: MRS, **134**.

Hwang, W.F., Wiff, D.R., Benner, C.L. and Helminiak, T. E., 1983, *J. Macromol. Sci., Phys.*, **B22**, 231.

Iimura, K., Koide, N. and Ohta, R., 1981, *Rep. Prog. Polym. Phys., Jap.*, **24**, 231.

Imai, Y., Taoka, J., Uno, K. and Iwakura, Y., 1965, *Makromol. Chem.*, **83**, 167.

Inai, S., Suzuki, H., Asai, K. and Ueno, K., 1982, *U.S.Pat.*, 4,311,823.

Irvine, P.A. and Flory, P.J., 1984, *J. Chem. Soc., Faraday Trans.*, **80**, 1821.

Isayev, A.I., 1996, in *Liquid-Crystalline Polymer Systems*, ed. A.I. Isayev, T. Kyu and S.Z.D. Cheng, Washington, DC: ACS.

Isayev, A.I. and Modic, M., 1987, *Polym. Compos.*, **8**, 158.

Jackson Jr., W.J., 1988, in *Polymers for Advanced Technology.* ed. M. Lewin, New York: VCH.

—— 1989, *Mol. Cryst. Liq. Cryst.*, **169**, 23.

—— 1992, *Chinese Journal of Polymer Science*, **3**, 195.

Jackson, Jr., W.J. and Kuhfuss, H.F., 1973, *U.S.Pat.*, 3,778,410.

—— 1976, *Journal of Polymer Science, Polymer Chemistry Edition*, **14**, 2043.

Jackson Jr., W.J. and Kuhfuss, H.F., 1982, *U.S.Pat.*, 4,360,658.

Jackson Jr., W.J., Gebeau, G.G. and Kuhfuss, H.F., 1980, *U.S.Pat.*, 4,242,496.

Jahnig, F., 1981, *Mol. Cryst. Liq. Cryst.*, **63**, 157.

Jarry, J.P. and Monnerie, L., 1979, *Macromolecules*, **12**, 316.

Jo, B.W., Lenz, R.W. and Jin, J.I., 1982, *Makromol. Chem., Rapid commun.*, **3**, 23.

Jones, J.L., 1968, *J. Macromol. Sci.*, **C2**, 303.

Joseph, E.G., Wilkes, G.L. and Baird, D.G., 1983, *Polymer Preprints*, **24**, 304.

—— 1985, in *Polymeric Liquid Crystals*, ed. A. Blumstein, New York: Plenum.

Josson, H., Werner, P.E., Gedde, U.W. and Hult, A., 1989, *Macromolecules*, **22**, 1683.

Kajiyama, T., Washizu, S. and Tehayange, M., 1984, *J. Appl. Polym. Sci.*, **29**, 3955.

Kaneda, T., Ishikawa, S., Daimon, H., Kaisura, T., Ueda, M., Oda, K. and Horio, M., 1981, *Makromol. Chem.*, **183**, 417.

Kaneda, T., Ishikawa, S., Daimon, H., Kaisura, Hondo, T. and Uenda, M., 1983, *U.S.Pat.* 4,373,087.

Kaneko, E., 1987, *Liquid Crystal TV Displays: Principle and Application*, Tokyo: KTK.

Kapitza, H., *et al.*, 1990, *Adv. Mater.*, **2**, 539.

Kardos, J.L. and Raisoni, J., 1975, *Polym. Eng. Sci.*, **15**, 183.

Ke, B. and Vernon, L., 1971, in *Photochromism*, ed. G.H. Brown, New York: Wiley.

Keller, A., 1957, *Philos. Mag.*, **2**, 1171.

Keller, P., Hardouin, R., Mauzac, M. and Achard, M., 1988, *Mol. Cryst. Liq. Cryst.*, **155**, 71.

Khokhlov, A.R. and Semenov, A.N., 1982, *Physica*, **112A**, 605.

Kimura, H., Hoshino, M. and Nakano, H., 1979, *J. Phys. (Paris)*, **40**, C3-174;

—— 1982, *J. Phys. Soc. Jpn.*, **51**, 1584.

Kirst, R.G. and Ohm, H.G., 1985, *Makromol. Chem., Rapid Commun.*, **6**, 179.

Kishi, R., Suzuki, Y., Ichijo, H. and Hirasa, O., 1994, *Chem. Lett.*, 2257.

Kiss, G., 1987, *Polymer Engineering and Science*, **27**, 410.

Kiss, G. and Porter, R.S., 1980a, *J. Polym. Sci. Phys. Ed.*, **18**, 361.

—— 1980b, *Mol. Cryst. Liq. Cryst.*, **60**, 267.

Klein, P.G., Evans, B.W. and Ward, I.M., 1996, in *Liquid-Crystalline Polymer Systems*, ed. A.I. Isayev, T. Kyu and S.Z.D. Cheng, Washington DC: ACS.

Kleman, M., 1991, in *Liquid Crystallinity in Polymers: Principles and Fundamental Properties*, ed. A. Cifferi, New York: VCH.

Kleman, M. and Friedel, J., 1969, *J. Phys. (Paris)*, **20**, 43.

Kofler, L. and Kofler, A., 1954, *Thermo-Mikro-Methoden Z. Kennzeichnung Organischer Stoffe und Stoffgemische*, Weinheim: Verlag Chemie.

Kohlhammer, K., Muller, K. and Kothe, G., 1989, *Liquid Crystals*, **5**, 1525.

Koide, N., Ogura, S., Aoyama, Y., Amano, N. and Kaino, T., 1991, *Mol. Cryst. Liq. Cryst.*, **198**, 323.

Korshak, V.V., 1969, *Heat Resistant Polymers*, Moscow.

Kostromin, S.G., Talroze, R.V., Shibaev, V.P. and Plate, N.A., 1982, *Makromol. Chem., Rapid Commun.*, **3**, 803.

Kostromin, S.G., Simitsyn, V.V., Talroze, R.V. and Shibaev, V.P., 1984, *Polym. Sci. USSR*, **26**, 370.

Kovacs, A.J., Aklonis, J.J. and Hutchinson, J.M., 1979, *J. Polym. Sci., Polym. Phys. Ed.*, **17**, 2031.

Kovar, R.F. and Arnold, F.E., 1976, *J. Polym. Sci., Polym. Chem.*, **14**, 2807.

Kratky, O. and Porod, G., 1949, *Red. Trav. Chim. Paye-Bas.*, **68**, 1106.

Krause, S.J., Haddock, T., Price, G.E., Lenhert, P.G., O'Brien, J.F., Helminiak, T.E. and Adams, W.W., 1986, *J. Polym. Sci.: Part B: Polym. Phys.*, **24**, 1991.

Krigbaum, W.R., 1982, *Polymer Liquid Crystal*, ed. A. Ciferri, W.R. Krigbaum and R.B. Meyer, New York: Academic Press.

Kumar, U., Kato, T. and Frechet, M.J., 1992, *J. Am. Chem. Soc.*, **114**, 6630.

Kundler, I. and Finkelmann, H., 1995, *Macromol. Chem., Rapid Commun.*, **16**, 679.

Kurik, M.V. and Lavrentovich, O.D., 1988, *Sov. Phys. Usp.*, **31**, 196.

Kutsumizu, S., Yamada, M. and Yano, S., 1994, *Liquid Crystals*, **16**, 1109.

Kuzuu, N. and Doi, M., 1983, *J. Phys. Soc. Jpn.*, **52**, 3486.

—— 1984, *ibid*, **53**, 1031.

Kwolek, S.L., Morgan, P.W. and Sorenson, W.R., 1962, *U.S.Pat.* 3,063,966.

Kwolek, S.L., Morgan, P.W., Schaefgen, J.R. and Gulrich, L.W., 1977, *Macromolecules*, **10**, 1390.

Kwolek, S.L., Memeger, W. and Van Trump, J.E., 1988, in *Polymers for Advanced Technologies*, ed. M. Lewin, New York: VCH.

Lagarde, M., Moisan, J.Y. and Dubois, J.C., 1991, *Molec. Eng.*, **1**, 221.

Lagerwall, S.T., 1993, *Liquid Crystal Today*, **3**, 3.

Lam, L., 1982, *Wuli*, **11**, 171.

Larson, R.G. and Archer, L.A., 1995, *Liquid Crystals*, **19**, 883.

Laupretre, F. and Noel, C., 1991, in *Liquid Crystallinity in Polymers*, ed. A. Ciferri, New York: VCH.

Le Barny, P. and Dubois, J.C., 1989, in *Side Chain Liquid Crystal Polymers*, ed. C.B. McArdle, New York: Blackie and Son.

Le Barny, P., Ravanx, G., Dubois, J.C., Parneix, J.P, Njenmo, R., Legrand, C. and Levelut, A.M., 1986, *SPIE*, **682**, 56.

Lee, A.G., 1975, *Eudeavour*, **34**, 67.

Lee, S.D., 1987, *J. Chem. Phys.*, **87**, 4972.

—— 1988, *J. Chem. Phys.*, **88**, 5196.

—— 1991, in *Liquid Crystallinity in Polymers: Principles and Fundamental Properties*, ed. A. Ciferri, New York: VCH.

Lee, S.D. and Meyer, R.B., 1988, *Phys. Rev. Lett.*, **61**, 2217.

—— 1990, *Liquid Crystals*, **7**, 15.

Legge, C.G., Mitchell, G, R. and Davis, F.J., 1991, *J. Phys. II (Paris)*, **10**, 1253.

Lehmann, O., 1900, *Verhandl., d. Deutschen Phys. Ges., Sitzung* **16**. 3., p.1.

Lenz, R.W. and Feichtinger, K.A., 1979, *Polymer Preprints*, **20**, 114.

Leroux, N., Keller, P., Achard, M.F., Noirez, L. and Hardouin, F., 1993, *J. Phys. II (Paris)*, **3**, 1289.

Leroux, N., Mauzac, M., Noirez, L. and Hardouin, F., 1994, *Liquid Crystals*, **16**, 421.

Leslie, F.M., 1966, *Q. J. Mech Appl. Math.*, **19**, 357.

—— 1968, *Arch. Ration. Mech. Anal.*, **28**, 265.

Levine, B.F. and Bethea, C.G., 1976, *J. Chem. Phys.*, **65**, 1989.

Lysenko, Z., 1986, *U.S.Pat.Appl.*, 925,358.

—— 1988, *Eur.Pat.Appl.* EP 266,222.

Madhusudana, N.V. and Sumathy, K.R., 1983, *Mol. Cryst. Liq. Cryst.*, **92**, 179.

Magagnini, P.L., Marchetti, A., Matsa, F., Pizzirani, G. and Turchi, G., 1974, *Eur. Polym. J.*, **10**, 585.

Maier, W. and Saupe, A., 1959, *Z. Naturforsch.*, **12a**, 882.

Maret, G. and Blumstein, A., 1982, *Mol. Cryst. Liq. Cryst.*, **88**, 295.

Marruci, G., 1982, *Mol. Cryst. Liq. Cryst.*, **72**, 153.

Martins, A.F., Esnault, P. and Volino, F., 1986, *Phys. Rev. Lett.*, **57**, 1745.

Matheson, R.R. Jr. and Flory, P.J., 1981, *Macromolecules*, **14**, 954.

Mattossi, M., Ober, R., Veyssie, M. and Finkelmann, H., 1986, *Europhys. Lett.*, **2**, 233.

McArdle, C.B., 1989, *Side Chain Liquid Crystal Polymers*, New York: Blackie and Son.

McCulloch, I.A. and Bailey, R.T., 1991, *Mol. Cryst. Liq. Cryst.*, **200**, 157.

Medrano, J.M., 1989, *Symposium on Materials Science and Engineering of Rigid Rod Polymers*, MRS, Proceedings, **134**.

Meesiri, W., Menozel, J., Gaur, U. and Wunderlich, B., 1982, *J. Polym. Sci., Polym. Phys. Ed.*, **20**, 719.

Mehta, S. and Deopura, B.L., 1993, *J. Appl. Polym. Sci.*, **47**, 857.

Menges, G. and Hahn, G., 1981, *Modern Plastics*, October, 56.

Meredish, G.R., Van Dusen, J.G. and Williams, D.J., 1982, *Macromolecules*, **15**, 1385.

Mermin, N.D., 1979, *Review of Modern Physics*, **51**, 591.

Meyer, R.B., 1982, in *Polymer Liquid Crystals*, ed. A. Ciferri, W.R. Krigbaum and R.B. Meyer, New York: Academic Press.

Millaud, B., Thierry, A. and Skoulios, A., 1978, *Mol. Cryst. Liq. Cryst. (Lett.)*, **41**, 263

Miller, W.G., Wu, C.C., Wee, E.L., Santee, G.L., Ray, T.H. and Goebel, K., 1974, *Pure & Appl. Chem.*, **38**, 37.

Mitchell, G.R., Coutter, M., Davis, F.J. and Guo, W., 1992, *J. Phys. II (Paris)*, **2**, 1121.

Mitchell, G.R., Davis, F.J. and Guo, W., 1993, *Phys. Rev. Lett.*, **71**, 2947.

Miyasato, K., *et al.*, 1983, *Jpn. J. Appl. Phys.*, **22**, L661.

Morgan, P.W., 1977, *Macromolecules*, **10**, 1381.

Moussa, F., *et al.*, 1987, *J. Phys. (Paris)*, **48**, 1079.

Muramatsu, H. and Krigbaum, W.R., 1986, *Macromolecules*, **19**, 2850.

Nakagawa, Y., Noma, T. and Mera, H., 1977, *U.S.Pat.*, 4,018,735.

Nakai, A., Shiwaku, T., Hasegawa, H. and Hashimoto, T., 1986, *Macromolecules*, **19**, 3010.

Nakajama, A., Hayashi, T. and Ohmori, M., 1968, *Biopolymers*, **6**, 973.

Nakamura, T. and Ueno, T., Proc. of 12th Japanese Symp. on Liquid Crystals.

Navard, P., Haudin, J.M., Dayan, S. and Sixon, P., 1981, *J. Polym. Sci., Polym. Lett. Ed.*, **19**, 379.

Needham, J., 1950, *Biochemistry and Morphogenesis*, Cambridge: Cambridge University Press.

Nehring, J. and Saupe, A., 1972, *J. Chem. Soc., Faraday Trans.*, **II 68**, 1.

Nielsen, L.E., 1975, *Mechanical Properties of Polymers and Composites*, New York: Marcel Dekker.

Niori, T., Adachi, S. and Watanabe, J., 1995, *Liquid Crystals*, **19**, 139.

Noel, C. and Billard, J., 1978, *Mol. Cryst. Liq. Cryst. (Lett.)*, **41**, 269

Noel, C., 1985, in *Polymeric Liquid Crystals*, ed. A. Blumstein, New York: Plenum.

Noel, C., 1989, in *Side Chain Liquid Crystal Polymers*, ed. C.B. McArdle, Glasgow: Blackie.

Northolt, M.G. and Van Aartsen, J.J., 1973, *J. Polym Sci., Polym. Lett. Ed.*, **11**, 333.

Nyitrai, K., Cser, F., Lengyell, M., Seyfried, E. and Hardy, G., 1977, *Eur. Polym. J.*, **13**, 673.

Ober, C.K., Jin, J.-I. and Lenz, R.W., 1983, *Makromol. Chem., Rapid. Commun.*, **4**, 49.

Ober, C., Lenz, R.W., Galli, G. and Chiellini, E., 1983, *Macromolecules*, **16**, 1034.

Ober, C., Jin, J.I., Zhou, Q.F. and Lenz, R.W., 1984, *Advances in Polymer Science*, **59**, 103.

Odijk, T., 1985, *Polym. Commun.*, **26**, 197.

—— 1986a, *Liquid Crystals*, **1**, 553.

—— 1986b, *Macromolecules*, **19**, 2313.

Onagi, Y., White, J. and Feller, J., 1980, *J. Polym. Sci., Polym. Chem. Ed.*, **18**, 663.

Onsager, L., 1931, *Phys. Rev.*, **37**, 405.

—— 1932, *ibid*, **38**, 2265.

—— 1949, *Ann. N. Y. Acad. Soc.*, **51**, 627.

Oseen, C.W., 1933, *Trans. Faraday Soc.*, **29**, 883.

Ozawa, S., Nakagawa, Y., Matsuda, K., Nishihara, T. and Yunoki, H., 1978, *U.S.Pat.*, 4,075,172.

Painter, P.C., Tang, W., Graf, J.F., Thomson, B. and Coleman, M.M., 1991, *Macromolecules*, **24**, 3929.

Pak, H. and Flory, P.J., 1979, *J. Polymer Sci.*, **17**, 1845.

Pake, G.E., 1948, *J. Chem. Phys.*, **16**, 327.

Papkov, S.P., Kulichikhin, V. G., Kalmykova, V. D. and Malkin, A. Y., 1974, *J. Polym. Sci., Polym. Phys. Ed.*, **12**, 1753.

Papkov, S.P., 1977, *Vysokomol. Soyed.*, **A19**, 3.

—— 1982, *Vysokomol. Soedin.*, **A24**, 233.

Parker, G., Chen, W., Tsou, L. and Hara, M., 1996, in *Liquid-Crystalline Polymer Systems*, ed. A.I. Isayev, T. Kyu and S.Z.D. Cheng, Washington, DC: ACS.

Parodi, O., 1970, *J. Phys. (Paris)*, **31**, 581.

Parsons, J.D., 1979, *Phys. Rev. A*, **19**, 1225.

Parthasarathy, R., Houpt, D.J. and DuPre, D.B., 1988, *Liquid Crystals*, **3**, 1073.

Paschke, R., 1994, *Liquid Crystals*, **16**, 1105.

Payet, C.R., 1979, *U.S.Pat.*, 4,159,365.

Pedorov, A.A., Savinov, V.M. and Sololov, I.B., 1970, *Vysokomol. Soyed.* **A12**, 2183.

Pennings, A.J. and Kiel, A.M., 1965, *Kolloid Z. Z. Polym.*, **205**, 160.

Pennings, A.J., Van der Mark, J.M.A.A. and Kiel, A.M., 1970, *Kolloid Z. Polym.*, **237**, 336.

Percec, V., 1988, *Mol. Cryst. Liq. Cryst.*, **155**, 1.

Percec, V. and Nave, H., 1987, *J. Polym. Sci., Polym. Chem. Ed.*, **25**, 405.

Percec, V. and Pugh, C., 1989, in *Side Chain Liquid Crystal Polymers*, ed. C.B. McArdle, New York: Blackie and Son.

Percec, V., Tomazos, D. and Pugh, C., 1989, *Macromolecules*, **22**, 3259.

Percec, V. and Tsuda, Y., 1991, *Polymer*, **32**, 673.

Percec, V. and Yourd, R., 1988, *Macromolecules*, **21**, 3379.

Piercourt, S., Lacoudre, N., Borgne, A.L and Spassky, N., 1992, *Makromol. Chem.*, **193**, 705.

Pinsl, J., Brauchle, C. and Kreuzer, F.H., 1987, *J. Mol. Elect.*, **3**, 9.

Plate, N.A. and Shibaev, V.P., 1980, *Grebneobraznye polimeri I zhidkie kristally* (Comb-like polymers and liquid crystals), Moscow: Khimiya.

Porter, R.S. and Johnson, J.F., 1967, in *Rheology*, ed. F.R. Eirich, vol. 4, New York: Academic Press.

Portugall, M., Ringsdorf, H. and Zentel, R., 1982, *Makromol. Chem.*, **183**, 2311.

Prasad, P.N., 1988, in *Nonlinear Optical and Electroactive Polymers*, ed. P.N. Prasad and D.R. Ulrich, New York: Plenum.

Prevorsek, D.C., 1988, in *Polymers for Advanced Technology*, ed. M. Lewin, New York: VCH.

Priest, R.G., 1973, *Phys. Rev. A*, **7**, 720.

Pugh, C. and Schrock, R.R., 1993, *Polymer Preprints*, **34**, 180.

Qian, R., Chen, S. and Song, W., 1995, in *Macromolecular Symposia*, ed. Xin-Jiu Wang, **96**, Zug: Huthig & Wept Verlag.

Qian, R.Y., Shen, D.Y. and Li, H.M., 1989, *Chinese Journal of Polymer Science*, **7**, 150.

Rastogi, S., Newman, M. and Keller, A., 1991, *Nature*, **353**, 5.

Reinitzer, F., 1988, *Monatsh*, **9**, 421.

Renn, S.R. and Lubensky, T.C., 1988, *Phys. Rev. A*, **38**, 2132.

Renz, W. and Warner, M., 1986, *Phys. Rev. Lett.*, **56**, 1268.

Ringsdorf, H. and Schneller, A., 1981, *Br. Polym. J.*, **13**, 43.

Ringsdorf, H., Schmidt, H.W., and Schneller, A., 1982, *Makromol. Chem., Rapid Commun.*, **3**, 745.

Ritter, A.P., 1986, unpublished work.

Rivin, R.S. and Saunders, D.W., 1951, *Philos. Trans. R. Soc. London A*, **243**, 251.

Robinson, C., 1955, *Trans. Faraday Soc.*, **52**, 571.

—— 1961, *Tetrahedren*, **13**, 219.

Robinson, C., Ward, J.C. and Beevers, R.B., 1958, *Discus. Faraday Soc.*, **25**, 29.

Rowell, J.C., Pillips, W.D., Melby, L.R. and Panar, M., 1965, *J. Chem. Phys.*, **43**, 3442.

Ryan, J.W. and Speier, J.L., 1959, *J. Org. Chem.*, **24**, 2052.

Sackmann, H. and Demus, D., 1965, *Mol. Cryst.*, **2**, 81.

—— 1973, *Mol. Cryst. Liq. Cryst.*, **21**, 239.

Schadt, M. and Gerber, P.G., 1982, *Z. Naturforsch.*, **37A**, 167.

Schadt, M., 1986, Lecture Note, Qingtao.

Schatzle, J., Kaufhold, W. and Finkelmann, H., 1989, *Makromol. Chem.*, **190**, 3269.

Scherowsky, G., *et al.*, 1989, *Liquid Crystals*, **5**, 1281; 1297;

—— 1991, *Makromolekulaves Kolloquium Freiburg.*

Sekiya, T., *et al.*, 1993, *Liquid Crystals*, **14**, 1255.

Semenov, A.N., 1988, *Sov. Phys. JETP*, **66**, 712.

Shibaev, V.P., *et al.*, 1984, *Polym. Bulletin*, **12**, 299.

Shibaev, V.P. and Plate, N.A., 1984a, in *Liquid Crystal Polymers II/III*, ed. M. Gordon, Berlin: Springer-Verlag.

—— 1984b, *Adv. Polym. Sci.*, **60/61**, 173.

—— 1985, *Pure & Appl. Chem.*, **57**, 1589.

Shibaev, V.P., Kozlovsky, M., Beresnev, L., Blinov, L. and Plate, N.A., 1984, *Polym. Bullet.*, **12**, 299.

Shimamura, K., White, J. and Feller, J., 1981, *J. Appl. Polym. Sci.*, **26**, 2165.

Shiwaku, T., Nakai, A., Wang, W., Hasegawa, H. and Hashimoto, T., 1995, *Liquid Crystals*, **19**, 679.

Siegmann, A., Dagan, A. and Kenig, S., 1985, *Polymer*, **26**, 1325.

Sigaud, G., Achard, M.F., Hardouin, F., Mauzac, M., Richard, H. and Gasparoux, H., 1987, *Macromolecules*, **20**, 578.

Singer, K.D., *et al.*, 1988, *Appl. Phys. Lett.*, **19**, 1800.

Singer, S.J. and Nicholson, G.L., 1972, *Science*, **175**, 720.

Sirigu, A., 1991, in *Liquid Crystallinity in Polymers: Principles and Fundamental Properties*, ed. A. Ciferri, New York: VCH.

—— 1993, *Liquid Crystals*, **14**, 15.

Smith, P. and Lemstra, P.J., 1979, *Makromol. Chem.*, **180**, 2983.

Spassky, N., *et al.*, 1989, *Makromol. Chem. Makromol. Symp.*, **24**, 271.

Stamatoff, J., *et al.*, 1990, *Angew. Makromol. Chemie*, **183**, 151.

Stevens, H., Rehage, G. and Finkelmann, H., 1984, *Macromolecules*, **17**, 851.

Straley, J.P., 1973, *Phys. Rev. A*, **8**, 2181.

Suenaga, J.I., 1990, *Polymer News*, **15**, 201.

Suenaga, J.I. and Okada, T., 1989, *Mol. Cryst. Liq. Cryst.*, **169**, 97.

Sweet, G.E. and Bell, J.P., 1973, *J. Polym. Sci.*, **A2**, 1273.

Takanayagi, M. and Goto, K., 1984, *J. Appl. Polym. Sci.*, **29**, 2547.

Takayanagi, M., Ogata, T., Morikawa, M. and Kai, T., 1980, *J. Macromol. Sci. Phys.*, **B17(4)**, 591.

Tanner, D.W. and Berry, G.C., 1974, *J. Polym. Sci. Polym. Phys. Ed*, 941.

Taratuta, V., Hurd, A.J. and Meyer, R.B., 1985, *Phys. Rev. Lett.*, **55**, 246.

Tashiro, K., Kobayashi, M. and Tadokoro, H., 1977, *Macromolecules*, **10**, 413.

Treloar, L.R.G., 1975, *The Physics of Rubber Elasticity*, 3rd edition, Oxford: Clarendon.

Tsai, T.T., Arnold, F.E. and Hwang, W.F., 1985, *Polymer Preprints*, **26**, 144.

Tsutsui, T. and Tanaka, R., 1980, *J. Polym. Sci., Polym. Lett. Ed.*, **18**, 17.

Tsvetkov, V.N., 1989, *Rigid-Chain Polymers*, Consultant Bureau, N.Y.

Tsvetkov, V.N., Andreeva, L.N., Bushin, S.V., Mashoshin, A.I., Cherkasov, V.A., Yedlinski, Z. and Sek, D., 1984, *Polym. Sci. USSR*, **26**, 2569.

Uchida, S., *et al.*, 1988, *Mol. Cryst. Liq. Cryst.*, **155**, 93.

Uematsu, I. and Uematsu, Y., 1981, *Polymer*, **2**, 117.

—— 1984, *Adv. Polym. Sci.*, **59**, 37.

Ueno, K., Sugimoto, H. and Hayatsu, K., 1985, *U.S.Pat.*, 4,503,005; *EP Pat.*, 92,843.

Ueno, T., Nakamura, N. and Tani, C., 1986, Proc. Japan Display, 290.

Ulrich, D.R., 1988, *in Nonlinear Optical and Electroactive Polymers*, ed. P.N. Prasad and D.R. Ulrich, New York: Plenum.

Van Luyen, D. and Strzelecki, L., 1980, *Europ. Polym. J.*, **16**, 303.

Van Luyen, D., Liebert, L. and Strzelecki, L, 1980, *Europ. Polym. J.*, **16**, 307.

Vogel, H., and Marvel, C.S., 1961, *J. Polym. Sci.*, **50**, 511.

Volkenstein, M.V. and Sharonov, Y.A., 1961, *Vysokomol. Soed.*, **3**, 1739.

Volokhina, A.V. and Kudryavtsev, G.I., 1988, in *Liquid Crystal Polymers*, ed. N.A. Plate, Moscow: Khimia.

Vorlander, D., 1908, *Kristallinisch-flussige Substanzen*, Stuttgart: Enke Verlag.

—— 1923, *Z. Phys. Chem.*, **105**, 211.

—— 1927, *Z. Phys.Chem.*, **A126**, 449.

Wan, X., Zhang, F., Wu, P., Zhang, D., Feng, X. and Zhou, Q.F., 1995, in *Macromolecular Symposia*, ed. X.J. Wang, **96**, Zug: Huthig & Wepf Verlag.

Wang, C.S., Goldfarb, I.J. and Helminiak, T.E., 1988, *Polymer*, **29**, 825.

Wang, X.J., 1990, *Wuli*, **19**, 685.

—— 1995a, *Chinese Journal of Polymer Science*, **13**, 361.

—— 1995b, *Acta Polymerica Sinica*, no. **2**, 228.

—— 1997, *Prog. Polym. Sci.*, **22**, 735.

Wang, X.J. and Lam, L., 1992, *Liquid Crystals*, **11**, 411.

Wang, X.J. and Warner, M., 1986, *J. Phys. A*, **19**, 2215.

—— 1987, *J. Phys. A*, **20**, 713.

—— 1992a, *Liquid Crystals*, **12**, 385.

—— 1992b, in *Phase Transitions in Liquid Crystals*, ed. S. Martellucci and A. Chester, New York: Plenum.

—— 1997, *Macromol. Theory Simul.*, **6**, 37.

Wang, X.J. and Zhao, J.A., 1986, *Progress in Physics*, **6**, 451.

Wang, X.J., Leadbetter, A.J. and Etherington, G., 1986, *Journal of Tsinghua University*, **26**(6), 48.

Wang, X.J., Tao, K, Zhao, J.A. and Wang, L.Y., 1989, *Liquid Crystals*, **5**, 563.

Warner, M. and Flory, P.J., 1980, *J. Chem. Phys.*, **73**, 6327.

Warner, M., Gelling, K.P. and Vilgis, T.A., 1988, *J. Chem. Phys.* **88**, 4008.

Warner, M., Gunn, J.M.F. and Baumgartner, A., 1985, *J. Phys. A*, **18**, 3007.

Warner, M. and Wang, X.J., 1991, *Macromolecules*, **24**, 4932.

—— 1992a, *Macromolecules*, **25**, 445.

—— 1992b, in *Elastomeric Polymer Networks*, ed. J.E. Mark and B. Erman, Englewood Cliffs: Prentice Hall.

—— 1992c, *J. Phys. A*, **25**, 2831.

Watanabe, J. and Hayashi, M., 1989, *Macromolecules*, **22**, 4083.

Watanabe, J. and Krigbaum, W.R., 1985, *J. Polym. Sci., Folym. Phys. Ed.*, **23**, 565.

Watanabe, J., Kishida, H. and Uematsu, I., 1981, *Polymer. Preprints. Japan*, **30**, 279.

Watanabe, J., Hayashi, M., Morita, A. and Niori, T., 1992, *Mol. Cryst. Liq. Cryst.*, **254**, 221.

Wee, E.L. and Miller W.G., 1971, *J. Phys. Chem.*, **75**, 1446.

Weiss, R.A., Huh, W. and Nicolais, L., 1987, *Polymer Engineering and Science*, **27**, 684.

Welsh, W.J., 1987, in *Current Topics in Polymer Science*, ed. R. Ottenbrite, L.A. Utracki and S. Inoue, Munich: Hanser Verlag.

Wen, Z.Q., Shen, D.Y., and Zhou, Q.F., 1988, *Fen Xi Ce Shi Tong Bao* (Chinese), **7**(6), 14.

Wendorff, J.H., 1978, in *Liquid Crystalline Order in Polymers*, ed. A. Blumstein, New York: Academic Press.

Wendorff, J.H., Finkelmann, H. and Ringsdorf, H., 1978, in *Mesomorphic Order in Polymers and Polymerization in Liquid Crystalline Media*, ed. A. Blumstein, Washington, DC: ACS.

Wolfe, J.F. and Loo, B.H., 1980, *U.S.Pat.*, 4,225,700.

Wolfe, J.F. and Arnold, F.E., 1981, *Macromolecules*, **14**, 909.

Wolfe, J.F., Loo, B.H. and Arnold, F.E., 1981, *Macromolecules*, **14**, 915.

Wolfe, J.F. and Sybert, P.D., 1985, *U.S.Pat.*, 4,533,693.

—— 1987, *U.S.Pat.*, 4,703,103.

Wu, D. C., Xie, X. G. and Xu, J. J., 1988, *Polymeric Liquid Crystals*, Chengdu: Shichun Education Press.

Wu, P.P., Hsu, X.L., Thomas, O. and Blumstein, A., 1986, *J. Polym. Sci., Polym. Phys. Ed.*, **24**, 827.

Wunderlich, B., Moller, M., Grebowicz, J. and Baur, H., 1988, *Adv. Polym. Sci.*, **87**, 1.

Xu, G., Wu, W., Shen, D., Hou, J., Zhang, S., Xu, M. and Zhou, Q.F., 1993, *Polymer*, **34**, 1818.

Yang, H.H., 1989, *Aromatic High-Strength Fibers*, New York: John Wiley & Sons.

Yoon, D.Y. and Bruckner, S., 1985, *Macromolecules*, **18**, 651.

Yoon, Y., Ho, R.M., Savitski, E.P., Li, F., Cheng, S.Z. D., Percec, V. and Chu, P., 1996, in *Liquid-Crystalline Polymer Systems*, ed. A.I. Isayev, T. Kyu and S.Z.D. Cheng, Washington, DC: ACS.

Yoshida, C., *et al.*, 1972, *Rept. Prog. Polym. Phys. Japan*, **15**, 645.

Yuasa, K., Uchida, S., Sekiya, T., Hashimoto, K. and Kawasaki, K., *Ferroelectrics*, in press.

Yurasova, T.A. and Semenov, A.N., 1991, *Mol. Cryst. Liq. Cryst.* **199**, 301.

Zbinden, R., 1964, *Infrared Spectroscopy of High Polymers*, New York: Academic Press.

Zentel, Z., 1986, *Liquid Crystals*, **1**, 589.

Zhang, C.X., Li, Z.F., Zhou, Q.F. and Zhou, H.B., 1993, *Chinese Journal of Polymer Science*, **11**, 348.

Zhang, D., Zhou, Q.F., Ma, Y.G., Wan, X.H. and Feng, X. D., 1996, *Polymers For Advanced Technologies* (in press).

Zhou, Q.F. and Lenz, R.W., 1983, *J. Polym. Sci., Polym. Chem. Ed.*, **21**, 3313.

Zhou, Q.F., Jin, J.I. and Lenz, R.W., 1985, *Canadian Journal of Chemistry*, **63**, 181.

Zhou, Q.F., Lenz, R.W. and Jin, J.-I., 1985, in *Polymeric Liquid Crystals*, ed. A. Blumstein, New York: Plenum.

Zhou, Q.F., Duan, X.Q. and Liu, Y.L., 1986, *Macromolecules*, **19**, 247.

Zhou, Q.F., Li, H.M. and Feng, X.D., 1987, *Macromolecules*, **20**, 233.

Zhou, Q.F., Zhu, X.L. and Wen, Z.Q., 1989, *Macromolecules*, **22**, 491.

Zhou, Q.F., Li, Z.F., Zhang, Z.Y. and Pei, X.Y., 1989, *Macromolecules*, **22**, 3821.

Zhou, Q.F., Wan, X., Zhu, X., Zhang, F. and Feng, X., 1993, *Mol. Cryst. Liq. Cryst.*, **231**, 107.

Zhou, Q.F., Wan, X.H., Zhang, F., Zhang, D., Wu, Z. and Feng, X., 1993, *Liquid Crystals*, **13**, 851.

Zhou, Q.F., Wan, X.H., Zhang, D. and Feng X.D., 1996, in *Liquid-Crystalline Polymer Systems*, ed. A.I. Isayev, T. Kyu and S.Z.D. Cheng, Washington DC: ACS.

Zhou, Q.F., Wan, X.H., Zhang, D. and Feng, X.D., 1996, in *Recent Advances in Liquid Crystal Polymers*, ed. A.I. Isayev *et al.*, Washington, DC: ACS.

Zocker, H., 1933, *Trans. Faraday Soc.*, **29**, 945.

This page intentionally left blank

Index